Australian Geomechanics Society

ENGINEERS AUSTRALIA

ISSN 0818-9110

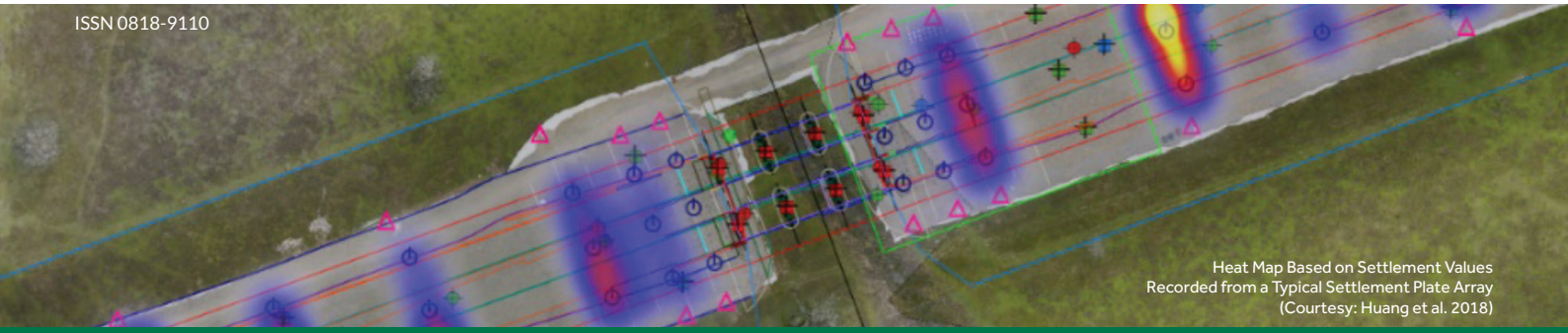

Heat Map Based on Settlement Values Recorded from a Typical Settlement Plate Array (Courtesy: Huang et al. 2018)

ADVANCES IN SITE INVESTIGATIONS, MONITORING AND INSTRUMENTATION

PROCEEDINGS OF THE 2018 AGS SYMPOSIUM HELD IN AUSTRALIAN NATIONAL MARITIME MUSEUM, DARLING HARBOUR, NSW ON NOVEMBER 16TH 2018

Low-cost Autonomous Global Navigation Satellite System (GNSS) Monitoring Installation (Courtesy: Nicholson, 2018)

ORGANISING COMMITTEE:
A. Parsa, H. Khabbaz, S. Mirlatifi, C. Rujikiatkamjorn,
A. Hulskamp, AHMK Zaman, and P. Rajarathnam

EDITORS:
H. Khabbaz, A. Parsa, AHMK. Zaman, and C. Rujikiatkamjorn

ENGINEERS AUSTRALIA

Published by The Australian Geomechanics Society,
National Secretariat,
P.O. Box 955, ST IVES, NSW 2075

AusIMM THE MINERALS INSTITUTE

The Australian Geomechanics Society (AGS) is jointly sponsored by: Engineers, Australia and The Australasian Institute of Mining and Metallurgy

Responsibility for the content of this publication rests upon the authors and not on Engineers Australia, the International Association of Hydrogeologists nor the Australian Geomechanics Society. Data presented and conclusions developed by the authors are for information only and are not intended for use without independent substantiating investigation on the part of the potential user.

Australian Geomechanics Society

Geomechanics is the application of engineering principles to the earth sciences to improve continually the accuracy, efficiency, cost-effectiveness and safety of construction projects both above and below ground, including the recovery of the earth's mineral resources. It remains an imprecise discipline due to the infinite variety of conditions in the earth's crust but correspondingly offers a fascinating and rewarding field of research and practice.

The Australian Geomechanics Society was founded in 1970. Its origins lie in the National Committee of Soil Mechanics of the Institution of Engineers, Australia, established in 1953 and the call for a corresponding society in rock mechanics. In 1973 the society was expanded to include the third discipline of engineering geology and has remained substantially unchanged since that date.

The society is affiliated to the International society of Soil Mechanics and Geotechnical Engineering (ISSMGE), the International Society for Rock mechanics (ISRM) and the International Association for Engineering Geology and the Environment (IAEG).

CORPORATE MEMBERSHIP OF THE AGS

$770.00 and look at what your organisation gets -
Membership for two nominees who each receive:

- Membership fee ($209)
- Membership of the three International Societies ($176)
- IAEG Bulletin ($44)

An extra copy of *Australian Geomechanics* for company library ($154)

Acknowledgement in front section of every issue of *Australian Geomechanics*

Total benefit is $836 All prices include GST.

Contact Peter Robinson on secretary@australiangeomechanics.org or go to www.australiangeomechanics.org **for application forms and more information**.

(c) Australian Geomechanics Society

All rights reserved. Other than brief extracts, no part of this publication may be produced in any form without the written consent of the publisher. The Society encourages reproduction of its publications and consent is usually looked upon favourably. It is a requirement that full and complete acknowledgement be cited when referencing articles published by AGS.

TIMETABLE

8:00 Registration

8:45 Opening Address

SESSION I:
ADVANCES IN INSTRUMENTATION AND MONITORING (MINING AND INFRASTRUCTURE)

9:00 Keynote Lecture

Advances in Ground Monitoring Techniques – A Surveyor's Perspective

M. Nicholson (Michael Nicholson Consulting)

9:30 Presentation

Continuous Monitoring of Landslides and Infrastructure for Asset Management

P. Flentje (UOW)

9:50 Presentation

Monitoring of Mining Induced Movements Between Bridge Components with Fibre Bragg Grating Sensors

M. Brunton (Monitor Optics System)

10:05 Questions

10:20 Morining Tea

SESSION II:
ADVANCES IN MEASUREMENT OF GROUNDWATER AND ROCK IN-SITU STRESSES

10:50 Presentation

Groundwater Drawdown Related Settlement and Pump Test Interpretation

R. Best (Coffey)

11:10 Presentation

In situ Stress Testing for Tunnel Design in Sydney – Hydraulic Fracturing and Overcoring

A. Suchowerska (Golder Associates)

11:25 Presentation

Standpipe Piezometer Installation - Lessons Learnt

S. Thorin (AECOM)

11:40 Presentation

Development of computer code to optimise the downloading of data loggers and the production of hydrographs in Sydney, Australia

C. Murphy (AECOM)

11:55 Questions

12:15 Lunch

SESSION III:
INNOVATIONS IN SITE INVESTIGATIONS AND TESTING

13:00 Keynote Lecture

CPT-based Soil Behavior Type (SBT) Classification System: recent updates and applications

P. Robertson

13:30 Presentation

Sampling disturbance in soft ground: implications in geotechnical design

J. Pineda (UON)

13:50 Presentation

Hard Drilling – Overcoming challenging ground conditions with a diverse and integrated ground investigation campaign for the new bridge over the Clarence River, Harwood NSW

J. Care (Arup)

14:05 Presentation

An Innovative Method of Assessing the Capacity of Existing Wharf Piles

P. Wong (PKW Solutions)

14:20 Questions

14:40 Afternoon Tea

SESSION IV:
ADVANCES IN INSTRUMENTATION AND MONITORING (DATA MANAGEMENT SYSTEMS FIBRE OPTICS, AND GEOPHYSICS)

15:10 Presentation

Real time monitoring of a road embankment subject to coastal erosion and slope instability

H. Buys (AECOM)

15:30 Presentation

Satellite InSAR technique for urban tunnelling monitoring: the Crossrail project case study

B. Payas (SIXENSE)

15:45 Presentation

Woolgoolga to Ballina Pacific Highway Upgrade – Embankment Performance Monitoring

V. D. Nguyen (Coffey)

16:00 Presentation

The use of ultra-wide band GPR for the detection of voiding and other artefacts in bridge abutments and related retaining structures

R.Newton (RMS)

16:15 Presentation

GeoView – An Advanced Instrumentation and Monitoring Data Management System

D. Huang (EIC)

16:30 Questions

16:50 Closing Address

17:00 Close

IGS

reducing geotechnical uncertainty

In Situ Testing

CPT, CPTu, SCPTu, Tee-Bar
DMT, SDMT, Vane Shear

Sampling

PPI Piston Sampler
Vibracore & other sediment samplers
Vertek & Window samplers, etc

Other Things

piezos, standpipes & permeabilities

0417-748-669
allan@insitu.com.au
www.insitu.com.au

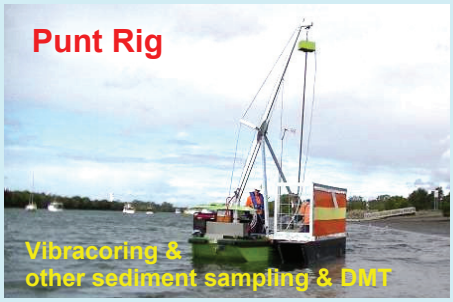

Melbourne *Sydney* *Newcastle* *Brisbane* *Townsville* *PNG*

SMEC
Member of the Surbana Jurong Group

local people
global experience

SMEC and Surbana Jurong Group's partnership provides a talent pool of 14,000 people working across a network of 120 offices in more than 40 countries.

SMEC has provided geotechnical engineering and geological services on a diverse range of projects for over 40 years.

Our expertise includes soft ground engineering, underground space development, soil-structure interaction and slope assessment and design.

Our capability spreads across all aspects of geotechnical and geological engineering, from planning, investigation and feasibility studies, through to design, construction surveillance and operations and maintenance.

—

www.smec.com

GROUND BREAKING SOLUTIONS

Taking on projects at any scale, our integrated team cuts through complex issues in design, construction, site investigations and tunnelling to deliver transformational outcomes for our clients.

AECOM's ground engineering specialists understand the challenges of delivering complex projects. For further information visit **aecom.com**

AECOM Imagine it. Delivered.

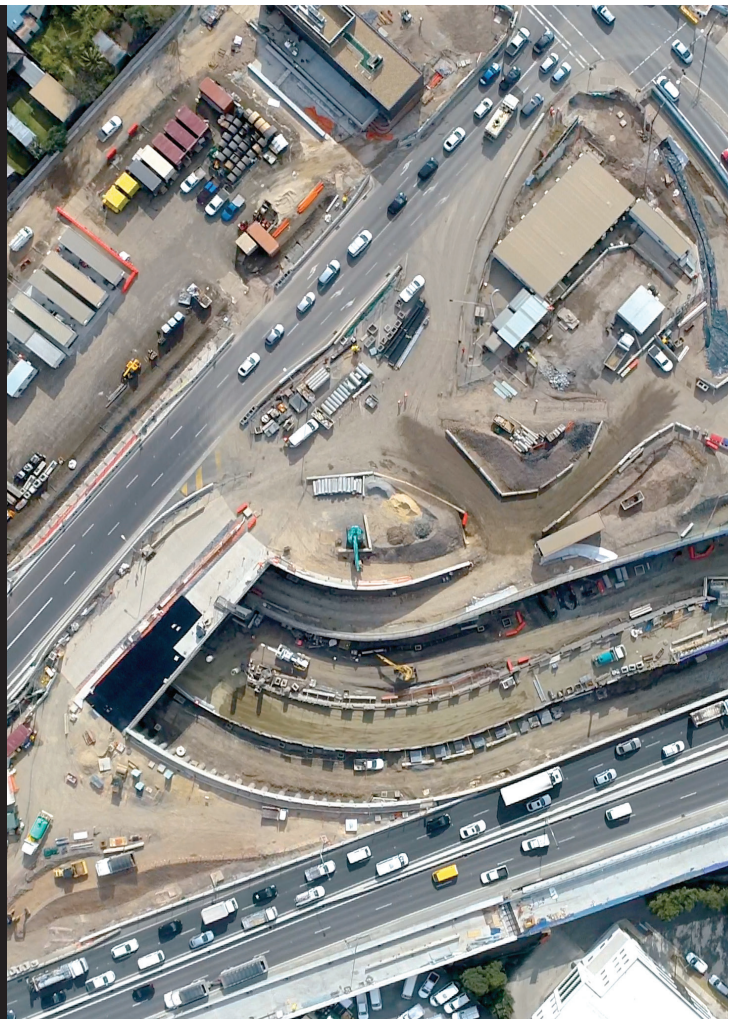

We drive forward expertise in the structure and behaviour of all ground conditions, to become better managers of our built and natural world.

As an acknowledged leader in geotechnics, Arup is often asked to push the essential skill and science of designing and building structures in the ground. Wherever difficult ground conditions, sensitive environments or ambitious projects present geotechnical challenges, Arup provides robust and advanced solutions.

Our geotechnical expertise underpins Arup's work on projects from building design to infrastructure for water, energy, mining, rail, highways and aviation. To the full range of geotechnical needs, we bring interconnected skills in *foundation and landfill engineering*, *environmental geotechnics*, *hydrogeology*, *tunnel and seismic design*, *geographic information systems*, *engineering geology* and many specialised services.

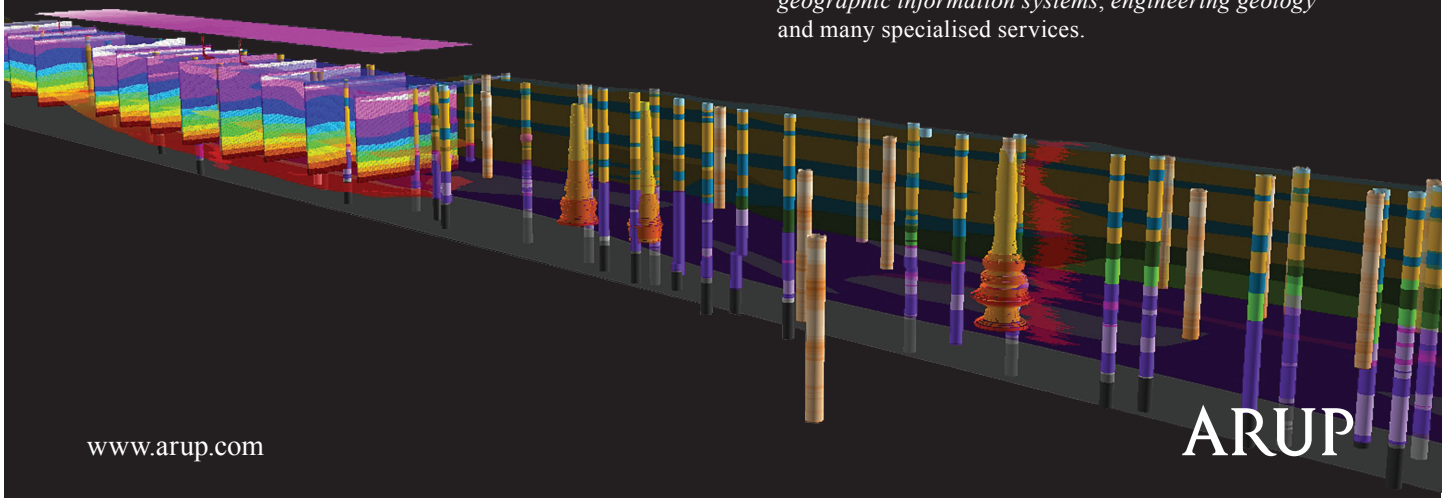

www.arup.com

ARUP

coffey

A TETRA TECH COMPANY

Coffey harnesses nearly 60 years of specialist geotechnical engineering experience to help our clients deliver their projects successfully.

We take great care to hone and nurture the passion, knowledge and expertise that sits with our people to instil a culture of collaboration and ingenuity.

Our team thrives on the tricky, the complex and the challenging projects and take pride in working closely with our Clients.

coffey.com

Douglas Partners

Geotechnics / Environment / Groundwater

Understanding and Solutions from the Earth's Surface Down

Geotechnical Engineering
Engineering Geology
Rock Mechanics
Environment
Geophysics
Groundwater
Construction Monitoring
Earthworks

BALLINA - BRISBANE - CAIRNS - CANBERRA
CENTRAL COAST COFFS HARBOUR - DARWIN
GEELONG - GOULBURN - GOLD COAST - MACARTHUR
MELBOURNE - NEWCASTLE - NTH WEST SYDNEY
PERTH - PORT MACQUARIE - SUNSHINE COAST
SYDNEY - TOWNSVILLE - WOLLONGONG

www.douglaspartners.com.au

EIC ACTIVITIES

A MEMBER OF THE CIMIC GROUP
CIMIC

Trusted experience. Integrated solutions.

EIC Activities is proudly part of the CIMIC Group. We are connecting our expertise with the diversity of skill and specialisation across our family of industry leaders to drive insight and deliver enduring value, together.

CIMIC GROUP INCLUDES CPB CONTRACTORS · LEIGHTON · BROAD CONSTRUCTION · THIESS · SEDGMAN · UGL · PACIFIC partnerships

JK Geotechnics

Industry Leading Geotechnical Engineers & Engineering Geologists

Investigations for proposed riverbank stabilisation works in Wolgan Valley, NSW. Geotechnical issues include collapsible and deep 'soft' soils.

Servicing the following markets:

Residential • Commercial/Industrial • Infrastructure • Construction • Legal & Insurance • Councils • Government • Education

www.jkgeotechnics.com.au 115 Wicks Road, Macquarie Park, 2113 Ph: +61 2 9888 5000

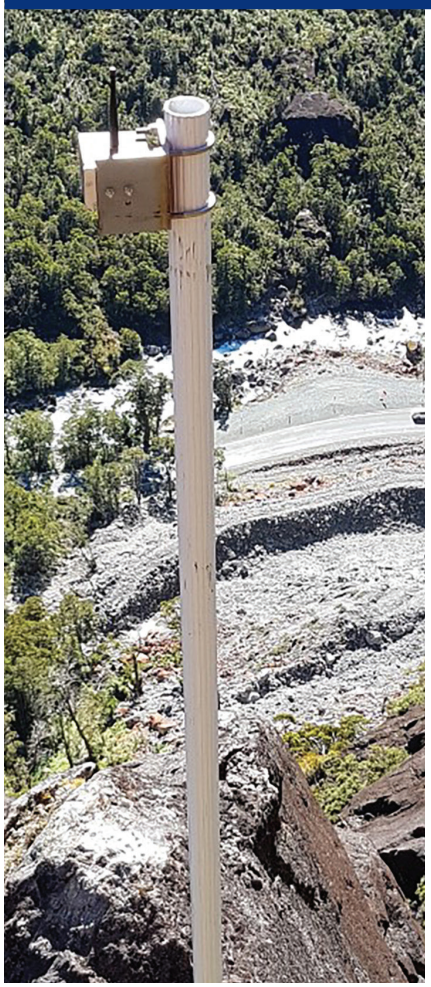

Wireless Monitoring

Any Site.Any Scale

Scalable • Reliable • Robust

Monitor any structure or landscape, without prisms and entirely wire free!

Senceive is an innovative deformation monitoring solution that delivers unparalleled accuracy and reliability, with the ability to fit to almost any structure or landscape and be scaled to any size of project.

Ideal for:

- Roads
- Tunnels
- Bridges
- Rail
- Façades

Senceive
Wireless condition monitoring

Get in touch today:

1300 867 266

info@positionpartners.com.au

www.positionpartners.com.au

Australia • New Zealand • SE Asia

Position Partners

Shaping New Dimensions

NSW GOVERNMENT | Transport Roads & Maritime Services

Did you know?

WSP is solving geotechnics and tunnelling challenges for:

- / the largest freight rail project in Australia
- / the light rail that's revitalising Newcastle
- / Australia's largest regional public infrastructure project
- / the longest road tunnel in New Zealand
- / the widest underground metro platforms in the world
- / Australia's deepest urban basement in St Leonards.

2018 Winner! International Road Federation's **Global Road Achievement Award – Design** (Waterview Connection)

wsp

Advances in Site Investigations, Monitoring and Instrumentation

PREFACE

This document contains the accepted papers submitted and peer reviewed for the 22nd annual symposium organised by the Sydney Chapter of the Australian Geomechanics Society (AGS). It is hoped that the symposium will keep practicing geotechnical engineers, engineering geologists, and other engineering professionals informed of recent developments in this field. It also recognises the need to gather the experience of those practicing throughout Australia and to allow transfer of knowledge and sharing of their experiences.

These symposia continue to be one of the best forms for bringing together the key stakeholders of the Australian geological and geotechnical community. The main objective of the symposium, held on 16 November 2018, is to present overviews of current geotechnical investigation and instrumentation challenges, state-of-the-art practices, innovative technologies, new research results and case histories demonstrating applications of advanced techniques and cost effective approaches in site investigation and verification of long-term performance of earth and earth supported structures. Papers are invited on geotechnical aspects of site investigation, real time monitoring and new insights into experiences, technologies and strategies.

This symposium is the cooperative effort of many authors and qualified reviewers. The editors and organising committee wish to thank the authors, who have generously contributed their time to prepare the various papers and the colleagues of the authors, who have assisted with time, secretarial, drafting and other facilities. Appreciation is also extended to our sponsors for their support. Without them, the Symposium would not be possibly the best ongoing forum for the Australian Geomechanics and groundwater community.

Ali Parsa, Sam Mirlatifi, Cholachat Rujikiatkamjorn, Hadi Khabbaz, Adrian Hulskamp, AHMK Zaman and Puvaneswary Rajarathnam

On behalf of the AGS Symposium Organising Committee,
The Australian Geomechanics Society, Sydney Chapter

Annual Seminars of AGS Sydney Chapter

No.	Date	Topic	Chairman & Organising Team
1	1997	Pavement Design Beyond 2000	A Leventhal
2	1998	Recent Developments in Piling Practice in Sydney	P Andrews
3	1999	Flexible Retaining Walls: Design to Prevent Failure	P Andrews and P Hewitt
4	2000	Computer Methods	P Hewitt and J Carter
5	2001	Excavation Retention	T Walker and P Hewitt
6	2002	Landslide Risk Management	B Walker and T Walker
7	2003	Geotechnical Instrumentation and Construction Works Compliance Testing	G Scholey and T Walker
8	2004	The Engineering Geology of the Sydney Region – Revisited	G Scholey, M Parmar, G Young and G McNally
9	2005	Geotechnical Aspects of Tunnelling	H Buys and T Gourlay
10	2006	Soft Ground Engineering	H Buys, R Moyle and P Hewitt
11	2007	Engineering Advances in Earthworks	R Moyle, R Lindbeck and H Liu
12	2008	Foundation Design and Construction	R Moyle, R Lamont and B Ewers
13	2009	Geosynthetics – New Materials for Modern Infrastructure	B Ewers, H Buys and H Liu
14	2010	Seismic Engineering- Design for Management of Geohazards	C Rujikiatkamjorn, J McIlveen, R Lamont and M Haysler
15	2011	Coastal and Marine Geotechnics- Foundations for Trade	C Rujikiatkamjorn, J McIlveen, G Blumberg, J Smith and C Y Tey
16	2012	Advances in Geotechnical Aspects of Roads and Railways	H Khabbaz, C Y Tey, O Stahlhut and C Rujikiatkamjorn
17	2013	Retaining Structures: Recent Advances and Past Experiences	H Khabbaz, C Rujikiatkamjorn, M van Uden, C McColgan and S Mirlatifi
18	2014	Resilient Geotechnics	H Khabbaz, C Rujikiatkamjorn, S Mirlatifi, C McColgan and M van Uden
19	2015	Recent Developments and Experiences with Groundwater and Excavation	C Rujikiatkamjorn, S Mirlatifi, Katarina David, A. Hulskamp, and M van Uden
20	2016	Ground Stabilisation Techniques for Problematic Soils and Unstable Rocks	C Rujikiatkamjorn, S Mirlatifi, A. Hulskamp, T Mcwilliam and H Khabbaz
21	2017	Geotechnical innovations and challenges for transport infrastructure	S Mirlatifi, , C Rujikiatkamjorn, G Vorobieff, D Airey, A Parsa, A Hulskamp, H Khabbaz, H Buys and K Oj,
22	2018	Advances in Site Investigations, Monitoring and Instrumentation	A. Parsa, H. Khabbaz, S. Mirlatifi, C. Rujikiatkamjorn, A. Hulskamp, AHMK Zaman, and P. Rajarathnam

TABLE OF CONTENTS

PROGRAM i

SPONSORS ii

PREFACE viii

TABLE OF CONTENTS x

KEYNOTE PAPER: 1
SOIL BEHAVIOR TYPE CLASSIFICATION SYSTEM BASED ON CONE PENETRATION TEST
Peter K. Robertson

KEYNOTE PAPER: 30
ADVANCES IN GROUND MONITORING TECHNIQUES – A SURVEYORS PERSPECTIVE
Michael Nicholson

CONTINUOUS MONITORING OF LANDSLIDES AND INFRASTRUCTURE FOR ASSET MANAGEMENT 43
Phil Flentje, David Arnold, Dhammika Ruberu, Andrew Monk, Peter Tobin, Kevin Bogie and Raymond Piatek

MONITORING OF MINING INDUCED MOVEMENTS BETWEEN BRIDGE COMPONENTS WITH FIBRE BRAGG GRATING SENSORS 60
M. Brunton and B. E. Whelan

GROUNDWATER DRAWDOWN RELATED SETTLEMENT AND PUMP TEST INTERPRETATION 70
Ross James Best

IN SITU STRESS TESTING FOR TUNNEL DESIGN IN SYDNEY – HYDRAULIC FRACTURING AND OVERCORING 83
Anastasia Suchowerska, Les McQueen and Mahdi Zoorabadi

STANDPIPE PIEZOMETER INSTALLATIONS - LESSONS LEARNT 92
Sven Thorin, Angus McFarlane, Alasdair Hamilton

DEVELOPMENT OF COMPUTER CODE TO OPTIMISE THE PRODUCTION OF HYDROGRAPHS IN SYDNEY, AUSTRALIA 105
Cassandra Murphy

SAMPLING DISTURBANCE IN SOFT GROUND: IMPLICATIONS IN GEOTECHNICAL DESIGN 113
Jubert Pineda, Richard Kelly, Laxmi Suwal, Guan Tor Lim and Kaiwen Ouyang

A COMPREHENSIVE GEOTECHNICAL INVESTIGATION FOR THE NEW BRIDGE OVER THE CLARENCE RIVER AT HARWOOD 131
James Care and Michelle Watson

AN INNOVATIVE METHOD OF ASSESSING THE CAPACITY OF EXISTING WHARF PILES 141
Patrick Wong and Peter Hitchcock

REAL TIME MONITORING OF A ROAD EMBANKMENT SUBJECT TO COASTAL EROSION AND SLOPE INSTABILITY 149
Henk Buys and Puvaneswary Rajarathnam

SATELLITE INSAR TECHNIQUE FOR URBAN TUNNELLING MONITORING: THE CROSSRAIL PROJECT CASE STUDY 162
Nuria Devanthery, Javier González Martí, Blanca Payas, Eric Audigé

WOOLGOOLGA TO BALLINAPACIFIC HIGHWAY UPGRADE –EMBANKMENT PERFORMANCE MONITORING AND BACK-ANALYSIS 171
Viet D. Nguyen, Patrick K. Wong, Henry Zhang

THE USE OF ULTRA-WIDE BAND GPR FOR THE DETECTION OF VOIDING AND OTHER ARTEFACTS IN BRIDGE ABUTMENTS AND RELATED RETAINING STRUCTURES 180
Reagan Newton

AN ADVANCED WEB-BASED MANAGEMENT SYSTEM FOR INSTRUMENTATION AND MONITORING DATA 205
Darren Huang, Idy Li and Jeff His

A CASE STUDY – GEOTECHNICAL AND GEOPHYSICAL INVESTIGATIONS OF AN OLD STONE HERITAGE BRIDGE AT PARRAMATTA, GREATER WESTERN SYDNEY NSW, AUSTRALIA 216
Yogeshwaran Arumugam, Peter Hitchcock, Rolf Rohleder and Simon Stewart

DEVELOPMENT AND APPLICATION OF GEOTECHNICAL MONITORING AND DATA MANAGEMENT FOR WOOLGOOLGA TO BALLINA PACIFIC HIGHWAY UPGRADE 223
1Henry Zhang, Paul Hewitt, Graham Yip, Stephen Summerell, Sudar Aryal, Chris Davis, David Groth, & James Tyrrell

EXPERIENCE OF OVERCORING THE ANZI STRAIN CELL IN HQ EXPLORATION BOREHOLES TO DETERMINE THE THREE DIMENSIONAL IN SITU STRESSES AT DEPTHS APPROACHING 1KM 234
Kenneth W. Mills and Jesse W. Puller

VIBRATION TRANSFER MOBILITY MEASUREMENTSCOMBINING FALLING WEIGHT AND IMPACT HAMMER EXCITATION METHODS 244
Giovanni Farotto and Alexis Bigot

MONITORING OF SPRAYED CONCRETE LINED TUNNELS USING FIBRE BRAGG GRATING SENSORS 258
M Brunton, J Preston, BE Whelan

ASSESSMENT OF METHODOLOGIES FOR REBURIAL OF EXCAVATED ACID SULFATE SOFT SOILS WITHIN SHELL COVE BOAT HARBOUR ZONE 268
Kourosh Kianfar, Scott Morrison, Glenn Colquhoun

[All papers have been refereed in accordance with the full DETYA (Department of Education, Training and Youth Affairs) review process, unless stated otherwise.]

SOIL BEHAVIOR TYPE CLASSIFICATION SYSTEM BASED ON CONE PENETRATION TEST

Peter K. Robertson
Technical Advisor, Gregg Drilling & Testing Inc., California, USA

ABSTRACT

A soil classification system is used to group soils according to shared qualities or characteristics based on simple cost effective tests. The most common soil classification systems used in geotechnical engineering are based on physical (textural) characteristics such as grain size and plasticity. Ideally, geotechnical engineers would also like to classify soils based on behavior characteristics that have a strong link to fundamental in-situ behavior. Existing textural-based classification systems have a weak link to in-situ behavior since they are measured on disturbed and remolded samples. The cone penetration test (CPT) has been gaining in popularity for site investigations due to the cost effective, rapid, continuous and reliable measurements. The most common CPT-based classification systems are based on behavior characteristics and are often referred to as a Soil Behavior Type (SBT) classification. This paper presents an update of popular CPT-based SBT classification systems to use behavior-based descriptions. The update includes a method to identify the existence of microstructure in soils and examples are used to illustrate the advantages and limitations of such a system.

1 INTRODUCTION

This paper is a shorter version of a paper in the Canadian Geotechnical Journal (Robertson, 2016). A soil classification system is used to group soils according to shared qualities or characteristics based on simple cost effective tests. The most common soil classification systems used in geotechnical engineering are based on physical (textural) characteristics such as grain size and plasticity (e.g. Unified Soil Classification System). These textural-based classification systems have been used for over 70 years to provide general guidance through empirical correlations based on past field experience. Unfortunately, empirical correlations between simple physical index properties measured on remolded samples and in-situ soil behavior have significant uncertainty. Ideally, geotechnical engineers should also classify soils based on fundamental behavior characteristics that have a strong link to in-situ behavior. A combined classification based on both physical and behavior characteristics would be very helpful for many geotechnical projects.

The cone penetration test (CPT) has been gaining in popularity for site investigations due to the cost effective, rapid, continuous and reliable measurements. The most common CPT-based classification systems are based on behavior characteristics and are often referred to as a Soil Behavior Type (SBT) classification (e.g. Robertson, 1990). However, most CPT-based SBT classification systems use textural-based descriptions, such as sand and clay that can cause some confusion in geotechnical practice. The objective of this paper is to present an update to the Robertson (1990, 2009) and Schneider et al (2008) CPT-based SBT classification system with behavior-based descriptions for each soil group. The importance of microstructure and how it can influence CPT-based classification is also discussed. The paper will also collate, update and summarize the growing experience that exists to guide in the classification of soils based on CPT measurements.

2 SOIL CLASSIFICATION

The most common soil classification system used by engineers and geologists in North America is the Unified Soil Classification System, USCS (ASTM D 2487-11). The system, similar to others used around the world, is based on physical characteristics of grain-size distribution and plasticity (Atterberg Limits) measured on disturbed and remolded samples. The USCS groups soils into two broad groups: coarse-grained (sand and gravel) and fine-grained (silt and clay). Coarse-grained soils are those with more than 50% retained on or above the #200 sieve (>0.075mm) and are further grouped based on grain size and fines content (e.g. silty sand). Fine-grained soils are those with 50% or more passing the #200 sieve and are further grouped based on plasticity (high or low).

The actual in-situ soil behavior depends on many other factors such as geologic processes related to origin, environmental factors (such as stress history) as well as physical and chemical processes. In general, soils tend to become stiffer and stronger with age. The successful link between simple physical characteristics and in-situ behavior is strongly influenced by geologic factors such as age and cementation. Typically, the link is most successful when applied to young (Holocene and Pleistocene-age), uncemented silica-based deposits with limited stress and strain history (e.g. older heavily overconsolidated clays can have similar strength and compressibility characteristics to younger uncemented sands).

3 GENERALIZED SOIL BEHAVIOR

The behavior of natural soils is complex with many extensive publications attempting to describe this behavior (e.g. Leroueil and Hight, 2003). The following is a very short summary of some key features of soil behavior as it relates to a possible behavior type classification system.

The following features describe the essential elements of soil behavior (e.g. Atkinson, 2007):

- Soil can change in volume due to rearrangement of grains and void space changes.
- Soil is essentially frictional where strength and stiffness increases with normal stress and with depth in the ground.
- Soil is essentially inelastic where response is non-linear to loading beyond an initial very small threshold strain.

As stated above, in-situ soil behavior depends on many factors such as geologic processes related to origin (e.g. depositional and compositional features), environmental factors (e.g. stress and temperature), as well as physical and chemical processes (e.g. aging and cementation). The powerful early concepts of Critical State Soil Mechanics (CSSM) were based on tests performed on isotropically consolidated reconstituted (clay) samples and can be representative of saturated '*ideal soils'* (Leroueil and Hight, 2003). Many natural soils have some form of structure that can make the in-situ behavior different from those of '*ideal soils'*. The term structure can be used to describe features either at the deposit scale (macrostructure), e.g. layering and fissures, or at the particle scale (microstructure), e.g. bonding/cementation. Older natural soils tend to have some microstructure caused by post depositional factors, of which the primary ones tend to be age and bonding (cementation).

Many authors have discussed the effects of microstructure (e.g. Burland, 1990, Leroueil, 1992, Leroueil and Hight, 2003). Microstructure can be caused by many factors such as: secondary compression, thixotropy, cementation, cold welding, and aging (Leroueil and Hight, 2003). Microstructure tends to give a soil a strength and stiffness that cannot be accounted for by void ratio and stress history alone. Compared to the same '*ideal soil*' at the same void ratio, the *'structured soil'* with microstructure has higher yield stress, peak strength and small strain stiffness. At larger strains, when the effects of microstructure can be destroyed due to factors such as; compression, shearing, swelling, weathering and fatigue, the soil becomes '*destructured*' (Leroueil and Hight, 2003). The term *'ideal soil'* will be used to describe soils with little or no microstructure that are predominately young and uncemented. The term *'structured soil'* will be used to describe soils with extensive microstructure, such as caused by aging and cementation.

CSSM is based on the observation that soils ultimately reach critical state (CS) at large strains and at critical state there is a unique relationship between shear stress, normal effective stress and void ratio. Since critical state is independent of the initial state, the parameters that define critical state depend only on the nature of the grains of the soils and can be linked to basic soil classification (e.g. Atkinson, 2007). The current in-situ state of a soil can be defined in a number of ways. In fine-grained soil, it is common to define the current state in terms of overconsolidation ratio (OCR) that is related to the normal compression line (NCL), since fine-grained '*ideal soils'* tend to have a unique NCL that is essentially parallel to the CSL. In coarse-grained soil, it is still common to define in-situ state in terms of relative density (or density index), especially for clean sands. However, it is becoming more common to define the current state in terms of a state parameter (ψ) that is related to the CSL, since the NCL is not unique (e.g. Been and Jefferies, 1985). At low confining stress the CSL for many clean silica-based sands can be very flat in terms of void ratio versus log mean effective stress and hence, there is an approximate link between relative density and state parameter. However, state parameter can capture the current state for most coarse-grained soils over a wide range of stress.

There is an important difference between the behavior of '*ideal soils'* that are either 'loose' or 'dense' of CS. Soils that are 'loose' of CS tend to contract on drained loading (or where pore pressures rise on undrained shear). Soils that are 'dense' of CS tend to dilate at large shear strains (or where pore pressures can decrease in undrained loading). The tendency of soils to change volume while shearing is called dilatancy and is a fundamental aspect of soil behavior.

The behavior of soil in shear prior to failure can be classified into two groups; soils that dilate at large strains and soils that contract at large strains. Saturated soils that contract at large strains have a shear strength in undrained loading that is lower than the strength in drained loading, whereas saturated soils that dilate at large strains tend to have a shear strength in undrained loading that is either equal to or larger than in drained loading. When saturated soils contract at large strain, they may also show a strain softening response in undrained shearing, although not all soils that contract show a strain softening response in undrained shear. This strength loss in undrained shear can result in instability given an appropriate geometry, such as flow liquefaction (e.g. Robertson, 2010). Hence, classification of soils that are either contractive or dilative at large strains can be an important behavior characteristic for many geotechnical problems.

Jefferies and Been (2006) had suggested that coarse-grained *'ideal soils'* with a state parameter $\psi < -0.05$ will tend to dilate at large strains when loaded in drained shear. Hence, coarse-grained saturated *'ideal soils'* with $\psi < -0.05$ will tend to generate a decrease in pore pressure and an increase in effective stress at larger strains in undrained shear and tend to be strain hardening. Likewise, fine-grained saturated '*ideal soils'* with an OCR > 4 tend to dilate when loaded in drained shear and also tend to generate a decrease in pore pressure in undrained shear. Most soils tend to contract at small strains (i.e. develop positive pore pressures under undrained loading), which is a major feature in soils that experience cyclic liquefaction. Clearly classifying soils by their tendency to dilate or contract at large strains under shearing is an important behavior characteristic since it can guide the engineer in terms of appropriate behavior parameters and critical loading conditions.

Idriss and Boulanger (2008) classified soils as either sand-like or clay-like in their behavior, where sand-like soils are susceptible to cyclic liquefaction and clay-like soils are not susceptible to cyclic liquefaction. Idriss and Boulanger (2008) also suggested that fine-grained soils transition from behavior that is more fundamentally like sands to behavior that is more fundamentally like clays over a fairly narrow range of plasticity index (PI). Sand-like soils tend to have PI < 10% and clay-like soils tend to have PI > 18% (Bray and Sancio, 2006). The transition from more sand-like to more clay-like behavior is conceptually similar to the transition in the USCS from coarse-grained (non-plastic) to fine-grained (plastic) soils, although some low or non-plastic fine-grained soils (e.g. ML and CL) can behave more sand-like, as suggested by Idriss and Boulanger (2008). Likewise, the transition from saturated soils that are more sand-like to more clay-like typically corresponds to a response that transitions from one that is predominately drained under most static loading to a response that is predominately undrained under most static loading, although the rate of loading also has a major role.

A modified classification system based on behavior characteristics can be built around groupings that divide soils that show either dilative or contractive behavior at large strains and soils that are predominately more sand-like or more clay-like. There can also be a group that captures soils that are in transition from more sand-like to more clay-like, since the change occurs over a range of behavior type.

Since natural soil behavior is complex, any classification system based on behavior characteristics should involve multiple measurements that are repeatable and capture different aspects of in-situ soil behavior. For classification systems to be effective and easy to use they must also be based on rather simple, cost effective repeatable tests. For an in-situ test to meet these demands, the test should be simple, cost effective and provide several repeatable independent measurements. One of the most popular modern in-situ test that is applicable to most uncemented soil is the cone penetration test (CPT). The CPT is fast (20mm/s), cost effective and provides continuous and repeatable measurements of several parameters. The basic CPT records tip resistance (q_c) and sleeve resistance (f_s). The CPTu provides the addition of penetration pore pressure (u), often in the u_2 location just behind the tip, combined with a measure of the rate of pore pressure dissipation during a pause in the penetration process, often expressed as the time required to dissipate 50% of the excess pore pressure (t_{50}). The CPTu can also provide in-situ equilibrium pore pressure after 100% dissipation (u_o) that is helpful

to define the in-situ piezometric profile at the time of the CPTu. The seismic CPTu (SCPTu) provides the additional measurement of in-situ shear wave velocity (V_s) and, in some conditions, in-situ compression wave velocity (V_p). Hence, the SCPTu can provide up to 7 independent measurements in one cost effective test. Ideally a classification system should include all these measurements to be fully effective. However, a practical classification system can still be effective based on either 2 or 3 measurements, provided limits are placed on the range of applicable soils (e.g. restricted to predominately '*ideal soils'*).

Any behavior based classification systems will tend to apply primarily to '*ideal soils'* that have little or no microstructure. Hence, it can be important to have a system and associated in-situ test that can also provide a method to identify if the soil to be classified has a behavior similar to most '*ideal soils'*, i.e. has little or no microstructure. It will be shown that the SCPTu measurements have the potential to identify soils with significant microstructure.

4 EXISTING CPT-BASED CLASSIFICATION

One of the major applications of the CPT has been the determination of soil stratigraphy and the identification of soil type. This has been accomplished using charts that link cone measurements to soil type. The early charts developed in the Netherlands were based on measured cone resistance, q_c and sleeve resistance, f_s using a mechanical cone (e.g. Begemann, 1965) and showed that there is an approximate linear link between q_c and f_s for a given soil type. Early charts using q_c and friction ratio ($R_f = f_s/q_c$ in percent) where proposed by Douglas and Olsen (1981), but the charts proposed by Robertson et al. (1986) and Robertson (1990, 2009) have become very popular. Robertson et al (1986) and Robertson (1990, 2009) stressed that the charts were predictive of Soil Behavior Type (SBT), since the cone responds to the in-situ mechanical behavior of the soil (e.g. strength, stiffness, compressibility and drainage) and not directly to classification criteria based on physical characteristics, such as grain-size distribution and soil plasticity.

The CPT-based normalized Soil Behavior Type (SBTn) method suggested by Robertson (1990) was based on the following normalized parameters:

$$Q_{t1} = (q_t - \sigma_{vo})/\sigma'_{vo} \quad (1)$$

$$F_r = [(f_s/(q_t - \sigma_{vo})] \, 100\% \quad (2)$$

$$B_q = (u_2 - u_0) / (q_t - \sigma_{vo}) = \Delta u / (q_t - \sigma_{vo}) \quad (3)$$

where:
q_t = cone resistance corrected for water effects, where $q_t = q_c + u_2(1\text{-}a)$
a = cone area ratio, typically around 0.8
σ_{vo} = current in-situ total vertical stress
σ'_{vo} = current in-situ effective vertical stress
u_2 = penetration pore pressure (immediately behind cone tip)
u_0 = current in-situ equilibrium water pressure
Δu = excess penetration pore pressure = $(u_2 - u_o)$

Robertson (1990) suggested two charts based on either Q_{t1} - F_r and Q_{t1} - B_q but recommended that the Q_{t1} - F_r chart (illustrated in Figure 1) was generally more reliable, since the CPT penetration pore pressures (u_2) can suffer from lack of repeatability due to loss of saturation, especially when performed onshore at locations where the water table is deep and/or in very stiff soils. The sleeve resistance (f_s) is often considered less reliable than the cone resistance (q_c) due to variations in cone design (e.g. Lunne et al, 1986). However, Boggess and Robertson (2010) provided recommendations on methods to improve the repeatability and reliability of sleeve resistance measurements by using cone designs with separate load cells, equal end areas sleeves, attention to tolerance requirements and careful test procedures. Robertson (2009) also showed that, in softer soils, the SBTn charts are not overly sensitive to variations in f_s. The chart shown in Figure 1 is based on the corrected cone resistance (q_t) that requires pore pressure measurements to make the correction. However, the difference between q_c and q_t is generally small, except in very soft fine-grained soils. Hence, the chart in Figure 1 is often used successfully with the basic CPT data of q_c and f_s in most soils (i.e. q_c used in equation 1). Since soils are essentially frictional and both strength and stiffness increase with depth, normalized parameters are more consistent with in-situ soil behavior. The chart in Figure 1 is often referred to as the *Robertson SBTn* chart.

Since 1990 there have been other CPT soil behavior type charts developed (e.g. Jefferies and Davies, 1991; Olsen and Mitchell, 1995; Eslami and Fellenius, 1997; Ramsey, 2002; Schneider et al, 2008; Schneider et al, 2012). Each chart tends to have advantages and limitations some of which were briefly discussed by Robertson (2009). A common feature in many of these CPT-based methods is that the classification system uses groupings based on traditional physical descriptions (e.g. sand and clay) even though the methods are based on behavior measurements (e.g. either q_c or q_t and f_s). This has resulted in some confusion in geotechnical practice.

Jefferies and Davies (1993) identified that a Soil Behavior Type Index, I_c, could represent the SBTn zones in the Q_{t1} - F_r chart where I_c is essentially the radius of concentric circles that define the boundaries of soil type. Robertson and Wride, (1998) modified the definition of I_c to apply to the Robertson (1990) $Q_{t1} – F_r$ chart, as defined by:

$$I_c = [(3.47 - \log Q_{t1})^2 + (\log F_r + 1.22)^2]^{0.5} \quad (4)$$

The contours of I_c can be used to approximate the SBTn boundaries. The circular shape of the I_c boundaries provides a reasonable fit to the SBTn boundaries in the center of the chart where much of the data exists for most normally to lightly overconsolidated *'ideal soils'*. For some soils, the circular shape is a less effective fit to the original SBT boundaries, as illustrated in Figure 1 for $I_c = 2.6$ and discussed by Robertson (2009). Robertson and Wride (1998) had suggested that $I_c = 2.6$ was an approximate boundary between soils that were either more sand-like or more clay-like, based on cyclic liquefaction case histories that were limited to predominately silica-based *'ideal soils'* that were essentially normally consolidated. However, experience has shown that the $I_c = 2.6$ boundary is not always effective in soils with significant microstructure.

Robertson (2009) updated the normalized cone resistance and the associated SBTn chart, using a normalization with a variable stress exponent, n; where:

$$Q_{tn} = [(q_t – \sigma_v)/p_a](p_a/\sigma'_{vo})^n \quad (5)$$

where: $(q_t – \sigma_v)/p_a$ = dimensionless net cone resistance

$(p_a/\sigma'_{vo})^n$ = stress normalization factor

p_a = atmospheric reference pressure in same units as q_t and σ_v

n = stress exponent that varies with SBTn, and defined by;

$$n = 0.381 (I_c) + 0.05 (\sigma'_{vo}/p_a) – 0.15 \quad (6)$$

where $n \leq 1.0$

The chart shown in Figure 1 uses Q_{tn}, instead of the original Q_{t1} suggested by Robertson (1990), and where I_c is also determined using Q_{tn} (Robertson, 2009). In most fine-gained soils when $I_c > 2.6$, $Q_{t1} \sim Q_{tn}$ since n ~ 1.0. Likewise, when σ'_{vo} = 1atm (100kPa) and σ'_{vo} > 10atm (1MPa), $Q_{t1} = Q_{tn}$. The largest difference between Q_{t1} and Q_{tn} occurs in coarse-grained soils at shallow depth (σ'_{vo} < 1atm), when $Q_{t1} > Q_{tn}$, (since n < 1.0). Jefferies and Been (2006) had suggested that the stress exponent in equation 5 should always be n = 1.0. However, due to the non-linear variation of shear stiffness (G) with depth, the effective stress exponent in coarse-grained soil can be less than 1.0, as indicated by equation 6.

The original method suggested by Robertson (1990) included a chart based on Q_{t1} and B_q. However, Schneider et al (2008) showed that B_q may not be the best form of normalized CPT pore pressure to identify soil type and suggested a chart based on Q_{t1} and U_2 (where $U_2 = \Delta u_2/\sigma'_{vo}$). The Schneider et al (2008) pore pressure chart applies mostly to clay-like soils since it requires a measured excess penetration pore pressure (Δu_2) and was developed primarily to aid in separating whether CPT penetration is drained, undrained or partially drained. The Schneider et al (2008) $Q_{t1} – U_2$ chart uses slightly different grouping of soil type (and description terms) compared to the Robertson (1990) chart, which can also lead to some confusion when applying both.

There is now more than 25years experience using the *Robertson SBTn* chart and in general, the chart provides good agreement between USCS-based classification and CPT-based SBTn (e.g. Molle, 2005) for most soils with little microstructure. Robertson (2009) discussed several examples where there can be observed

differences. In summary, the *Robertson SBTn* chart tends to work well in *'ideal soils'* (i.e. unstructured soils) but can be less effective in *'structured soils'*. Schneider et al (2012) and Saye et al (2017) suggested adjusting the boundaries to be more hyperbolic in shape so that they are steeper in the region of higher F_r values. Based on the accumulated experience using the SBTn chart it is possible to update the chart and to modify the descriptions of 'soil type' to use terms based more on soil behavior. It is also possible to identify soils with significant microstructure using additional CPT-based measurements (e.g. SCPT).

5 PROPOSED MODIFIED SBTN CHARTS

As discussed in the section on soil behavior, a major factor in any classification system can be the effects of post deposition processes that can generate microstructure. Hence, it can be important to first identify if soils have significant microstructure, since this can influence the in-situ behavior and ultimately the effectiveness of any classification system based on in-situ tests. Some understanding of the geologic background of the soil is always a required starting point for reliable classification based on CPT data, since geology provides a framework for interpretation.

The combined information from the SCPT has the potential to aid in identification of possible microstructure in soils to either supplement existing geologic information or when geologic information maybe either lacking or uncertain. Eslaamizaad and Robertson (1996) and Schnaid (2009) suggested that the SCPT can be helpful to identify soils with microstructure based on a link between G_o/q_t and Q_{tn}, since both aging and bonding tend to increase the small strain stiffness (G_o) significantly more than they increase the large strain strength of a soil (reflected in both q_t and Q_{tn}). Hence, for a given soil, age and bonding both tend to increase G_o more than the larger strain cone resistance (q_t), all other factors (in-situ stress state, etc.) being constant. Schneider and Moss (2011) extended the link between CPT and G_o to establish a method to identify sandy soils with microstructure. Schneider and Moss (2011) suggested using an empirical parameter, K_G defined in equation 7 (modified from Rix and Stokoe, 1991):

$$K_G = (G_o/q_t)\,(Q_{tn})^{0.75} \tag{7}$$

where G_o is in same units as q_t and Q_{tn} is dimensionless:
G_o = small strain shear modulus = $\rho\,(V_s)^2$
V_s = shear wave velocity
ρ = soil mass density = γ/g
γ = soil unit weight
g = acceleration due to gravity

Schnaid (2009) and Robertson (2009) proposed similar relationships but with slightly different exponents for Q_{tn}. The ratio G_o/q_t is essentially a small strain rigidity index (I_G), since it defines stiffness to strength ratio, where G_o is the small strain stiffness and q_t is a measure of soil strength. Robertson (2015) had suggested that K_G is essentially a normalized rigidity index, since it normalizes the small strain rigidity index (G_o/q_t) with in-situ soil state reflected by Q_{tn}. The works by Eslaamizaad and Robertson (1996), Schnaid (2009) and Schneider and Moss (2011) were focused primarily on coarse-grained soils. Robertson (2009) suggested that the small strain rigidity index (I_G) can be extended to include fine-grained soils and should be defined based on net cone resistance q_n, since q_n is a more correct measure of soil strength, to be:

$$I_G = G_o/q_n \tag{8}$$

where $q_n = (q_t - \sigma_v)$

Hence, a modified normalized small strain rigidity index, K^*_G is defined as:

$$K^*_G = (G_o/q_n)\,(Q_{tn})^{0.75} \tag{9}$$

Figure 2 presents a plot of Q_{tn} versus I_G similar to that shown by Schneider and Moss (2011) but extended to cover a wider range of soils. Schneider and Moss (2011) showed that most young, uncemented (*ideal*) silica-based sands have $100 < K_G < 330$, with an average value of around 215. In most coarse-grained soils $q_t \sim q_n$ since $q_t > \sigma_v$, hence the data presented by Schneider and Moss (2011) in terms of K_G also plot in the same region in terms of K^*_G on the modified plot shown in Figure 2. Since Figure 2 has been extended to include

soft clays the modification to use G_o/q_n becomes important, since q_n is a direct measure of soil strength in clay-like soils and can be significantly smaller than q_t in soft clay.

Most of the existing empirical correlations developed for interpretation of CPT results are predominately based on experience in silica-based soils with little or no microstructure (e.g. Robertson, 2009; Mayne, 2014). Hence, if soils have $K^*_G < 330$ the soils are likely young and uncemented (i.e. have little or no microstructure) and can be classified as '*ideal soils'* (unstructured) where many traditional CPT-based empirical correlations likely apply. Soils with $K^*_G > 330$, tend to have significant microstructure and the higher the value of K^*_G, the more microstructure is likely present. Hence, if a soil has $K^*_G > 330$ the soils can be classified as '*structured soils'* where traditional generalized CPT-based empirical correlations may have less reliability and where local modification may be needed. The influence of increasing microstructure on in-situ soil behavior is often gradual and any separating criteria can be somewhat arbitrary. Data suggests that very young uncemented soils tend to have K^*_G values closer to 100, whereas soils with some microstructure (e.g. older deposits) tend to have K^*_G values closer to 330. As will be shown later, soils with $K^*_G < 330$ tend to have little or no microstructure where existing empirical CPT-based correlations tend to provide good estimates of soil behavior.

A challenge when calculating K^*_G, that will be illustrated later, is that the CPT parameters (q_t and Q_{tn}) and V_s are often measured over different depth intervals. For example, CPT measurements are typically made at 10 to 50mm depth intervals, whereas V_s (and hence, G_o) is typically measured over 500 to 1000mm (or larger) depth intervals. Hence, there can be a scale effect when combining the two parameters (G_o/q_n), where the CPT parameters respond to smaller features and variability in the ground and V_s (G_o) tend to respond in a more subdued average manner. In the examples shown later, the CPT data (q_n) was averaged over the depth interval that was used to obtain the V_s measurement (e.g. if V_s was taken at 1m intervals, the associated q_n value was taken as the average value over the same 1m interval). Hence, the calculated value of K^*_G can show some variability in non-homogenous soils.

Natural soils can also be anisotropic where the small strain stiffness can vary depending on the direction of loading where G_{oVH} (and V_{sVH}) may not be equal to G_{oHH} (and V_{sHH}). The subscript VH applies to stiffness that is measured in the vertical and horizontal direction, which is the most commonly measured in-situ shear wave velocity (V_{sVH}), i.e. either a vertically propagating wave with particle motion in the horizontal direction (V_{sVH}) or a horizontal propagating wave with particle motion in the vertical direction ($V_{sHV} = V_{sVH}$). The suggested relationship shown in Figure 2 is based on G_{oVH} (and V_{sVH}) that is measured primarily using the SCPT. For simplicity, the relationship is shown in terms of G_o but is intended to apply G_{oVH}.

Robertson (2009) presented contours of state parameter (ψ) for young uncemented coarse-grained (*unstructured*) soils on the normalized SBTn ($Q_{tn} - F_r$) chart and suggested that the contour for $\psi < -0.05$ could be used to separate coarse-grained *'ideal soils'* that are either contractive or dilative at large strains. This was supported by case histories where flow liquefaction had occurred (Robertson, 2010).

Robertson (2009), Mayne (2014) and others have shown that most fine-grained *'ideal soils'* with an OCR > 4 should have $Q_{tn} > 12$ and are predominately dilative at large shear strains. Hence, combining these two criteria it is possible to develop a simple $Q_{tn} - F_r$ based boundary that would separate *'ideal soils'* that are either contractive or dilative at large shear strains, as shown on Figure 3 by the solid line (marked CD = 70). The contractive-dilative (CD) boundary can be represented by the following simplified expression:

$$CD = 70 = (Q_{tn} - 11)(1 + 0.06\ F_r)^{17} \qquad (10)$$

When CD > 70 the soils are likely dilative at large shear strains, as shown on Figure 3. Equation 10 is a simplified fitting relationship to capture the generalized shape of the contractive-dilative boundary on the $Q_{tn} - F_r$ chart. Figure 3 also includes (as light dashed lines) the original SBTn boundaries suggested by Robertson (1990, 2009) for comparison and to retain the original grouping based on physical characteristic descriptions (e.g. sand and clay). Because Figure 3 shows behavior based descriptions and boundaries, it applies primarily to soils that have little or no microstructure (i.e. *'ideal soils'*).

A CPT-based boundary between contractive and dilative soils depends on many variables (e.g. in-situ stress state, soil plastic hardening) and there is a transition between *'ideal soils'* that are predominately contractive to soils that are predominately dilative at large shear strains. Robertson (2010) indicated that the flow liquefaction case histories showed that the suggested boundary (represented by CD = 70) was slightly conservative (i.e. soils with some data slightly lower Q_{tn} values could be dilative at larger strains). The dashed line in Figure 3 shows an approximate lower limit, based on the case histories presented by Robertson (2010) for *'ideal soils'* that are predominately dilative at large strains that can be represented by the following simplified expression:

$$CD \text{ (lower bound)} = 60 = (Q_{tn} - 9.5)(1 + 0.06\ F_r)^{17} \quad (11)$$

In general, it is recommended to apply the upper boundary (CD = 70) for most geotechnical interpretation, since this is often slightly conservative. The CD = 70 boundary shown in Figure 3 applies only to *'ideal soils'* with little or no microstructure, since some aged and/or cemented soils can be contractive at large strains but produce relatively high values of Q_{tn} due to the increased stiffness and strength from aging and/or cementation. Examples will be presented later to illustrate this point.

The boundary between the original (Robertson, 1990) SBTn zones 4 (silt-mixtures) and 5 (sand-mixtures) is the approximate boundary between soils that are either more clay-like or more sand-like and can be approximated by $I_c = 2.6$ (Figure 1). However, the simple circular shape of I_c is not always a good fit to the original boundary, except for predominately young uncemented, essentially normally consolidated (*ideal*) soils, as suggested by Robertson and Wride (1998).

Schneider et al (2012) had suggested a more hyperbolic shape (in terms of log Q_t and log F_r) to better capture the SBT boundaries. Figure 3 shows suggested modified main SBTn boundaries based on a more hyperbolic shape using a Modified Soil Behavior Type Index, I_B, defined as:

$$I_B = 100(Q_{tn} + 10) / (Q_{tn}\ F_r + 70) \quad (12)$$

The boundary shown on Figure 3 represented by $I_B = 32$ represents the lower boundary for most sand-like *'ideal soils'* and is similar to the original boundary between SBTn zones 4 and 5 for normally consolidated soils. The boundary represented by $I_B = 22$ represents the upper boundary for most clay-like *'ideal soils'*, and is similar to the original boundary between SBTn zones 3 and 4 for normally consolidated soils. The value of $I_B = 22$ represents the approximate boundary for a plasticity index PI ~ 18% in fine-grained *'ideal soils'*.

The region represented by $22 < I_B < 32$ is defined as *'transitional soil'* which are soils that can have a behavior somewhere between that of either sand-like or clay-like *'ideal soil'* (e.g. low plasticity fine-grained soils, such as silt). Some *'transitional soils'* can also respond in a partially drained manner during the CPT (e.g. DeJong and Randolph, 2014) and are sometimes referred to as '*intermediate soils'*. The modified boundaries shown in Figure 3 are similar to the original boundaries for zones 3, 4 and 5 in the central part of the chart, where most young uncemented, normally consolidated *'ideal soils'* plot.

The soil close to the friction sleeve of the cone has experienced very large shear strains and tends to be fully '*destructured*' and/or remolded. Based on this observation, Robertson (2009) had suggested that sensitivity (S_t) in most fine-grained *'ideal soils'* could be estimated using the simplified expression:

$$S_t = 7.1 / F_r \quad (13)$$

Hence, soils with $F_r < 2\%$ tend to have a sensitivity $S_t > 3$ to 4. This boundary has been included in Figure 3 as an approximate separation between clay-like-contractive (CC) soils with moderate to low sensitivity ($S_t < 3$) from clay-like-contractive soils with higher sensitivity, $S_t > 3$ (CCS). This value of sensitivity is somewhat conservative but considered appropriate for basic classification purposes. Any boundary based on sensitivity is somewhat arbitrary, but can be helpful to warn users when a soil may have higher sensitivity to disturbance with associated risk of strength loss. As shown in Figure 3 the boundary between CC and CCS is slightly more conservative than the previous boundary suggested by Robertson (1990).

Eslami and Fellenius (1997) had suggested that charts based on Q_t and F_r were not mathematically correct for any statistical analyses since both Q_{tn} and F_r use q_t. Figure 4 shows the same boundaries as Figure 3 but represented on a modified SBTn chart based on Q_{tn} and F (where F is the normalized sleeve resistance, $F = f_s/\sigma'_{vo}$). Figure 4 (dashed lines) shows the original boundaries suggested by Robertson (1990), for comparison. The format shown in Figure 4 has the advantage that the normalized parameters are independent, but the disadvantage that data becomes more compressed. For most applications, there is no difference between Figures 3 and 4 and either format can be used, although the $Q_{tn} – F_r$ format (Figure 3) is preferred and for the examples shown later, this format is used. Figure 4 is similar to the earliest normalized CPT 'characterization' chart that was suggested by Olsen (1984).

The $Q_{tn} – F_r$ chart can also be used when no pore pressure (u_2) data are available (i.e. basic CPT data), since $q_c \sim q_t$ for most soils, except soft fine-grained soils ($Q_{t1} < 10$). Although the basic $Q_{tn} – F_r$ charts tend to be more popular for most onshore projects, since they do not require accurate CPT pore pressure measurements, it can be helpful to include CPT measured pore pressures into the interpretation of soil behavior type. Since Schneider et al (2008) showed that a slightly better form for the normalized pore pressure is U_2, Figure 5 shows a proposed modified Schneider et al (2012) chart using the same behavior type terms applied in Figure 3 but using the generalized normalized cone resistance, Q_{tn}, instead of Q_{t1}. The equations to define the boundaries shown in Figure 5 were provided by Schneider et al (2008) but replacing Q_{t1} with Q_{tn}. For most clay-like soils there is little difference between Q_{tn} and Q_{t1}, since $n \sim 1.0$, but for consistency it is preferred to use Q_{tn}. Pore pressures measured in the u_2 location (just behind the cone tip) are dominated by soil behavior in shear at large strains, hence U_2 tends to reflect the behavior of the soil in shear at large strain (i.e. destructured). In general, positive U_2 values tend to reflect large strain contractive behavior and negative U_2 values tend to reflect large strain dilative behavior. Hence, mostly 'contractive' behavior descriptions are shown on Figure 5 for positive values of U_2. Based on the $Q_{tn} – F_r$ chart (Figure 3), most fine-grained *'ideal soils'* with $Q_{tn} > 12$ will have negative values of U_2 since they are generally dilative at large shear strains. However, *'structured soils'* can have $Q_{tn} > 12$, due to the increased strength and stiffness, combined with large positive values of U_2 due to the loss of structure resulting in a contractive behavior at large strains. Hence, if data plot in the region represented by $Q_{tn} > \sim 12$ combined with high positive U_2 values ($U_2 > 4$), the soils likely have significant microstructure (i.e. '*structured soils'*) and are contractive at large shear strains. Increasing values of Q_{tn} combined with increasing positive U_2 values indicate increasing microstructure, as indicated in Figure 5. This will be illustrated later with some examples. Schneider et al (2008) showed that soils with increasing coefficient of consolidation (c_v) tend to show a decrease in U_2 with increasing Q_{tn}, due in part to an increase in drainage during the CPT but also an increased tendency for dilative behavior. For a given soil, increasing OCR can be associated with increasing c_v, hence *'ideal soil'* with increasing OCR tend to show a decrease in U_2 combined with an increase in Q_{tn}, as illustrated in Figure 5.

The $Q_{tn} – F_r$ chart has a modified SBTn Index I_B that can be used to define the main boundaries in soil SBTn. Likewise, the $Q_{tn} – U_2$ chart can use B_q as an approximate SBTn index to define the main boundaries, as shown in Figure 5. Hence, soils with $0.2 < B_q < 0.6$ tend to be CC and soils with $0.6 < B_q < 1.0$ and $Q_{tn} > 4$ tend to be CCS, as shown in Figure 5. Likewise, soils in the region defined by $U_2 > 0$ with $Q_{tn} = 20$ and $U_2 > 10$ with $Q_{tn} = 10$ appear to have significant microstructure. The combination of $Q_{tn} – F_r$ (Figure 3) and $Q_{tn} – U_2$ (Figure 5) can aid in identification of soils with microstructure since '*structured soils'* tend to have different classification between the two charts.

A major challenge for any classification method based on CPT pore pressures is the risk that the measured pore pressures may be unreliable due to loss of saturation (Robertson, 2009). This is an issue for CPT profiles performed onshore either in soils that are dilative or when the water table is deep and the cone is required to penetrate unsaturated and/or dilative soils for some depth.

Ideally, the above three charts (Figures 2, 3 and 5) should be used together to improve soil classification. Figure 2 ($Q_{tn} - G_o/q_n$) can be used to identify soils with significant microstructure (e.g. age and/or cementation), i.e. $K^*_G > 330$, provided V_s data are available. If the soils have little or no microstructure (i.e. '*ideal soil'*), Figure 3 ($Q_{tn} – F_r$) should apply. Figure 5 ($Q_{tn} – U_2$) can be used primarily in fine-grained soils, when V_s data are either not available or as a supplement to Figure 3, to evaluate if soils have significant microstructure and to evaluate large strain behavior, provided reliable pore pressure measurements are made.

The following section will illustrate the main features of the above approach using mostly published SCPTu data from well-documented sites. Schneider and Moss (2011) have essentially demonstrated the effectiveness of the $Q_{tn} - G_o/q_t$ chart for a wide range of coarse-grained soils and Schneider et al (2008) have essentially demonstrated the effectiveness of the $Q_{tn} - U_2$ chart for a wide range of fine-grained soils, hence the focus will tend to be more on the $Q_{tn} - F_r$ chart, although data will be presented on all three charts for each example site.

6 CASE HISTORY EXAMPLES

Selected representative case histories are presented to identify specific features that illustrate key points. Table 1 presents a summary of the selected deposits used to evaluate the proposed modified SBTn charts. The sites shown in Table 1 were selected to represent a wide range of deposits ranging from very recent fill and/or tailings to older very stiff soil/soft rock. The deposits have been listed by increasing value of K^*_G that essentially capture increasing microstructure. SCPTu data will be presented in the three normalized charts (Q_{tn}–F_r; Q_{tn}–U_2 and Q_{tn}–I_G).

Figure 6, 7 and 8 presents a summary of the average values for all the case history example deposits on the Q_{tn}–I_G, Q_{tn}–F_r and Q_{tn}–U_2 charts, respectively. Figure 6 (Q_{tn}–I_G) shows that the value of $K^*_G = 330$ suggested by Schneider and Moss (2011) provides a good separation between soils with little or no microstructure and soils with significant microstructure. Also, $K^*_G = 330$ appears to separate predominately silica-based soils from carbonate-based soil. Figure 7 (Q_{tn}–F_r) shows that, in general, soils with significant microstructure tend to plot in the dilative region of the chart. Figure 8 (Q_{tn}–U_2) shows that fine-grained contractive soils with significant microstructure plot in a region defined approximately by $U_2 > 0$ when $Q_{tn} = 20$ and $U_2 > 10$ when $Q_{tn} = 10$.

The following examples were selected to illustrate the variation and trends in the SCPTu data in the selected deposits.

6.1 SOILS WITH LITTLE OR NO MICROSTRUCTURE

Figure 9 shows SCPTu data to a depth of 40m at the KIDD site near Vancouver, BC, that was part of the CANLEX research project (Robertson et al, 2000, Wride et al., 2000). The soils are essentially normally consolidated, uncemented Holocene-age natural (silica-based) deposits from the Fraser River delta and represent both sand-like and clay-like soils in one profile. The SCPTu was carried out at a part of the site where the soils from a depth of about 4 to 22.7m are relatively uniform medium dense fine sand overlying uniform sensitive marine clay with the water table at a depth of 1m and V_s measurements were made every 0.5m starting at 3.25m. The sand (4 to 22.7m) plots predominately in the sand-like-dilative (SD) region consistent with the detailed results from the CANLEX project with an average $K^*_G = 214$. The underlying normally consolidated sensitive marine clay (22.9 to 40m) plots in the clay-like-contractive-sensitive (CCS) region on both the Q_{tn} - F_r and Q_{tn} - U_2 charts, with an average $K^*_G = 215$. The K^*_G values are consistent with the Holocene-age with no evidence of cementation. Figure 9 shows that the original descriptions used by Robertson (1990) also provide a good classification of both the sand and clay deposits. The CPT data transitions from the sand to the clay between 22.7 and 22.9m and is incorrectly classified. The issue of data in transition from sand-like to clay-like was discussed by Robertson (2009).

Figure 10 shows SCPTu data to a depth of 35m at a site in the San Francisco Bay area near Vallejo. The test location was pre-drilled using a hand auger to a depth of 1.5m after which the SCPTu was started and V_s measurements were made every 1m starting at a depth of 2m. The groundwater table is at a depth of 2m. The site is composed of about 1.5m of fill overlying Young Bay Mud (YBM) to a depth of around 12m. General details about YBM are provided by Bonaparte & Mitchell (1979). At this location, the YBM is late Holocene-age and lightly overconsolidated below a depth of 4m (OCR < 1.5) with a desiccated surface crust due to groundwater fluctuations. Below the YBM is Old Bay Clay (OBC) to the final depth of the SCPTu at 36m. SCPTu data from 2 to 11m in the YBM are shown in Figure 10a and from 12 to 35m in the OBC on Figure 10b. The average K^*_G value for the YBM at this site is around 85 consistent with the young geologic age and lack of microstructure. The OBC has slightly higher K^*_G values of around 300 consistent with the older geologic age (late Pleistocene). The YBM below the desiccated crust plots in the clay-like-contractive-sensitive (CCS) region on the $Q_{tn} - F_r$ chart and in the clay-like-contractive (CC) region of the $Q_{tn} - U_2$ chart. The YBM has a sensitivity of around 4 to 6 based on field vane tests that is consistent with the classification of CCS. The difference in classification between the $Q_{tn} - F_r$ and $Q_{tn} - U_2$ charts is partly due to a somewhat

slow pore pressure response in the upper 11m of the profile after recording small negative pore pressures in the desiccated crust. In the YBM desiccated crust the normalized cone resistance (Q_{tn}) moves higher and plots in the transitional soil region (TC and TD) of the $Q_{tn} – F_r$ chart. As desiccation increases closer to the ground surface, with associated increase in apparent OCR, the CPT data plots higher on both the $Q_{tn} – F_r$ and $Q_{tn} – U_2$ charts. As Schneider et al (2008) identified the U_2 values decrease with increasing Q_{tn} due to a more dilative behavior and increasing c_v (and possible partial drainage during the CPT). Close to the ground surface (at a depth of about 2m) some of the SCPTu data plot in the sand-like-dilative (SD) region due in part to the very dilative behavior of the very stiff desiccated clay and the almost drained penetration during the CPT, however, most of the SCPTu data for the desiccated crust plot in the transitional-dilative (TD) region. The OBC is more stratified and variable as indicated by the wide range in normalized CPT values shown in Figure 10b. Much of the OBC data plot on the boundary between clay-like and transitional soils and contractive to dilative behavior, consistent with the variable nature of this predominately stiff overconsolidated sandy clay.

Figure 11 shows SCPTu data from the Madingley site near Cambridge, UK (Lunne et al, 1997) from 2 to 12m. The Madingley site is underlain by Gault clay that is very stiff overconsolidated fissured clay of the Cretaceous period (~110 million years ago) with OCR > 10. The high overconsolidation ratio is derived from significant stress removal with no evidence of cementation. The SCPTu data correctly plot predominately in the clay-like-dilative (CD) region of the $Q_{tn} – F_r$ chart but plot close to the sand region of the $Q_{tn} – U_2$ chart, due to the negative values of U_2. This trend of small or negative U_2 values was illustrated in Figure 6 for 'ideal soils' with high OCR. The average $K^*_G = 360$ indicates some microstructure consistent with the significant age of the deposit but no cementation. The K^*_G value of 360 puts this clay close to the boundary between a soil with little or no microstructure and a soil with significant microstructure. Given that the existing empirical correlations provide a reasonably good estimation of soil behavior (Lunne et al, 1997), the clay can be considered to be close to the limit of the suggested boundary for *'ideal soils'*.

The above examples, where $K^*_G < 330$, were soils with little or no microstructure and where the proposed SBTn charts provided general good classification in terms of behavior type.

6.2 SOILS WITH SIGNIFICANT MICROSTRUCTURE

The following examples illustrate soils with significant microstructure, where $K^*_G > 330$ and where the CPTu data does not always fit well on the SBTn charts.

Figure 12 shows SCPTu data to a depth of 50m at the Cooper River Bridge site in Charleston, SC, (Camp et al, 2002) where the soil below a depth of 22m is Cooper Marl, that is a stiff calcareous plastic clay or silt of Eocene to Oligocene-age (~30 to 40 million years ago). The SCPTu data from 22 to 50m plot predominately in the transitional-contractive (TC) region of the $Q_{tn}–F_r$ chart and the clay-like-contractive (CC) region of the $Q_{tn}–U_2$ chart with an average $K^*_G = 580$. Dissipations tests provided t_{50} values ranging from 90 to 850s that indicate predominately undrained cone penetration. Data from a nearby site in the same Cooper Marl but at a shallow depth (less than 9m) have higher values of $Q_{tn} > 40$ and plot more in the SC and SD regions and with values of U_2 as high as 50. The high K^*_G and U_2 values indicate significant microstructure consistent with cementation from the high carbonate content (Camp et al, 2002). The high Q_{tn} values suggest a relatively high apparent OCR (>4) and possible dilative behavior whereas the high U_2 values show a more contractive behavior at high shear strains consistent with a cemented soil. The high level of cementation is consistent with a very stiff behavior at small strains followed by a contractive behavior at high shear strains when the cementation is broken and the soil becomes destructured.

Figure 13 shows SCPTu data from a site in Atlanta, Georgia in the Piedmont residual soil (Mayne, 2009). The site served as a test area for instrumented piles (Harris and Mayne, 1994) and consists of silty fine sand derived from the weathering of the underlying gneiss and schist bedrock. The SCPTu data from 4 to 19m plot predominately on the boundary between sand-like-dilative (SD) and transitional-dilative (TD) region of the $Q_{tn}–F_r$ chart with an average $K^*_G = 520$. The excess pore pressures are generally negative with values close to -100kPa and hence close to the saturation limit of the sensor. Dissipations tests provided t_{50} values ranging from 20 to 100s that indicate a potentially partially drained cone penetration. The negative pore pressures and the potential for partially drained penetration can explain why the data plot toward the sand region of the Q_{tn}-U_2 chart. The high K^*_G values indicate significant microstructure consistent with the remaining cementation in the residual soil. Residual soils derived from granite bedrock in Porto, Portugal have similar high K^*_G

values and plot in TD region of the Q_{tn}–F_r chart whereas data from a fine grained clayey silt residual soil in Campinas, Brazil plot in the CD region of the Q_{tn}–F_r chart (De Mio et al, 2010). The significant microstructure present in many residual soils tends to explain why the current SBTn charts often misinterpret their classification.

Figure 14 shows SCPTu data from a site near downtown Los Angeles composed of a uniform siltstone from 3 to 10m. The siltstone is part of the Fernando formation of Pliocene age (~3 to 5 million years ago). The SCPTu data plot in the sand-like-dilative region (SD) on the Q_{tn}–F_r chart but in the clay-like-contractive (CC) region of the Q_{tn}–U_2 chart (note that the U_2 values are between 18 to 40 and are mostly off the scale of the Q_{tn}–U_2 chart at the scale shown). The average $K^*_G = 635$ is consistent with the old age of the deposit combined with the cemented nature of this soft rock. The Q_{tn}–U_2 chart is correctly classifying the behavior as contractive at large strain that is different to the dilative behavior suggested by the Q_{tn}–F_r chart. The difference is explained by the significant microstructure (cementation) identified by the high K^*_G values.

Figure 15 shows SCPT data from a site in Tangiers, Morocco (Debats et al, 2015) composed of hydraulically placed calcareous sand. The sand has a high carbonate content ranging from 75 to 95% and is composed of shell fragments and carbonate algae mixed with grains of silica and mica (Debats et al, 2015). The highly compressible nature of the carbonate (shell) mineralogy produces small friction ratio values ($F_r < 0.3\%$) but high small strain stiffness with $K^*_G \sim 380$. Soils with high carbonate content have a tendency to develop rapid calcium cementation resulting in some microstructure and high values of K^*_G. However, it is also possible that an apparent microstructure is caused by the highly compressible nature of the carbonate grains. The resulting 'microstructure' often makes CPT interpretation difficult using traditional empirical correlations based on predominately silica-based soils.

In some parts of the middle east where calcareous sands exist it has become common practice to correct the CPT cone resistance to 'equivalent silica-sand' values using a Shell Correction Factor (SCF) where:

$$q_{c(ss)} = SCF\ q_c \tag{14}$$

where $q_{c(ss)}$ = equivalent silica-sand cone resistance

The SCF has been estimated based on calibration chamber studies that have been costly and provide limited results. Debats et al (2015) suggested that the SCF could be estimated from SCPT data by adjusting q_c, using an iterative approach with variable SCF values, until the measured V_s agrees with an estimated V_s using the empirical CPT-based correlation suggested by Robertson (2009) using the adjusted q_c. Since the average K^*_G for most young, uncemented silica-based sands is about 215 (Schneider and Moss, 2011), it is also possible to estimate the SCF based on SCPT data using the following simplified relationship:

$$SCF = (K^*_G/215)^{1.334} \tag{15}$$

where K^*_G = the average measured normalized small strain rigidity index.

Application of equation 15 is conceptually similar to the approach used by Debats et al (2015) but avoids the need for iteration to obtain the SCF. For the data shown in Figure 15, the SCF based on equation 15 is 2.1 compared to the average value of about 2.0 suggested by Debats et al (2015).

7 DISCUSSION

The above examples illustrate that the modified Q_{tn}–F_r and Q_{tn}–U_2 charts provide good classification in terms of soil behavior type for soils with little or no microstructure when $K^*_G < 330$. The Q_{tn}–U_2 chart can be somewhat sensitive to minor loss of saturation of the pore pressure sensor in some soils, especially in stiffer onshore soils. In soils and soft rock where there is significant microstructure (i.e. *'structured'* soils) with $K^*_G > 330$ the classification of soil behavior type becomes less reliable and some judgment is required. If *'structured'* soils and/or soft rocks are sufficiently fine-grained to develop reliable excess pore pressures, the Q_{tn}–U_2 chart provides a better classification of soil behavior type at large strains and can be used to identify significant microstructure. Geomaterials with significant microstructure tend to be cemented/bonded and can

be very stiff at small strains (producing high Q_{tn} values) but can be contractive at large shear strains (producing high U_2 values) when the cementation is destroyed and the material becomes destructured.

As discussed by Robertson (1990) the addition of dissipation tests to measure the rate of dissipation of any excess pore pressures (e.g. t_{50}) can also aid in the correct classification of soil behavior, as well as drainage conditions during the CPT. DeJong and Randolph (2014) suggested that when $t_{50} > 50$s the cone penetration (1000 mm^2 cone at standard rate of 20mm/s) is essentially undrained.

Soil behavior is controlled by the in-situ effective stress hence CPT parameters normalized in terms of effective stress can better capture in-situ behavior for classification. However, the normalization process is not always perfect due to uncertainty in estimating in-situ stress. Conceptually, any normalization should also account for the important influence of horizontal effective stresses, since penetration resistance is strongly influenced by the horizontal effective stresses. However, this continues to have little practical benefit for most projects without a prior knowledge of in-situ horizontal stresses (Robertson, 2009). Uncertainty in estimating in-situ vertical stresses can also result from uncertainty in soil unit weight (γ) as well as the in-situ piezometric profile (u_o). This uncertainty typically has a minor effect in coarse-grained soils (e.g. SD and SC) where the measured CPT parameters (q_c and f_s) tend to be large relative to σ_{vo} and u_o. However, the normalized parameters (Q_{tn}, F_r and I_G) can become sensitive to uncertainty in σ_{vo} and u_o in very soft fine-grained soils (e.g. CC and CCS). Likewise, the normalized CPT parameters can also be sensitive to measurement uncertainty in soft fine-grained soil where the measured CPT parameters (q_c and f_s) can be close to the limits of accuracy/repeatability for the CPT equipment (Robertson, 2009). One method to identify when the normalized parameters (e.g. Q_{tn} and F_r) may not be correct is when the data plot outside some of the limits shown on the charts. For example, $Q_{tn} < 1$ when pushing in soil is rare and is often the result of an overly high estimate for σ_{vo}. Soft soils with high organic content can have very low soil unit weight that can result in apparent low values of q_n and Q_{tn} due to over-estimated values of σ_{vo}. In soft fine-grained soil, it is also rare to obtain $B_q > 1.2$, since this requires an excess pore pressure higher than the net cone resistance (q_n). Hence, if data plot lower than the line identified by $B_q = 1.0$ in the $Q_{tn} – U_2$ chart, there may be some uncertainty in the low values of Q_{tn}. In soft soil, the uncertainties in estimating σ_{vo} and u_o often outweigh the uncertainty in horizontal stress ratio (K_o), since variations in K_o tend to be captured by the empirical correlations (e.g. OCR). The normalized parameter I_G requires in-situ shear wave velocity measurements that can be difficult to obtain accurately in the upper 1 to 2m and at depths greater than about 50m using a downhole method like the SCPT. Likewise, scatter in I_G can also result from scale effects between the measured V_s and CPT measurements in heterogeneous deposits.

CPT measurements taken over water often require special care to ensure correct data normalization. Typically, CPT work overwater is referenced to the mudline (i.e. point where soil starts), since the effective stress is zero at the mudline and the cone zero load readings are also taken at the mudline. Hence, σ_{vo} and u_o are also referenced to mudline (i.e. equivalent to assuming piezometric surface at the mudline). If the CPT zero load readings are taken at the water surface (e.g. for shallow over water work), the cone (q_t and u_2) will measure the water pressure when lowered through water (with $f_s \sim 0$). Hence, σ_{vo} and u_o must be selected to produce $\sigma'_{vo} = 0$ at the mudline, that may require using the unit weight of water for the section of CPT data in water.

Calculation of Q_{tn} requires an iterative procedure to determine the stress exponent (n) using I_c. The proposed modified SBTn chart based on Q_{tn} and F_r contains a modified soil behavior type index (I_B) to define the main boundaries between sand-like and clay-like behavior, however it is recommended to continue using I_c in the iterative procedure to determine Q_{tn}, since I_c adequately captures the variation of soil behavior to estimate the stress exponent as well as other current applications of I_c (e.g. Robertson, 2009 and Mayne, 2014).

8 SUMMARY AND CONCLUSIONS

Updated and modified charts have been proposed to estimate soil behavior type based on either CPT, CPTu or SCPTu data. Ideally these charts should be used in conjunction with the traditional textural-based classification system (e.g. USCS) based on samples. The charts utilize normalized parameters in an effort to capture in-situ soil behavior. New behavior descriptions are suggested in an effort to be consistent with the concept of a behavior type classification. The method is based on CPT (i.e. electric cones of either 500, 1000 or 1500 mm^2 area) at the standard penetration rate of 20mm/s. The Q_{tn}–F_r chart does not apply to data from a

mechanical CPT, since both the tip and sleeve resistance values from a mechanical CPT can be different than an electric CPT.

Since soil behavior can be complex, it is recommended to apply multiple CPT-based measurements to improve behavior classification. The SCPTu offers the opportunity to obtain anywhere from 3 to 6 independent measurements to improve classification. However, classification is still possible using either 2 (q_c and f_s) or 3 (q_c, f_s and u_2) measurements from the standard CPT or CPTu. Classification based on only 2 measurements (q_c and f_s) is generally less reliable and should be limited to predominately silica-based, young, uncemented soil (i.e. *'ideal soil'*). Classification is improved if 3 measurements are used (q_c, f_s and u_2) especially in more fine-grained soils. Ideally classification should be based on 4 measurements (q_c, f_s, u_2 and V_s) since this allows identification of possible microstructure. In fine-grained soils, dissipation tests that provided an added measurement (t_{50}) is also valuable and recommended where possible. Dissipation tests in coarse-grained layers, where 100% dissipation can be rapid and cost effective, are recommended so that the correct equilibrium piezometric pressure (u_0) can be determined.

The geologic history of the deposit is always a helpful starting point for correct classification. If the geologic history supports the potential that the soils are predominately silica-based, young (i.e. Holocene to Pleistocene-age) and likely uncemented, the basic SBTn charts based on Q_{tn} and F_r will generally provide reliable classification.

The link between behavior characteristics (e.g. strength, stiffness and compressibility) that is reflected in the CPT measurements and physical characteristics (e.g. grain size and plasticity) can be very good in soils with little or no microstructure (i.e. '*ideal soils'*). Hence, it can be important to identify the level of microstructure in a deposit. If V_s (and hence G_o) data are available, ideally using SCPT, the proposed Q_{tn}–I_G chart can be used to evaluate the level of microstructure in a deposit with supporting evidence from the geologic background. The modified Q_{tn}–U_2 can also be helpful in fine-grained soils where CPT penetration is essentially undrained.

If soils have little or no microstructure, the proposed SBTn charts and existing empirical correlations (e.g. Robertson, 2009) tend to apply and can provide reasonable estimates of soil behavior. However, if soils have significant microstructure (e.g. $K^*_G > 330$) the proposed SBTn charts and most existing empirical correlations may not always apply and site or geologic specific modifications may be required.

9 ACKNOWLEDGMENTS

This research could not have been carried out without the support, encouragement and input from John Gregg, Kelly Cabal and other staff at Gregg Drilling and Testing Inc. The sharing of ideas and data by Prof. Paul Mayne, Prof. Fernando Schnaid, Dr. James Schneider, M. Jefferies and others has also been helpful and is appreciated.

10 REFERENCES

Al-Homoud AS. and Wehr W., (2006). Experience of vibrocompaction in calcareous sand of UAE. *Geotechnical and Geological Engineering*; **24**: 757-774.

ASTM-D 2487-11. Standard Method for Classifying Soils for Engineering Purposes (Unified Soil Classification System). ASTM International. www.astm.org.

Atkinson, J.H., (2007). The Mechanics of Soils and Foundations. Taylor & Fancis, London

Bastani, S.A., Silver, P. and Atkinson, D.R., 2014. CPT based settlement prediction over California soft rock, Proceedings of Third International Symposium of Cone Penetration Testing, CPT'14, Las Vegas, Nevada. Gregg Drilling & Testing. www.cpt14.com.

Begemann, H. K. S., (1965). The friction jacket cone as an aid in determining the soil profile. Proceedings of the 6th ICSMFE, Montreal, Vol. 2, 17-20.

Been, K. & Jefferies, M.G., (1985). A state parameter for sands. Géotechnique, 35(2): 99–112

Boggess, R., and Robertson, P.K. (2010). CPT for soft sediments and deepwater investigations. In Proceedings International Symposium on Cone Penetration Testing, CPT'10, Huntington Beach, Calif., paper 1-17.

Boneparte, R. and Mitchell, J.K., (1979). The Properties of San Francisco May Mud at Hamilton Air Force Base, California. Department of Civil Engineering, University of California, Berkeley.

Bray, J.D. & Sancio, R.B. (2006). Assessment of the liquefaction susceptibility of fine grained soils. Journal of Geotechnical and Geoenvironmental Engineering 132 (9): 1165-1177.

Burland, J.B. 1990. On the compressibility and shear strength of natural clays. Géotechnique 40(3): 329–378.

Camp, W.M., Mayne, P.W. and Brown, D.A., (2002). Drilled shaft axial design values: Predicted versus measured response in Calcareous Clay. Proceedings of Deep Foundations, ASCE GSP No. 116, pp. 1518-1532.

Campanella, R. G., Robertson, P. K., and Gillespie, D. (1983). Cone penetration testing in deltaic soils. Can. Geotech. J., 20-1, 23–35.

Debats, J., Pardessus, N., Racinais, J. and Olgun, C. (2015). InSitu determination of the Shell Correction Factor in Carbonate Sands. Proceedings of 6th International Conference on Earthquake Geotechnical Engineering, Christchurch, New Zealand. Paper 742, 9 pages.

DeGroot, D.J. & Lutenegger, A.J. (2003). Geology and engineering properties of Connecticut Valley Varved Clay. Characterization and Engineering Properties of Natural Soils, Vol. 1, Swets and Zeitlinger, Lisse: 695-724.

DeJong, J. T. and Randolph, M., (2014). Influence of partial consolidation during Cone Penetration on estimated soil behavior type and pore pressure dissipation measurements, Journal of Geotechnical and Geoenvironmental Engineering, ASCE, 138(7): 777-788

Douglas, B.J., and Olsen, R.S., 1981. Soil classification using electric cone penetrometer. *In* Proceedings of Symposium on Cone Penetration Testing and Experience, Geotechnical Engineering Division, ASCE. St. Louis, Missouri, October 1981, pp. 209-227.

Di Mio, G., Giacheti, H.L., Viana da Fonseca, A. and Ferreira, C., (2010). CPTu interpretation for stratigraphic logging differences between sedimentary and residual soils. Proceedings of Second International Symposium of Cone Penetration Testing, CPT'10, Huntington Beach, CA. Gregg Drilling & Testing. www.cpt10.com.

Eslaamizaad, S., and Robertson, P.K., (1996). Seismic cone penetration test to identify cemented sands. In Proceedings of the 49th Canadian Geotechnical Conference. St. John's, Newfoundland. September, pp. 352 – 360.

Eslami, A., and Fellenius, B.H., (1997). Pile Capacity by direct CPT and CPTu methods applied to 102 case histories. Canadian Geotechnical Journal, 34(6): 880-898.

Finno, R.J., Gassman, S.L. and Cavello, M. (2000). The NGES at Northwestern Univ., National Geotechnical Experimentation Sites, GSP 93, ASCE, Reston/Virginia, 130-159.

Harris, D.E., and Mayne, P.W., (1994). Axial compression behavior of two drilled shafts in Piedmont residual soils, Proceedings International Conference on Design and Construction of Deep Foundations, Vol. 2 (Orlando), Federal Highway Administration, Washington, D.C., 352-367.

Hight, D. W. and Leroueil, S., (2003). Characterization of soils for engineering purposes. Characterization and Engineering Properties of Natural Soils, Tan et al. (eds.). Swets and Zeitlinger, pp. 255-360.

Idriss, I. M., and Boulanger, R. W., 2008. Soil liquefaction during earthquakes. Monograph MNO-12, Earthquake Engineering Research Institute, Oakland, CA, 261 pp.

Jefferies, M.G., and Davies, M.P., (1993). Use of CPTu to estimate equivalent SPT N_{60}. Geotechnical Testing Journal, ASTM, 16(4): 458-468.

Jefferies, M.G. and Been, K., (2006). Soil Liquefaction – A critical state approach. Taylor & Francis, ISBN 0-419-16170-8 478 pages.

Ku, T., Mayne, P. W. and Cargill, E., (2013). Continuous interval shear wave velocity profiling by auto-source and seismic cone tests, Canadian Geotechnical Journal, 50(2): 382-390.

Leroueil, S. 1992. A framework for the mechanical behavior of structured soils, from soft clays to weak rocks. Proc. US-Brazil NSF Geotechnical Workshop on Applicability of Classical Soil Mechanics Principles to Structured Soils, Belo Horizonte: 107–128.

Leroueil, S. and Hight, D.W., (2003). Behavior and properties of natural soils and soft rocks. Characterization and Engineering Properties of Natural Soils, Tan et al. (eds.). Swets and Zeitlinger, pp. 29-253.

Lunne, T., Eidsmoen, T., Gillespie, D., and Howland, J.D., (1986). Laboratory and field evaluation on cone penetrometers. Proceedings of ASCE Specialty Conference In Situ'86: Use of In Situ Tests in Geotechnical Engineering. Blacksburg, ASCE, 714-729

Lunne, T., Robertson, P.K., and Powell, J.J.M., (1997). Cone penetration testing in geotechnical practice. Blackie Academic, EF Spon/Routledge Publ., New York, 1997, 312 pp.

Lunne, T., Long, M., and Forsberg, C.F., (2003). Characterization and Engineering properties of Holmen, Drammen sand. Characterization and Engineering Properties of Natural Soils, Vol. 2, Swets & Zeitlinger, Lisse, pp. 1121-1148.

Mayne, P.W., (2000). Enhanced Geotechnical Site Characterization by Seismic Piezocone Penetration Test. Invited lecture, Fourth International Geotechnical Conference, Cairo University. pp 95-120.

Mayne, P.W., (2005). Integrated Ground Behavior: In-Situ and Lab Tests, Deformation Characteristics of Geomaterials, Vol. 2 (Proc. Lyon), Taylor & Francis, London, pp. 155-177

Mayne, P.W., (2009), Engineering Design using the Cone Penetration Test: Geotechnical Applications Guide. ConeTec Investigation Inc., 165 pages.

Mayne, P.W., (2014), Interpretation of Geotechnical Paramaters from seismic piezocone tests, Proceedings of 3rd International Symposium on Cone Penetration Testing, CPT14, Las Vegas, Nevada, Gregg Drilling & Testing, Inc., www.cpt14.com.

Mayne, P.W. and Pearce, R.A., 2005, Site characterization of Bootlegger Cove Clay for Port of Anchorage, Proceedings of ISFOG, Anchorage.

Mayne, P.W. and Woeller, D.J., (2008), O-Cell response using elastic pile and seismic piezocone tests, Proceedings of the Second British Geotechnical Association International Conference of Foundations – ICOF (2008), Dundee, Scotland, Edited by Brown, M.J., Bransby, M.F., Brennan, A.J. and Knappett, J.A. Published by HIS BRE Press, UK., Vol. 1:235-246.

Molle, J., 2005. The accuracy of the interpretation of CPT-based soil classification methods in soft soils. MSc Thesis, Section for Engineering Geology, Department of Applied Earth Sciences, Delft University of Technology, Report No. 242, Report AES/IG/05-25, December

Olsen, R.S. (1984). Liquefaction analysis using the cone penetration test. Proceedings of 8th World Conference on Earthquake Engineering. Vol. III, Prentice-Hall Inc., Englewoods Cliffs, NJ, 247-254.

Olsen, R.S., and Mitchell, J.K., (1995). CPT stress normalization and prediction of soil classification. Proceedings of the International Symposium on Cone Penetration Testing, Vol.2, Swedish Geotechnical Society, Linkoping, pp. 257-262.

Ramsey, N., 2002. A calibrated model for the interpretation of cone penetration tests (CPTs) in North Sea Quaternary soils. Offshore site investigation and geotechnics – diversity and sustainability. London: Society for Underwater Technology, pp. 341–356.

Randolph, M.F. (2004). Characterization of soft sediments for offshore applications. Geotechnical and Geophysical Site Characterization, Vol. 1 (Proc. ISC-2, Porto), Millpress, Rotterdam: 209-232.

Rix, G. J. & Stokoe K. H. II., (1991). Correlation of initial tangent modulus and cone penetration resistance. In Calibration chamber testing. New York: Elsevier, pp. 351–361.

Robertson, P.K., (1990). Soil classification using the cone penetration test. Canadian Geotechnical Journal, 27(1): 151-158.

Robertson, P.K., (2009). Interpretation of Cone Penetration Tests – a unified approach. Canadian Geotechnical Journal, 46: 1-19

Robertson, P.K., (2010). Evaluation of Flow Liquefaction and Liquefied strength using the Cone Penetration Test. Journal of Geotechnical and Geoenvironmental Engineering, ASCE, 136(6): 842-853

Robertson, P.K., (2015). Comparing CPT and Vs Liquefaction Triggering Methods. Journal of Geotechnical and Geoenvironmental Engineering, ASCE, 141(9): 842-853

Robertson, P.K., (2016), Cone penetration test (CPT)-based soil behaviour type (SBT) classification system: an update. Canadian Geotechnical Journal, 53(12); pp 1910-1927

Robertson. P.K., Campanella, R.G., Gillespie, D., and Greig, J., (1986). Use of Piezometer Cone data. In-Situ'86 Use of Ins-itu testing in Geotechnical Engineering, GSP 6, ASCE, Reston, VA, Specialty Publication, SM 92, pp 1263-1280.

Robertson, P.K. and Wride, C.E., (1998). Evaluating cyclic liquefaction potential using the cone penetration test. Canadian Geotechnical Journal, Ottawa, **35**(3): 442-459.

Robertson, P.K., Wride (Fear), C.E., List, B.R., Atukorala, U., Biggar, K.W., Byrne, P.M., Campanella, R.G., Cathro, D.C., Chan, D.H., Czajewski, K., Finn, W.D.L., Gu, W.H., Hammamji, Y., Hofmann, B.A., Howie, J.A., Hughes, J., Imrie, A.S., Konrad, J.-M., Küpper, A., Law, T., Lord, E.R.F., Monahan, P.A., Morgenstern, N.R., Phillips, R., Piché, R., Plewes, H.D., Scott, D., Sego, D.C., Sobkowicz, J., Stewart, R.A., Watts, B.D., Woeller, D.J., Youd, T.L., and Zavodni, Z. (2000). The CANLEX project: summary and conclusions. Canadian Geotechnical Journal, 37: 563–591.

Safner, D.A., Jung, Y., Hryciw, R.D. and Green, M., (2011), Comparison of predicted cyclic resistance ratios from CPT, DMT and shear wave velocity tests in Griffin, Indiana. Proceedings of Geo-Frontiers, ASCE, pp 2298-2307.

Saye, S. R., Santos, J., Olson, S.M. and Leigh, R.D. (2017). Linear trendlines to assess soil classification from cone penetration test data. J. Geotech. Geoenviron. Eng. 143(9): 04017060.

Schnaid, F. 2009. In-Situ Testing in Geomechanics – the main tests. Taylor & Francis Group, London: 327 p.

Schnaid, F. & Odebrecht, E. (2015) Challenges in the interpretation of the DMT in tailings. The 3rd Int. Conf. on the Flat Dilatometer DMT-15, Rome, 13-24.

Schneider, J.A., Randolph, M.F., Mayne, P.W. and Ramsey, N. R., (2008). Analysis of Factors Influencing Soil Classification using Normalized Piezocone Tip Resistance and Pore Pressure Parameters. Journal of Geotechnical and Geoenvironmental Engineering, ASCE, 134(11): 1569-1586.

Schneider, J.A. and Lehane, B.M., (2010). Evaluation of cone penetration testing from a calcareous sand dune. Proceedings International Symposium on Cone Penetration Testing, CPT'10, Huntington Beach, CA, paper 2-28, www.cpt10.com

Schneider, J.A. and Moss, R.E.S., (2011). Linking cyclic stress and cyclic strain based methods for assessment of cyclic liquefaction triggering in sands. Geotechnique Letters, Institute of Civil Engineers, UK

Schneider, J.A., Hotstream, J.N., Mayne, P.W. and Radolph, M.F., 2012, Comparing CPTU Q-F and Q-$\Delta u_2/\sigma'_{vo}$ soil classification charts. Geotechnique Letters 000, 1–7, http://dx.doi.org/10.1680/geolett.12.00044, 7 pages.

Simonini, P., (2004), Characterization of Venice lagoon silts from in-situ tests and performance of a test embankment. Proceedings 2nd International Conference on Site Characterization, ISC'2, Geotechnical & Geophysical Site Characterization, Porto, Vol. 1, 187-207.

Wride, C.E., Robertson, P.K., Biggar, K.W., Campanella, R.G., Hofmann, B.A., Hughes, J.M.O., Küpper, A., and Woeller, D.J. (2000) In-Situ testing program at the CANLEX test sites. Canadian Geotechnical Journal, Vol. 37, No. 3, June, pp. 505-529.

Table 1: Selected representative examples

Ref #	Site	Description	Geologic Age	Q_{tn}	F_r	U_2	I_G	K^*_G	References
1	San Francisco (USA)	Young Bay Mud NC-LOC Clay	Holocene	4.0 (3.0-5.0)	1.0 (0.5-2.0)	2.0 (1.5-3.0)	30 (25-35)	85 (70-100)	Robertson (personal files)
2	Burswood Perth (Australia)	NC-LOC Clay	Holocene	6.5 (5.5-8.0)	2.0 (1.0-3.0)	2.5 (1.5-3.5)	22 (18-30)	90 (75-122)	Randolph, 2004
3	Syncrude (Canada)	NC Tailing Sand	Recent	30 (20-65)	0.7 (0.4-1.0)	0	8 (6-10)	105 (100-110)	Wride et al, 2000
4	Highmont (Canada)	NC Tailing Sand	Recent	40 (20-70)	0.3 (0.1-0.6)	0	8 (6-12)	130 (120-140)	Wride et al, 2000
5	LL Dam (Canada)	NC Tailing Sand	Recent	45 (30-60)	0.4 (0.1-0.8)	0	8 (6-12)	140 (130-150)	Wride et al, 2000
6	Holmen (Norway)	Drammen River NC Sand	Holocene	30 (20-60)	0.4 (0.2-0.7)	0	12 (10-18)	155 (125-205)	Lunne et al., 2003
7	Onsoy (Norway)	NC-LOC Clay	Holocene	4.5 (4.0-5.0)	1.8 (1.2-2.2)	3.0 (2.5-3.5)	60 (50-70)	185 (155-215)	Lunne et al., 1997
8	Tabarao (Brazil)	NC-LOC Clay	Holocene	4.0 (3.0-5.0)	1.3 (1.1-1.5)	1.7 (1.0-2.2)	65 (50-80)	185 (140-225)	Schnaid et al., 2015
9	UBC McD. (Canada)	Fraser River NC Sand	Holocene	100 (50-150)	0.3 (0.2-0.5)	0	5 (3-9)	200 (100-300)	Campanella et al, 1983
10	KIDD (Canada)	Fraser River NC Sand	Holocene	80 (40-150)	0.6 (0.3-1.0)	0.1 (-0.1-0.5)	8 (5-12)	214 (130-310)	Wride et al, 2000
11	J-Pit (Canada)	NC Tailing Sand	Recent	35 (20-50)	0.7 (0.6-1.0)	0	15 (9-25)	215 (170-270)	Wride et al, 2000
12	KIDD (Canada)	Fraser River NC-LOC Clay	Holocene	3.5 (3.0-4.0)	1.1 (0.9-1.4)	3.0 (2.0-3.5)	85 (60-110)	215 (155-280)	Wride et al, 2000
13	Bothkennar (UK)	LOC silty Clay	Holocene	6.5 (5.5-8.0)	1.6 (1.0-2.5)	3.6 (2.5-4.5)	60 (50-70)	240 (205-290)	Hight et al, 2003
14	UBC McD. (Canada)	Fraser River NC-LOC Clay	Holocene	4.0 (3.0-5.0)	1.8 (1.5-2.2)	2.5 (2.0-3.0)	100 (80-120)	280 (230-320)	Campanella et al, 1983
15	San Francisco (USA)	Old Bay Clay OC Clay	Late Pleistocene	12.0 (5-30)	2.5 (1.5-5.0)	2.5 (-1.5-5.0)	45 (30-100)	300 (195-600)	Robertson (personal files)
16	Venice (Italy)	NC-LOC Clayey Silt	Holocene	7.5 (5.0-10.0)	2.0 (1.3-2.8)	1.0 (0.1-1.8)	70 (60-80)	315 (270-350)	Simonini et al., 2004
17	Amherst (USA)	Varved clay	Late Pleistocene	7.5 (6.5-9.0)	1.5 (0.8-3.0)	5.0 (3.0-6.0)	70 (50-90)	325 (225-400)	DeGroot & Lutenegger, 2003
18	Ford Center (USA)	LOC Clay	Pleistocene	7 (5.5-9.0)	3.0 (2.5-43.5)	3.8 (3.0-4.5)	78 (70-90)	330 (300-380)	Finno et al 2000
19	Madingley (UK)	HOC Clay	Cretaceous	35 (30-45)	4.5 (3.0-6.0)	-1	25 (15-30)	360 (330-430)	Lunne et al, 1997
20	Griffin (USA)	Dense Sand	Pleistocene	150 (80-400)	0.6 (0.3-1.0)	0	9 (4-20)	380 (215-800)	Safner et al, 2011
21	Tangiers (Morocco)	Calcareous sand	Recent	100 (60-200)	0.2 (0.1-0.8)	0	12 (7-20)	380 (215-560)	Debats et al, 2015
22	Campinas (Brazil)	Residual soil	-	20 (15-25)	6.0 (5.0-8.0)	1 (0-4)	45 (40-60)	425 (375-565)	De Mio et al, 2010
23	Dubai (UAE)	Calcareous sand	Recent	70 (60-80)	0.2 (0.1-0.3)	0	18 (15-21)	435 (360-500)	Robertson, (personal files)
24	Porto (Portugal)	Residual soil	-	40 (30-50)	5.0 (3.0-7.0)	0	30 (20-40)	475 (320-640)	De Mio et al, 2010
25	Ledge Point (W. Australia)	Calcareous sand	Holocene	150 (80-300)	0.5 (0.2-0.8)	0	10 (5-20)	500 (330-800)	Schneider & Lehane, 2010
26	Houston (USA)	Beaumont OC Clay	Pleistocene	25 (20-30)	4 (3.5-4.5)	-0.5 (-1.0 – 0)	48 (35-50)	535 (425-640)	Mayne, 2009
27	Atlanta (USA)	Piedmont Residual soil	-	45 (25-65)	2.2 (1.2-3.0)	-0.5 (-1.0-0)	33 (25-40)	570 (470-640)	Mayne, 2009
28	Charleston (USA)	Cooper Marl Calcareous Clay	Oligocene	12 (8-25)	0.6 (0.4-1.4)	6 (4.5-11)	90 (50-200)	580 (330-1200)	Camp et al 2002
29	Los Angeles (USA)	Fernando Siltstone	Miocene	75 (60-100)	1.5 (1.0-2.0)	33 (20-40)	30 (17-40)	635 (510-1,020)	Robertson, (personal files)
30	Anchorage (USA)	Bootlegger Cove HOC Clay	Pleistocene	20 (10-50)	1.3 (1.0-2.0)	1.7 (1.0-5.5)	80 (50-110)	750 (450-1,400)	Mayne & Pearce, 2005
31	Windsor (USA)	Calcareous cemented clay	Miocene	45 (40-50)	2.5 (2.0-3.0)	12 (5-16)	48 (40-65)	830 (690-1,150)	Ku et al, 2013
32	Calgary (Canada)	Glacial clay Till	Pleistocene	40 (35-50)	3.0 (2.5-3.5)	5 (0-7.0)	55 (40-70)	850 (600-1,100)	Mayne & Woeller, 2008
33	Newport Beach (USA)	Monterey Sandstone/siltstone	Miocene	150 (50-400)	2.5 (0.8-5.0)	1 (0-15)	20 (8-200)	860 (350-4,000)	Bastani et al, 2014

Values shown are mean values with range in bracket
NC Normally consolidated
LOC Lightly overconsolidated (OCR < 4)
HOC Heavily overconsolidated (OCR >4)

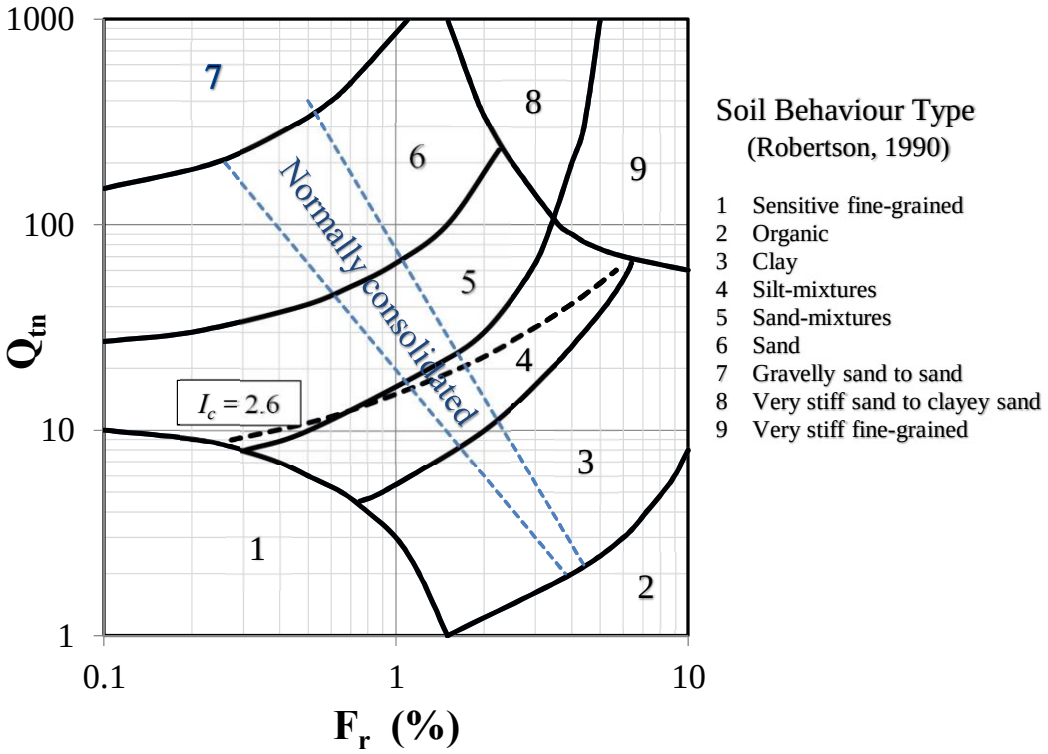

Figure 1: CPT-based SBTn chart suggested by Robertson (1990) and updated by Robertson (2009)

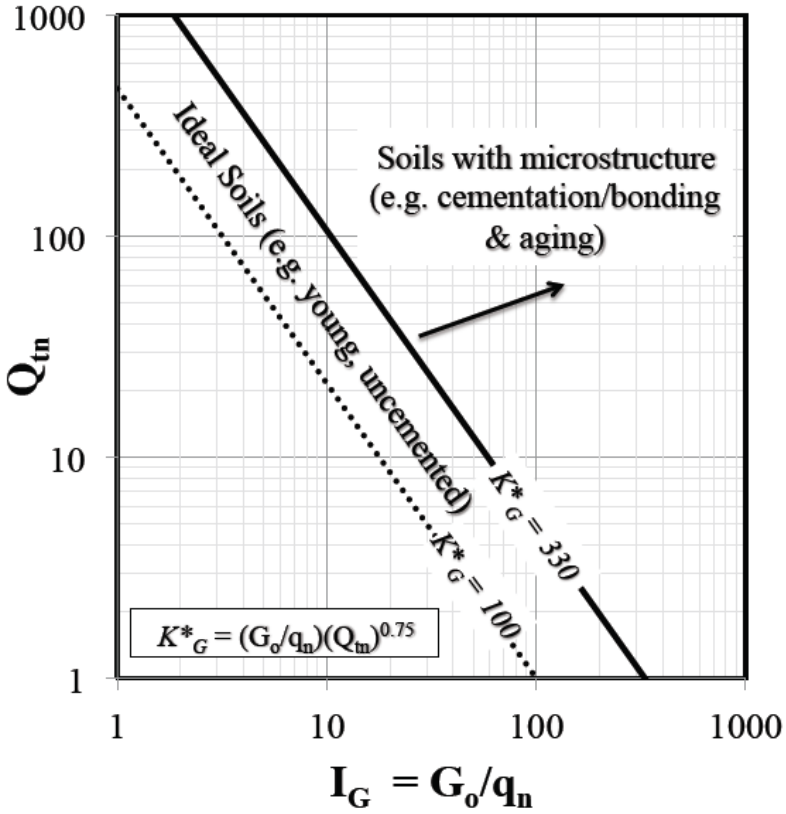

Figure 2: Proposed Q_{tn} – I_G chart to identify soils with microstructure

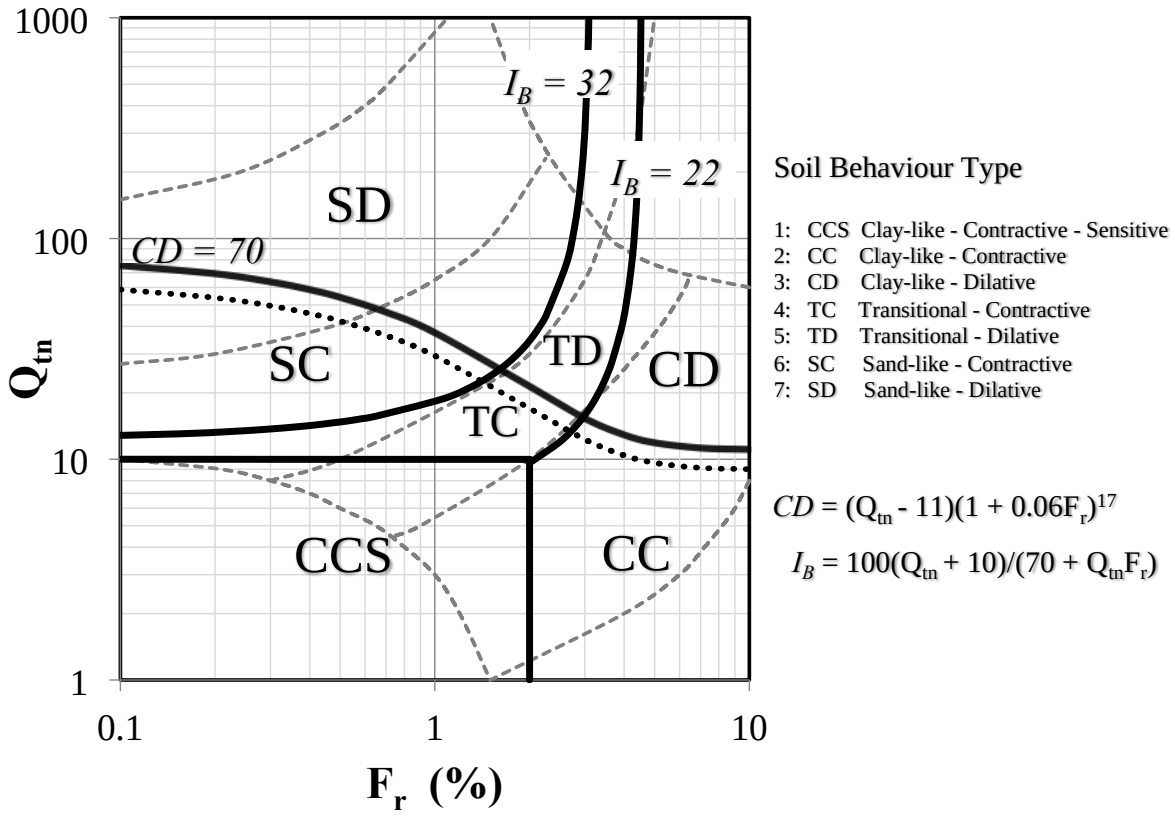

Figure 3: Proposed updated SBTn chart based on $Q_{tn} – F_r$ (solid lines show proposed new soil behavior type boundaries and dashed lines show boundaries suggested by Robertson, 1990)

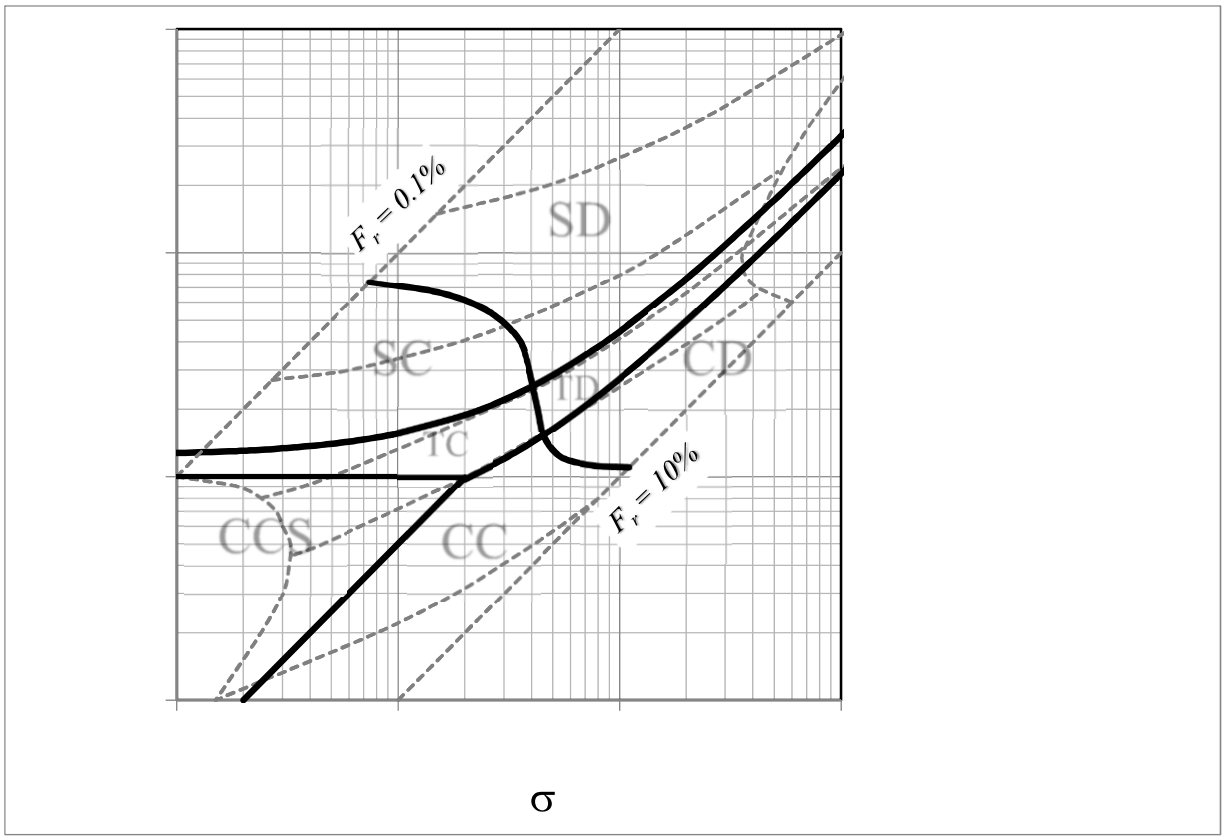

Figure 4: Proposed alternate format SBTn chart based on Q_{tn} – F (solid lines show proposed new soil behavior type boundaries and dashed lines show boundaries suggested by Robertson, 1990)

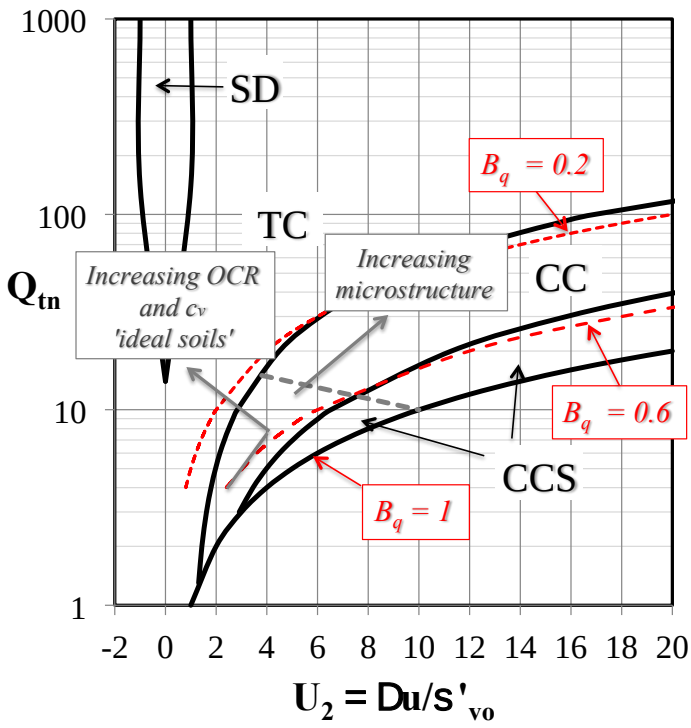

Figure 5: Proposed updated Schnieder et al (2008) chart based on Q_{tn} – U_2 with proposed new soil behavior type boundaries (B_q lines in red)

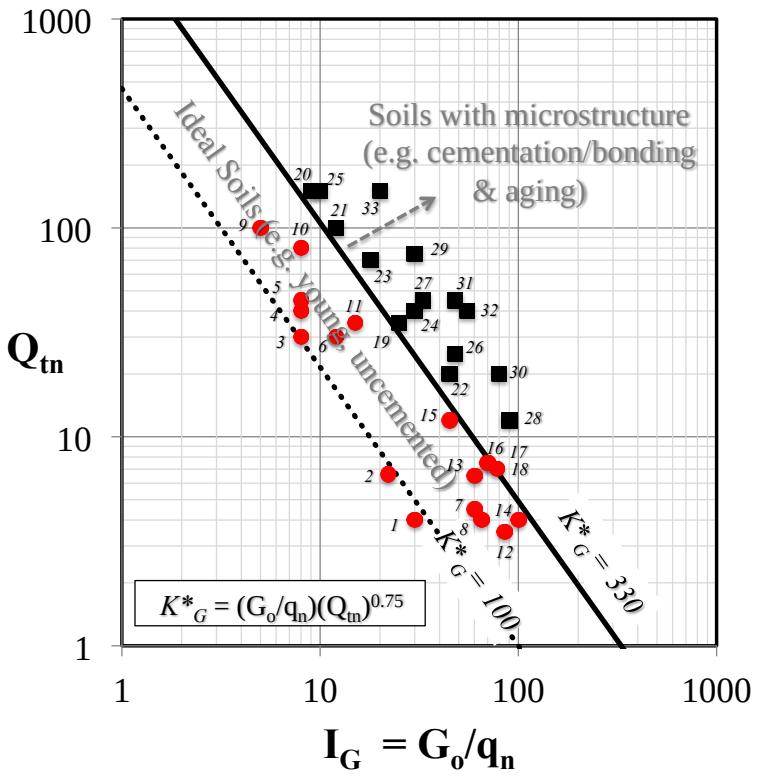

Figure 6: Proposed Q_{tn} – I_G chart with case history examples (details in Table 1). Red circles are young uncemented, and Black squares are soils with microstructure or calcareous.

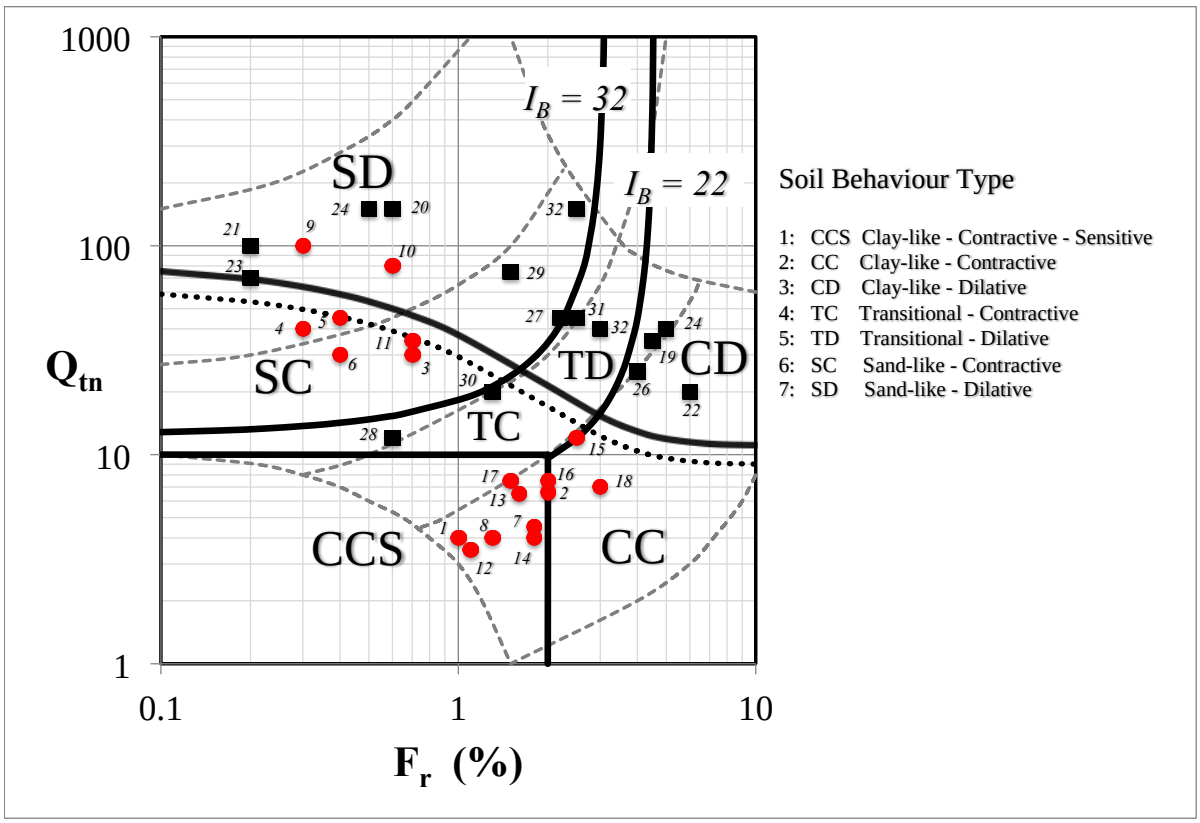

Figure 7: Proposed updated SBTn chart based on $Q_{tn} - F_r$ with case history examples (details in Table 1). Red circles are young uncemented; and Black squares are soils with microstructure or calcareous.

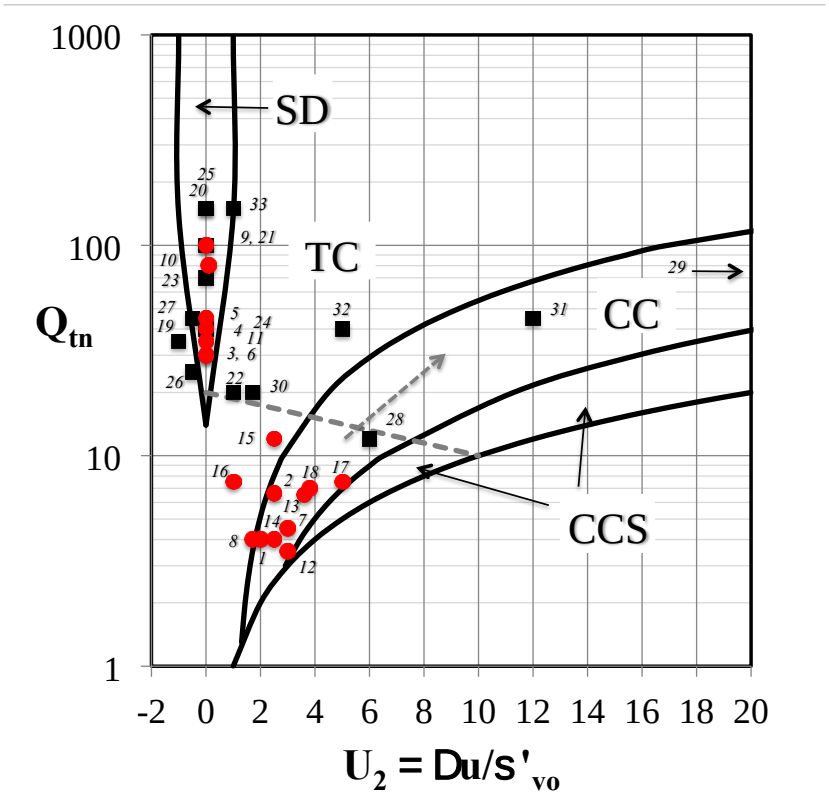

Figure 8: Proposed updated Schnieder et al (2008) chart based on $Q_{tn} – U_2$ with case history examples (details in Table 1. Red circles are young uncemented, Black squares are soils with microstructure or calcareous)

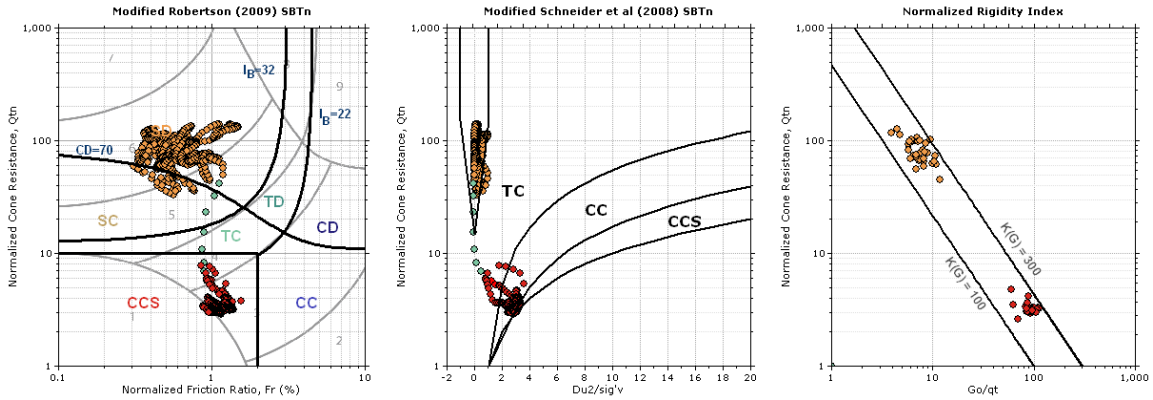

Figure 9: Example of normalized SCPTu data from 4m to 40m at the KIDD site in the Fraser River delta near Vancouver, BC, (orange dots for the sand from 4m to 22.7m, red dots for clay from 22.9 to 40m, green dots for the transition zone from 22.7 to 22.9m)

(a)

(b)

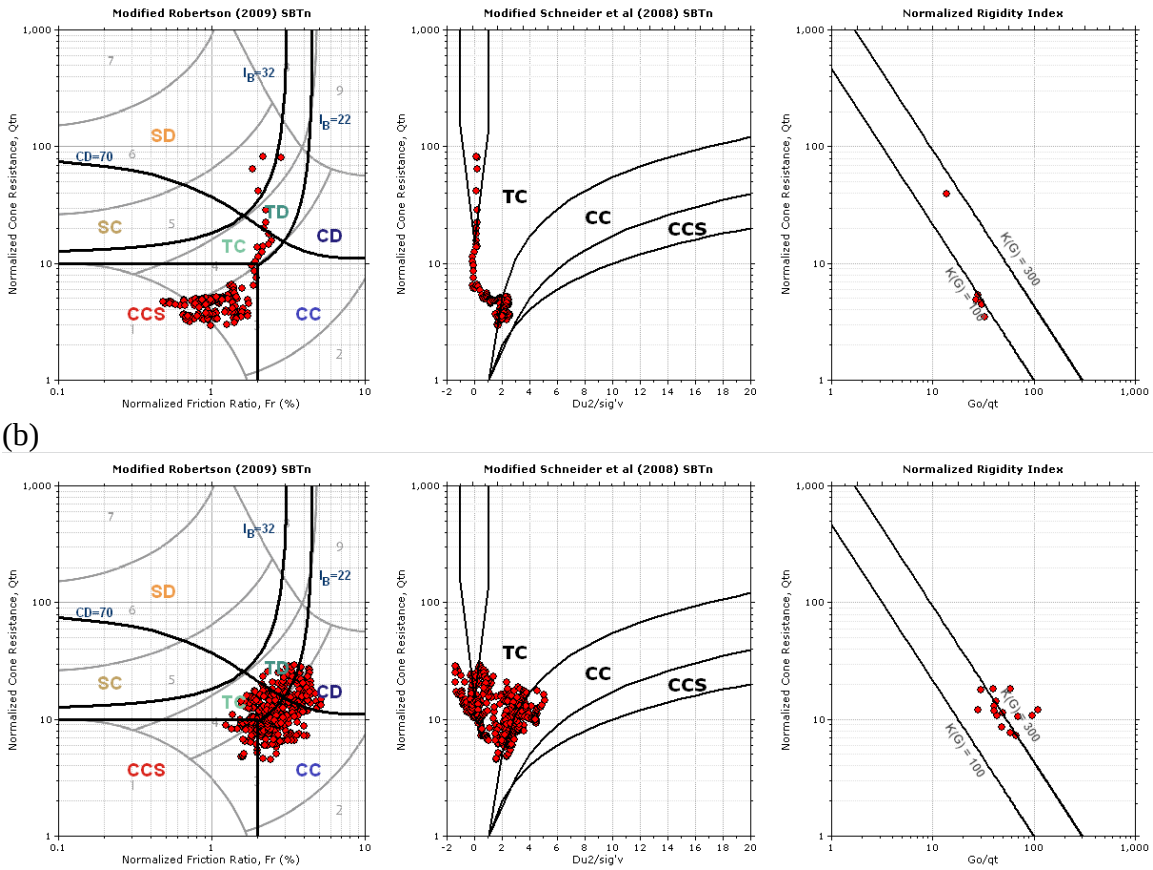

Figure 10: Example normalized SCPTu data from San Francisco Bay, California, USA; (a) Young Bay Mud with desiccated crust (2m to 11m) and (b) Old Bay Clay (12 to 35m)

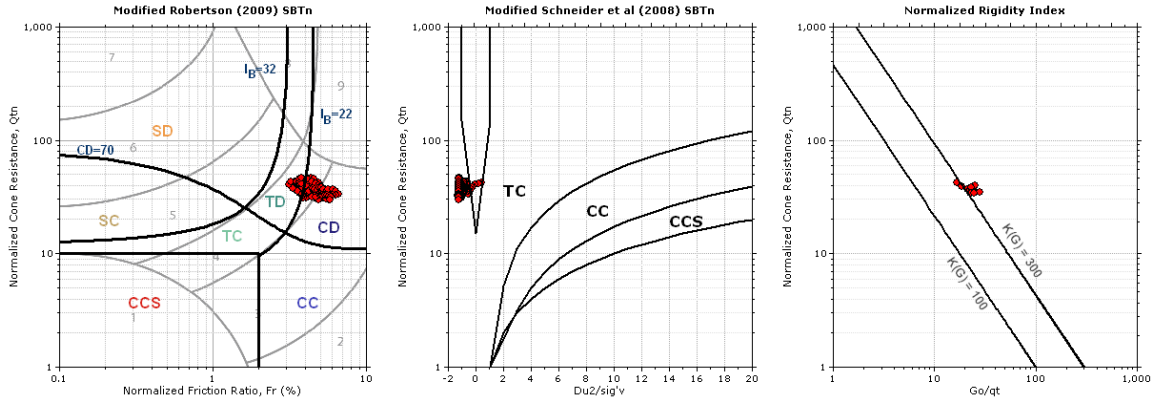

Figure 11: Example normalized SCPTu data from 2m to 12m at the Madingley stiff clay site, Cambridge, UK

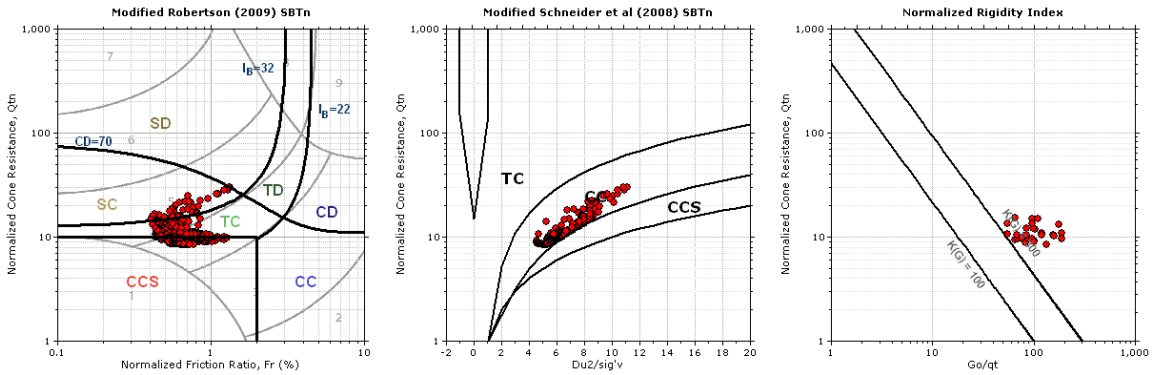

Figure 12: Example normalized SCPTu data from 22m to 50m in Cooper Marl (calcareous cemented clay), Charleston, South Carolina, USA

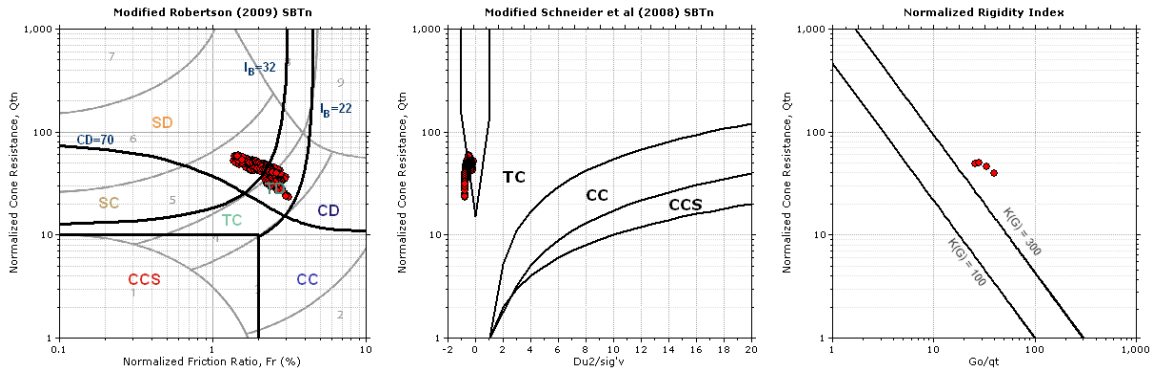

Figure 13: Example normalized SCPTu data from 4m to 19m in Piedmont residual soil at a site in Atlanta, Georgia

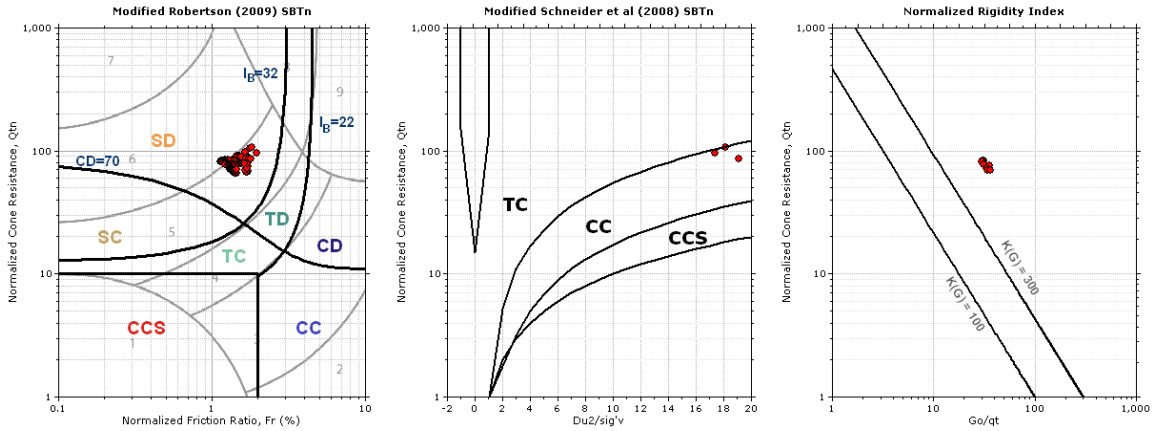

Figure 14: Example normalized SCPTu data from 3m to 10m in siltstone at a downtown Los Angeles site, California

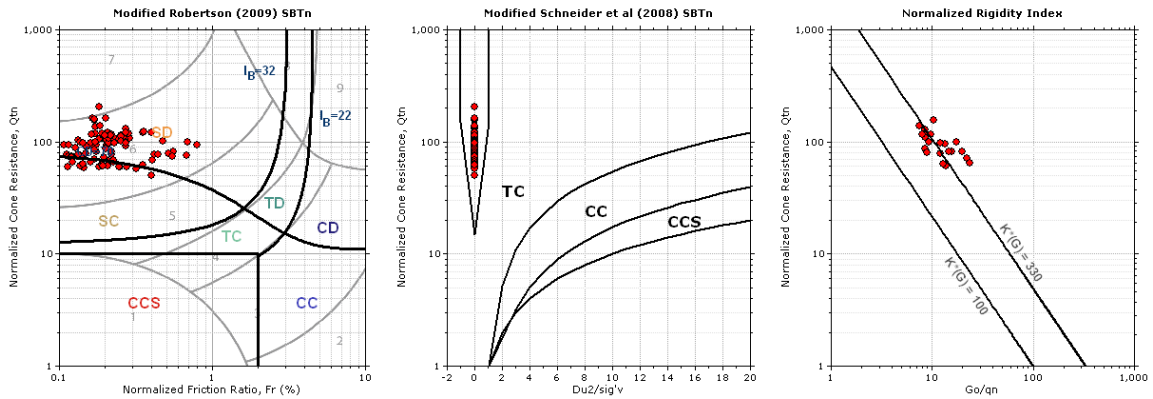

Figure 15: Example normalized SCPT data from 4m to 14m in hydraulically placed calcareous sand in Tangier, Morocco (data from Debats et al, 2015)

ADVANCES IN GROUND MONITORING TECHNIQUES – A SURVEYORS PERSPECTIVE

Michael Nicholson
Director, Michael Nicholson Consulting Pty Ltd

ABSTRACT

In essence 'Surveying' is simply the science of measuring positions on Earth. Surveying has been a key element in the development of the human environment since we stepped out of the caves. The relationship between surveying and geotechnical engineering principles arguably dates back just as far. There is a real synergy between these disciplines / professions that, in the main, is often not fully appreciated.

The core mathematical foundations upon which surveying is based are essentially unchanged. What has changed enormously over the centuries and dramatically over the past decade or two are the technologies available to Surveyors to aid them in measuring the 'Earth', and anything built on / in it.

This paper touches on a range of current survey measurement methodologies, some of which may be considered 'tried and true' traditional techniques along with a number of exciting newer technologies such as LiDAR (Light Distance and Ranging), DInSAR (Differential Interferometric Synthetic Aperture Radar), GNSS* (Global Navigation Satellite System) based real-time 3D measurements, with particular attention given to drone (Unmanned Aerial Vehicle - UAV) based digital photogrammetry.

Like many measurement techniques, digital photogrammetry is a technological evolution of a well understood and developed traditional analogue approach. With the advent of laser scanning (LiDAR) measurement technologies in the late 1990's, analogue photogrammetry rapidly fell out of favour for all but a few niche measurement applications. However, over the past few years there has been a dramatic shift back to 'digital' photogrammetry. This re-emergence has been facilitated by advances in digital photogrammetry autocorrelation algorithms, increases in computing power, relatively affordable PC based software solutions, digital SLR cameras and most recently, the development of commercially available drone (UAV) based digital camera systems. Modern digital photogrammetry solutions are now capable of very quickly capturing high resolution, high accuracy and generally high quality measurements with flexible outputs ideally suited to 3D surface modelling and measurement problems. These technical attributes in tandem with affordable digital cameras and modern UAV platforms has opened up a wide range of applications, many of which are in mining, engineering and monitoring fields.

More important than any particular measurement technology, effective survey monitoring, or any type of monitoring, starts with clearly understanding: what has to be measured (critical parameter(s)), how accurately it needs to be measured, and at what frequency are the measurements required? Only once these factors are crystal clear should we start to consider which technology or combination of measurement techniques is most suitable for the project. In many cases, an integrated approach utilizing a blend of 'surveying' and 'geotechnical' measurements will deliver the optimal monitoring strategy.

1 INTRODUCTION

Surveying now takes many forms. We've probably all heard the claims that the latest piece of technology or instrument is revolutionising practises…*throw out all your conventional gear; Total stations, Global Positioning Systems (GPS), Laser scanners, drones, etcetera, can do everything better, you don't need anything else!* These various technologies are indeed marvellous but to suggest that any one of them is the best tool for every job is simply not correct.

All too often we see examples where instrument manufacturers, clients, or consultants push a particular technology solution or instrument rather than focussing first on really understanding and defining what needs to be measured. Knowing what needs to be measured sounds relatively straightforward, and in many cases it is. However, in some instances, especially the more challenging projects, gaining a clear understanding of exactly what and how accurately something needs to be measured can be half the battle. Understanding deformation / failure mechanisms is the key to developing an appropriate measurement / monitoring strategy.

This paper aims to provide Geotechnical Engineers and associated professionals with a greater understanding of the various surveying factors to consider. In many cases, these same fundamental considerations transfer equally to other disciplines. In addition to providing general information on some fundamental measurement concepts the paper gives an overview of the current status of drone (UAV) based digital photogrammetry, as well as autonomous GNSS based real-time three dimensional (3D) movement monitors.

2 DEVELOPING A MEASUREMENT / MONITORING STRATEGY

We should not focus on how measurements will be made or what technology to use. Only once the answers to the questions below are completely understood should consideration be given to 'how'!

2.1 WHAT TO MEASURE?

Irrespective of whether a feature is natural or man-made one of the first steps in developing an appropriate monitoring strategy is gaining an understanding of the possible failure mechanism(s) of the feature. For example tension cracks is an earth wall dam have the potential to lead to a piping failure, differential leg movement of a steel truss high voltage (HV) transmission tower leads to change in stress distribution in structure members which could readily lead to a collapse of the structure, compression of a rock bar or bound highway pavement can lead to a sudden step failure.

The engineering characteristics, and likely behaviour of man-made features is generally easier to define than natural features. Civil and geotechnical engineers often play critical roles in determining failure modes. The determination of failure mechanisms leads to the definition of the key parameter(s) that need to be measured. Referring to previous examples: change in length along the dam wall, differential settlement of HV transmission tower legs, change in stress within rock / pavement. From a surveying perspective, we are often simply looking for relative movement between one structural element and another.

2.2 HOW ACCURATELY TO MEASURE?

How much movement is too much? The answer to this question informs how accurately something needs to be measured. There is no point measuring something to an accuracy of ± 5mm if a 1mm change could cause a failure. Similarly, a feature that is not sensitive to change at the ± 100mm level does not need the effort and (enormous) expense of a ± 1mm monitoring system. As a general rule, as survey monitoring accuracy requirements increase the cost increases exponentially.

2.3 HOW FREQUENTLY TO MEASURE?

How quickly can movements occur? The answer to this question leads to understanding what sort of measurement frequency is required. If the measured parameters can go from safe levels to dangerous levels quickly them high frequency monitoring is required to allow time to respond. However, if changes are slow and /or the risks are low then lower frequency monitoring may be more appropriate. A great example of this involves the measurement of underground longwall induced mine subsidence in the southern coalfield of NSW. The actual ground movement (subsidence) occurs relatively slowly, generally < 20mm / day. However, the Hume Freeway which has been undermined by longwall mining operations has the very real potential to experience a compressive stress 'build-up' within the pavement in response to the slow ground movements acting on the pavement structure to a point where a sudden brittle failure could occur. To aid in the management of a 'sudden' failure, pavement stress is monitored continuously by a real-time system whereas the ground movements only need to be monitored weekly.

2.4 ACCURACY, PRECISION, RESOLUTION – KNOW THE DIFFERENCE

Accuracy can be most simply defined as: how close a measurement / observation is to its true value.

Precision refers to how consistent results are when measurements / observations are repeated. It is entirely possible that measurements / observations can be precise but inaccurate.

Resolution is often defined as the minimum distance existing between two objects when those objects can still be observed as separate entities i.e the level of detail that can be detected – 'resolved'. With respect to photogrammetry, resolution is perhaps best thought of as: the pixel size of imagery or 3D renders produced, and / or the density (and precision) of the 3D point clouds generated.

2.4.1 Precision is the key

Survey monitoring aims to detect change. For this reason, precision is the key not accuracy. How precisely (or repeatable) a series of measurements can be made essentially quantifies of how accurately differences (change) can be defined. For survey monitoring, 'differences' is usually in terms of change in length, height or spatial position.

Using a real world example of this concept: a line of discrete fixed survey prisms installed to monitor ground deformations caused by mine subsidence can be repeatedly measured with only very small variations in the measured values, say ± 2mm, the measurements are very precise. However, the line of survey prisms may have only been approximately connected to the National Map Grid Australia (MGA) / Australian Height Datum (AHD) coordinate systems, say ± 1m. The reported MGA / AHD coordinate values for each prism are not very accurate i.e. close to their true spatial position. As mining related ground movements begin the survey repeatability remains the same and ground movements are calculated by comparing the initial (base) values for each prism location verses subsequent measurements of the prism location. The precision and accuracy of the reported movements (differences) is nominally < ± 5mm i.e. the true magnitude of the movement (change in coordinate values) is equal to the combination of the measurement precisions.

2.4.2 Absolute vs Relative Accuracy

Expanding on the definitions of accuracy, precision and resolution presented above, another key concept is the notion of absolute accuracy and relative accuracy. In typical deformation surveying applications, absolute and relative accuracy can be thought of in a very similar vein as the accuracy and precision discussion in section 2.4.1 above. Absolute Accuracy is defined as how close the data is to its true value. In the surveying context absolute, or global accuracy as it is sometimes known, generally refers to how close a reported 3D coordinate is to its true position with respect to a recognised coordinate framework, for example MGA / AHD. Relative accuracy refers to how true the spatial relationship (geometry) of the data is relative to other elements in the same dataset. Alternatively, more specifically, how accurate the reported 3D coordinates of one survey point are relative to other points reported within the same survey / monitoring network.

Differential movements of one piece of ground or one structural component relative to adjacent components effectively equate to 'deformation'. Deformation often leads to an increase in risk of failures. By way of example, continental tectonic movements might see might see a dam on the Australian continent moving 40mm North per year. This global (absolute) movement poses no risk to the integrity of the dam. However, if the dam wall moves 40mm relative to the adjoining abutment this most certainly would raise concerns about structural integrity.

For deformation monitoring surveys relative accuracy and survey precision are far more important than absolute accuracy as they directly influence the ability to detect change.

2.5 DISCRETE POINTS VS CONTINUOUS DATA

Traditionally surveying has involved the measurement of particular 'points of interest' – discrete points in space. Such discrete points can include: survey pegs on property boundaries, buildings, fence intersections and so on. The common element is the discrete points are always tangible physical features. In the survey-monitoring context, discrete points can take many forms: fixed survey prisms, pins or threads in rock / concrete, photography / scanner targets, permanently mounted GNSS receiver hardware to name just a few. The central idea being that the same point can be remeasured time and time again (i.e. multiple epochs in time) allowing a direct comparison of the measured data for each point. Discrete point measurements usually have simple well-defined accuracy and precision estimates. Total station measurements to fixed monitoring prisms and GNSS measurements to monitoring pins are two common examples of discrete point monitoring methodologies.

Within the surveying, mapping and remote sensing context 'continuous' data or non-discrete data as it is sometimes known, are datasets that are comprised of many, often millions, of individual arbitrary (blind) observations that are examined / viewed together as a surface(s). While the surveyor may have some control over the point distribution or density they typically have no ability to control exactly where individual points within the cloud will fall (i.e. the exact opposite of discrete point measurements where the surveyor knows precisely the point where each individual observation will be made). Many 'raster' datasets are effectively continuous. Perhaps the most prevalent current example of continuous surveying data would be 3D point clouds generated by LiDAR or digital photogrammetry and the Triangulated Irregular Network (TIN) meshes computed from point cloud datasets.

The accuracy and precision of continuous data is often more difficult to define and / or understand in practical terms. To date remote sensing derived raster datasets often have their quality described in terms of resolution or a mathematical computation of accuracy based on specific instrumentation, measurement parameters and processing methodologies. Mathematical computation based accuracy / precision / resolution statements are particularly common with interferometry based technologies such as Differential Interferometric Synthetic Aperture Radar (DInSAR). In the author's experience

the practical (real world) accuracy / precision of these data is often significantly lower than the mathematical computation statements suggest.

LiDAR or digital photogrammetry derived continuous point cloud datasets often have their accuracies defined by the nominal quality of each individual data point within the cloud. The problem with this approach is that at the individual data point level the stated accuracy does not necessarily provide a fair indication of the accuracy of the continuous dataset as a whole. High density point clouds are capable of yielding extremely accurate shape / surface definitions. The key is that high point data density (usually millions) combined with high relative accuracy can often more than compensate for lower absolute accuracy of individual points in the cloud. A great way to illustrate this is to consider two measurement scenarios for a complicated, say 1 km² area of interest.

a. The first measurement method involves extremely high accuracy (say ± 3mm) total station observations, but in a full day of fieldwork, the surveyor can only measure 500 points to define the surface. Even though the surveyed points have been carefully selected by the surveyor and measured very accurately the overall accuracy of the surface shape of the landform is not likely to be great as there are simply not enough measured points to yield anything other than a very generalised definition of the 1 km² topographic surface.
b. The second measurement technique involves using digital photogrammetry from drone-based imagery. The same surveyor could comfortably survey the same area in a single day. The vertical accuracy of the individual points that make up the photogrammetry derived point cloud may only be accurate to ± 30mm however the data density would be nominally 30 points / m². Thus the 1 km² topographic surface would be defined by 30 million points at ± 30mm, rather than 500 points at ± 3mm.

Given the very high density of typical point cloud datasets the 'continuous surface' derived from the data points is far more accurately defined than official accuracy statements may suggest. The more complex the surface / shape to be surveyed the more influential data density is rather than individual point measurement accuracy.

3 GNSS BASED REAL-TIME 3D MOVEMENT MONITORS

GNSS based 3D monitoring systems as described below are a great example of discrete point measurement.

Real-time 3D movement monitoring systems come in many forms and can be based on a variety of measurement technologies such as: GNSS, Total Station, Radar, LiDAR and many others. In addition to these surveying based 3D movement monitoring systems there's an equally wide range of geotechnical sensors such as extensometers, inclinometers and so on that are also highly effective at detecting movement.

This section will focus on GNSS based 3D monitoring systems with particular emphasis on the latest low cost options. GPS (Global Positioning System) based technology has been widely used in monitoring applications for over 30 years. Some of the earliest applications in the late 1980's involved monitoring ground movements associated with active volcanoes. By studying the rate of change of key points around the volcano, volcanologists were able to develop predictions as to when eruptions were imminent. More recently, fixed real-time GNSS stations played a critical role in providing up to the minute survey control data during the construction of the world's tallest building, the Burji Dubai Tower completed in 2008.

The technical capabilities of such systems are well understood and have been successfully applied to a broad range of surveying and monitoring applications. However, up until very recently GNSS based systems have been relatively costly as the unit cost for the hardware was quite high and each point to be measured requires its own hardware. On this basis such systems have been largely out of reach for all but the highest priority / value projects.

The rapid proliferation, particularly over the past decade, of consumer grade GPS and GNSS receivers for integration in mainstream devices such as mobile phones, watches, cameras and so on has led to enormous development and a dramatic reduction in cost of GNSS receivers, associated peripherals and software. These developments, together with powerful, compact computer hardware and simple telemetry options have facilitated the development of very low cost GNSS based 3D monitoring systems. As the cost of such systems has reduced the number of potential applications has expanded proportionally. One such arrangement that the author has extensive experience with is a completely autonomous system with each monitoring unit consisting of: GNSS receiver, computer board, telemetry module and solar / battery power supply. As shown in Figure 1 below, the entire stand-alone unit is not much larger than a shoebox with a dedicated solar panel. The measurement unit and solar panel are typically mounted on fixed posts in the ground or directly to structures.

Figure 1: Low-cost Autonomous GNSS Monitoring Installation

The key site constraints are that the mounting point is free of large amplitude vibrations and has a reasonably clear 'sky window' (i.e. view of the sky). This later point is the biggest limitation of any GNSS based measurement / navigation solution as a compromised sky window can have a significant impact on the quality / accuracy of 3D positioning, with the height coordinate being the most affected. When these systems are installed in suitable locations the daily 3D survey accuracies achieved are in the order of ±3 – 5mm. Each unit sends data back to a central computer multiple times per day with results uploaded to an internet site where they can be viewed and downloaded by clients, consultants, regulators and any other authorised parties (internet sites are all password protected). Figure 2 below illustrates some simple graphical representations of deformation data taken directly from a project internet site. In addition to the internet based data, the system is also able to be programmed to send automated SMS or email alerts in the event predefined movement triggers are reached.

As noted above, GNSS based monitoring systems with the functionality and measurement accuracy described are not new. However, with the latest systems now costing 5 to 10 times less the more traditional brand name systems this methodology now represents a very cost effective option for many applications. Another very appealing aspect of these newer systems is that additional sensors can be readily integrated into the same 3D position monitoring unit. To date tilt meters have been added to these systems and the latest work is looking at integrating a range of geotechnical sensors, such as piezometers, inclinometers and extensometers. In the very near future, we will see affordable fully integrated monitoring units capable of measuring, logging and uploading to an internet site, a whole range of surveying and geotechnical data.

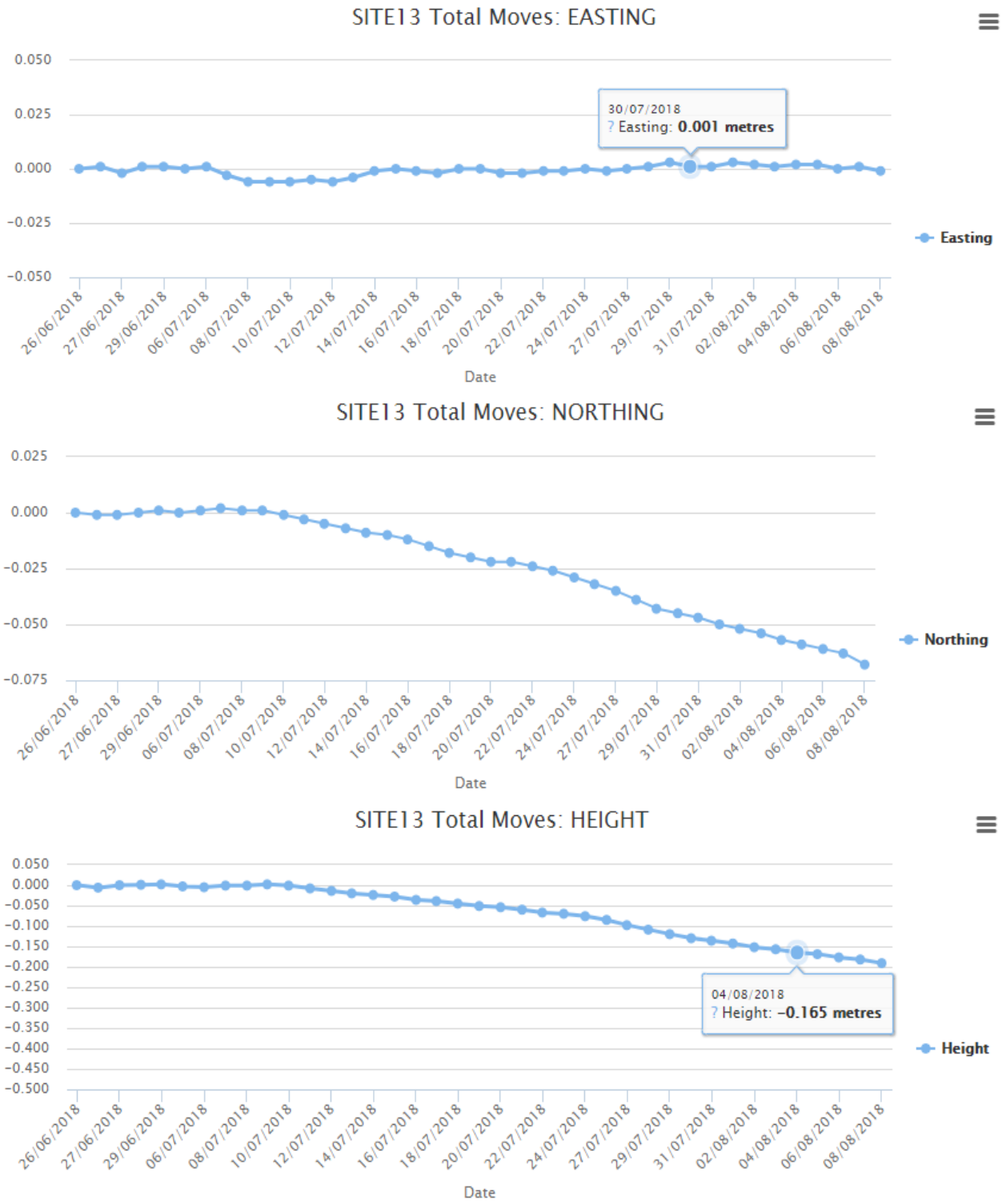

Figure 2: Typical Internet based deformation data represented in graphical form

4 DIGITAL PHOTOGRAMMETRY

Digital photogrammetry as described below is a great example of a technology that yields continuous data. However it should also be noted that discrete point measurements are also readily achievable using photogrammetric techniques.

4.1 BACKGROUND

Photogrammetry is most simply defined as: *the science of making measurements from photographs*. The key concepts and mathematical principles photogrammetry is based on date back hundreds of years. However, photogrammetry really emerged shortly after the advent of photography in the mid-19th century. Like many technologies before and since, photogrammetry developed quickly on the back of military investment. By the 1990's photogrammetry and photogrammetric principles were at the height of their powers, not only being well established as the primary mapping and remote sensing technology but also increasingly used for a wide range of terrestrial surveying applications.

The mainstream emergence of laser scanning, now referred to almost universally as LiDAR (Light Detection And Ranging), around the turn of the millennium resulted in a rapid shift away from photogrammetry for many applications. This shift was most notable in surveying where LiDAR and other alternate technologies very quickly replaced photogrammetry for all but a small number of specific applications. After almost fifteen years of relatively little use, photogrammetry has come back in to favour. This re-emergence has been facilitated by advances in digital photogrammetry autocorrelation algorithms, increases in computing power, relatively affordable personal computer (PC) based software solutions and most recently, the development of commercially available drone (UAV) based digital camera systems.

It is beyond the scope of this paper to focus on the hard, dry mathematics that is at the heart of digital photogrammetry technology. However, for context it should be noted that computer based image matching or 'autocorrelation' as it is now commonly known, is a term, which refers to automated raster-based identification of common points in two or more overlapping images. Digital photogrammetry projects generally adopt much higher photography overlaps than traditional film based analogue conventions. High overlaps together with rigorous autocorrelation based image matching protocols lead to high levels of redundancy such that sub-pixel accuracy is readily achievable.

So, with foundations in basic mathematical principles over 100 years old, along with modern day advances in digital techniques and computing power what is photogrammetry capable of today? Somewhat paradoxically, it is still a rapidly evolving technology. The rise in consumer level drones / UAVs has not only provided the obvious advancement in affordable image acquisition, but even more importantly, stimulated significant further software development.

The latest digital photogrammetry hardware and software is still advancing rapidly. As such, it is difficult at this stage to put bounds on what is possible in terms of both resolution and accuracy. Sub 10 millimetre (<10mm) resolution and accuracies are certainly possible for small localised sites / objects while many square kilometres can be covered at sub 50mm (<50mm) resolution and accuracy. The accuracy of control networks is often the limiting factor, particularly in terms of absolute accuracy. Like the resolution and accuracy parameters, there is a broad range of vertical and oblique (or combinations of both) methodologies available. The various techniques can cover almost any size / shape object, from kilometres of pancake flat desert through to small (<1m), highly complex natural or manmade shapes.
There is an equally broad range of outputs possible including (but certainly not limited to):

- 3D point clouds
- Triangulated Irregular Network (TIN) mesh surfaces
- Contours
- 3D rendered animations
- Ortho-photos
- Deformation models
- Cross sections
- Tabular data
- 3D virtual reality

4.2 APPLICATIONS

Applications for digital photogrammetry based methodologies are many and varied, ranging from traditional topographic mapping through to the creation of spatially and geometrically correct photographically rendered 3D CAD models.

4.2.1 Traditional Applications

Fundamentally, for most of the past 100+ years photogrammetry has been primarily used to create topographic maps. The native photographs were also often useful – particularly when viewed stereoscopically, but really it was all about making maps. Topographic mapping techniques were then applied to mapping open cut mining operations and large earthworks

projects to quantify material movements, measure stockpile volumes and so on. The good news is that these traditional applications have all benefitted from the transition to, and ongoing refinement of, digital photogrammetry. Even stereoscopic viewing is still accommodated in some digital photogrammetry workflows.

4.2.2 Cliff Mapping

As per section 4.2.1 above, most traditional photogrammetric applications involved taking overlapping photographs looking vertically down in order to digitize a 3D model of the earth's surface – a topographic map. In analogue photogrammetry it was exponentially more difficult to effectively 'tip' the entire methodology on its side and use oblique photography to map vertical, or near vertical surfaces such as cliffs, mine batters or building facades. Digital photogrammetry and very recently, drone based camera systems have made this once extremely challenging application very doable and highly effective.

There have now been several cliff mapping projects aimed at quantifying and generating accurate 3D models of many kilometres of difficult to access cliff lines. In most cases these models are used to accurately, and in high resolution, quantify the baseline (pre-mining) status of these natural features. Follow-up mapping surveys can be undertaken at any time with any changes (geometric or aesthetic), disturbances or deformations measured, quantified and documented. Figure 3 is a still image of an extensive and complex 3D rendered cliff line model in the Western Coalfield of NSW. Over twenty similar cliffs were mapped during this project. Figure 4 is a similar 3D rendered model of a cliff collapse on the Illawarra escarpment.

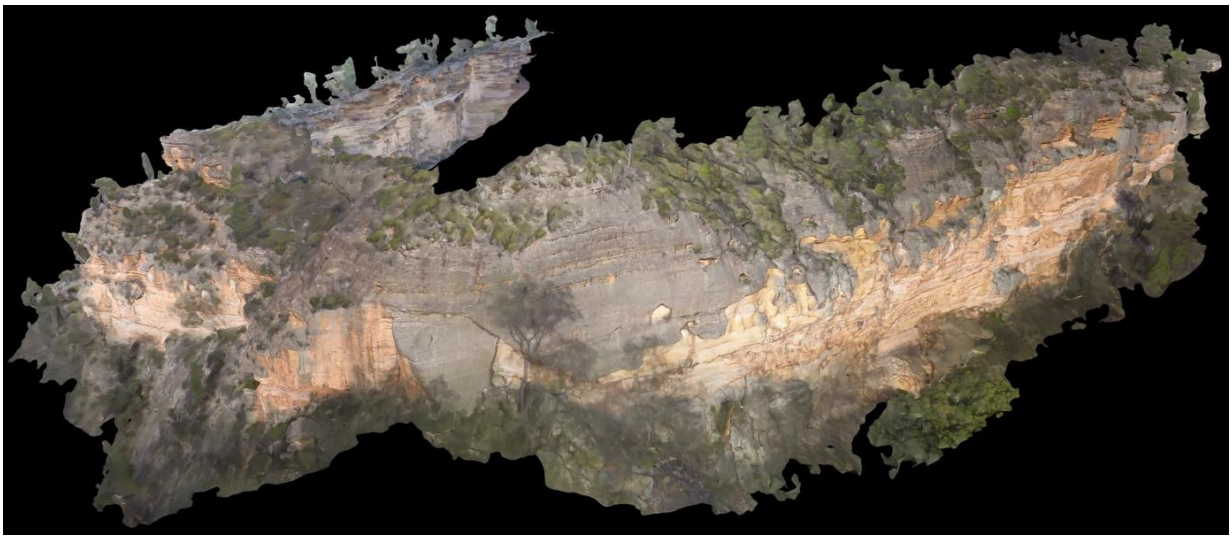

Figure 3: Cliff line model

Figure 4: Modelled cliff collapse on Illawarra escarpment

4.2.3 Highwall Mapping and Batter Monitoring

Using essentially the same methodology as that used for cliff mapping, mine highwalls and batters can also be mapped. Generally highwall and batter mapping is much simpler than cliffs as they are usually clear of vegetation and other obstructions which can often complicate cliff mapping. One of the key advantages of using photogrammetry for detailed highwall and batter mapping is the ability for geologists and geotechnical engineers to use both the 3D point clouds and the photographically rendered models to accurately define measure and map geological features such as joints, faults, lineaments etc., along with areas of potential or previous instability. Figure 5 is a very high resolution (<10mm) 3D rendered point cloud of a section of batter in a Victorian brown coal mine before and after the controlled failure of a small section of clay in the coal seam.

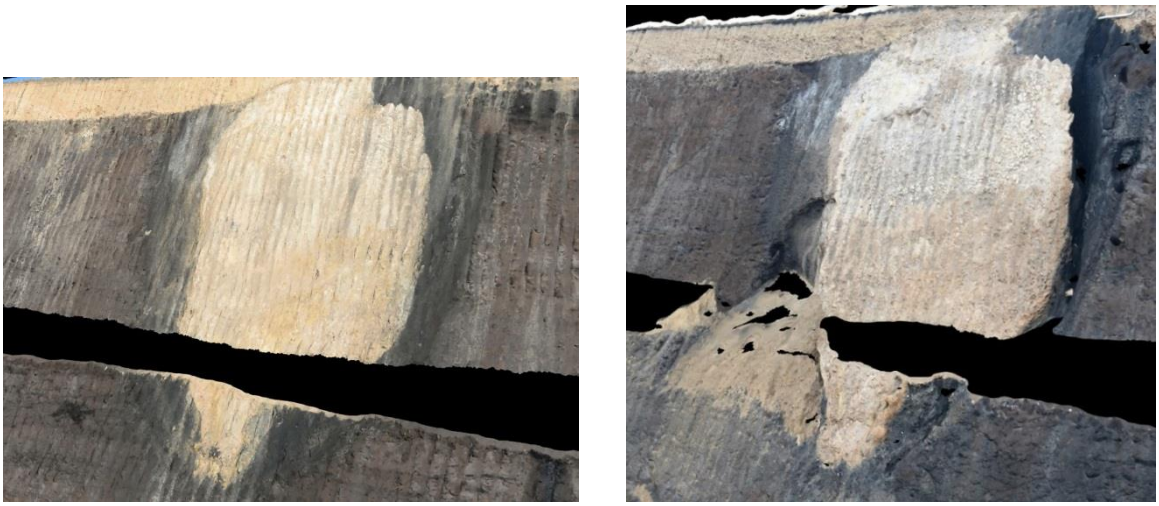

Figure 5: Before and after models of batter deformation

In benchmark trials against more conventional, discrete point prism monitoring, 3D drone based mapping of batters has proven to be effective in identifying areas of batter movement and deformation. On the basis of these extremely

encouraging results, further trials are planned with a view to drone based photogrammetric mapping playing a significant role in future Ground Control Management for this site.

4.2.4 High Resolution Orthoimagery

It's only fair to note that orthophotos were routinely produced well before digital photogrammetry emerged. However, these 'analogue' orthophotos were really only available as hardcopies and were relatively expensive and difficult to produce.

An orthophoto or orthoimagery, as it is now often referred to, can be defined as an orthogonally rectified photographic image (either digital or hardcopy). The perspective projection of the raw photographs has been removed resulting in orthogonal, map accurate imagery. In almost all cases, the orthoimagery is made up of a large number of raw images where only the optimal central portion of each individual image is used in the production of the final overall product.

Digital photogrammetry together with GNSS positioning of airborne sensors (cameras etc.) has meant that the once very difficult task of orthophoto production is now just another step in the same digital workflow.

4.2.5 3D Modelling of Man-made Structures

Photogrammetric techniques can be applied to man-made structures such as viaducts, buildings, bridges, statues, as readily as natural features. It should be noted however that in many cases man-made features such as the examples given, represent more challenging photogrammetry projects as they are often no longer fundamentally planar, as is the case with traditional applications or cliff lines and highwalls. Rather, man-made features often involve full 360 degree complex photography networks which can be considerably more difficult, and require much more photography than simpler, nominally planar projects. Having said that, and perhaps because of the added complexity, the 3D models that are created of man-made features can be among the most visually impressive, whilst also retaining the backbone of a fully spatially and geometrically correct 3D survey.

Objects / structures that can be particularly difficult to model are those of long, slender proportions. Generally the more 'massive' the object the easier it will be to model. For example, an old sandstone railway viaduct would be much easier than say the Sydney Harbour Bridge.

Figures 6a and 6b are an old gold smelting stack of considerable historical significance. Figure 6a shows the underlying, photogrammetry derived 3D point cloud framework, while Figure 6b provides an overview with photography based 3D render applied to the frame.

Figure 6a: Underlying point cloud

Figure 6b: Photographically rendered historic stack model

4.2.6 Rock Shelter / Rock Bar Modelling

As with the man-made features discussed in section 4.2.5 above, rock bars and rock shelters are ideal applications for digital photogrammetry based 3D modelling. These features are generally quite complex in geometry, lighting and accessibility, making them very difficult to accurately record / survey using more conventions methods. These sensitive features are regularly the focus of mining companies and related stakeholders as their sensitivity means they may be more susceptible to impact resulting from ground movements.

The benefits to all parties of accurate, high resolution 3D modelling of such sites is twofold: firstly a baseline condition record, both geometric and visual (photographic), can prove extremely valuable for both qualitative and quantitative assessment of any impacts which may occur; secondly, in the event the features are damaged or even destroyed the 3D models can facilitate the accurate restoration of the site, and / or provide a permanent high quality record of what the site was like prior to being damaged. Figure 7 shows a recently completed 3D model of a combined rock bar and rock shelter site in the NSW Southern Coalfield.

4.2.7 Archaeology & Heritage Recording

Photogrammetry based modelling has been used for a range of environment and heritage features. In the rock bar model in Figure 7 there are numerous Aboriginal grinding grooves which have been modelled. Likewise, rock art has been recorded in shelters where the real benefit is that not only does the photogrammetric model yield a photographic quality record of the art / grinding etc., but the 3D model provides a complete geometric and spatial context of the site. Similarly, man-made features of historical significance such as the previously referenced stack or abandoned buildings, entire facilities, ruins can be readily modelled and recorded.

Unfortunately, time is often the enemy of both Indigenous and built heritage sites. In many cases, full 3D rendered computer aided design (CAD) models of these sites may become the only record available. One of the really exciting aspects of this application, will be the ability of the 3D rendered models to be experienced in a virtual reality environment (refer section 4.3.2).

Figure 7: Combined rock bar and rock shelter 3D Model

4.3 FUTURE DIRECTIONS

4.3.1 Deformation Monitoring without control

Like virtually all survey and mapping activities, control points are required to provide an accurate framework for photogrammetric mapping and modelling surveys. The most accurate, versatile and reliable way of controlling photogrammetry networks is by adding targeted control points at / around the site that are visible in the photography. Typically, control points are surveyed in using either total station instruments, GNSS receivers or a combination of both. In many cases, especially inaccessible areas such as cliffs, rock shelters and creek lines, the provision of survey control points is substantially more difficult, time consuming and costly than the rest of the digital photogrammetric modelling process.

It should be stressed that 'control' in the context discussed above refers to absolute control. Controlling models in a relative sense is far simpler and can also include an approximate (± 3m) absolute location without imposing too much additional expense on the project.

An exciting advancement in drone technology is the integration of full differential real-time kinematic (RTK) or post-processed kinematic (PPK) GNSS sensor positioning and rotation determination. The addition of this accurate positioning technology onto relatively affordability drones (from ~ $30K) means that 3D models with an absolute 3D accuracy of better than ±50mm is now possible with little to no ground control.

Even more interesting is using a form of autocorrelation on two (or more) 3D point clouds that have no absolute control at all, to determine and quantify areas of difference – deformation. A large open cut coal mine is currently trialling and benchmarking the effectiveness of using uncontrolled drone derived 3D point clouds for deformation monitoring of mine batters. Initial results have been extremely encouraging. Figure 8 provides a visualisation of two auto-correlated point clouds on a section of open cut coal mine, where white / light grey shows areas where point cloud correlation agrees to better than 50mm whilst coloured regions identify areas where the point clouds diverge indicating change in the shape of the surface. These deviations between surfaces can be represented and quantified in a range formats including: colour coded images such as Figures 8a and 8b, contours of deformation, cross sections, right through to simple tabular data.

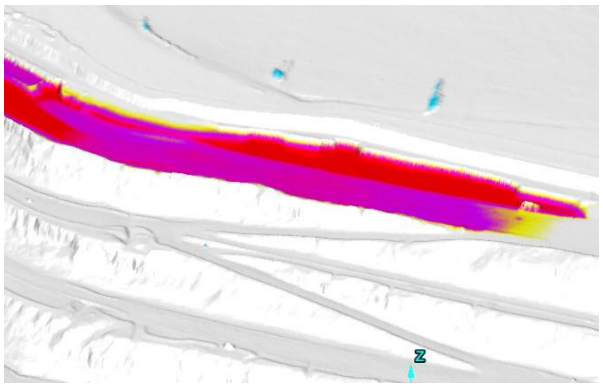

Figure 8a: Point cloud autocorrelation – civil site

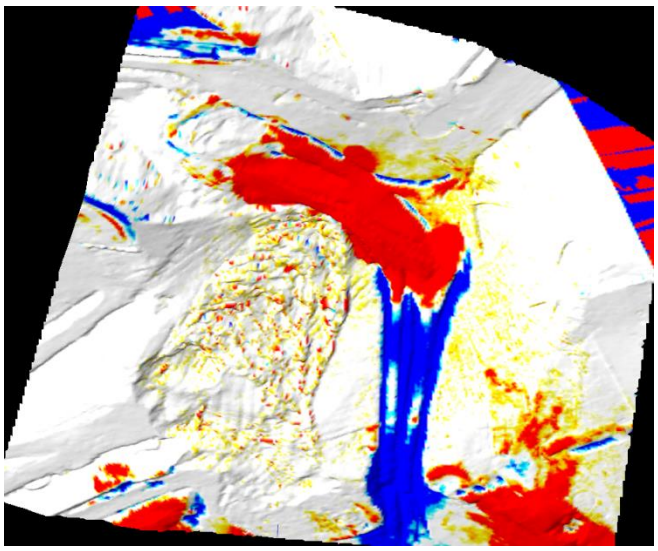

Figure 8b: Point cloud autocorrelation – deformation site

The same auto-correlated point cloud principle has great potential to yield extremely accurate (<±5mm) deformations from a given baseline surface. To this end, trials are ongoing to gain a greater understanding of the full potential and limitations of this very promising methodology.

In addition to using the continuous point cloud data, trials are also under way to automatically extract discrete point monitoring information from the same raw overlapping photography.

4.3.2 Virtual Reality

Currently, hi-resolution 3D rendered animations are routinely produced and only really limited by our imagination (and file size). These animations are visually spectacular and it is easy to forget they are actually built from survey quality, geometrically accurate datasets. These datasets have all the functionality of traditional survey data, but with the added bonus of being able to yield such high-resolution qualitative data formats that are easily accessible to everybody, not just surveyors and engineers.

It is a relatively small step to move from the current predefined video animations to a fully immersive 3D virtual reality experience. Perhaps the most exciting aspect of the virtual reality solution is that users can experience sites in a way that is second only to being there in real life. When we consider that many of the best Indigenous rock art sites for example are, quite rightly, off limits to the general public, virtual reality allows people to still engage with, and hopefully appreciate such sites in ways that are simply not possible from more conventional imagery. Taking one-step further, many culturally significant sites have a finite lifespan and may well be lost to the future. 3D survey quality rendered models such as those produced by modern digital photogrammetry provide us with a way of 'digitally preserving' these sites indefinitely.

Please note that some elements of this section: **Digital Photogrammetry** have been taken directly from the author's 2017 paper - *Re-emergence of Photogrammetry for Hi-Resolution 3D Surface Modelling and Measurement.*

5 CONCLUSIONS

With the seemingly ever-increasing rate of technological advancement, it is interesting to note that two of the most exciting areas of development in survey monitoring involve the evolution of older technologies. GNSS (formerly GPS) position monitoring solutions have very recently become dramatically more cost effective and can now incorporate a range of additional sensors such that they are an integrated hub reporting a variety of measured data autonomously to a central internet site. Digital photogrammetry is an extremely powerful measurement / monitoring technique capable of simultaneously yielding continuous point cloud datasets and the numerous derivatives along with accurate discrete point data. Stand-alone GNSS + monitoring units and digital photogrammetry are just two areas of recent development, there are many more across the surveying, mapping and remote sensing disciplines. Irrespective of the measurement technologies available, it needs to be reinforced that carefully defining what has to be measured, how accurate the measurements need to be and how frequently measurements need to be taken is by far the most important step in any measurement / monitoring task. Only once these parameters are clearly understood should specific measurement methodologies be considered.

* GNSS stands for ***Global Navigation Satellite System*** and is the new naming convention for what was previously referred to as GPS. The reason for the change in terminology was that GPS referred directly to the United States Global Positioning System (Satellites) whereas GNSS refers to the combined satellite positioning systems (e.g. GloNass (Russia), BeiDou (China), Galileo (Europe)).

6 REFERENCES

Han S. and Rizos C. (1996) GPS network design and error mitigation for real-time continuous array monitoring systems. *Proceedings of 9th Int. Tech. Meeting of the Sat. Div. of the U.S Inst. of Navigation,* Kansas City, Missouri

Hayes D., Sparks I., Cranenbroeck J., (2006). Core Wall Control System for High Rise Buildings. *Proceedings of XXIII FIG Congress: Shaping the Change*, Munich Germany

Kelley D. and Loecherbach T. (2007). A comparison of LiDAR terrain data with auto-correlated DSM extracted from digitally acquired high overlap photography. *Proceedings of ASPRS Conference on Safety, Security and the Environment through Remote Sensing*, Ottawa, Ontario, Canada.

McGlone C. J., Mikhail E. M., Bethel J.S. (2004). *Manual of Photogrammetry*. American Society for Photogrammetry and Remote Sensing (ASPRS)

Nicholson M. 2017. Re-emergence of Photogrammetry for Hi-Resolution 3D Surface Modelling and Measurement. *Proceedings of Mine Subsidence Technological Society 10th Triennial Conference – Mine Subsidence: Adaptive Innovation for Managing Challenges*

CONTINUOUS MONITORING OF LANDSLIDES AND INFRASTRUCTURE FOR ASSET MANAGEMENT

Phil Flentje[1], David Arnold[2], Dhammika Ruberu[3], Andrew Monk[4], Peter Tobin[5], Kevin Bogie[6] and Raymond Piatek[7]

1. *Senior Research Fellow, Faculty of Engineering and Information Sciences, University of Wollongong*
2. *Communications Engineer, IMTS, University of Wollongong*
3. *Manager, Educational Systems Development, Technology Enhanced Learning*
4. *Corridor Maintenance Planner, NSW Roads and Maritime*
5. *Senior Geotechnical Engineer, Wollongong City Council*
6. *Geotechnical Engineer, Wollongong City Council*
7. *Civil Engineer, Wollongong City Council*

ABSTRACT

The University of Wollongong Faculty of Engineering and Information Sciences Landslide Research Team (UoW), with our industry partners, Wollongong City Council, Roads and Maritime and Sydney Trains, has developed a network of thirty one currently active Continuous near Real-Time Monitoring (CRTM) stations within NSW.

This paper provides a general overview of the field monitoring equipment used, the monitoring strategies employed, wireless and mobile communications employed and a brief mention of the monitoring server setup and the related IT setup. The second part of the paper focuses a more detailed summary of two site installations, the acquired monitoring history and how this has expanded our knowledge and understanding of the site geological models and allowed progress towards site remediation and ongoing management. A brief mention of several interesting and emerging technologies in the fields of the Internet of Things (IoT) and Low Power, Wide Area Network (LoRaWAN) instrumentation is made.

The paper concludes by highlighting some critical issues related to the development of site monitoring strategies that experience has shown are sometimes not well managed. These include the reason for monitoring, the awareness of ongoing maintenance costs for the life of the monitoring, the duration of monitoring and reasons to either continue, modify and cease a monitoring program.

1 INTRODUCTION

Developed with our industry partners, Wollongong City Council, Roads and Maritime and Sydney Trains, the University of Wollongong Faculty of Engineering and Information Sciences Landslide Research Team (UoW) has developed a network of thirty one currently active Continuous near Real-Time Monitoring (CRTM) stations within NSW. Installed initially at landslide sites to monitor landslide and or asset performance in response to landslide movement, most of these sites report in real-time to a University of Wollongong Data Centre Server. The monitoring frequency is either 5 minutes or hourly and the field data is automatically stored in site specific databases with the aid of custom software so that the full history of data is available for querying in real-time via a custom designed, secure password protected web-based graphical user interface we have developed. The earliest installations now have up to fifteen years of continuous monitoring history. We have already developed and continue to roll out smart alerts for some of the stations, based on rainfall, pore water pressure and movement thresholds.

Landslides in the area have been mapped by the first author of this paper as one focus of research at the University of Wollongong. The University of Wollongong NSW Landslide Inventory includes 1867 landslides (134 falls, 278 flows and 1455 slides) to date. Wollongong is the 10th largest city in Australia, and the surrounding terrain includes a range of long linear urban, road and rail infrastructure distributed over several hundred kilometres along the NSW south coast. The monitored locations represent important sites to asset and or geotechnical managers from our industry partners, co-authors of this paper and the summary histories of two sites are discussed in this paper. The community is fortunate to have a strong proactive group of multi-disciplinary geotechnical and asset managers and staff within our industry partners who are aware of the hazardous terrain, in a hazardous climatic and hydrogeological environment who support the university based research to develop and maintain this extensive network.

2 MONITORING STRATEGIES

As an engineering geologist, the first thing to do on any site investigation is to make a desk top assembly of available data and review of any relevant information from all sources available. Of note here, for Australia is Trove, a free online

library database with its own search engine hosted by the National Library of Australia which has scanned just about every newspaper printed in Australia. This of course will develop as part of the wider geotechnical/engineering geological investigation of any site that may develop over time. It is also essential to visit any rock outcrops/exposures in cuttings, cliff lines, coastal exposures etc that the site mapping and desktop research has highlighted, to start developing a conceptual geological model of the site. Landslide investigations must always be tailored to the site and the attendant budget and the issues they relate to. The budget allowed should be tailored to the perceived risk and the sites priority in the list of planned works. That perception may or not be correct, and it may need to be adjusted as part of your investigation work.

During the initial site visit the site, a 'walkover' of the entire site is essential. If the site is small and confined, and relatively straight forward, your first visit may also be your last, although some landslide sites may become part of your routine work flow and they may get visited many times over. Mapping may be with a pencil sketching in a field book or on an immaculately prepared Geographic Information System (GIS) base map and involve identifying relevant pertinent features on and around the site, or it may be using the latest Global Navigation Satellite System (GNSS) tablet device with a streamlined workflow feeding into a GIS-based desktop environment Landslide Inventory (where all landslide mapping should be stored). It may even involve high definition lidar, captured by a small unmanned aerial vehicles (UAV – drone) producing high resolution point clouds (500 points per m^2 are cost effective and available today). With landslides you just have to get the dimensions known, the length downslope, the width across slope, and depth (often a hard one) as components of the total affected area, and of course the timing and magnitude of past and/or recent failures. The number of past failures and the corresponding frequency, that's typically next to impossible, but ongoing investigations will target, in part at least, refining that. After defining the landslide feature itself, in landslide risk assessments, it's really all about understanding the frequency and magnitude of displacement, at least to start with. If this work has been done, periodic landslide monitoring has commenced. If it is not a landslide site, rather perhaps urban, road and or rail infrastructure, all the relevant site features, geomorphic and infrastructure related, should be recorded.

The investigation work may involve some subsurface investigations to find out more of the subsurface beyond what the mapping has shown, to further enhance the engineering geological model. It is also only after the initial walkover and desktop investigations that a subsurface investigation plan can be developed, to try and ensure the maximum understanding is achieved for the smallest commercial outlay. This may include installation of some instruments, most likely dependant on the landslide and the assets considered to be at risk if movement were to continue. If installed, then some periodic monitoring can be done to value add to the field mapping and inspections, which are also a form of periodic monitoring. This will often include inclinometer monitoring and measuring water levels in standpipes or possibly vibrating wire piezometer readings. Monitoring is only part of any investigation, it certainly does not fix anything. It is primarily used to help understand the mechanisms of failure (depth to slide surface, rate of movement along the slide surface, pore water pressures at various depth above, at, and below the slide surface) and it can also be used to help manage things in the short to medium term. It is more than likely that remedial and/or avoidance works will be required in the longer term. Even then, monitoring has a role to play, to assess the performance and effectiveness of installed works - this will be demonstrated in the first case study discussed below.

Where the site is important to an asset or geotechnical manager, funding may be available to install a logger and collect some continuous data for a period of time. One, of the many decisions, at this point will revolve around the frequency of monitoring, (i.e., hertz, minutes, hours or even daily). If the asset or perceived risk is really important, or alternatively, sending a human out to collect the data is time consuming, or considered dangerous, a communications device (radio or router, both in some instances) to facilitate collecting the continuous data remotely can be added. At the University of Wollongong, with the ongoing support of our industry partners, we have automated this process and added a secure password protected web-based graphical user interface (GUI) to deliver the information in real-time (subject only to the monitoring frequency) for our industry partners. It is now being done increasingly more often as time goes by, but we have been doing it in Wollongong now since 2004.

3 BACK TO BASE REPORTING CONCEPT

The initial monitoring project was conceptualised as shown in Figure 1, with a range of monitoring sites reporting back to a centralised 'control centre'. A simple, ideal concept indeed. The reality of having road, rail and other urban infrastructure assets built on landslide affected, geomorphologically and hydrologically hazardous terrains introduces a wide number of site based and external constraints that seriously complicates the ideal concept. Some of these complicating issues are highlighted in Figure 2. Here, the landslide (or any other asset) situated in the field ideally delivers data to a computer database, which is in turn accessed by a web-based graphical user interface such that any user can

access, view and manipulate data, a process symbolised in Figure 2 by the blue arrow. Already this involves project, site and monitoring based constraints with additional constraints regarding design of the data structure and the web-based graphical user interface including its design and the computer systems ongoing storage and backup facilities. Challenging enough on their own, other challenges such a system must address and manage include site based communication choices, computer/server data management and legal/insurance issues.

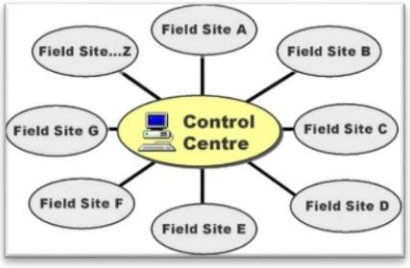

Figure 1: Idealised 'back to base' remote monitoring concept used in the initial proposal

Back to base field communications can take many forms. Over the last decade, the University of Wollongong has opted to use Internet Protocol (IP) based communications facilitated by a Private Internet Protocol Wide Area Network (IPWAN) service on the Telstra network, and this is currently rolling over to the National Broadband Network (NBN). This has proved to be an excellent solution that is still the preferred option today, but it brings Telstra in as a site constraint and despite purchasing a higher data quality, five nines level reliability (99.999%), the IPWAN has not been without issues (beyond the scope of this paper).

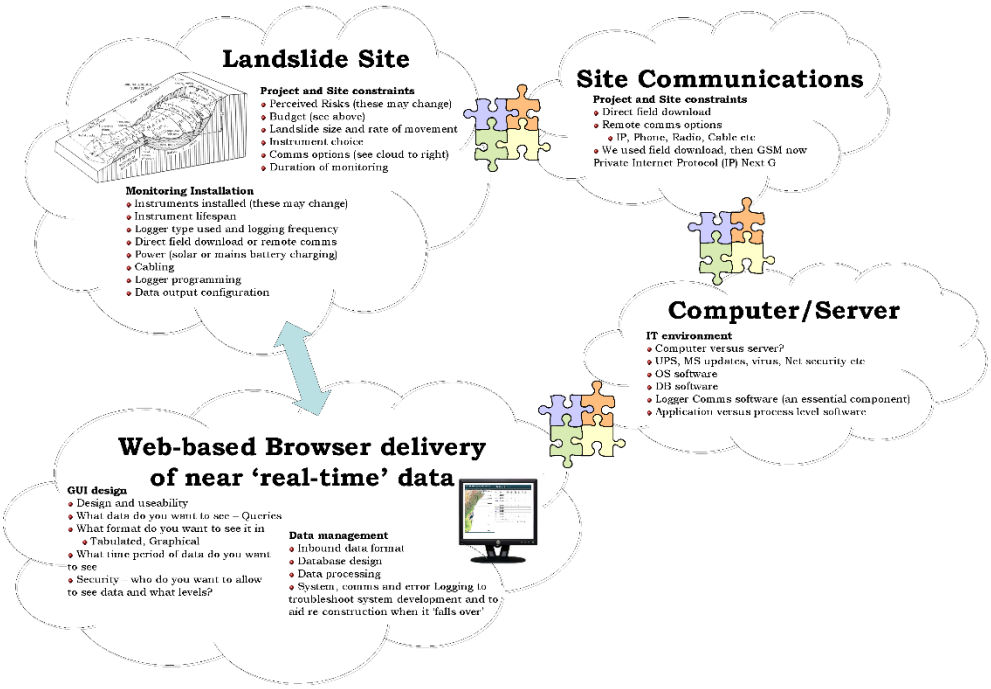

Figure 2: The desired remote site direct to web-based data access (blue arrow), in practice involves numerous additional types of constraints

Computer or Server and Information Technology based issues provide a major constraint in this type of system and indeed they have been integral concerns during the development of the UoW landslide monitoring network. The reliability requirements our industry partners place on the UoW landslide monitoring network of course is far beyond the acceptable reliability of a desktop computer on a staff member's desk (although that is exactly where it started), instead requiring

the reliability of a computer server housed within an IT data centre with 24/7 IT support. The Information Management and Technology Services (IMTS) is the internal University of Wollongong's central information management and technology service provider. A dedicated IMTS managed server within the University of Wollongong Server Farm has been setup and developed to manage the landslide monitoring network and this is summarised in Figure 3. The IMTS Team manages all the IT issues this system requires, and the second author of this paper manages this facility on behalf of the first author and our industry partners. The software used to manage the inbound data, placing it in site specific data bases, together with the graphical user interface (GUI) that provides the portal to access and display the data for our industry partners, has all been custom developed within the UoW space, by the third author of this paper. It is this stack of services/applications that really sets our system up and apart from most others, as it does work within a fully-fledged IT environment.

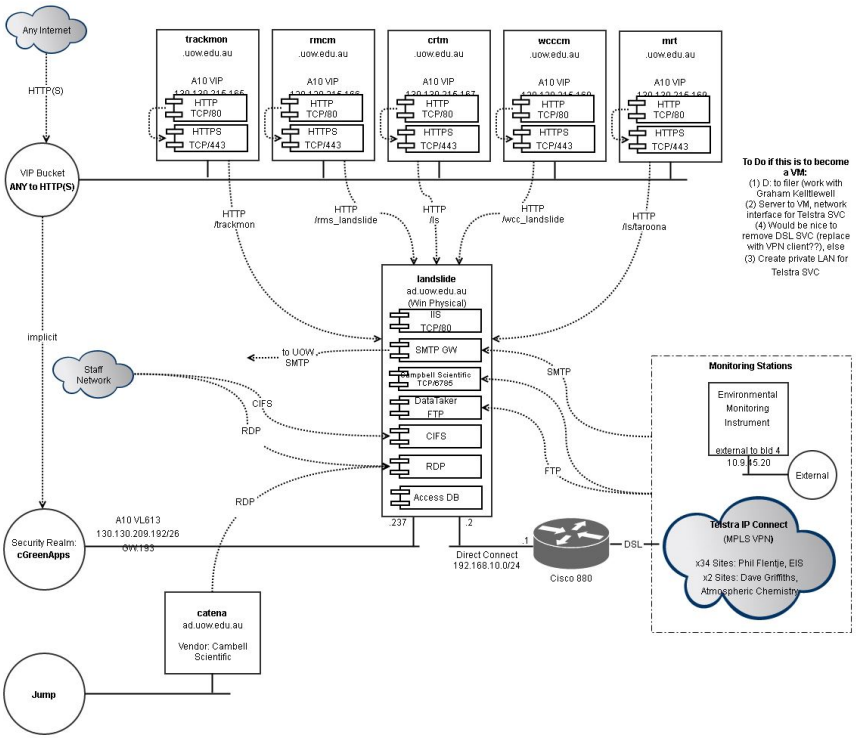

Figure 3: University of Wollongong IMTS server configuration

Our datalogger of choice is the Campbell Scientific CR1000, and the recent upgrade to the CR1000X. This logger is superbly manufactured, highly reliable and moderately easy to program. The company has a strong presence within Australia and provides very good technical support. The very strong element in favour of the Campbell Scientific devices, is the communications management software LoggerNet. This software facilitates the communications and is purpose designed for the server/IT environment. However, we do also incorporate data from other dataloggers, as we have a number of DataTaker loggers remotely sending us data.

Several smaller management issues arise from time to time. Data logger time management with respect to daylight saving is worthy of note. Australian Eastern Standard Time (AEST) is maintained throughout the year on all the data loggers used on the UoW Monitoring Network. The data loggers are not changed for daylight saving/summer time AEDT, so during summer months the data is reported in AEST. Most of our sites are powered by 12 or 24volt lead acid batteries. The batteries themselves are charged by mains power supplied chargers or solar panels with voltage regulators. Therefore, annual syncing of time stamps must happen outside of daylight saving time.

A significant issue includes the periodic update of communications devices. When this system first developed, cellular Wavecom modems were the comms device of choice. The system migrated quickly through Code Division Multiple Access (CDMA) devices, then Global System for Mobiles (GSM), to the Internet Protocol (IP) based comms (as mentioned above), initially using the 3G Call Direct routers and then the NetComm 3G 6908 devices. Recently they have also been discontinued, so new stations currently under construction are now using a new router (that will remain confidential). Each of these requires development and their installations require a level of quality insurance (as an engineering geologist, installing this level of IT does require assistance). The issues of telecommunications reliability is

critical, yet often ignored. The normal sim in a mobile phone is about 97% reliable and that's one of the issues signed up to when purchasing a mobile sim contract (it's in the fine print and buyers here do need to be aware). For data contracts for this type of monitoring, higher reliability contracts may be desirable and they come at a cost, of course. The UoW Industry monitoring project has a private IPWAN mobile contract with 'five nines' reliability specified (99.999%) as mentioned previously.

4 FIELD MONITORING EQUIPMENT

The Campbell Scientific CR1000 data logger has been mentioned above. That really is the brains of each field station. It requires a power source, typically a 12 volt battery charged by photo voltaic solar panels, of if mains power is available some form of trickle charger. In our experience, power supply is the source of about half the site based problems. The instrumentation used will then include in ground instruments to measure displacement (in place inclinometers and extensometers) and above ground instruments, such a extensometers, tipping bucket rainfall pluviometers, and weather station equipment (wind direction and strength, temperature, relative humidity and perhaps even air pressure). Basically any instrument with a digital output most likely can be connected to a Capmbell Scientific logger.

The data loggers can easily be configured to output to warning devices, such as flashing lights and boom gates if required. The UoW team and our industry partners are increasingly setting up multiple level warnings based on the monitoring data using thresholds. Mutliple level warnings (perhaps a warning and then an alert) and this is just terminology here, they are all based on thresholds, can be sent via the router as emails and or as sms. Take note here though, that sms are essentially redundant already. Smart alerts are a really important tool and very useful as a value added service extension. For example, if pore pressure (logged hourly) is rising towards a 50kPa thresholds, the current data, if it exceeds say a 40kPa threshold, can be compared with data from say, 1 hour ago, and also perhaps 6 hours ago and report in an email (and or an sms if they are still being used) "*pore pressure exceeded 40kPa, 1hr data ave time to 50kPa 3hrs, 6hr data ave time to 50kPa 13hrs"* is so much more informative than a *"40kPa threshold reached"* message from Site xyz. Similarly for rainfall and even battery voltage.

5 MOUNT OUSLEY ROAD, SITE 153 - THE MOUNT PLEASANT LANDSLIDE

5.1 HISTORICAL BACKGROUND

Mount Ousley Road was built during World War 2 as a special defence route in response to the fear of war operations arriving on the east coast of Australia and the need for better, faster and more direct transportation routes. The main route between Sydney and Wollongong up to that time was the Princess Highway via Bulli Pass. Construction proceeded throughout 1942 whilst the attendant property boundaries and acquisition were determined later. Landslides were noted (locations not specified) in 1949 and 1950, but a major movement of this landslide was reported in 1952 and Figure 4 shows a photograph of the landslide area at that time (Main Roads, 1952). The road was officially 'opened' in 1955. Interestingly, the 1904 Parish of Wollongong County of Camden 1904 map shows a sympathetic deviation of the original Mt Pleasant Road alignment around this landslide (the green dashed line below the landslide in Figure 5), suggesting the landslide may already have been active in 1904.

Figure 4: 1950 Landslide displacement reported as 30ft laterally with 6ft of subsidence.

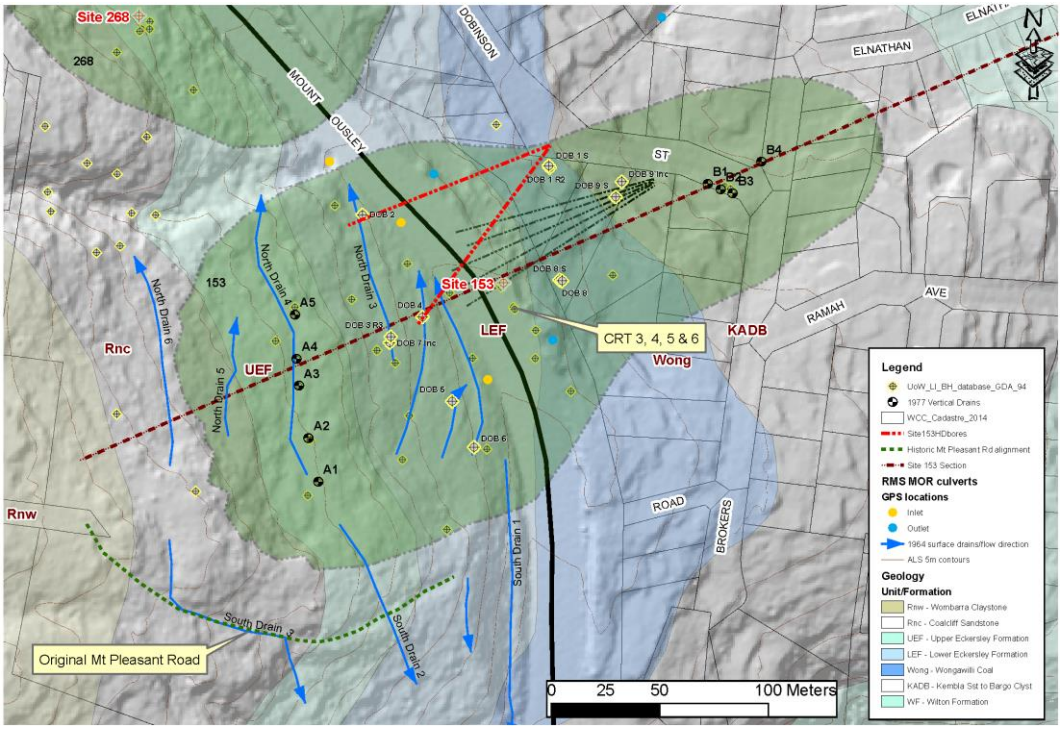

Figure 5: The Mount Pleasant landslide, Site 153 on Mount Ousley Road.

5.2 POST 1964 REMEDIAL WORKS

In 1964, portions of the ground surface within the upper half of the landslide area were reshaped to promote better surface drainage, including the 'cutting' of a series of six surface contour drains (Figure 5). From 1972 up to 1977 the Department of Main Roads investigated this site, and another landslide in the Razorback Ranges area (Nyland, 1977, Suine, 1978, Forrester and Nyland, 1980) and opted to install a series of horizontal drains at both sites. At the Mt Pleasant landslide, geotechnical investigations had shown the 10m plus depth of the colluvium across the head area of the landslide would make the installation of a trench drainage system difficult, such that horizontal drains were seen as the 'only possible treatment'. The concept rational involved installing a subsurface drainage system that enabled the ground water to flow more quickly through the landslide site. This was achieved by drilling a series of larger diameter 32m deep vertical drains upslope of the rear main scarp (the A wells, to intercept ground water, Figure 5) and allowing the ground water to flow vertically into the underlying Wongawilli Coal Seam. The intention was that the coal seam was to be targeted by the ~100m long horizontal drains thereby allowing the groundwater to flow into the drains to their outlet. Another series of six vertical drains (the B wells, Figure 5) were planned below the horizontal drain outlets to intercept groundwater across the toe area of the landslide (not clearly identified) allowing it to flow vertically down to a lower coal seam. During the 1977 remedial works, in addition to the A wells, four vertical B wells were installed, and five horizontal drains were drilled from an undeveloped, albeit urban, block facing Dobinson Road, downslope of Mount Ousley Road, into the landslide area, as shown in the black dashed lines in Figure 5. The horizontal drains reached the road (one actually exited the pavement) and two showed good initial flows (drains 3 and 5 flowed at 25 and 40 and litres per minute in September 1977), but both had dropped substantially by the end of the year (to 1.5 and 12 litres per minute respectively). Four vertical wells were drilled below the horizontal drain outlet, but it was never clear how the link between the horizontal drain outlet and the lower B vertical wells was to be achieved. The upslope extent of the horizontal drains was also approximately 80m short of the five vertical A wells, although both (A wells and the horizontal drains) targeted the same coal seam. The PVC lining of the drains was also reported to be of insufficient strength during installation and some of the holes were collapsing during the monitoring period.

5.3 URBAN ENCROACHMENT

The most important changes at this site, since the 1970s, has been the encroachment of urban development and the attendant development of Mount Ousley Road into a 5 lane expressway. After the remedial works were installed in the late 1970's, and with the apparent success of the remedial works and lack of any landslide movement since, the site had disappeared into obscurity. There is no evidence of any ongoing monitoring after December 1977 with a final report dated

January 1978 (Suine, 1978). With the construction of a new northbound lane in 2001, the site growing in prominence in the eyes of RTA Asset Management and the first authors landslide research work growing, the site again attracted attention. Desktop reviews of the available RTA reporting and site inspections were undertaken to assess the sites performance. It was apparent that the horizontal drains may have been compromised with urban development. A house had been built over the drain outlets, with no caveats being placed over the land parcel, or any noticeable headwall structure being documented. A saturated footpath pit was cleared and inspected and two 100mm pvc inlets were found to be flowing at rates of between 2.5 and 4 litres per minute total inflow into the pit (2005 – 2015). On questioning, the adjacent land owner reported to the RTA that some unexpected pipes were encountered during the foundation construction works and they were diverted around the dwelling and back into the roadside pit. The RTA did investigate by trenching along the property boundary to unearth the pipes and inspected them with cameras only to find them closed up/squashed only metres up. Two UoW landslide monitoring stations were constructed on Mount Ousley Road in March 2004, funded by the RTA. One of these was installed at this site. This landslide, and the monitoring station are known as Site 153 in the UoW landslide inventory.

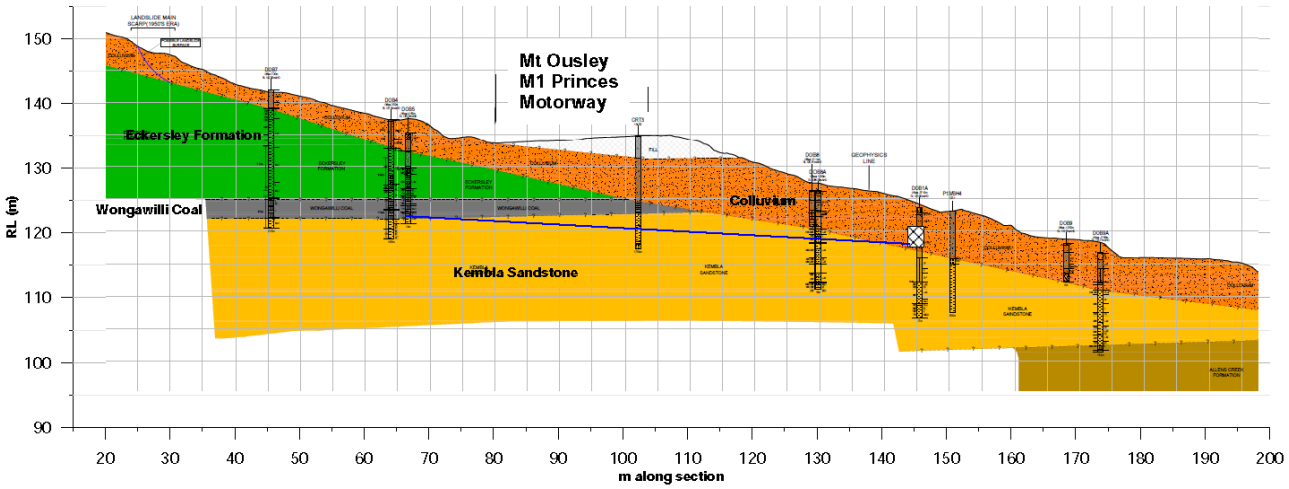

Figure 6: Central cross section of the Site 153 landslide, after Coffeys (2016) and showing the offset Dobinson Street Pit and schematic trend of the micro tunnels.

5.4 NEW MICROTUNNELING BORES IN MID 2018

During 2014 and 2015 the RMS Southern Region Asset Management decided the existing horizontal wells at this site warranted replacement. Following careful review of all the existing information, including the two detailed Department of Main Roads reports (Nyland, 1977 and Suine, 1978), the UoW monitoring data and site inspections, it was clear that a new hydrogeological investigation combined with a review of horizontal drilling and micro tunnelling techniques was required to establish the scope of works and design the new solution. The RMS engaged the NSW Public Works to manage development of the new solution at this site and they also engaged Coffey Geotechnics to undertake a new Hydrogeological Investigation of the site, supported by the first author.

To summarise, the investigations clearly defined the subsurface profiles, hydrogeology and target permeability zones and identified that a precise laser guided micro tunnelling technique would deliver the required horizontal bores of approximately 100m length. The two micro tunnels (MTs) were bored from a 4.5m deep pit, founded in colluvium on the side of Dobinson Road in May and June 2018 as shown in Figure 6. The results of the hydrogeological investigation and drilling operations will be discussed in a more detailed and focused paper in the future, but the total costs of these works was approximately $1.7 million including the mid-term purchase of two properties, which will likely be sold in the future.

5.5 UOW MONITORING EQUIPMENT

The Site 153 monitoring station comprises a cabinet on the noise wall on the northeastern side of Mount Ousley Road in the middle of this landslide site. The cabinet houses the CR1000 datalogger, a NetComm router, a 75 AmpHour 12 volt battery, solar regulator and the instrumentation peripherals such as the vibrating wire interface, a multiplexer for the five local vibrating wire piezometers (vwp) instruments and three in place inclinometers, and a radio receiver for the 3 remote vwp stations. An 80 Watt solar panel and a 0.2mm tipping bucket rainfall pluviometer are mounted 80m south of the cabinet with a clear view of the sky, with the cabling running along the side of the noise walls. Four boreholes (CRT 3, 4, 5 and 6 in Figure 5) have been drilled along the side of the road, between the fog line and the noise walls. Boreholes

CRT 3 and 4 were both cored holes drilled in March 2004, only 1m apart, and boreholes CRT 5 and 6 were augured holes, drilled in May 2007 to install three additional vwp devices, 10.5m south of CRT 4. CRT 3 is an inclinometer casing to 17m and now houses one (initially 3) MEMs In Place Inclinometer installed in the casing at 9-10m depth. Borehole CRT 4 has two vwp's installed at 7.8m and 12.1m respectively. CRT 5 has two vwp's installed at 5m and 9.8m respectively, whilst CRT6 has one vwp suspended in an open standpipe at 11m.

Workplace Safety requirements have evolved within the RTA/RMS and on the Mount Ousley Road and associated network specifically, such that since about 2012, workers cannot access sites on the downhill, southbound lanes outside of full road closures. Hence, the monitoring site has suffered from periodic maintenance, as opposed to on-demand maintenance and in early 2016 the cabinet and all the instrument cables were relocated from the road side of the noise walls, to the urban side of the noise walls facilitating much easier access.

As part of the mid 2016 Coffeys Hyrogeological Investigation, a total of nine new sonic and cored boreholes were drilled across the site, to install inclinometers and new vibrating wire piezometers whilst ensuring comprehensive detail was collected of the colluvium and subsurface bedrock profile. Two new vibrating wire piezometers were installed in both boreholes DOB 1 (adjacent to the eventual MT Pit) and DOB 3 (adjacent to DOB 7, 17m upslope of DOB 4 and the ultimate target of one of the MTs). These four new vwp's have subsequently been connected to the UoW Site 153 monitoring station with radio links and some quite impressive data from these is presented below.

5.6 MONITORING DATA RECORD – SITE PERFORMANCE

Continuous, hourly monitored rainfall, pore water pressure, rainfall and battery voltage data have been recorded at this site since 31st July 2004. The site monitoring has evolved over this period as new information has become available, and as new information has been required to aid investigations and design of a new remedial solution, as discussed above. The inclinometers installed since 2000 have not shown any defining shear movement to date, which is great information in itself, but not particularly helpful in building our models. Hence no In Place Inclinometer data is included in this discussion. In the confined space of this paper, the authors have selected two periods of data to present. Figure 7 presents data from January 2007 to October 2009. This period is important as it includes two sizeable rainfall events in April - June 2007 and early February 2008, both events where the 60 day cumulative rainfall almost reached 600mm. This graph also shows the two borehole CRT 4 vwp data, the shallow 7.8m piezo in the colluvium profile showing no pore pressure, and the deeper vwp at 12.1m in bedrock, ~ 2m below the base of the colluvium, showing pore pressures consistently between 40 and 50kPa and rising to 60kPa during these rainfall events. The graph also shows the 3 additional vwp installed in CRT 5 and 6 appearing in late 2007. The two vwps in CRT 5 are installed in the colluvium and at the bedrock colluvium interface, whilst the one is CRT 6 was suspended near the base of an open standpipe at 11m. The CRT6 was intended so we can test the logging system and the groundwater, should the vwp in CRT provide no pore pressure, as the upper piezo in CRT4. As shown in Figure 5, these boreholes are located on the southern side and very close to the original horizontal

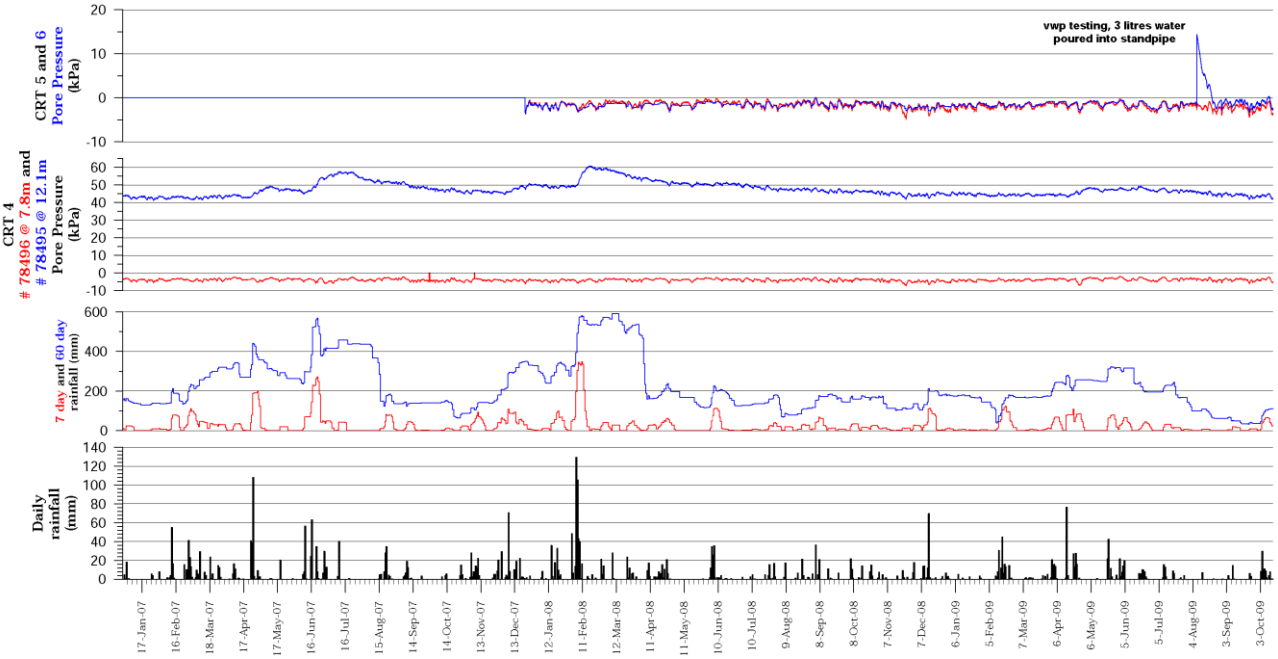

Figure 7: Site 153 hourly monitoring record from 1st January 2007 to 30th October 2009.

drains. CRT 5 and 6 were positioned 10m further south, away from the horizontal drains to see if any pore pressure was indicated along the colluvium bedrock interface (whilst also noting, at that time and even still today we have no confirmed indication from the inclinometers as to the depth of sliding). As Figure 7 shows, the boreholes CRT 5 and 6 show no pore pressure at all. In early August 2009, 3 litres of water was poured into the 50mm standpipe (and again in late June 2014) and this resulted in the ~ 1.5m (15kPa) rise of water in the standpipe and in the indicated pore pressure, confirming that the vwp instruments are indeed working and that this area is just dry. The vwp instruments were also checked using the Campbell Scientific Device Configuration Utility spectrum anaylsis, and they were found to be working, and other vwp instruments were connected to the same ports and tested with various water levels in a PVC casing and the results confirmed the system to be working. This indicates that this central area of the landslide and this section of the subsurface profile are likely located within the zone of influence of the five 1977 horizontal wells.

Figure 8 shows the hourly monitoring record from Site 153 from the 1st February 2014 to the 30th October 2018. Firstly, this period shows an extended data outage between August 2015 and September 2016. Before the outage period, a period of vwp data was lost, and troubleshooting investigations commenced. The site became infested with ants which were cleaned out on several occasions, but each time they returned in greater numbers ultimately damaging the router and several of the components. After the repairs, reconfiguration and relocation to the outside of the noise wall, including updating the cabinet from a fibreglass enclosure, to the latest style vermin proof stainless steel cabinet, the system was reactivated in time for the upgrades contributing to the hydrogeological investigation and impending remedial works – although at this stage we did not know exactly what form the remedial works were going to take. This graph highlights the wet weather experienced during February and March 2017, with the 60 day cumulative rainfall reaching almost 700mm, and the corresponding CRT 4 deep vwp pressure reaching 70kPa. For the first time since its installation the borehole CRT 5 vwp at the colluvium bedrock interface also showed a rise to 8.5kPa, almost 1m head of pressure on the slide surface at this location, if indeed that is where the slide surface is located. The top axis in this graph shows the borehole DOB 1 data stream from September 2017 and DOB 3 vwp data from mid February 2018 – after a significant troubleshooting experience with this remote station. Prior to the micro tunnelling works, the DOB 3 pore pressures in the bedrock intervals below the head area of this landslide are significant, with the deeper vwp at 15m reading pressures between 60 and 70kPa, and the shallower vwp at 8m (the base of colluvium here is at 6.5m) reading pressures between 50 and 60kPa. The deeper vwp in DOB 1 reading the highest pressures on the site at between 80 and 100kPa and the shallower vwp at 8m, just in bedrock below the base of the colluvium reading pressures of between 20 and 35kPa.

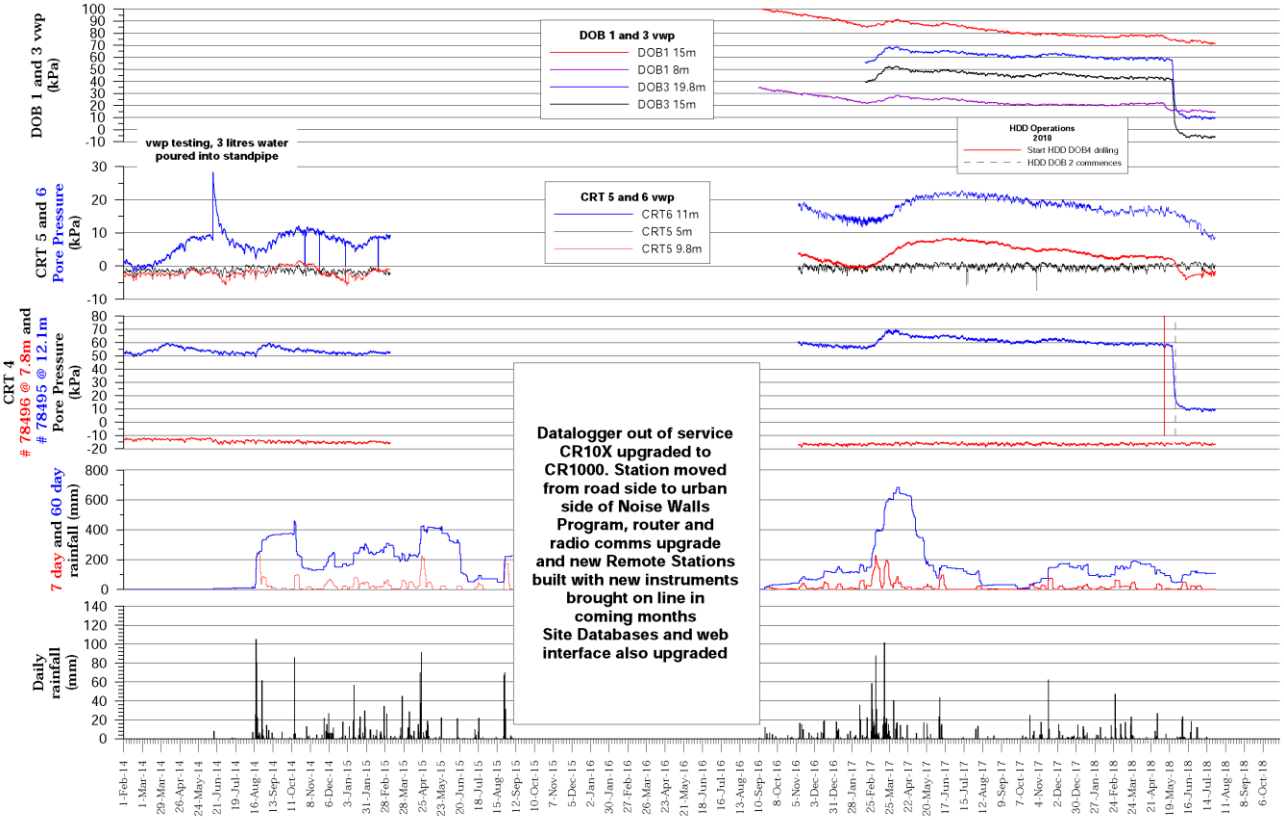

Figure 8: Site 153 hourly monitoring record from 1st February 2014 to 30th October 2018

Table 1 summarises the flow data from the micro tunnel outlets. There is little flow data unfortunately, as it was a crowded and busy excavation pit and the data was difficult to collect. The few values do show an interesting trend, and the early flow of about 45,000 litres per day from the DOB 4 collar was extraordinary. They may have both settled down to around 4-5,000 litres per day by early August and it will be interesting to see how this develops over the next few years and watch how it varies during rainfall events. Whilst there is no monitoring in place, the first writer will be trying to retro fit two small V notch weirs to the outlets and monitor water depth in each small weir reservoir using LoRaWAN IoT sensors over the next 12 months.

Figures 8 and 9 highlights the commencement of the micro tunnelling works with a vertical red line, and a vertical dashed black line when the northern mico tunnel was commenced. The pore pressure drawdown shown in Figure 8, and highlighted in Figure 9 are the results of the pit excavation and the micro tunnelling works, and these drawdowns are significant. Figure 8 shows these vwp traces as continuous curves. As the pit excavation was completed and the MT commenced, battery voltage on site was struggling with the low winter sun angles, and a Eucalyptus tree had started to shade the 65 Watt solar panel. Figure 9 highlights the faltering battery voltage over this period. A new 75 Amphour deep cycle battery solved the initial problem, but not the shading issue. Swapping and cycling batteries over the next month allowed the site to continue logging without significant further interruptions until the offending tree was trimmed. Figure 9 has the vwp curves as discontinuous (other than the DOB 3 15m vwp) showing the interuptions where battery voltage dropped below the radio transmitter operational frequency. The DOB 3 15m vwp shows simply exceptional response the drilling operations dropping over the 3 day outage from 45kPa to approximately 5kPa and continuing to drop since to small negative values.

Table 1: Micro-tunnel water flows

Date	DOB4 (litres/m and litres/day)	DOB2 (litres/m and litres/day)
29-May-18	32.4/46656	
31-May-18	25.7/37028	
2-Jun-18	17.3/24883	
19-Jun-18	4.2/6056	5.9/8516

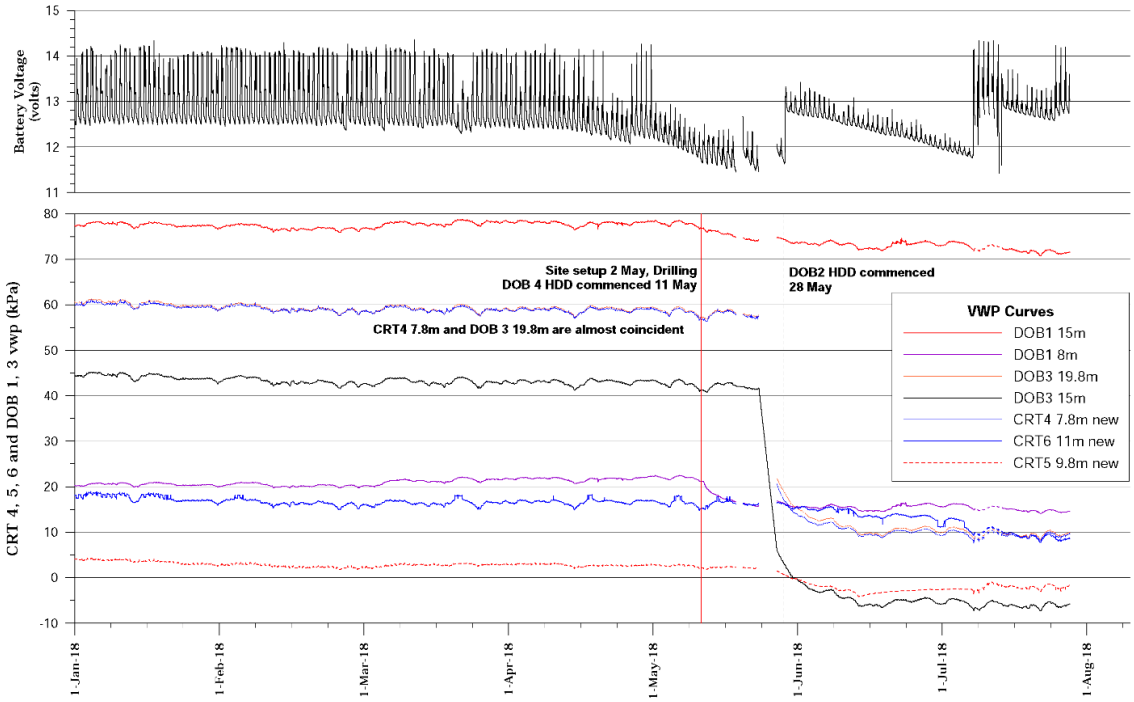

Figure 9: Site 153 hourly vwp monitoring record throughout 2018, highlighting the MTs installation and the effect this has had on the groundwater, and also the impact of site power on the operations.

The drops in pore pressure are clear in Figures 8 and 9, but one of the key issues, is the spread of the drawdown effect across the site. The DOB 3 borehole is 14m upslope from the upper end of the DOB 4 MT, and the CRT 3 borehole is 20m south of the DOB4 MT. DOB 1 is located 10m south of the MT outlet pit and the shallow vwp is approximately 0.5m below the base of the pit and the deep vwp is at 15m and both have shown 5 – 10kPa reductions in pore water pressures. The real test of the success of these works will be seen into the future during prolonged and intense wet events of the 20, 50 and even 100 year Average Recurrence Interval magnitudes. It is clearly hopeful that these works will have successfully remediated this site for the long term into the future. The RMS are currently sorting out easements across the subject sites to ensure the 1970's experience of development encroaching upon the installed remedial works is not repeated.

6 MOUNT KEIRA ROAD, SITE 229 LANDSLIDE

6.1 HISTORICAL BACKGROUND

The landslide site 229 on Mount Keira Road has proven to be problematic for the owner, Wollongong City Council (WCC), due to numerous landslides and rockfalls causing damage to the road and forcing its closure to the public on several occasions due to an elevated risk to public safety. Site 229 is located approximately 4km west of Wollongong along a section of Mount Keira Road in Mount Keira, NSW between the archery range and the first hairpin turn and is approximately 200m in length a shown in Figure 10. Mount Keira Road was first formed in 1835 using convict labour although the hairpin bend was introduced in a later re-alignment to avoid steeps grades and potentially this very landslide. The route was chosen in 1834 by Surveyor General Mitchell due to the absence of rocky outcrops which reduced the amount of labour required to construct the road (WCC, 2015). Until the construction of Mount Ousley Road in 1942, Mount Keira Road was the primary route in and out of Wollongong, to the west.

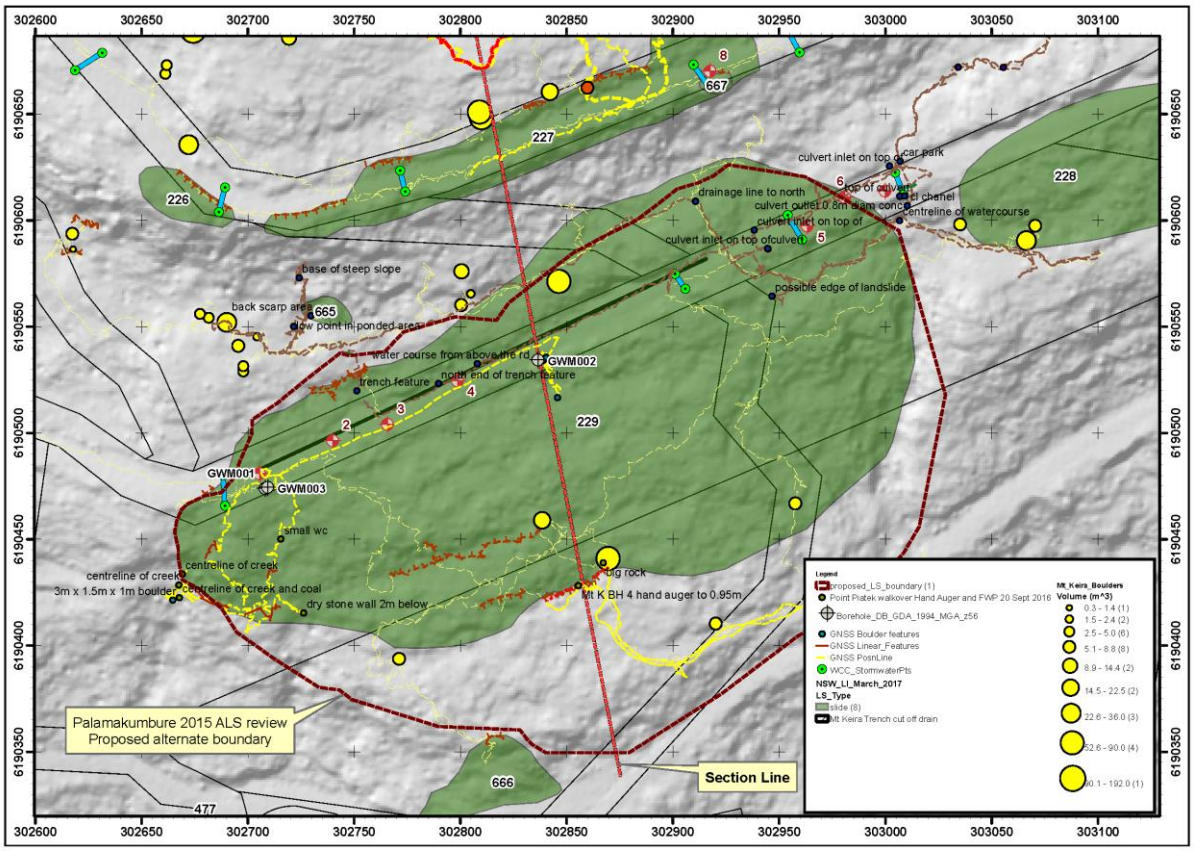

Figure 10: Site 229 Palamakumbure 2016

In 2000, the WCC geotechnical group performed an in-house landslide risk assessment for Mount Keira Road and identified four sites requiring remediation (WCC, 2016). One of the identified sites was site 229 and remediation works

were completed in 2013 which included installation of a longitudinal subsurface cut-off drainage slot (that intersected claystone bedrock at all of the inspected locations) with a concrete swale drain above along the uphill side of the road, road stabilisation works and re-paving (Figures 10 - 13). The adjoining landowner (NPWS) would not permit any works on their land, so all the remedial works were restricted to the road easement. The road has once again begun to undergo some deformation, due to landsliding after a number of rainfall events since the completion of the remedial works.

Figure 11: 2013 Excavation of a 4m deep cut-off drain along the road, with a concrete swale gutter above

This site now uses a landslide CRTM station for continuous assessment of the landslide performance and status. Instruments installed at this station include a 0.2mm tipping bucket pluviometer, three vibrating wire piezometers (one has now been sheared), two extensometers and three inclinometer casings (one has now sheared) for manual operation and reading of probe inclinometers (Figure 14). The inclinometer casings are also used as open standpipe piezometers for manual data collection.

Figure 12: The image on the left shows obvious undulations on Mt Keira Rd at site 229 in 2012 (WCC, 2012) whilst on the right image the undulations are beginning to return in August 2017, 6 years after the work

6.2 SITE INVESTIGATIONS

The first, fifth and six authors of this paper have been investigating this site and the nearby upper escarpment slopes since the early 1990's, with the help of many university students over that time. This site was a PhD case study site (Palamakumbure, 2016) and a number of high achieving undergraduate students have also studied this site in recent years (Piatek 2016, Newman 2017). Investigation works undertaken across this site include the following:

1. Site walk-overs and mapping of features, over the last decade using Trimble Geo 7 GNSS device (once off the road, mapping within the forest is challenging) and importing of all data into an ArcGIS project folder;
2. Three separate rounds of state government sourced regional Lidar data are available and have been downloaded and analysed, and a surface change analysis has been conducted, nothing clear was detected;
3. Develop a cross section of the site, which has now been iterated numerous times;
4. Drilling 3 cored boreholes with inclinometers, with periodic manual inclinometer monitoring, two drilled in November 2000, one sheared by late 2006, new replacement hole drilled in June 2013;
5. Installation of a Continuous Real-time Monitoring system near GWM002 with 10m high folding pole for solar panel and rain gauge;
6. Retrofit Geokon Long Range extensometer to bottom of sheared inclinometer casing;
7. Auguring of a new borehole and dynamic cone penetrometer (DCP) testing;
8. Periodically recorded water table levels;
9. Progressive movement data and determination of the depth to the slip plane of the landslide using inclinometer readings; and
10. Use of data collected from the CRTM system including rainfall, extensometer and piezometer readings to develop a better understanding of site mechanisms and management of the station infrastructure.

The site 229 landslide is classified as an *episodically active, complex, extremely slow, moist – debris slide* as based on the landslide classification system developed by refined by Cruden and Varnes (1996). The volume involved was determined to be approximately 135,000m^3. Interestingly, despite all this work, this landslide has not moved a significant amount, such that mapping its boundary is difficult. Tension cracks across the road are clear of course, but throughout the rest of the landslide, across the leaf and vegetation laden forest floor, identifying the margins and internal features of this landslide is certainly challenging.

6.3 MONITORING DATA RECORD – SITE PERFORMANCE

The inclinometer displacement data shows that the landslide has moved 73mm in boreholes GWM001 between November 2000 and November 2006, 62 mm in GWM002 between November 2000 and July 2017 (Figure 14) and 37 mm in GWM003 between June 2012 to July 2017, with average rates of 12mm/year, 4mm/year and 9mm/year respectively (Table 2). Using the AGS (2007) landslide velocity scale, the Site 229 landslide velocity is classified as extremely slow. In BH2, the sliding plane is located at a depth of approximately 4.5-5.0m, and in BH1 and BH3 (1m apart) sliding occurs from 4m to 5m.

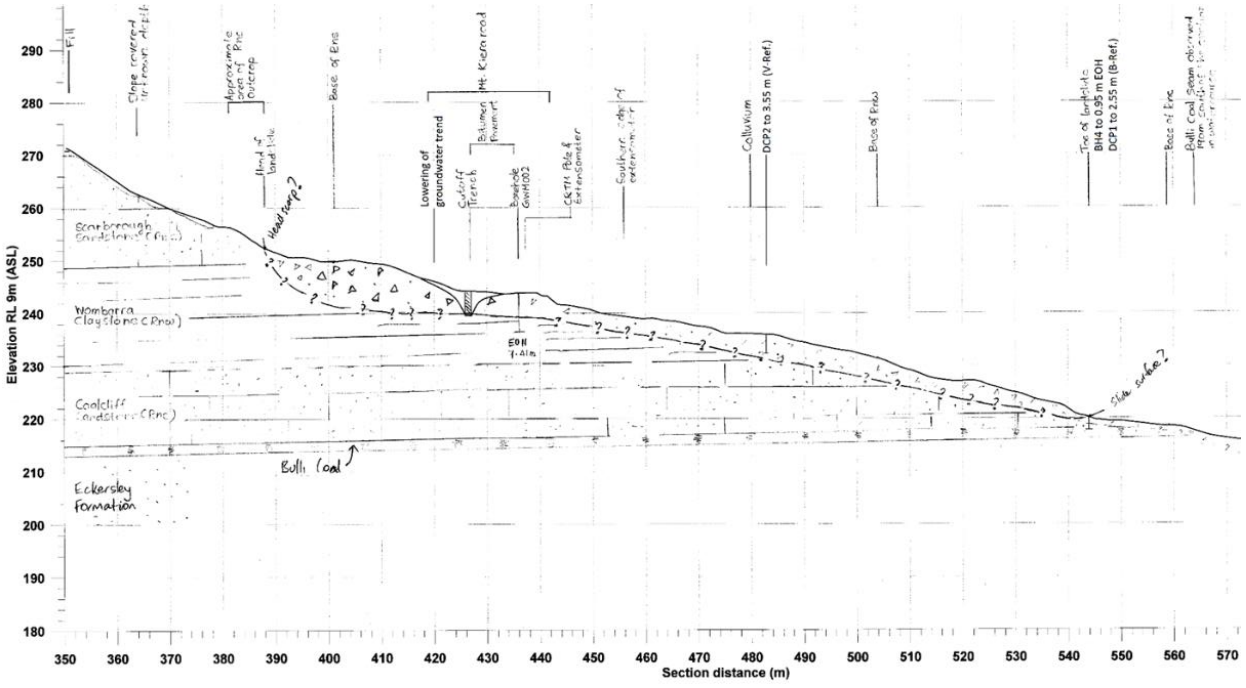

Figure 13: Site 229 cross-section developed by Flentje, Palamakumbure, Piatek and the Newman (Piatek, 2016)

The Site 229 monitoring summary shown in Figure 15 includes a comparison of rainfall, pore water pressure (pwp), extensometer displacements and BH2 and BH3 inclinometer displacements. The pwp response to rainfall events is

proportional to the size of the event but is relatively small. Vibrating wire piezometer (vwp) 3564, located in BH1 at a depth of 4.3 m, shows the greatest pwp of the three vwp's. This high pwp may be the cause of the significant landslide displacement at this location which has caused the inclinometer casing to shear and sever the cable connected to vwp3564. vwp18143, located in BH3 adjacent to BH1 at a depth of 6.2 m, shows very low pwp values and doesn't follow the same trend as vwp3564. This may be due to the vwp being placed in bedrock at a point where groundwater pressure is not well expressed. vwp3562, located in BH2 at a depth of 4.9 m, follows a similar trend in pwp as vwp3564 but is consistently 5kPa lower. The lower pwp at BH2 may help explain the lower rate of displacement of the landslide at BH2 compared to BH3.

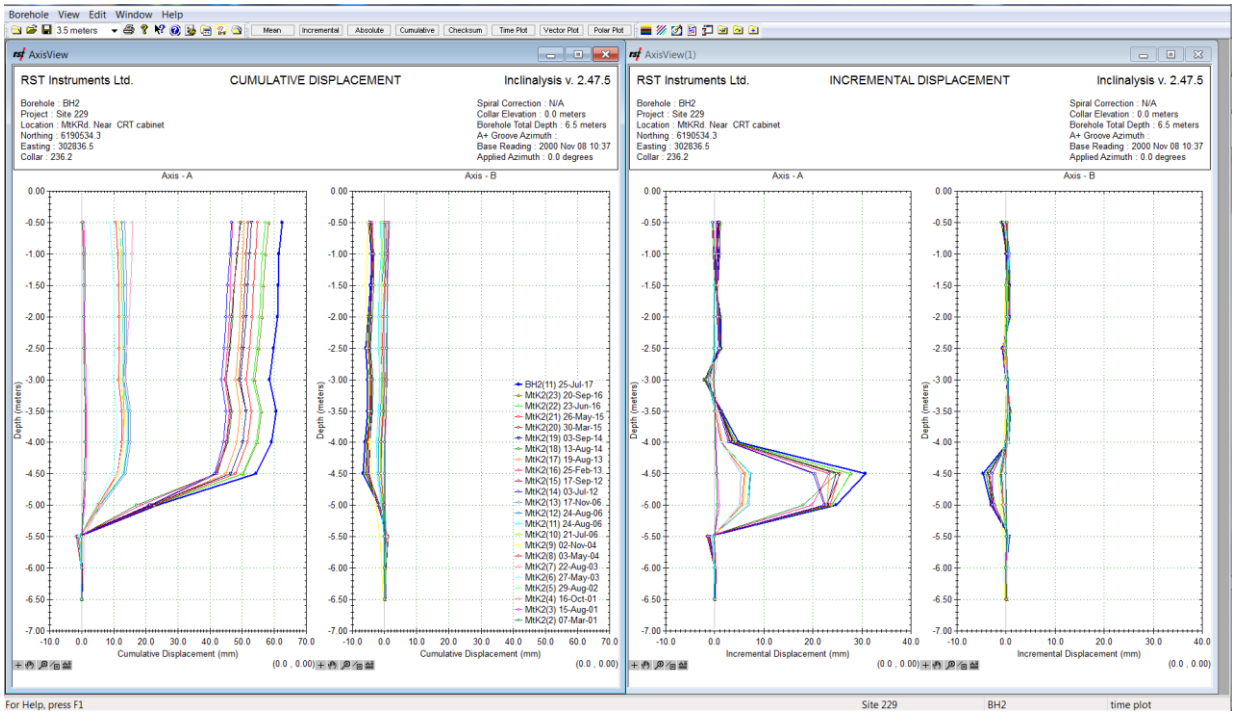

Figure 14: BH GWM002 near the centre of site 229

Table 2: Site 229 BH 1, BH2 and BH3 Displacement-Time Relationship

Borehole	Number of Days	Displacement (mm)	Rate of Movement (mm/day)	Rate of Movement (mm/year)
BH1	2200	72.95	0.03316	12.11
BH2	6104	61	0.00999	3.65
BH3	1505	37.5	0.02492	**9.09**

The extensometer data does not display any obvious landslide events, although the downhole Extensometer 1 is now expected to start to show more landslide like movement (the cable tension after a difficult custom retrofit into a shear inclinometer casing is now likely to be fully in place – despite a motor vehicle accident that completely demolished the installation in early January 2018) over the last 6 months. The extensometer 2 cable on the other hand is only attached to a star picket 20m downslope from the sensor, in the hope it will see some differential movement.

From the rainfall data and inclinometer data collected, a tentative displacement-time relationship and rainfall-displacement relationship has been established. The displacement-time relationship was found to be highly variable between periods, however, the long-term relationship showed that BH3 was displacing much faster than BH2 with velocities of 9.09 mm/year and 3.65 mm/year respectively. A relationship between total rainfall and displacement was explored unsuccessfully for both boreholes. It was discovered though that for the three periods analysed, the period with the peak 30-60-90-day rainfall values produced the most displacement in the landslide. From this data, it was also concluded that 30, 60 and 90-day rainfall peaks of 330 mm, 420 mm and 480 mm are likely triggering events for small

annual magnitude displacements. To assess 1 in 10 year and even higher return period events, the authors and wider project team will need to monitor the landslide through those type of events and examine the performance. The cut off drain along the roadway was being installed at the same time as this continuous monitoring station. So the monitoring data now shows the sites performance in its current configuration.

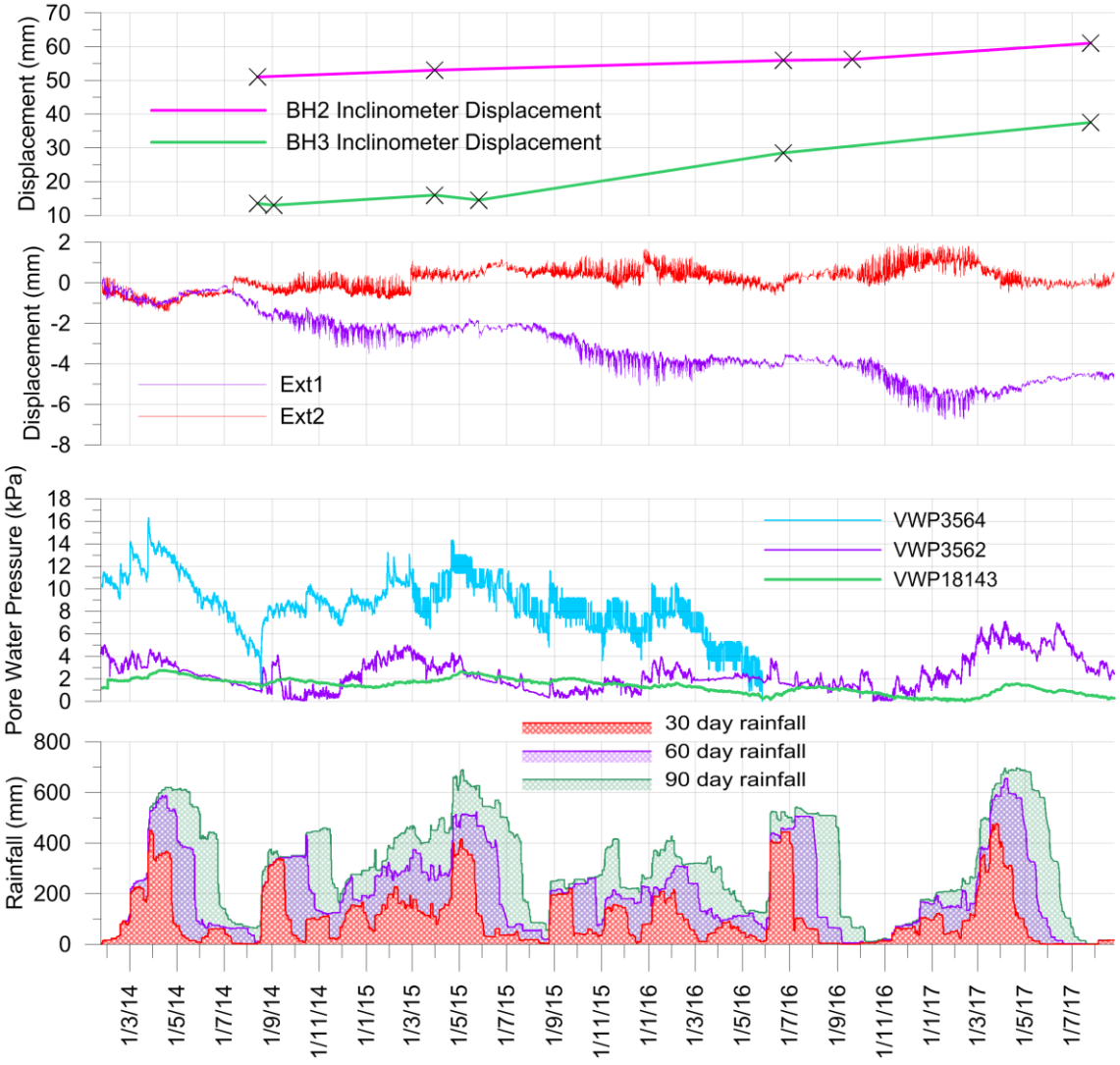

Figure 15: Site 229 Monitoring Summary 1/1/2014 – 1/8/2017

6.4 POWER MANAGEMENT AT SITE 229

Battery voltage data is important as the site battery is solar charged and it indicates the health of the power components of the monitoring system. Figure 16 shows the battery voltage from 24/01/2014 to 12/08/2018 where it can be seen that during the winter solstice the battery voltage drops to under 12 volts at times. The router does not work with power less than 12 volts thus resulting in the station being offline. If the voltage drops below 9.6 volts, the logger will cease working and data is actually not recorded. Whilst this has only happened occasionally, the drop on voltage is certainly an issue that needs addressing. Some logger program modifications have been made to switch the power off to the router, from the logger 12 volt power ports, between 7pm and 9am, outside of available sun hours, only during the winter months to help prolong the daily power supply, and the life of the battery. A new 75 Amphour battery was installed during the 2018 winter period and the night time switching off of the router has definitely reduced the sites power consumption. The site is located within a forest environment and trimming the nearby trees is not an option. The rain gauge and the solar panel have been mounted on a 10m high folding pole, but unfortunately many of the surrounding trees are 15m plus in height, so its likely to be an ongoing issue at this site. We may even install a small wind turbine generator on the pole to compliment the charging options.

7 FUTURE DEVELOPMENTS

The web-based delivery of monitoring data to a widely distributed audience is now pretty standard and the done thing in many organisations today. But that still requires that audience to log in to the graphical user interface (GUI) and check the data. Of course, the distributed audience may also be using a desktop PC, and Apple Mac, or a Windows based laptop, an iPad (2, 3, 4 or iPad Pro), a Samsung Galaxy 6 or 7, an iPhone 5, 6, 7 (regular or Plus format), or X etc. So the today the GUI must be platform independent and typically not involve software installations (as the corporate/government world just won't allow that these days, heaven forbid). Dashboards are now quite common and alas we haven't completed ours yet, but its on the way. In a nutshell, a dashboard is a simple icon that may live on your desktop, or tablet/phone home screen that will give the user immediate access to the networks monitoring status. It may reside in the taskbar on a PC/laptop/windows machine, or simply on your desktop and if every site is online, current and all data is under thresholds levels, the button will remain green. Thus at a simple glance you can be confident everything is working. If something is wrong, the icon can change through shades to orange to red, and or flash or even beep. Tapping on the icon in such situations can open, with more clicks a series of cacscading icons, menus and tables taking the user to where the issue(s) may be.

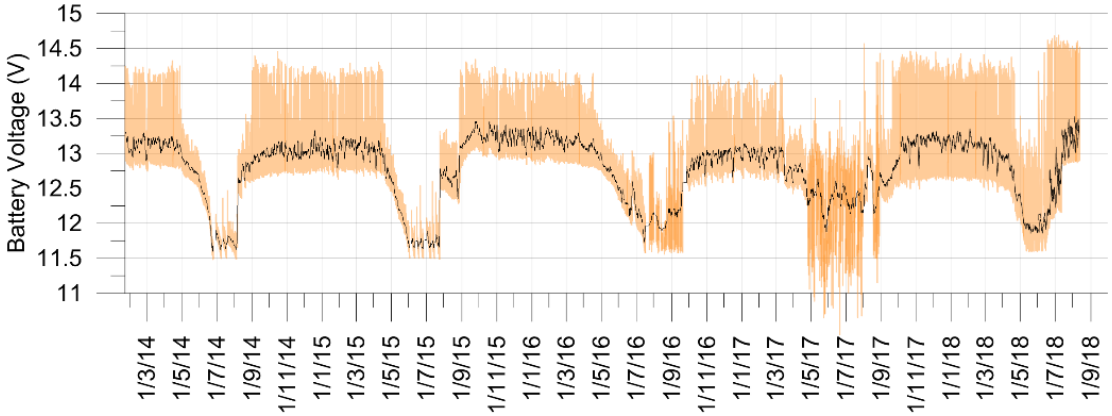

Figure 16: Site 229 monitoring station battery voltage

The internet of things (IoT) is a moderately new area of live data awareness, where sensors are embedded in just about everything and integrated, or connected through cloud computing supplying data essentially live to anyone who wants it. One of many methods enabling this is LoRaWAN, a network architecture, which uses license free sub-gigahertz radio frequency communications to send data. The University of Wollongong has teamed up with numerous partners, including Wollongong City Council and Sydney Water, and others to provide a free LoRaWAN across much of the Wollongong area. The simple attractiveness of this technology is the low power, long range free transmission of small data packets. The UoW Digital Living Lab and the UoW landslide team are currently investigating a number of monitoring strategies in this area at present. Imagine button sized sensors with matchbox sized transmitters, transmitting free over many kilometres. No data loggers, no solar panels, no routers or sim cards or monthly fees. This technology is a revolution that is upon us now.

8 SUMMARY AND CONCLUSIONS

Continuous monitoring is the best way to gain an accurate understanding of a landscape site and its performance today. The site will behave very differently over the lifetime of the investigation and of the lifetime of the project being planned or designed, as it will surely be exposed to drought and or deluge, as well as human intervention. The data presented here shows very clearly how this data can help build an understanding of a site over time and how one can measure how this performance may change as site works are performed. The value of this data to quantitative risk assessments is clear.

However, installed devices reach their end of life, in ground devices get damaged easily, above ground devices also get damaged by vandalism or by critters (ants and cockatoos are common culprits) or just by the environment (sun, wind, dust, rain and lightning are all foes). Communication fees and equipment upgrades are also ongoing so all such issues must be considered in recurring budgets. Therefore, it is very important to acknowledge that monitoring installations do have an ongoing cost and must be maintained to continue the monitoring job they were setup to do. It is also important to consider, at the setup stage, what the expected life of the monitoring will be and a stage at which that can be reviewed and the opportunity for the monitoring to be stopped if and when necessary.

9 ACKNOWLEDGEMENTS

The authors gratefully acknowledge our Industry Partners, in this case the Roads and Maritime Services and Wollongong City Council, and your approval to publish this paper and we acknowledge all those dedicated staff that have worked on these projects. The first author also needs to thank the growing list of students who have collaborated and worked on these monitoring sites, Rostam Sohaili, Darshika Palamakumbure, Raymond Piatek and Jake Newman – your level of enthusiasm and eagerness to contribute, collaborate and learn is always inspiring.

10 REFERENCES

AGS, (2007). Guidelines for Landslide susceptibility, Hazard and Risk Zoning for Land Use Planning. Australian Geomechanics Journal, 42(1), 23.

Cruden, D. M, and Varnes, D. J., (1996). Landslide Types and Processes. In Turner and Schuster, 1996. Turner, A. K. and Schuster, R. L., (1996). Landslides, Investigation and Mitigation. Special Report 247. Transportation Research Board, National Research Council. National Academy Press Washington DC.

Forrester, K and Nyland, G., (1980). Two landslides on New South Wales Highways. Proceedings of the International Symposium of Landslides, New Delhi, India. Vol. 1, pages 181 to 184.

Main Roads, (1952). Landslides on the Razorback Range near Wollongong 1949 and 1950. Quarterly Department of Main Roads, Australia, Vol. 17, No 3, pages 77 to 83, with 1 map, 3 figs, 6 photos.

Newman, J., (2017). Assessment of Landslide Hazard and Performance Using Periodic and Continuous Monitoring. Bachelor of Engineering Thesis. Faculty of Engineering and Information Sciences, School of Civil, Mining and Environmental Engineering. Unpublished, University of Wollongong.

Nyland, G., (1977). Landslide Areas Below Mt Pleasant Overbridge, Site Investigation, Department of Main Roads, Job 457.

Palamakumbure, D., (2016). GIS based Landslide Inventory and Landslide Susceptibility Modelling across the Sydney Basin PhD, University of Wollongong, Faculty of Engineering and Information Sciences. Retrieved from http://ro.uow.edu.au/theses/4642/

Piatek, R., (2016). Assessment of Landslide Hazard and Performance Using Periodic and Continuous Monitoring. Bachelor of Engineering Thesis. Faculty of Engineering and Information Sciences, School of Civil, Mining and Environmental Engineering. Unpublished, University of Wollongong.

Suine, P., (1978). Landslide Area below Mt Pleasant Overbridge, Report on Remedial Measures, Department of Main Roads, Job 622, January.

WCC, (2015). Wollongong City Council Library - Mount Keira. [Online] Available at: http://www.wollongong.nsw.gov.au/library/onlineresources/suburbprofiles/pages/mountkeira.aspx [Accessed 02 September 2016].

WCC, (2016). Wollongong City Council Works and Maintenance: Mt Keira Road. August 14, (2016). Retrieved from http://www.wollongong.nsw.gov.au/services/maintenance/Pages/mtkeiraroad.aspx

MONITORING OF MINING INDUCED MOVEMENTS BETWEEN BRIDGE COMPONENTS WITH FIBRE BRAGG GRATING SENSORS

M. Brunton and B. E. Whelan
Monitor Optics Systems Pty. Ltd.

ABSTRACT

This paper outlines a novel use of Monitor Optics Systems' (MOS) Fibre Bragg Grating (FBG) sensor cables to monitor relative movements between bridge components. Twin bridges that form part of the M1 Motorway in Helensburgh were to be subjected to ground movements caused by subsidence from planned underground Longwall coal mining parallel to the bridges. An engineering assessment was carried out to determine the risk of movements of bridge pier and abutment footings relative to the bridges' headstocks, abutments and deck. It showed that relative movements of 5mm or more between headstocks and abutments could cause cracking in areas that cannot be visually inspected and that are difficult to repair, and relative movements of more than 16mm could lead to structural failure. A technical committee formed to manage subsidence effects on RMS infrastructure agreed that a surveying accuracy of 2mm was the minimum requirement to determine trends in movements between bridge components. As conventional relative 3D survey has a tolerance of +/- 2.5mm, it was agreed that a more accurate monitoring solution was required.

MOS initially proposed using their FBG sensor cables between bridge footings to measure relative movements, but it was deemed impractical and expensive due to the difficulties associated with installing sensor cables underground. MOS then proposed using their sensor cables held in tension between headstocks and abutments to measure relative horizontal movements. The solution would provide measurements of relative horizontal orthogonal shifts at the corner of each abutment and headstock at an accuracy of approximately 0.02mm. Sensor cables could not be installed between headstocks and the bottom of piers due to the risk of vandalism, so tilt meters were proposed to measure in-plane transverse tilts of the outer piers instead, and traditional 3D surveying for all other measurements. The technical committee concluded that the proposed solution would be adequate for their requirements.

A clamping system was developed for the sensor cables and the monitoring system was installed in 2016. The sensors are monitored at pre-determined times with demodulation equipment that is battery powered. Data is automatically sent to key personnel which is post processed by engineers to determine stresses in key bridge components.

1 INTRODUCTION

Longwall mines LW301-303 are located west of the M1 Motorway and northwest of Helensburgh, with extraction to be approximately parallel to the motorway from north to south. LW301 is located closest to the motorway at a distance that varies between 210m and 335m. Two bridges that form part of the northbound and southbound carriageways of the motorway are also located parallel to the mines, with LW301 located approximately 330m from the bridges. The bridges, formally known as BN616 and BN617, but more commonly referred to collectively as "Bridge 2", carry traffic over the old Princes Highway. Figure 1 illustrates the above.

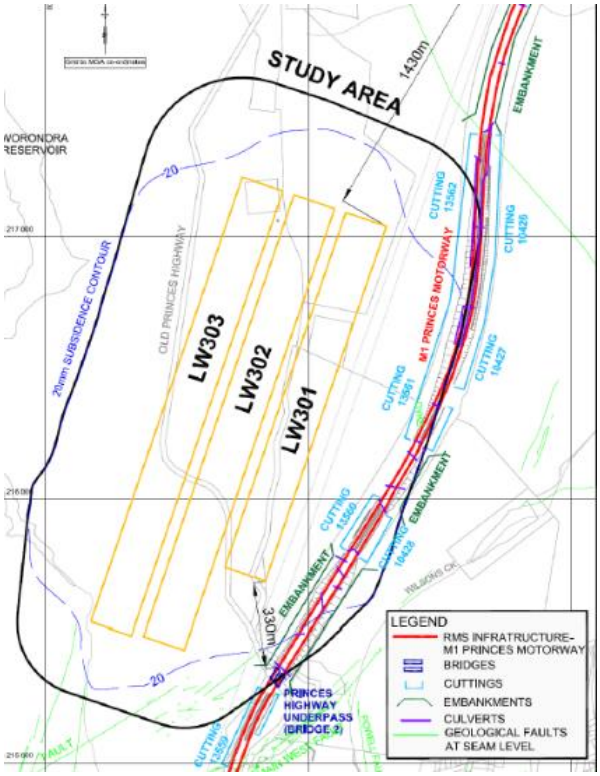

Figure 1: LW301-303 Plan

The RMS formed a technical committee comprising of various consulting engineers and experts to predict and manage the effects of subsidence on Bridge 2 and other RMS infrastructure. One of the requirements for the technical committee was to gain an understanding of the effects of subsidence induced ground movements on Bridge 2 with magnitudes that have a 1 in 100 and 1 in 2000 probability of occurring. The technical committee determined the absolute horizontal movement to be approximately 95mm with a 95% confidence level (1 in 20 probability), but the differential horizontal movements were more of interest as they are more significant to the bridge structures. Incremental relative opening and closing and mid-ordinate deviation was determined by analysing far-field horizontal movement data, and the results for different confidence levels is shown in Table 1.

Table 1: Incremental Relative Opening, Closing and Mid-Ordinate Deviation at 330m from Active Longwall

	1 in 20 probability (95% confidence level)	1 in 100 probability (99% confidence level)	1 in 2000 probability (99.95% confidence level)
Opening	8mm	14mm	44mm
Closing	6mm	13mm	44mm
Mid-Ordinate Deviation	9mm	15mm	32mm

The effects of the predicted movements on Bridge 2 were assessed, and it was determined that the bridge superstructure and bearings would not be adversely affected by differential ground movements. However, it was also determined that there is potential for local crushing of the girder concrete at the contact point of the dowel restraints on the pier headstocks. The 1 in 100 probability movements at the bridge dowels could cause cracking between 0.1mm and 1mm, but this cracking would be structurally acceptable as the girders would continue to be adequately supported. However, the 1 in 2000 probability movements at the bridge dowels could cause cracking above 1mm, which could lead to structural failure.

As the concrete at the dowel joints cannot be visually inspected, monitoring of the relative movements between bridge components was required. The 1 in 100 probability movements between the bridge and abutment footings translate to movements of 6-15mm at bridge headstocks and abutments. The technical committee agreed that a surveying accuracy of no less than 2mm was required. As conventional 3D surveying has a tolerance of +/- 2.5mm, a more accurate solution was sought out. Monitor Optics Systems (MOS) was asked to propose a Fibre Bragg Grating (FBG) based monitoring system to monitor the movements between bridge components.

2 MONITORING PROPOSAL

2.1 APPROACHES TO MONITORING

Ideally, the concrete around the dowels would be monitored for strains and crack growth. However, the dowel restraints in the pier headstock are inaccessible, so there is no way to monitor for concrete strains or visually inspect the area.

The next best approach is to monitor the ground movements that are occurring between the bridge footings. This information can be used to calculate the forces at the dowel locations. The installation of Fibre Bragg Grating (FBG) based sensor cables between pier footings under the Princes Highway was considered, but this would have required road closures and destructive installation procedures, which was deemed unacceptable. Additionally, this technique would have only monitored changes in distance between the pier footings as the abutment footings are inaccessible, providing only limited information of the bridge distortion.

It was also possible to monitor movements between the outer pier and abutment headstocks to calculate forces at the dowel locations. MOS proposed a monitoring system that would measure relative movements between key bridge components using their FBG-based Glass Fibre Reinforced Composite (GFRC) sensor cables, which could achieve an accuracy better than 0.1mm. The technical committee decided to proceed with this approach.

2.2 FIBRE BRAGG GRATINGS TECHNOLOGY BACKGROUND

Bragg Gratings are periodic perturbations of an optical fibre that results in the reflection of a narrow bandwidth of light when illuminated by a broadband light. The reflected central peak wavelength is a function of both the grating's period and the refractive index of the fibre's core. If strain is applied to the grating, the grating period changes, changing the reflected wavelength as a linear function to the strain applied. If the fibre undergoes a temperature change, the refractive index of the fibre will change, which also changes the reflected wavelength as a linear function of temperature. This linear response makes FBGs ideal strain and temperature transducers.

FBGs are often packaged to protect the delicate optical fibre, with some packages including a mechanism to convert other measurement types (e.g. pressure, acceleration) to a strain on the fibre. MOS developed its own proprietary method of embedding one or more optical fibre into a glass fibre reinforced composite (GFRC) cable, which protects the optical fibre while maintaining excellent strain transfer.

2.3 MONITORING OF RELATIVE MOVEMENTS

MOS proposed suspending their GFRC sensor cables between key bridge components, held under tension, to measure the opening and closing between anchor points using one FBG between the anchor points.

The proposed installation points were between:

1. The outer pier and abutment headstocks on each side of the bridge, longitudinally and diagonally relative to the bridge deck, as shown in Figure 2
2. The outer headstock corners and bottom of piers, as shown in Figure 3

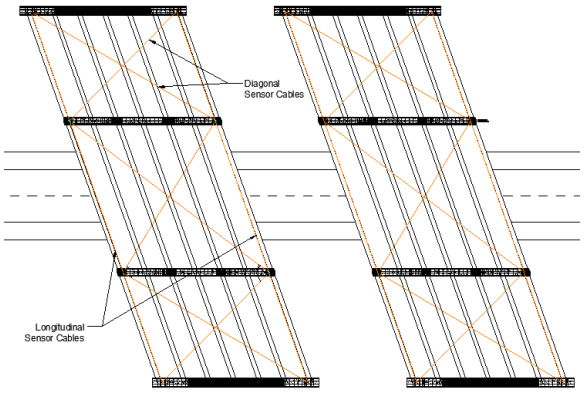

Figure 2: Longitudinal and Diagonal Sensor Cables Suspended between Outer Piers and Abutments

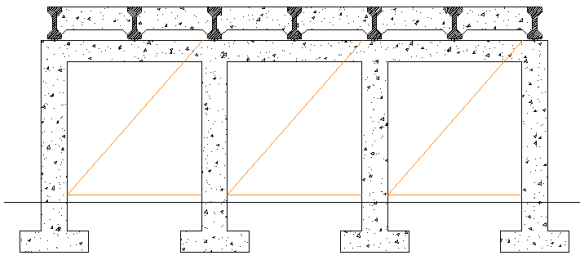

Figure 3: Sensor Cables Suspended between Headstock and Piers

The sensor cables between the outer pier and abutment headstocks are used to calculate orthogonal horizontal measurements at each anchor point relative to one of the abutments.

The sensor cables suspended between the outer headstock corners and bottom of piers was considered impractical due to the risk of vandalism. Tilt meters were proposed as an alternative, with tilt meters located on one side of the outer piers to determine transverse tilt, and in turn, transverse movements of the outer piers, as shown in Figure 4. This was considered as an acceptable alternative.

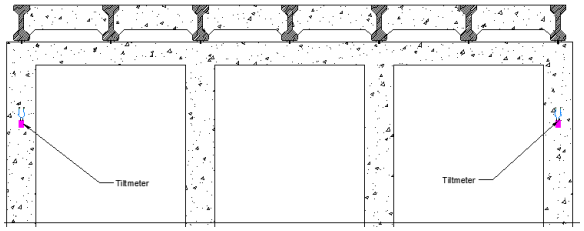

Figure 4: Tilt meters Located on Outer Piers

It was noted that although these approaches would provide valuable high accuracy data of the relative movements of bridge components, it was not a comprehensive system, and was to be conducted in conjunction with 3D surveying of the bridge.

2.4 SENSOR CABLE ACCURACY

The change in length of the sensor cables between anchor points is determined by the change in strain multiplied by the original length, or:

$$\Delta l = \Delta\varepsilon_{FBG} \times l_o \tag{1}$$

The original length is obtained by surveying the distance between anchor points, and the FBG strain is monitored using an optical interrogation unit, which can measure FBGs to an accuracy of 1 x 10^{-3}mm/m. From equation (1), the accuracy of the change in length is dependent on the length of the anchor points. The distance between anchor points is between 13m and 27m, which results in an accuracy of between 0.013mm and 0.027mm.

The accuracy of the FBGs were not brought into question by the technical committee because of their previous experience with MOS sensor cables on a different project. MOS sensor cables were embedded into the shoulders of a major highway pavement to monitor for changes in strain caused by mining-induced subsidence from a longwall coal mine that ran beneath the highway. The MOS sensor cables were tested in Universities and in the field prior to their deployment into the highway, and were further validated after their embedment into the highway by surveying results during the active subsidence period.

2.5 MONITORING REQUIREMENTS

The sensor cables were required to measure orthogonal movements at the abutment and pier headstock corners with suitable allowance for +/- 15mm movements longitudinally relative to the bridge deck and +/- 30mm movements transversely relative to the bridge deck. The required accuracy is +/- 0.5mm, which the sensor cables can easily achieve.

The tilt meters were required to measure tilts of the piers with a minimum accuracy of 0.01° and a resolution of 0.001°. The Smartec Tilt meter have these exact measuring capabilities and were deemed adequate. The tilt meters were to be installed 2m below the headstock.

As FBG sensors respond to changes in temperature as well as strain, temperature sensors were also required to compensate for temperature induced changes to the strain FBGs. Temperature sensor cables were to be installed alongside the longitudinal sensor cables in all cases, with the temperature FBG located alongside the strain FBG. The diagonal sensor cables were to be compensated using the average of the two temperature sensors that are located in their bay.

3 INSTALLATION

3.1 PROTECTION OF SENSOR CABLES

Prior to the installation of the sensor cables, ducting was installed to protect the sensor cables from wildlife and other environmental factors. The longitudinal sensor cable ducting was simple to install as it could be attached directly to the bridge girders, as shown in Figure 5.

Figure 5: Longitudinal Sensor Cable Ducting

The installation of ducting to protect the diagonal sensor cables was more challenging as there were sections of up to 2.5m that were not supported. To prevent sagging, aluminium angle was attached to the girders and the ducting was attached to the angles. The aluminium angle and ducting is shown in Figure 6.

Figure 6: Diagonal Sensor Cable Ducting Attached Using Aluminium Angle

Junction boxes were also fitted over the clamping plates on the headstocks to protect the sensor cable egress from the clamping plates, as shown in Figure 7.

Figure 7: Junction Box Fitted Over Headstock Clamps

3.2 CLAMPING SYSTEM

A clamping system was developed to anchor the sensor cables and apply an appropriate amount of tension to the cables. In all cases, the 1mm diameter sensor cable was glued into the groove of an aluminium clamp that was attached to a steel plate that in turn was attached to the bridge. The clamping system consisted of:

- 30mm x 6mm aluminium "slug" with a 1.2mm x 3mm deep groove
- Aluminium clamp with a 1.2mm wide groove, which varied in dimensional and groove depth depending on location
- Steel plate which the aluminium clamp is attached to, which attaches to the bridge
- Tensioning tool

The slug was glued to one end of the sensor cable in all cases. Once the sensor cable was suspended between anchor points, the end without the slug was glued into the aluminium clamp that is attached to the steel plate. Once the glue on the first clamp was set, the slug was fitted into the tensioning tool, which was placed behind the second aluminium clamp. Figure 8 shows an example of the tensioning tool being setup

Figure 8: Sensor Cable in Clamping System with Tensioning Tool

Suitable tension was then applied and the sensor cable was glued into the second clamps' groove. Once the glue was set, the tensioning tool was redeployed to tension other cables.

3.3 TENSIONING OF SENSOR CABLES

The MOS sensor cables have a tensile capacity of 10,000με, allowing for a potential of +/-5,000με. From equation (1), a shorter length between anchor points requires a larger pre-tension strain for a given measurement allowance. The shortest distance between clamp locations is 13m; suitable tension to allow 30mm of closure over this distance is 2,400με.

As there was significant capacity, MOS decided to tension the longitudinal sensor cables to 30mm between anchor points and tension the diagonal sensor cables so they had allowance to move 40mm longitudinally, and 50mm transversely.

The assigned pre-tension strain on each sensor cable was achieved by monitoring the tensioning process using an interrogation unit. Once the required strain was obtained, the tensioning tool maintained the tension while the cable was glued into the groove of the clamp. The tensioning of S_B1_DNE1 (Bridge 1 NE diagonal cable in the northern bay) is shown in Figure 9.

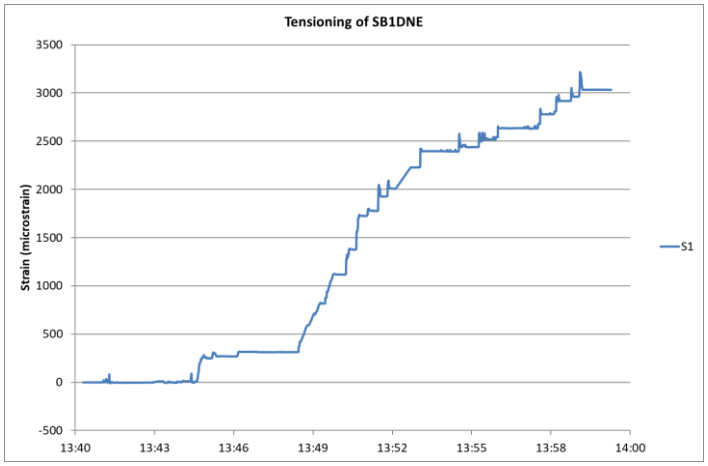

Figure 9: Tensioning S_B1_DNE1

3.4 TILT METERS

All tilt meters were installed 2m below the headstock on the outer piers of each bridge and were installed into junction boxes. The tilt meters were installed away from the Princes Highway for discretion. Cages were then installed over the junction boxes for protection from vandalism. The tilt meter installation is shown in Figures 10 and 11.

Figure 10: Tilt Meter Installation

Figure 11: Cage Installation Over Tilt Meters

3.5 SECUIRTY FENCING

Security fencing was installed at all abutments so the sensor cables were out of reach from the public, and to provide a safe place to install the interrogator cabinet. The security fencing is shown in Figure 12.

Figure 12: Security Fencing

4 CALCULATION OF ORTHOGONAL MEASURMENTS

A fixed reference system was defined for each bridge that uses the northern abutment as its reference point so the orthogonal movements of each bridge component could be calculated from the sensor cable values. Within this frame of reference, the northern abutment is assumed as fixed. The co-ordinate system is displayed in Figure 13.

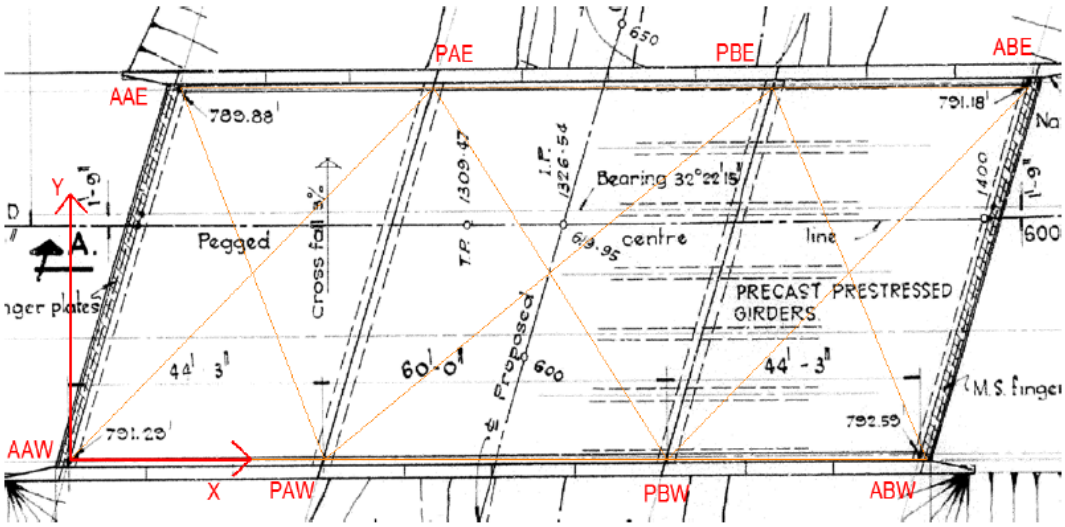

Figure 13: Fixed Reference System (Similar for each Bridge)

Within this reference frame, AAW and AAE are the corners of the northern abutment (Abutment A), which are considered fixed. The orthogonal values of PAE and PAW are first calculated using the four sensor cable values in the northern bay, and the surveyed distance between AAE and AAW, in the Cosine Rule. PBE and PBW are calculated using the Cosine Rule again with the four sensor cable values in the middle bay, except the distance between PAE and PAW is calculated from the results of PAE and PAW. This approach is also used for the measurements of ABE and ABW, using the calculated distance between PBE and PBW as well as the four southern bay sensor cable values. This ensures all measurements are relative to Abutment A.

The distances between clamp points were all surveyed following their installation, so are known to within +/- 2.5mm accuracy.

5 MONITORING SYSTEM

5.1 FBG SENSOR NETWORK

To make efficient use of interrogator bandwidth, the FBGs were serially multiplexed into two strings per bridge; one with 15 FBGs, and one with 11 FBGs. Multiplexing of the network was achieved through patch-cords between sensor locations that did not have a common focal point. Redundancy was also allowed for, with signal cables connecting to both ends of the four sensor strings. The signal cables terminate in the interrogator cabinet which is located in the north abutment of the northbound carriageway.

5.2 DEMODULATION SYSTEM AND POWER

The optical interrogation unit is a Micron Optics Inc. sm125 static interrogator, which has an acquisition frequency of 2Hz. The interrogator is connected to an industrial PC with monitoring software.

The monitoring system is powered by a battery with inverter that is programmed to switch on at specific times and days during the week to acquire data. As the inverter draws power from the battery, the switch is located between the battery and the inverter. Two batteries are dedicated to the project and are swapped on a monthly basis.

5.3 DATA ACQUISITION AND PROCESSING

FBG central peak wavelengths are acquired by the interrogator and converted to relative displacement, temperature and tilt measurements using acquisition software provided by Micron Optics Inc. Custom Utility Software designed by MOS then processes the data to calculate the total orthogonal movements of each bridge component relative to Abutment A of each bridge. The data is then sent to key technical committee members at an agreed frequency, typically monthly. This data is then fed into a computer along with the survey data to understand the stresses at the dowel joints and other key areas of the bridge.

6 RESULTS

6.1 SYSTEM PERFORMANCE

The monitoring system has been in operation since June 2016 and acquired data since. No sensors have gone offline or slipped in tension over this time.

The software provided by Micron Optics Inc. was initially used to calculate the orthogonal values from the sensor cable data. However, when performing this task, the load time for the software was more than 20 minutes from boot up. This is likely due to the calculation heavy dependant nature of the results. As the monitoring system runs off batteries, software was developed in Labview to perform the complex calculations to reduce the required system run-time.

6.2 ORTHOGONAL SHIFTS

The orthogonal shift range for each bridge component has been approximately 6mm in the longitudinal x-direction and approximately 4mm for the transverse y-direction. Some examples of data are shown in Figure 14. Seasonal trends can be observed in the results.

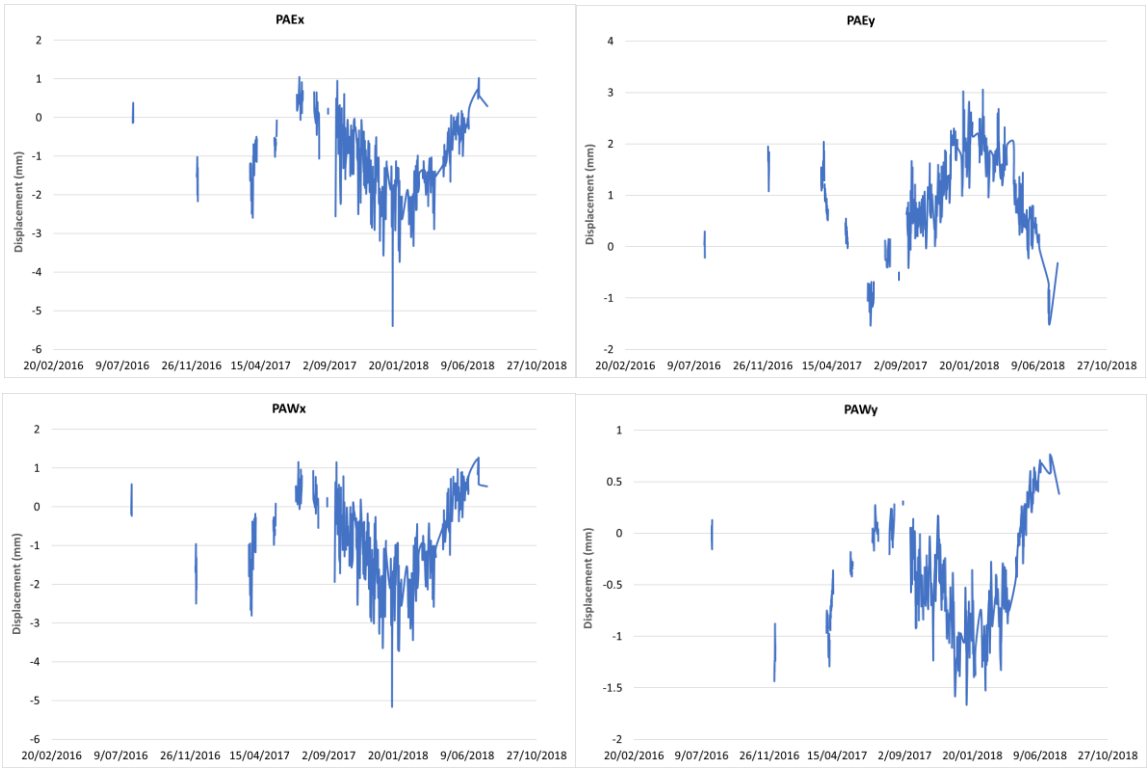

Figure 14: Orthogonal Shifts for Bridge 1

6.3 TILT MEASUREMENTS

The tilt measurements have been susceptible to noise from traffic that uses the bridge, and as such, the tilt meter data has been averaged to obtain more accurate results. Occasional outliers are still evident, however, there are seasonal trends in the results, as shown in Figure 15.

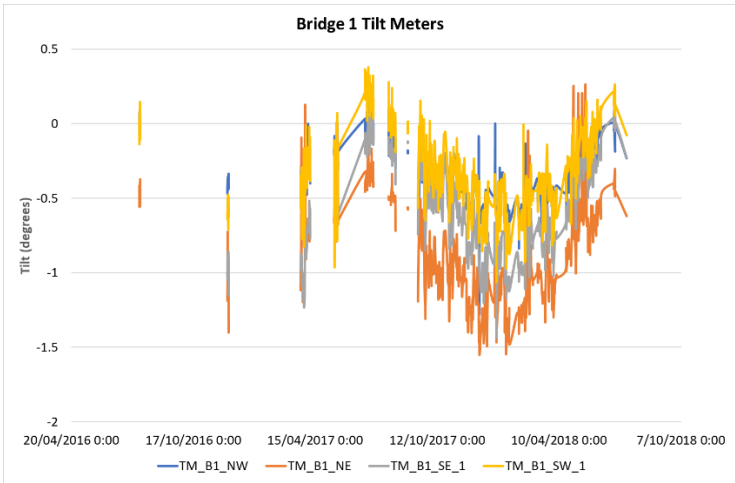

Figure 15: Tilt Meter Results

7 CONCLUSIONS

An optical fibre sensing system that comprises of 44 FBGs has been installed onto two bridges in Helensburgh to monitor differential movements between bridge components caused by subsidence induced ground movements. The monitoring system installation was concluded in June 2016, and data has been acquired since.

The monitoring system uses MOS FBG sensor cables for highly accurate measurements between bridge components, which is converted to orthogonal movements of each end of the pier and abutment headstocks for each bridge. Tilt meters are also employed to monitor pier tilt to deduce transverse movements of the piers. The data is used to calculate stresses in the concrete in the bridge girders at the headstock dowel restraints. Pre-tension was applied to all sensor cables to allow opening and closing between bridge components using a tensioning system developed by MOS. The tensioning system has proven to be robust since installation, with no slip in tension or losses occurring.

The FBG sensors are monitored using a Micron Optics Inc. sm125 interrogator and industrial PC. The monitoring system will monitor for bridge distortion for the duration of three Longwalls, ensuring the bridges' on-going safety and serviceability.

8 ACKNOWLEDGEMENT

The on-going success of this monitoring project relies on the valuable contributions of a team of specialists in bridge engineering, geotechnical and subsidence engineering, and project management, acting under the auspices of the RMS and mining company.

9 REFERENCES

Allwood, G., Wild, G., Lubansky, A., Hinckley, S. (2015). A Highly Sensitive Fiber Bragg Grating Diaphragm Pressure Transducer. *Optical Fiber Technology*, Vol 25, 25-32

Lee, J., Cann, N. (2016). Arup 2016 Report. 20161107 RMS LW301-303 Report – ISSUE, report to RMS, Wollongong 7th November, 2016

Nosenzo, G., Whelan, B.E., Brunton, M., Kay, D., Buys, H. (2012). Continuous Monitoring of Mining Induced Strain in a Road Pavement Using Fiber Bragg Grating Sensors. *Photonic Sensors*, DOI: 10.1007/s13320-012-0077-0

Woods, R. (2016). BFMP-RMS 301-303 Figures Removed - Cardno Changes RW3, report to RMS September 2016

GROUNDWATER DRAWDOWN RELATED SETTLEMENT AND PUMP TEST INTERPRETATION

Ross James Best

Senior Principal, Coffey Geotechnics Pty Ltd

ABSTRACT

Settlement associated with groundwater drawdown can be an important design factor for construction below the watertable. As a result, prediction of the extent and magnitude of groundwater drawdown is an essential part of the evaluation of potential impacts of deep structures. Pump test analysis is routinely employed to for assessment of hydraulic properties of aquifer units affected by deep excavation. Interpretation of pump tests makes use of the rate of groundwater extraction and the drawdown measured in the pumping bores and at other locations. Settlement is not usually considered during interpretation of pump tests. This paper discusses settlement due to dewatering and proposes use of settlement monitoring for interpretation of pump test results.

1 INTRODUCTION

Prediction of groundwater impacts arising from deep excavations is an essential part of the excavation design for excavations below the groundwater table. It involves assessment of groundwater inflow and prediction of drawdown response and generally is a requirement for development approvals. In mining applications, the same basic considerations apply.

Assessments involve development of a conceptual model drawn from the geological interpretation of ground conditions and monitoring of pre-development groundwater levels to evaluate the depth of drawdown and background variation in groundwater levels in response to factors such as rainfall, tidal effects and nearby activities. Where existing developments are present below the groundwater there may be variations in groundwater level associated with basement drainage in rural settings there may be drawdown associated with groundwater use for irrigation. In this paper, settlement due to drawdown is discussed and the use of settlement monitoring to improve the interpretation of test pumping is described.

2 SETTLEMENT DUE TO DEWATERING

Settlement is often a factor of primary important in assessment of the groundwater impacts associated deep excavations where compressible sediments are present. In Melbourne, Australia, settlement associated with construction of major building developments and civil infrastructure has resulted in observed settlement and lead to protracted legal disputes. Groundwater seepage to the Burnley Tunnel in South Melbourne results in continuing significant seepage and permanent groundwater injection is used to prevent ongoing settlement of the compressible Coode Island Silt. In Sydney, settlement associated with dewatering during construction of the Eastern Distributor resulted in damage distance from the works areas and construction of the Northside Storage Tunnel resulted in settlement beneath Middle Harbour, which raised concerns regarding potential impacts on a main sewer pipeline along the harbour floor supported on piles into the channel sediments.

There are many other examples where deep excavation or groundwater extraction as resulted in substantial settlement. Well-known examples are subsidence in Venice and Bangkok. The following examples are among a large number noted by Poland (1984):

- Latrobe Valley, Victoria. Settlement of in excess of 1.6 m has been recorded around coalmines in a thick shallow brown coal deposit with settlement in excess of 200 mm over an area of 100 km^2 as a result of groundwater extraction to prevent floor heave.
- Shanghai, China. Settlement of 2.6 m occurred from 1921 to 1965 within the upper 300 m of freshwater and marine sediments due to extraction of water for domestic and industrial use.
- Taipei Basin, Taiwan. Settlement of 1.9 occurred between 1955 and 1974 because of groundwater extraction from a deep alluvial deposit.

One example of groundwater drawdown related settlement of major settlement due to groundwater extraction in California occurred in Antelope Valley 80 km northeast of Los Angeles. Hoffmann *et al* (2003) describe regional land subsidence within a basin filled to depths of more than 2 km with fluvial and lacustrine sediments used to supply water for agriculture and town water. Settlement in the aquifer is estimated to be up to 2.5 m since the start of groundwater extraction. Groundwater use commenced following an investigation in 1911, which indicated water resources, which could support substantial agricultural development. As groundwater levels fell, agricultural use became uneconomic and

currently use is primarily for municipal and industrial purposes. Figure 1 from Hoffmann *et al* (2003) illustrates the drawdown and settlement, which has occurred.

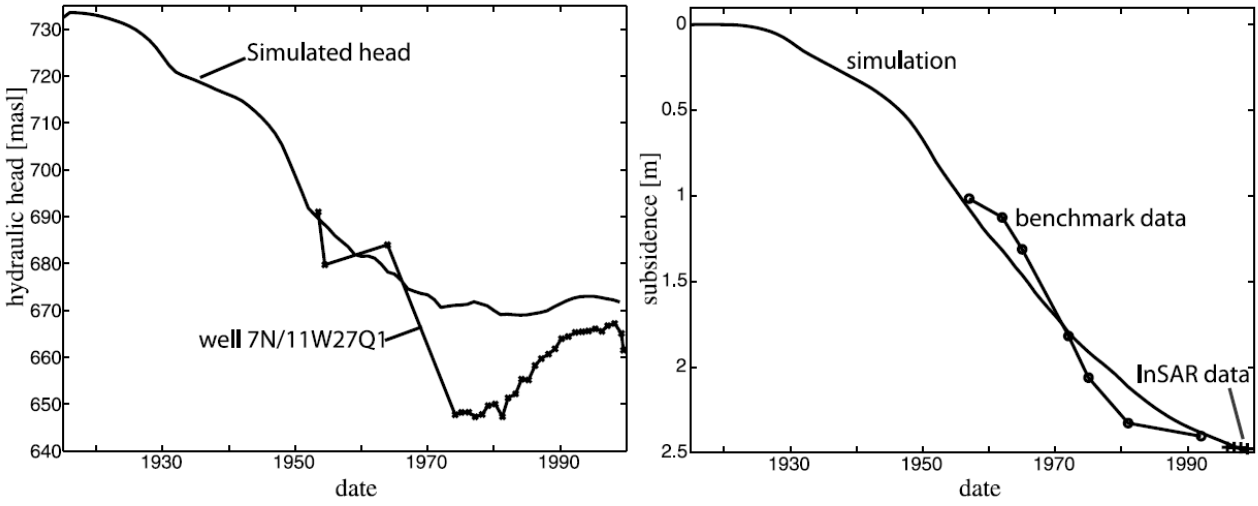

Figure 1: Groundwater drawdown and subsidence in Antelope Valley (Hoffmann *et al* 2003)

Hoffmann *et al* carried out a study using ground movement records from extensometer monitoring and InSAR satellite monitoring combined with groundwater monitoring to assess storage characteristics of the ground profile and in particular inelastic components of storage. Three high yielding aquifers are present separated by compressible low yielding sediments. Water is drawn from the upper unconfined aquifer and the middle aquifer. The study made use of conventional groundwater modelling to assess distribution of groundwater level changes in the main aquifer and one-dimensional consolidation theory to interpret delays in response. The study demonstrated the utility of InSAR monitoring to measure ground movement over wide areas. The InSAR measurements were in good agreement with the extensometer results. The results illustrated in Figure 2 demonstrate the link between annual groundwater level variations and ground movement. The InSAR measurements show good resolution of the pattern of movement over a 20 mm range over a period of four years and indicate movement below the level of anchorage of the reference extensometer (anchored at 363 m depth). Based on the results of the study zones of rapid and slow response to groundwater level changes were identified ranging from essentially instantaneous to over 200 years and estimates of inelastic storage coefficients were made.

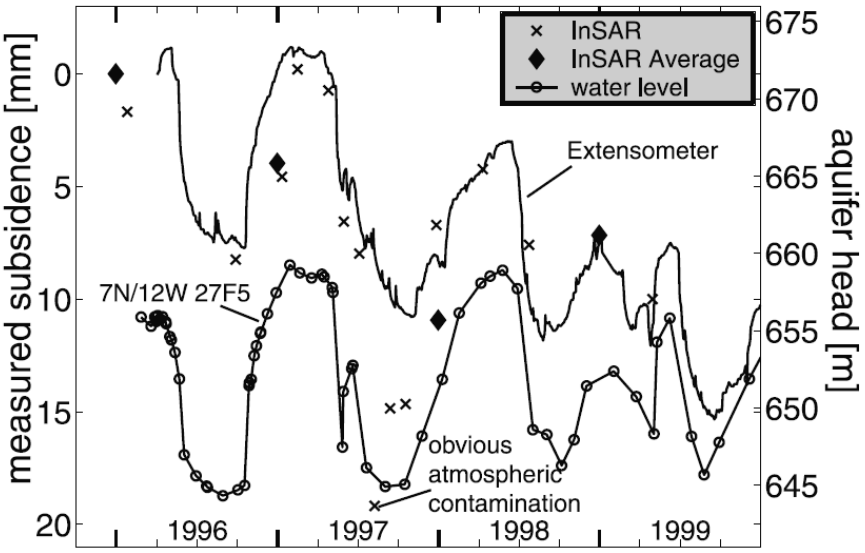

Figure 2: Monitoring of drawdown and subsidence - Antelope Valley, California (Hoffmann *et al* (2003)

During construction of the Sydney Northside Storage Tunnel to carry sewer overflows, seepage to the part of the tunnel in sandstone rock beneath a palaeochannel at Middle Harbour resulted in significant drawdown beneath the 70 m thick palaeochannel sediments and the development of settlement over a period of five years.

During investigation of the area, test pumping was carried out to provide information to predict behaviour during tunnelling the test involve pumping for a well screened in rock and monitoring of piezometric response in the rock and in the base of palaeochannel. In addition, settlement was monitored at a series of locations. Settlement of 5 mm occurred during the test pumping. This result, together with the piezometric response, allowed prediction of settlement for nominated inflow rates and was an important input to the design of a grouting program to reduce the rate of seepage to the tunnel.

The settlement resulted in movement of a sewer main installed across the floor of Middle Harbour supported by friction piles into the channel sediments. Figure 3 (after Best and Parker 2005) shows the variation in drawdown at the base of the palaeochannel and the measured settlement over a five-year period spanning construction and operation of the Northside Storage Tunnel. A major programme of grouting was carried out during tunnelling of a section at the floor of palaeochannel where the sandstone was broken as a result of valley bulging. The effects of grouting after tunnel construction are apparent in the record resulting in a sharp reduction in drawdown. The drawdown reduced briefly during periods of surcharge when the tunnel was filled with sewer overflows during high rainfall events while the treatment plant at North Head treated the accumulated flows. It is also interesting to note the gradual reduction in drawdown over time after construction indicating seepage to the tunnel gradually reduced as a result of a clogging process. Settlement stabilised at about 85 mm for the result illustrated in Figure 3 though higher settlements were recorded (up to about 110 mm) at other locations.

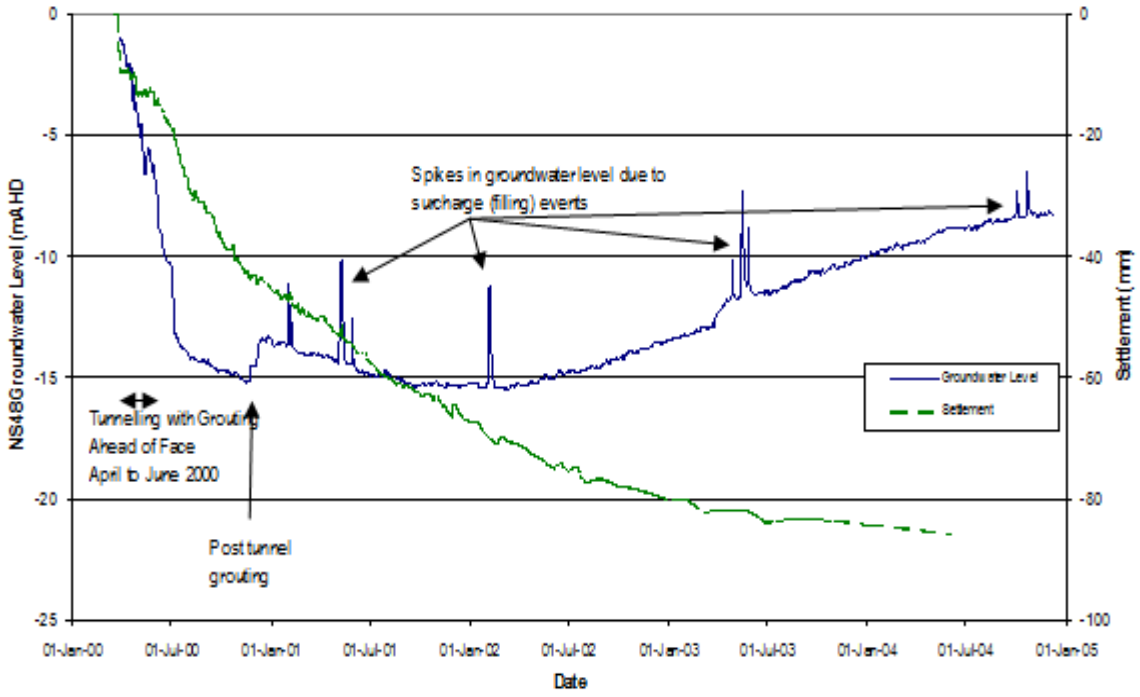

Figure 3: Drawdown and settlement - Middle Harbour Palaeochannel due to Northside Storage Tunnel

Coal seam gas extraction is being carried out in the Surat and Bowen Basins in Queensland. This involved extraction of groundwater to reduce pore pressure at depths of up to several hundred metres to release the gas (methane and propane) contained in coal seams. This groundwater extraction results in settlement and interferometric synthetic aperture radar (InSAR) methods are used to track settlement over vast areas. The power of this method, which involves comparison of phase difference in satellite radar images of the ground surface is illustrated in a report by Altamira (2012) which provided a baseline assessment of background settlement. Figure 4 shows the extent of the coverage where settlement monitoring over a four year period was interpreted from satellite images.

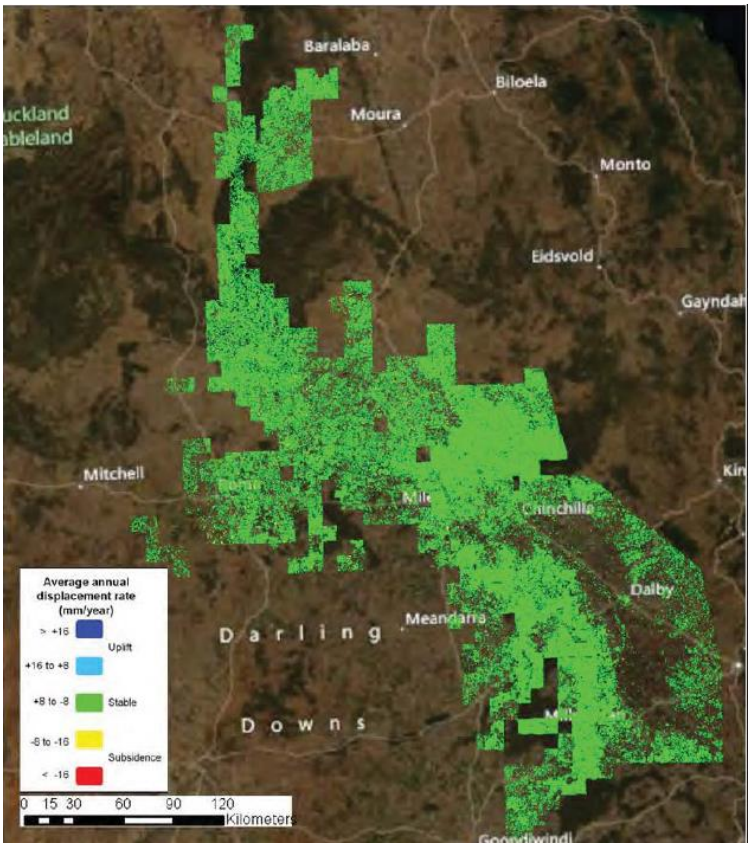

Figure 4: Coverage of InSAR settlement monitoring - Surat Basin (Altamira 2012)

The coverage of the method is vast and movements with sub-10 mm resolution are discriminated. Figure 5 taken from the Altamira report illustrates the response interpreted at one location selected from the area covered in Figure 4. Each settlement point represents a pass of the monitoring satellite.

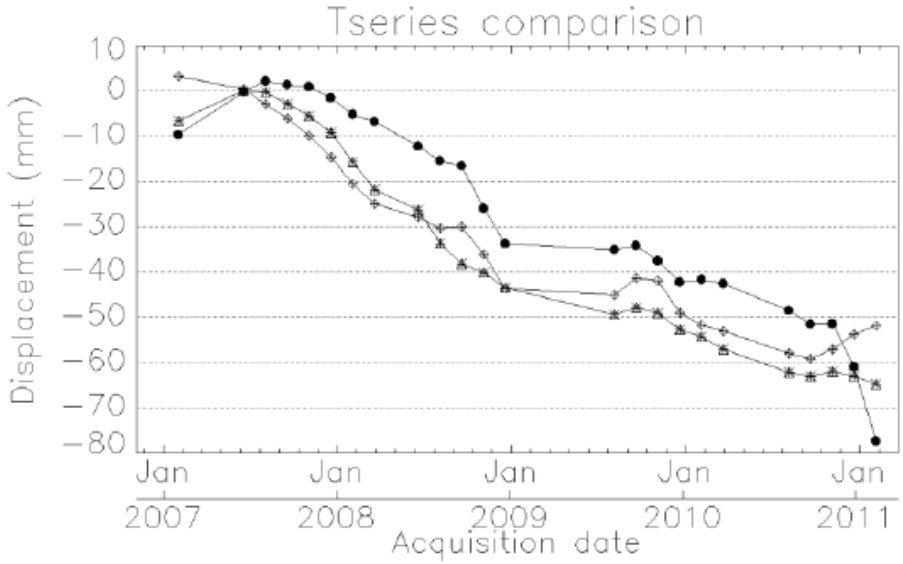

Figure 5: Selected interpretation record using InSAR (Altamira 2012)

Averaging methods are used to reduce scatter and some areas are unsuitable for interpretation such as areas of ploughed fields. The capacity to resolve movement over such a wide area provides a powerful tool, which is being used to interpret movement associated with coal seam gas extraction.

3 APPROACH FOR EXTENDING PUMP TEST ANALYSIS

Groundwater investigations are typically in the form of testing of response to changes in conditions at monitoring bores. This can be in the form of packer testing, falling or rising head testing or response to test pumping. Standard methods are employed for interpretation of these tests. In the case of interpretation of response to test pumping a wide range of interpretation methods are available depending upon the hydrogeological model of the groundwater system. Kruseman and De Ridder (2000) provide an excellent description of method for interpretation of test pumping results, which can be applied to conditions ranging from extensive confined aquifers, to leaky aquifers and aquifers bounded by low or high permeability features. Interpretation software is available which can carry our automatic curve fitting using a variety of hydrogeological models.

Pump testing is often carried out to assess hydraulic parameters for design for major mining and civil infrastructure developments. It provides a means of assessing the transmissivity of dominant aquifers and can provide some information about geological units overlying or underlying the dominant aquifer.

3.1 USE OF SETTLEMENT MONITORING TO ENHANCE TEST INTERPRETATION

Use of settlement monitoring to extend interpretation of the results for test pumping is proposed. This would provide more complete use of spatial response induced by testing. Typically, test pumping involves a pumping bore and a small number of monitoring piezometers. The results of testing provide limited information regarding spatial response. In formations which are extensive and hydraulic properties are expected to be consistent testing for a pumping bore with a few monitoring bores would typically provide a sound basis for interpretation of the properties of a single aquifer and some information regarding overlying or underlying units of lower permeability. Where there is strong directional behaviour as can occur in palaeochannels or in faulted rock systems, multiple monitoring piezometers are required to provide information regarding the distribution of the drawdown. In urban settings, the locations available for installation of monitoring bores are typically limited and delays in securing approval for installation can be problematic.

The paper proposes use of settlement monitoring to extend the interpretation of test pumping results. This would involve monitoring of settlement at high resolution in the area surrounding the test. This offers a number of potential benefits:

- Identification of directional behaviour (such as that resulting from the present of structures such as dykes and faults)
- Interpretation of vertical consolidation characteristics of compressible units overlying the aquifer tested
- Improvement of the overall interpretation by allowing clearer discrimination of the radial extent of response
- Allowing improvement in test analysis where there are constraints on installation of monitoring piezometers.

Surface settlement monitoring only requires access to the ground surface and typically involves minimal interference to other activities. Approvals for conduct of conventional survey are much less restrictive than those required for installation of monitoring piezometers.

In order to take advantage of settlement monitoring to extend the results of test pumping, analytical tools beyond those normally employed for test pump interpretation are required. Theory is available which allows prediction of drawdown for extensive layered aquifer systems subject to pumping. These are readily extended to allow prediction of surface settlement. Approaches by others have included employment of standard consolidation theory to assess surface settlement from dewatering. An approach described by Niu *et al* (2013) involved assessment of settlement associated with vertical consolidate of a compressible unit overlying an aquifer in which drawdown was considered stable with time in the aquifer and settlement of the overlying compressible sediment was obtained by integration. The results were for use in estimation of surface settlement at the pumping bore.

An analysis method for calculation of drawdown in a layered aquifer system was developed by Neuman (1975) and a similar approach was followed by Booker and Best (1990) and Best and Booker (2000) who extended the application of this method for calculation of settlement associated with groundwater extraction. These methods allow calculation of drawdown in a system of aquifers separated by lower permeability beds. The method involves solution of the problem in the Laplace transform domain and numerical inversion to obtain the result in the time domain.

There are many methods for numerical Laplace inversion. Two which have been demonstrated to be effective for layered groundwater flow are Talbot's method (1939) and the Gaver-Stehfast method (Gaver 1966). This process involves evaluation of the result for selected values of the transform variable and combining these results using inversion algorithms to obtain results at particular times. The Talbot method involves evaluation for a number of complex values

of the transform variable while the Gaver-Stehfast has the advantage that evaluations are for real values of the transform variable.

Layered groundwater flow models predict drawdown and flow from the low permeability beds to the aquifers and settlement is obtained analytically using the integral of flow from the low permeability beds and the head reduction in the aquifers. For soil strength material, it is reasonable to approximate settlement as the volume of water removed from a soil column below the watertable. The theory is provided in Appendix A setting out the formulation. For rocks a minor adjustment is required to account for compressibility of water and Biot's coefficient linking settlement with pore pressure change.

An example is illustrated in Figure 6 for the case of a transmissive aquifer overlain by a compressible unit.

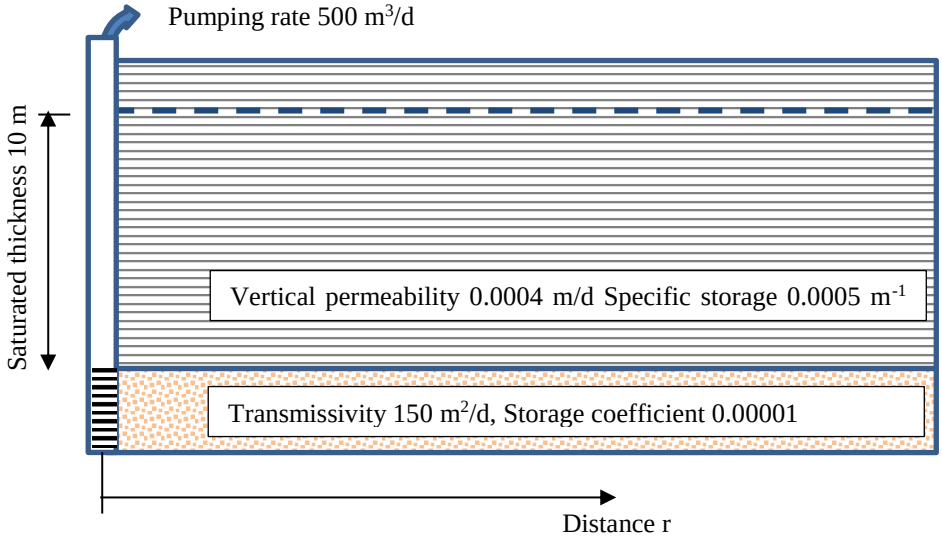

Figure 6: Example aquifer and consolidating layer case

Figure 7 shows the modelled drawdown in the base aquifer and the surface settlement for the case illustrated in Figure 6 for distances of 5 m and 20 m from the pumping bore.

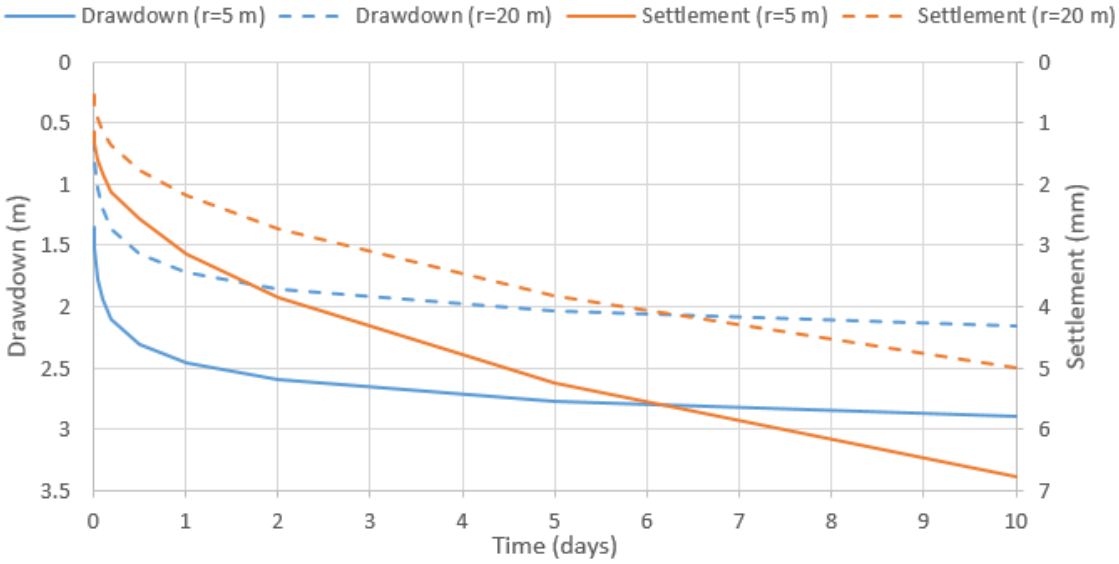

Figure 7: Modelled drawdown and settlement for sample case

The case illustrates that settlement continues to occur after drawdown as begun to stabilise. The settlement response with time provides a means of assessing the vertical consolidation parameters for the compressible formation as well as the

transmissivity of the aquifer underlying the compressible unit. The utility of the approach depends upon the capacity to measure settlement to millimetre (or preferably sub-millimetre) resolution.

Assessment of parameters from test results can be carried out by testing trial choices against measured response.

4 INSTRUMENTATION

The measurements traditionally employed for interpretation of test pumping are:

- Measurement of the pumping rate over the duration of the test
- Measurement of piezometric level in the pumping bore and in piezometers near the pumping bore.
- Water quality can also be measured and can be helpful in assessing the origin of the water pumped and identifying the presence of contamination.

Measurements are made at regular intervals over the course of the test including a period after pumping has ceased. The results at the pumping bore during the recovery period after pumping ceases is particularly useful as groundwater recovery is not affected by the losses through the screen and formation in close proximity to the well as occurs during pumping.

Measurements of drawdown are typically made using pressure monitors installed in the pumping bores and the observation piezometers. These are typically recorded automatically by a downhole logger or by a telemetry system. These methods are well established.

Measurement of settlement is not typically carried out for pump tests but a number of methods are widely used for assessment of settlement for engineering projects and for large-scale response to groundwater extraction these include:

- Conventional survey using total station equipment – resolution to approximately 1 mm can be achieved over limited areas
- GPS based survey – resolution of several millimetres can be achieved over a wide area
- InSAR satellite based imaging – resolution at sub 10 mm resolution can be achieved over vast areas
- Tiltmeters – are employed during fracturing of coal seam gas bearing horizons to assess the extent of fracturing (seismic monitoring is also employed for this purpose but is not helpful for assessment of ground movement). Tiltmeters are commercially available with quoted resolution of 0.0013^{o}.
- Hydrostatic profiler – a pressure measuring instrument is drawn through a tube containing water. The difference in pressure is a measure of relative elevation. This can resolve movement of about 2 cm.
- High resolution can be obtained using a partly fill pipe with high precision force transducers to record changes in level at selected location. These can achieve resolution of 0.025 mm. It requires a rigid pipe partly filled with water to a tightly controlled level corrected for temperature effects.
- Laser methods are available to measure the vertical movement of structures to about 1 mm resolution.

In addition to these methods, extensometers can be used to measure the settlement profile at particular locations.

In order to extend interpretation of test pumping results to include treatment of settlement methods for measurement of settlement to a resolution of 1 mm or better are required. In urban settings, creation of settlement in excess of about 20 mm for testing purposes would generally be unacceptable. Ideally monitoring settlement to sub-millimetre resolution at a multiple times per days would allow evaluation of response in stiff ground conditions.

Settlement of sub-millimetre resolution is not readily available to be routinely deployed for monitoring of test pumping but a range of methods offer promise. For the present conventional survey is considered to be the most practical method for monitoring of settlement for test pumping and thus the use of settlement monitoring to enhance test pumping analysis is limited to situations where settlement of up to 8 to 20 mm is anticipated. Where higher resolution is required use of high resolution tiltmeters offer the possibility of obtaining sub-millimetre resolution using a series of tiltmeters.

5 CONCLUSIONS

A method for enhancing interpretation of test pumping interpretation is provided. This offers potential to provide additional information regarding the consolidation properties of compressible units overlying aquifer, identification of directional response in groundwater systems and clearer indications of the location of hydraulic boundaries and extent of drawdown influence. The approach is considered to have immediate applicability where settlement of the order of 10 mm can be induced by pumping or where project needs can support use of high precision settlement monitoring. Use of tiltmeters offers the potential for interpretation of testing where settlement of only a few millimetres takes place. The method is illustrated for a practical case. The theory presented in this paper can readily be employed to assess settlement associated with deep excavations or pumping from deep aquifers.

6 ACKNOWLEDGEMENTS

The author gratefully acknowledges the support and encouragement of the late Professor John Booker during the development of the theoretical basis for the work.

7 REFERENCES

Altamira. *Baseline report on InSAR monitoring on the Surat-Bowen Basin*, (2012) contained in Santos. *GLNG Gas Field Development Project's EIS Documents – Appendix AE-E Ground deformation monitoring and management program* – (https://www.statedevelopment.qld.gov.au/assessments-and-approvals/santos-glng-environmental-impact-statements.html, 22 August 2018))

Best, R.J. and Booker J.R. (2000). *Groundwater flow in layered systems.* Developments in Theoretical Soil Mechanics – The John Booker Memorial Symposium, Balkima.

Best R.J and Parker C.J. *Groundwater in Sydney – Tunnel inflows and settlement – Theory and experience.* 12th Australian Tunnelling Conference (2005). The Australian Underground Construction and Tunnelling Association. 2005.

Boulton, N.S. (1954). *Unsteady radial flow to a pumped well allowing for delayed yield from storage*. International Association of Science and Hydrology, Volume 2, pp 472-476, Rome.

Booker, J.R. and Best, R.J. (1990). *Analysis of layered aquifer systems*. The Institution of Engineers Australia, Conference on Hydraulics in Civil Engineering, pp 1-5. Sydney.

Gaver, D.P. (1996). (Jr) *Observing stochastic processes, and approximate transform inversion.* Operations Research, 14: 444-459.

Hoffmann, J., Galloway D.L., Zebker, H.A. (2003). *Inverse modeling of interbed storage parameters using land subsidence observations, Antelope Valley, California,* Water Resources Research 39 (2) 1031.

Kruseman, G.P. and De Ridder, N.A. *Analysis and evaluation of pump test data – Second Edition,* Publication 47, International Institute for Land Reclamation and Improvement, Wageningen, The Netherlands, 2000.

Neuman, S.P. (1975). *Analysis of pumping test data from anisotropic aquifers considering gravity response.* Water Resources Research. Volume 23, Number 8, pp 1683-1688.

Niu Wen-jie, Wang Zhenyu, Chen Feng and Li Hongran. (2013). *Settlement analysis of a confined sand aquifer overlain by a clay layer due to single well pumping.* Mathematical Problems in Engineering, Vol 2013. Hindawai Publishing Corporation.

Talbot (1939). A. *The accurate numerical inversion of Laplace transforms.* Journal of Institution of Mathematics Applications, Volume 23, pp 97-120.

Wen-jieNiu, Zhenyu Wang, Feng Chen, and Hongran Li, (2013). *Settlement Analysis of a Confined Sand Aquifer Overlain by a Clay Layer due to Single Well Pumping*, Mathematical Problems in Engineering Volume 2013.

8 APPENDIX – ANALYSIS OF MULTILAYER GROUNDWATER SYSTEMS

The background theory below follows the treatment presented by Booker and Best (1990) and Best and Booker (2000) similar approaches are described by Neuman (1975).

THEORY:

This paper provides an extension to the results presented in Booker & Best (1990) and includes treatment of a ring source and a circular source and takes account of multiple radial boundary conditions.

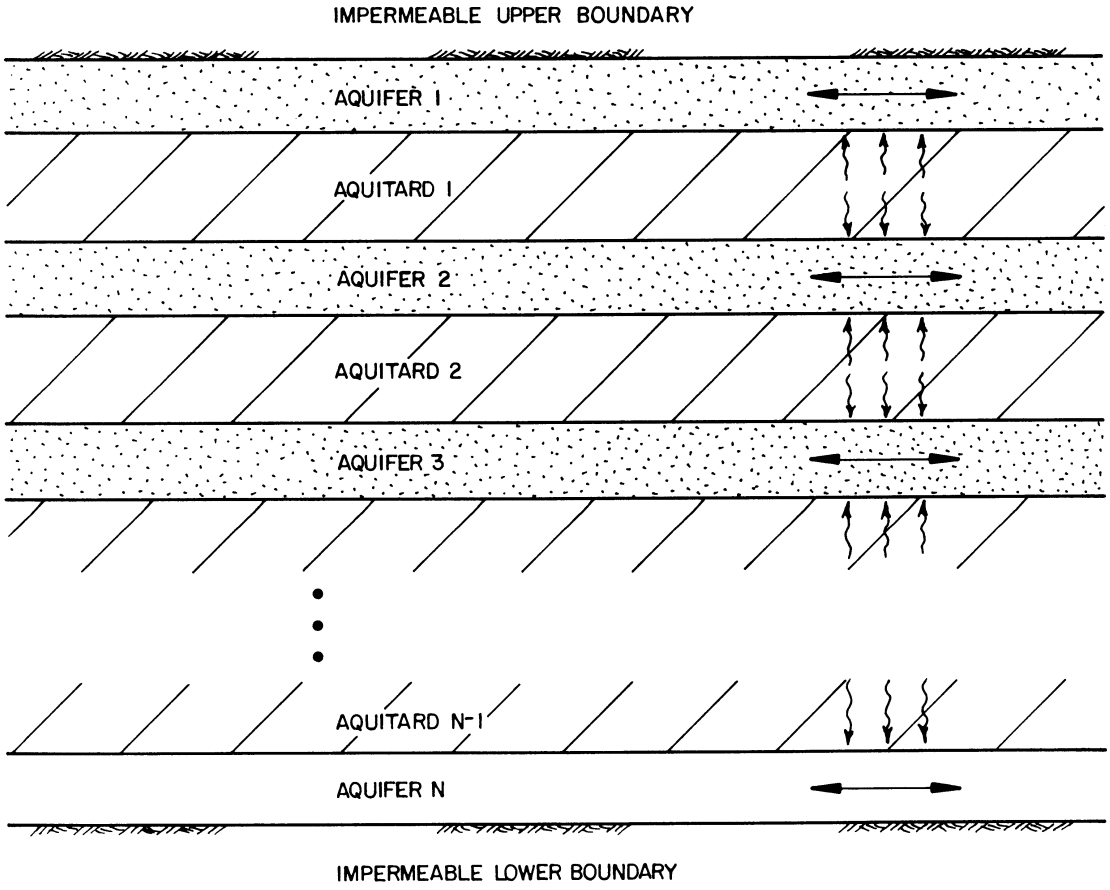

Figure 1A: Layered aquifer system.

8.1 FINITE LAYER APPROACH

The aquifer system is assumed to be made up on alternating aquifer and aquitard layers as shown in Figure 1. Flow is taken as purely horizontal in the aquifer layers and purely vertical in the aquitard layers. Impermeable boundaries are assumed above and below the layered system. Material properties are considered to be uniform within each layer. No account is taken of unsaturated flow.

The vertical flow within the aquitard unit below aquifer i is governed by Darcy's law:

$$k\frac{\partial^2\phi}{\partial z^2} = S_s\frac{\partial\phi}{\partial t} \tag{1}$$

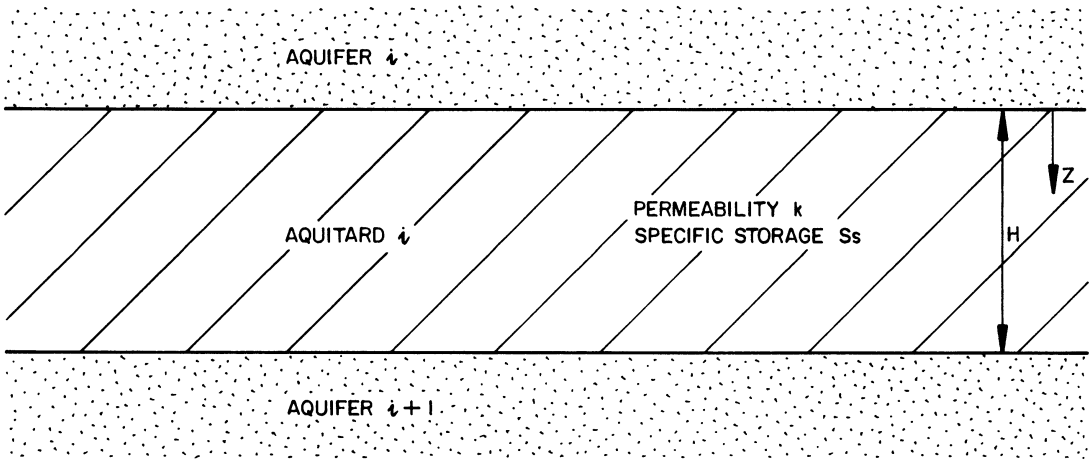

Figure 2A: Component aquitard

Where k, z and S_s are defined in Figure 2, t is time and ϕ is potentiometric head. Flow into the aquifer overlying the aquitard, q_i is given by:

$$q_i = k\frac{\partial \phi}{\partial z} \qquad \text{at} \quad z = 0 \tag{2}$$

Flow into the lower aquifer from the aquitard, q_{i+1}, is given by:

$$q_{i+1} = -k\frac{\partial \phi}{\partial z} \qquad \text{at} \quad z = H \tag{3}$$

Where H is the aquitard thickness. Taking the Laplace transform of Equation 1 and assuming that head is zero at time zero gives:

$$k\frac{\partial^2 \bar{\phi}}{\partial z^2} = S_s \rho \bar{\phi} \tag{4}$$

Where the superior bar indicates the Laplace transform and ρ is the Laplace transform variable. This has solution:

$$\bar{\phi} = \bar{\phi}_i\left(\cosh \mu z - \frac{\cosh \mu H \sinh \mu z}{\sinh \mu H}\right) + \bar{\phi}_{i+1}\left(\frac{\sinh \mu z}{\sinh \mu H}\right) \tag{5}$$

Where:

$\mu^2 = \dfrac{\rho S}{k}$ and μ is taken as having a positive real part

$\bar{\phi}_i$ is the Laplace transform of the head in the overlying aquifer

$\bar{\phi}_{i+1}$ is the Laplace transform of the head in the underlying aquifer

It follows that:

$$\begin{Bmatrix} \bar{q}_i \\ \bar{q}_{i+1} \end{Bmatrix} = -\frac{k\mu}{\sinh \mu H} \begin{bmatrix} \cosh \mu H & -1 \\ -1 & \cosh \mu H \end{bmatrix} \begin{Bmatrix} \bar{\phi}_i \\ \bar{\phi}_{i+1} \end{Bmatrix} \tag{6}$$

Assembling for each aquifer in the profile gives the following relationship between aquifer head and flow into the aquifers from the aquitards:

$$\begin{Bmatrix} \bar{q}_1 \\ \bar{q}_2 \\ \bar{q}_3 \\ \vdots \\ \bar{q}_{n-1} \\ \bar{q}_n \end{Bmatrix} = -\begin{bmatrix} A_1 & B_1 & & & & \\ B_1 & A_1 + A_2 & B_2 & & & \\ & B_2 & A_2 + A_3 & & & \\ & & & \ddots & & \\ & & & & A_{n-2} + A_{n-1} & B_{n-1} \\ & & & & B_{n-1} & A_{n-1} \end{bmatrix} \begin{Bmatrix} \bar{\phi}_1 \\ \bar{\phi}_2 \\ \bar{\phi}_3 \\ \vdots \\ \bar{\phi}_{n-1} \\ \bar{\phi}_n \end{Bmatrix} \tag{7}$$

Using matrix notation Equation 7 becomes:

$$\{\bar{q}\} = -[A]\{\bar{\phi}\} \tag{8}$$

8.2 RADIAL FLOW

Assuming purely radial flow in the aquifers the equation for flow in aquifer i can be written:

$$T_i\left(\frac{\partial^2 \phi_i}{\partial r^2} + \frac{1}{r}\frac{\partial \phi_i}{\partial r}\right) = -q_i + S_i \frac{\partial \phi_i}{\partial t} \tag{9}$$

Where

T_i is the transmissivity of aquifer i

S_i is the storage coefficient of aquifer i

r is the distance from the centre of axisymmetry of the radial flow

In matrix notation the system of equations relating head and aquifer inflow becomes:

$$[T]\left(\frac{\partial^2 \{\phi\}}{\partial r^2} + \frac{1}{r}\frac{\partial \{\phi\}}{\partial r}\right) = -\{q\} + [S]\frac{\partial \{\phi\}}{\partial t} \tag{10}$$

Where:

$[T]$ is the diagonal matrix of aquifer transmissivities

$[S]$ is the diagonal matrix of aquifer storage coefficients

$\{\phi\}$ is the vector of aquifer heads

$\{q\}$ is the vector of inflows into each aquifer

Taking the Laplace transform of Equation 10 and assuming zero head at time zero gives:

$$[T]\left(\frac{\partial^2\{\bar{\phi}\}}{\partial r^2}+\frac{1}{r}\frac{\partial\{\bar{\phi}\}}{\partial r}\right)=-\{\bar{q}\}+\rho[S]\{\bar{\phi}\} \tag{11}$$

Substituting Equation 8 gives:

$$[T]\left(\frac{\partial^2\{\bar{\phi}\}}{\partial r^2}+\frac{1}{r}\frac{\partial\{\bar{\phi}\}}{\partial r}\right)=[B]\{\bar{\phi}\} \tag{12}$$

Where $[B]$ is given by:

$$[B]=[A]+\rho[S] \tag{13}$$

Equation 12 has solutions of the form:

$$\{\bar{\phi}\}=X\ K_0(\omega r)\{v\}+Y\ I_0(\omega r)\{v\} \tag{14}$$

Where X and Y are constants and

K_0, I_0 are the zeroth order modified Bessel functions

ω^2 is an eigenvalue and

$\{v\}$ is the corresponding eigenvector satisfying

$$\omega^2[T]\{v\}-[B]\{v\}=0 \tag{15}$$

and ω is taken as having a positive real part.

The n eigenvalues and n eigenvectors of Equation 15 can be found analytically for $n<5$ and numerical methods can be employed for $n>4$. The solution to Equation 12 can be written:

$$\{\bar{\phi}\}=\sum_{i=1}^{n}\left(X_i\ K_0(\omega_i r)\{v_i\}+Y_i\ I_0(\omega_i r)\{v_i\}\right) \tag{16}$$

Where:

$\omega^2{}_i$ is the i'th eigenvalue of Equation 15

$\{v_i\}$ is the i'th eigenvector of Equation 15

X_i, Y_i are constants chosen to satisfy the radial boundary conditions

Rewriting Equation 16 in matrix form gives:

$$\{\bar{\phi}\}=[v][K_0(\omega r)]\{X\}+[v][I_0(\omega r)]\{Y\} \tag{17}$$

Where:

$[K_0(\omega r)]$ is a diagonal matrix with $K_0(\omega r)_{ii}=K_0(\omega_i r)$

$[I_0(\omega r)]$ is a diagonal matrix with $I_0(\omega r)_{ii}=I_0(\omega_i r)$

$[v]$ is the matrix of eigenvectors of Equation 15

8.2.1 Point source

For a series of point sources in each aquifer at $r=0$ of varying strengths with Laplace transforms given by $\{\bar{Q}\}$:

$$\{\overline{Q}\} = \lim_{r \to 0} -2\pi r[T]\frac{\partial\{\overline{\phi}\}}{\partial r}$$

$$\{\overline{Q}\} = \lim_{r \to 0} -2\pi r[T][v]\left[\frac{\partial K_0(\omega r)}{\partial r}\right]\{X\}$$

$$\{\overline{Q}\} = 2\pi[T][v]\{X\}$$

so that:

$$\{X\} = \frac{1}{2\pi}[v]^{-1}[T]^{-1}\{\overline{Q}\} \tag{18}$$

Numerical inversion of the matrix of eigenvalues is not necessary due to the orthogonality of the eigenvectors with respect to $[T]$. Provided that the eigenvectors are scaled such that:

$$\{v_i\}^T\{v_i\} = 1 \tag{19}$$

whence Equation 18 becomes:

$$\{X\} = \frac{1}{2\pi}[v]^T[T]^{-1}\{\overline{Q}\} \tag{20}$$

The inverse of the diagonal matrix of transmissivities is simply the diagonal matrix of inverse transmissivities.

For an extensive aquifer system $\{\overline{\phi}\} = 0$ at great distance from the point source. This implies $\{Y\} = 0$. It follows that for point aquifer sources in an extensive aquifer system:

$$\{\overline{\phi}\} = \frac{1}{2\pi}[v][K_0(\omega r)][v]^T[T]^{-1}\{\overline{Q}\} \tag{21}$$

For a source $\{Q_0\}$ that is constant with time the Laplace transformed source vector is given by:

$$\{\overline{Q}\} = \frac{\{Q_0\}}{\rho}$$

8.3 CALCULATION OF SETTLEMENT

Settlement can be calculated at the surface or at aquifer boundaries. Settlement at the surface is given by the sum of the settlements within each aquifer and aquitard. Aquifer settlement can be calculated by multiplying the head change by the aquifer storage coefficient. Aquitard settlement can be calculated as the integral of the flow to the overlying and underlying aquifers. Surface settlement is calculated as the sum of settlements from all the aquifers and aquitards:

$$\delta = \sum_{i=1}^{n} S_{si}\phi + \sum_{i=1}^{n}\int_0^t q_i \, dt \tag{22}$$

In the Laplace transform domain the time integral of vertical flow into the aquifers simplifies to become the transformed vertical flow divided by the Laplace transform variable.

$$\overline{\delta} = \sum_{i=1}^{n} S_{si}\overline{\phi} + \frac{\overline{q}_i}{\rho} \tag{23}$$

Settlements at particular times can be obtained by numerical inversion.

IN SITU STRESS TESTING FOR TUNNEL DESIGN IN SYDNEY – HYDRAULIC FRACTURING AND OVERCORING

Anastasia Suchowerska, Les McQueen and Mahdi Zoorabadi

Golder Associates

ABSTRACT

Over the last decade there have been several road and rail tunnels designed within the Sydney Metropolitan area that are now well into construction. For these tunnelling projects, a key design input has been an estimate of the magnitude and orientation of the *in situ* stress. Designers typically consider the measurement of *in situ* stress from boreholes located along the project alignment and also from published stress measurements and empirically derived relationships for the Sydney Basin. This is because there is often significant variability in the results obtained from limited stress measurements for a given project and a reasonable interpretation of these results needs to take into account a number of factors such as geological and topographical situation. Measurement technique is also a source of variation and practitioners need to be aware of the limitations and advantages of these to ensure that a stress measurement program has the opportunity to deliver the required project needs. This paper considers *in situ* measurements made within boreholes in Sydney using the commonly-used hydraulic fracturing method and the more recently used overcoring method by the Sigra IST tool. Results from two infrastructure projects, where these two methods were used, are presented and the possible reasons for differences obtained between the two methods are discussed. The process of overcoring is a focus including the factors that influence the determination of the elastic properties of the rock for the calculation of the *in situ* major horizontal stress. Numerical modelling is used to examine the potential for brittle microcracking in the porous Sydney sandstones, which can damage an overcored sample and invalidate elastic parameters obtained.

1. INTRODUCTION

Measurements of *in situ* stresses in the Sydney metropolitan have been collected for many decades and are well documented (Enever et al 1990; Enever 1999; McQueen, 2004). Subsequently there have been multiple linear correlations made between stress and depth data for deep excavations and tunnels (Pells, 1990; Enever, 1999; Bertuzzi, 2014). Even with the plethora of data available within the Sydney area, the influences on rock stress such as topography, geological structure and varying stiffness of sedimentary strata, *in situ* rock stress estimation is still a challenge. This is not just in Sydney, as John Hudson identified in his paper on what faces the International Society of Rock Mechanics (ISRM) in the next 50 years, 'rock stress is one of the major unsolved problems in rock mechanics' (Hudson, 2012). The ISRM Suggested Methods for Rock Stress Estimation, after discussing measurement techniques, puts *in situ* stress in the wholistic context of topography, soils, rock mass lithology, structural geology, hydrogeology and mechanical data (including rock stress) to arrive at a 3D Final Rock Stress Model (Stephansson and Zang, 2012).

This measurement of rock stress faces the key challenge, that stress cannot be measured directly, but requires us to measure some response that comes from the relief of stress or applied additional stress to the rock mass. Typically, this response measurement is undertaken in a stress-disturbed zone such as a borehole or wall of a tunnel. Therefore, we are changing the rock attribute we wish to measure. For this reason, calculated *in situ* stress from measurements of other rock properties are estimates at best. This paper aims to further the discussion on some of the key test measurement issues, to assist the practitioner in the interpretation of the stress measurements.

Elevated horizontal stress has been deduced from stress measurements in the Sydney area, and also from observations and measurements of displacements in deep excavations (Hewitt, 1999; Pells, 1990; Braybrooke, 1990) and failures in underground openings (Pells, 2004; McQueen, 2004). Spalling brittle failure of Hawkesbury Sandstone has been observed in the crown of the M5 East, Malabar Sewerage Outfall, Cataract, Pipehead to Potts Hill, Cross City and Northside Storage tunnels and Elgas Cavern, (Enever et al., 1990, Pells, 2002, De Ambrosis and Kotze 2004, McQueen, 2004, Bertuzzi, 2015). Spalling has also occurred in sandstones from other formations encountered in tunnels such as the Bringelly Shale and Newport Formation where these sandstones are interbedded with lower stiffness finer grained more jointed rocks. Certain conditions are required to elevate the stress to brittle failure levels (McQueen et al. 2017), such as stiffer beds in a stratified sequence, as recognised in Sydney stratified rocks by Enever et al. (1990) from CSIRO Hollow Inclusion Cell stress measurements in the Malabar Ocean Outfall Sewerage Tunnel. Another consequence of these elevated horizontal stress conditions is the potential for slip or shear between the varying stiffness layers. This has occurred in Sydney on a broad scale from folding in geological time, resulting in clay lined or sheared bedding partings.

On a smaller scale shear on these weaker bedding planes also occurs in tunnels walls on excavation, which can influence stability and tunnel support elements.

2. RECENT STRESS MEASUREMENTS IN SYDNEY

Variability in the magnitude of measurements of *in situ* stress between different techniques at the same site have been encountered elsewhere as well as in Sydney (Pells, 2004). Variations may be due to factors, as indicated by Hudson (1993), such as the theory used (assumes homogeneous, isotropic, linear elastic materials), presence of rock discontinuities, inhomogeneous rock, topography, anisotropic rock conditions and measurement error including temperature effects. Different measurement techniques also affect a different volume of rock and address a different rock property.

The variability in magnitudes of stress measurements is evident when reviewing recent data from two Sydney projects. The estimates of major horizontal principal stress from these two projects are presented in Figure 1. The data indicates a wide range in magnitudes and presents a challenge for interpretation without a detailed examination of individual tests, methods and the geological situation. A first pass differentiation of the data in Figure 1 can be made by grouping according to the test method used. Hydraulic fracturing and Sigra IST overcoring was used on both projects. The graph suggests two databases of measurements with hydraulic fracture results tending to be higher and Sigra IST results tending to be lower. Also shown in Figure 1 is the mean trend line from Bertuzzi (2014) for 0 to 50 m depth and the trend line of Pells (1990) representing the stress field for deep excavations in the Sydney CBD. The Pells (1990) stress trend is also supported by Oliveira and Wong (2012) from measured displacements for excavations in the upper 10 to 20 m in the Sydney CBD. Compared with these trend lines the Sigra overcoring results are generally low.

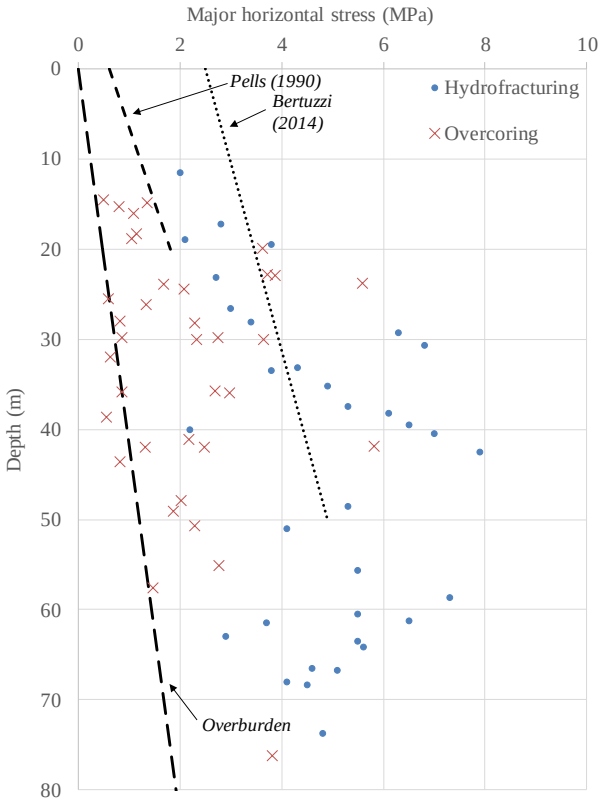

Figure 1: Estimates of major principal horizontal stress versus depth from two Sydney projects

Hydraulic fracturing has been the primary method of in situ stress testing in the Sydney area over the last few decades. Some overcoring has been carried out by the CSIRO Hollow Inclusion Cell and, predominately in the mining field, by the ANZI cell (Mills, 1997, Mills et al., 2016). Sigra IST overcoring has been a more recent addition. This overcoring technique, which can be carried out in boreholes to the depths required for Sydney tunnels, is a form of USBM apparatus (Hooker and Bickel, 1974). It measures the two dimensional strain response of a pilot hole during overcoring by the drilling of a larger diameter hole. Elastic parameters of the overcored rock are then required, from testing of the overcored sample, to calculate the in situ stress.

Some of the limitations of the hydraulic fracture and Sigra IST overcoring techniques in the Sydney sandstone, are discussed below, particularly overcoring since it is relatively recent. Detailed reviews on the advantages and disadvantages of in situ stress testing methods has been reviewed by others (e.g., Fairhurst, 2003; Ljunggren et al., 2003; Doe et al., 2006).

The hydraulic fracture technique has been the subject of discussion due to high results obtained for the horizontal major stress in Sydney tunnelling projects. Enever (2008) indicates that the validity of the framework behind the theory of the stress calculations has been established by laboratory studies. Pells (2004) discusses this and quotes from Fairhurst (1986) and others on the limitations of the hydraulic fracture test. Principle limitations peculiar to this test relate to the action of pore pressures during the test in the porous Sydney sandstone and the determination of the tensile strength, which is required to calculate the major horizontal stress. The Borehole Slotter was introduced as an alternative technique for two projects where high hydraulic fracture test results were obtained (Pells, 2004).

The IST overcoring tool is placed in a pilot hole approximately 26 mm in diameter and is overcored by a HQ core barrel which cuts approximately a 61 mm diameter core with a 96 mm borehole diameter. Mechanical gauges measure the 2D strain in the pilot hole. The overcored hollow cylinder core sample is recovered from the borehole and transported to the laboratory where strain gauges are fixed to the outside of the cylindrical sample and it is subjected to cyclical uniaxial loading to calculate the elastic parameters. Factors that could affect the determination of these elastic parameters and the calculation of the *in situ* stress normal to the borehole, include:

- Elastic parameters are obtained from the low end of the uniaxial stress-strain curve, which is considered to be the seating zone for closure of pore space in the sandstone. The cyclical loading and unloading of the hollow cylinder of relatively low strength sandstone may also aggravate this effect.
- Strain gauges are fixed to the outside of the cylindrical sample, whereas *in situ* strain measurements are made in the pilot hole, i.e., the inside of the hollow sample.
- The IST gauges measure pilot hole closure during horizontal unloading. The laboratory test is a vertical loading case.
- The IST gauge with mechanical pins are susceptible to inhomogeneities on the scale of a grain.
- Development of microcracks in the rock sample during the overcoring process

The authors consider that the above factors have contributed to low modulus determinations and hence to low *in situ* stress estimation.

ISRM Suggested methods (Sjoberg et al., 2007) specify that a biaxial test be carried out on site on the core sample with the overcored cell still bonded within, as soon as possible after it is recovered from the borehole. The elastic parameters are then determined from the same gauges that measured the *in situ* strains and in the same direction. The difference from the *in situ* test is that this is a loading situation not an unloading one.

The determination of the elastic parameters of the overcored rock has been scrutinised by the operators of the ANZI overcoring cell. The procedure for determining the elastic properties involves three tests: a pressuremeter test in the pilot hole prior to overcoring; a biaxial test on the overcored hollow cylindrical sample; and a uniaxial test on a solid core sample retrieved from drilling of the pilot hole (Mills, 1997 and Mills et al., 2016). The variability in the magnitude of Young's modulus from these tests in some cases have been reported to be up to 2 fold. Thus, further investigation is warranted to identify how the approach to obtaining elastic parameters from overcore samples can be improved.

It is informative to note the paper by Anderson and Christiansson (2003) who compared hydraulic fracture and overcore stress measurements in the same borehole in a medium grained crystalline rock. Some of their conclusions are relevant to overcoring in our weaker sandstone, including the large scatter in the overcoring measurements due to the size of the strain gauges in relation to the crystals. They also questioned the validity of overcoring in high stress conditions compared to the rock strength and suggested that microcracking may be induced during overcoring resulting in a low Young's modulus during biaxial testing. Thus, they concluded that the determination of this elastic parameter using core samples may not be trivial.

3 TRANSIENT STRESS AND EXTENSIONAL STRAIN IN OVERCORED SAMPLE

3.1 THE POTENTIAL FOR MICROCRACKING

The variation of the measured strains throughout the overcoring process show that the rock core experiences a transient stress path due to stress concentration ahead of the drill bit and stress release when overcoring passes the measuring point (Mills et al., 2016). Some studies, utilising 3D modelling, have been conducted to better understand the transient stresses and strains and the nature of stress-induced microcracking in a core sample during the drilling and overcoring process (eg. Hakala, 1999; Hakala, 2006; Lundholm et al. 2000). The process of drilling the overcore can result in stress-induced microcracking that permanently alters the physical state of the rock (Eberhardt et al. 1999), which changes the elastic properties of the sample. Based on the critical extensional strain criterion (Stacey, 1981), microcracking of brittle rock will occur when the extension strain exceeds a critical limit that is characteristic of the rock. If these cracks propagate under higher strain levels in drill core then the ultimate result is a macro phenomenon of fracturing known such as core disking, or ring disking in the case of the overcored hollow cylinder core.

As indicated in the introduction, Hawkesbury Sandstone has been observed to behave in a brittle manner leading to spalling failure in Sydney tunnels. Pells (2002) indicates a critical extensional strain for Hawkesbury Sandstone of about 500 microstrains when considering stress-induced tunnel failures. A similar extensional strain is obtained on interrogating the back analysis model from McQueen et al. (2017) of the M5E tunnel spalling failure at a stress level of about 0.5xUnconfined Compressive Strength. The extensional strain in these cases results from a compressive stress situation in the walls of a tunnel, unlike a stress relief situation during overcoring.

In the case of overcoring that is being considered here, the release of stress in transient conditions during drilling a pilot hole and then overcoring to create an unconfined situation sets up a scenario for failure under axial extension. Extensional strain will also vary with position around the circumference of a borehole in an unbalanced stress field. This was investigated for the Sydney overcoring case, using numerical modelling using 3D and 2D axisymmetric methods, as reported in the next section.

3.2 NUMERICAL MODELLING

The tensile stress and the extensional strain during the transient overcoring process was considered in the wall of a hollow core sample with the borehole dimensions from the Sigra IST. The modelling was carried out as a parametric study of various *in situ* stress conditions using elastic stress analysis. The aim is to consider the *in situ* stress level that could generate a tensile stress that would exceed the tensile strength and critical extensional stain limit and thus the potential for microcracking in the overcored sample. This condition would result in the invalidation of the assumed linear elastic behaviour of the rock and the reliability of the calculated stress.

The two modelling approaches were employed, viz. a two-dimensional axisymmetric plane strain model using the RS2 software (Rocscience Inc.) and a three-dimensional model using the FLAC3D software (Itasca Consulting Group Inc.). The problem definition is presented in Figure 2. The parameters used in the models are listed in Table 1. The rock material was modelled as an elastic material. Both the 2D and 3D numerical models were staged to include an initial step where *in situ* stresses were applied, the borehole was then drilled followed by the pilot hole, and then subsequent incremental excavations of the rock to replicate the overcoring process. The size of the smallest incremental removal of rock in the overcoring process corresponded to 1 mm thickness, and this was applied around the nominated enquiry point for both models. The enquiry point was located on the edge of the pilot hole approximately 200 mm from the start of the pilot hole where a strain gauge would be located. The results present compression as positive values.

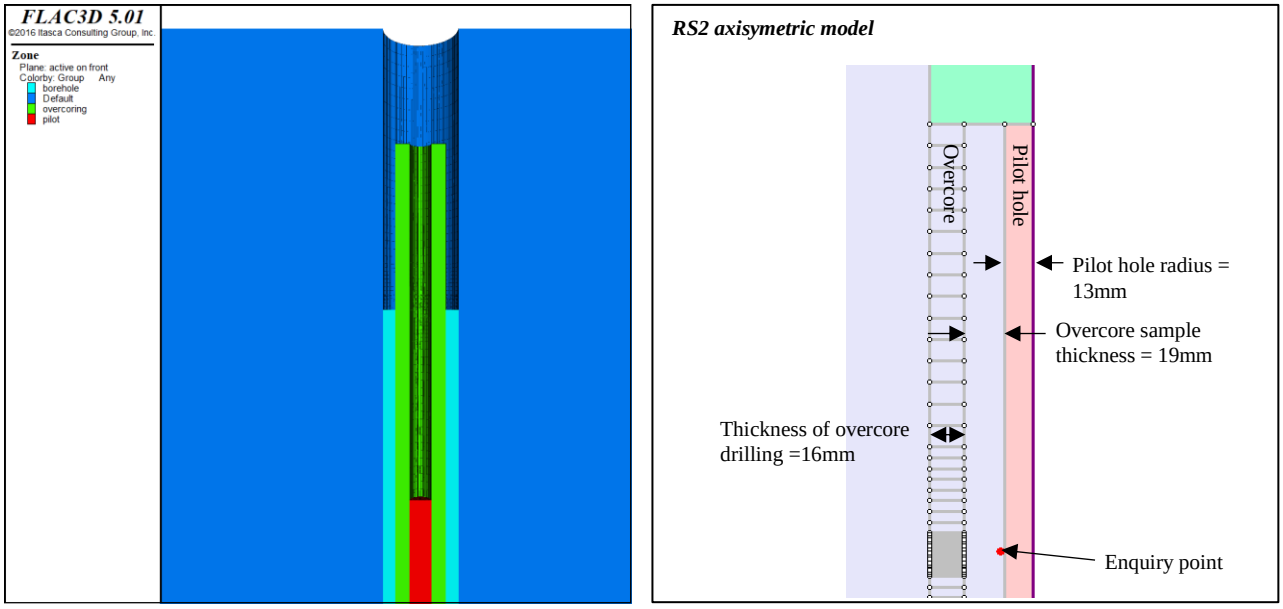

Figure 2: Snapshots from FLAC3D and RS2 showing the model setup and geometry

Table 1: Summary of magnitudes of parameters used in both the FLAC3D and RS2 numerical models

Parameter	**Magnitude**
Depth of analysis (z)	60 m
Major horizontal *in situ* stress (σ_H)	Varied from 2 to 8 MPa
Minor horizontal *in situ* stress (σ_h)	= 0.625σ_H
Vertical *in situ* stress (σ_v)	= 0.024 x depth (MPa)
Poisson's ratio (v)	0.2
Young's modulus (E)	8000 MPa
Diameter of pilot hole	26 mm
Internal diameter of overcore	64 mm
External diameter of overcore	96 mm

3.1 RESULTS OF 2D AXISSYMETRIC ANALYSIS

The axial stress and axial strain induced into a point in the 2D model throughout the overcoring process is presented in Figure 3. The results are presented as the overcoring proceeds from 250 mm prior to the enquiry point through to 100 mm past that point. These results are for the case of 60 m depth where vertical *in situ* stress was assumed to be 1.44 MPa.

The initial axial compressive stress starts from the vertical *in situ* stress (Figure 3 at -250mm). The transient stress path dramatically changes to tensile stress within 40 mm of the enquiry point. The highest tensile stress is induced in the case of the highest major horizontal *in situ* stress. After the enquiry point axial compressive stresses are once again induced prior to the axial stress decaying to zero. These models indicate that axial strains in the rock are exposed to extensional strains with the overcore within 50 mm of the enquiry point. The higher the *in situ* horizontal stress the higher the induced extensional strain.

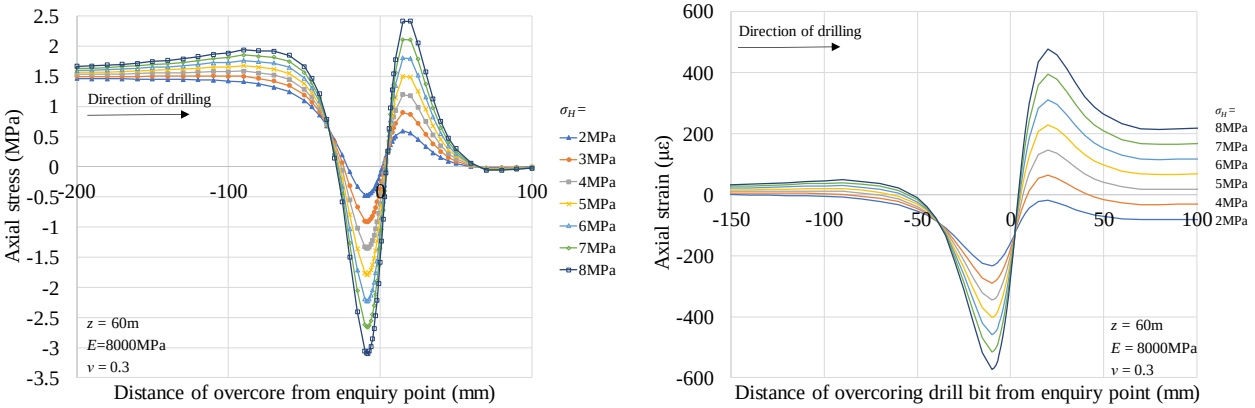

Figure 3: 2D model results of axial stress and strain at the enquiry point during overcoring

3.2 RESULTS OF 3D ANALYSIS

When the axial stress for enquiry points around the circumference of the pilot hole, at 200 mm from the start of the pilot hole, are plotted against distance around the borehole, they were found to vary roughly sinusoidally, being located 90 degrees from each other. Figure 4 presents the transient axial stress and axial strain path induced around the pilot hole. In contrast, the axial strain showed almost no variation in magnitude for the enquiry points located around the pilot hole. The 2D results for the same parameters are also shown for comparison. The results from the 3D and 2D analyses where further compared for three magnitudes of major *in situ* horizontal stress (Figure 5).

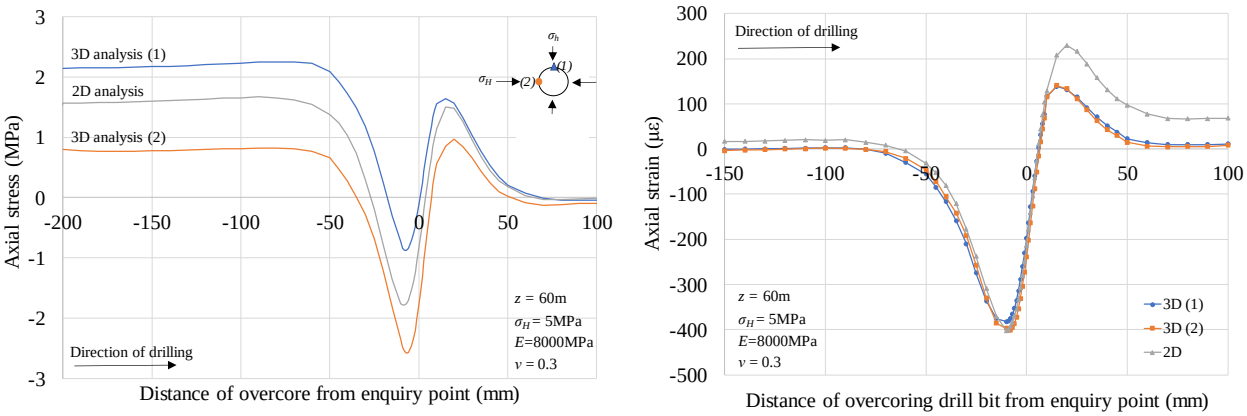

Figure 4: 3D model results of axial stress and strain at the enquiry points around the pilot hole during overcoring for 60 m depth with 2D model results for comparison

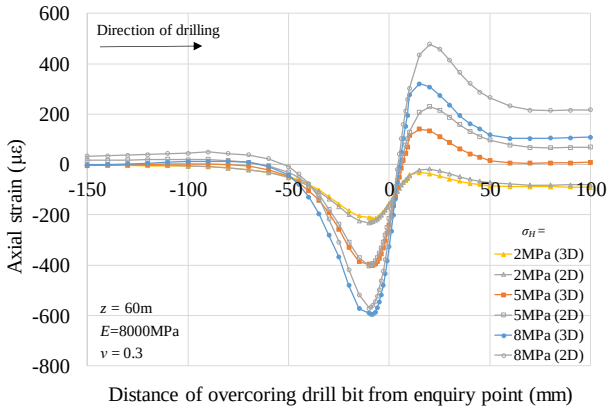

Figure 5: Comparison of axial strain from 2D and 3D models for the enquiry point in the pilot hole for varying *in situ* horizontal stress levels

3. DISCUSSION

The numerical modelling indicates that for a major horizontal stress ranging from 2 to 8 MPa and overburden stress for 60 m depth, the tensile stress is within the range of 0.5 to 4.5 MPa and extensional strain of 200 to 600 με, respectively (Figure 6). For a major horizontal stress ranging from 2 to 5 MPa and overburden stress for 30 m depth, the tensile stress is within the range of 1 to 3 MPa and an extensional strain of 150 to 350 με, respectively (Figure 6).

A direct tensile strength of about 1.5 to 2 MPa has been assumed, from Brazilian tensile strength of 2 to 3 MPa for the better classes of sandstone (Pells, 2002) and applying a factor of 0.7 (Perras and Diederichs, 2014) to estimate the direct tensile strength. The transient tensile stress that exceeds that limit occurs above about 3 to 4 MPa *in situ* major horizontal stress. Extensional strain at this *in situ* stress level is about 250 to 330 microstrain for the assumed Young's modulus of 8 GPa. Higher extension strains would be expected for lower modulus rocks.

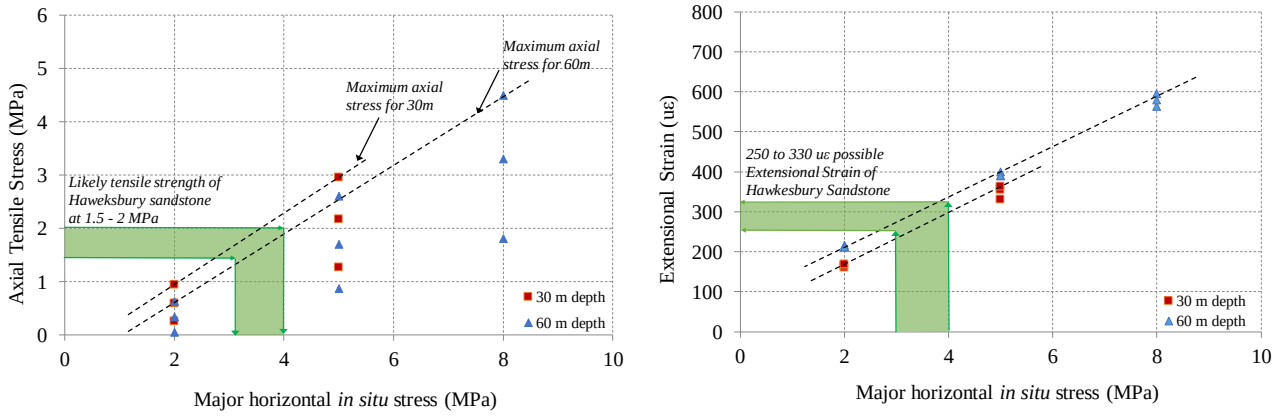

Figure 6: Peak axial stress and extension strain obtained from the 3D model

The 2D model cannot capture the variation in stress in an unbalanced horizontal stress field, however, the results trend midway between the axial stress results of the 3D model. There is good agreement between the peak extensional strain determined by the two numerical models. Thus given this comparative study of the overcoring process, a parametric analysis can be run with the quicker 2D model with confidence. The obtained extensional strains from the 2D analyses are shown in Figure 7. To assist in the interpretation of this graph, Bertuzzi's (2014) *in situ* stress trend line is shown. The peak extensional strain between 250 and 30 microstrain has been shaded to show the zone where there is a high likelihood that microcracking may start to take place during the overcoring process.

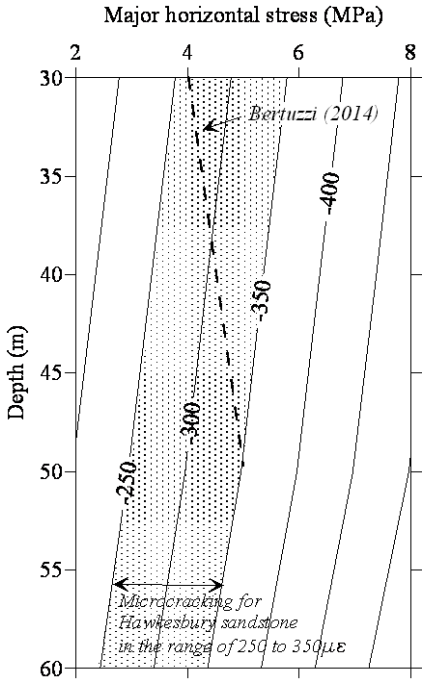

Figure 7: Maximum extensional strain induced into the overcored rock sample obtained from the 2D analysis

4. CONCLUSIONS

This paper has considered *in situ* major horizontal stress measurements made within boreholes in Sydney sandstone by the different techniques of hydraulic fracturing and overcoring. It was initially prompted by lower results obtained from Sigra IST overcoring than generally accepted in Sydney from the experience of stress-induced displacements and failure in deep excavations and tunnels. The process of overcoring was then examined along with experience elsewhere in the literature of overcoring in relatively high stress conditions compared with the strength of the rock.

Numerical modelling of the transient stress path at the measurement point during overcoring indicates the presence of a tensile stress level that can exceed the tensile strength of the rock and thus the potential for microcracking in the overcored sample. If this occurs, the measured elastic properties of the rock sample will be affected and thus the calculated *in situ* stress. The stress path and extensional strain was modelled for different *in situ* stress conditions to provide an indication of the conditions in which microcracking can occur.

Further work is required to model the influence of different *in situ* stress regimes and different rock conditions (anisotropic strength, presence of discontinuities adjacent to an overcore) on the stress path and the extensional strain, which can result in microcrack sample damage. Physical testing of the overcored hollow cylindrical samples, from which elastic parameters are obtained, could also be carried out to examine for the presence of microcracks.

REFERENCES

Anderson, C. and Christiansson, R. (2003) Variability of hydraulic fracturing rock stress measurements and comparisons to triaxial overcoring results made in the same borehole. *Rock Stress*, Sugawara, Obara and Sato (eds), Swets and Zeitlinger, Lisse.

Bertuzzi R.P. (2014) Sydney sandstone and shale parameters for tunnel design. *Australian Geomechanics,* pp. Vol 49, 95-104.

Bertuzzi R.P. (2015) Forming a view of the rock mass strength of Hawkesbury Sandstone from tunnelling case histories, in *13th Int. Congress of Rock Mechanics,* May; Montreal, Canada.

Braybrooke J., (1990) Some geotechnical phenomena related to high stress in Hawkesbury Sandstone., *Proceedings of the 24th Symposium on Advances in the study of the Sydney Basin* University of Newcastle, pp. 97-104.

De Ambrosis L.P. and Kotze G.P. (2004) Stress induced roof collapses during construction of the Sydney LPG storage cavern. *Proc. 9th ANZ Conf on Geomechanics*, Auckland, February,159-165.

Doe T., Zieger M., Enachescu C. and Bohner J. (2006) In situ stress measurements in exploratory boreholes. *Felsbau - Rock and Soil Engineering,* pp. 39-47.

Eberhardt, E., Stead, D. and Stimpson, B. (1999) Effects of sample disturbance on the stress-induced microfracturing characteristics of brittle rock. *Can Geotech. J.,* (36) 239-250.

Enever J.R., Walton R.J., and Windsor C. (1990) Stress regime in the Sydney Basin and its implication for excavation design and construction. *Inst. Eng. Aust. VII Tunnelling Conf*., Sydney, pp. 49-59.

Enever J.R. (1999) Near Surface In-situ stress and its counterpart at Depth in the Sydney Metropolitan Area. Hobart, *Australian Geomechanics Journal*, pp. 591-597.

Enever J.R. (2008) A life in stress – the Reliability of Rock Stress Measurements, *EAGCG meeting 'Stress Measurements, Monitoring and Modelling Techniques and their Design Applications'*

Fairhurst C. (2003) Stress estimation in rock: a brief histroy and review. *International Journal of Rock Mechanics and Mining Sciences,* pp. 957-973.

Fairhurst C. (1986) In situ stress determination – an appraisal of its significance in rock mechanics. *Proc. Int. Sym. Rock Stress and Rock Stress Measurements*, Stockholm

Hakala, M. (1999) Numerical study on core damage and interpretation of *in situ* state of stress. Posiva 99-25.

Hakala, M. (2006) Quality control for overcoring stress measurement data. Posiva 2006-03.

Hewitt P.B., McQueen L. and Davies P. (1999) Genting Centre, Sydney - Deep Excavation Adjacent to Railway Tunnels. *Proceedings of the 8th Australia New Zealand Conference on Geomechanics,* pp. 611-617.

Hooker V. and Bickel D.L. (1974) Overcoring equipment and techniques used in rock stress determination, *USBM Circ. 8618*.

Hudson J.A. (2012) The next 50 years of the ISRM and antcipated future progress in rock mechanics. In: *Harmonising Rock Engineering and the Environment.* London: Taylor and Francis Group, pp. 47-55.

Hudson J.A. (1993) Rock Properties, Testing Methods and Site Characterisation. *Comprehensive Rock Engineering, Vol. 3*, Ed. John Hudson, Pergamon Press.

Ljunggren,C., Yanting Chang, Janson, T., Christiansson, R. (2003) An overview of rock stress measurements methods. *I. J. Rock Mech. Mining Sci*., (40) pp. 975-989.

Lundholm, B. E. and Nordlund E. (2000) The effect of overcoring on elastic properties and evaluated stress components. GeoEng2000, *ISRM International Symposium*, 19-24 November, Melbourne.

Mills K.W. (1997) In Situ Stress Measurement using the ANZI Stress Cell, *Rock Stress*, Edited by Sugawara & Obara, Balkema, Rotterdam.

Mills K., Zoorabadi M., Puller J. (2016) A Strategy to Compensate for Axial Strains Induced by Drilling During Overcoring. *7th International Symposium on In-Situ Rock Stress*, Finland.

McQueen L. (2004) In situ rock stress and its effect in tunnels and deep excavations in Sydney. *Australian Geomechanics Society*, pp. 43-58.

McQueen L.B., Bewick R.P., Sutton J. and Morrow A. (2017) Stress-induced Brittle Failure of the Hawkesbury Sandstone – Case Study from Crack Initiation to Tunnel Support. Australian Tunnelling Society, ATS2017, *16th Australian Tunnelling Conference.*

Oliveira D.A.F. and Wong P.K. (2012) Selection of Rock Mass Design Parameters for Assessing Excavation Induced movements in the Sydney CBD. *Proc. ANZ Conf. Melbourne*.

Pells, P.J.N. (1990) Stresses and displacements around deep excavations in the Sydney area. *Australian Tunneling Conference*, Institute of Engineers Australia, pp. 241-249.

Pells P.J.N. (2002) Developments in the design of tunnels and caverns in the Triassic rocks of the Sydney region. *Int. J. Rock Mech. & Mining Sciences*.(39) pp. 569-587.

Pells P.J.N. (2004) Substance and Mass Properties for the Design of Engineering Structures in the Hawkesbury Sandstone. *Australian Geomechanics Society*, pp. 1-21.

Perras, M.A. & Diederichs, M.S. (2014) A review of the tensile strength of rock: concepts and testing. *Geotechnical and Geological Engineering*, (32) pp. 525–546.

Sjoberg J., Christiansso R. and Hudson J.A. (2007) ISRM Suggested Methods for rock stress estimation - Part 2 Overcoring methods. *The Complete ISRM Suggested Methods for Rock Characterization, Testing and Monitoring:1974-2006.*

Stacey T. (1981) A simple extension strain criterion for fracture of brittle rock. *International Journal of Rock Mechanics and Mining Sciences and Geomechanical Abstracts*, pp. 469 – 474.

Stephansson, O. and Zang A. (2012) ISRM Suggested Methods for rock stress estimation - Part 5: Establishing a Model for the In Situ Stress at a Given Site. *Rock Mech.Rock Eng*. Springer,

STANDPIPE PIEZOMETER INSTALLATIONS - LESSONS LEARNT

Sven Thorin[1], Angus McFarlane[2], Alasdair Hamilton[3]

[1]Principal Geotechnical Engineer AECOM Australia Pty Ltd sven.thorin@aecom.com,
[2]Senior Hydrogeologist, AECOM Australia Pty Ltd,
[3]Manager, Terratest Pty Ltd

ABSTRACT

Standpipe piezometer installations are frequently commissioned as part of site investigations to monitor groundwater levels and chemistry. On a recent site investigation for a large tunnel infrastructure project in Sydney, Australia, 15 standpipe piezometers were installed and developed. Some of the well screen depths exceeded 100 m below ground surface. Several of these wells, especially the deeper ones, returned unexpectedly high pH values after development and sampling. The values were potentially misleading for the assessment of infrastructure durability and environmental impacts.

A hypothesis for these high pH readings was the potential ingress of the cement-bentonite grout in the annulus to the standpipe piezometer via the bentonite seal and/or the casing threads. The latter was confirmed by borehole imaging. Following this observation, a literature review and trials were carried out to investigate the impacts of typical well construction methodology and materials on the pH of the groundwater sampled. In particular, threads from several PN18 nominal pressure rated casing were tested, with their elastomeric joints, at different confining pressures. The effectiveness of the bentonite seal above the screened section was also tested by varying curing time and seal thickness for different overburden pressures. This paper discusses the results of these trials and describes measures to reduce the risk of groundwater contamination induced by cement-bentonite grout leakage.

1 INTRODUCTION

Well installations are frequently commissioned as part of site investigations to monitor groundwater levels. These usually take the form of standpipe or vibrating wire piezometers. Standpipe piezometers constructed with 50 mm internal diameter (DN50) casings are particularly common as they are economical and enable both instrumented groundwater level monitoring and sampling.

During a recent site investigation for a large road and tunnel infrastructure project in Sydney, Australia, Terratest Pty Ltd (Terratest) and AECOM Australia Pty Ltd (AECOM) installed standpipe piezometers following standard industry practice. Terratest is an experienced site investigation contractor and has installed more than 10,000 wells in Australia in the last 20 years. AECOM's ground engineering, hydrological and environmental teams have delivered many large geotechnical and environmental site investigations that have included monitoring well design and installation.

Most of the piezometers installed as part of this project were screened within the Hawkesbury Sandstone, a medium to coarse Triassic sandstone, with the base of the screens varying from 20 m to 140 m below ground surface. Groundwater quality was tested in the field during piezometer development and during the monthly groundwater contamination sampling regime. Several of these wells, especially the deeper ones, returned pH (potential of Hydrogen) readings well in excess of the 5 to 8 range expected. A hypothesis for the high pH values measured in the sampled water was the potential ingress of the cement-bentonite grout in the annulus to the standpipe piezometer via the casing threads and/or the bentonite seal. Ingress via the casing threads was confirmed by borehole imaging. Subsequent trials and a literature review were conducted by the authors to investigate the impacts of typical well construction methodology and materials on the pH of the groundwater sampled.

This paper presents current well design and installation practices in Australia, and then describes project-specific groundwater quality testing results. Measures to reduce the risk of groundwater contamination induced by cement-bentonite grout leakage are then presented.

2 TYPICAL WELL DESIGN AND INSTALLATION PRACTICE IN AUSTRALIA

2.1 TYPICAL WELL DESIGN

An example of a standpipe piezometer is shown in Figure 1. The standpipe is typically made of unplasticised Polyvinyl Chloride (PVC-U), and is a continuous casing which is locally slotted to form a well "screen" along the section of

aquifer of interest. The annulus adjacent to the screen is filled with a filter pack of uniform gravel or sand to allow the water of the targeted aquifer to rise hydrostatically in the standpipe. Above and below the filter pack, bentonite seals can be constructed to avoid contact with the annulus grout and isolate the target formation. The annulus section above is backfilled with cement-bentonite grout until close to the surface, where a bentonite seal typically avoids surface water ingress. A sump can be constructed under the screen with a PVC cap and a blank casing riser to capture fines without blocking the slotted screen.

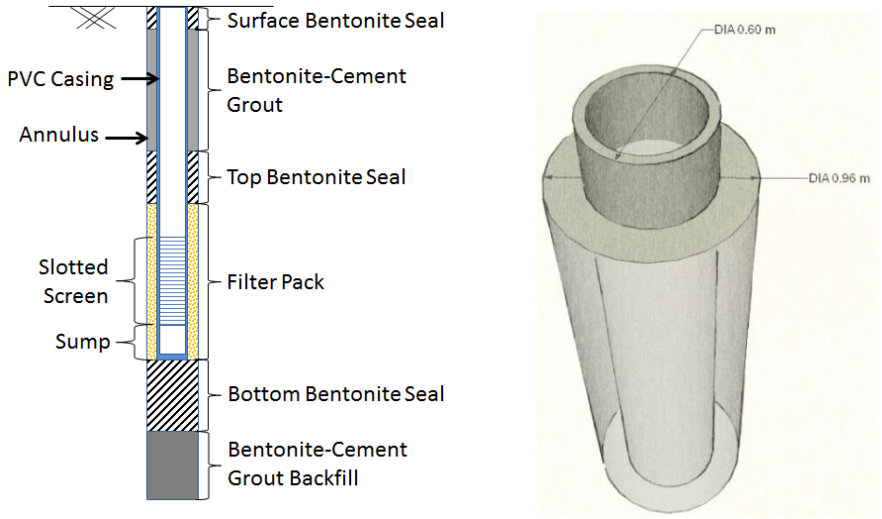

Figure 1: Typical 50 mm internal diameter (DN50) standpipe piezometer in 96 mm diameter (HQ) hole

2.2 STANDARD REQUIREMENTS

Boreholes and monitoring wells in Australia are typically constructed in accordance with the methodologies and practices outlined in NULDC 2012. Selected mandatory requirements of particular relevance to this paper are:

- PVC-U casing must comply with AS/NZS 1477:2017 (AS1477)
- The casing and casing joints shall "withstand the pressures imposed during the installation and operation of a water bore" and "all casing joints shall be aligned, secure and leak-proof"
- The cement grout annulus should have a minimum annular thickness of 15 mm (20 mm if artesian) above the maximum diameter of the casing to provide "adequate clearance"
- Bentonite pellets/chips shall only be used below the fluid level when sealing the annulus.

Additionally, the casing should be centred in the hole by means of centralisers at the top and bottom of screen and at a maximum spacing of 6 m for "long lengths". The annular thickness must be greater than four times the graded size of the filter sand or gravel. There is no specific requirement for bentonite seals.

2.3 TYPICAL MATERIALS AND INSTALLATION METHODOLOGY

The initial step is to drill and flush the borehole. Geotechnical drilling typically consists of non-destructive drilling, augering above the water table in soil, rotary non-core with casing advance below the water table in soil, and coring in rock. Environmental drilling often uses direct push drilling techniques instead of augering to avoid mixing contamination. Rock is typically cored with triple-barrel wireline HQ3 (96 mm hole diameter). Once the drilling is complete, the hole is flushed by pumping fresh water into the hole until clean water runs from the top of the borehole to reduce the likelihood of contamination of the groundwater by drilling chemicals, polymer and sediment.

The well installation methodology then consists of backfilling the base of the hole (if required), installing the PVC casing and backfilling the annulus. Typical materials and installation methodology are summarised as follows:

2.3.2 Casing

Casing is usually AS1477 Series 1 white DN50 PVC-U rated to a nominal pressure of PN12 or PN18, corresponding to respective nominal internal working pressures of 1200 kPa and 1800 kPa at 20° C.

This casing is typically installed in 3 m long sections, which are clamped and assembled during the installation down the hole. AS1477 describes two types of moulded spigot and socket (bell) joints for Series 1 casing: solvent cement

jointing (SCJ) and elastomeric seal joints, also called rubber ring joints (RRJ). In practice, typical piezometer casings joints are however Male/Female (M/F) threads with an O-ring, rather than moulded joints (Figure 5).

Centralisers are rarely used. Depending on the contractor, the drilling rig availability and the casing length, the casing either rests at the base of the hole or is suspended from the ground surface. Once the PVC casing is installed, the annulus is backfilled with a filter pack, bentonite seals and cement-bentonite grout.

2.3.3 Filter pack

The annulus adjacent to the screen is filled with a filter pack that is usually composed of uniform coarse sand and fine gravel ranging from 2 mm to 4 mm. The maximum size of the particles is limited by the (radial) annular thickness and the grainsize of the aquifer. The filter pack usually extends 0.5 m to 1.0 m above and below the screen, creating a buffer zone, to avoid swelling of the bentonite seal in the slotted screen and allow for settlement of the filter pack. Filter socks, which slide over the screen to keep out fines, are generally not used due to the risk of clogging by algal growth.

2.3.4 Bentonite Seal

Subject to well design, a bentonite seal can be installed in the annulus above and below the filter pack to create a relatively impervious barrier between the cement-bentonite grout and the filter pack. Compressed bentonite pellets or chips are used as bentonite powder is not appropriate to create a seal (Mikkelsen 2002). When hydrated, these swell and can reach hydraulic conductivities of 10^{-10} m/s (Mikkelsen 2002). Pellets used for bentonite seals are generally coated to retard the start of the hydration so they can reach the intended depth of the seal prior to swelling. In practice, the bentonite seal is typically 0.5 m to 1.0 m thick where present and left to hydrate from 45 minutes to 1.5 hours. Frequently, no water is added down the hole to help hydration, unless water loss occurred during drilling.

Pellets are usually placed in the annulus by hand from the surface (gravity method) or poured down a polypropylene pipe. The hand installation is often far quicker but can lead to bridging off of the pellets in the annulus above the intended depth of the seal, even if coated (Kaempffer 2003). Once bridging has occurred, there is no option but to redrill (Mikkelsen 2002).

Dropping the pellets via a tremie pipe to the required depth mitigates the risk of annulus bridging and is often used below 30 m or in challenging installation environments (e.g. artesian flow). To limit pipe blockage, the pellets must be placed slowly. A pump can usually clear pipe blockage. The tremie pipe diameter typically exceeds the annular space and has to be flattened as it is lowered. To place the tremie pipe at the correct depths, it is often secured to the PVC casing during installation, about 2 m above the target depth. The tremie pipe is usually removed after installation of the seal to avoid acting as a conduit for gas or water.

2.3.5 Cement-Bentonite Grouting

Cement-bentonite grouting is typically carried out in the annulus above the screen section/bentonite seal, but also in the annulus below the screen section/bentonite seal in the case of a sump. If the base of the borehole is substantially deeper than the depth of the screen, the bottom grout is left to set overnight prior to placement of the standpipe.

The grout typically comprises water, cement and bentonite powder. The cement increases the compressive strength of the grout and reduces the swelling of the bentonite. The bentonite quickly decreases hydraulic conductivity of the grout, increases the viscosity of the mix and also its stability by preventing segregation of the cement particles (“bleeding”) (Mikkelsen 2003). The grout can have highly variable properties depending on the proportions of the constituents and the mixing process (Bruce 1997). Typically, drillers use a bentonite/cement mass ratio ranging from 3 % to 5 % for borehole and annulus backfilling. However, this ratio can reach 30 % when proportions of 2.5 (water) to 1 (cement) to 0.3 (bentonite) are used, as proposed by Mikkelsen 2003 for fully grouted piezometers.

Two approaches can be used by the drillers to prepare the cement-bentonite grout. Mixing bentonite and water first, then adding cement, is more economical (Mikkelsen 2002) and enables an ideal pH range for bentonite hydration (Kelessidis *et al.* 2007). Mix ratios presented in NUDLC, 2012 are based on this method. However, hydrating and shearing the bentonite early increases viscosity, which decreases pumpability and limits working times. The typical approach is therefore to initially mix cement and water, which enables to control the stiffness and strength of the grout first and then adjust the hydraulic conductivity and viscosity by increasing the quantity of bentonite (Mikkelsen 2002).

Ideally, a colloidal mixer should be used to quickly produce a homogeneous mix. However, common practice is to use a flexible drive pump suction line and output in the same tank. An additional positive displacement pump can be used to deliver the grout to the hole via the tremie pipe. Tremie pipes should be slightly raised during each batch volume to keep pumping pressures as low as possible (Mikkelsen 2002) and rinsed prior to retrieval to avoid grout smearing.

2.4 TYPICAL WELL DEVELOPMENT METHODOLOGY

Groundwater monitoring wells are usually developed using either disposable polyethylene bailers, submersible pump or by air lifting. Submersible pumps are generally suitable for well development above 30 m, but air lifting methods should be preferred when significant amounts of sediment are expected. Compressed air can be used effectively when the casing is connected to a PVC T-piece to divert the purge water down to a drum and the air pressure is slowly increased until a steady stream of purge water is lifted. The wells should be purged until returned groundwater is sediment-free. However, often the wells are bailed dry and left to recharge until three well volumes are completed.

3 PROJECT GROUNDWATER QUALITY TESTING

3.1 BACKGROUND

The Hawkesbury Sandstone in Sydney is a medium to coarse grained quartzose sandstone of the Triassic period. This 200 m thick formation acts as a semi-confined dual porosity regional aquifer typically varying from acidic to slightly alkaline (pH of 5 to 8) and is probably influenced by leakage from the saline groundwater present in the overlying Wianamatta Group shales and mudstones, where present (Hawkes *et al*. 2009, McLean & Ross 2009).

3.2 METHODOLOGY

Along the project alignment, 15 standpipe piezometers were installed in HQ3 boreholes by two highly experienced and licenced groundwater drillers under the direction of experienced field engineers. Of the piezometers, 12 were screened in the Hawkesbury Sandstone, while the others were screened in fill and alluvium. The piezometers were installed using standard monitoring well installation techniques and the materials below:

- Casing: DN50 PN18 PVC-U manufactured by Waterscreens Pty Ltd in 3 m or 6 m long M/F threaded sections with an O-ring, machine slotted to 0.5 mm
- Filter pack: 2 mm Boral Blue Circle Specialised Sand extended by 0.5 m to 2 m above and below screen
- Cement-bentonite grout: bentonite/cement mass ratio varying from 5% to 30%. Boral Blue Circle General Purpose Cement and Halliburton Aquagel bentonite powder
- Bentonite seals: 6.35 mm Pel-Plug TR30 natural sodium bentonite pellets, mined in Texas, single-coated in order not to stick together for up to 30 minutes when poured in standing water.

Bentonite pellets were dropped by hand for wells shallower than 40 m and tremied for deeper wells. No water was added for hydration. Centralisers were installed at 9 m intervals in some of the initial deeper wells (BH1, BH4, BH5) but only two were placed above and below the screen in the other wells following issues with lowering the tremie pipe.

Development by air lifting and pumping was carried out until three well volumes of water were removed from the monitoring well. Due to consistently slow recharge conditions in most wells across the alignment (no level changes within 10 minutes during slug testing except in BH7), multiple development rounds were required over several days.

3.3 GROUNDWATER QUALITY TESTING RESULTS

Groundwater samples were retrieved with a bailer and field parameters including Electrical Conductivity (EC) and pH were measured using a calibrated and decontaminated water quality meter. The field-testing of 8 of the 15 piezometers, described in Table 1, indicated higher-than-expected pH values. Figure 2 shows the pH evolution for these piezometers. With the exception of BH1, elevated pH values remained high, even months after the end of development.

Table 1: Installation Details and pH and EC results

Well	Length (m)	Screen Section (m below ground level)	Backfill (below sump)	Seal thickness (m)		After development		Long-term	
				Top	Base	pH	EC (mS/cm)	pH	EC (mS/cm)
BH1	66.5	62.5 – 65.5	Pellets	1.0	n/a	9.6	1.42	5.5	1.35
BH2	49.7	45.7 – 48.7	Grout	2.1	1.0	11.2	1.75	n/a	n/a
BH3	137	121.0 – 127.3	Pellets	0.5	0.8	9.3	0.62	n/a	n/a
BH4	103.5	99.5 – 102.5	Grout	0.5	None	11.3	0.47	n/a	n/a
BH5	52.2	48.2 – 51.2	Grout	1.0	None	11.6	1.27	n/a	n/a
BH6	65.0	59.0 – 64.0	Pellets	4.1*	n/a	11.9	3.46	11.4	1.22
BH7	29.0	24.0 – 27.0	Pellets	2.0	4.0	9.6	1.43	11.3	0.80
BH8	139.0	135.0 – 138.0	Pellets	1.0	n/a	9.0	0.52	n/a	n/a

*left to cure for 12 hours

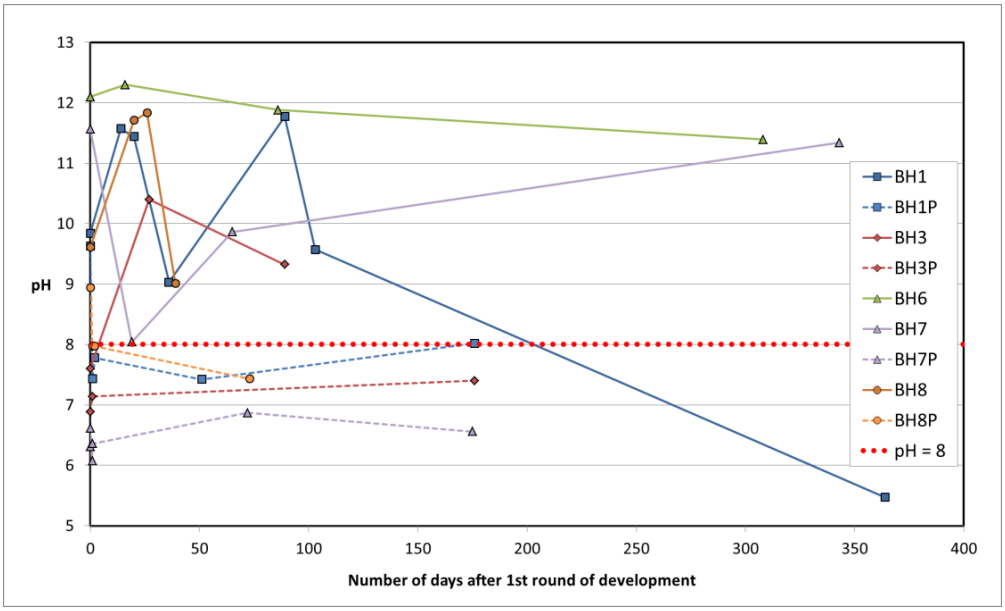

Figure 2: Groundwater pH readings during and after development

3.4 TELEVIEWER RESULTS AND REDRILLING

The elevated pH readings were not expected to reflect aquifer conditions but rather to be caused by direct or indirect contact with the installation materials. Nielsen 1991 states that even hard set grouts can bleed very alkaline water down into the well screen area. Cement contains calcium hydroxide, which has a pH of about 12.4, and is therefore expected to be the most likely material to impact the pH readings. Based on the absence of water-bearing discontinuities in the rock between the annulus grout and the screen in the eight piezometers, the most probable contact mechanism between the grout and the sampled groundwater is either an absent or ineffective bentonite seal, or ingress inside the casing from the annulus via the threads or a fissure in the casing.

To investigate potential grout ingress, Terratest completed post-development downhole optical televiewer imaging inside the PVC casing in BH3 and BH6. The imaging in BH3 (Figure 3) suggests a breach of casing thread by dark material, expected to be cement-bentonite grout from the annulus, at 65.2 m and 68.4 m below top of casing. The quality of the water did not enable confirmation of leakage via the deeper threads. The casing also seemed full of grout from 112 m to 120 m. The imaging in BH5 showed material from 62.8 m to the base of the casing. The annulus was backfilled with grout only above 55 m, suggesting leakage from either a shallower thread or the bentonite seal.

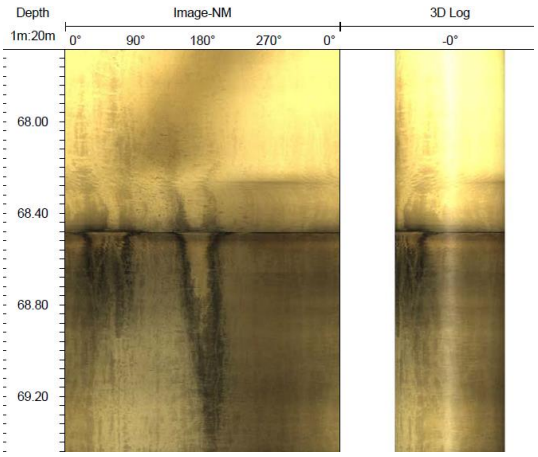

Figure 3: Evidence of material ingress through PVC thread in BH3

Four selected wells were redrilled at about 10 m from their original position and extended about 1 m below the required screen depth. The filter pack was installed from the base of the 1 m sump interval to at least 2 m above the top of the screen. A 2 m thick bentonite seal was installed above the filter pack and left to hydrate for at least 2 hours. The

remaining annular space was sealed with bentonite pellets installed in multiple batches of maximum 30 m thickness, each allowed to hydrate for at least 2 hours. No bentonite-cement grout was used.

These wells are labelled with a "P" suffix on Figure 2. Despite similarly slow recharge compared to the original wells, the measured pH stayed within a 6 to 8 range after development, confirming that the high pH of the original wells did not reflect true aquifer conditions and were likely to be due to contact with bentonite-cement-grout.

Whilst this methodology was apparently successful, the approach of replacing the cement-bentonite grout with pure bentonite pellets is time-consuming, can create substantial external pressures on the PVC casing due to swelling, and can cause issues if intersected during construction (e.g. tunnelling blowout). Pure bentonite is not volumetrically stable (Mikkelsen 2002) and can be affected by the water chemistry, even after curing. Trials were therefore carried out and lessons learnt are presented in the following section.

4 FIELD TRIALS AND LESSONS LEARNT

The impact of the piezometer installation methodology on the pH of the sampled groundwater was investigated both through a literature review and trials. The tests were completed using the project materials listed earlier and are relevant to single standpipe piezometers. The findings were not correlated with the project-specific results due to the number of unknowns and the variability of the readings.

4.1 IMPACT OF DRILLING ON WELL PERFORMANCE

4.1.1 Drilling diameter

The external diameter of DN50 casing varies from 60.2 mm to 60.5 mm. DN50 PN18 casing requires a wall thickness of about 5 mm, leading to an average internal diameter of 50.5 mm. Assuming that the casing is centred, the resultant annular thickness is only 18 mm in an HQ borehole. Despite fulfilling NUDLC 2012 requirements, this annular thickness can impede annulus backfilling by preventing the lowering of the tremie pipe and increases the risk of bridging. Besides, using 6.35 mm diameter bentonite pellets in such an annular thickness exceeds the recommendations from DEP 1992 to limit pellet size to a fifth of the annular thickness. Installing DN50 in HQ borehole also precludes the use of moulded spigot and socket joints due to the increase in external diameter at the socket.

Most available guidelines recommend a minimal annular thickness of 50 mm or 60 mm (e.g. EPA 2013, DPI 2010). For a M/F threaded DN50 casing, this would require reaming the borehole diameter to 160 mm. If this is not practicable, we recommend reaming boreholes to at least 123 mm (PQ) diameter if the screen base exceeds 30 m.

4.1.2 Borehole depth

The difficulty of successfully installing a well increases with borehole depth. Standpipe piezometers are often installed in existing geotechnical boreholes which are deeper than the target zone, requiring backfilling of the base with cement-bentonite grout. The economy of using an existing hole compared to redrilling an adjacent well terminating at the base of the target zone should be balanced against the risk of grout ingress along the walls of the borehole during backfilling, the grout curing time (unless a plug is installed) and the additional flushing required. As outlined above, reaming the borehole prior to well installation should also be considered in deep wells.

4.1.3 Flushing

Insufficient flushing is common and negatively impacts optical televiewer imaging and well development. As well as installing the surface casing deep enough to avoid material ingress, it is recommended that at least 1000-2000 L of clean potable water are available and that the well installation is carried out at least two hours after water pressure testing if the losses exceed one Lugeon. Flushing should be completed before and after any bottom backfilling.

4.1.4 Construction records

As-built details cannot be checked post installation and should be recorded during each installation stage and signed by the drillers. Whilst the thicknesses of the backfilling sequence are usually measured at each stage, the details of the installation methodology are often not recorded. These should include type and brand of all materials used, position of any centralisers, bentonite seal installation methodology and curing time, grout mix proportions and mixing methodology and a comparison of calculated and actual material quantities to identify potential bridging.

4.2 IMPACT OF BACKFILLING MATERIALS

The filter pack and bentonite are in direct contact with the aquifer and were investigated to assess if these materials could have impacted the pH of the groundwater drawn into the casing.

4.2.1 Filter pack

The Safety Data Sheet for the Boral Blue Circle Specialised 2 mm Sand states that the quartz content is more than 60% but no information could be found on the potential other constituents or the pH range. The addition of 100 grams of sand to 250 cm^3 of tap water was found to increase the pH from 6.7 to 7.5 in 10 minutes, decreasing to 7.4 after 3 hours. Six tests on three different batches of sand also confirmed that the sand is only slightly alkaline. This suggests that the sand is not likely to have caused the high pH measurements.

4.2.2 Bentonite

Na-bentonites are alkaline due to the formation of sodium hydroxide (NaOH) in water. The typical pH range of natural Na-bentonites is 9 to 10 and the material data sheet for the Pel-Plug TR30 used on the project reports a pH ranging from 7 to 11 in a 0.5% solution (PDS 2017). Na-bentonites were found to increase the pH of a solution for at least several months, even in relatively small concentrations (Muurinene & Clarsson 2013). The evolution of the pH was recorded after adding 15 grams of Pel-Plug TR30 pellets to 225 cm^3 of tap water. Results are presented in Table 2 and show a significant pH increase within the first hour, followed by stabilisation. Similar proportions of Na-bentonite in various solutions increased the pH from about 8.2 to more than 9 even after 3 months (Melamed & Pitkanen 1996).

Table 2: Impact of Pel-plug TR30 bentonite on solution pH

Time after addition	0 s	30 s	1 min	5 min	10 min	20 min	1 h	24 h	48 h
pH	6.14	6.23	6.38	8.05	8.80	9.19	9.53	9.74	9.35

The recorded increase in pH could explain the wells with a slightly alkaline pH but does not explain the pH>11 occurrences. Bentonite seals are in direct contact with the filter pack in most wells and further testing would be required to assess the impact of a real-scale hydrated bentonite seal on the pH of the sampled water pH at various recharge rates.

4.3 PERFORMANCE OF BENTONITE SEAL

4.3.1 Lack of bentonite seal

Well designers do not often require a bottom bentonite seal between the cement-bentonite grout and the filter pack. To investigate the impact of the lack of a bentonite seal, a vertical 4 metre long piezometer was constructed within a Class 12 DN100 PVC-U casing (representing the hole) using the project methodology and materials presented previously but with no bentonite seal. The filter pack was saturated with tap water with a pH of about 6.5. Within an hour, the pH of the water sampled reached 11.9, reflecting the pH of the calcium hydroxide contained in the cement-bentonite grout.

Bentonite pellets should typically only be placed below groundwater level (NULDC 2012) due to hydration and desiccation. Neat cement or bentonite-cement grouts can have sufficiently low hydraulic conductivities compared to the aquifer to act as a seal. However, we recommend the systematic placement of bentonite seals between any cement-containing grout and the filter pack to limit surface contact between the cement and the water in the screen. WRP 1993 recommends installing a 150 mm thick bentonite seal above the filter pack if the screen if above the water table.

4.3.2 Bentonite seal hydration

As discussed above, bentonite chips or compressed pellets are used to form seals above and below the filter pack. Often, water is not added down the annulus to hydrate the bentonite, unless water loss occurred during drilling. However, the water levels in the annulus at the time of placement might not be sufficient to hydrate the seal. This section summarises why the addition of soft water during installation is usually required to successfully create a seal.

The hydraulic conductivity of the bentonite decreases with swelling (Pusch *et al.* 2010). The expected swelling mechanism of bentonite is described by Savage 1999, Tripathy 2004, Morodome & Kawamura 2009, Ferrage *et al.* 2010, Hensen & Smit 2002, Svensson 2015, Ahmed *et al.* 2015.

The swelling behaviour of bentonite is explained by its mineralogy. By definition, the main component of bentonite is montmorillonite, which is an aluminium phyllosilicate clay mineral with a 2:1 structure: each clay platelet comprises one aluminium octahedral sheet sandwiched between two silica tetrahedral sheets. Isomorphic substitutions in the octahedral and tetrahedral sheets (Lavikainen, 2016) create a negative charge along the surface of the platelet. This charge inequality is balanced by cation exchange in an interlayer between the clay platelets.

The first type of swelling to occur, called “crystalline” swelling, is an increase in the thickness of this interlayer due to the adsorption of water molecules in the interlayer. The thickness of the interlayer increases in steps with moisture content and can double when four layers of hydration are reached.

Once the interlayer has reached a certain thickness, another process called “diffuse double-layer” swelling is expected to occur. This swelling is caused by the difference in concentration between the cations close to the surface particles and of the solution, creating an osmotic pressure. Importantly, the thickness of the diffuse double-layer decreases with

the electrolyte concentration of the water solution and the valence of the cations. The first point entails that to enable swelling, the bentonite should be hydrated with soft water. The second is that Na-bentonite, containing mostly monovalent sodium Na^+, will, at a given water content, swell more than Ca-bentonite, containing mostly divalent calcium Ca^{2+}. Na-bentonite is therefore typically used to create seals.

Na-bentonites can be natural or sodium activated. Natural Na-bentonites are mined and rarely monoionic. PDS Pel-plug TR60 (similar to TR30 but with double-coating) cations were found to be 60% sodium and 30% calcium (RWM 2016). Alternatively, Ca-bentonite can be activated by adding sodium to improve the swelling properties by exchanging Ca^{2+} for Na^+. In a similar process, contact between the Na-bentonite with material containing divalent cations, such as hard water present in the ground or cement from the grout, can greatly decrease the swelling and increase the hydraulic conductivity of the seal. This ion exchange will occur even after bentonite hydration, for the life of the seal (Benson & Meer 2009, Melanmed & Pitkanen 1996). Hydration with soft water is therefore essential for good seal performance.

Hydration is also influenced by the thickness of the bentonite layers. RWM 2016 tested hydration of bentonite pellets placed in columns and found that the swelling occurred mainly in the top 50 mm to 100 mm. This is expected to be due to the limited access to water for the underlying pellets following the swelling of the top pellets. We therefore recommend to place and hydrate bentonite pellets in batches, for instance 0.5 m thick.

4.3.3 Groundwater Salinity

Despite not being usually checked prior to piezometer installation, groundwater salinity can have a detrimental effect on the performance of the bentonite seal.

In Sydney, the salinity of the Hawkesbury Sandstone aquifer is typically higher in its upper part, particularly where it is overlain by the Wianamatta Group shales. Measured Electrical Conductivity (EC) readings can be as high as 1.7 mS/cm but typically decreasing with depth to about 0.3 mS/cm (McLean & Ross 2009). The shales from the Wianamatta Group are generally saline and in the range of 5,000 to 50,000 mg/L – total dissolved solids (McNally 2009) which corresponds to approximately 8 mS/cm to 80 mS/cm. However, much higher values can be expected when the aquifer is hydraulically connected to saltwater, such as in joint swarms associated with faulting close to Sydney Harbour.

As discussed previously, the diffuse double-layer swelling decreases with the valence of the cations and the electrolyte concentration in the water solution. This swelling can be suppressed in relatively saline solutions (Rao *et al.* 2013, Shirazi *et al.* 2011). With a compressed or inexistent diffuse double-layer, attractive forces cause the clay particles to flocculate, effectively disintegrating the pellets and increasing the hydraulic conductivity of the seal.

Dispersion and flocculation depend on the soil's Electrical Conductivity (EC) and Sodium Absorption Ratio (SAR). The SAR is the ratio of the Na^+ concentration divided by the square root of the Ca^{2+} and Mg^{2+} concentration (in mmol/L). The bentonite will flocculate if the SAR decreases but also if the EC increase. Even a soil with a SAR higher than 13 will tend to flocculate if the EC is more than 4 mS/cm (EMU). A study on bentonite pellets by RWM 2016 concluded that the EC has a greater influence on the stability of the clay than the SAR.

The coating from coated bentonite pellets was found to slow but not suppress flocculation in various saline solutions (RWM2016). After 10 minute exposure in an 0.1M (about 10 mS/cm) solution, Pel-plug uncoated pellets were almost completely disintegrated. Single coating coated pellets (Pel-plug TR30) were highly disintegrated in a 1M (about 100 mS/cm) solution after 10 min. Even double-coated pellets were highly disintegrated in a 0.1M (about 10 mS/cm) solution after 30 min. Disintegration of the pellets reduced their sinking speed, increasing the risk of bridging.

We therefore recommend measuring the groundwater salinity after borehole flushing and recharge. If the salinity is high enough to compromise the effectiveness of the bentonite seals, neat cement can be used as a seal at certain water/cement ratios (NUDL 2012) but the groundwater pH readings will be affected. A similar approach should be taken in contaminated sites, as certain chemicals such as hydrocarbons are known to affect bentonite (Nielsen 1991).

4.3.4 Bentonite seal thickness and hydration time

Typically, bentonite hydration times varied from 45 minutes to 1.5 hour on the project. However, Pel-plug recommends a minimum of 4 hours (PDS 2017). This recommendation is not generally displayed on the containers or bags but can be found on an online data sheet that only a few suppliers provide on their website.

The curing duration should conservatively start after the pellets have reached the base of the hole. The average sinking rate of pellets in water is 0.30 to 0.45 m/s (RWM 2016).

To assess the impact of the thickness of the top bentonite seal and its curing time, a vertical steel or PVC-U HWT (102 mm internal diameter) casing with pressure sealed end caps was packed with 2 mm diameter wet sand. A bentonite seal of varying thickness was installed (Figure 4). The bentonite seal was hydrated and allowed to cure for various durations before cement-bentonite grout was added and pressurised for a nominal duration of 25 minutes to simulate overburden.

A sample of the water from the filter pack was then analysed in the field with a water quality meter. Results are presented in Table 3.

Figure 4: Bentonite seal testing (Left, Middle); PVC thread testing (Right)

Table 3: Bentonite Seal Pressure

Seal thickness (m)	Seal Curing time (min)	Grout Pressure	Equivalent grout head (assuming 14 kN/m^3)	Breaching comments (original water pH: 6.8)
0.5	45	760 kPa (110 psi)	54 m	No breach observed (pH = 8.8*)
0.5	120	1240 kPa (180 psi)	89 m	Breach (pH = 11.2)
2.0	120			No breach observed (pH = 8.1*)

*expected to be due to the Na-bentonite

More testing would be required to characterise the behaviour of 0.5 m and 2 m thick bentonite seals at a range of pressures. However, this preliminary testing suggests that even after curing for 2 hours, a 0.5 m thick bentonite seal does not resist an overburden of 1240 kPa, corresponding to a grout head of 89 m. As a result, we recommend a top seal thickness of at least 2 m with a minimum curing time of 2 hours for depths of screen base in excess of 50 m.

4.4 PERFORMANCE OF PVC CASING

4.4.1 Standard requirements

As discussed previously, AS1477 Series 1 DN50 (50 mm) PVC-U casing is typically used. AS1477 describes two types of moulded spigot and socket joints, rubber joints (RRJ) or solvent cement joints (SCJ).

SCJ exist in a wide range of nominal diameters and ratings and require Type P (for Pressure) solvent cements compliant with AS/NZS 3879. However, solvent cements are usually proscribed as some of the solvents can migrate in the groundwater and affect its chemistry for months despite development (Barcelona *et al.* 1983). More testing would be required to confirm that the cement solvents used become inert once fully cured. AECOM observed no change in pH within an hour of adding 100 grams of solvent cement Type P in 250 mL of water with a pH of 6.6.

RRJ do not require solvents, but are typically manufactured to DN80 upwards and can require a lubricant and bactericidal fluid, potentially affecting hydrochemistry. Also, the annulus thickness, already reduced by the spigot, is further reduced by the thickness of the ring cavity. Rubber rings should comply with AS 1646.

As a result, casings are usually AS1477 DN50 PN18 or PN12 which is then threaded straight Male/Female and supplied with an O-ring, instead of moulded spigot and socket joints. The compression of the ring is meant to create the seal (fastening thread) since the threads are parallel to each other. NUDLC, 2012 recommends the use of a sealastic or flexible sealant for threaded PVC so that the joints are watertight. This is, however, not expected to be applicable to fastening threads.

AS1477 only briefly mentions threaded joints and states that the threads need to be of Whitworth form, and require a minimum number of fully engaged threads. For 50 mm diameter fastening threads, at least 4 full threads should be engaged. Reference is made to AS1722:2 for fastening threads in terms of type and dimensioning. AS1477 refers to various parts of AS1462 for testing joint performance, most of which are however relevant to socketed joints.

4.4.2 Manufacturing

Two major Australian casing manufacturers were approached. One manufacturer mentioned that, despite being widespread, the cutting of threads on PVC casings (without a moulded thread adaptor) is not an acceptable practice due to performance issues. As a result, they only provide moulded spigot and socket joints. Another manufacturer confirmed verbally that although their casings are rated to AS1477, they did not manufacture the threads and O-rings to any particular standard.

Threads from several manufacturers were counted and measured and were found to be inconsistent. The male thread varied in length across four DN50 casings by a total 4 mm deviation for a same manufacturer. The number of fully engaged threads was typically less than the minimum of 4 required by AS1477 for DN50 casing with fastening threads.

4.4.3 Trials

A 1.5 m long section of M/F threaded DN50 PN18 PVC-U casing was tested for both water and cement-bentonite grout breaching under varying external pressures. This casing section comprised one M/F threaded joint in the middle, with the 1.7 mm annular diameter O-ring supplied and two end caps. Primer and cement solvent was used to seal the end caps only. The caps were tested separately at 1725 kPa to ascertain that potential breaches would happen via the middle thread and not the end caps. The same operator applied torsion to the threads for consistency; however the torsion was not measured.

This casing section was placed in a horizontal custom-made steel pressurised HWT (102 mm internal diameter) casing. The annulus between the DN50 casing and the HWT casing was filled either with water with a blue dye, or cement-bentonite grout. The grout comprised 27.5 L of water, 20 kg of cement and 1 kg of bentonite (5% bentonite), yielding a 34 L mix with a unit weight of 14 kN/m^3. The pressure was applied to the water or the grout to a nominal 3 or 10 minutes.

The inside of the DN50 PVC casing was left empty: neglecting viscosity effects, the pressure applied to the middle joint was therefore equal to the pressure applied to the water or grout in the annulus.

Breaching examples are shown in Figure 5. The results in 00 m with a PVC full of water. To reduce the likelihood of a breach, it is recommended that the PVC casing should be filled with water during well installation until the annulus backfill has set.

Table 4 show water and cement grout consistently breaching between 795 kPa and 830 kPa, corresponding to a grout head of about 60 m with an empty PVC casing and about 200 m with a PVC full of water. To reduce the likelihood of a breach, it is recommended that the PVC casing should be filled with water during well installation until the annulus backfill has set.

Table 4: Water and grout breaching trials

Pressure applied to water in annulus	Pressure applied to grout in annulus
795 kPa (115 psi) for 10 min – NO BREACH OBSERVED 830 kPa (120 psi) for 10 min – BREACH* 860 kPa (125 psi) for 10 min – BREACH 135 psi, 150 psi, 175 psi, 220 psi for 10 min – BREACH 1515 kPa (220 PSI) for 3 min – BREACH* 1725 kPa (250 PSI) for 3 min – BREACH	795 kPa for 10 min – NO BREACH OBSERVED 830 kPa for 10 min – BREACH, grout solids visible 930 kPa for 10 minutes – BREACH, no solids 1725 kPa for 10 minutes – BREACH, grout solids visible

* water only on threads past O-ring, not in casing

Figure 5: M/F thread with O-ring: Water breach (Left); Grout breach (Middle, Right)

4.4.4 Use of centralisers

NULDC 2012 recommends centralisers above and below the screen at a maximum spacing of 6 m for "long lengths". However, pipe buckling under its own weight when resting on the base of the hole could lead to contact between the casing and the side of the borehole even above the screen, causing backfilling issues, which could compromise the integrity of the well and connect different aquifers. AECOM estimated the quantity of centralisers required due to self-buckling of a vertical DN50 PN18 PVC casing. Euler's critical load for a long slender column was calculated assuming a uniform modulus of elasticity of 3000 MPa and a unit weight of 13.6 kN/m^3. Results suggest that intermediate centralisers are required for casings longer than 11.5 m. The longer the pipe, the higher the axial loads and 50 and 100 m long casings would require a respective maximal centraliser spacing decreasing to about 5 m and 3 m at their base.

The conclusion of this theoretical exercise is that centralisers are required if DN50 PN18 PVC casing longer than 10 m is resting on the base of the hole, and that their required frequency increases substantially with casing length. The recommendation is to install one centraliser above and below the screen but also systematically suspend the casing from the ground surface until the annulus backfill has set.

5 SUMMARY AND CONCLUSIONS

Unexpectedly high pH readings of groundwater sampled in standpipe piezometers during a large infrastructure project triggered a review of current standpipe piezometer installation practice and identified potential issues with the manufacturing of PVC casing threads and areas of improvement for future installations. These recommendations are summarised in the table below.

Table 5: Standpipe piezometer installations - hazards and recommendations for future installations

Item	Hazard	Recommendations
Hole	Incorrect piezometer type selection	- Install fully grouted vibrating wire piezometers instead of standpipe piezometer unless groundwater sampling is required.
	Insufficient annular thickness	- Aim for 50 mm annular thickness if feasible - For DN50 PVC casing, ream HQ boreholes deeper than 30 m to PQ diameter (30 mm annular thickness) as a minimum
	Lack of flushing	- 1000-2000 L of clean water to be available on site - Flush before and after any bottom backfilling - Observe cleanliness of water return not just well volume
Casing	Leakage via M/F threaded joints	- Request evidence from casing supplier/manufacturer of M/F threaded joint compliance with existing standards and evidence of testing for leakage when submitted to a appropriate range of pressures - Fill casing with freshwater to decrease overburden via threads - Do not place clamp on thread - Use 6 m casing sections where feasible to limit number of joints
	Casing not centralised	- For lengths > 11 m, suspend PVC casing until the grout has set
Tremie	Smearing of grout along screen	- Rinse tremie prior to retrieval
Filter pack	Lack of specified pH	- Seek confirmation from supplier or check pH of filter pack
Bentonite	Bridging	- Use coated Na-bentonite pellets - Use tremie pipe to install pellets in holes deeper than 30 m
	High pH	- Be aware of the potential impact of Na-bentonite on pH
	Poor hydration	- Add soft water in the annulus during bentonite seal installation - Install seal in 0.5 m thick layers, hydrated separately
	Insufficient curing time or thickness	- Curing time of at least 2 hours and 2 m thick seal below 50 m - Install even above groundwater table
Groundwater	Groundwater salinity (and chemistry)	- Check groundwater salinity prior to well installation - Use alternative materials such as neat cement in saline environments
Records	Lack of information	- Record full installation methodology, not only as-built details

6 ACKNOWLEDGEMENTS

The Authors wish to thank the Roads and Maritime Services for authorising this paper and Graham Hawkes, Marco Rafanelli, Peter Waddell, Giovanny Alvarado, Antony Tam, Michael Cardell (AECOM) and Jon Maguire (Terratest).

7 REFERENCES

Ahmed A. A., Saaid I. M., Akhir N.A.M., Rashedi M. (2015), Influence of Various Cation Valence, Salinity, pH and Temperature on Bentonite Swelling Behaviour, International Conference on Advanced Science, Engineering and Technology (ICASET) 2015 IP Conf. Proc. 1774, 040005-1–040005-8;

Australian/New Zealand Standard AS/NZS 1462, Methods of test for plastics pipes and fittings

Australian Standard AS/NZS 1477:2017, PVC pipes and fittings for pressure applications, ISBN 978176035779 5

Australian Standard AS/NZS 1646:2007, Elastomeric Seals for waterworks purposes

Australian/New Zealand Standard AS/NZS 3879:2006, Solvent cements and priming fluids for PVC (PVC-U and PVC-M) and ABS casings and fittings, ISBN 0733778933

Barcelona M.J., Gibb J. P., Miller R. A. (1983). A Guide to the Selection of Materials for Monitoring Well Construction and Ground-Water Sampling, Illinois State Water Survey Department of Energy and Natural Resources Champaign, Illinois, SWS Contract Report 327.

Benson C.H., Meer S. R., Relative (2009). Abundance of Monovalent and Divalent Cations and the Impact of Desiccation on Geosynthetic Clay Liners, Journal of Geotechnical And Geo-environmental Engineering, ASCE, 10.1061/ASCE1090-0241 2009135:3 34.

Boral, Boral Blue Circle 2 mm Safety Data Sheet 30/07/2010

Bruce D.A., Littlejohn S., Naudts A. M.C. (1997), Grouting Materials for ground treatment, A Practitioner's guide, Grouting: Compaction, Remediation and Testing, Geotechnical Special Publication No.66, ASCE, January 1997

DPI (Department of Primary Industries) (2011), Standards/Guidelines for Installation and Management of Testwells and Piezometers, Implementation of the Mallee Regional Irrigation Development Guidelines – 2010/1, Victorian Mallee Irrigation.

DEQ (Department of Environmental Quality), State of Oregon, *Groundwater Monitoring Well Drilling*, *Construction, and Decommissioning* August 24, 1992

EMU (Eastern Mediterranean University), Flocculation and Dispersion, Lecture 12

Ferrage E., Lanson B., Michot L., Robert J-L. (2010), Hydration Properties and Interlayer Organization of Water and Ions in Synthetic Na-Smectite with Tetrahedral Layer Charge. Part 1. Results from X-ray Diffraction Profile Modelling, . Phys. Chem. C 2010, 114, pp. 4515–4526

Hawkes G., Ross J.B. and Gleeson L. (2009), Hydrogeological resource investigations – to supplement Sydney's water supply at Leonay, western Sydney, NSW, Australia IAH NSW, Groundwater in the Sydney Basin Symposium, Sydney, NSW, Australia, 4-5 Aug. 2009, W.A.Milne-Home (Ed) ISBN 978 0 646 51709 4.

Hensen E. J. M, Smit B., (2002). Why Clays Swell, University of Amsterdam, Nieuwe Achtergracht 166, 1018 WV Amsterdam, The Netherlands, 2002, J. Phys. Chem. B 2002,106, 12664-12667, 2002

Kaempffer (2003), Update on Bentonite chips and pellets for sealing piezometers in boreholes, Geotechnical News 21(4):32-37 December 2003.

Keledissis V. C., Tsamantaki C., Dalamarinis P. (2007), Effect of pH and electrolyte on the rheology of aqueous Wyoming bentonite dispersions, Appl. Clay Science.

Lavikainen L. (2016), The structure and surfaces of 2:1 phyllosilicate clay minerals, Department of Chemistry University of Eastern Finland, Finland.

McLean, W., Ross, J., Hydrochemistry of the Hawkesbury Sandstone Aquifers in Western Sydney and the Upper Nepean catchment, (20090. IAH NSW, Groundwater in the Sydney Basin Symposium, Sydney, NSW, Australia, 4-5 Aug. 2009, W.A.Milne-Home (Ed) ISBN 978 0 646 51709 4

McNally G., Soil and groundwater salinity in the shales of western Sydney. In: Milne-Home WA (ed.) Groundwater in the Sydney Basin Symposium. International Association of Hydrogeologists NSW, 228–233, 2009

Melanmed, A., Pitkanen P. (1996), Chemical and mineralogical aspects of water-bentonite interaction in nuclear fuel disposal conditions, Espoo 1996, Technical Research Centre of Finland, VTT Tiedotteita – Melanmed – Research Notes 1766. 41 p.

Morodome S. and Kawamura K., Swelling Behavior Of Na- And Ca-Montmorillonite Up To 150ºc By In Situ X-Ray Diffraction Experiments, Clays and Clay Minerals, Vol. 57, No. 2, 150–160, 2009

Mikkelsen, P.E. (2002), Cement-Bentonite Grout Backfill for Borehole Instruments. Geotechnical News, Vol.20, No.4, December: 38-42.

Mikkelsen, P.E., Green G.E., Piezometers in Fully Grouted Boreholes, Symposium on Field Measurements in Geomechanics, FMGM 2003, Oslo, Norway, September 2003

Muurinen A., Carlsson T. (2013). A Method for on-Line Measurements of pH in Compacted Bentonite, VTT Technical Research Centre of Finland.

NUDLC (National Uniform Drillers Licensing Committee) Minimum Requirements for Water Bores in Australia, Edition 3, 2012. ISBN 9780646569178

Nielsen D. M., (1991). Practical Handbook of Ground-Water Monitoring, Taylor & Francis Inc, ISBN 0873711246, March 1991.

PDS (2017). Pel-plug data sheet, http://pdscoinc.com/wp-content/uploads/2017/07/PEL-PLUG-TR30.pdf.

Pusch R., Kasbohm J. & Thao H.T.M. (2010). Chemical stability of montmorillonite buffer clay under repository-like conditions – A synthesis of relevant experimental data. Applied Clay Science , 47, 113–119.

Rao, S.M., Thyagaraj, T. & Raghuveer Rao, P. (2013). Crystalline and Osmotic Swelling of an Expansive Clay Inundated with Sodium Chloride Solutions, Geotech Geol Eng 31: 1399.

RWM (Radioactive Waste Management) (2016), Sealing Site Investigation Boreholes: Phase 2. Stage 1 laboratory programme, reference RWM/03/046, Amec Foster Wheeler, 23 December 2016.

Savage, D. Review of the potential effects of alkaline plume migration from a cementitious repository for radioactive waste. Implications for performance assessment. UK Environment Agency Report P60, 1997

Shirazi S.M., Wiwat S., Kazama H., Kuwano, Shaaban M.G. (2011), Salinity effect on swelling characteristics of compacted bentonite, Environ. Protect. Eng. Jpn., 37 (2011), p. 2.

Svensson, D., The Bentonite Barrier (2015) - Swelling Properties, Redox Chemistry and Mineral Evolution Centre for Analysis and Synthesis, Lund University, January 2015

Tripathy S., Sridharan A., Schanz T, (2004). Swelling pressures of compacted bentonites from diffuse double layer theory, Can. Geotech. J. 41: 437–450

WRP, Installing Monitoring Wells/Piezometers in Wetlands (1993), WRP Technical Note HY-IA-3.1, August 1993.

DEVELOPMENT OF COMPUTER CODE TO OPTIMISE THE PRODUCTION OF HYDROGRAPHS IN SYDNEY, AUSTRALIA

Cassandra Murphy
Environmental Engineer,
AECOM, PO Box Q410, QVB PO, Sydney, 1230, AUSTRALIA
Cassandra.murphy@aecom.com

ABSTRACT

Long term groundwater level monitoring has been conducted in support of the environmental impact statement (EIS) prepared for the WestConnex M4-M5 Link project (RMS, 2017). The M4-M5 Link will connect two predominately underground twin drained motorway tunnels and multiple interchanges which will be excavated from the Hawkesbury Sandstone and Ashfield Shale. In order to assess the impacts of the tunnels and associated infrastructure on the local groundwater systems, a groundwater level baseline data set is being developed to characterise natural seasonal and tidal variations in the existing hydrogeological regimes.

A network of data loggers have been installed in groundwater wells screened in alluvium, Ashfield Shale and Hawkesbury Sandstone and are programmed to monitor groundwater levels through hydrostatic pressure fluctuations at an hourly interval. Barometric monitoring was also undertaken to correct for atmospheric pressure variations. Due to the large amount of data generated by the project and the shortcomings of Microsoft Excel as a streamlined graphing tool, innovation was required on the traditional method of using Excel for data analysis. As such, a custom R code was created to automate the process of hydrograph generation. The code imports folders of raw data logger files, barometrically corrects the data, identifies the groundwater well location of each raw data logger file, matches each file to the manually recorded standing water levels, and converts the groundwater level to m AHD from the raw pressure files. The code then produces hydrographs, plotting the reduced standing water levels against rainfall, exporting a fully formatted combined PDF of each hydrograph. This process significantly reduces the time spent on data manipulation and graphing and the potential for human error during the data manipulation phase.

This visualisation of the data has allowed groundwater trends within the measured time to be observed, including the tidal and rainfall dependant nature of recharge. In the Hawkesbury Sandstone, groundwater fluctuations shown in the hydrographs display a high correlation with rainfall patterns observed over the monitoring period. The alluvium is primarily controlled by local recharge and discharge conditions within the measured time. Several hydrographs also show tidal oscillations, suggesting hydraulic connections with nearby canals, creeks and Sydney Harbour. The creation of this data processing code has greatly reduced the time required for data manipulation in assessing groundwater patterns in the area of the M4-M5 Link WestConnex project. For other large groundwater monitoring projects, investing time early in the development of data processing codes could add similar benefits.

1 INTRODUCTION

Long term groundwater monitoring was conducted in support of the EIS prepared for the WestConnex M4-M5 Link project. The project location and attributes are shown in Figure 1 and comprise of:

- Twin mainline tunnels between the M4 East at Haberfield and the New M5 at St Peters;
- The Rozelle interchange;
- Connections and tunnels between the M4 East and New M5 and the proposed future Western Harbour Tunnel and Beaches Link;
- The Iron Cove Link between Victoria Road and Anzac Bridge; and
- Tunnel ventilation systems (RMS, 2017).

The project will be constructed in alluvium, Hawkesbury Sandstone and Ashfield Shale below the water table. In order to assess the impacts of the tunnels and associated infrastructure on local groundwater systems, a monthly groundwater monitoring program was conducted between June 2016 and June 2018. This program aimed to characterise the existing hydrogeological regimes in the three aquifers by collecting standing water levels and groundwater quality parameters.

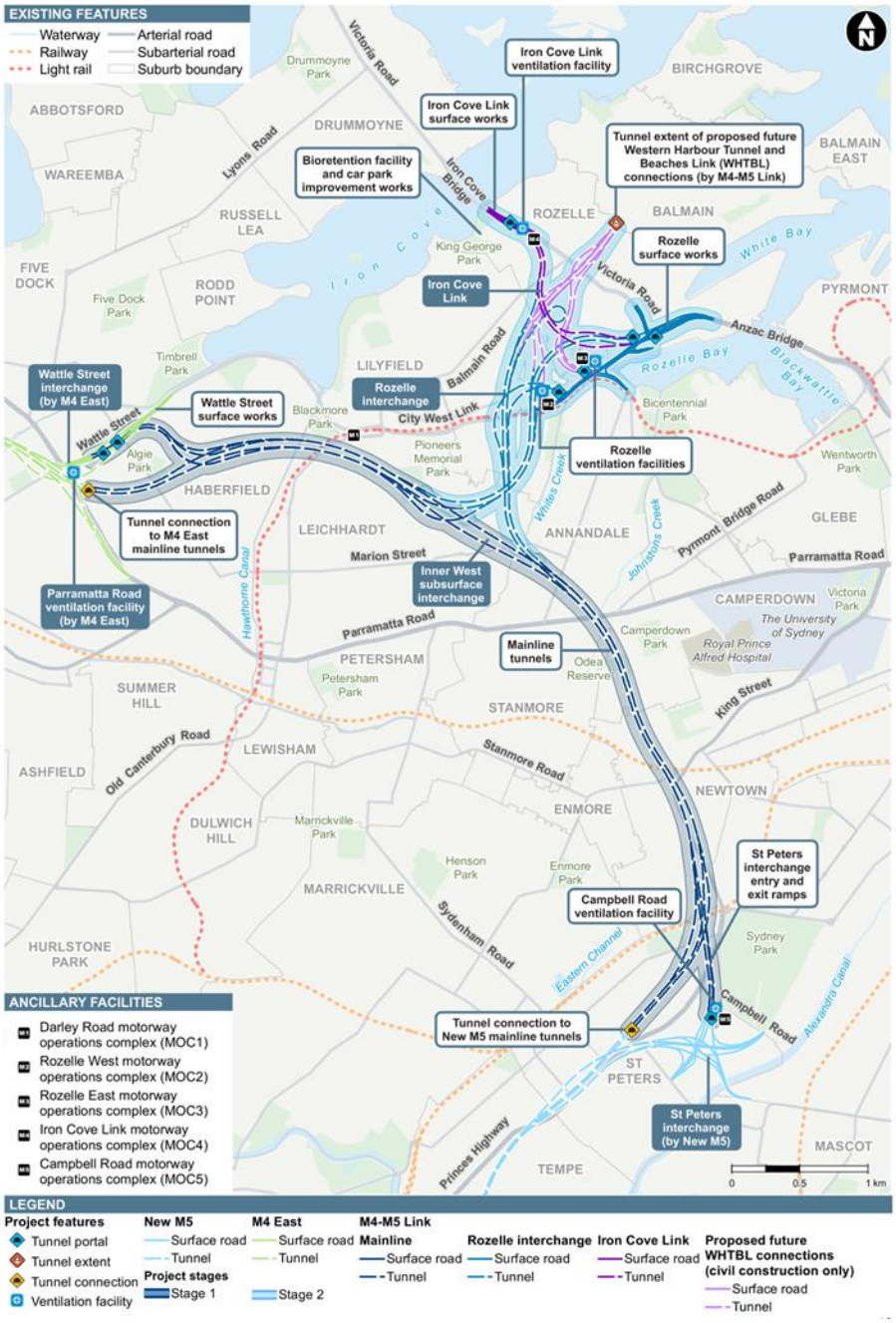

Figure 1: Overview of M4-M5 Link (RMS, 2017)

To assess changes in groundwater levels over time, hydrographs were created for each monitoring well. Hydrographs are time series graphs showing groundwater elevation as a line graph and rainfall as a bar graph. Hydrographs are most commonly used for visually determining hydrologic flow patterns in river and stream systems, but have also been used to present groundwater data and estimate groundwater recharge patterns globally (Moon et al. 2004; Cai and Ofterdinger 2016). For this project, hydrographs were used to identify a correlation between rainfall and groundwater levels and to aid groundwater model development.

The collection of long term groundwater monitoring data is crucial as an input to groundwater model calibration. However, manipulating and visualising large datasets is often time consuming and can potentially be prone to human error. Due to the large amount of data generated by the groundwater monitoring program and the shortcomings of Microsoft Excel as a streamlined graphing tool, innovation was required to replace the traditional method of using Excel. As such, a custom R code was created to automate the process of hydrograph generation.

2 GROUNDWATER MONITORING NETWORK

The groundwater monitoring network comprised of 58 monitoring wells installed between May 2016 and May 2017 in four lithologies: alluvium (10), Mittagong Formation (1), Ashfield Shale (8) and Hawkesbury Sandstone (39). The monitoring wells were screened at secondary structural features in the expected tunnel zones and sealed with bentonite above and below the well screens. Once installed, these wells were developed to remove drilling mud and establish connection with the aquifer.

The locations of the monitoring wells are shown in Figure 2.

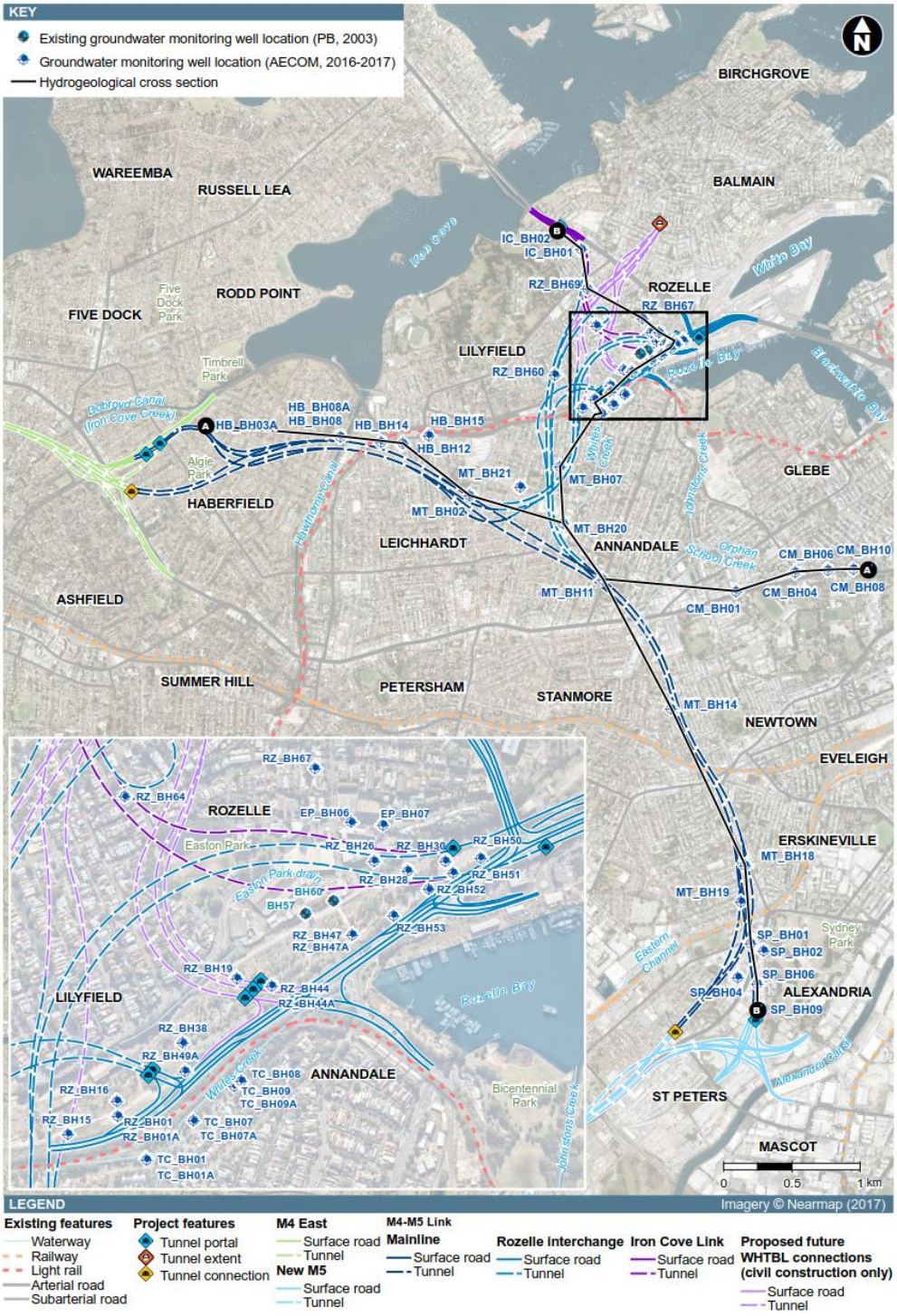

Figure 2: Groundwater Monitoring Well Locations (RMS, 2017)

Monthly groundwater gauging and sampling occurred over two to three days each month. Standing water levels were measured, along with the field parameters of electrical conductivity, temperature, dissolved oxygen, pH, and redox potential. Samples were routinely analysed for a suite of inorganic and organic analytes including heavy metals, nutrients, cations and anions.

A network of groundwater level data loggers were installed in the monitoring wells to automatically monitor groundwater level trends. Manual groundwater levels were monitored monthly with an electronic dip meter to calibrate the logger traces. The data loggers monitored groundwater levels through hydrostatic pressure fluctuations and were programed to record at hourly intervals.

Barometric monitoring was also undertaken to correct for atmospheric pressure variations. The barometric pressure logger was placed within the extent of the network and recorded ambient air pressure throughout the program.

The climate within the project area is temperate. Rainfall is measured daily at Bureau of Meteorology Station 66062 located at the Sydney Observatory. More rainfall is recorded in the late summer and early autumn months, with March receiving the maximum monthly rainfall of 129.6 mm and August receiving the minimum monthly rainfall of 68.4 mm. Over the time period of this project, yearly rainfall levels were above average. The rainfall residual mass, or difference between expected annual rainfall and experienced rainfall, can be seen in Figure 3.

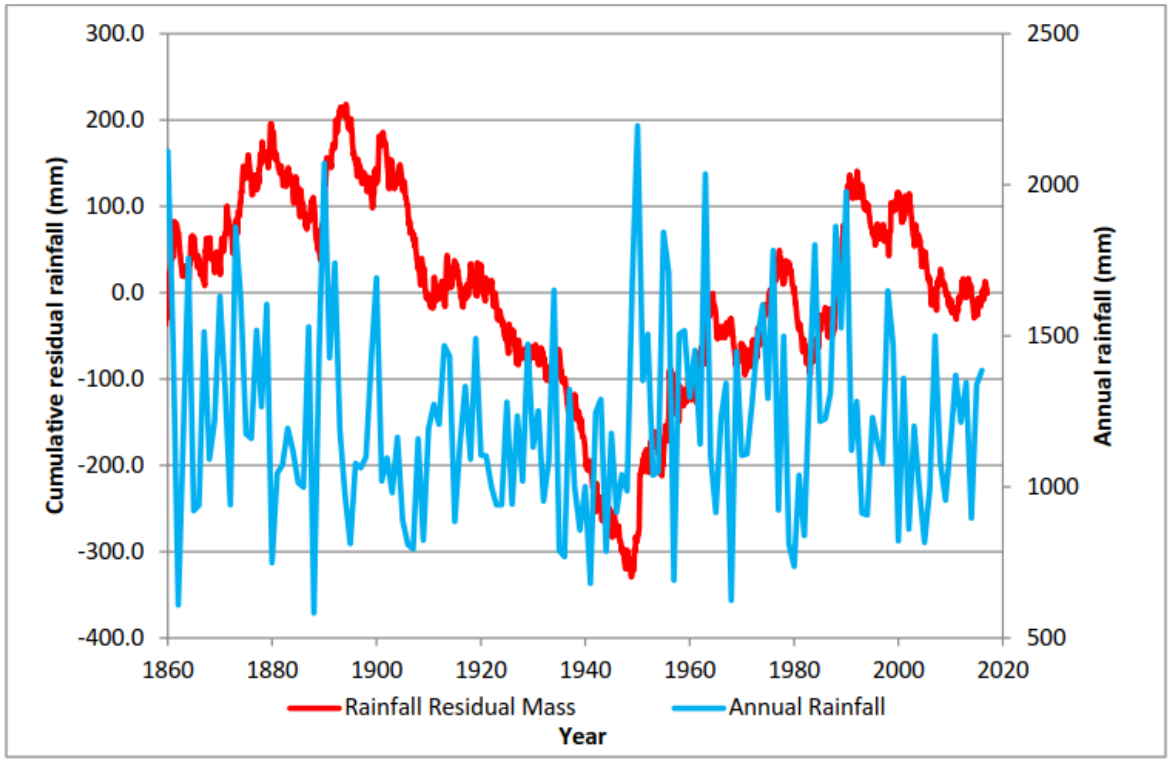

Figure 3: Sydney Residual Rainfall Mass (Station 66062) (RMS, 2017)

3 R SCRIPT

To streamline data manipulation and graphing, a custom R script was written to automate the process of hydrograph generation. R is a programming language that specialises in statistical computing and graphics and an R script is a file containing all the commands that would be typed into R as a combined document to allow for more complex data manipulation (R Core Team, 2017).

The script imports folders of raw data logger files, barometrically corrects the data, identifies the groundwater well location of each raw data logger file, matches each file to the manually recorded standing water levels, and converts the groundwater level to m AHD from the raw pressure files. The script then produces hydrographs, plotting the standing water levels against rainfall, exporting a fully formatted combined PDF of each hydrograph. This process is described in more detail in the following sections.

3.1 FILE IMPORT

The initial step is to import the relevant data. Data manipulation in Excel begins with formatting the data, writing formulas or the input of data into a template. In contrast, R is able to import and read files of data directly into the program as tables ready to be edited. R is also able to read the file names within a specified folder and import them when prompted.

Rainfall measurements were extracted from the publicly available climate records at Sydney Observatory. These are presented in CSV files with days, months and years separated into different columns. Once imported into R, these were able to be transformed into one column containing the date.

R is also able to read a variety of date formats during import. This removes the need to format time series into a common date format and allows data to be combined by time and date in future steps.

3.2 DATA MANIPULATION

Data manipulation can occur in R by applying operations to whole columns instead of copying formulas down to each row as in Excel, reducing mistranslations of data or typographical errors in formulas, like the lack of cell reference locks when they are copied.

Pressure readings, recorded as the length of the water column above the logger, were translated to standing water levels with barometric correction and the monthly groundwater gauging data that accompanied the download of the data loggers.

Barometric correction of the data loggers is required to gain accurate readings of groundwater height. As hydrostatic data loggers record the pressure above them and translate that into length of a water column, additional pressure experienced by the logger may be erroneously attributed to a groundwater flux. Barometric correction removes the pressure associated with atmospheric changes from the pressure recorded above the logger. Commercially available data loggers often have dedicated software that is able to barometrically correct the data logger files. This process is able to be done in R, as pressure can be described as a length measurement of a fluid as shown in the formula below:

$$\mathrm{WC} = \mathrm{P}_{\text{Data logger}} - \mathrm{P}_{\text{Barometric logger}} \quad (1)$$

where WC = Water Column (cm H_2O);

P = pressure (cm H_2O)

Barometric correction can therefore be applied by subtracting the pressure of the atmosphere from the total pressure experienced by the logger. As R is able to merge two data sets based on a shared column of variables, in this case date and time, a combined data set with both relevant pressures matched for each time step is able to be quickly and accurately produced.

Once the pressure data has been corrected, it can then be translated into a standing water level elevation in m AHD. The groundwater elevation recorded just prior to the data logger removal and download will reflect the height of water measured above the logger. As the data logger is stationary, changes to the height of water detected can be applied to the measured groundwater elevation. This can be seen in the formula below:

$$\mathrm{SWL} = \frac{(WC_i - WC_e)}{100} + \mathrm{GWL_m} \quad (2)$$

where SWL = Standing Water Level (m AHD);

WC_i = Water Column of time step under inspection (cmH_2O)

WC_e = Water Column of the last time step (cmH_2O)

GWL_m =Manual Groundwater Level (m AHD)

For example, if the height of water above the data logger increases by 2 cm from recording just prior to the data logger removal, the groundwater elevation will also increase by 2 cm from the groundwater elevation measured just prior to data logger removal. Using this reference point, the whole data set is able to be transformed.

A loop, or programming tool that repeats a section of code, can be created in R to import and manipulate each file sequentially, without the need for each file to be handled independently. This ability is key to saving time during data manipulation.

If multiple data sets have been imported into R, matching the groundwater elevation to the data logger can either be done manually or with a search function. The raw CSV files exported by commercial data logger programs typically contain some form of data logger identification, like the monitoring well identification number. If these can be isolated for each data set they can be used to match to a corresponding manual groundwater level measurement in a combined reference table, automating the process and allowing the correction to occur within the loop.

3.3 GRAPH GENERATION

Within Excel, plotting bar and line graph types on one graph is possible. However, both data sets rarely align correctly without the creation of a secondary horizontal axis and the selection of only relevant rainfall data for the bar graph. As this usually has to be hidden for formatting, checking that the graphs are displaying the correct data is time consuming and not intuitive, as the axis has to be unhidden for viewing within each Excel file.

As previously mentioned, R can combine multiple data sets based on one column of data. If matched by the date and time column, data sets of transformed standing water levels can be matched to the corresponding rainfall recordings for the time periods that the data loggers were recording. The timescale of this merged data set will be set to when the data logger was operational for both variables.

Graphs can be overlapped, allowing both standing water levels and rainfall to be plotted. The creation of these figures can also occur within a loop, saving time and creating consistency. Features like titles can be numbered during the looping process, allowing them to be labelled with figure numbers in a sequence or the name of the monitoring well specific to data set being transformed.

3.4 BARRIERS TO USE

Although R allows the rapid manipulation of raw data files, it also has several limitations. As the steps of data manipulation are not as readily visible as in Excel, small errors may occur during the development of the code. To prevent this from occurring, data can be exported from each step to allow for checking. The format of R also may present a barrier to its use, as a knowledge of the R programming language is required. Detailed code comments or potentially making a user interface could aid the learning process for inexperienced users.

4 HYDROGRAPH INTERPRATATION

The production of the hydrographs has allowed groundwater trends within the measured time to be observed in the three aquifers. This can be seen in more detail in the M4-M5 Link EIS (RMS, 2017), with a small subset shown below.

4.1 HAWKESBURY SANDSTONE

In the Hawkesbury Sandstone, groundwater fluctuations shown in the hydrographs appear to respond to the rainfall patterns observed over the monitoring period. Groundwater elevations in EP_BH06, located in Rozelle, can be seen to increase after all large rainfall events, with a large increase in February 2017 to March 2017 following several rainfall events of over 20 mm/day (Figure 4). RZ_BH16, located at Rozelle also shows these general trends (Figure 4).

While EP_BH06 appears to experience small daily fluctuations, RZ_BH16 experiences more pronounced daily fluctuations in groundwater elevation of approximately 150 mm. These are attributed to tidal influences from Sydney Harbour.

Over the time period of the project, the groundwater elevations vary less than 1 m, indicating that the rainfall infiltrating and recharging the aquifer is approximately equal to the discharge to adjacent water bodies, including Sydney Harbour, and evapotranspiration.

4.2 ALLUVIUM

The alluvium is primarily controlled by local recharge and discharge conditions. In both TC_BH01S and TC_BH08, groundwater elevations increase after rainfall and decrease over the drier period between September 2016 to February 2017 (Figure 4). The pronounced tidal oscillations of TC_BH08 suggests hydraulic connections with the nearby Sydney Harbour. The relationship between the groundwater elevations of both TC_BH01S and TC_BH08 with rainfall events indicates a strong connection between infiltration and recharge.

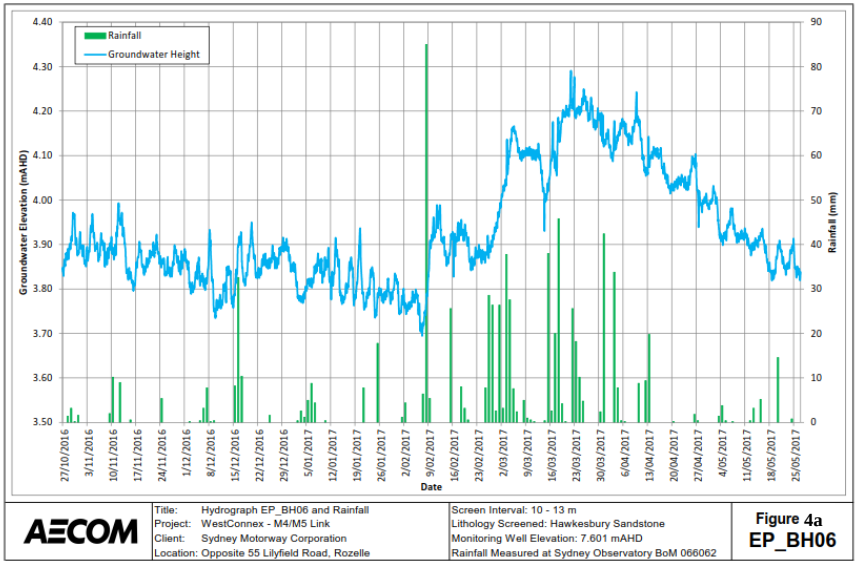

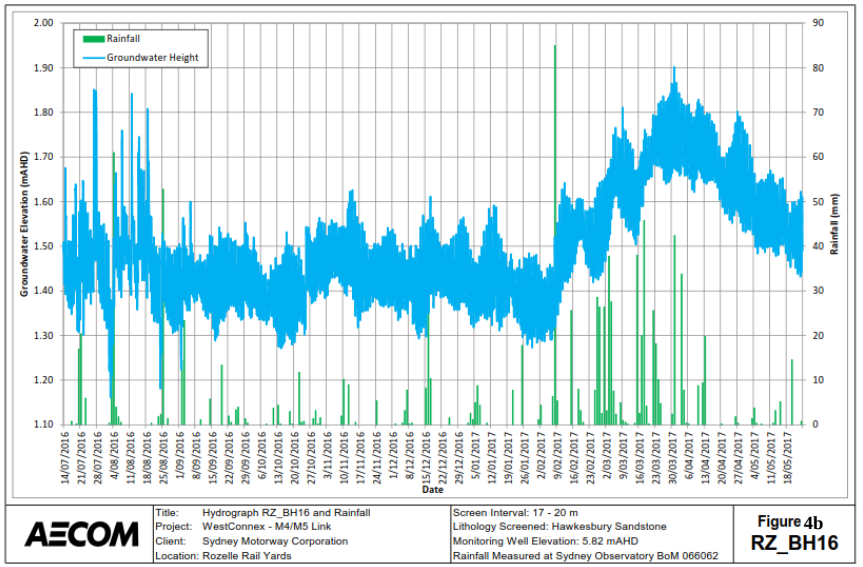

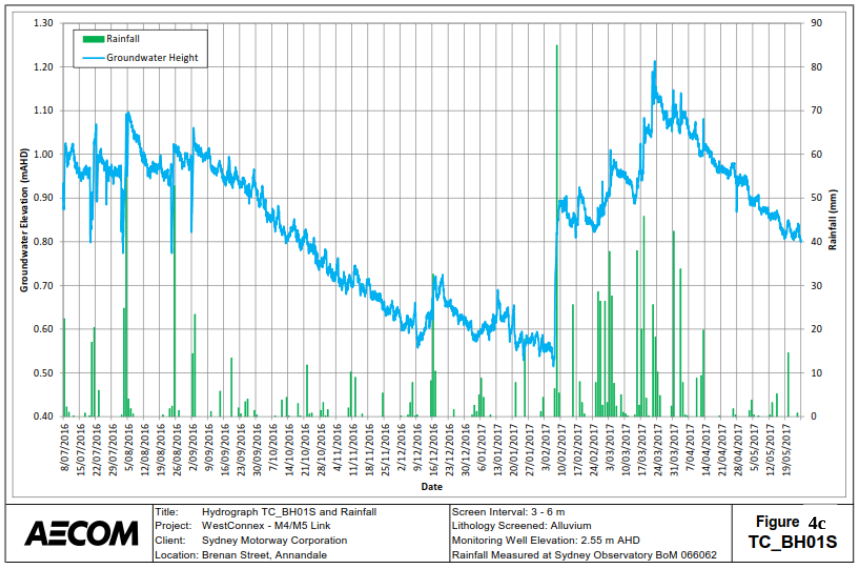

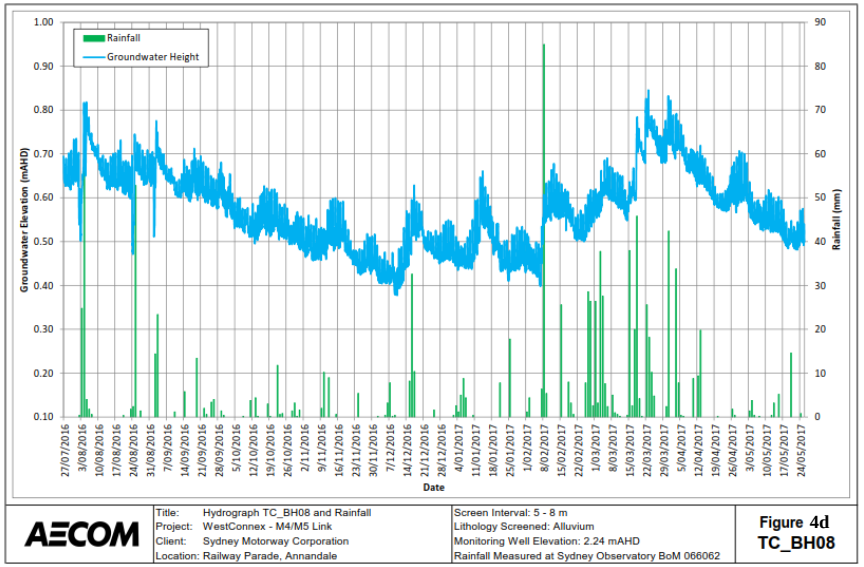

Figure 4: Hydrographs of EP_BH06 (a), RZ_BH16 (b), TC_BH01s (c) and TC_BH08 (d) (RMS, 2017)

5 CONCLUSIONS

As part of the routine groundwater monitoring that was undertaken to support the EIS for the M4-M5 Link motorway project, a network of hydrostatic pressure data loggers were installed in groundwater wells screened in alluvium, Ashfield Shale and Hawkesbury Sandstone. The ongoing monitoring associated with this project has resulted in a large amount of data that is cumbersome to efficiently manipulate in Excel. As such, an R script was developed for the purpose of data manipulation and visualisation.

The script imports, barometrically corrects, and transforms the raw data logger data into standing water levels in m AHD. It then plots the hydrographs of groundwater elevations against rainfall and exports a pdf of the figures. These figures have aided in the interpretation of groundwater level trends in the three aquifers, revealing that both rainfall recharge and tides influence groundwater level fluctuations.

The creation of this data processing code has greatly reduced the time dedicated to data manipulation as well as aided in assessing groundwater patterns within the measured time in the area of the M4-M5 Link. For other large groundwater monitoring projects, investing time early in the development of data processing codes could add similar benefits.

6 ACKNOWLEDGEMENTS

The Author wishes to thank the NSW Roads and Maritime Service for permission to publish some of the results of this investigation. The experience and professionalism of our subcontractors also contributed to the success of this investigation, namely TerraTest, Hagstrom Drilling and Numac Drilling (drilling contractors). The Author also gratefully acknowledges the efforts of RMS project managers Angelique Easton and Verity Humble-Crofts, AECOM Technical Director Andrew Cook and AECOM hydrogeologists Brad Eismen and Graham Hawkes.

7 REFERENCES

Cai, Z., & Ofterdinger, U. (2016) *Analysis of groundwater-level response to rainfall and estimation of annual recharge in fractured hard rock aquifers, NW Ireland*. Journal of Hydrolog, **535*:*** pp. 71-84.

Moon, S. K., Woo, N. C., & Lee, K. S. (2004. *Statistical analysis of hydrographs and water-table fluctuation to estimate groundwater recharge.* Journal of Hydrology, **292(1-4):** pp. 198-209.

R Core Team (2017). *R: A language and environment for statistical computing.* R Foundation for Statistical Computing, Vienna, Austria, 2017. URL: https://www.R-project.org/.

Roads and Maritime Services (2017). *WestConnex – M4-M5 Link Environmental Impact Statement Appendix T - Technical Working Paper: Groundwater*, August 2017.

SAMPLING DISTURBANCE IN SOFT GROUND: IMPLICATIONS IN GEOTECHNICAL DESIGN

Jubert Pineda[1*], Richard Kelly[1,2], Laxmi Suwal[1], Guan Tor Lim[3,4] and Kaiwen Ouyang[1]

[1]Priority Research Centre for Geotechnical Science and Engineering, University of Newcastle, Callaghan, NSW, Australia
[2]Chief Technical Principal, SMEC, Australia
[3]SRK Consulting (Australasia) Pty Ltd., Perth, WA, Australia
[4]Centre for Offshore Foundation Systems, The University of Western Australia, Perth, WA, Australia

ABSTRACT

This paper discusses the main mechanisms of sampling disturbance in soft ground and their implications in geotechnical design. In addition to the mechanical disturbance associated with the type of sampler, the influence of other factors frequently overlooked in practice such as thermal loading due to waxing as well as biological effects due to long-term storage, are evaluated. The paper discusses three methodologies for assessing sample quality in soft soils, which may be easily incorporated in practice. In the last section, mechanical soil properties derived from specimens retrieved using four different samplers are used in the prediction of the total settlement and excess pore water pressure underneath an embankment. The results of the prediction exercise demonstrate the negative effects of poor sampling in geotechnical design. It demonstrated that reliable and cost-effective predictions of geotechnical infrastructure are possible with minimum improvements to the current practice for sampling and testing of soft clays.

1. INTRODUCTION

Safe and cost-effective geotechnical design is critically dependent on the precise determination of soil parameters, as these effect the accuracy of the associated numerical analysis (which is now ubiquitous in geotechnical practice). Laboratory tests are a key to the characterization process, especially to measure input parameters for numerical soil models, but they need high quality samples which are often hard to obtain in soft and problematic soils. Poor quality sampling changes the state and properties of the soil, and hence the representativeness of the *in situ* material. This, in turn, has been shown to affect safe and cost-effective designs for much of civil infrastructure (e.g., Rowe, 1972; Clayton, 2001; Tor Lim et al., 2018a).

Despite of being a very old problem in geotechnical engineering, sampling disturbance is a common issue observed in current practice worldwide. The answers to the sampling issues are local, because they need to be grounded in the local practice of drilling and sounding and be adapted to suit the local geological and geochemical conditions. In Australia, where light geotechnical structures are frequently located along the east coast on soft estuarine clays, rigorous guidelines for undisturbed sampling in soft soils are still not available.

A typical soil sampling process is composed of eight stages as follows: (i) drilling, (ii) sampler penetration or block trimming, (iii) sampler extraction or block retrieval, (iv) tube/block sealing, (v) tube/block transport, (vi) tube/block storage, (vii) soil extrusion (only tube specimens) and, (viii) sample preparation. Figure 1 shows a schematic representation of the stress path followed by a soil specimen subjected to tube sampling. As observed in this figure, soil sampling reduces the *in situ* mean effective stress, $p'_{in\text{-}situ}$, even if soil disturbance is 'avoided'. Every stage of the sampling process may cause some degree of disturbance that changes further the stress state as well as the structure of natural soils. Some of the interactions that occur during different steps in a tube sampling campaign are represented in Figure 2. The degree that each stage of the sampling process contributes to the total disturbance in a given soil is, even nowadays, largely unknown. One of the main reasons for this is the profound lack of knowledge about the coupled phenomena that occur during each stage of sampling. Stress relief, undrained compression and extension paths, suction effects, thermal gradients, time-dependent dissipation phenomena and biogeochemical processes take place during and/or after soil sampling. According to Hight (1986) soil disturbance is associated with:

- Changes in the soil stress state (i.e. reduction in p' and q)
- Mechanical deformation

- Moisture content redistribution
- Chemical reactions
- Mixing and segregation of soil constituents

Clearly, soil disturbance is not solely associated with the mechanical deformation caused by each sampler type, an aspect that has been extensively investigated over last decades. Other effects like tube penetration and tube extraction rates, sealing methods, transport and storage methods, rarely described and frequently ignored in geotechnical practice, may also adversely affect measured soil properties in a major way.

The aim of this paper is to identify the negative effects of sampling disturbance in geotechnical design. Emphasis is given to Australian soft soils (clays and silts), particularly to the estuarine soft soil deposits from the National Soft Soil Field Testing Facility located in Ballina (NSW) (Kelly et al., 2017). These deposits represent the natural soft soils commonly encountered along the eastern and southern Australian coastlines. The consequence of poor sampling in practice are evaluated in the last part of the paper via a prediction exercise of surface settlements and excess pore water pressure underneath an embankment built on estuarine soft clay. It is important to remark here that although laboratory testing procedures are also key to obtaining reliable soil parameters this topic is beyond the scope of this paper.

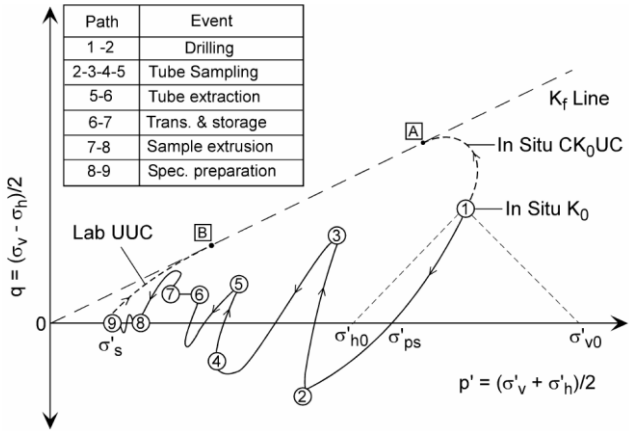

Figure 1: Hypothetical stress path during tube sampling in low OCR clay (Ladd & DeGroot, 2003)

2. MECHANICAL DISTURBANCE: EFFECT OF THE SAMPLER TYPE

The open sampler (Shelby tube) is the most common sampling method in soft soils due to its simple operational principle (Figure 3). However, specimens retrieved using Shelby tubes are significantly influenced by mechanical deformation as a consequence of the entrance of disturbed soils from the bottom of the borehole. Baligh et al. (1987) studied the undrained penetration of a rigid open sampler (S-sampler) in saturated clay using the strain path method (Baligh, 1985). Neglecting the differences in the geometry of the cutting edge between the S-sampler and open (Shelby) tubes, it was shown that: (i) large shear strains (and strain non-uniformity) take place in the outer zone of the tube, mainly at the soil-tube interface, and (ii) the vertical strain component is dominant at locations closer to the centreline. Three deformation stages were identified for soil located at the centreline of the sampler: (a) compression, ahead of the sampler, (b) extension, near to the cutting edge and (c) compression, inside the sampler. Clayton et al. (1998) complemented the work done by Baligh and co-workers by considering more realistic geometries for the cutting edge of the sampler. The results were analysed in terms of the geometric descriptors introduced by Hvorslev (1949) to quantify the effects of tube sampling caused by different tools. They showed that the area ratio (AR = area of the annulus of the tube sampler divided by the area of the tube specimen), as well as the angle of the cutting edge (α), dominate the compression component ahead of the sampler (see Figure 4(a) and (b)). The axial compression increases with the increasing of AR and α. On the other hand, the inside clearance ratio (ICR), which refers to the enhancement of the internal tube diameter behind the cutting edge, has a strong influence on the extension component inside the sampler.

Another issue with Shelby tubes is the difficulty of the check valve to maintain the vacuum during sampler retrieval which affects the total recovery (e.g., Clayton et al., 1995). This phenomenon is associated with suction created at the bottom of the sampler during retrieval. Figure 5 shows the key role of sampler retrieval on soil disturbance (Tor Lim et al., 2018b). The Authors took advantage of the symmetry of the problem to push in half Shelby tubes in reconstituted

calcareous silt against a transparent Perspex window. Three mechanisms may be recognized: (i) the progressive development of a shear plane at the sampler tip, (ii) the soil heave at the bottom of the borehole (due to the interaction between the uplift force and soil suction), and (iii) the creation of tension cracks, due to the loss of lateral support for the soil located at the bottom of the sampler, which leads to low soil recovery.

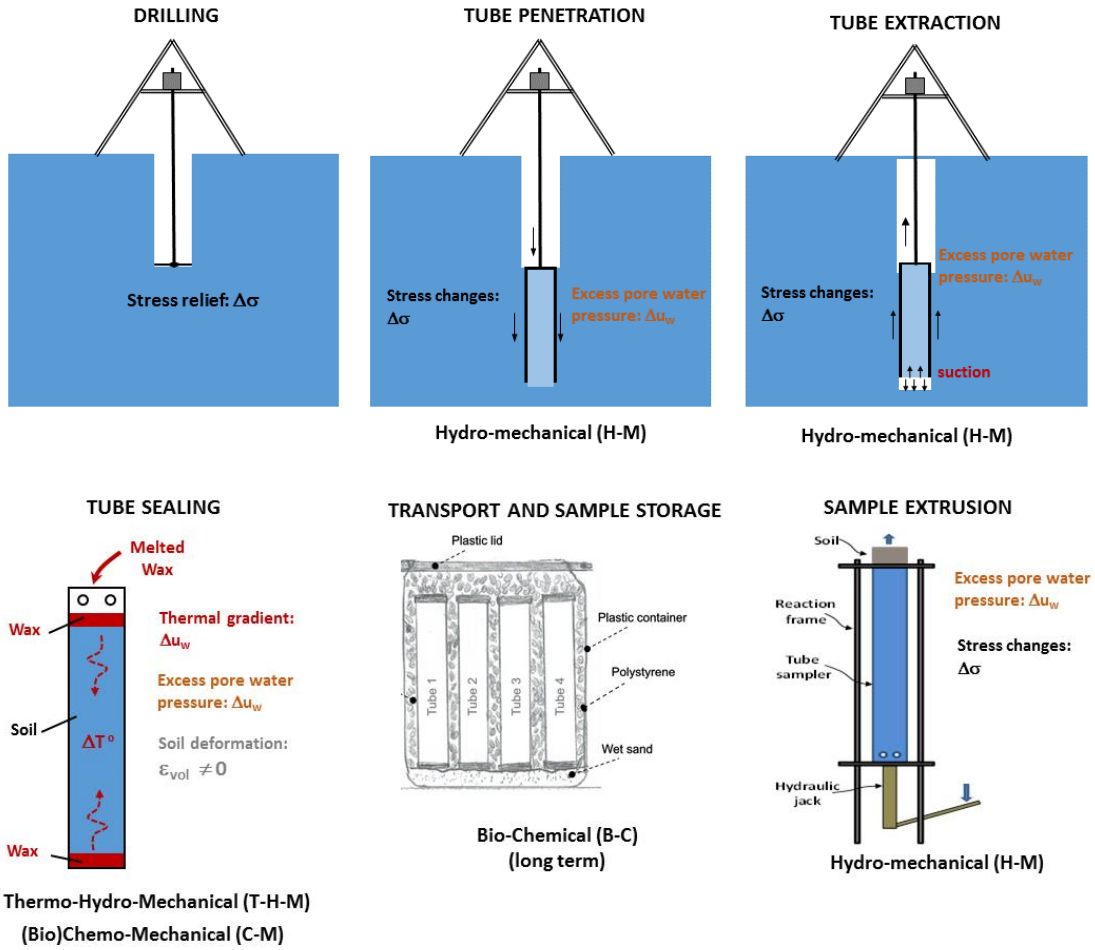

Figure 2: Physical and (bio)chemical processes that may occur in a tube sampling campaign

To overcome those issues, Österberg (1973) designed the hydraulic fixed-piston sampler which has catalysed the development of several devices of its kind during subsequent decades. Although the working principle of the hydraulic fixed-piston sampler is a bit more complicated than the Shelby sampler, it is still simple enough to be adapted to conventional practice without major modifications (Figure 3). The main differences between these two samplers are: (i) the presence of an internal fixed piston to prevent the entrance of disturbed soil during lowering to the sampling depth, (ii) the presence of an internal thin-walled tube sampler that is pushed into the ground using a floating piston via hydraulic pressure. After full penetration, the hydraulic fluid flows up (through the hollow piston rod) and down (through the cutting toe) to ensure the same static pressure inside the sampler and at the bottom base. It helps to minimize suction at the bottom of the sampler during withdrawn. The NGI 54-mm sampler (Andersen & Kolstad, 1979) and the JPN 75-mm sampler (e.g., Tanaka et al., 1996) are examples of hydraulic fixed-piston samplers that have been incorporated into practice in Norway and Japan, respectively.

Fixed-piston samplers are known for providing specimens of better quality compared with other tube sampling techniques (e.g., Andersen and Kolstand, 1979; Lacasse et al., 1985; Tanaka et al., 1996; Lunne et al., 1997; Ladd & DeGroot, 2003; Lunne et al., 2006; Landon et al., 2007; Donohue & Long, 2010; Pineda et al., 2016b; to name a few). Despite their well-documented advantages, the use of fixed piston samplers is still not well established in practice. In Australia, for instance, Shelby tubes (50 – 75 mm in diameter) are the typical choices, mainly due to their simple operational principle. However, mechanical parameters obtained from laboratory tests performed on Shelby tubes in most cases do not represent the *in situ* conditions. Laboratory testing is expensive and involves long testing times, so additional sampling and laboratory campaigns tend to be avoided in practice, even if the quality of soil specimens does

not fulfil the recommendations given in the literature. Therefore, there is a concern about the influence of soil disturbance as a result of sampling on predicted soil behaviour for typical geotechnical infrastructure.

A set of recommendations to select the proper tube sampler and minimize mechanical disturbance was given by Ladd & DeGroot (2003) (see Table 1). They suggest the use of sampler tubes with ratio B/t (B: outer diameter and t: thickness of the tube wall) higher than 40, area ratio lower than 10%, no inside clearance ratio and angle of the cutting shoe lower than 10 degrees. Moreover, they suggest avoiding top and bottom ends in tube specimens (≈ 1.5 B each) for mechanical testing due to the large degree of soil disturbance. Soil from top and bottom ends should be used for characterization purposed only.

Even if fixed-piston samplers are used in practice, the quality of the retrieved sample is also influenced by the skills of drillers. Tanaka (2008) reported a benchmark exercise carried out to assess by how much driller skills may affect the undrained shear strength of a soft clay from Japan found in a site with an homogeneous soil profile up to 20 m depth devoted to port construction works. Seven drilling companies (A to G) were requested to obtain tube specimens using the JNP sampler, a 75-mm fixed-piston sampler recommended in the specifications given by the Japanese Geotechnical Society (JGS). Figure 6 compares the undrained shear strength profiles obtained by each company. There is a clear effect of the driller's skill on the measured undrained shear strength, even in homogeneous soil profiles. Although it is commonly overlooked, results shown in this figure highlight the importance of good training for drillers and technicians in order to obtain high quality soft soil specimens for laboratory testing.

Table 1: Recommended criteria for the selection of tube samplers (Ladd & DeGroot, 2003)

B/t	Area Ratio AR (%)	Inside Clearance Ratio ICR (%)	Angle of the cutting shoe α (º)
> 40	< 10	0	< 10

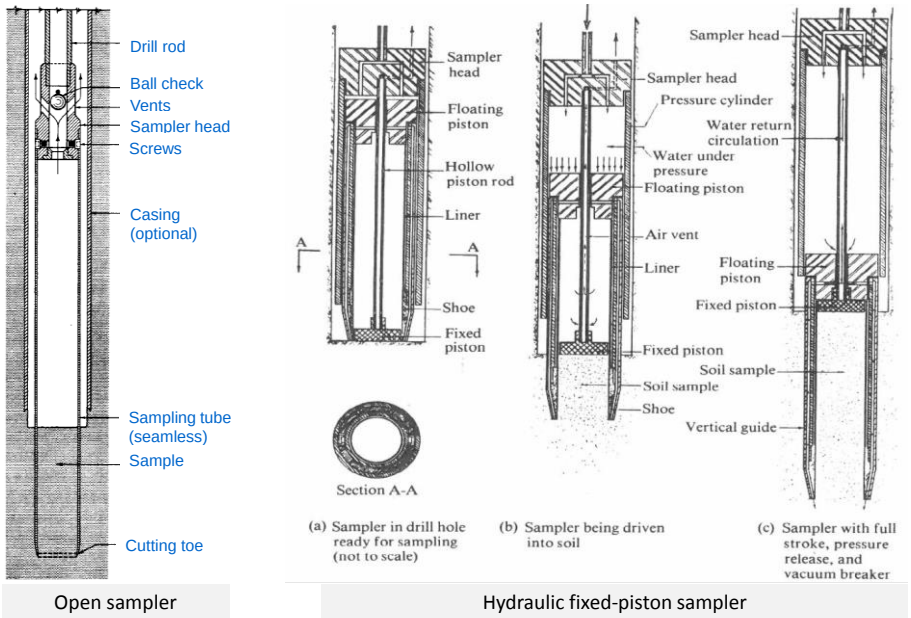

Figure 3: Shelby tubes and hydraulic fixed-piston sampler (from Clayton et al., 1995)

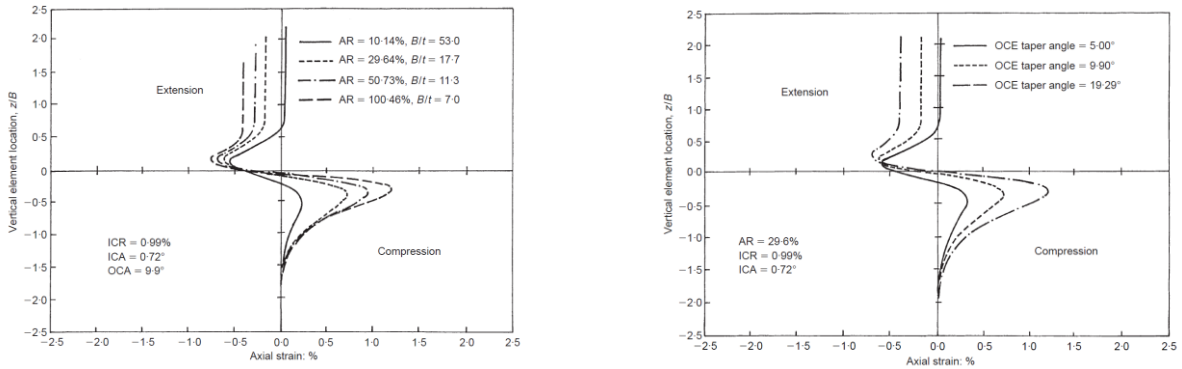

(a) (b)

Figure 4: Deformations during undrained tube sampling in saturated clay. (a) Influence of AR on centreline vertical strains. (b) Influence of ICR and a on centreline vertical strains (from Clayton et al., 1998)

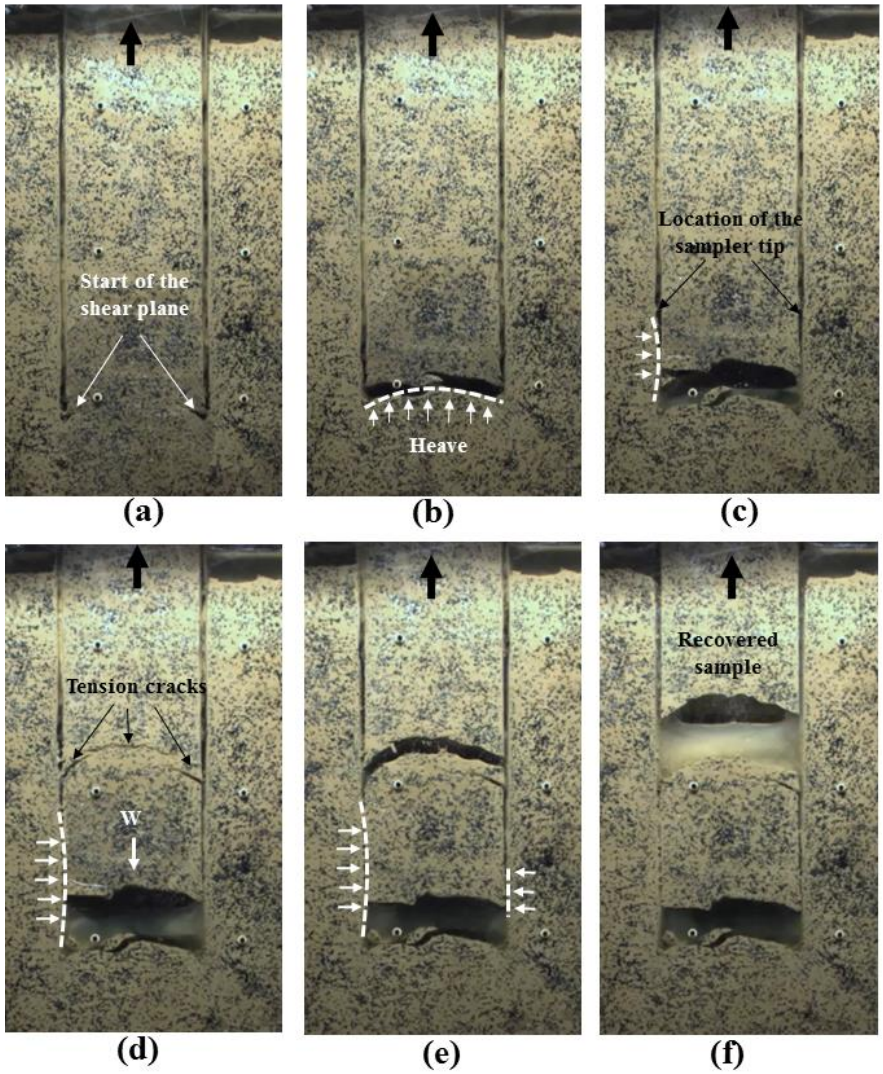

Figure 5: Effects of sampler retrieval in calcareous silt

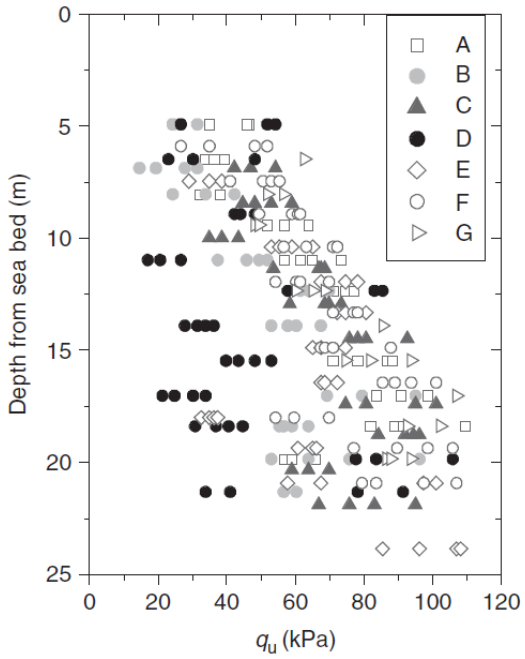

Figure 6: Effects of driller's skills on the measured undrained shear strength of a soft clay from Japan (Tanaka, 2008)

3. THERMAL DISTURBANCE: EFFECTS OF WAXING

Little attention has been given in the past to the influence of the thermal gradients generated by waxing when sealing tubes and block specimens after sampling. This was recognized by Hvorslev (1949) as a potential problem and led to complementary work (Lefebvre & Poulin, 1979; La Rochelle et al., 1986) that focused almost exclusively on the performance of the wax composite in avoiding moisture losses. However, soil disturbance caused by the thermal gradient was neglected. This gradient dissipates with time as wax hardens, but generates excess pore water pressure under undrained conditions as the pore water is not allowed to drain out. This may lead to significant moisture redistribution within the clay. Biological processes (e.g., methane release) and chemical reactions may also be triggered by thermal fluctuations, but are rarely evaluated in practice.

A pilot test was carried out on Ballina soft clay from the National Field Testing Facility (NSW, Australia) to highlight the importance of the thermal gradients caused by waxing in soft soils. The upper slice of a tube specimen, previously waxed and stored for six months in a controlled relative humidity room, was used. To perform the experiment, the layer of solidified wax applied *in situ* was first removed. Then, thermocouples were inserted into the soft clay to monitor variations in temperature along the specimen (see Figure 7a). Additional thermocouples were attached externally to the sampler wall to monitor the changes in temperature along the tube. Melted wax was then poured onto the top of the sample to reproduce the procedure used *in situ*, and created a final layer thickness of around 15mm. As observed in Figure 7(b), the temperature of the wax reached 85ºC after pouring and then reduced slowly with time. The soil located closer to the top boundary cooled to around 34ºC in less than 1h, while soil at the bottom of the specimen (75mm from the heat source) reached 28ºC after 2h. It took about 1 day for the temperature to come back to room conditions. This specimen was re-opened after one week and a clear oxidation front could be observed.

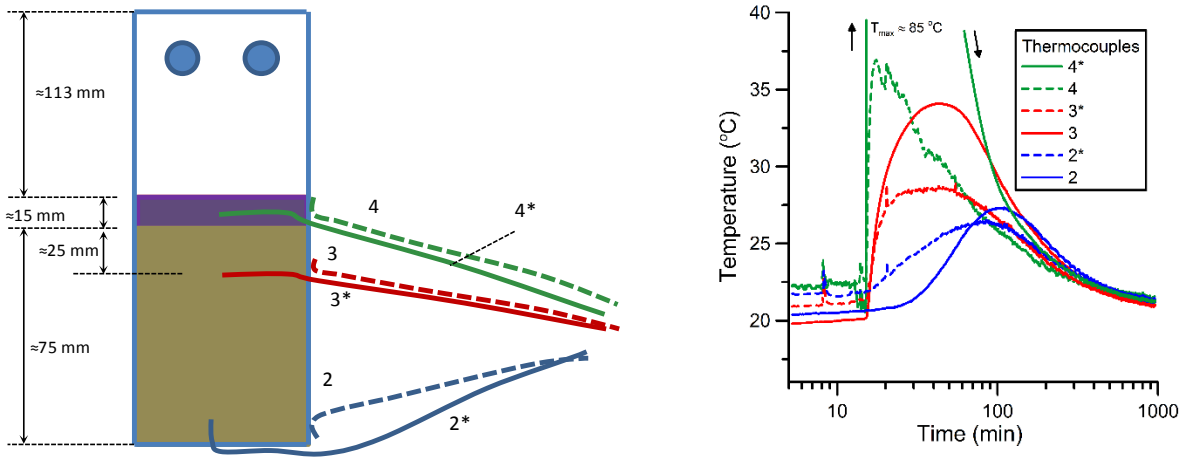

Figure 7: Thermal test in Ballina clay. (a) Experimental set up. (b) Temperature variations with time

To get a better understanding of the evolution of the thermal gradient generated by waxing in tube samples, a simple numerical modelling of the thermal loading was performed using the finite element analysis program ABAQUS FEA 6.14. For the sake of simplicity, it was assumed that conduction is the only factor that controls the temperature field within the sample. Therefore, the basic energy balance equation is given by

$$\int_V \rho \dot{U} dV = \int_S q dS - \int_V r dV \quad (1)$$

where V is the volume of the solid material with surface area S, ρ is the density of the material, $\dot{U}$ is the rate of inertial energy; q is the heat flux per unit area of the body; r is the heat supplied internally into the body per unit volume. The heat flux and the variation of the internal energy are computed via Fourier's law and the internal energy equation as follows:

$$q = -\lambda \nabla T \quad (2)$$

$$dU = c \cdot dT \quad (3)$$

where λ is the thermal conductivity of the material, ∇T is the thermal gradient and c is the heat capacity of the material. The latent heat of the wax was also considered in the calculation of the internal energy to account for the phase change that occurs as wax hardness. Table 2 summarizes the set of parameters used in the numerical simulations.

Table 2: Thermal parameters for the materials

Material	Heat capacity (10^3J/kg · K)	Thermal conductivity ($W/(m \cdot K)$	Density (kg/m^3)	Latent Heat (10^5J/kg)
Wax[1]	2.9	0.25	900	2
S.S. tube	0.502[2]	16[3]	7480[3]	-
Soil[3]	1.381	1	1348	-

[1] Haji-Seik et al. (1982) [2] https://www.engineersedge.com [3] https://www.engineeringtoolbox.com

In practice, there is a heat loss starting as soon as the wax is poured as a consequence of the difference in temperature between the system (wax+tube+soil) and the environment. This scenario was simulated by introducing a convection-type boundary condition. The heat flux at the boundary is given by

$$q = c_{conv}(T - T_0) \quad (4)$$

where q is the heat flux at the boundary; c_{conv} is the convection coefficient at the boundary, T is the temperature of the boundary surface and T_0 is the temperature of the environment. Figure 8(a) shows the geometry and set up used in the numerical simulations. The experimental results described in Figure 7 were used here to calibrate the numerical model.

A back-analysis procedure was followed to estimate the convection coefficient for Ballina clay which controls the heat loss during the experiments. 2D axisymmetric analyses were carried out using 4-node linear heat transfer elements. The boundary condition at the axisymmetric axis was set as zero heat flux boundary, while other boundaries were set as convection-type. The contact conditions between the wax, soil and sampler were set as "tie" as suggested by (Fiedler et al., 2015). Figures 8(b) and (c) show screenshots that correspond, respectively, to the thermal fields at the beginning of the simulation (t=0) and after a reduction of about 50% in the initial wax temperature. The convection coefficient obtained from the back analysis was equal to 10 W/m^2.K.

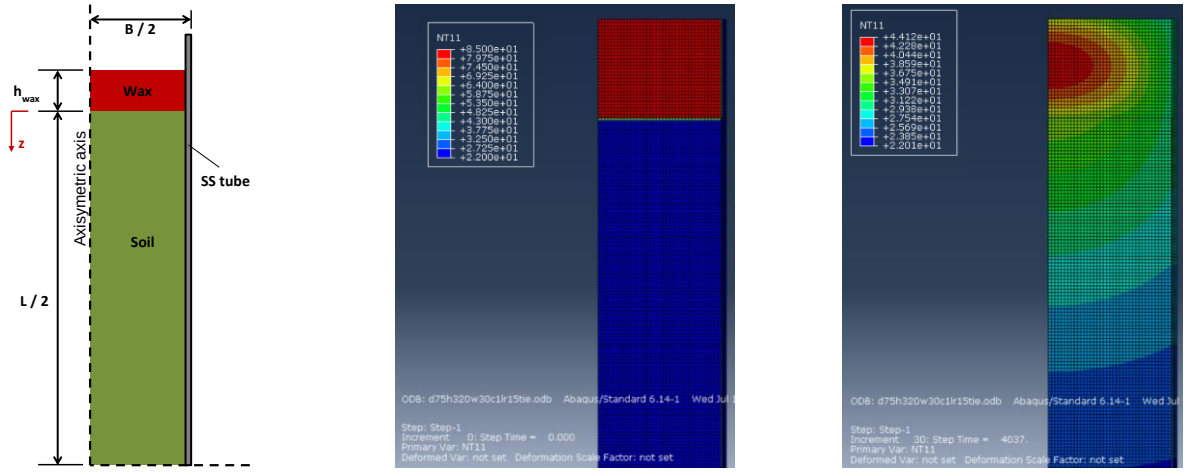

(a) (b) (c)

Figure 8: Modelling of thermal effects in tube samples. (a) Model set up. (b) and (c) Generated thermal profiles

A parametric analysis was then performed in order to evaluate: (i) the influence of the amount of heat applied to the system, which is controlled by the height of the wax layer, and (ii) the thermal field generated in samples of different sizes. The second aspect was studied by applying the same volume of heat to tube specimens of different diameters.

Figure 9(a) shows the variation of the maximum temperature, T_{max}, estimated at the centreline of a U75 tube specimen (commonly used in Australian practice), with the sample depth. The three profiles observed in this figure represent thicknesses of the wax layer of 10 mm, 30 mm and 50 mm. As expected, the influence of the thermal loading on the soil mass enhances with h_{max}. At the wax/soil interface, the soil reach temperatures up to 45ºC which dissipates at different rates depending on h_{max}. There is a zone affected by the thermal loading which varies from $0.15 < z/L < 0.25$, depending on the thickness of the wax layer. For $h_{max} \geq 30$ mm, the numerical results presented in Figure 8(a) indicate that around 50% of the sample is (directly) affected by the thermal gradient. Therefore, only about 250 mm of the tube (assuming full recovery) could be used in advanced laboratory testing (e.g., triaxial, consolidation). The results presented in Figure 9(b) indicate that, if the same volume of heat is applied to the system, the zone affected by the thermal loading reduces with increasing the sampler diameter. Hence, specimens retrieved using U50 samplers are more prone to be affected by waxing.

One of the limitations of the numerical analysis described above is the lack of information regarding to the excess pore pressure generated by the thermal loading. Waxing is used to avoid moisture losses in soil samples. This implies that undrained conditions prevail during the thermal loading as the pore water is not allowed to drain out. A rough estimate of the maximum excess pore water pressures generated by the thermal load was carried out here by using the following expression (e.g., Mitchell & Soga, 2005)

$$\Delta u_w = \frac{n\Delta T(\alpha_{solids} - \alpha_{water}) + \alpha_{st}\Delta T}{m_v} \quad (5)$$

where n is the soil porosity, α_{solids}, α_{water} and α_{st} refer to the thermal expansion coefficients of solids, water and soil structure, respectively, whereas m_v is the volumetric compressibility of the soil. $\alpha_{st} = 1.x10^{-4}\ e^{-0.014PI}$, where PI is the plasticity index of the soil. Figure 9(c) shows the estimated excess pore water pressure caused by an increase in temperature in Ballina clay. Values of n, PI and mv were obtained from laboratory data given in Pineda et al. (2016b) and Tor Lim et al. (2018a) whereas α_{solids} and α_{water} were selected from values reported by Mitchell and Soga (2005). The rate of excess pore water pressure due to thermal heating is around 0.46 kPa/ºC. Maximum temperatures estimated

from the numerical modelling at the top boundary of the tube sample lies around 40-45ºC, i.e., $\Delta T_{max} \approx$ 20-22 ºC. According to Eq. 5 such an increase in temperature would generate a maximum excess pore water pressure of 10 kPa (from top and bottom ends), travelling towards the centre of the tube sample. For a natural soft clay with values of undrained shear strength between 10-15 kPa (see Pineda et al., 2016) an increase in excess pore pressure of that amount may cause the failure of the soil located closer to the heating source but also modifications in soil fabric (due to moisture redistribution) along the entire specimen.

The results of the numerical analyses remark the need of using insulating materials to separate the soil from the wax. This approach was intuitively adopted by Pineda et al. (2014, 2016b) who used a foam plate (10 mm in thickness) to minimize the effects of waxing on tube specimens of Ballina clay. Preliminary numerical analyses including the foam plate suggest that the effects of the thermal loading on tube specimens may reduce by around 40-50%. This simple approach could be adopted in practice. Further research is still required in order to get a proper understanding of the effects of waxing in natural soft soils.

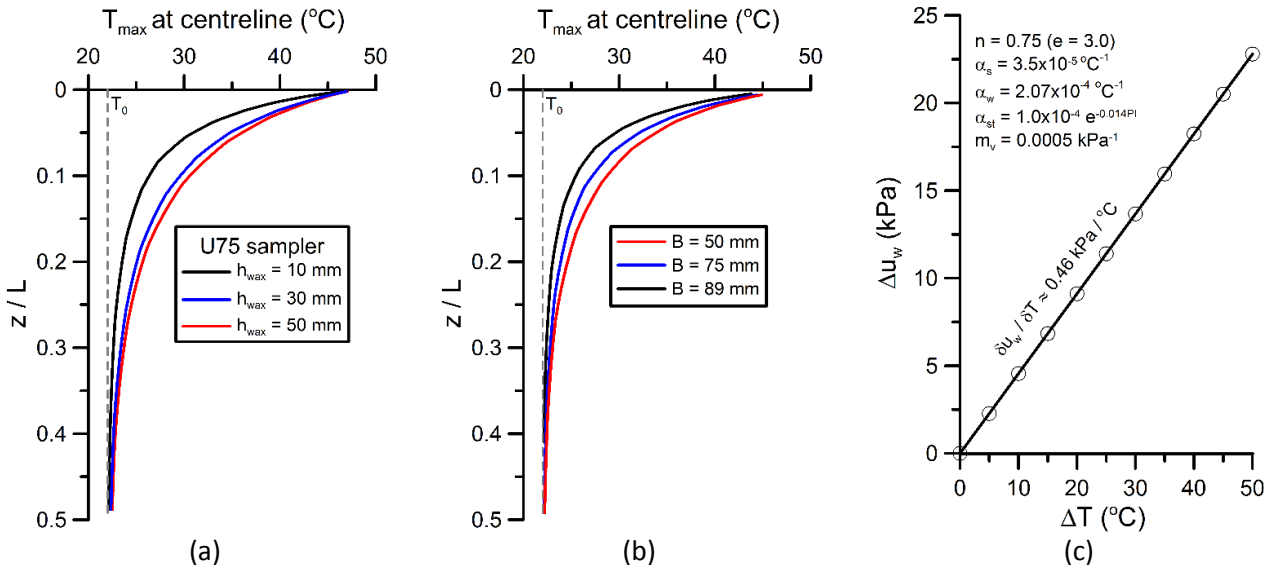

Figure 9: Thermal effects in Ballina clay; (a) Effects of the volume of wax and (b) Effects of the sample diameter. (c) Estimated excess pore water pressure

4. (BIO)CHEMICAL DISTURBANCE: EFFECTS OF THE SOIL STORAGE

The sample storage method and storage time have a major influence on the behaviour of soft soils (e.g., see Bjerrum & Rosenqvist, 1956; Thakur, 2014). Indeed, sample storage may activate biological processes, such as methane release and the oxidation of organic matter. This may lead to a progressive change of the undrained shear strength and preconsolidation pressure as reported by Arman and MacManis (1976) for clay and silty clay specimens from Louisiana (USA) (Figure 10). A reduction about 50% in undrained shear strength is observed after 4 months of storage. Preconsolidation pressure decreases drastically after only three months of storage. Unfortunately, the alteration of natural soft clays during long-term storage is still an unsolved issue due to the lack of understanding of the key physical-biogeochemical interactions involved. Even small thermal variations may activate or accelerate biogeochemical reactions and alter the hydraulic (permeability) and mechanical (compressibility, strength, stiffness) properties of soft soils (e.g., see Mitchell and Santamarina, 2005). Chemical changes may also take place under isothermal conditions if enough oxygen is present. This aspect is frequently neglected in practice, despite its major effect on the mechanical response of natural soils. Therefore, it is recommended to test soil specimens soon after sampling in order to minimize the aforementioned effects. Regarding to the laboratory testing techniques, it is important to use pore water with similar salinity to natural water in order to minimize changes in the mechanical behaviour of the soil as a consequence of chemical reactions.

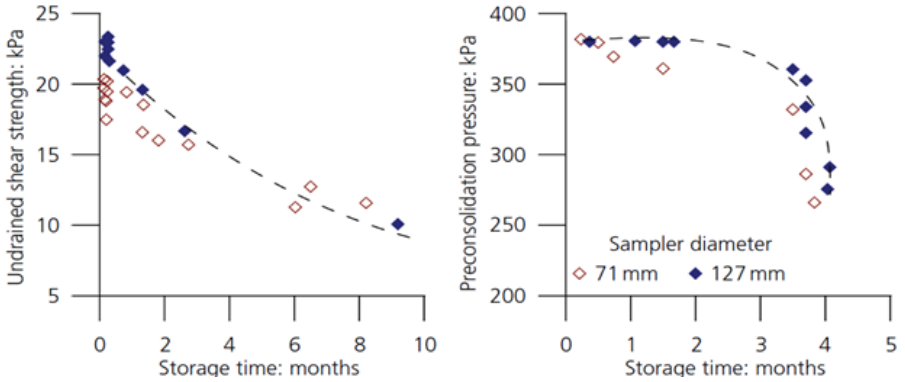

Figure 10: Effects of storage time on undrained shear strength and preconsolidation pressure in soft soils (Arman and MacManin, 1976)

5. SAMPLE QUALITY ASSESSMENT

A key issue in the characterization of natural soft soil deposits lies in the selection of 'representative' soil specimens for laboratory testing. Sampling disturbance as well as the natural soil variability along tube/block specimens, may affect the results of laboratory tests and lead to considerable discrepancies between *in situ* and laboratory data. Non-destructive methods as well as conventional laboratory tests have been used over the last decades to assess sample quality in soft soils. The most common approaches are based on:

- Volume change due to soil recompression to the *in situ* effective stress
- Image analysis (X-ray analysis and CT scanning)
- Shear wave velocity measurements

The proposals by Andersen & Kolstad (1979) (see also Terzaghi et al., 1996) and more recently by Lunne et al. (1997) have a good track record as indicators of sample quality in soft soils. Both approaches are based on the recompression deformation (ε_v or $\Delta e/e_0$) required to bring the sample to the *in situ* vertical effective stress. Sample quality is ranked using four levels (see Table 3): (1) very good to excellent, (2) good to fair, (3) poor and (4) very poor. The method by Lunne et al. (1997) also considers the influence of OCR and therefore it has become popular in the assessment of sample quality in soft soils.

Table 3: Methods for sample quality assessment based on ε_v and void ratio

Level	Andersen & Kolstad (1979)		Lunne et al. (1997)		
	ε_v (%)	Rating	1 < OCR < 2 $\Delta e/e0$	2 < OCR < 4 $\Delta e/e0$	Rating
1	< 1	Very good to excellent	<0.04	<0.03	Very good to excellent
2	1-2	Good to fair	0.04-0.07	0.03-0.05	Good to fair
3	2-4	Poor	0.07-0.14	0.05-0.10	Poor
4	4-8	Very poor	>0.14	>0.10	Very poor

Nevertheless, both approaches were developed using laboratory results obtained primarily for marine clays (6% < PI < 43%) retrieved from relatively shallow depths (< 25 m). Although the influence of OCR is accounted for by Lunne et al. (1997), no correction is considered for the recompression to *in situ* stress in specimens with high overburden stresses, subjected to large stress relief due to sampling. This issue was evaluated by Krage et al. (2016) using reconstituted specimens made of silica silt-kaolin mixtures with PIs ranging from 0 to 31%. Oedometer specimens were subjected to a wide range of overburden stresses ($20 < \sigma'_{v0} < 500$ kPa) to establish a depositional stress history. Two levels of disturbance were then induced as follows: 1D 'perfect sampling' (1DPS) and highly disturbed (HD) states. 1D 'Perfect sampling' condition was achieved via removal of the deviatoric stress to get K_0=1. Highly disturbed specimens were produced by applying a freezing-thawing cycle under unstressed conditions. HD samples were subsequently loaded beyond the preconsolidation stress, followed by unloading until achieve K_0=1, as imposed to 1DPS specimens. Finally, both 1DPS and HD samples were loaded further to a vertical effective stress of 2500 kPa. Figure 11(a) and 11(b) shows the compressibility curves obtained from 1DPS and HD specimens, respectively. It can be seen the strong influence of

the previous freezing-thawing cycle on the compressibility of HD specimens which also affects the preconsolidation stress. Figure 11(c) shows the variation of the normalized void ratio ($\Delta e/e_0$) against the overburden stress obtained from 1DPS and HD specimens. The quality of HD specimens ranges from *very good to excellent* to *poor* sample quality. These results are clearly inconsistent with level of disturbance induced to each specimen and highlight the need for considering the influence of the stress relief (overburden stress) on $\Delta e/e_0$. Therefore, caution should be taken when using these methodologies to assess sample quality in low plasticity silty deposits.

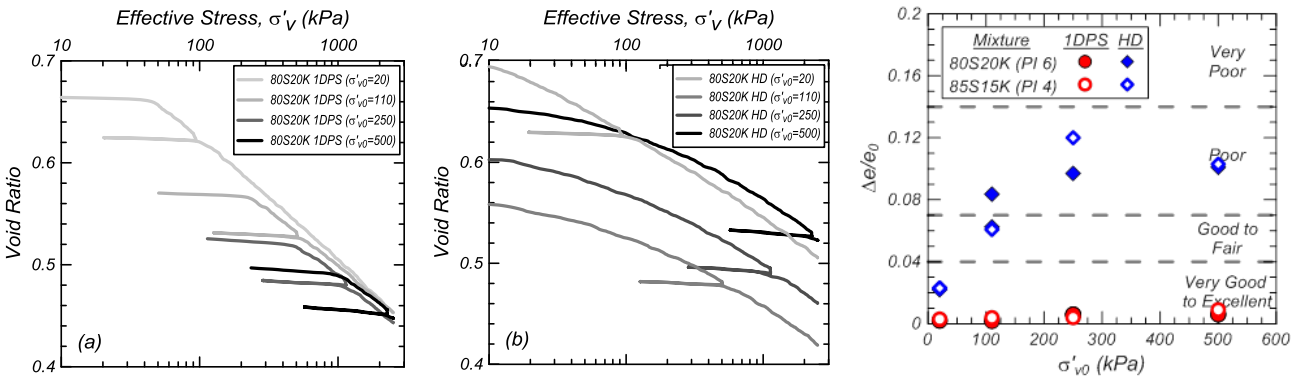

(a) (b) (c)

Figure 11: Sample disturbance in low-plasticity soil. (a) Compressibility curves of 1DPS specimens. (b) Compressibility curves of HD specimens. (c) Sample quality rating for 1D perfect sampled (1DPS) and highly disturbed (HD) specimens (Krage et al., 2016)

The main drawback of the volume change-based sample quality methods is the testing time which, in some cases, makes them unsuitable for a quick assessment of sample disturbance. This fact has prompted interest on non-destructive sample quality examination techniques. X-Ray or Computer Axial Tomography (CAT) analysis are becoming popular in geotechnical engineering due to their non-destructive nature and simple procedure. The main drawback of the X-Ray technique is that all features of the specimen are superimposed into a 2D image whereas a 3D reconstruction is obtained from CAT analysis. It gives a 3D picture of the sedimentary structures but also natural heterogeneities (fissures, inclusions, cavities) and allows selection of high-quality specimens for laboratory testing.

The maximum energy of medical CT scanners ranges between 120 – 140 keV. These devices are designed for use on human subjects to image soft tissue and bones. Human bones have similar density as natural soft soils (~ 2 Mg/m^3) and therefore it might be reasonable to use them on soft soil deposits. CT scanning is nowadays common practice at the University of Newcastle (Australia) to examine qualitatively the internal structure of tube samples. Figure 12 shows the vertical sections of two tube specimens, retrieved from two near-by boreholes at the National Soft Soil Testing Facility using a fixed-piston sampler as well as a Shelby tube. Both tube specimens were retrieved from a depth of 7.5 m - 8.1m. The fixed-piston sampler has an outer diameter of 89mm, 5-degree cutting edge and area ratio equal to 9%. The U75 (Shelby), commonly used in Australian practice, has an outer diameter of 75mm and an area ratio of 8%. The cutting edge is 15 degrees. The inside clearance ratio is zero in both cases. Particular emphasis was made here on the detection of possible heterogeneities and their potential influence on laboratory testing. The free software Gimias® (Gimias, 2011) was employed for image post-processing. The attenuation scale shown in Figure 13 varies from white (maximum attenuation or high material density) to black (minimum attenuation or low density).

The comparison of the vertical sections shows clear differences between the two tube specimens. The specimen retrieved using the fixed-piston sampler seems quite homogeneous with a few sub-horizontal cracks observed at top and bottom ends. A highly disturbed specimen is obtained with the Shelby tube. Sub-horizontal cracks as well as vertical fissures and cavities are clearly identified along the 75-mm Shelby tube caused by the absence of a fixed-piston, which helps to compensate suction effects created at the bottom of the sampler during retrieval as discussed above. Figure 12 also shows cross-section images obtained at different depths along the tubes. It can be noted that the presence of fissures, cavities and shells in the Shelby tube which makes difficult to obtain representative specimens for laboratory testing (i.e., oedometer and triaxial tests). The black hole located at the top of the tube represents a cavity, which is assumed to be induced during sampling. In the case of the specimen retrieved with the fixed-piston sampler, the inspection of Figure 12 suggest that soil from slice 2 to 7 could be used for laboratory testing whereas top and bottom ends should be employed only for characterization purposes as suggested by Ladd & DeGroot (2003). Overall, CT images indicate that open sampler U75 induces higher soil disturbance than fixed-piston samplers despite its lower area ratio.

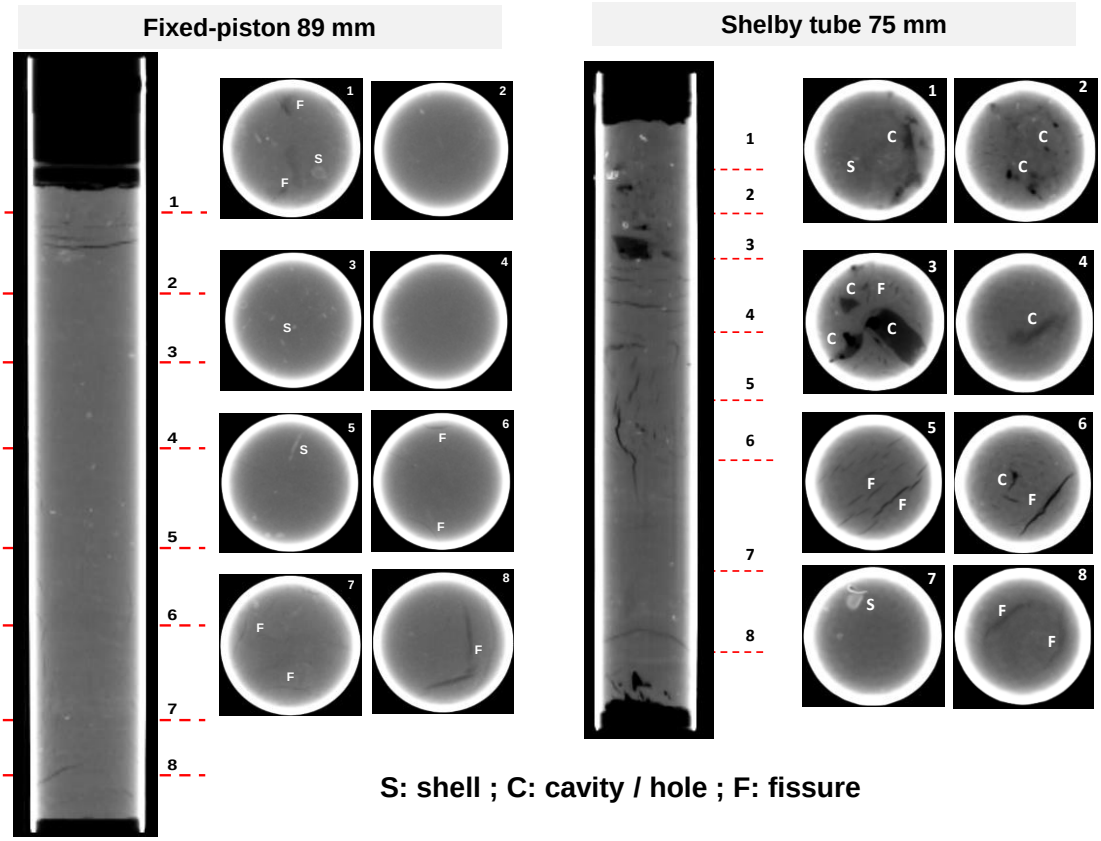

Figure 12: Qualitative CAT analysis in Ballina clay (Australia)

Sample quality assessment via shear wave propagation is becoming a common procedure in several laboratories worldwide. Shear waves, Vs, are preferred against compressional waves, Vp, as they can only propagate through the soil skeleton and therefore they provide useful information about changes in soil fabric, like those caused by sampling. Laboratory measurements are conveniently normalized against *in situ* values (e.g. CPTu, SDMT) in order to have an estimation of the reduction in soil stiffness due to sampling. Values of shear wave velocity measured at unconfined conditions (e.g., Landon et al., 2007; Donahue & Long, 2010) as well as at *in situ* stress conditions (e.g., Arroyo et al., 2015; Pineda et al., 2016b) are the two procedures followed in laboratory to check variations in soil stiffness due to sampling. Both have shown good correlation with sample quality descriptors ε_v and $\Delta e/e_0$ for a wide variety of soils.

Figure 13 shows V_s estimates for three natural soils: low plasticity Boston Blue clay (USA) (Landon & DeGroot, 2007), low plasticity silty deposits from Spain (Arroyo et al., 2015) as well as high-plasticity Ballina clay (Pineda et al., 2016). Block (Sherbrooke) specimens as well as tube samples (fixed-piston, Shelby tube and SPT samplers) are included in this figure. Good correlation between shear wave velocity, normalized against *in situ* values obtained from seismic dilatometer tests, $Vs_{(BE)}/Vs_{(SDMT)}$, and sample quality indicator $\Delta e/e_0$ is observed. Results shown in Figure 13(a) correspond to Vs estimates after recompression to the *in situ* vertical effective stress in CRS tests. Values of Vs measured at unconfined conditions are shown in Figure 13(b). Sherbrooke specimens show the lowest reduction in shear wave velocity followed by fixed-piston samplers and Shelby tubes. Recompression to the *in situ* stress in high-plasticity Ballina clay gives shear wave velocities close to the *in situ* measures. In the case of the low plasticity silty deposits, recompression bring the shear wave velocity to 0.80 $Vs_{(SMDT)}$ for $\Delta e/e_0=0$. Arroyo et al. (2015) observed that the normalized shear wave measurements showed a better correlation with sample quality when taken after recompression than when taken after re-saturation. Values reported by Landon et al. (2007) for Boston Blue Clay show a clear ordering of Vs with sample quality, with the Sherbrooke rating above the piston tubes, those above the Shelby and SPT. Vs reduces to $0.35Vs_{(SDMT)}$ and 0.15 $Vs_{(SDMT)}$ in specimens retrieved with Shelby tube and SPT sampler, respectively.

Despite the simplicity of the shear wave propagation technique, it is important to recognize that sampling may affect the soil stiffness in two opposite ways. Whereas soil stiffness may decrease due to soil destructuration it may increase if soil destructuration causes a reduction in porosity (compression). The latter has been reported in silty deposits (e.g. Long, 2006; Tor Lim et al., 2018b).

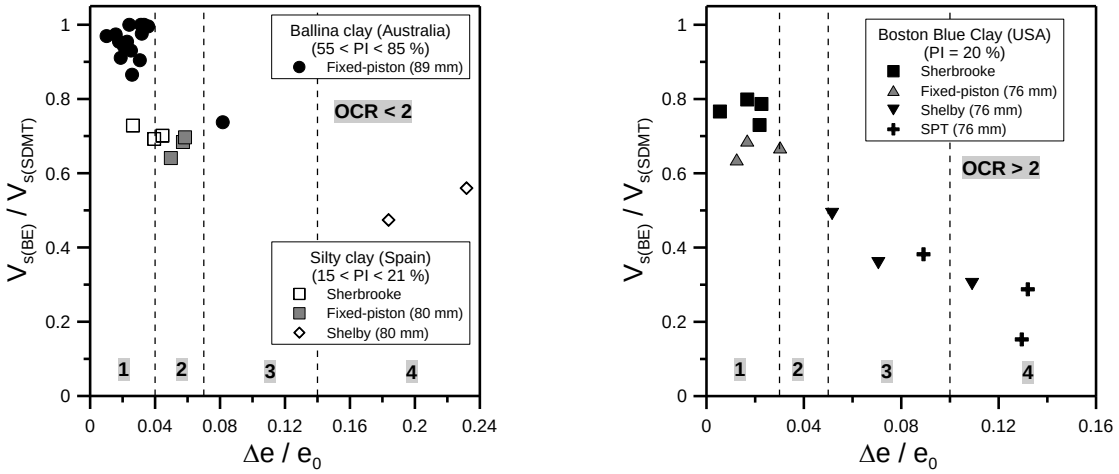

Figure 13: Normalized shear wave velocity vs Lunne's et al. sample quality indicator. (a) Ballina clay (Pineda et al., 2016b) and silty deposits (Arroyo et al., 2015). (b) Boston Blue Clay (Landon et al., 2007)

6. IMPLICATIONS OF SAMPLING DISTURBANCE IN GEOTECHNICAL DESIGN

Recently, Tor Lim et al. (2018a) evaluated the effects of sampling disturbance on the predicted behaviour of geotechnical infrastructure. Laboratory tests were performed on Ballina clay specimens retrieved from the National Soft Soil Testing Facility in Ballina (NSW) using four different samplers: (i) the U75 Shelby sampler (commonly used in Australian practice), (ii) the 100 mm free-piston sampler, (iii) the 89 mm hydraulic fixed-piston sampler and (iv) the 250 mm Sherbrooke (block) sampler. Block specimens were used to obtain reference soil parameters as the Sherbrooke sampler is recognized to provide specimens of the highest quality in soft soils (e.g., Terzaghi et al., 1996; Lunne et al., 1997). Results obtained from 1D Constant Rate of Strain (CRS) compression tests are shown in Figure 14(a). The inspection of the compressibility curves (e-log σ'_v) shows two main trends. Block and O89 specimens have the lowest volumetric deformation at $\sigma'_{v\text{-in situ}}$ followed by the P100 and U75 specimens. The small deformation that has been required to reach $\sigma'_{v\text{-in situ}}$ implies less degree of soil destructuration. This is consistent with the larger yield stress σ'_{yield} as well as the steeper slope of the compressibility curve post-yielding observed in block and O89 specimens. σ'_{yield} ranges from 20 kPa to 65 kPa. The value obtained from the U75 specimen, which is even lower than the $\sigma'_{v\text{-in situ}}$ (i.e. OCR<1), is incompatible with the stress history of the marine deposits at the Ballina site. Specimen P100 shows a σ'_{yield} slightly higher than $\sigma'_{v\text{-in situ}}$, thus, much lower than the level of overconsolidation ratio (1.5 < OCR < 1.6) reported by Pineda et al. (2016b). The oedometric modulus, $M=\delta\sigma'_v/\delta\varepsilon$, reduces from 2.72 MPa (block sample) to 0.25 MPa (U75 sample) in the overconsolidated range. Block and the O89 specimens show a similar trend which is followed by the P100 specimen only at larger stress levels. The variation of the compression index, $C_c=-\partial e/\partial\log(\sigma'_v)$, with σ'_v is highly non-linear, characterized by a peak value reached between 1.20 – 2.0 σ'_{yield}. As expected, strong non-linearity is observed in the block and O89 specimens, with a peak Cc values of 2.95 and 2.25, respectively. Lower peak values of C_c are reported for P100 and U75 specimens (1.83 and 1.38, respectively) for which a more gentle post peak reduction in C_c is observed. The post peak value seems to be similar for all specimens tested ($C_c \approx 1.30$), except for the U75 sample ($C_c \approx 1.0$).

Laboratory results were used to estimate the ratio $\Delta e/e_0$ used by Lunne et al. (1997) as sample quality descriptor (see Table 3). Figure 14(b) compares the estimated σ'_{yield}, M and $C_{c\text{-peak}}$ against $\Delta e/e_0$ obtained from CRS tests. The trend shown in this figure is qualitatively consistent with published data, i.e. the estimated σ'_{yield}, initial M and $C_{c\text{-peak}}$ decrease with reducing sample quality. σ'_{yield} reduces 30 % and 67 % in P100 and U75 specimens respectively. The reduction of M and $C_{c\text{-peak}}$ is even more dramatic. It may be noted that the P100 specimen has a good to fair quality according to the adopted sample quality criterion. This would imply that results from this specimen could be used with confidence in design, which would appear to be a misleading outcome judging by the comparison against mechanical properties measured in either block or O89 specimens.

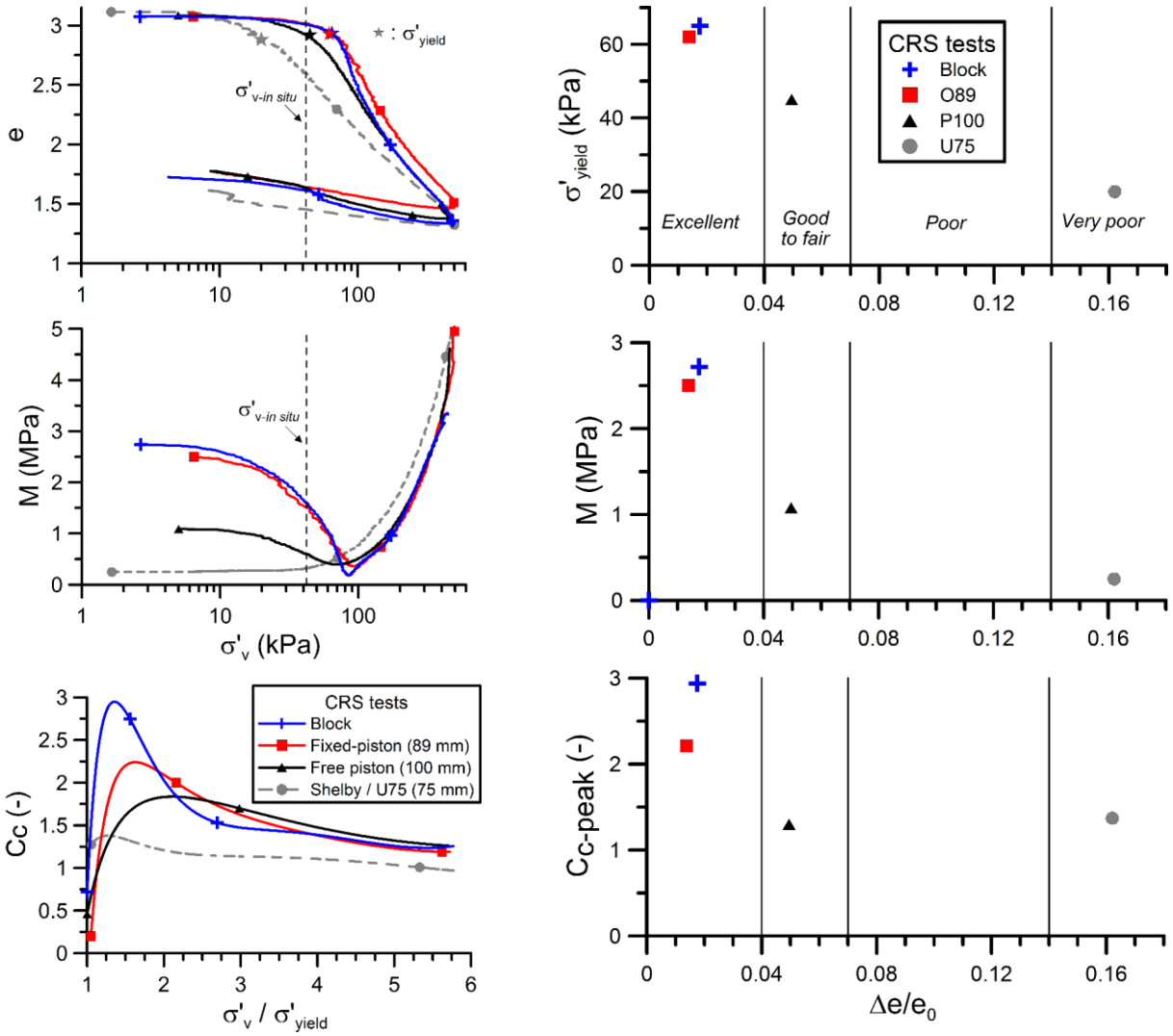

(a) (b)

Figure 14: (a) CRS test results on Ballina clay specimens. (b) Sample quality assessment

Compressibility parameters estimated from CRS tests were used by Tor Lim et al. (2018a) to assess the effects of sampling disturbance on the predicted surface settlement and excess pore pressure underneath an embankment built on Ballina clay. The geometry of the trial embankment constructed at Ballina site by the ARC Centre of Excellence for Geotechnical Science and Engineering (CGSE) was adopted here (Kelly et al., 2018) (see Figure 15). With the aim of emphasizing the effects of sampling disturbance on predicted soil behaviour, a few simplifications were made in the predictions presented below. Vertical drains, included in the trial embankment constructed at Ballina site, were neglected in the predictions described below. Moreover, a single layer soil profile was adopted. The predictions made include: (i) the end-of-primary consolidation settlement due to the weight of the embankment using 1-D consolidation theory, and (ii) the time variation of excess pore water pressure, degree of consolidation and consolidation settlement due to the construction of the embankment via the Finite Difference Method (FDM). Only total settlements are discussed here.

Figure 16 compares the predicted surface settlements using the set of parameters determined from CRS tests for each sampler type. Larger total settlement is predicted when using parameters obtained from block or O89 specimens, which had sample quality indexes of *excellent*. The settlement curve predicted for the P100 specimen is similar to those obtained for the block and O89. Although this result would be considered in agreement with its sample quality index of *good to fair*, it may be noted the important differences in soil properties between this sample and block and O89 specimens shown in Figure 14(a). Total settlement is mainly controlled by σ'_{yield} and C_c. The 'good' prediction obtained for the P100 specimen is attributed here to the counterbalance effects of a lower compression index (that reduced the predicted total settlement) and a lower yield stress (that increased the predicted total settlement). Figure 16(a) also

shows an important underestimation of total settlement when soil parameters are obtained using disturbed specimens such as those obtained with the U75 sampler. In this case, the reduction in C_c had more effect on the predicted total settlement than the reduction in σ'_{yield}. Underestimation of total settlement caused by embankment construction on soft clay has been commonly observed in Australian practice. This result is likely, to a large extent, due to the use of inappropriate sampling techniques, such as the U75 Shelby tube.

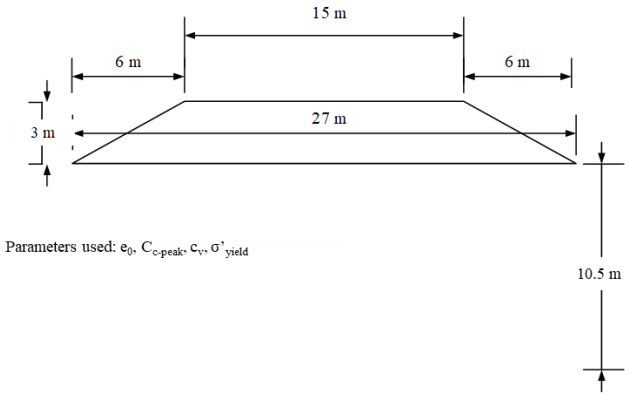

Figure 15: Embankment geometry

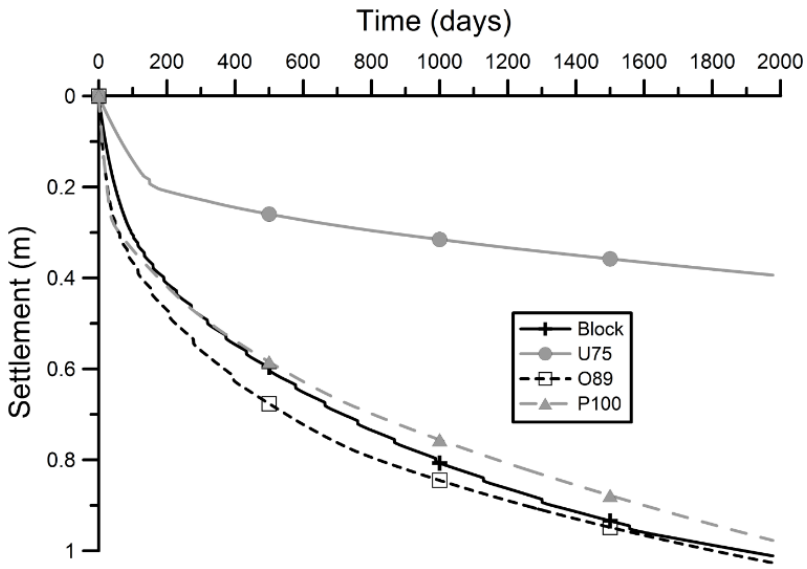

Figure 16: Predicted embankment surface settlement

7. CONCLUDING REMARKS

The paper discussed the factors influencing sampling disturbance and its consequences on the predicted behaviour of geotechnical infrastructure. It was showed that total settlement prediction underneath an embankment is strongly affected by sampling disturbance as a consequence of the important variation in σ'_{yield} and Cc (but also the cv which controls the excess pore pressure dissipation). Practitioners have to be aware of the fact that there are cases where correct predictions can be achieved, but for the wrong reasons, which by no means reflects good practice. It may occur, for instance, when the reduction in C_c is largely compensated for by the reduction in σ'_{yield}.

Relatively simple, relatively low cost steps can be taken to improve the quality of tested samples and hence the reliability of soil properties measured in the laboratory. It is recommended that these steps, below, be incorporated into routine practice.

- Use fixed-piston samplers for sampling soft soils (Shelby tubes should be avoided).
- The diameter of the tube sampler should be ≥ 63 mm. (50 mm tube diameters should be avoided).

- Use insulating materials, such as polystyrene plate, to separate the soil from the wax. In the case of block samples, aluminium foil and plastic film could be used as insulating materials.
- Tube/block specimens should be tested soon after sampling. In organic soils, storage for more than 3 months seems problematic.
- When possible, use either X-Ray or (conventional) medical CT scanning to assess sample quality and select the best zone of the tube for (mechanical) laboratory testing.
- Check sample quality using volume change relationships (either ε_v or $\Delta e/e_0$) and potentially laboratory shear wave velocity measurements (e.g. bender elements) correlated with $V_{s\text{-}in\ situ}$. This allows engineers to make judgement on the sensitivity of analysis to laboratory test inputs
- Regarding to the laboratory testing techniques (not discussed here), it is important to use pore water with similar salinity to natural water as it plays a key role on the mechanical behaviour of the soil.

8. ACKNOWLEDGEMENTS

The authors are grateful for support by all contributing partners to the ARC Centre of Excellence in Geotechnical Science and Engineering at the University of Newcastle, Australia. These partners include Advanced Geomechanics, Coffey Geotechnics and Douglas Partners. The senior author also acknowledges funding provided by the NSW Science Leveraging Fund. The first and fifth authors acknowledge the support given by the University of Newcastle through the *Research Advantage* Program, *ECR-HDR Scholarship* (2018-2022) scheme.

9. REFERENCES

Andersen A, Kolstad P. The NGI 54-mm samplers for undisturbed sampling of clays and representative sampling of coarser materials. In: Proc. Int. Symp. Soil Sampling, Singapore, 1979. 13–21.

ABAQUS/Standard User Manual. Version 6.14. 2016.

Arroyo, M, Pineda, J, Sau, N, Devincenzi, M & Pérez, N. Sample quality examination on silty soils. In 16th European Conf. on Soil Mechanics and Geotechnical Engineering, Thomas Telford Ltd, Edinburgh, Scotland, 2015. 2873-2878.

Arman A. & McManis K.L. Effects of storage and extrusion on sample properties, ASTM, 1976. STP 599: 66–87.

Baligh, M.M., Azzouz, AS & Chin, C.T. Disturbances due to "ideal" tube sampling. Journal of Geotechnical Engineering, 1987. 113, 7, 739-757.

Balinh, M. M. Strain path method. J. Geotech. & Eng. Div., Am. Soc. Civ. Engrs, 1985. 111, No. GT9, 1108-1136.

Bjerrum L. & Rosenqvist T.H. Some Experiments With Artificially Sedimented Clays, Géotechnique, 1956. 6: 124–136.

Clayton, C.R.I., Simmons N.E., Matthews M.C. Site investigation. 3rd Ed., University of Surrey, London, United Kingdom, 1995.

Clayton, C. R. I., Siddique, A. & Hopper, R. J. Effects of sampler design on tube sampler disturbance-numerical and analytical investigations. Géotechnique, 1998. 48(6), 847-867.

Clayton C.R.I. Managing geotechnical risk: time for change? Proceedings of the Institution of Civil Engineers, Geotechnical Engineering, 2001. 149(1), 3-11.

Donohue S. and Long M. Assessment of sample quality in soft clay using shear wave velocity and suction measurements. Geotechnique, 2010. 60 (11), 883-889.

Fiedler T., Belova I. and Murch G. On the thermal properties of expanded perlite – Metallic syntactic foam. International Journal of Heat and Mass Transfer, 2015. 90, 1009-1014.

Haji-Sheikh A., Eftekhar, J. Lou, D. Some thermophysical properties of paraffin wax as a thermal storage medium. 3rd Joint Thermophysics, Fluids, Plasma and Heat Transfer Conference, St. Louis, MO, USA, 1982. 1-10.

Hight, D. W. Laboratory testing: assessing BS 5930. Proc. 20th regional meeting of the Engineering Group of the Geological Society, University of Surrey, 1986. 43-52.

Hvorslev M.J. Subsurface exploration and sampling of soil for civil engineering purposes U.S. Army Corps of Engineers, Vicksburg, 1949.

Kelly, R.B., Pineda, J.A., Bates, L., Suwal, L. and Fitzallen, I. Site characterisation for the Ballina field testing facility. Géotechnique, 2017. 67(4), 279-300.

Kelly, R.B., Sloan, S.W., Pineda, J.A., Kouretzis, G. and Huang J. Outcomes of the Newcastle Symposium for the prediction of embankment behaviour on soft soil. Computers and Geotechnics, 2018. 93, 9-41.

Krage, C, Albin, B, DeJong, J & DeGroot, D. The influence of *in situ* effective stress on sample quality for intermediate soils. In Proc. 5th international conference in geotechnical and geophysical site characterization, ISC5, McConnell, Kelly & Lehane (eds), Gold Coast, Australia, 2016. Vol 1, pp. 565-570.

Lacasse, S., Berre, T., and Lefebvre, G. Block sampling of sensitive clays. Proceedings, 11th International Conference on Soil Mechanics and Foundations Engineering (2), San Francisco, 1985. 887-892.

Ladd, C.C. and DeGroot, D.J. Recommended practice for soft ground site characterization: Arthur Casagrande Lecture. Proc. 12th Pan American Conference on Soil Mechanics & Geotechnical Engineering, 2003. Vol. 1, Verlag Glückauf GMBH, Essen: 3-57.

Landon M., DeGroot D. and Sheanan T.C. Nondestructive sample quality assessment of a soft clay using shear wave velocity. J. Geotechnical and Geoenvironmental Engineering, 2007. 133(4), 424-432.

La Rochelle P., Leroueil S.& Tavenas F. A technique for long term storage of clay samples, Canadian Geotech. Journal, 1986. 23(4), 602-605.

Lefebvre, G. and Poulin, C. A new method of sampling in sensitive clay. Canadian Geotechnical Journal, 1979. 16(1), 226-233.

Long, M. Sample disturbance effects on medium plasticity clay/silt. In Proc. Inst. Civ. Eng. Geotech. Eng, 2006. 99-111.

Lunne, T., Berre, T. and Strandvik, S. Sample disturbance effects in soft low plasticity Norwegian Clay, Proc. Recent developments in soil and pavement mechanics, Rio de Janeiro, Brazil, 1997. 81-102

Lunne, T., Berre, T., Andersen, K., Strandvick, S. and Sjursen, M. Effects of sample disturbance and consolidation procedures on measured shear strength of soft marine Norwegian clays. Canadian Geotechnical Journal, 2006. 43(7), 726-750.

Mitchell J.K. & Soga K. Fundamentals of soil behaviour. Wiley & Sons, 2005.

Mitchell J.K. & Santamarina J.C. Biological considerations in geotechnical engineering, J. Geot. Geoenv. Eng., 2005. 131(5): 1222–1233.

Osterberg J. The new hydraulic piston sampler. Proc. 8th Int. Conf. Soil Mech. and Foundation Eng., 1973. Vol 1.2, 317-321.

Pineda, J.A., Liu, X-F. and Sloan S.W. Effects of tube sampling in soft clay: a microstructral insight. Geotechnique, 2016a. 66(12), 969-983.

Pineda, J.A., Suwal, L.P., Kelly, R.B., Bates, L. and Sloan, S.W. Characterisation of Ballina clay. Géotechnique, 2016b. 66(7), 556-577.

Rowe P.W. The relevance of soil fabric to site investigation practice. 12th Rankine Lecture, Geotechnique, 1972. 22(2), 195-300.

Thakur V. Can we assess the effect of storage time on fine-grained soil samples?, Environmental Geotechnics, 2014. 1(4), 1-4.

Tanaka, H., Sharma, P., Tsuchida T. and Tanaka, M. Comparative study on sample quality using several types of samplers. Soils and foundations, 1996. 36(2), 57-68.

Terzaghi, K., Peck, R. and Mesri, G. Soil Mechanics in Engineering Practice, Wiley & Sons, 1996.

Tor Lim G., Pineda J.A., Boukpeti N., Carraro J.A.H. and Fourie A. Effects of sampling disturbance in geotechnical design. Canadian Geotechnical Journal (in print), 2018a. https://doi.org/10.1139/cgj-2018-0016.

Tor Lim G., Pineda J.A., Boukpeti N., Carraro J.A.H. and Fourie A. Experimental assessment of sampling disturbance in calcareous silt. Geotechnique Letters (in print), 2018b.

A COMPREHENSIVE GEOTECHNICAL INVESTIGATION FOR THE NEW BRIDGE OVER THE CLARENCE RIVER AT HARWOOD

James Care[1] and Michelle Watson[2]

[1]Arup Pty Ltd, Email: james.care@arup.com

[2]Arup Pty Ltd, Email: michelle.watson@arup.com

ABSTRACT

The new bridge over the Clarence River at Harwood forms an integral part of the Pacific Highway upgrade in northern NSW and is currently under construction by the Acciona-Ferrovial Harwood Joint Venture (AFHJV). The proposed bridge extends 1.5km between abutments, spans the Clarence River with a water span of approximately 560m and is founded on 2m to 2.4m diameter driven hollow steel tubular piles to over 60m depth in some areas.

The underlying geology of the site consists of 30 to 40m of soft estuarine silts, clays and loose to medium dense sands underlain by saturated basal sands, gravel and cobbles up to 25m in thickness. Historical ground investigation information has thus far failed to provide confidence in the characterisation and engineering properties of this basal gravel and cobble layer due to limitations with conventional SPT, CPT and drilling techniques. The focus of this paper is primarily on characterisation of the basal sand and gravel units encountered in the River and North portions which largely drove the selection of innovative ground investigation techniques and methodologies.

A comprehensive ground investigation (GI) scope was proposed to support the bridge detailed design phase undertaken in parallel with the field works. This paper presents a perspective on the challenges of developing a ground model within this complex geological sequence and how this was addressed through a diverse, state-of-art GI campaign. It presents a methodology to derive ground profiles and soil parameters from advanced geotechnical testing and provides comparison of these innovative techniques against industry standard approaches.

1 INTRODUCTION

1.1 PROJECT DESCRIPTION

The new bridge over the Clarence River at Harwood forms an integral part of the Pacific Highway upgrade in northern NSW and is currently under construction by the Acciona-Ferrovial Harwood Joint Venture (AFHJV). The proposed bridge extends 1.5km between abutments, spans the Clarence River with a water span of approximately 560m and is intended to replace the existing lifting deck bridge located 30m upstream of the proposed alignment. The base of the proposed bridge deck is to be positioned at a level coincident with the top of the existing bridge lifting towers, some 30m above mean tidal water level. The bridge deck is supported by 35 piers at 36m to 45m spacing, each founded on two 2.4m diameter (land) or five 2.0m diameter (river) hollow tube steel driven piles. The bridge design evolved in parallel with the ground investigation (GI) which imposed further logistical constraints and prioritisation on the investigation program.

2 SITE GEOLOGY

2.1 GEOLOGICAL SETTING

The project site is located within the Clarence-Moreton Basin, an extensive on-shore Mesozoic sedimentary basin in northeast New South Wales and southeast Queensland. The basin comprises a sequence of fluvial sediments that rest on Palaeozoic basement of the New England Fold Belt. The site is situated within the southern region of the Clarence-Moreton Basin and is underlain by the bedrock of the Bundamba Group.

The portion of the Clarence River at Harwood is influenced by tidal movements and thus the site geology has characteristics of both a meandering river floodplain as well as estuarine environments. A deep paleochannel has been incised into the surface of the bedrock and is in-filled with Pleistocene age fluvial and estuarine sediments. The Pleistocene sediments have been further incised by a paleochannel and in-filled with younger Holocene age sands, silts and clays. The site is thus underlain by a complex sequence of fluvial and estuarine deposits of Holocene to Pleistocene age with soil depths ranging from 30m to over 80m in soil depth.

2.2 HISTORICAL GROUND INFORMATION

Given the long history of the Pacific Highway Upgrade project, ground investigation data at the site is available from historical GIs from 1962 through to 2016. Available data ranged from test pits and conventional boreholes to more advanced ground soundings such as cone penetration tests (CPT) and seismic dilatometers (sDMT).

Of interest for developing a suitable GI scope was the reported constraints regarding the deepest soil layer in the sequence. This material was summarised as medium dense to very dense sandy gravels and cobbles overlying bedrock. This basal sand and gravel layer was encountered in thicknesses from only a few metres at the midspan of the Clarence river to over 25m in thickness at the Northern abutment. It was noted that the depth and nature of the deposit resulted in poor sample recovery and therefore; no laboratory test data was available and significant uncertainty remained regarding the mechanical properties of the materials. The material was not encountered south of the Clarence River providing insight into the location and extent of the paleochannel incision and high energy flow environment required to deposit material of this nature.

2.3 SIMILARITIES TO MACLEAY RIVER FLOODPLAIN BRIDGE

Supplementing site specific ground information, prior experience from the Macleay River floodplain bridge, part of the Kempsey Bypass Project (2011). This experience identified similarities in geological conditions between the two sites where at both locations, a deep gravel and cobble dominant unit was encountered logged as medium dense to very dense. However, key field observations such as drilling resistance and observations of pile driving behaviour at the Macleay River site suggested the material performed as a loose formation under pile driving conditions, providing a contrast of information to that presented on borehole logs.

2.4 SUMMARY OF GROUND CONDITIONS

Ground conditions varied across the site however were generally distinct between the South, North and River crossing locations. Soil depth generally increased towards the north with average soil depths of 32m, 38m and 56m for the South, River and North locations, respectively. The focus of this paper is primarily on the basal sand and gravel units encountered in the River and North portions, which largely drove the selection of innovative ground investigation techniques and methodologies.

The underlying geology consists of 30 to 40m of soft estuarine silts and clays and loose to medium dense sands of Holocene to Pleistocene age. This is underlain by a layer of saturated basal sands, gravel and cobbles up to 25m in thickness with gravel grains and cobbles comprised of rounded high strength meta-siltstone.

The final interpreted geological long section is presented in Figure 1 (Arup, 2017) with simplified geological units descriptions listed in Table 1 to provide context for the remainder of this paper.

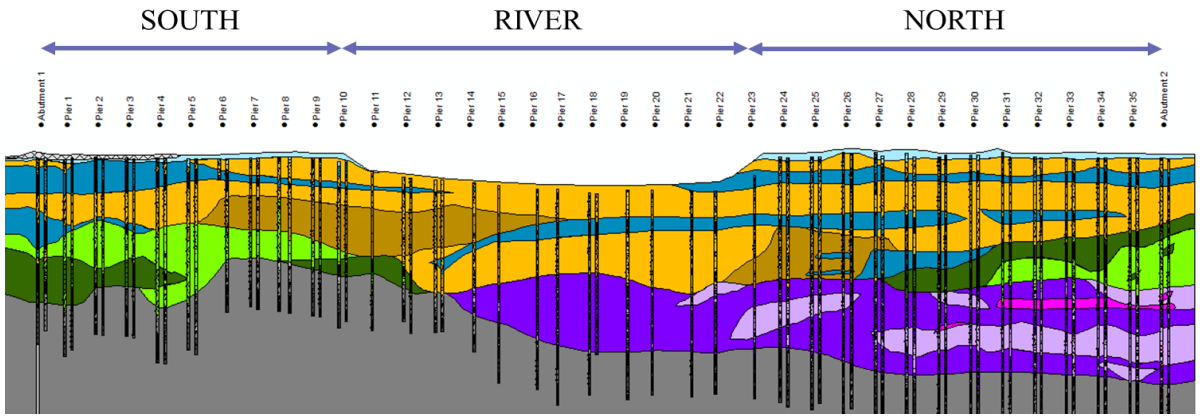

Figure 1: Final interpreted geological long section exaggerated by five times in vertical orientation (Arup, 2017)

Table 1: Summary of geological units at the site in relation to Figure 1 (Arup, 2017)

Geological sequence	Colour	Unit	Material description
Holocene (Clarence River floodplain)		Estuarine Clay	Dark grey silts and clays, very soft to stiff, with shells and minor organics
		Estuarine/Alluvial Sand and Clayey Sand	Grey to dark grey sands and clayey sands, very loose to medium dense, with shells and minor organics
		Estuarine/Alluvial and Clayey Sand	As above – medium dense to dense
Pleistocene (Clarence River floodplain)		Pleistocene Clay	Grey, pale grey and orange/red brown clay (often mottled and fissured), typically stiff to very stiff
		Pleistocene Sand and Clayey Sand	Clean grey, brown and yellow/orange brown sands and dark grey estuarine sands and clayey sands with minor organics, loose to very dense
		Basal Clays	Dark grey and grey-brown clay, trace of gravel, variable consistency
		Basal Sands	Pale grey to dark grey sands, silty sands and gravelly sands, medium dense to dense
		Basal Gravels	Gravels and sandy gravels to cobbles, rounded to sub-rounded, comprised of extremely high strength meta-siltstone grains
Bundamba Group		Rock	Interbedded siltstone and sandstone

3 GROUND INVESTIGATION SCOPE

A critical design uncertainty was the suitability of the basal sand and gravel layer for pile founding capacity and drivability assessments. Ground information available at the start of design was deemed insufficient to provide confidence in engineering design for foundations within the basal layer and thus the proposed GI was critical.

3.1 BOREHOLE DRILLING TECHNIQUES

Given the well-known difficulties penetrating gravel and cobble materials via conventional drilling methods, it was proposed that two boreholes be drilled at each bridge pier (one per pile, 10m spacing) consisting of one conventional borehole and one sonic borehole. Sonic boreholes allowed for continuous large diameter (80 to 120mm) soil cores to be recovered and sampled, appropriate for the larger grain sizes of gravel and cobble materials. This method provided an improved resolution of all soil units and in many instances identified lenses and layers, which would otherwise be missed by 1.5m interval SPTs. Conventional HQ sized boreholes were drilled to provide mechanical SPT testing as well as piston and push tube samplers for granular and cohesive materials respectively. Both conventional and sonic boreholes were switched to HQ sized rock coring below soil horizons. Table 2 summarises the borehole diameters and purposes utilised on the project.

Table 2: Summary of geological units at the site in relation to Figure 1 (Arup, 2017)

Borehole Technique	Size	Casing Outer Diameter (mm)	Core Outer Diameter (mm)	Application
Conventional Rig	HQ / HW	114.3	88.9	SPT tests and piston/tube sampling. PVC casing installed for Crosshole geophysics receiver
Sonic Rig	6inch	160.0	107.0	Continuous geological profile
Sonic Rig	8inch	210.0	152.0	Continuous geological profiling and installing PVC casing for Crosshole geophysics source

Wherever possible, conventional boreholes were scheduled in advance of sonic at each pier to limit potential disturbance and impact to SPT testing from the high frequency sonic vibration. It is acknowledged that limited published data is available on the zone of influence of sonic drilling, which may adversely impact subsequent SPT, CPT

or other ground sounding test results; and may be an opportunity for further study. The paired conventional boreholes provided SPT information for design engineers estimates of relative density of granular horizons and other soil units.

3.2 GEOPHYSICAL TESTING

A key limitation of both conventional and sonic drilling methods is the inability to provide reliable information on the density or mechanical properties of gravel and cobble dominant layers. Traditional SPT tests are well known to be unsuitable, CPTs and DMTs are unable to penetrate, and the high frequency vibration of sonic drilling effectively liquefies the soil matrix making meaningful measurements of density impossible.

As such the following series of geophysical test methods were proposed to provide insight into the density, stiffness and spatial characteristics of these materials:

- Cross-hole seismic testing at five selected land-based piers in the North site. PVC casing was installed in paired conventional boreholes (65mm inner diameter PVC) and sonic boreholes (100mm inner diameter PVC) to house the seismic geophone receiver and signal source, respectively.
- Natural gamma logging (QL40-GR Probe) within select boreholes to provide a mapping of relative levels of potassium, thorium and uranium gamma radiation signals. These elements typically occur in higher concentrations within clay soils and conversely in lower concentrations in clean sands (correspondence with Alpha Geoscience). Logging was undertaken through PVC casing for all cross-hole locations and groundwater monitoring wells and prior to pulling steel drilling casing from select over-water boreholes.
- Marine geophysical suite including sub-bottom profiling (SBP), continuous marine seismic refraction (CMSR) and the mapping of riverbed levels using bathymetric survey. This study provided a sub-surface profile by density, which was correlated against borehole information and natural gamma logs to support ground model development.

4 DEVELOPING THE GEOTECHNICAL MODEL

The geotechnical model summarises the spatial distribution and engineering properties of all materials below the ground surface. It is the fundamental basis for all geotechnical analysis and design. A high quality geotechnical model, which addresses the key geotechnical aspects of a project is essential to undertaking meaningful, efficient and cost-effective design. This section summarises how the ground investigation techniques described above were used to develop key aspects of the geotechnical model, focusing in particular on the basal sands and gravels.

A preliminary set of characteristics for the basal sand and gravel layer was based on the regional geology, tender stage ground investigation and previous projects in similar geology such as Kempsey Bypass. It was theorised that this unit comprised a high energy meandering river deposition comprising predominantly gravels, and likely including lenses of sands and/or clays. It was unknown whether the material would behave as loose or dense under pile driving conditions. The ground investigation was targeted to develop a sufficiently detailed ground model, addressing the following key uncertainties:

- Stratigraphy - soil grading, heterogeneity, clast supported or matrix supported gravels;
- Engineering properties - strength and stiffness;

This geotechnical model was developed in parallel with the ongoing field investigation and to inform design of pile capacity and settlement and drivability assessments (details of these calculations are not covered in this paper).

4.1 STRATIGRAPHY

A model of the basal sand and gravel stratigraphy was developed by plotting the borehole stratigraphy, SPT ‘N’ values and shear wave velocity measurements in 2D and 3D. Geological interpretation was undertaken between data points to understand the distribution of ground materials.

The recovered sonic cores confirmed that the basal sand and gravel unit comprised predominantly rounded coarse gravel to cobbles, which appeared to be clast supported. Extensive lenses of saturated sands and occasional 1m to 2m thick lenses of clay were also identified as part of the soil matrix. The gravel and cobble layers were noted to vary in thickness

from a few metres in the southern portion of the river to over 20m at the northern abutment. The composition of these gravel and cobble materials was later observed to be partially metamorphosed siltstone displaying extremely high strength based on point load testing of some suitably sized cobbles where failure was not achieved. Example sonic cores containing basal gravel, sand and clay material are shown in Figure 2.

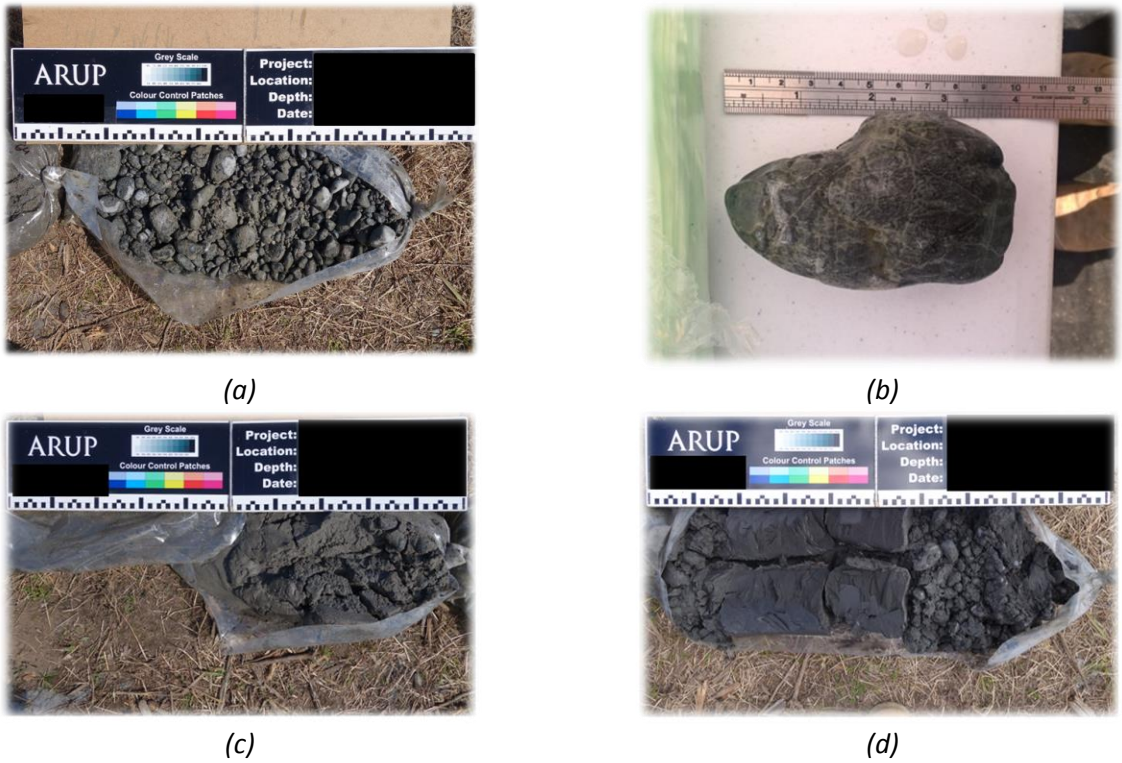

Figure 2: Example sonic soil core containing (a) gravel and cobble material, (b) recovered cobblestone, (c) sand material and (d) silty clay material

The sonic core provided a high resolution, continuous geological profile. The technique was ideal for the gravelly material which is challenging to penetrate and sample using conventional wash bore or coring techniques and ground soundings using cone penetration or dilatometer probes. The adjacent conventional wash-bored boreholes with SPT samples under-represented sand lenses and did not identify any of the clay lenses, which were able to be detected using sonic drilling.

4.2 STIFFNESS

The stiffness of the basal sand and gravel unit was assessed using typical empirical correlations and using the cross-hole and marine geophysics measurements. In this section stiffness will be discussed using the working shear modulus (G) and small strain shear modulus (G_{max}).

4.2.1 Derivation of stiffness using empirical correlations

Empirical correlations are widely adopted in industry for classifying soil stiffness. The working elastic modulus (E) was approximated by empirical correlation of SPT 'N' values from the conventional boreholes using Eq. (1) below:

$$E = 1000N_{60} \text{ (CIRIA, 1995)} \quad (1)$$

The working shear modulus was then calculated using Hooke's Law:

$$G = \frac{E}{2(1+\nu)} \quad (2)$$

4.2.2 Derivation of stiffness using geophysics

The small strain shear modulus of the soil (G_{max}) can be directly calculated from the shear wave velocity. The shear wave velocity of a homogenous, isotropic solid is related to the small strain shear modulus (G_{max}) using Eq. (3) below:

$$G_{max} = \rho V_s^2 \text{ (Lunne et. al. 1997)} \quad (3)$$

Where ρ is the soil mass density and V_s is the shear wave velocity.

The small strain shear modulus is related to the working shear modulus by shear modulus ratio G/G_{max}. The measured shear wave velocity and constrained modulus values from available seismic dilatometer testing were used to establish a site-specific shear modulus ratio for each unit using the approach presented in Varcoe et al. (2015).

4.2.2 Comparison of empirical correlation and geophysics

The cross-hole and marine geophysics indicate a much greater for the basal unit's in-situ stiffness than that derived from the SPT data, shown in Figure 3 below. Due to difficulties in obtaining accurate measurements of basal gravel densities, sensitivity checks were performed assuming various densities from very loose to very dense based on correlation with the SPT data. The increase in stiffness inferred from the geophysical testing was up to 8 times greater at lower relative densities (very loose to loose) and 1.5 to 3 times greater at higher relative densities (medium dense to very dense).

The higher soil stiffness calculated from geophysics was believed to be more representative as the calculation of G_{max} is not reliant on empirical correlations. This has been demonstrated on previous projects in similar geology such the Kempsey Bypass (Terzaghi et al. 2015). The higher soil stiffness was important to prove that the proposed pile design satisfied the strict project settlement criteria. The higher stiffness also attracts additional bending moments for the lateral pile design. Adopting the lower stiffness from empirical correlations can under-estimate the bending moments generated in the piles.

The ability to determine stiffness parameters directly using geophysics for coarse grained materials is valuable as it is site specific, provides higher confidence in the determined parameters and offers programme and cost savings where higher stiffness allows for a more efficient design. The empirical correlations commonly used in industry are typically conservative, in many cases are derived from case histories, which are not representative of the project.

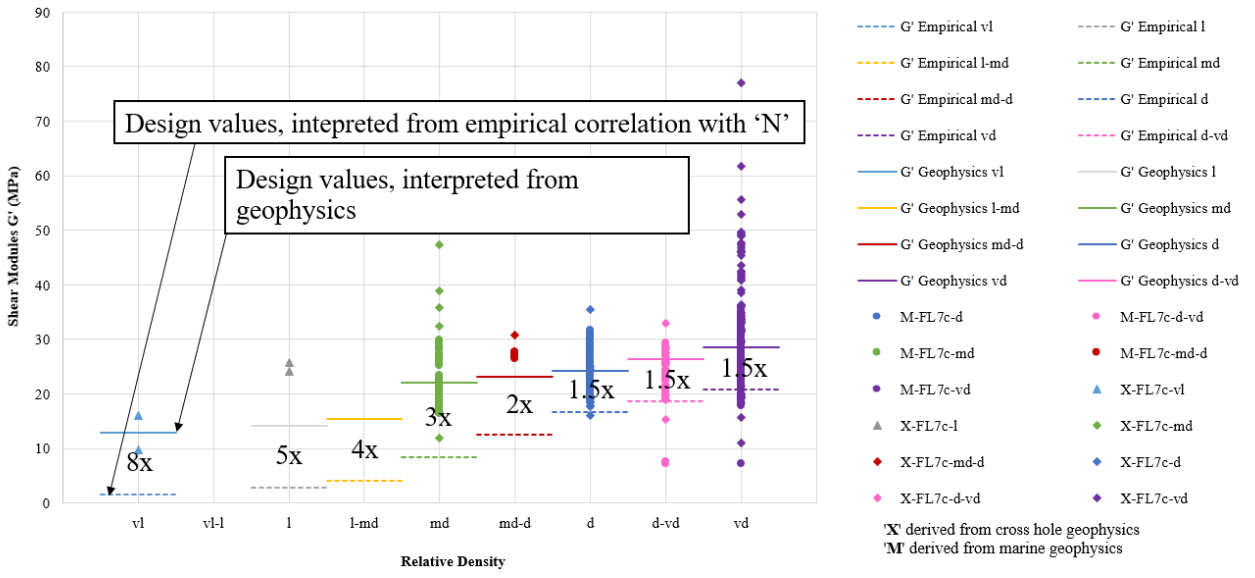

Figure 3: Comparison of stiffness estimate obtained from empirical correlation with SPT 'N' and geophysics for Basal Gravel unit

4.3 STRENGTH

4.3.1 Derivation of strength using SPT 'N'

The Mohr-Coulomb framework is widely adopted in industry for classifying soil strength using effective friction angle (ϕ') and effective cohesion (c'). The effective friction angle of granular materials is often estimated empirically using published empirical correlations with SPT 'N'. The relationship presented by Peck et al. (Peck 1963, cited in Tomlinson, 2001) has been adopted and is shown in Figure 4 below. As the basal sand and gravel layer is predominantly granular, the effective cohesion was not assessed.

4.3.2 Derivation of strength using geophysics

The critical state framework provides an alternative method of deriving soil strength from the shear wave velocity measured by cross-hole and marine geophysics. In the critical state framework, strength is understood using the critical state parameter ψ, which can be empirically correlated to a Mohr-Coulomb friction angle.

The soil void ratio (e) was calculated empirically from the small strain shear modulus derived using Eq. (1). A number of empirical relationships exist from small strain shear modulus to void ratio. A modification of the Hardin & Black equation (Hardin and Black 1968, cited in Das 1993) presented in Eq. (4) has been adopted for sands and gravel units at the project site.

$$e = \frac{2\omega + \kappa \pm \sqrt{(-2\omega - \kappa)^2 - \omega(\omega^2 - \kappa)}}{2} \quad (4)$$

Where $\kappa = \frac{G_{max}}{A} * \left(\frac{p'}{p_{ref}}\right)^{-m}$, $\omega = 2.17$, $A = 80$, $m = 0.5$, p' = mean effective stress and p_{ref} = reference pressure

The state parameter can then be calculated at any depth using Eq. (5). The critical state void ratio (e_c) can be obtained by laboratory testing. To allow for comparison with conventional Mohr-Coulomb strength parameters, the peak effective friction angle can then be approximated using Eq. (6)

$$\psi = e - e_c \text{ (Jeffries and Been, 2016)} \quad (5)$$

$$\phi' = -45 \times \psi + 32 \text{ (Jeffries and Been, 2016)} \quad (6)$$

4.3.3 Comparison of friction angle derived from SPT 'N' and geophysics

A comparison of ϕ' derived from empirical correlation with SPT 'N', and geophysical testing at five pier locations is presented in Figure 5. A number of useful observations can be made:

- The estimated friction angle is loosely correlated between the two approaches, however; the SPT 'N' indicates a denser soil profile and geophysics indicates a looser soil profile;
- High estimated friction angles generally corresponded with gravel layers. Where SPT refusal occurred (represented by the horizontal cluster of data points at a friction angle of 54°), the estimated friction angle is typically larger than the estimated friction angle derived from geophysics;
- Low estimated friction angles generally corresponded with sand lenses. Where low SPT 'N' values were obtained (SPT 'N'=0-5) geophysics confirmed that these values were representative of loose layers within the profile. Care should be taken in the interpretation of occasional low SPT 'N' values within a gravelly profile. Low SPT 'N' values should not be simply dismissed as outliers or errors in testing;
- Sonic drilling was essential to understanding friction angles interpreted from both methods within the context of the geological model. The ground model derived from widely spaced SPT tests can be misleading as significant sand and clay lenses are not able to be identified.

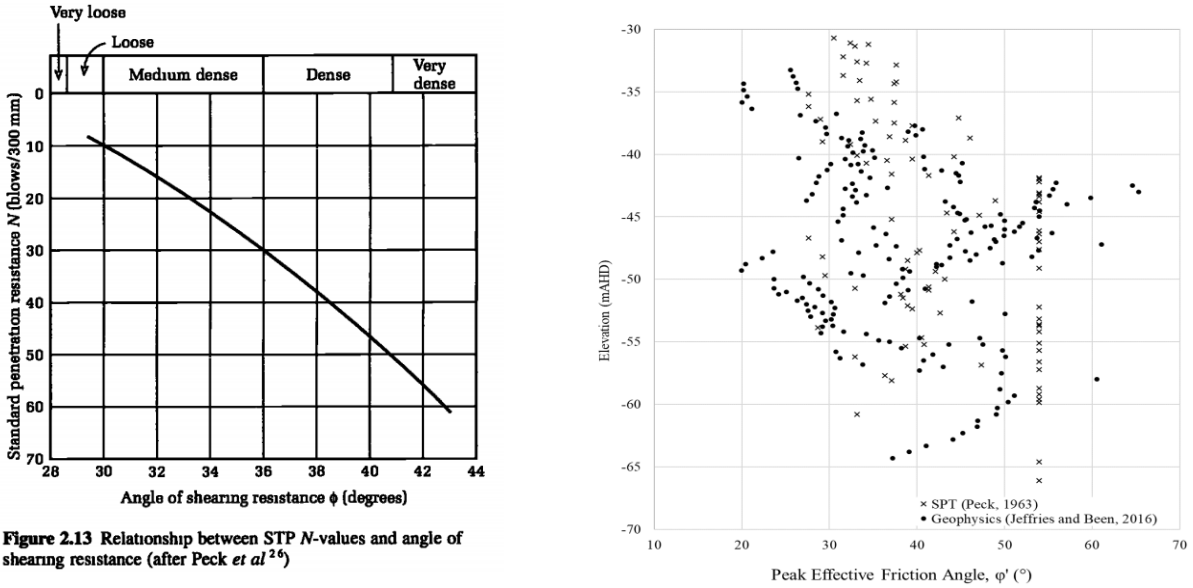

Figure 2.13 Relationship between STP *N*-values and angle of shearing resistance (after Peck *et al* [26])

Figure 4: (Left) Relationship between SPT 'N' value and angle of friction (Peck 1963, cited in Tomlinson, 2001) (Right) Peak effective friction angle versus elevation for the basal sand and gravel unit, derived using SPT N60 (Peck et. al) and geophysics (Jeffries and Been, 2016)

5 TECHNICAL SUCCESSES

5.1 DRILLING RESISTANCE OF BASAL GRAVELS

Despite the physical difficulties progressing conventional drilling methods in gravel materials, valuable observations could be made and recorded by the supervising engineer and drillers of drilling resistance through various strata. The interbedded nature of the basal deposits and distinctive 'crunch' on first strike of gravel or cobbles, allowed relatively accurate measurements of layer thickness and transitions.

As the drill string was advanced, it was often necessary to pull back and re-drill to prevent locking up of the drill bit between large cobbles. It was often the case that after multiple drill passes, the similarities in resistance of each pass suggested that the gravel and cobble grains were merely being pushed aside and thus the material was sufficiently loose to allow for this movement. These observations were recorded on borehole logs as a valuable piece of information, which would be otherwise ignored to the design engineer scanning SPT values of refusal.

Both tri-cone and diamond tipped coring drill-bits were trialled in the basal gravels, each with degrees of success. Whilst tri-cone bits are more suitable for progression and tend to survive longer, soil returned in drilling fluid is generally crushed and provides little information on the true size of the gravel and cobble grains. Diamond tip drill bits on the other hand can core through larger cobbles and pickup gravels providing some indication of size up to the core barrel diameter (PQ in this case), albeit with a shorter lifespan and thus additional cost.

5.2 NATURAL GAMMA LOGGING

One of the more unique techniques employed was natural gamma logging, which is more often deployed in the minerals, oil and gas industries. The method relies on the detection of gamma emission spectra of primarily potassium occurring naturally in clay dominant rocks such as siltstones, and shales. Whilst natural gamma logging does not provide distinct 'geological logs', the interbedded nature of the soil sequence at the site coupled with complete sonic soil cores provided a supplementary source of information regarding layer transitions. Seawater was observed to have a relatively insignificant gamma emission signature and thus the depth to mudline could be easily confirmed from gamma traces.

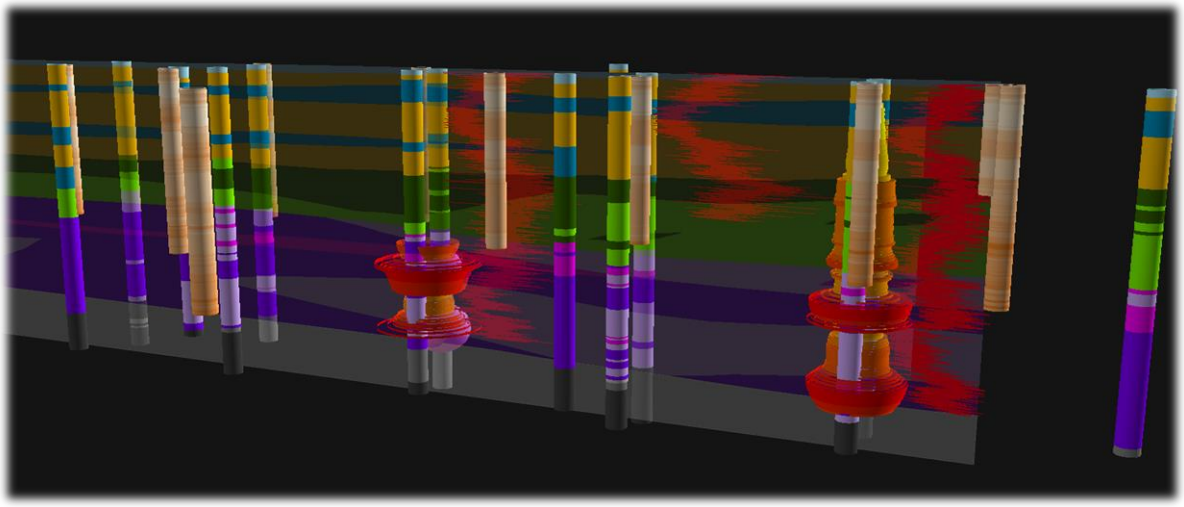

Figure 5: Example of natural gamma traces (red lines) overlayed on a 3D geological model

Natural gamma logging was undertaken within boreholes following installation of PVC for cross-hole geophysics or groundwater monitoring wells as well as prior to pulling up steel casing for overwater boreholes. To test the potential signal attenuation through steel, a comparison was undertaken on a land-based hole through steel casing and then again through PVC with determined a minor attenuation of about 2%.

The equipment was easily operated by a field engineer or geologist following supplier training requiring only operation of a wireline winch and data logger, powered by a 12volt battery or mains supply. For the probe supplied for this project, a winch speed of 3m/min was used, and a trace was obtained on both the up and down legs and undertaken twice at each location. Comparison of the up, down and different passes showed only natural variability with the overall trace shapes largely consistent.

A few useful observations of trends and patterns of natural gamma traces on the project were:

- Generally higher emission signatures at depths coinciding with logged clays and sandy clays and conversely lower signatures in sand dominant materials. Very low relative signatures were recorded for clean sands observed on the South portion of the site.

- A relatively larger range and scatter of emission signatures at depths coinciding with logged gravel and cobble materials. The authors suspect that the scatter is a result of the relatively high concentration of clay particles within the meta-siltstone gravel contrasted with void/water space between the grains.

An example of natural gamma logs within the context of a 3D ground model is presented in Figure 5 showing higher relative readings within clay dominant materials (shown in darker colour sets, see Table 1).

The typical time from setup to pack-down for a 65m borehole was one hour; a month hire cost of the equipment totalled A$6000 thus making this technique remarkably efficient. This leads the authors to conclude that for complex interbedded sequences, the return on investment and value add to geological logs from an accompanying natural gamma log is substantial and hopes to see the technique more widely researched and employed for use in the geotechnical industry.

6 CONCLUSIONS AND RECOMMENDATIONS

A comprehensive and diverse GI campaign was completed for the proposed bridge over the Clarence River at Harwood which included conventional and sonic drilling and geophysical test methods. The scope of works was developed and delivered to manage the technical and physical challenges of obtaining reliable material information of deep gravel deposits. Reflecting on these challenges and successes, the author draws the following conclusions and recommendations:

- Substantial value can be added for designers, clients and projects by pursuing non-traditional investigation techniques such as sonic drilling and geophysical surveys. The best outcomes occur where emphasis on a 'right tool for the right job' approach is adopted and by utilising a diverse range of techniques to build sound evidence-based ground models.

- Sonic drilling coupled with cross-hole seismic testing and marine geophysics is a viable strategy for obtaining meaningful engineering properties for gravel and cobble dominant beds where conventional SPTs are unsuitable. Sonic cores provide engineers and geologists with meaningful observation of grain size and characteristics whilst geophysics can provide small strain material behaviour properties and densities.

- Natural gamma logging presents a time and cost-efficient technique for sub-surface profiling and is a valuable supplement to a borehole log, particularly in complex and interbedded sequences.

- Observations of drilling resistance and physical challenges of penetrating gravel and cobble materials should always be recorded on logs as they can provide insight into relative density to contextualise refusing or outlier SPTs.

6.1 AREAS FOR FURTHER RESEARCH

- Investigation of the zone of influence of sonic drilling vibration to determine whether results of SPT, CPT or geophysical tests adjacent to a previously drilled sonic borehole are compromised.

- Further research into the application of natural gamma logging and other easily deployed and efficient geophysical test methods to extract additional geological and geotechnical data from drilled boreholes.

- Feasibility of positioning geophone arrays at ground surface to detect SPT blows at depth as a seismic source providing a "reverse down-hole seismic" test during conventional borehole drilling. Such a method could be reasonably and cost efficiently deployed for many ground investigations to capture data on material properties.

- Evaluation of design methodologies adopted and comparison with results of pile driving.

7 REFERENCES

Arup. *Pacific Highway Upgrade – W2B – Bridge over Clarence River at Harwood - Geotechnical Factual Report. (Ref: W2B-AFV-E-GX-RPT-00004).* 2017a.

Arup. *Pacific Highway Upgrade – W2B – Bridge over Clarence River at Harwood - Geotechnical Interpretive Report. (Ref: W2B-AFV-E-GX-RPT-00003 I02).* 2017b.

Construction Industry Research Information Association (CIRIA). *Report 143: The Standard Penetration Test (SPT) Methods and Use*. 1995. 144p.

Das, B. M. *Principles of soil dynamics.* PWS-KENT Publishing Company, 1993. 570p.

Jefferies, M., Been, K. Soil Liquefaction: A Critical State Approach. Environmental Earth Sciences, 2nd Ed, 2016. **169**(3): p.317

Lunne, T., Robertson, P. and Powell, J. *Cone Penetration Testing in Geotechnical Practice*. CRC Press, First Ed. 1997. 352p.

Parry, S. Baynes, F, J. Culshaw, M, G. Eggers, M. Keaton, J, F. Lentfer, K. Novotny, J. Paul, D. *Engineering geological models: an introduction: IAEG commission 25.* Bulletin of Engineering Geology and the Environment, 2014. 34p.

Tomlinson, M. *Foundation Design and Construction*, Pearson Education Limited, 7th Ed. 2001. 584p.

Varcoe, J., Nation, K., Nunn, K. and Terzaghi, S. *Application of modern ground investigation techniques to characterise Quaternary sediments in Kempsey.* 2015. 8p.

AN INNOVATIVE METHOD OF ASSESSING THE CAPACITY OF EXISTING WHARF PILES

Patrick Wong[1] and Peter Hitchcock[2]

[1]Senior Consultant, Coffey Services Australia Pty Ltd, NSW, Australia, patrick.wong@coffey.com and Senior Principal, PKW Geosolutions Pty Ltd, NSW, Australia, pwong@pkwgeosolutions.com.au

[2]Geophysicist, Coffey Services Australia Pty Ltd, NSW, Australia, peter.hitchcock@coffey.com

ABSTRACT

North Queensland Bulk Ports (NQBP) is upgrading the Mackay Outer Harbour wharves. The work involves a fender replacement and bollard upgrading programme. As a result of the proposed upgrade, the axial capacity of the fender piles at Wharves 1, 4 and 5 is increased from the original design requirements.

The existing piles beneath the wharf deck are driven steel tubular piles and they range in diameter from 0.457 m for Wharves 1 and 4, to 1.0 m for Wharf 5. Unfortunately, no construction records could be found in relation to as-constructed pile toe levels, final driving energy and sets or pile load testing. Therefore, the as-installed pile capacities could not be readily assessed. Using conventional theoretical assessment methods, the design consultant concluded the existing piles would not have adequate capacity to support the increased axial loads. The challenge was to investigate and assess whether the existing fender piles can support the increased axial loads associated with the wharf upgrade, and if not, what are the options for remediation.

This paper describes the investigation and assessment of the axial capacity of the existing piles using a combination of innovative downhole magnetic testing adjacent to the existing piles to assess the as-constructed pile toe levels, conventional coring to assess the founding materials, and dynamic pile load tests on new prototype piles driven close to the existing piles. Using the innovative investigation and assessment technique, the existing piles were assessed to have adequate capacity and successfully avoided the costly option of remedial works for the client.

1. INTRODUCTION

The Mackay Outer Harbour is situated in Northern Queensland of Australia, and was officially opened on 26 August 1939 (see Figure 1). The deep water port became an important facility for the thriving trade of a growing district. In 1957, the bulk sugar handling terminal was open, servicing the sugar industry that started in the region in 1865.

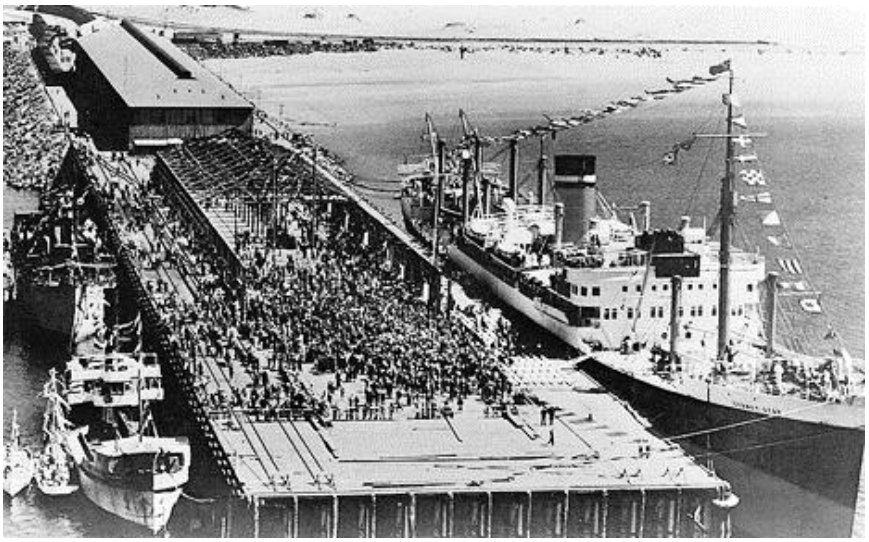

Figure 1: Official Opening of Mackay Outer Harbour in 1939 (source: Daily Mercury https://www.dailymercury.com.au/news/mackay-harbour-70-today/304046/)

Since its opening, various phases of harbor expansion took place under McKay Harbour Board. Wharf No. 4 was constructed circa 1967 and Wharf No. 5 followed later under McKay Harbour Ltd which changed to North Queensland Bulk Ports in 2009. The locations of Wharves 1, 4 and 5 are shown in Figure 2.

Figure 2: Site Plan showing Wharf and Borehole Locations

In 2017, NQBP commenced upgrade work on wharves 1, 4 and 5 involves a fender replacement and bollard upgrading programme. As a result of the proposed upgrade, the axial capacity of the fender piles at Wharves 1, 4 and 5 is increased from the original design requirements. The piles supporting the wharves are driven tubular steel piles ranging from 457 mm diameter at Wharves Nos. 1 and 4, to 1000 mm diameter at Wharf No. 5. The required pile capacities are compared to estimated pile capacities made in 2016 by another geotechnical consultant as summarized in Table 1.

Table 1: Pile Loads and Initial Estimate of Capacity

Statistics	Design Ultimate (kN)	Available Design Ultimate Capacity[(1)] (kN)
Compression Row C	1,135	650
Compression Row D	1,364	975
Tension	426	225

[(1)] Estimated by another geotechnical consultant in 2016

Due to the lack of information on as-constructed pile toe levels, final driving energy and sets or pile load testing at the wharves in question, doubts were raised on the ability of the existing piles to carry the revised loads based on the theoretical assessment results shown in Table 1. Contrary to the theoretical assessment, however, a previous dynamic pile load test with CAPWAP assessment on a pile installed at Wharf 3 gave a compression capacity of a 1000mm diameter pile of 1,900 kN in shaft resistance and 5,380 kN end resistance, i.e. 7,280 kN total capacity (or a design ultimate capacity of 798 kN in tension and 5,096 kN using a tension to compression capacity ratio, R_{st} of 0.6 (based on De Nicola and Randolph (1993) and a geotechnical strength reduction factor ϕ_g of 0.7). This is significantly higher than the theoretical estimate made by the other consultant and therefore gave at least some confidence that the existing piles may be able to carry the revised loading associated with the upgrade without remedial works. To confirm this initially assessment, the following programme of investigation was carried out:

- Drilling of 3 boreholes, one at each of Wharf 1, 4 and 5 adjacent to existing piles at the locations shown in Figure 2.
- Conduct downhole magnetic testing in PVC access tubes installed at the completion of the boreholes to assess the toe levels of the adjacent piles.
- Install 457 mm diameter tubular steel test piles to the assessed pile toe levels.
- Conduct dynamic pile load testing and CAPWAP analyses (Rausche et al, 1985) to assess the ultimate pile capacity of the test piles.

The test results and subsequent interpretations are discussed below.

2. BOREHOLE AND DOWNHOLE MAGNETIC TESTING

Three boreholes were drilled at the approximate locations shown in Figure 2. It had originally been intended to drill the boreholes within 1 m of the external face of the existing pile for the downhole magnetic testing. Unfortunately, that was not possible due to site access constraints and the boreholes were drilled at distances ranging from 1.3 m to 1.6 m. Beyond 1 m distance, the accuracy of the magnetics testing reduces.

Downhole magnetics testing is a passive method based on the measurement of localised perpetrations of the Earth's magnetic field measured in nano-tesla's (nT). These may be caused by geological features and buried ferrous targets (eg, pipes, cables, drums, iron sheets, steel reinforcement etc).

The magnetics testing was completed in-situ using pre-drilled, PVC cased boreholes. A Bartington 3-component fluxgate magnetometer was used to measure the magnetic field variations at 0.5m intervals to the maximum depth of the borehole. The magnetic data was acquired with Spectromag-6 software.

The borehole magnetometer was lowered from the top of each borehole (from the wharf deck) and repeated magnetic measurements were made at each depth to assist assessment of any external magnetic noise.

The borehole magnetometer measures magnetic field intensity in three dimensions (X, Y and Z) with the vertical (Z) component of the magnetic field typically providing the clearest indication of the base of steel piles and hence the approximate depth of the pile. Furthermore, the vertical first derivative of the vertical component of the magnetic field can also reliably indicate the base of a steel pile. Figure 3 shows a typical magnetic response of a pile as sensed from a proximal borehole adjacent to the pile, including the vertical component and vertical first derivative of the magnetic response. This shows that a magnetic anomaly indicates the approximate base of the pile.

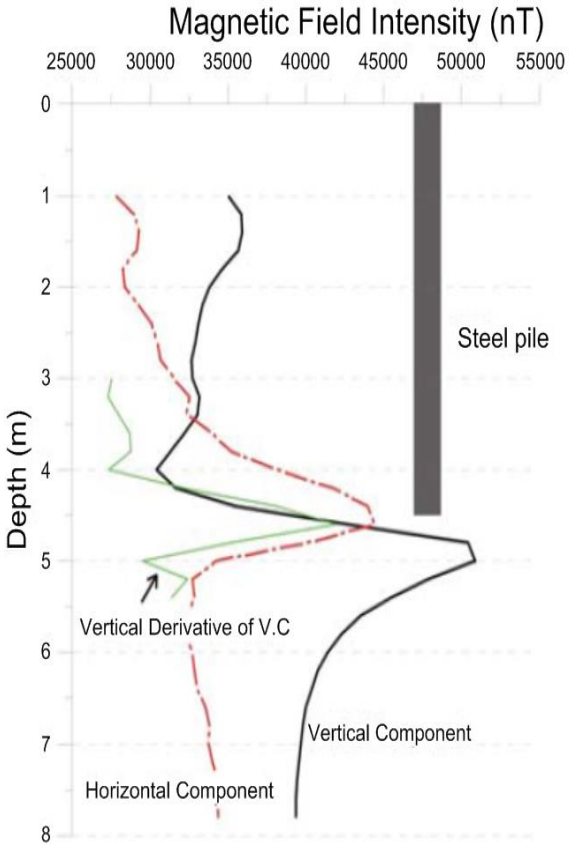

Figure 3: Typical Magnetic Response of a Steel Pile (from Jo. *et al.*, 2003)

3. SUBSURFACE PROFILE AND INFERRED PILE TOE LEVELS

The results and interpretation of the downhole magnetics testing are shown in Figure 4 below. It can be seen that the clearest magnetic response change was obtained at Wharf 4 where the borehole was at the least distance away from the face of the nearest pile.

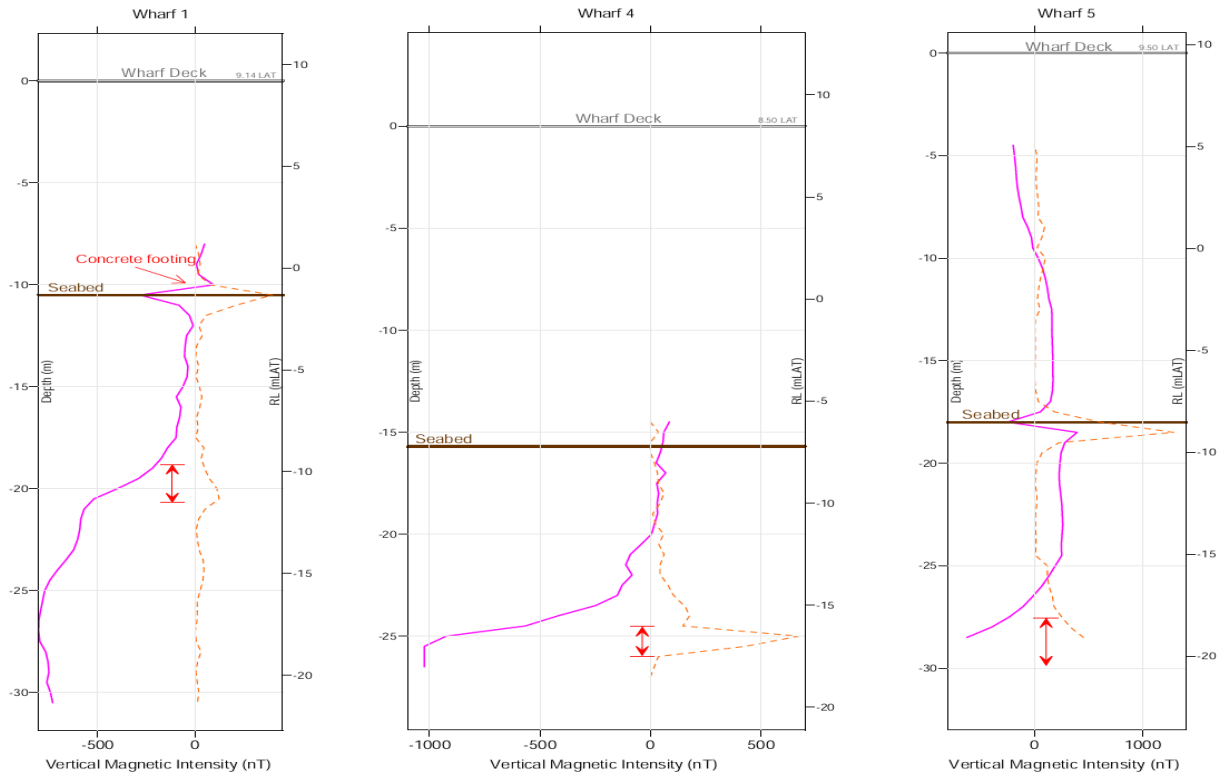

Figure 4: Results of Downhole Magnetics Testing

The results of the borehole drilling and inferred pile toe levels at each borehole location based on interpretation of the downhole magnetics testing are summarized in Table 2.

Table 2: Summary of Borehole and Downhole Magnetics Investigation Results

Borehole	Approximate Distance to Nearest Existing Pile (m)	Inferred Pile Toe Level Range[1] from Magnetics Testing (mLAT)	Materials Recorded in Borehole and Standard Penetration Test Results
Wharf 1	1.4	-9.7 to -11.6 (-12.8)[2]	Gravelly Clayey Sand and Clayey Sand, SPT- N = 21 and 26 above -11.6 m LAT SPT-N = 39 at -12.8 m LAT
Wharf 4	1.3	-15.0 to -17.4	Gravelly Sand and Clayey Gravelly Sand (Residual Soil), SPT-N = "R" (30 blows per 145 mm penetration)
Wharf 5	1.6	Below -18.1	Sandy Gravelly Clay and Sandy Gravel, SPT-N = "R" (30 blows per 100 mm penetration)

(1) Definitive levels cannot be inferred due to attenuation of magnetic intensity with distance away from the pile, and potential influence from other piles that have different toe levels.

(2) Based on SPT-N value, it is unlikely that the pile would have terminated in SP-N of 21 to 26 material. Therefore, the next SPT of N = 39 at 22 m depth (-12.8 mLAT) is considered to be a more reasonable estimate.

4. TEST PILE AND CAPWAP ANALYSES

The proposed methodology of testing originally proposed was that the test piles should have been installed to a similar pile toe level as assessed by the magnetics testing. However, due to logistics reasons, the test piles were installed before the magnetics testing took place, and they were generally driven to a level lower than the pile toe levels inferred from the magnetics testing.

The test piles comprised 457 mm OD steel tubular piles with a wall thickness of 15.9 mm, and they were driven using a Junttan HHK7A hammer. The average final sets under a final drop height of 1.2 m and the corresponding materials at the end of drive toe level from the nearest boreholes are tabulated in Table 3 and the CAPWAP analysis results of the test piles are summarized in Table 4.

Table 3: Test Pile Average Final Set and Founding Material

Test Pile	Installed Pile Toe Level (mLAT)	Average Final Set (mm/blow)	Founding Material Inferred from Nearest Boreholes
TP1 – Wharf 1	-16.553	1.6	Clayey Sandy Gravel, Residual Soil, SPT-N = "R" (30 blows / 60 mm penetration)
TP4 – Wharf 4	-17.558	2.1	Extremely Weathered Rock, SPT-N = "R" (30 blows / 60 mm penetration)
TP5 – Wharf 5	-19.169	2.2	Sandy Gravel, SPT-N = "R" (30 blows / 100 mm penetration)

Table 4: Results of Test Pile CAPWAP Analysis

Test Pile	Inferred EOD Capacity(1) (kN)			Inferred Restrike Capacity(2) (kN)		
	Shaft	Base	Total	Shaft	Base	Total
TP1 – Wharf 1	-	-	-	2273	2685	4958
TP4 – Wharf 4	1674	2053	3727	1716	2304	4020
TP5 – Wharf 5	2169	2385	4554	1984	2338	4332

It can be seen from Table 4 that the test pile capacities are sufficiently high (even after accounting for geotechnical strength reduction and tension to compression reduction factors) to deal with the increased loads associated with the wharf upgrade work. However, because the test piles are driven into rock and founded below the existing pile toe levels inferred from the downhole magnetics testing, direct application of the dynamic pile load testing to assess the existing pile capacities was not possible. Further assessment of the pile capacities by correlation of shaft friction and end bearing capacities for the soil and rock layers intersected by the boreholes was necessary as discussed in the following section.

5. ASSESSMENT OF EXISTING PILE CAPACITIES

As a cautious approach, an assumption was made to assess the situation where the pile toes of the existing piles are not founded into or close to rock level. The assessment was made as follows:

- Assume the pile toe is located at the average of the range assessed by the magnetics testing, or the best estimate for TP1 as shown in Note 2 of Table 2.

- For driven steel tubular piles, the phenomenon of "friction fatigue" as described by White and Lehane (2004) results in the pile shaft capacity mainly derived from about 10 x pile diameters (i.e. say 4.5 m) above the pile toe. This is the section where adjustment of SPT-N value and shaft capacity will take place. The ultimate shaft friction in this section were back-analysed from the CAPWAP results using the correlation of SPT-N values by DeCourt (1982) who suggested $f_s = K_sN + 10$ (kPa) where K_s is typically about 3.3 for displacement piles, although this was later reduced to 2.8 in Decourt (1995). Based on the CAPWAP results, however, we inferred a K_s value of about 3.4 at this site as shown in Figure 5.

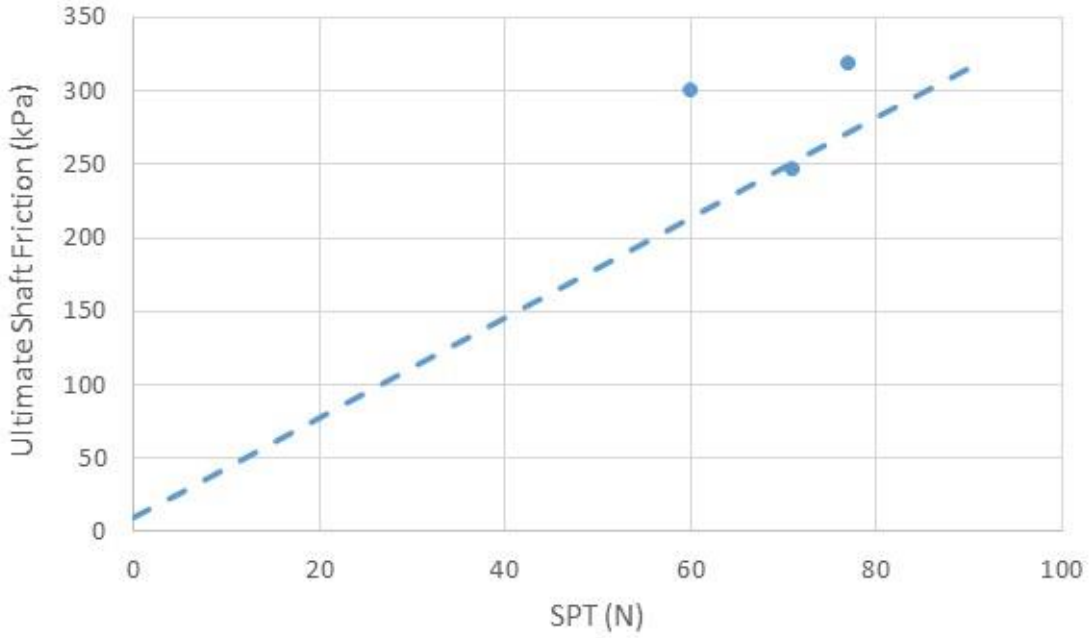

Figure 5: Back-analysed Relationship between Ultimate Shaft Friction and SPT-N

- For the shaft above 4.5 m above the test pile toe, the shaft friction from the CAPWAP testing was relatively low, and based on the SPT results, average values of 28 kPa to 45 kPa was adopted for the pile assessment for the upper part of the pile shaft, ignoring any shaft friction in soft to firm soils.

- For the ultimate end bearing pressure, the CAPWAP results were back-analysed using the correlation of SPT-N values by Decourt (1982) who suggested $f_b = K_bN$ (kPa) for driven piles where $K_b = 250$ for sandy silt and 400 for sands, although the value for sands was later reduced to 325 for sands in Decourt (1995). From the test results, we adopted a correlation of $f_b = 300\ N^{0.77}$ as shown in Figure 6. This relationship was then applied to the inferred existing pile toe levels where SPT values may be lower than those below the toes of the test piles.

- Finally, reduction factors, ϕ_g and R_{st} as described in Section 1 above were applied to compute the design ultimate pile capacity presented in Table 5.

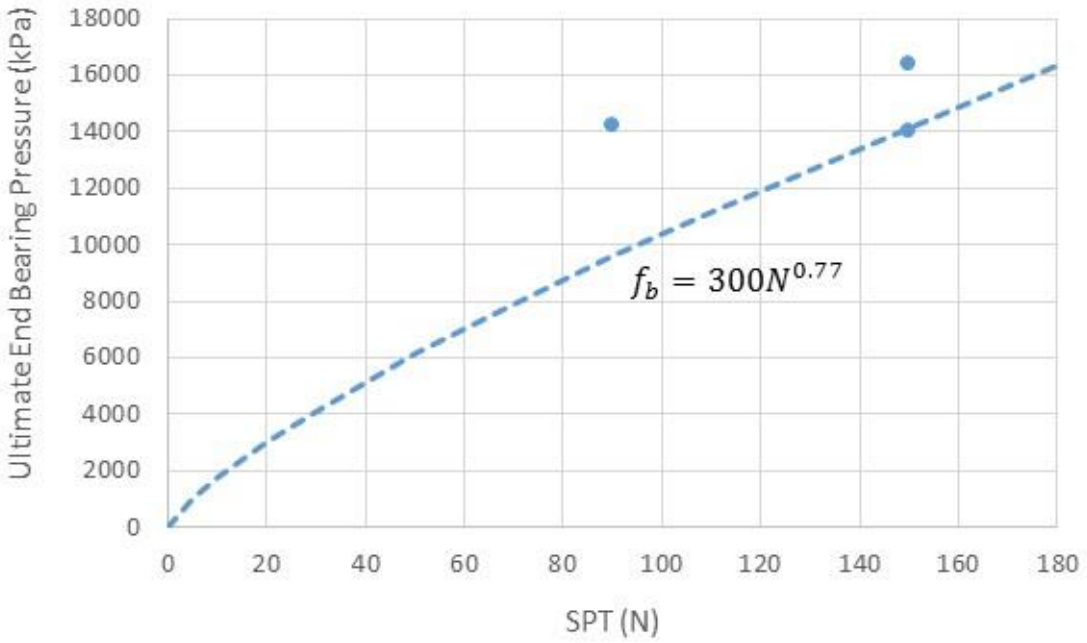

Figure 6: Back-analysed Relationship between Ultimate End Bearing Pressure and SPT-N

Table 5: Pile Capacity Assessment Results

Statistics	Wharf 1	Wharf 4	Wharf 5
Length of bottom 4.5 m	4.5	4.5	4.5
Length of upper pile shaft	5.5	3.2	4.5
Ultimate End Bearing Pressure (kPa)	4,255	5,804	6,514
Ultimate Compression Shaft Friction in upper section of pile shaft (kPa)	28	34	45
Ultimate Compression Shaft Friction in bottom 4.5 m of pile shaft (kPa)	120	185	202
Assessed Ultimate Shaft Compression Capacity (kN)	997	1,351	2,382[(2)]
Assessed Ultimate Compression Base Capacity (kN)	698	952	5,116[(2)]
Assessed Ultimate Compression Pile Capacity (kN)	1,695	2,304	7,498[(2)]
Assessed Design Ultimate Compression Capacity[(3)] (kN)	1,187	1,613	5,249[(2)]
Assessed Design Ultimate Tension Capacity[(3)] (kN)	419	568	1,000[(2)]

[(1)] Based on restrike CAPWAP analysis result (see Table 4)

[(2)] Based on 1,000 mm diameter existing pile at Wharf 5. Pile diameter = 457 mm for all other piles

[(3)] Design ultimate values including a ϕ_g value of 0.7 and a R_{st} ratio of 0.6 for tension capacity

Based on the assessment results shown in Table 5, only the Wharf 1 Row D piles were found to have design ultimate capacities slightly less than the required capacity of 1,364 kN for compression and 426 kN in tension. Following a review of the results with the marine/structural engineer for the project, it was considered that the existing piles are considered to be acceptable based on the following reason:

- The test piles were installed off the existing wharf and therefore slightly more seawards compared to the existing piles and the boreholes which were drilled from the wharf decks. Therefore, it is feasible that the bedrock is slightly deeper at the test pile locations compared to the existing piles which may also have been driven to rock.
- The downhole magnetics testing may be influenced by other piles further in-shore and which are shorter due to shallower depth to bedrock.
- The ultimate static end bearing capacity of the test piles are likely to be higher than those inferred from the dynamic pile load testing because during dynamic testing, the steel tubular pile will behave in an "unplugged" manner. Under static loading conditions, the steel tubular pile is likely to behave in a "plugged" manner thereby giving a much greater end bearing area.
- The inferred ultimate shaft capacity of the test piles will provide a reasonable estimate of the lower-bound unit shaft resistance of existing piles because the piles would not have sufficient time to "set up" with the restrike testing conducted only 24 hrs to 48 hrs after end of drive. Furthermore, minor rusting/aging of the steel surface over time has been shown to increase the ultimate shaft resistance of tubular piles.

As a result, no remedial works were deemed to be required for the proposed wharf upgrade works.

6. CONCLUSIONS

The innovative approach of combining conventional investigations with geophysical techniques using downhole magnetics testing, and dynamic pile load testing has enabled the toe levels of existing wharf piles to be assessed. Through the interpretation of unit shaft and base resistance derived from the test piles and adjustments made according to standard penetration test values at the inferred pile toe levels, the capacity of the existing piles were able to be made and compared to the increased load requirements associated with the wharf upgrade. In doing so, the existing piles were assessed to have adequate capacity and successfully avoided the costly option of remedial works for the client.

7. ACKNOWLEDGEMENT

The authors are grateful to NQBP for their permission to publish the test data in this paper. We are thankful to Royal Haskoning DHV (marine/structural engineers for the project) for their valuable comments on the pile assessment interpretation and content of the paper.

8. REFERENCES

Decourt, L. (1982) *Prediction of the Bearing Capacity of Piles based exclusively on N values of the SPT*, Proceedings of the Second European Symposium on Penetration Testing, Amsterdam, 24-27 May 1982, pp 29-34.

Decourt, L. (1995) *Prediction of the Load-Settlement Relationships for Foundations on the basis of the SPT-T*, Ciclo De Conferencias Internacionales "Leonardo Zeevaert", pp 87-104

De Nicola, A. and Randolph, M.F. (1993). *Tensile and Compressive shaft Capacity of Piles in Sand*. ASCE Journal of Geotechnical Engineering, Vol. 119, No. 12, pp 1952-1973.

Jo, C.H.J,. Cha, Y.H., and Choi, J.H. (2003). *A Borehole Magnetic Logging Tool for Estimating Unknown Foundation Depths.* Presented at the 3rd International Conference on Applied Geophysics, Orlando Fla., Dec. 8-12 2003.

Rausche, F., Goble, G.G. and Likins, G.E. (1985) *Dynamic Determination of Pile Capacity*. ASCE Journal of Geotechnical Engineering, Vol. 111, No. 3, pp 367-383.

White, D. J. and Lehane, B.M. (2004) *Friction Fatigue on Displacements in Sand*, Geotechnique, Vol. 54, No. 10, pp 645 – 658.

REAL TIME MONITORING OF A ROAD EMBANKMENT SUBJECT TO COASTAL EROSION AND SLOPE INSTABILITY

Henk Buys[1] and Puvaneswary Rajarathnam[2]
[1]Technical Director, [2]Geotechnical Engineer
Ground Engineering and Tunneling Team, AECOM Australia Pty Ltd (Sydney), Australia

ABSTRACT

In this paper, monitoring the stability of a road embankment at Lawrence Hargrave Drive along the Illawarra coast is discussed. The embankment supports a coastal road and had been subject to an ongoing process of coastal erosion at the embankment toe and instability due to elevated piezometric pressures after heavy or sustained rainfall. In this paper, the stability issues and potential failure mechanisms are discussed. In order to allow a long term solution to be developed, an interim real time, web based monitoring system was installed. An outline of the investigations and geotechnical conditions at the site is presented. The paper discusses the monitoring system, including the instrumentation used (in-place inclinometers, piezometers, rain gauge, wave height buoy and web cam, the development of monitoring plans, the integration of instrumentation to develop a Trigger Action Response Plan (TARP), the development of trigger levels based on antecedent monitoring data, and the successful operation of the system.

1 INTRODUCTION

Lawrence Hargrave Drive is a coastal road along the Illawarra coast north of Wollongong NSW. North of the Seacliff Bridge viaduct, the road is constructed on an embankment rising from the shore below. The site location is shown in Figure 1 and an oblique view of the site is presented in Figure 2. The embankment was originally constructed over old landslide debris and colluvium, which now forms the base of the slope. The slope has been subject to episodic instability, the formation of a slip zone due to elevated piezometric pressures within and behind the slope, and coastal erosion at the toe. The slip is located to the north of the Seacliff Bridge and south of a major drainage line. The slip is a cuspate slip with the back scarp located on the slope batter east of Lawrence Hargrave Drive and the toe located at the base of the slope, approximately at sea level. The toe has been over-steepened as a result of coastal erosion forces. With the development of further localised instability in the slope, this slip is referred to as the "main slip". Following heavy rain and high seas in July 2011, the main slip back scarp regressed towards the pedestrian footpath, and significant material was eroded from the toe of the slope by wave action. Surface monitoring results obtained from Roads and Maritime indicated a significant downward movement had occurred in the lower slope and flanks of the slipped mass, leading to more active management of the slope and acceleration of remedial option development. Heavy rain and wave action caused further movement of the slope in March 2012

By this time a 2.5m back scarp had formed at the rear of the main slip and slope movements had become more severe. There was a concern that the instability would regress further back into the embankment and endanger first the footpath and rest area immediately behind the slope and ultimately the road itself. Geotechnical investigations and analyses were carried out and monitoring and slope management programs were put in place as an interim measure to allow the development of permanent stabilisation measures.

Lawrence Hargrave drive is an iconic route on the Australian tourist map, and any remediation measures would need to be sensitive to this aspect in addition to the environmental, urban design and technical challenges at the site.

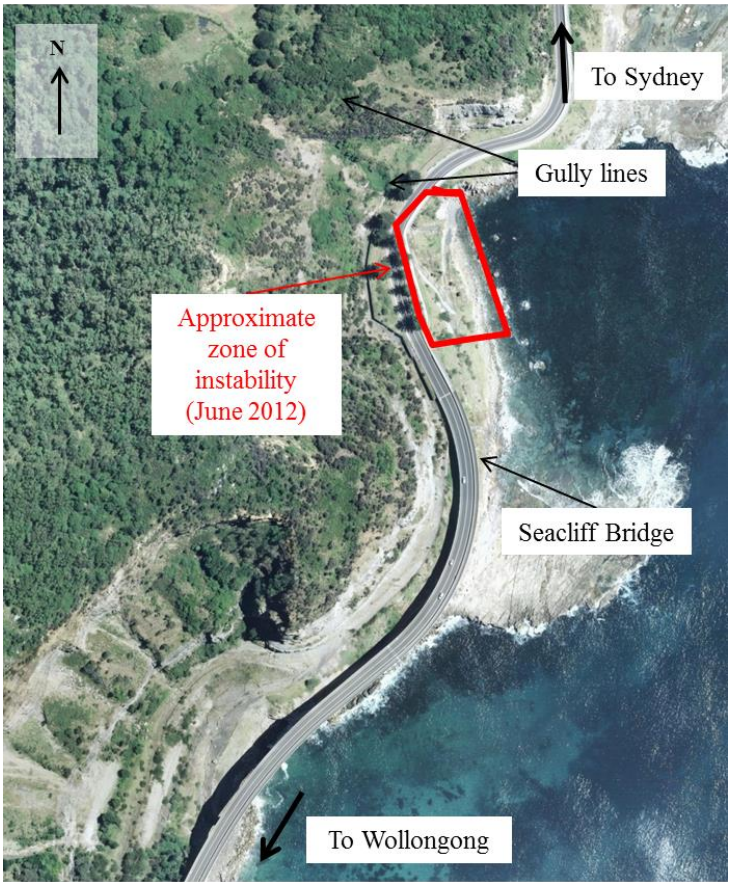

Figure 1: Site location

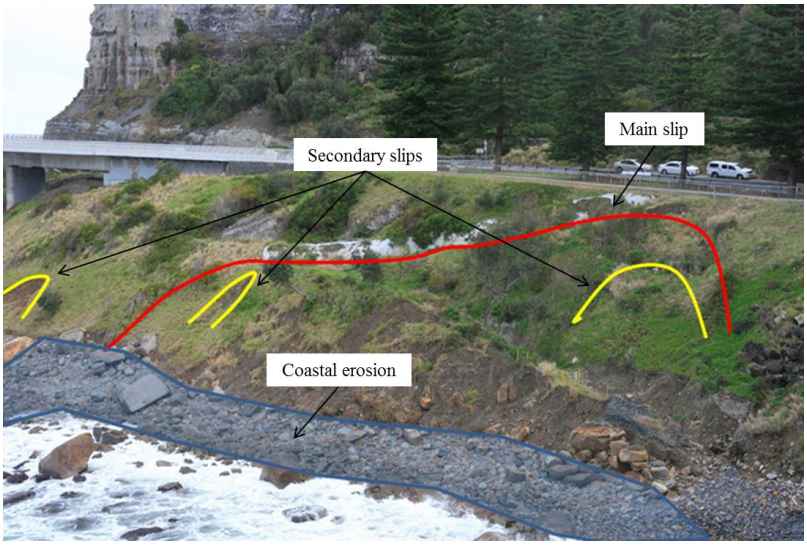

Figure 2: View of the main slip, showing secondary slip features and coastal erosion

2 GEOTECHNICAL CONDITIONS

Geotechnical investigations were carried out to assess subsurface conditions for stability analyses. A description of the ground conditions is presented in Table 1 and a cross section showing the inferred geotechnical conditions for analysis is shown in Figure 3.

Table 1: Summary of General Ground Conditions

Unit	Thickness of unit (m)	RL at base of unit (m AHD)	Description
Colluvium	0.5 to 21.0	-0.35 to -1.25	Highly variable but predominantly composed of Clayey Gravelly Sand and Clayey Sandy Gravel with numerous cobbles and boulders of sandstone (approx. 15%-20% by volume). Subordinate pockets of clay dominated the fine fractions. Generally moist, becoming wet with depth. Generally medium dense.
Gravelly Sandy clay (possible crushed zone)	0.05 to 0.4	-0.47 to -1.45	Generally Sandy Gravelly Clay of high plasticity, light grey. Generally firm to stiff, estimated moisture content greater than plastic limit. This is possibly a mix of crushed bedrock and colluvium.
Bedrock (Wombarra Claystone)	Base not seen	Base not seen	Generally interbedded fresh medium to high strength sandstone and siltstone, sub-horizontally bedded (possibly dipping northward at less than 5°).

Underlying the colluvium is a crushed zone interpreted as possible crushed / reworked bedrock and colluvium, which could have a lower shear strength than the overlying colluvium. Underlying the crushed zone is the Wombarra Claystone bedrock, which forms a gently northward dipping surface that is likely to represent a relict wave cut platform. The depth to the top of the bedrock below the surface is about 21.5 m at the embankment crest and about 1 m just beyond the toe of the main slip.

Two possible slope failure mechanisms were identified below the road:

- A deep seated failure, which could potentially result in tension cracks and ground displacement behind the crest of the slope and would be more likely to impact on the road.
- A shallow slip, which was less likely to have a direct impact on the road.

Back analyses were undertaken using the two failure modes described above. Both failure planes pass through the existing back scarp. The shallow failure plane remains within the colluvium. The deep seated failure plane passes through the previously identified crushed zone at the base of the slope. The ground model and geometry of the failure mechanisms is presented in Figure 3 below.

Monitoring, investigations and analyses combined to confirm that the shallow failure mode was more likely to occur. This was an important outcome as it suggested that other than local instability at the 2.5m high back scarp, there was a relatively stable zone behind the main slip. This zone could be managed by monitoring in the short term whilst stabilisation measures were developed. Stabilisation measures were likely to include substantial marine protection measures.

The analyses also indicated that slope stability could be improved by lowering the piezometric pressures in the slope. This provided an option to include depressurisation wells as an option for interim stability management of the slope. However, lower piezometric levels alone did not offer sufficient improvement in stability to meet the target design safety margins. Hence, drainage measures in isolation were not considered to be a feasible long term remediation option.

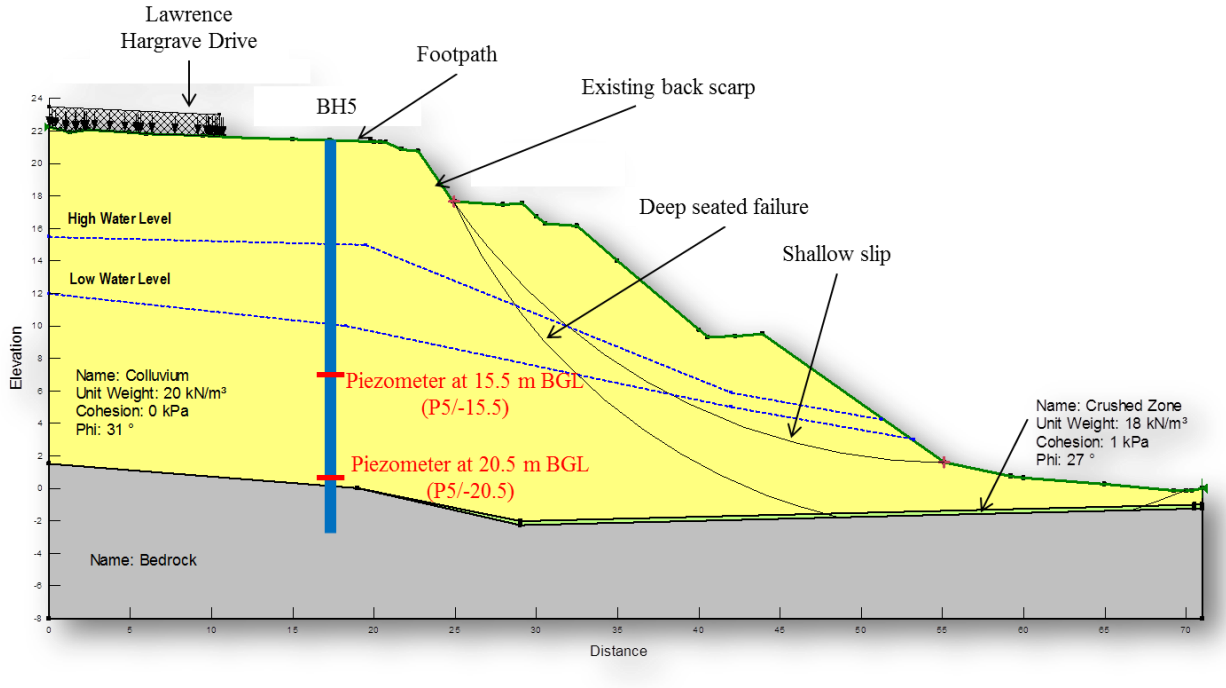

Figure 3: Ground model of main slips

The stability of the embankment is influenced by multiple factors including geotechnical, marine and environmental conditions. Therefore, it was necessary to develop a monitoring plan for this embankment to integrate these various aspects.

3 INTEGRATED MONITORING PROGRAM

A monitoring program was developed to provide information so that Roads and Maritime could manage the road asset on the embankment behind the main slip in such a way as to mitigate the landslip risks to road users and pedestrians. The monitoring program would be required as an interim measure as the development of permanent stabilisation measures were potentially time consuming due to the need for physical coastal modelling. The monitoring program was designed to manage the road asset behind the main slip. Local instability of cuts, fills and scarps on the slope were not captured as part of the program due to the dynamic nature of the slope.

The monitoring program was designed as an integrated system that would allow data from various monitoring instruments to be recorded by data loggers and transmitted to a web-based portal. This data could then be accessed by personnel involved in the project. This integrated, real-time monitoring program allowed the identification of relationships between the various parameters recorded by the monitoring devices.

3.1 INSTRUMENTATION

The borehole locations and the instrumentation in these boreholes are presented in Figure 4.

Figure 4:, Borehole locations and Instrumentation plan.

Boreholes BH5 and BH6, which contained the main geotechnical instrumentation (vibrating wire piezometers and SAA inclinometers), were located behind the slip failure. This was done for three reasons:

- It was likely that due to the dynamic nature of the slip zone, instrumentation located across the slip would be rendered inoperative in a short space of time
- The aim of the monitoring program was to manage risk to road users. Locating the instrumentation immediately behind the slip would allow any regression of the slip into the marginally stable area behind the slip zone to be detected by the instrumentation
- The ground behaviour in the slip zone was reasonably well understood. Further detailed monitoring in this area would provide little further useful information in relation to either slip behaviour or road user risk mitigation.

3.2 REMOTE REAL-TIME DATA COLLECTION SYSTEM

A web-based online portal with data base application, Vista Data Vision (VDV), was adopted to collect and manage monitoring data from the field instruments. The portal provided real-time updates of the incoming data and setting of pre-programmed triggers. It allowed automatic transmission of trigger exceedances via SMS and email to selected recipients.

3.3 MONITORING PLAN

A monitoring plan focussed on mitigating road user risk was developed for the instrumentation. The essential components of the monitoring plan are presented in Table 2 below. The table provided the basic monitoring requirements for each instrument so that all personnel involved in the project could quickly identify their responsibilities and understand the capabilities of the instrumentation. Also, if any amendment to instrumentation was required, the purpose of the existing instrumentation would be understood and considered.

Table 2: Monitoring Plan

Instrument	Accuracy	Frequency	Responsibility	Purpose
Rain Gauge	0.1 mm/hr	Recorded in mm/half hour intervals Transmitted to web portal every 15 minutes	AECOM	Provide rainfall intensity and duration data in the GD4 area
Piezometers	0.01 mm piezometric pressure	Transmitted to web portal every 15 minutes	AECOM	Provide piezometric pressure data at particular points within the main slip in GD4
Inclinometers (SAA type)	1 mm/m	Transmitted to web portal every 15 minutes	AECOM	Provide ground movement data west of the main slip
Inclinometers (Manual)	0.5 mm/m	Monthly	AECOM	Provide ground movement data in the slope below the piled roadway to the north of the slip
Bureau of Meteorology (BoM) rainfall predictions	BoM standard	Daily	AECOM	Provide predictions of rainfall and duration in slip area
Wave Buoys (Sydney and/or Port Kembla)	MHL standard	Daily	AECOM	Provide significant wave height information
Remote Camera		Transmitted to web portal every 15 minutes	AECOM	Provide visual image of slope

3.4 RELATIONSHIPS BETWEEN MONITORED PARAMETERS

3.4.1. GENERAL

Using the data obtained from the instrumentation in the monitoring plan, it was possible to develop relationships between the various monitored parameters. Data from various sets of instruments were plotted to the same time scale as in the example in Figure 4. The figure was plotted to assess the interaction between rainfall, piezometric pressure and wave height with inclinometer movement. The data set presented in the figure is from borehole BH5, located immediately behind the main slip. The following data are plotted from this borehole in Figure 4:

- Daily rainfall
- 30 day cumulative rainfall.
- Maximum, significant wave height and tide obtained from MHL.
- Piezometric pressure (15.5m (Piezometer P5/-15.5) and 20.5m (Piezometer P5/-20.5) below ground level (BGL)).
- SAA inclinometer movements at rock interface (20m below ground level), 10m below ground level and surface.
- Rate of pore pressure rise (rates of rise greater than +/-3m/day not shown in order to filter out anomalous responses due to the effects of surface water).

In the sections that follow, the relationship between piezometric pressure and inclinometer movement is discussed in some detail and in more general terms for other data. The storm event in March 2012 presented in Figure 4 provides much of the data for establishing relationships between the various monitored parameters and referred to from here on as ‘the storm event’.

3.4.2. RELATIONSHIP BETWEEN PIEZOMETRIC PRESSURE AND RAINFALL

Following rainfall, pore pressures rise rapidly at the piezometer at P5/-15.5 with very little lag, suggesting the recharge is close to the slope. The effect of surface water ingress can be clearly seen with sharp spikes in piezometric pressure associated with rainfall. It would not be practical to accommodate these spikes in a response plan. However, after relatively simple upgrades and repairs to surface drainage, it can be seen from the figure that these sharp spikes were

eliminated after February 2012. It illustrates graphically the importance of surface water management in slope risk management. After this time the rate of pore pressure rise associated with rainfall is approximately 1.4 m/day.

Lower piezometric pressures and flatter and smoother recharge curves lagging approximately three days behind rainfall were recorded at the piezometer at 20.5m BGL suggesting a longer flow path for groundwater at this level. The rate of piezometric pressure rise after rainfall at 20.5m BGL is approximately 0.4m/day, a significantly lower rate of rise than at P5/-15.5, and less critical in terms of response planning.

Towards the end of the monitoring period, piezometric pressures do not rise after rainfall due to the effects of the depressurisation wells.

3.4.3. RELATIONSHIP BETWEEN PIEZOMETRIC PRESSURE AND INCLINOMETER MOVEMENTS

It can be seen from Figure 5 that there are a number of distinct patterns of movement in the inclinometer at the three levels plotted in the figure.

At the rock interface (-20.5 m) there is distinct inclinometer movement of approximately 1 mm at the time of the storm event. From review of the full height time displacement curves for this inclinometer, this movement was interpreted as shear movement within the crushed zone at the base of the colluvium as a result of elevated piezometric pressures. It can be inferred from the data that once piezometric pressures at P5/-15.5 exceed approximately 14 m, there was a possibility of deep seated failure occurring. There was no further significant movement in this zone during the monitoring period.

At the slope mid-level (-10 m), piezometric pressures during the storm event once again result in mobilisation of the slope with movements in the order of 2 mm. Whilst there is some oscillating movement in the inclinometer after the storm event, the slope remains stable.

At the surface, the inclinometer records indicate that movement can occur at less severe rainfall events such as that in February 2012. However, the greatest sustained movement occurs during the storm event when piezometric pressures are in excess of approximately 14 m. These movements cease once piezometric pressures drop.

Further surface movement occurs during sustained rain in April. This movement was considered to be the result of saturation of the ground surface and subsequent movement towards the back scarp of the main slip as a result of lack of restraint at the free face of the scarp.

Surface movement occurred once again in June/July but with very little rainfall and without any associated rise in piezometric pressure. This was attributed to further ground movement within the main slip and subsequent movement of the ground behind.

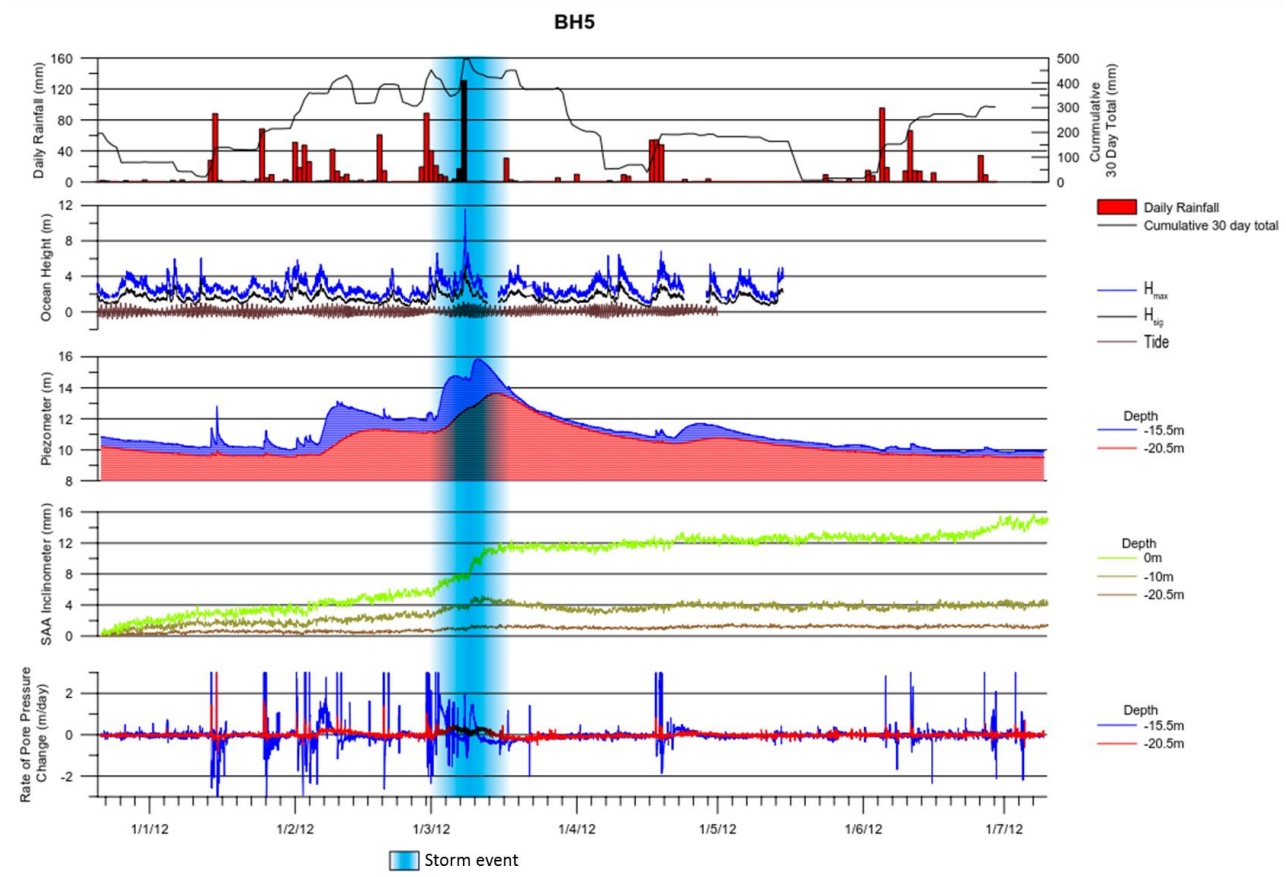

Figure 5: Temporal relationship between monitoring data at Borehole BH5.

Piezometric pressure peaks in P5/-20.5 generally lag approximately three days behind those in P5/-15.5 and the curve is substantially smoother. It is considered that this was due to recharge from further behind the slope or slow percolation through the slope.

Pressure at Piezometer P5/-20.5 did not appear to be a good predictor of the initiation of slope movement, but triggers were set for this piezometer as it was considered that there could be some contribution to ground movements with elevated pressures, and piezometric pressures here did track the piezometer above albeit with a lag. This lag could result in elevated piezometric pressures at depth some time after a rainfall event.

Piezometric rates of rise to establish trigger levels were modified from the values in Figure 5 to account for the following:

- Implementation of surface water control measures. It can be seen in Figure 5 above that after February 2012 the sharp spikes immediately following rainfall events have been eliminated.
- Installation of groundwater depressurisation wells. The impact of these wells can be seen in the muted response to rainfall in the piezometers after June 2012.

3.4.4. OFFSHORE WAVE HEIGHT AND EMBANKMENT TOE EROSION

Toe erosion due to wave action has been a contributor to slope instability and movement at the site. Hence, the potential for toe erosion due to wave action was monitored. However, no direct correlation between significant wave height and extent of erosion was established. Slope movements and erosion did occur during the storm event and towards the end of May 2012, in association with high tides and a significant wave height of approximately 5.5 m. However, no movements associated with slope instability or erosion were recorded during a sea storm with 8 m significant wave height. It is likely that the direction of the swell, which is not monitored at the buoy, is an important factor in toe erosion at this site.

4 TRIGGER ACTION RESPONSE PLAN

4.1 GENERAL

The purpose of the Trigger Action Response Plan (TARP) was to provide planned, graduated responses to changing slope conditions at the site in order to mitigate the landslip risks to road users/pedestrians. Clear and concise responses would be required at each trigger level to ensure that the correct actions were taken by responders, particularly those not directly involved in the formulation of the TARP. The points listed below were considered when developing trigger levels:

- The trigger levels need to reflect the urgency or criticality of the actions required.
- Realistic responses must be possible on receiving automated SMS / email alerts.
- These responses must be possible within a reasonable time frame.
- SMS / email trigger alerts must not occur so frequently that they are regarded as nuisance occurrences or important events are dismissed due to repeated false alarms.

Monitoring frequencies need to be consistent with trigger response times, particularly for electronic monitoring devices. If time is of the essence, the monitoring frequency must be reduced. The time taken to implement responses needs to be considered as well. The logistics of implementing a response may require frequent sampling to ensure the response can be implemented timeously.

4.2 TRIGGER STATUS

Trigger status or trigger levels for this project were set to provide escalating responses when each trigger level was exceeded. The general concept of the status for each trigger level is provided in Table 3.

Table 3: General concept of the status for each trigger

Trigger Status	Condition	Response
Green	Normal operation.	Monitor in accordance with monitoring plan.
Blue	Trends in data indicate that amber trigger may be exceeded.	Consider whether pre-emptive action is required, and implement where necessary.
Amber	Data indicates that unless action is taken within a predetermined time frame slope movement may take place.	Decide on and implement actions.
Red	Slope is potentially unstable.	Implement predetermined actions. Actions are prescriptive.
Grey	Loss of communication with web portal. Loss of data. Malfunctioning of instrumentation.	Response is targeted at reinstating instrumentation and action related to the slope is not necessarily required.

4.3 DEVELOPMENT OF TRIGGERS

4.3.1. GENERAL

A set of trigger levels were developed based on back analysis of the stability of the slope and review of monitoring data over the timeline of previous slope instability events. This review involved the assessment of the relationships between monitoring data such as piezometric pressure, inclinometer movement, antecedent rainfall (both daily and cumulative) and wave height as well changes in the slip area from remote camera images.

The slope movements were dependent on piezometric pressures, which in turn were dependent on rainfall intensity and duration, and antecedent piezometric pressures. Hence, triggers for rainfall could be varied depending on the piezometric pressures prevailing in the slope at the time. However, introducing interdependent triggers would have brought a level of complexity to the TARP, which could impact on reliability and risk.

Also, the slope was located in a very dynamic environment. Changes such as significant toe erosion leading to a reduction in slope stability, could change the piezometric level at which the slope is mobilised, rendering existing trigger values unconservative and requiring adjustment. Alternatively, pre-emptive action such as installing dewatering pumps to stabilise the slope could allow some relaxation in trigger levels. Hence, it was very likely that the trigger levels would be changed during the course of the monitoring program. Therefore, independent trigger levels were adopted for each monitoring device in this TARP.

4.3.2. SETTING PIEZOMETRIC TRIGGER LEVELS

Development of trigger levels for the piezometer at P5/-15.5 at borehole BH5 are discussed in some detail as an example of how trigger levels were set. Trigger levels for other instruments were developed in a similar fashion.

The critical piezometric level, the level which initiated approximately 5 mm of surface movement in the inclinometer during the storm event was set at 14.7 m BGL. From this level, there was a further rise in piezometric pressure of approximately 1.4 m. This represents one day's rate of pressure rise. The higher pressures did not lead to failures within the area of the footpath and Norfolk pines, although visual inspection indicated that significant further movement of the main slip had occurred. Survey carried out after the storm indicated ground movements of up to 1.5 m occurred in the main slip since a previous survey a week before the storm event. Some of these movements may have been associated with heavy rain and erosion due to high wave heights after the storm. This behaviour indicated that failure occurred as relatively shallow circular slip failure on the slope face, followed by ongoing creep movement identified by inclinometer data as shear at the rock/colluvium interface and stress relief in the upper section of the main slip. In view of this embankment behaviour behind the main slip when critical piezometric pressures were exceeded, it was considered that these pressures had been selected conservatively.

With the above in mind, red triggers were set to allow six hours of response time to execute management measures, such as closing the footpath, before the critical pressure was reached.

An amber trigger was set to allow one day for action before a red trigger was reached. Action could for instance include activating pumps in depressurisation wells which had recently been installed or assessing what further pre-emptive action could be taken to avert a red trigger.

A blue trigger was set to allow one day before an amber trigger was reached. Whilst no specified action was required on reaching a blue trigger, it allowed review of the data to identify trends which could result in further instability and consider possible pre-emptive actions.

To set the above trigger levels, the following process was followed:

Determine the piezometric pressure at which slope movement is initiated (critical pressure)

- The six hour rise is subtracted from the critical pressure to obtain the red trigger.
- The 24 hour rise is subtracted from the red trigger to obtain the amber trigger.
- The 24 hour rise is subtracted from the amber trigger to obtain the blue trigger.

The resulting raw trigger levels for a sample piezometer are presented in Table 4.

Table 4: Raw piezometric trigger levels.

Borehole	Piezometer	Critical Piezo level (mAHD)	Maximum Rate of rise (m/day)	Six hour rise	Red Trigger	24 hour rise	Amber Trigger	Blue Trigger
BH5	P5/-15.5	14.7	1.4	0.35	14..4	1.4	13.0	11.6

Table 5 below presents the piezometric trigger levels and response plan for the P5/-15.5 in BH5. Similar response plans were developed for the other instrumentation on site.

Table 5: Piezometric Pressure Trigger Levels at P5/-15.5.

Peizometric Triggers (mRL)			Maximum Response time from trigger notification
Grey	Loss of communication with web portal Loss of data Malfunctioning of instrumentation	Identify reason for malfunction and reinstate device	12 hours during green and blue status 2 hours during amber and red status
Green	N/A	Monitor in accordance with monitoring plan	N/A
Blue	10.8	Review data (AECOM) and meet with Roads and Maritime to agree if action is required. Review to include following data: Rain gauge information. BoM rainfall predictions. Wave height data. Tide data. camera images Evidence of erosion at the toe of the main slip. Piezometric pressures in BH5, BH6, and BH1. Rate of rise of piezometric pressures in BH5, BH6, and BH1.	24 hours
Amber	12.75	Inspect footpath, slope and road between bridge abutment at southern end of GD4 and BH4 (if safe to do so). Activate depressurization pumps and check discharge to confirm operation Review data (AECOM) and meet with Roads and Maritime to agree further action. Review to include following data: Rain gauge information. BoM rainfall predictions. Wave height data. Tide data. Camera images Site observations. Evidence of erosion at the toe of the main slip. Piezometric pressures in BH5, BH6, and BH1. Rate of rise of piezometric pressures in BH5, BH6, and BH1. Decide whether to run depressurisation pumps.	12 hours 12 hours 24 hours
Red	14.2	Inspect footpath, slope and road between bridge abutment at southern end of GD4 and BH4 (if safe to do so) Close footpath Activate pumps and check discharge to confirm operation Review data (AECOM) and meet with Roads and Maritime to agree further action. Review to include following data: Rain gauge information. BoM rainfall predictions. Wave height data. Tide data. Camera images. Evidence of erosion at the toe of the main slip. Piezometric pressures in BH5, BH6, and BH1. Rate of rise of piezometric pressures in BH5, BH6, and BH1.	6 hours 6 hours 6 hours 24 hours

4.4 PIEZOMETRIC TRIGGER REVIEW AGAINST HISTORICAL DATA

The piezometric data was assessed against the historical monitoring data to check the trigger levels under which the slope would have been managed had the TARP been in place from the installation of the piezometers. The assessment indicated that trigger levels would have been exceeded over the time frames listed below and the slope managed in accordance with those trigger levels in that time:

- Blue – approximately three and a half months
- Amber – approximately 30 days
- Red – approximately 10 days

Had these triggers been in place, the footpath would have been closed as a precautionary measure for a period of 10 days during the storm event. This would have been a reasonable management measure as there would have been very little pedestrian traffic in this area during that time. The need to manage the slope under an amber trigger for a period of 30 days would be undesirable, but it is likely that the depressurisation pumps would have been activated to avert this need. Hence, the risk to road users could be reasonably managed with the trigger levels developed for the site.

During the subsequent operation of the monitoring plan and TARP, the footpath was closed for one weekend due to high piezometric pressures and recorded inclinometer movements.

5 CONCLUSION

The road embankment at Lawrence Hargrave Drive, immediately north of Seacliff Bridge, was subject to instability due to elevated piezometric pressures and erosion due to wave action at the toe. Interim management measures which would not impact on the tourist value of this iconic route were required to ensure safety of the public whilst long term stabilisation solutions could be developed.

A comprehensive monitoring program was developed to provide an interim management tool to ensure public safety. The monitoring plan included detailed real-time monitoring of several parameters, which contributed to instability issues. These included rainfall measurements, piezometric pressures, slope movement, wave climate and toe erosion due to wave action. From the data collected as part of the monitoring program, it was possible to establish relationships between these parameters, leading to development of a comprehensive TARP, which allowed efficient interim management of the slope whilst long-term solutions were developed.

Management of the slope under the TARP has been a success and a permanent solution consisting of a rock revetment at the base of the slope, surface drainage measures and slope protection have now been installed. These measures are illustrated in Figure 6 below.

Figure 6: Slope showing rock revetment at the base of the slope, surface drainage measures and slope protection.

6 ACKNOWLEDGEMENTS

The authors wish to acknowledge the valuable contribution of Roads and Maritime Services of NSW in the operational management of this successful project, and for their permission to publish this paper.

7 REFERENCES

Roads and Maritime Services NSW. *Guide to Slope Risk Analysis (Version 4)*, 2014.

SATELLITE INSAR TECHNIQUE FOR URBAN TUNNELLING MONITORING: THE CROSSRAIL PROJECT CASE STUDY

Nuria Devanthery, SIXENSE SATELLITE, *Av. Carrilet 219, 08907 L'Hospitalet de Llobregat, Barcelona, +34 (93) 263 29 69, nuria.devantheryarasa@sixense-group.com*

Javier González Martí, *CRL, Location 5A – 7, Crossrail 1-14 Liverpool Street, London, EC2M 7NH, 02031975460, javiergonzalez-marti@crossrail.co.uk*

Blanca Payas, SIXENSE SATELLITE, *Av. Carrilet 219, 08907 L'Hospitalet de Llobregat, Barcelona +34 (93) 263 29 69, blanca.payas@sixense-group.com*

Eric Audigé, SIXENSE OCEANIA, *22 St Kilda Road, St Kilda, VIC 3182 , +61 (0)3 9510 0582, eric.audige@sixense-group.com*

ABSTRACT

One of the challenges in urban tunnelling projects is to guarantee that the infrastructure assets crossing or adjacent to the tunnel alignment and other new build elements are not affected by the construction activity.

Radar Satellite Interferometry (InSAR) is a non-invasive surveying technique, which uses a stack of synthetic aperture radar images (SAR) to measure millimetric deformations of terrain structures over wide areas. This technique allows a comprehensive and periodic vision, without any need to access site, with the same accuracy as manual levelling in cities for a fraction of the cost of traditional systems.

Sixense has been using its interferometric processing chain, ATLAS, with the aim of monitoring geotechnical and structural deformations linked to urban construction, specially aimed at tunnelling monitoring, using the experiences in geotechnical and automatic surveying.

ATLAS processing chain was successfully applied to Crossrail I, The Elisabeth Line, in London. In this context InSAR has proved to be a fundamental tool to: (i) present the historical ground/structure behaviour before the start of any construction was presented, (ii) monitor the movements during the construction works covering a huge extension for just a fraction of the cost and resources of what should be expended in order to be done by more traditional approaches, and (iii) keep a monitoring system in place for the long term movement performance of ground and structures, even years after the end of the construction phase.

In this paper, the technique will be briefly detailed and the application case of the monitoring of the different phases of the project will be shown.

1 INTRODUCTION

In urban tunnelling projects, one of the major challenges is to guarantee that the different infrastructure assets crossing or adjacent to the tunnel alignment and other new build elements are not affected by the construction activity (in the short or long term). This can be difficult because for traditional monitoring a good deal of installation and preparation is required, often not allowing much time between the time the instrumentation is installed and commissioned and the start of the construction works, which might not give enough background data to determine and properly understand each assets' natural movement behaviour.

Satellite remote sensing techniques can overcome these limitations and bring some new advantages to tunnelling monitoring due to the availability of historical data, the wider area imaging that allow monitoring over extended areas (and not only locally), and no need to access site. Radar satellite interferometry (InSAR) is a non-invasive surveying remote sensing technique based on the exploitation of synthetic aperture radar images (SAR), which is able to measure millimetric motion of terrain structures over wide areas in both urban and non-urban environments. Moreover, the large size of satellite images provides detailed information about areas outside the area of interest. For any point, satellite time series enable the follow-up of phenomena every few days during the monitoring period.

InSAR comes with no (or very limited) installation costs, minimal health and safety risks, and of course maintains a similar monitoring accuracy to other manual systems. The use of InSAR techniques provides huge cost saving whilst

maintaining all the technical/design requirements, since in terms of technical capabilities InSAR is entirely comparable with precise levelling. However, where the precise levelling is carried out in one specific area, and will only provide information in that area at a rate of around 100 points monitored per day, InSAR can provide more than 20,000 measurements points per km^2 in urbanised environments.

ATLAS Interferometry chain, has been developed with the aim of monitoring geotechnical and structural deformations linked to urban construction activities, specially aimed at tunnelling monitoring, using the experiences in geotechnical and automatic surveying. ATLAS has been used for measuring vertical ground and structure movements, specially to monitor ground settlement due to volume loss. Volume loss control is one of the main objectives in big tunnelling and excavation works on densely urbanized cities, where InSAR advantages complement more conventional approaches. ATLAS results can be integrated with other ground monitoring systems for global analysis.

ATLAS InSAR processing chain has been successfully applied in the ground settlement monitoring of CROSSRAIL C704 in UK, one of the largest infrastructures construction projects in Europe. This project comprises the construction of a new railway line which crosses Greater London from east to west, with five tunnelled sections totalling up to 42 km in length. Crossrail area of interest has been monitored with ATLAS using a set of high-resolution TerraSAR-X images (radar interferometry satellite constellation), acquired over London from 01/08/2013. ATLAS provided the accumulated deformation maps and the displacement time series for a dense net of points over the area of interest, during the extended observation time period.

2 TUNNELING MONITORING FROM SPACE: ATLAS PROCESSING CHAIN

2.1 RADAR SATELLITE INTERFEROMETRY

Radar Satellite Interferometry (InSAR) is a non-invasive surveying technique which uses a stack of synthetic aperture radar images (SAR) to measure millimetric deformations of terrain structures over wide areas (Bamler and Hartl, 1998 and Rosen et al., 2000).

Satellite monitoring techniques are based on the exploitation of synthetic aperture radar images (SAR). A SAR image is a complex picture in the mathematical sense. It contains amplitude and phase information. Solutions based on radar interferometry (InSAR) use this phase information to compare two SAR images acquired over the same area at different dates, and compute ground displacements information on the radar waves travel time, as described in figure 1, by means of the interferometric phase (Φ_{int}).

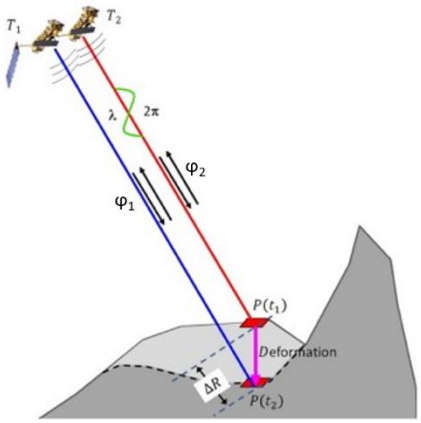

$$\emptyset_{int} = \Delta\varphi = \varphi_2 - \varphi_1$$

$$\emptyset_{int} = \emptyset_{Displacement} + \emptyset_{Topography} + \emptyset_{Orbital} + \emptyset_{Atmosphere} + \emptyset_{Noise}$$

Figure 1: Working principle of InSAR technique

Persistent scatterer interferometry (PSI) technique (Ferretti, 2001 and 2001) takes conventional InSAR a step further to get millimetric precision on the ground motion readings, that is done by correcting atmospheric, orbital and topographic components of the interferometric phase (see figure 1). This technique requires a database composed of more than fifteen images. The PSI algorithm identifies common points (geographical locations) in each image that reflect persistently the radar signal back to the sensor. These locations, called persistent scatterers (PS), are permanent highly reflective targets, whose reflections remain constant over the whole image stack during the duration of a project. They are generally man-made structures or rocks but can also be arid terrains and other ground features whose orientation and surface characteristics allow a perfect reflection of radar waves. In fact, their position and density depend strongly on the characteristics of the studied area. The number of natural permanent scatterers is usually around 20,000 points per km^2 in urban areas and up to thousands of points per km^2 in rural areas when using high resolution images from the last generation of sensors.

2.2 ATLAS PROCESSING CHAIN

Sixense has developed its own treatment processing chain, ATLAS, around the core software GAMMA (Werner et al., 2003). ATLAS allows for measuring vertical ground and structure movements, with special attention to urban works and critical non-linear movements, on permanent scatterers with millimetric accuracy.

For each measurement point, the Atlas solution provides: maps of accumulated displacement along the study period; time series of deformation for each point monitored; mean deformation velocity of deformation, and quality indexes of the measurements.

ATLAS PSI uses more than 15/20 SAR images with atmospheric compensation to derive highly accurate elevation and average displacement rate values for each stable point. The high-level of error compensation allows the generation of time series charts, visualizing the evolution of the displacement of each stable point. Urban, semi-urban or rural areas can be studied in detail (both in terms of high spatial resolution and the historical variation of the displacement) over long time periods.

The processing steps (figure 2) are summarized as follows:

Image extraction: SAR data is read from the original media and all the auxiliary parameters are retrieved from the product annotations into ASCII auxiliary files.

Image selection: Analyse the set of available images, quality control is done at this stage to detect images with acquisition defects (images altered by satellite manoeuvres, erroneous annotation file parameters and severe weather conditions during the acquisition, etc.).

Image co-registration: A stack of images must be co-registered to a geometry. One image is selected as master and then all the other data is aligned to have a common geometry. Every pixel in all the images must contain the radar response coming from the same ground resolution cell.

Generation of differential interferograms: Selection and generation of interferometric pairs based on the acquisition time, perpendicular baseline and Doppler centroid difference of every image.

PS selection: Selection of the initial stable points (PS like pixels). That is to choose the pixels with low noise level to retrieve reliable measurements of phase. This initial selection is based on the analysis of the radiometric and the phase stability of each pixel in all dataset/stack.

Ground motion estimation: This procedure assesses the ground motion, the vertical height, the atmospheric contribution and the quality index, based on the model coherence performed during the model adjustment, for each pixel selected as PS.

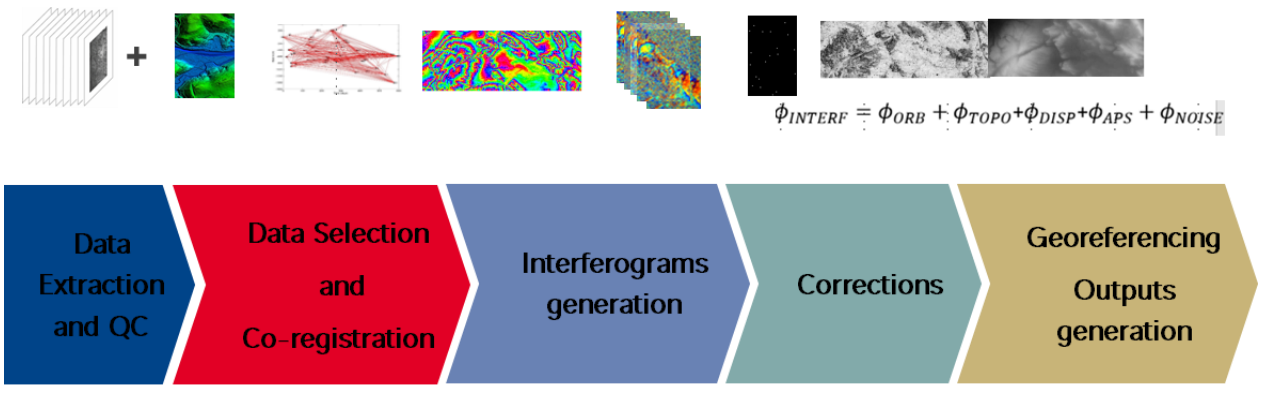

Figure 2: ATLAS processing steps scheme

3 CROSSRAIL MONITORING WITH ATLAS

CROSSRAIL C704, as one of the major tunnelling projects done in terms of impact in a heavily urbanised area consisting in the construction of a new railway line which crosses Greater London from east to west, with five tunnelled sections totalling up to 42 km in length, was the first one in implementing the InSAR technology as a non-intrusive technique to monitor the long-term movement in within the entire project extension. This came with a significant saving, but what is more important, it allowed the decommissioning of the physical instrument to be done in time while still monitoring the assets, and it prevented potential injures by using a monitoring system that was comparable to manual monitoring in terms of repetitivity, without having to have tenths of surveyor teams on site.

ATLAS was successfully applied to CROSSRAIL C704 using a set of high-resolution TerraSAR-X images (radar interferometry satellite constellation), acquired over London from 01/08/2013. The main uses of InSAR in CROSSRAIL have been: (a) a source of information for the ground/structure behaviour before the start of the construction activity; (b) a complementary source of settlement data, which could be considered as 'absolute' and in the same grid for the entire project, especially in big extension projects; (c) a check for the long term movements, right after the end of the construction activity, or after many years if claims are raised in a later stage.

ATLAS provided the accumulated deformation maps and the displacement time series for a dense net of points over the area of interest, during the extended observation time period, detecting: (i) the movements identified on the different ZOI and on tunnel sections, (ii) different seasonal effects on the area of interest, and (iii) subsidence and heave related to dewatering in different areas. In the following subsections, we will show the results of points (i) and (ii).

3.1 DEWATERING AROUND LIMMO/ CANARY WHARF AREA

Dewatering usually results in settlement as porewater pressures in the soil reduce. In this area historic pumping for the Canary Wharf development and the jubilee Line Extension suggested that approximately 1mm of settlement occurred for every 2 mm drawdown. 30m drawdown at Limmo (Figure 3) should therefore result in about 15mm of settlement at ground surface.

Figure 3: Limmo area while construction activity was taking place

For the Limmo shaft construction the lower aquifer level needed to be lowered by approximately 30m, later this pumping effort was reduced and other smaller pumping schemes were commissioned. The peak CROSSRAIL dewatering flow was 620l/sec from 37 wells in Jan 2014, and a peak flow radius to the 2m drawdown contour was 3.5 km. Figure 3 shows one of the active shafts at Limmo area, while the pumping was on-going. The shaft was necessary in order to access and build the SCL (Spray Concrete Lining) Tunnels.

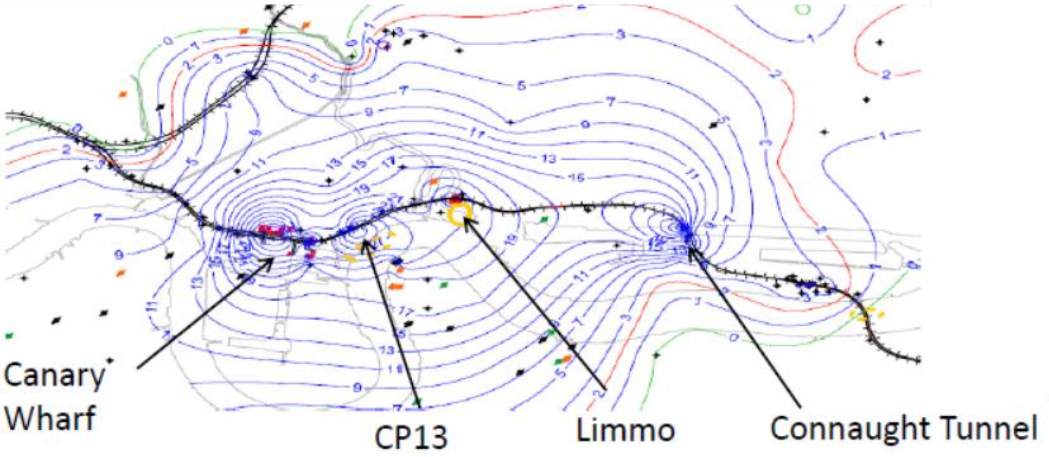

Figure 4: Ground settlement prediction due to dewatering

ATLAS was able to monitor the entire area exhaustively, much further away than originally predicted, and for a reasonable cost in a very unreliable ground were many other parties were working at the same time. The results were published internally in several papers, presentations, and even shared with other projects such as Lee Tunnel, which was affected by the dewatering.

Figure 4 shows the accumulated displacement map over Limmo area and its surroundings from August 2013 to March 2015. Yellow points show the shaft locations (CP13, CP14 and Limmo). The map is showing a big subsidence (in red and dark violet) reaching more than 30 mm since August 2013.

The tunnel alignment is highlighted and the map shows subsidence (in red and yellow) over it, related to the tunnelling activities. Moreover, the high density of measurement points available using InSAR, made possible the detection of a geological fault in the area that affected drastically the dewatering regime on either side of the fault (see dotted line in Figure 4).

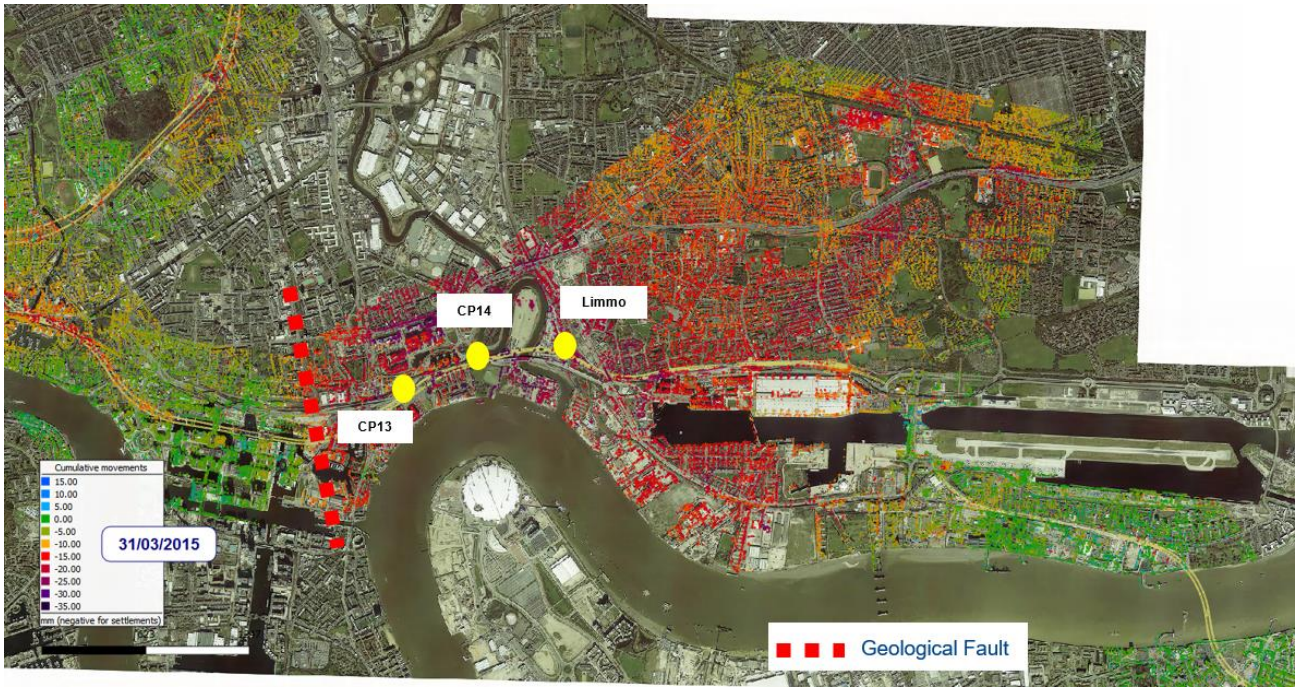

Figure 5: Ground settlement due to dewatering

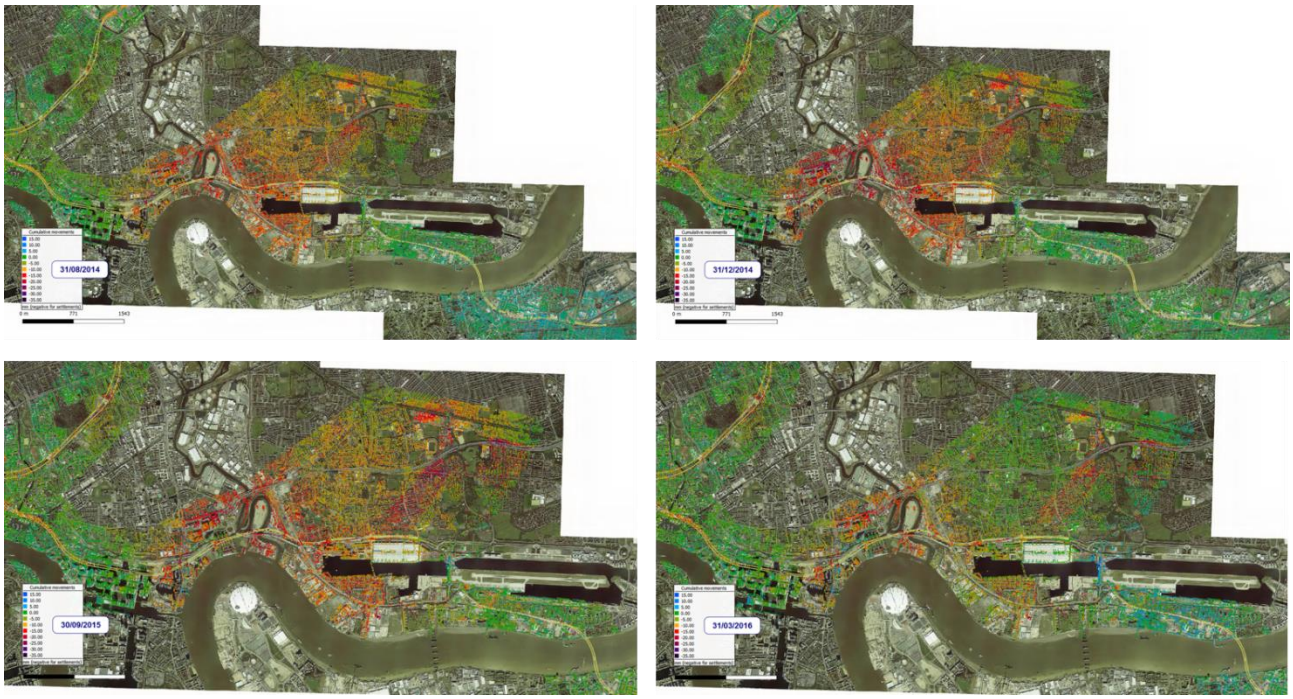

Figure 6: Ground settlement evolution due to dewatering

The evolution of the deformation measured in the area is depicted in Figure 6. The deformation map from August 2013 to August 2014 (upper-left), December 2014 (upper-right), September 2015 (bottom-left) and March 2016 (bottom-right) show the maximum intensity of the subsidence around end of 2014, and a decreasing intensity since this period.

3.2 LONG TERM MOVEMENTS AT LIVERPOOL STREET, FINSBURY CIRCUS

The area around Liverpool Street has been one of the most complicated ones in the project, not only because of the many SCL tunnels and shafts to be fitted, but as well the variable ground conditions, and the massive buildings around the main

shaft. Several years of ground treatment and compensation grouting while the excavation was being done were necessary. On the top of this, due to the many necessary works to be done, several projects needed to be working together, each of them with their own design in terms of ground settlement. Figure 7 shows the accumulated deformation map from August 2013 to June 2016 over Finsbury Circus area. The map shows subsidence up to more than 25 mm for 4 years (red to pink areas) coinciding with the tunnel alignment (depicted in yellow).

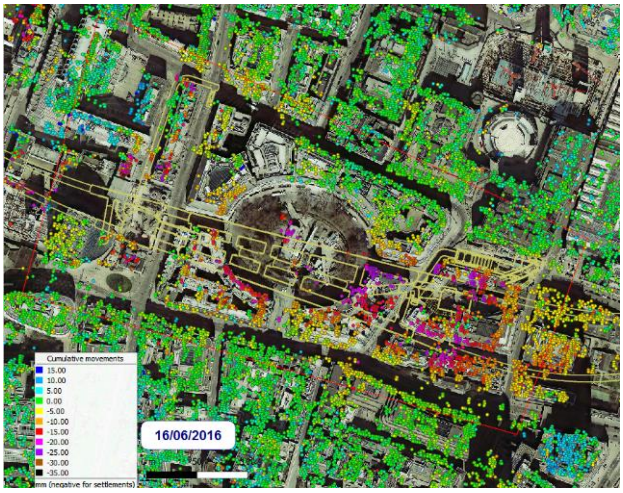

Figure 7. Recorded settlement at Finsbury Circus after almost 4 years of work

After more than 6 years of work, the tunnels were completed, and the new challenge was to demonstrate the ground stability, more commonly known as long term settlement. The pre-agreed according to the Crossrail Act was that there would not be more than 2mm per year once the construction will been finished. ATLAS gave assistance in several stages of the work:

(i) as a verification system to the more traditional ones, without taking in consideration splits in between the different contracts or contractors.

(ii) as a system to verify structural integrity. The huge properties around Finsbury Circus were divided in different data clusters and the data on those groups was analysed individually, and compared against the other monitoring systems. Figure 8a shows the accumulated deformation map from August 2013 to June 2016 over the area of maximum deformation, and Figure 8c shows the time series corresponding to each group of points (labelled with the number highlighted in the deformation maps from 1 to 8). The measured points show a behaviour tending to stability. InSAR outcome showed that the data coming from InSAR was comparable to the manual or automatic monitoring in place during the construction activity, as demonstrated in Figure 8b. Data coming from the area 1 of Figure 8a are depicted in the pink line, which show complete agreement with manual monitoring data (lines red and orange).

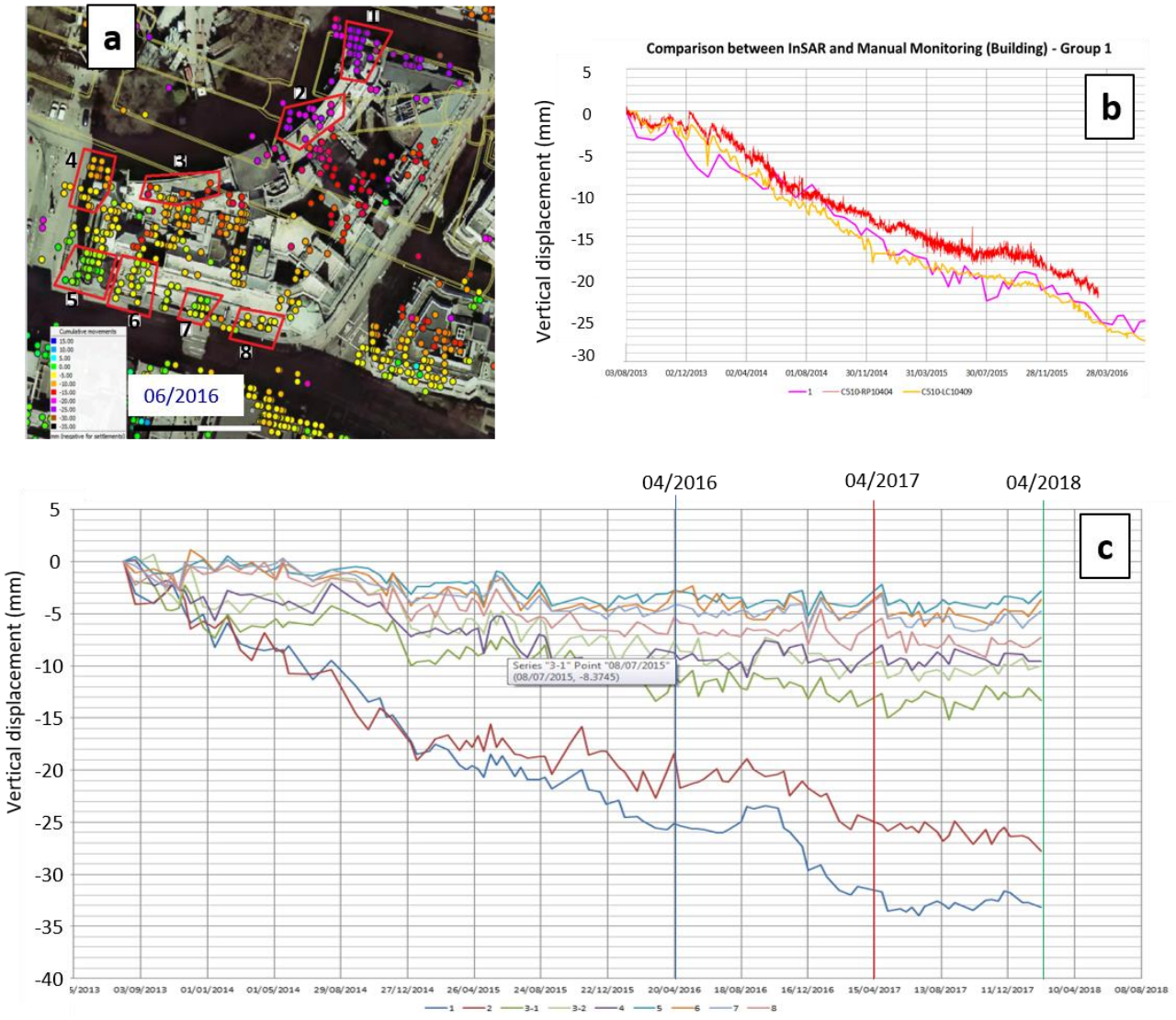

Figure 8. Recorded settlement at Finsbury Circus since August 2013

(iii) To be able to meet the key milestone of decommissioning and re-instatement of the specific equipment installed for the monitoring of the works, InSAR was used to assure the different stake holders that their assets were going to be monitored as long as necessary to prove ground and structure stability. It would provide the possibility of re-process images as well in years to come if an important volume of claims were to arrive.

4 CONCLUSIONS

Ground movements caused by major construction projects, such as tunnelling, have the potential of causing damage to overlying structures. This is even more probable when the project is done under or around heavily urbanised areas.

For this to be measured it is necessary to understand not only the ground behaviour before the start of the construction activity, but as well the structure behaviour. Synthetic Aperture Radar Interferometry (InSAR) has proven to be a suitable monitoring technique to monitor tunnelling activities. ATLAS, the Sixense's InSAR chain, has been and still is successfull to monitoring deformations related to CROSSRAIL activities, while the tunnelling activities were ongoing, and after they were finished until ground settlement will fade out.

In this paper, the results showing deformation maps related to dewatering in Canary Wharf and Limmo areas, and related to the tunnelling activities in Finsbury Circus have been presented, illustrating the advantages provided by the InSAR technique over big areas and a long period of time.

5 REFERENCES

Bamler, R., Hartl, P. (1998). Synthetic aperture radar interferometry. *Inverse Probl.*14, R1–R54

Ferretti, A., Prati, C., Rocca, F. (2000). Nonlinear subsidence rate estimation using permanent scatterers in differential SAR interferometry. *IEEE TGRS*, 38 (5), 2202–2212.

Ferretti, A., Prati, C., Rocca, F. (2001). Permanent scatterers in SAR interferometry. *IEEE TGRS*, 39 (1), 8–20.

Rosen, P.A., Hensley, S., Joughin, I.R., Li, F.K., Madsen, S.N., Rodriguez, E., Goldstein, R.M. (2000). Synthetic aperture radar interferometry. *Proc. IEEE*, 88 (3), 333–382.

Werner, C., Wegmüller, U., Strozzi, T., Wiesmann, A. (2003). Interferometric point target analysis for deformation mapping. *Proceedings of IGARSS*, Toulouse, France.

WOOLGOOLGA TO BALLINA PACIFIC HIGHWAY UPGRADE – EMBANKMENT PERFORMANCE MONITORING AND BACK-ANALYSIS

Viet D. Nguyen[1], Patrick K. Wong[2], Henry Zhang[3]
[1]Associate Geotechnical Engineer, Coffey Services Australia Pty Ltd
[2]Senior Consultant, Coffey Services Australia Pty Ltd & Senior Principal, PKW Geosolutions Pty Ltd
[3]Principal Geotechnical Engineer, WSP Australia Pty Ltd

ABSTRACT

The section of the Pacific Highway Upgrade project between Woolgoolga and Ballina (W2B) traverses areas having significant depths of soft soils. The presence of these soft soils causes significant risks in relation to timely project completion and potential cost blow out. To reduce these risks, soft ground treatment using wick drains and preloading was used in the form of Early Works to de-risk the project and to reduce the post construction settlement.

During the embankment construction and preloading period, instruments were installed to monitor the embankment performance. Monitoring was carried out using an innovative web-based system to enable continuous and real time monitoring of embankment performance, technical review and modifications of construction sequence as required.

Monitoring data were back analysed periodically to assess the embankment performance. Through this exercise, additional filling and stability measures were implemented over a number of embankment sections, where the monitored embankment settlements exceeded the design prediction. In addition to the innovative web-based monitoring system, advanced numerical modelling was used to predict future creep settlement using the back-analysed results. It was found that advanced numerical modelling of creep settlement must carefully consider the two-dimensional stress distribution beneath the embankment including toe berms in order to model accurately the stress history and over-consolidation effects on creep after surcharge removal. When the two-dimensional stress distribution is properly taken into account, the results of forward creep prediction matches well with one-dimensional analytical methods such as that proposed by Wong (2010).

1. INTRODUCTION

The section of the Pacific Highway Upgrade project between Woolgoolga and Ballina (W2B) traverses areas having significant depths of soft soils. The presence of these soft soils causes significant risks in relation to timely project completion and potential cost blow out. Early Works involved soft ground treatment and embankment preloading being undertaken ahead of the main upgrade construction works to reduce the cost of ground treatment and to provide certainty of delivery of the highway upgrade within a given time during the main contract. The Early Works also have other benefits such as improving long-term pavement performance and community benefits via improved safety and reduced maintenance.

Over the approximately 155 km project length from Woolgooga to Ballina, there are a total of eleven highway sections underlain by soft alluvium, with lengths ranging from about 0.5 km to 4 km. Three significant sections with deep soft soil are around Maclean, south and north of the Clarence River, and south of Ballina. At these areas, soft soil thickness ranges from 5 m up to approximately 26 m depth and extends over kilometer distance especially around Maclean and south of Clarence River areas.

To the south of Clarence River, the highway upgrade involves widening of the existing highway embankment toward north to the new bridge crossing Clarence River and construction of a new major interchange at Yamba Road.

This paper presents the process of the soft ground treatment design, instrumentation design, fill construction, monitoring and back analyses for an embankment section south of Clarence River Bridge. Lessons were learnt through the review and back analysis of the instrumentation. The advanced numerical modelling adopted to predict future creep settlement and comparison with one-dimensional analytical methods is also described.

2. PROJECT INFORMATION

Figure 1 shows the extent of areas underlain by soft alluvium along the highway upgrade alignment to the north and south of Clarence River. Figure 2 shows the proposed highway upgrade intersection to the south of Clarence River. Over this area, access ramps and new highway widening embankments up to 8.5 m high are to be constructed adjacent to the existing highway.

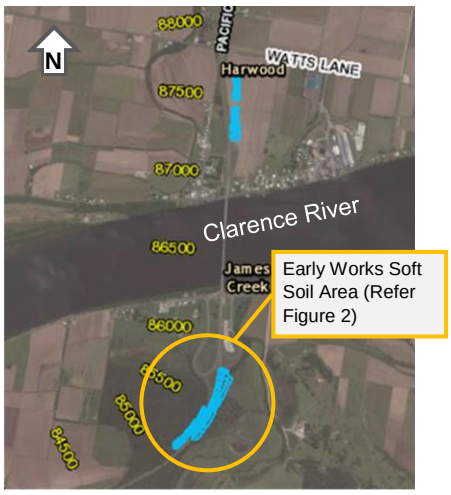

Figure 1: Location of soft soil areas south of Clarence River

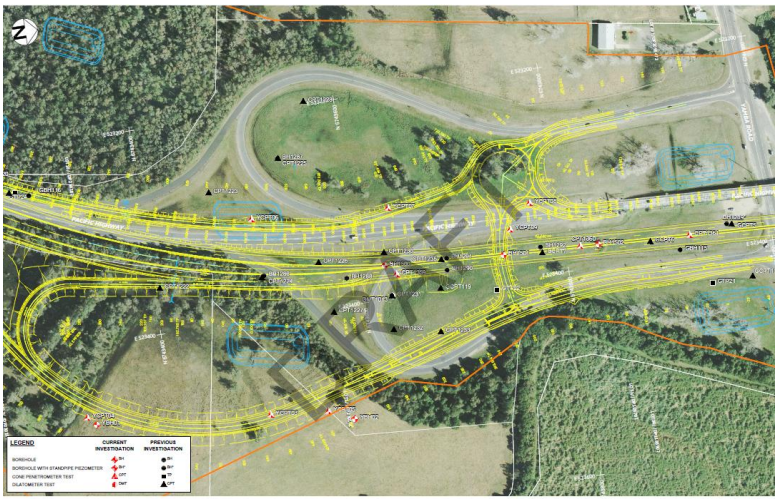

Figure 2: Proposed highway upgrade at south of Clarence River

3. GEOLOGICAL SETTING

The soft soil area to the south of the Clarence River is a large freshwater swamp associated with James Creek, which is part of the river floodplain. It has a natural ground surface elevation generally at approximately RL 0.0 m AHD and is inundated by the 1 in 20 year flood. Highway embankments over this area are underlain by Quaternary sediments, which are inferred to have been deposited as fluvial, deltaic, estuarine and marine sediments in approximately the last 200,000 years (Late Tertiary to Holocene). The sediment stratigraphy comprises recent, Holocene floodplain sediments (mud, silt, sands and local gravels) overlying extensive Holocene estuarine-deltaic sands and clays. These Holocene sediments overlie Pleistocene estuarine and lacustrine sediments (mottled clays) and basal fluvial gravels. The basal gravels are assessed to be pre-Pleistocene and directly overlie bedrock.

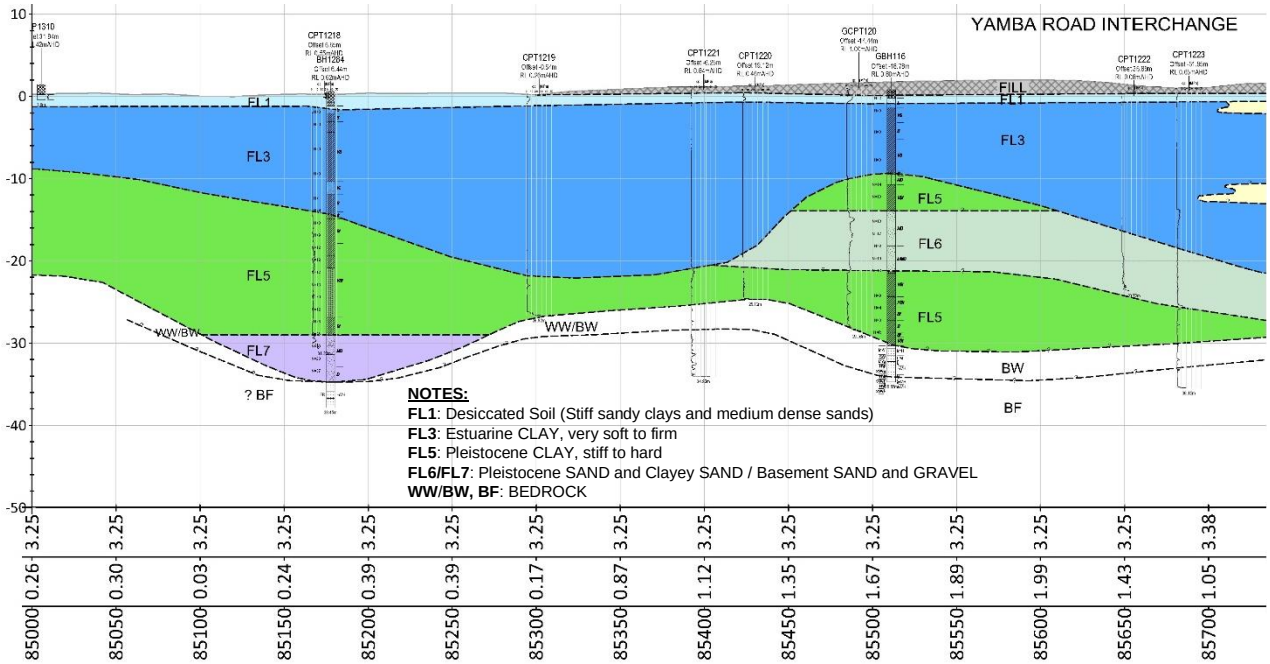

Figure 3: Geotechnical Long Section South of Clarence River (between CH 85000 and CH 85800 along the Pacific Highway Alignment)

Figure 3 shows a typical geotechnical long section along the highway main alignment (northbound lane control line) between CH 85000 and CH 85800. Soft Soil Unit FL3 is estuarine silts and clay, dark grey in color, very soft to firm, with shells and minor organics. This soft soil unit has the layer base level varying from RL -9 m AHD at CH 85000 to below RL -21 m AHD between approximately CH 85300 and CH 85400. It should be noted that this figure only shows the inferred soft soil thickness along the main alignment control line. Soft soil thickness and depth also vary transversely across the highway.

4. SOFT GROUND TREATMENT DESIGN

Soft ground treatment design and construction was carried out in advance of the main upgrade works. The design works were completed at the end of 2014 and construction of the early works commenced in Sept 2015 for target completion of the highway upgrade in 2019.

Soft ground treatment design was carried out using analytical and finite difference methods using the software CAOS (Consolidation Analysis of Soils) developed by Professor Harry Poulos with modification to include post surcharge creep reduction using the method described in Wong (2010). The design considers the following embankment preloading aspects:

- 2-dimensional stress distribution with depth under a fill embankment,
- ground consolidation with vertical drains including smear effect,
- large embankment deformation and settlement,
- time dependent settlement (creep settlement) and creep reduction due to surcharge removal and over consolidation effect, and
- Embankment construction staging.

5. INSTRUMENTATION AND MONITORING

Due to the complexity of fill placement and significant variation in the soft soil thickness, approximately 100 settlement plates, 26 inclinometers, 24 multi depth piezometers, and 13 extensometers were installed and monitored over this embankment area from CH 83400 to CH 85800.

Pacific Complete (PC), a Joint Venture of Lang O'Rourke and WSP, is the "Delivery Partner" engaged by RMS to manage delivery of the upgrade. PC developed an in-house online monitoring system (Zhang et al., 2016) because of the scale of this project with extensive soft ground treatment works. The system development was funded by Road and Maritime Services (RMS) and operated by PC.

PC set up the format and calculation process for each instrument type and the link between different instrument types, e.g. inclinometer and settlement plate, piezometer and settlement plate. Review levels were set up by the PC team to control short term slope instability and hold-point release.

PC developed the system using a data application for data uploading/editing/downloading, a Microsoft SQL Server database for all calculations and the Qlik Sense dashboard with the QlikMap GIS extension for visualisation. A screenshot of the Geotech Dashboard is shown in Figure 4 overleaf.

The tables, charts, graphs and maps used are interactively linked to the underlying data, so that selecting a project area, period, instrument type or instrument, will automatically filter the data being displayed on every control. The same session being open on multiple pages, screens or even computers and mobile devices will maintain a link to this dynamic filtering.

Features of this online monitoring system included:

- Automatic uploading using standard format for all instruments, either via email or a third-party website (e.g. VW piezometers owned by the suppliers).
- Automatic Alert System: an email was automatically sent to all relevant parties when the predetermined Review Levels were exceeded.
- A quick comprehensive review of all relevant instruments linked with a GIS Map to enable quick decision making, which is critical for short term slope stability.
- Open/flexible for further improvement.
- Automatic email reminders of late reading of any instruments.

Short term slope stability was monitored and delivered by PC adopting different trigger levels which addressed the rate of lateral displacement as shown in Table 1. With this online monitoring system, PC managed to build all the embankments safely without slip failure and 75% of all the preloading fills has been released for pavement construction on the whole project.

Table 1: Trigger levels for embankments with and without wick drains (Zhang et al., 2016)

Parameter	Wick drains		No wick drains	
	AL	WSL	AL	WSL
h_m/S (=DRc)	0.25	0.35	0.5	0.7
$\delta h_m/\delta S$ (=DRi)	0.5	0.7	N.A.	N.A.
δ_{hm}/δ_t (mm/day)	10	15	10	15
Action	Increase measurement frequency	Stop filling	Increase measurement frequency	Stop filling

Notes (for Table 1): h_m = max cumulative horizontal displacement from an inclinometer; S = cumulative settlement from adjacent settlement plate; δ = incremental; t = time in days; δ_{hm}/δ_t = daily lateral displacement; AL = Alert Level; WSL = Work Suspension Level; DRi only applies for high risk areas (Yamba and Maclean Interchanges)

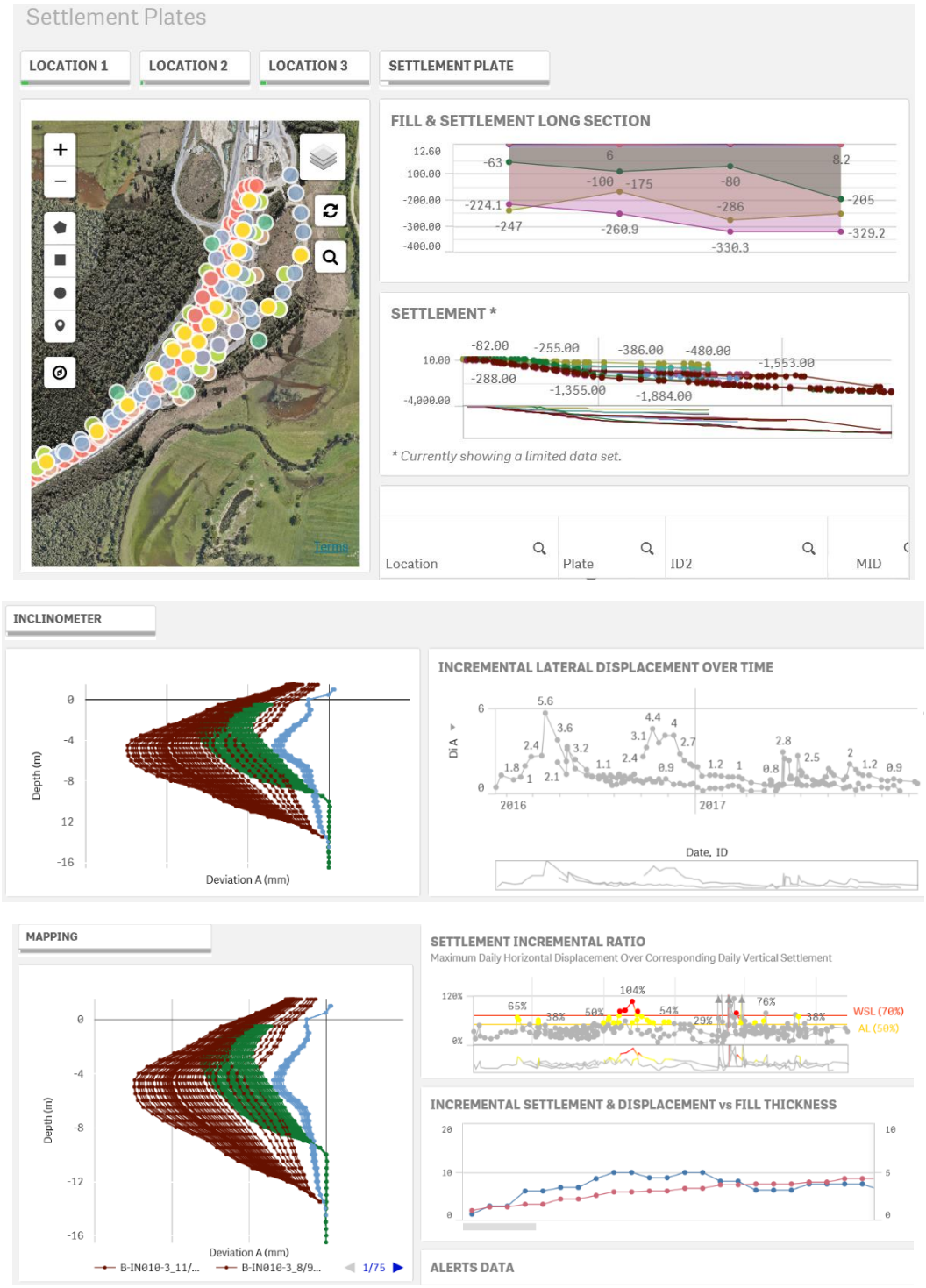

Figure 4: Web based monitoring dashboard of settlement plates and inclinometers

6. SETTLEMENT BACK ANALYSIS

6.1 TYPICAL EMBANKMENT SECTION

Back analysis results for a typical embankment section at approximate chainage CH 85290 are presented in this paper. At this location the following instruments were installed and monitored (1) Extensometer EM05007 with magnets at different depths; (2) Piezometers VP05014 at 6m, 12m, and 20m depths; (3) Inclinometer IN05015. In addition, there are

two settlement plates SP05057 and SP05058 at CH 85240 and CH 85330 respectively. The schematic of the embankment section is shown in Figure 5. A stability berm of 2 m height by 10 m width was used together with high strength reinforcement as stability measures for embankment construction.

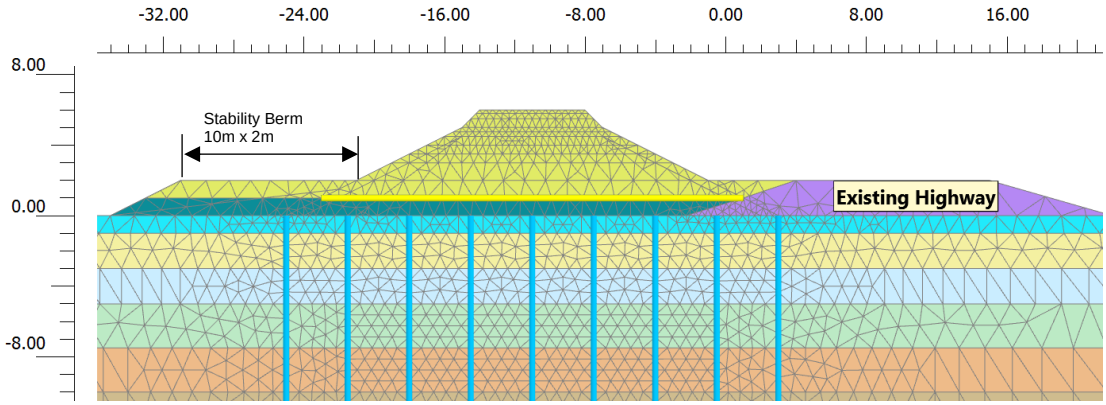

Figure 5: Geometry of Embankment Section at CH 85290

6.2 GEOTECHNICAL MODEL AND PARAMETERS

The back analysis involves settlement curve matching technique using Coffey in-house settlement software (CAOS) and PLAXIS 2D for settlement and consolidation. The primary parameters that were assessed in the settlement back analysis of the embankment performance are the compression and recompression ratios, pre-consolidation pressure, creep strain rate and the coefficient of consolidation. These parameters vary with depth so there are innumerous possible combinations of soil parameters that could match the measured ground settlement under the fill embankment. Finding the best fit parameters that matched excess pore pressure and settlement profiles with depth and embankment construction against time was extremely difficult and time consuming, and the resulting solution is by no means unique. The back analysed geotechnical model and soil parameters for ground under the embankment at CH 85290 are summarised in Figure 6.

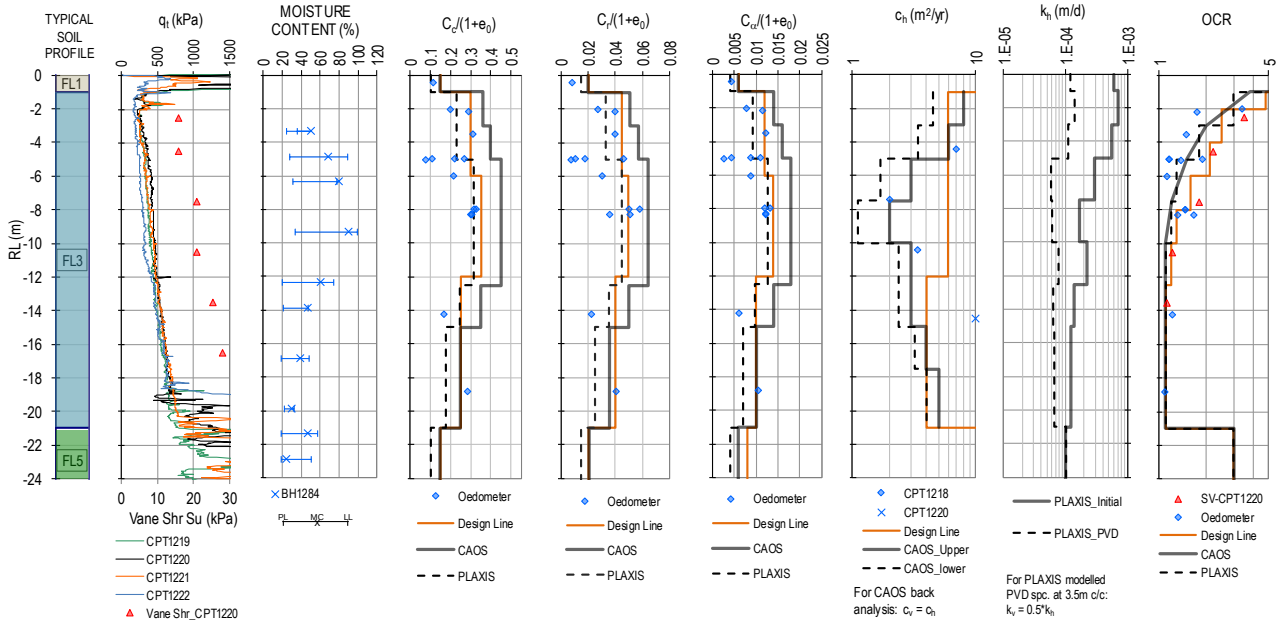

Figure 6: Back analysis parameters comparison with the interpreted design soil parameters.

The upper and lower values of the horizontal consolidation coefficient (c_h) are provided in Figure 6 for soft soil Unit FL3. These values are for soil behavior under the normal consolidated stress range. The adopted consolidation coefficient corresponding with the over consolidated stress range is 10 times the upper value of consolidation coefficient for the normal consolidated stress range. For soil Unit FL3 layer above 10 m depth, the lower value of consolidation coefficient is applied when the vertical effective stress increases more than approximately 20kPa beyond the pre-consolidation pressure. For soil Unit FL3 layer below 10 m depth, the lower value of consolidation coefficient is applied when the vertical effective stress increases more than approximately 10kPa beyond the pre-consolidation pressure. Vertical

consolidation coefficient has been assumed to be similar to the horizontal coefficient of consolidation (c_h), although the original design was based on $c_v = 0.5c_h$.

The initial ground level under this embankment section was at an approximately reduced level RL 0.0 m AHD. The initial groundwater level has been assumed at the initial ground surface in this back analysis. The groundwater level fluctuation with time has not been considered in the back analyses. Bulk unit weight of embankment fill has been assumed as 20 kN/m^3.

6.3 BACK ANALYSED SETTLEMENT RESULTS

In the back analysis using CAOS, Boussinesq equations were used to estimate the embankment induced vertical stress, which is calibrated with the induced stress from a PLAXIS 2D finite element analysis for this embankment. It was observed that the analytical method provides the embankment induced stress distribution within approximately 5% - 15% of that obtained from the PLAXIS 2D analysis.

Prefabricated Vertical Drains (PVD) were installed at 1.2 m center to centre in a triangular pattern. PVD were embedded approximately 3 m in very stiff clay layer (soil Unit FL5) below the base of the soft soil unit FL3. In the back analyses using CAOS software, PVD has been modelled as an equivalent radius of 0.026 m for the band type PVD. The smear zone has been assumed to extend to a radius of 0.13 m. The ratio of permeabilities of the undisturbed to remoulded soil is 5. In PLAXIS 2D, the equivalent 2D vertical spacing was assumed as 3.5 m to account for the plane strain (2D) modelling effect. Smear effect was accounted for in PLAXIS 2D by reducing the soil permeability within the vertical drain zone. In the PLAXIS 2D analysis, vertical permeability of half the horizontal permeability for the PVD zone has been adopted to minimize the impact of vertical consolidation due to the used of relatively large equivalent 2D PVD spacing of 3.5 m, especially for the soil layers within the top 5 m depth.

Figure 7 shows the back analysed settlement results at different depths for extensometer EM05007 at CH 85290 with forward prediction of settlements. The initial design embankment fill thickness was 5 m with the corresponding design settlement of 1.5 m at the end of 1.5 year preloading period. The back analyses indicate the actual ground settlement would have been approximately 1.8 m under a 5 m design height embankment at this location. Additional fill was recommended to compensate for the settlement and to speed up the preloading process.

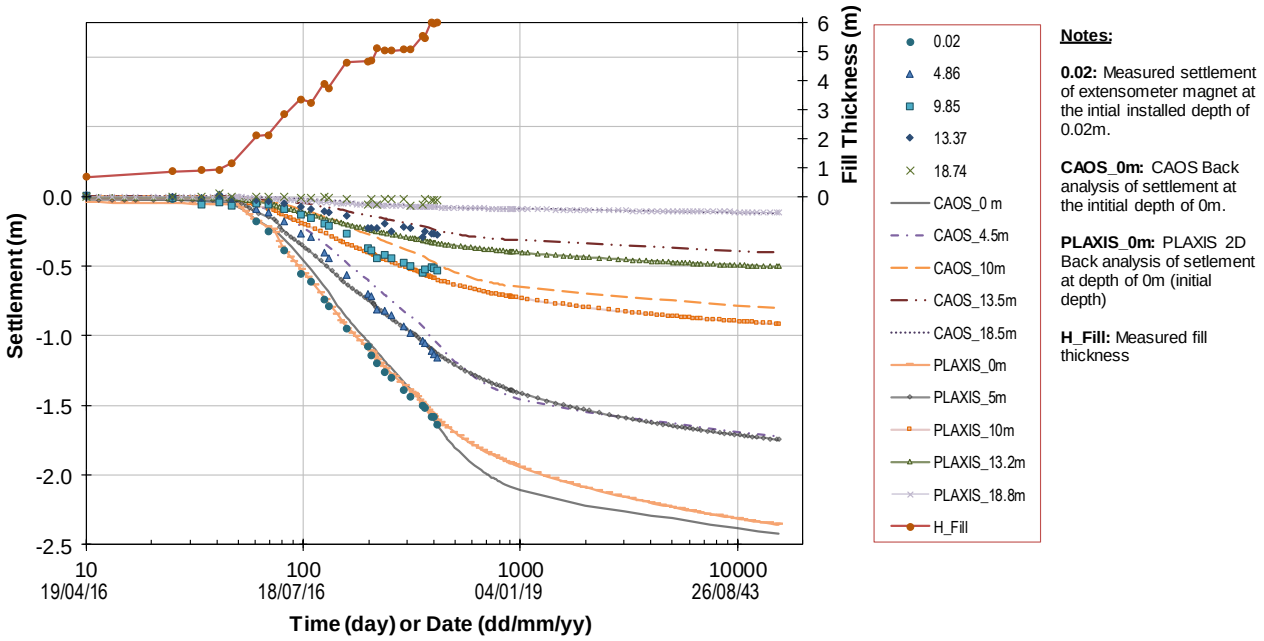

Figure 7: Back analysis of Extensometer EM05007 at CH 85290

As can be seen from the settlement curves at ground surface and at 10 m depth in **Figure 7**, the majority of the ground settlement (up to approximately 75% of the total ground surface settlement) occurred within 10 m depth. The remaining approximately 25% of ground settlement was due to the compression of the soil layer from 10 m to 19m depth. Relatively minor settlement occurred in soil layers below 19 m depth. This is partly because the average embankment induced vertical stress within 10 m depth is higher than those in the underlying soil layers. The average embankment induced vertical stress within 10 m depth is approximately 1.5 and 2 times higher than the average induced vertical stresses in soil layer from 10 m to 20 m and soil layer at below 20 m depth respectively. In addition, it appears from the back analysis

soil parameters and the investigation data that the soil layers within 10 m depth are softer than the soil layers below 10 m depth.

There have been no sensible extensometer reading available at this location beyond May 2017 as extensometer EM05007 was broken due to settlement. Further embankment settlement assessment has relied on settlement plate SP05058 installed at CH 85330. Embankment geometry (width, batter slope, wick drains, and stability berm) and ground condition at CH 85330 are generally similar to that at CH 85290, except that fill thickness at this settlement plate was at maximum 5.8 m. The monitored settlement of plate SP05058 and the corresponding back analysed settlements using CAOS and PLAXIS 2D are shown in **Figure 8Error! Reference source not found.**.

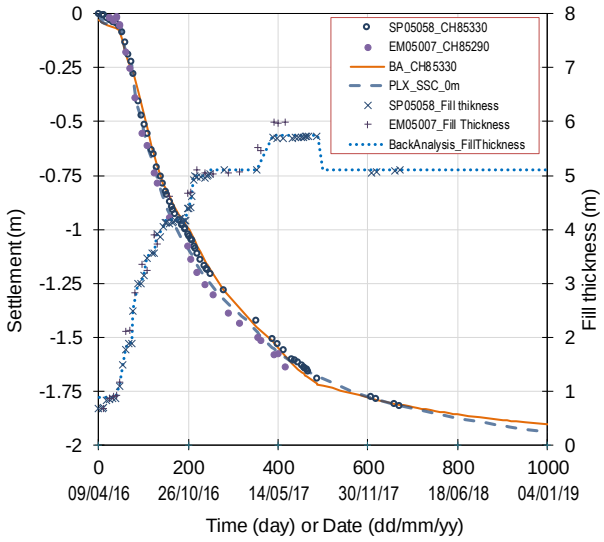

Figure 8: Back analysis of settlement plate SP05058 at CH 85330

The reduction in fill thickness shown in **Error! Reference source not found.** at 490 days was due to excavation for temporary traffic diversion but not at the completion of the preloading period. Approximately 0.7 m thick fill was excavated from the main embankment while an additional 2 m thick fill was stockpiled on the stability berm (over the whole berm width) for this embankment area. Embankment was restored to 6 m thick during June 2018 for further preloading, which has not been captured in the forward settlement prediction shown in Figures 7 and 8.

Figure 9 shows the measured pore pressure in the piezometers (VP05014) installed at 6 m and 12 m depth (installed depths below the initial ground surface) at CH 85290 and the back analysed pore pressures from CAOS and PLAXIS 2D. Groundwater table fluctuation with time was measured using a standpipe piezometer (WP05007) installed outside the embankment and stability berm footprint at CH 85180, i.e. approximately 110 m from the back analysed embankment section. The measured pore pressure in standpipe piezometer WP05007 at approximately CH 85180 are also included in Figure 9. The standpipe piezometer WP05007 was installed to 5.2 m depth below the initial ground surface level. The measured pore pressure fluctuation of up to approximately 14 kPa with time in the standpipe piezometer indicates the groundwater level fluctuation could be up to 1.4 m.

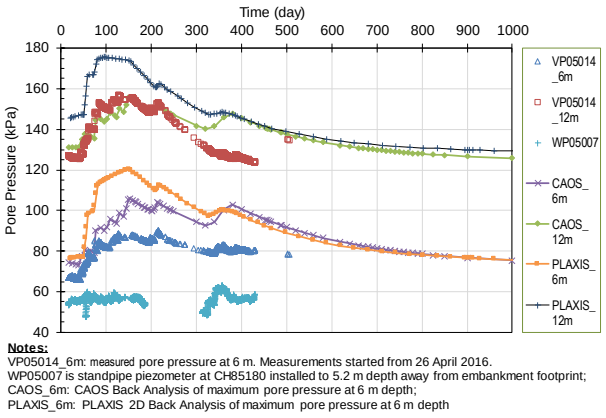

Figure 9: Measured pore pressures at CH 85290

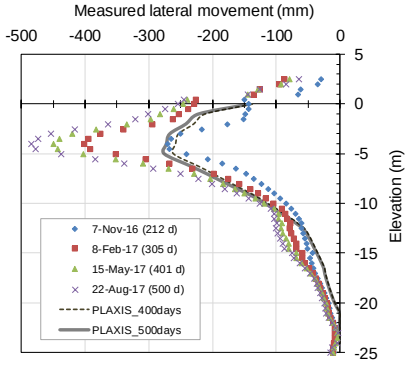

Figure 10: Lateral ground movement at CH 85290

Measured lateral ground movements versus depth at the toe of embankment fill at CH 85290 are presented in Figure 10 The measured lateral movements extended beyond 20 m depth below the initial ground surface level. Relatively large lateral movements occurred above 10m depth. The maximum lateral movements happened at approximately 4 m to 5m depth below the initial ground level. This indicates the soil layer within 0 m and 10 m depth could be significantly softer than the soft soil layer below 10 m depth. Overall, the measured maximum horizontal ground movement is 25% to 28% of the maximum vertical ground settlement at different times during the embankment construction and preloading period. It can be seen from Figure 10 that the lateral movement (negative implies outwards from the embankment toe) was significantly under-estimated by the numerical analyses. The authors believe that this under-estimation is caused by stress rotation effects on soil stiffness that have not been accounted for in the back-analyses.

6.4 BACK ANALYSIS PARAMETERS VS DESIGN SOIL PARAMETERS

Figure 6 shows the comparison between the back analysed compression ratios, over consolidated ratio (OCR), consolidation coefficient (c_h), and the interpreted design soil parameters for soft soil Unit FL3. The back analysed OCR and c_h are generally within the interpreted design parameters. Using CAOS, the back analysed compression ratios are approximately 30% higher than the interpreted design parameters from oedometer tests. However, using the Soft Soil Creep model in PLAXIS 2D, the back analysed compression ratios are within the oedometer test results.

It should be noted that there are more than one combination of back analysed soil parameters that could give reasonable matching with the actual settlement curves. A slightly lower OCR from 4 m to 8 m depth may also lower the compression ratios or lower consolidation ratio or permeability would result in higher compression ratios. It is possible that probabilistic and Bayesian updating methods such as those described by Huang et al (2010) and Kelly and Huang (2015) may provide better matching with quantifiable reliability of back-analyses using monitoring results.

7. CONCLUSION AND LESSONS LEARNT

Advanced instruments have been installed for embankment performance monitoring. Apart from surface settlement plates and inclinometer, extensometers and piezometers have been used for a more accurate back analysis that leads to more confidence in forwarded prediction of creep settlement.

Delicate instrument such as extensometer and piezometer are prone to being damaged during operation, when settlement or preloading time exceeds the design values respectively. They must be installed to accommodate contingency measures such as additional filling or can be operate at a significantly longer preloading time (long battery life).

The web-based monitoring system provides a tool to assist with early identifying problem area for review, assessment, and contingency measure action. Additional fill was identified for some area to compensate for embankment settlement in excess of the design and to accelerate the consolidation process.

Both conventional and advance soil models were utilized to assess and back analyse the monitored embankment performance. CAOS and PLAXIS 2D require different stiffness parameter input due to differences in the calculation approaches, particularly in the treatment of creep commencement time. However, they provide reasonably similar embankment settlement and long-term creep settlement under an embankment provided that comparable stiffness parameters have been input.

The use of CAOS for back analysis is fast and efficient to obtain a preliminary set of parameters that provide confident back analysis and prediction of embankment settlement. PLAXIS 2D with Soft Soil Creep model can be used subsequently to fine tune the back analysis and prediction to consider a more reasonable embankment filling and excavation stages. The use of PLAXIS 2D has a drawback to model consolidation with PVD and smear zone effect compared to using CAOS. Trial and error calibration of soil parameters is required to obtain the equivalent soil permeability for PVD zone in PLAXIS 2D. Future research of quantifying the reliability of back-analysed parameters and forward projection of settlement behavior may include probabilistic methods such as Bayesian updating of monitoring data.

8. ACKNOWLEDGEMENTS

The authors are grateful to the NSW Roads and Maritime Services and Pacific Complete for the use of the monitoring data and results and their approval for publishing this paper. Any opinions, findings, conclusions and recommendations in this paper are those of the authors only, and do not necessarily reflect the views of NSW Roads and Maritime Services.

9. REFERENCES

Huang, J., Griffiths, D.V. and Fenton, G.A. (2010) Probabilistic Analysis of Coupled Soil Consolidation. *Journal of Geotechnical and Geoenvironmental Engineering*, 136(3): 417-430.

Kelly, R. and Huang, J. (2015) Bayesian Updating for One-dimensional Consolidation Measurements, *Canadian Geotechnical Journal*, 52: 1318-1330.

Poulos, H.G. (2008) CAOS User Manual, Consolidation Analysis of Soils.

Zhang, H., Gombault, N., Choi, B. (2016) An innovative geotechnical monitoring system for soft ground treatment on W2B Pacific Highway Upgrade Project, *Australian Geomechanics Society Sydney Chapter Symposium*, Nov 2016, 194-203.

Wong, P. K., (2010). Comparison of experimental methods for assessing secondary consolidation settlement of soft soil after surcharging. *Australian Geomechanics Society Perth Chapter Symposium Ground Improvement Seminar*, June 2012.

THE USE OF ULTRA-WIDE BAND GPR FOR THE DETECTION OF VOIDING AND OTHER ARTEFACTS IN BRIDGE ABUTMENTS AND RELATED RETAINING STRUCTURES

Reagan Newton
Scientific Officer, Roads and Maritime Services

ABSTRACT

The structural integrity of bridge abutments and retaining structures can be compromised by the presence of voids. Structural deformations visible on the surface of structures that are indicative of voiding may not indicate the actual location of voids within the structure, therefore, pinpointing problem areas can be problematic. Traditional destructive methods of investigating these structures (including drilling and borescope inspection) generally only provide limited information at a single point; they also have the potential to cause damage to the structure during investigation.. Standard GPR (Ground Penetrating Radar) methods are utilised as a supplement and/or alternative to traditional methods of investigation but have limitation of depth and resolution. Ultra-wide band GPR methods provide an efficient non-destructive method for the detection of voiding while maintaining resolution over a broader depth range than that of other GPR methods.

Most GPR devices use an antenna that has a discrete peak frequency which provides a resolution at a specific depth. To investigate different depths, several different GPR antennae must be utilised with varying peak frequencies. As these antennae only have a peak frequency, resolution falls at depths which are outside of the specific depth related to the peak frequency of the respective antennae. Ultra-wide band GPR differs from standard GPR devices by having a range of peak frequencies that enable it to maintain the resolution over a broader depth range.

This paper provides a discussion on the feasibility of ultra-wide band GPR as a tool to investigate voiding of bridge abutments and retaining structures. It also provides a description of the methodology utilised for the assessment of ultra-wide band GPR technology and a description of its potential suitability for other uses.

1 INTRODUCTION

Roads and Maritime Services (RMS) currently maintains approximately 5100 bridges across NSW and proper maintenance of these structures is a vital priority. The RMS currently employs a rigorous maintenance and inspection scheme to ensure that these structures are properly maintained, including the inspection and investigation of bridge abutments and related retaining structures. However, this is no small task for an organisation that maintains approximately 5100 bridges, and due to the significant risk related to any deterioration in these structures, RMS has interest in investigating new methods to supplement the existing inspection and investigation system. Some of the key considerations when assessing a new technology engaged for this purpose include:

- increasing the efficiency of inspections while being cost effective
- increasing the confidence in data retrieved from investigations and inspections
- supplementing and aiding assessment interpretations

Ground Penetrating Radar (GPR) could be a viable technology for this purpose and help to increase the efficiency and accuracy of the current inspection and investigation system.

GPR has been established within the geophysics industry for a variety of purposes including archaeological, civil and geological purposes. In the civil arena, GPR has been widely utilised for scanning concrete structures for the purpose of locating defects, detecting reinforcement, finding concrete cancer, and other concrete integrity interpretations. Other civil applications include sub-surface imaging, ground profiling, utility location, pavement investigation, and void detection.

GPR does have limitations of depth and resolution, namely that there is a trade-off that states ‘with increased depth, there is a decrease in resolution’. The governing factor in this trade-off is the frequency of the GPR antenna; while lower frequency antennae reach deeper depths there is a reduction in resolution when compared to high frequency antennae. Selecting the correct antenna is critical in producing good results but often the sub-surface properties being scanned are either unknown or variable and depths of interest can therefore vary. The

ultra-wide GPR is a possible solution to this problem as it provides a range of frequencies and thus maintains a good resolution over a greater depth range from the surface.

2 THE PHYSICS OF GPR

2.1 GPR BASICS

GPR utilises radar waves in the electromagnetic spectrum via the transmission and subsequent detection of these waves to detect sub-surface layering, defects, objects, voids, and other artefacts. GPR devices can be of various constructions and sizes ranging from small hand held devices, to push cart/ vehicle mounted and aerial units. All GPR units have particular features in common such as transmitting and receiving antennae, processing computers and power sources. The GPR unit produces radar waves via the transmitting antenna in the direction of the surface to be investigated. The radar waves reflect off boundaries within the sub-surface and are detected at the receiving antenna (see Figure 1). The processing computer then produces a one dimensional plot of the amplitude (which can be negative or positive) of the detected radar waves (reflections) with time (measured from when the wave was produced by the transmitter to when it was received by the receiver - see the simplified version in Figure 1) which is known as a GPR trace. The GPR unit is then moved and the process is repeated which results in multiple traces along the direction of interest, the end output is known as a line.

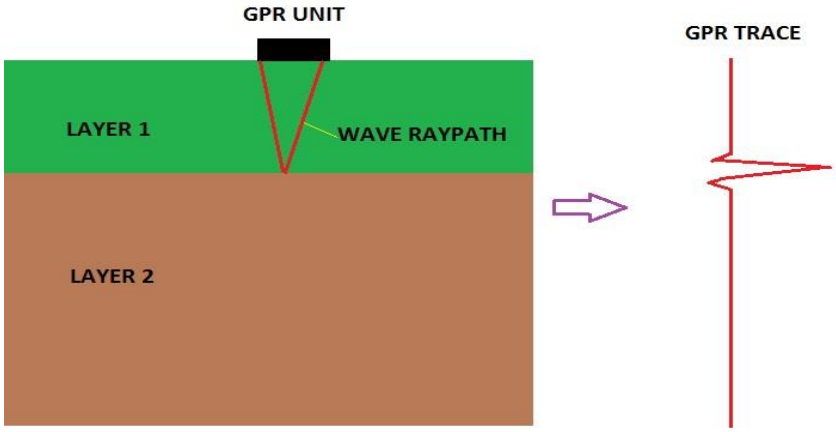

Figure 1: GPR radar waves being transmitted and reflections received and processed as a radar

The transmission, acquisition and processing of these traces occurs in very short time periods (in the order of nanoseconds) and as such the GPR unit can be moved at a relatively fast pace. When multiple traces are spliced together along a line, a GPR radargram or wiggle plot radargram is produced (see Figure 2). This shows the entirety of the line with amplitudes on traces representing the time the signal was detected after transmission.

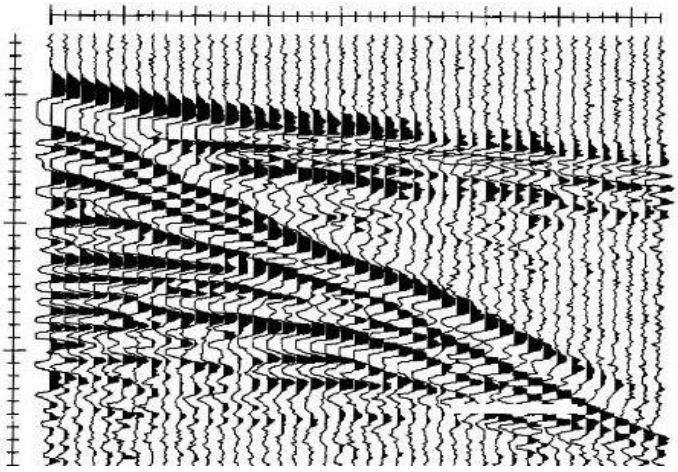

Figure 2: Wiggle plot GPR radargram

By displaying the radar traces representing the amplitude as a greyscale (with black representing the largest negative amplitude and white representing the largest positive amplitude) we can produce an image radargram (see Figure 3) to help visualise the time it takes for reflection signals to be received.

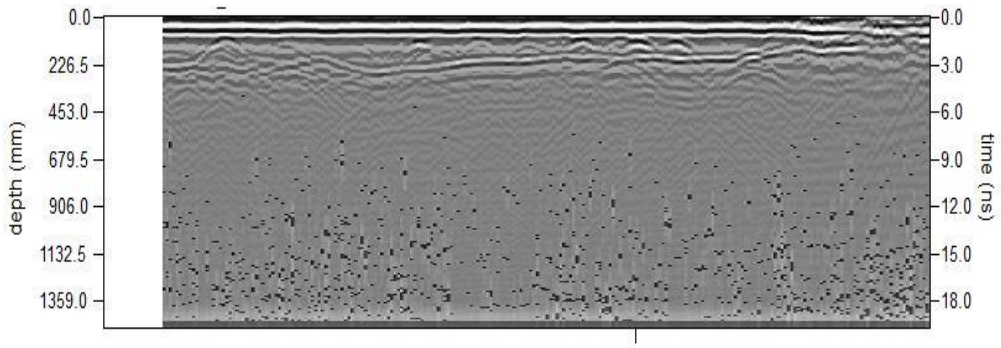

Figure 3: Image GPR radargram

Estimating the speed for radar waves to travel through predicated materials allows us to calculate the depth at which these reflections occur using the total travel time of the signal from transmitter to reflection to receiver (see Figure 4). By assessing where reflections occur at depth across the whole radargram, we can produce an interpretation of sub-surface features.

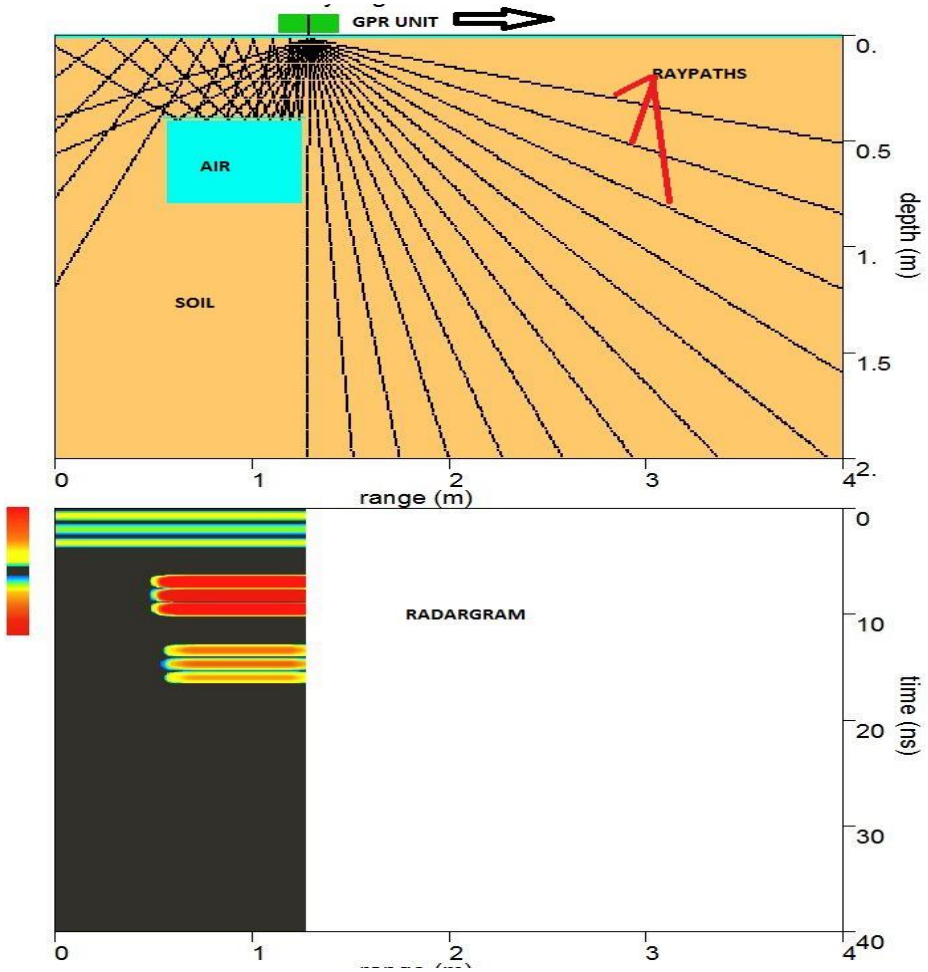

Figure 4: Reflection raypath and sub-surface interpretation

2.2 REFLECTIONS

As discussed in Section 2.1, GPR depends on reflections from sub-surface features to help us produce an image of the sub-surface profile; however, not all boundaries result in a reflection of radar waves. Reflections are

determined by the differences in relative permittivity or dielectric constant of the two materials forming the boundary. The equation for the dielectric constant is given in (1) where κ = dielectric constant of material, ε_r = relative permittivity of material, ε = absolute permittivity of material, and ε_0 = permittivity of vacuum.

$$\kappa = \epsilon_r = \frac{\varepsilon}{\epsilon_0} \tag{1}$$

$$R = \frac{\sqrt{\kappa_1}-\sqrt{\kappa_2}}{\sqrt{\kappa_1}+\sqrt{\kappa_2}} \tag{2}$$

$$T = \frac{2\sqrt{\kappa_2}}{\sqrt{\kappa_1}+\sqrt{\kappa_2}} \tag{3}$$

Equation 2 and Equation 3 show the reflection (R) and transmission (T) coefficients between a boundary interface formed by two materials dielectric constants κ_1 and κ_2 (assuming normal incidence on boundary interface with the wave moving from material κ_1 to material κ_2). These coefficients dictate the amplitude of the reflected and transmitted waves across a boundary. As shown by Equation 1, the larger the difference in dielectric constants, the larger the amplitude of the reflected wave. Boundaries where the dielectric constants are almost equal have very low reflection amplitudes and most of the wave is transmitted. The polarity of the reflected wave is governed by whether $\kappa_1 > \kappa_2$ or $\kappa_1 < \kappa_2$ and the difference in magnitude of κ_1 and κ_2 determines the amplitude of the reflected wave. A polarity shift may also occur in the reflected wave. If $\kappa_1 > \kappa_2$, then the reflected wave will have no change in polarity, if $\kappa_1 < \kappa_2$, then the reflected wave will have a change in polarity (see Figure 5). This is a fundamental principle of GPR as a GPR unit "sees" differences in dielectric constants.

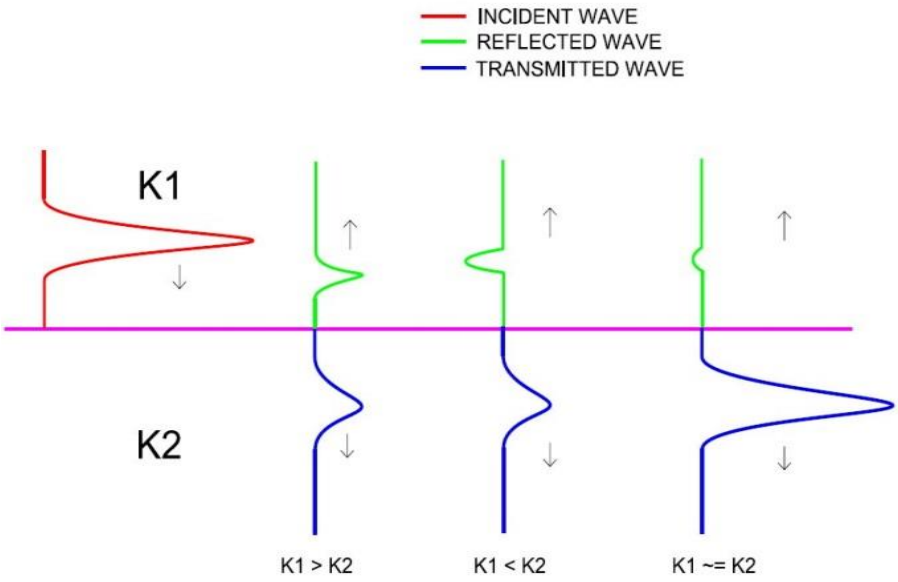

Figure 5: Reflection of waves at a boundary with varying dielectric constant combinations

2.3 FREQUENCY – BATTLE BETWEEN RESOLUTION AND DEPTH OF PENETRATION

A common discussion point when planning a GPR survey is what frequency of antenna is appropriate for the investigation. Resolution is affected by the medium composition, saturation, attenuation characteristics and other inherent properties of the investigation medium. For the most part, these factors cannot be controlled; however, what can be controlled is the frequency of the GPR unit. Resolution is divided into both vertical resolution and horizontal resolution where vertical resolution is the ability to resolve objects with depth and horizontal resolution is the the ability to resolve objects in the depth plane at a particular depth. Resolution is often calculated in terms of the wavelength (λ) which is inversely proportional to frequency (f) (Equation 4). As

described in Yilmaz and Doherty, 1997; it is generally accepted that the vertical resolution distance is equivalent to one quarter of the GPR wavelength.

$$\lambda \propto \frac{1}{f} \tag{4}$$

Figure 6 demonstrates the conical wave "footprint" of a GPR unit. This is based on the dispersing effect of propagating electromagnetic waves and the geometry of the GPR unit and its receiving and transmitting antennas. This footprint (Conyers and Goodman, 1997) is given mathematically by Equation 5, where A represents the horizontal spatial resolution distance at depth D, in medium with dielectric constant κ and GPR wavelength of λ.

$$A = \frac{\lambda}{4} + \frac{D}{\sqrt{\kappa+1}} \tag{5}$$

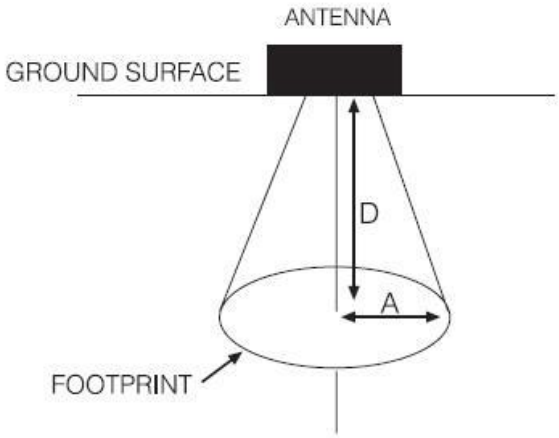

Figure 6: Geometry of conical "footprint" of GPR waves (Conyers and Goodman, 1997)

From Equation 5, we can see that an increase in wavelength (i.e. decrease in frequency) increases the horizontal spatial resolution distance. In addition to an increase in wavelength, Equation 5 shows that an increase in depth also results in an increase in horizontal spatial resolution distance.

Attenuation is also proportional to GPR frequency. Annan and Davis, 1989; demonstrates that attenuation (α) is directly proportional to frequency (f). Due to this relationship, the higher the frequency, the higher the attenuation and thus the lower the penetration depth.

Factoring in that vertical and horizontal resolution distance is smaller (able to resolve smaller objects) at higher frequencies, deeper depths increase the horizontal resolution distance, and that attenuation also increases with higher frequencies (affecting maximum depth) which is when the trade-off mentioned in Section 1 presents itself. Choosing a high frequency antenna reduces the minimum resolvable distance but also decreases the maximum penetration depth. Choosing a low frequency antenna allows an increased maximum penetration depth but increases the minimum resolvable distance. This reiterates the importance of choosing the right antenna for the right application.

3 ULTRA WIDE BAND GPR

Ultra-Wide Band (UWB) GPR has been in development and used for several years with the goal of finding a "one size fits all" GPR antenna. The benefit of a GPR antenna which can be utilised in all situations (rather than using multiple systems) is the efficiency. The UWB GPR has the potential to fulfil this role as a multi-purpose use GPR unit by utilising a range of frequencies rather than a singular frequency. All GPR antennas actually produce a range of frequencies but have peak amplitude at a central frequency, which is the antenna frequency. The UWB antenna has a range of frequencies that have peak amplitude and thus its central frequency is a range rather than a singular (see Figure 7). The broad range of frequencies allow a broader depth range while maintaining maximum resolution (as described in Section 2.3). Figure 8 displays two radargrams, one using a

single frequency antenna, the other using an ultra-wide band antenna. As it can be seen, the single frequency antenna has less resolution of features and imaging of sub-surface features.

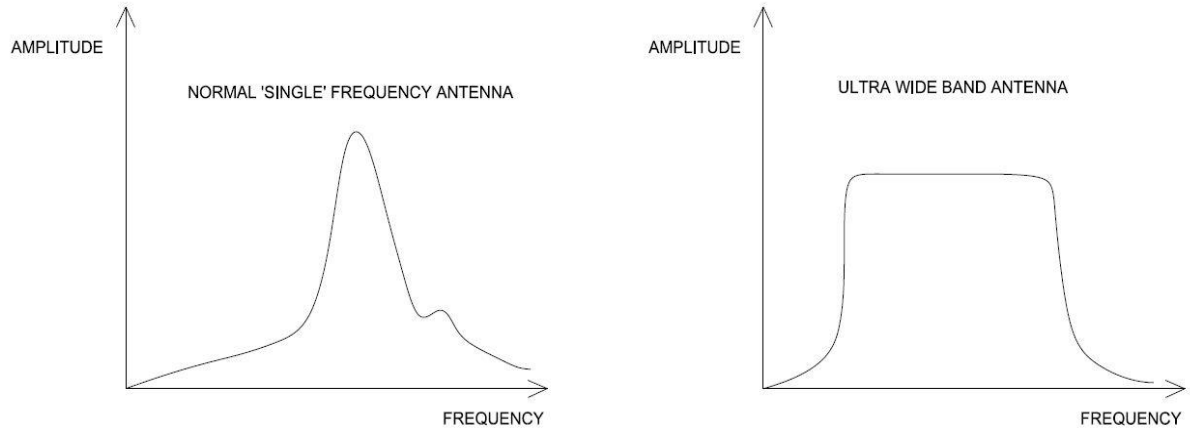

Figure 7: Frequency response for a regular 900MHz antenna and an UWB antenna

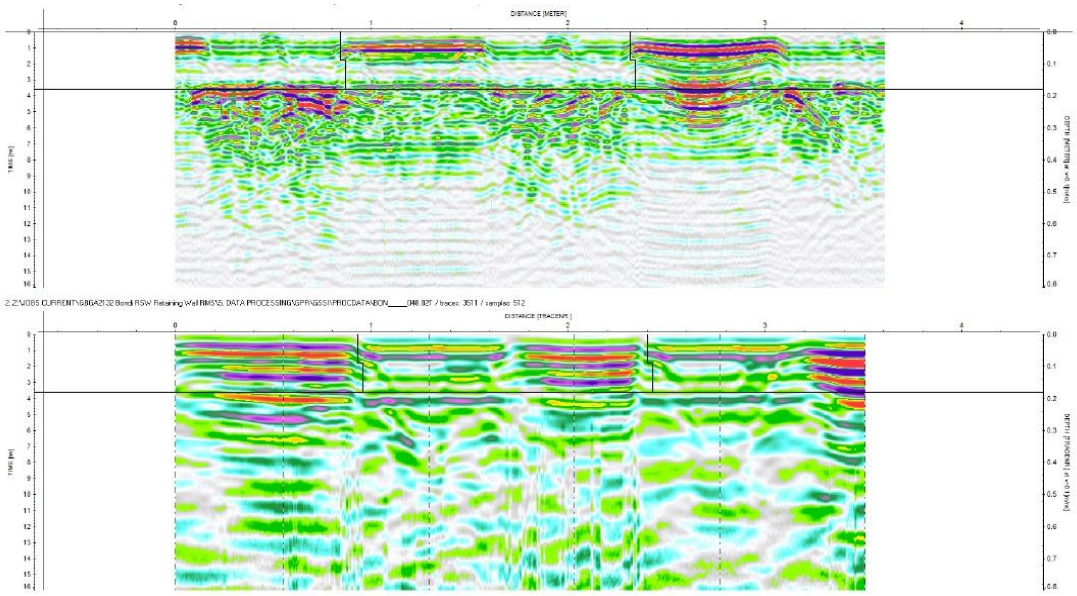

Figure 8: Comparison of UWB GPR radargram (top) and single frequency antenna (bottom) of the same line

4 GPR PROCESSING AND INTERPRETATION

4.1 GPR SIMULATIONS

GPR data requires a level of processing and interpretation to correctly produce a sub-surface model. Utilising a GPR simulation program (GPR-SIMM) we can produce several scenarios and produce artificial radargrams to aid in interpreting real world GPR radargrams. Figure 9 shows a simulated GPR radargram for detecting small subsurface metallic objects (such as a pipe or Iron block). The inverse "U" shape that appears on this radargram is known as a hyperbola. The crest of this hyperbola generally points to where the top of the subsurface feature is located in space (both horizontal and vertical). By analysing the gradient of the 'flukes' of the hyperbola, the velocity of waves within that medium can be determined using the distance-time relationship.

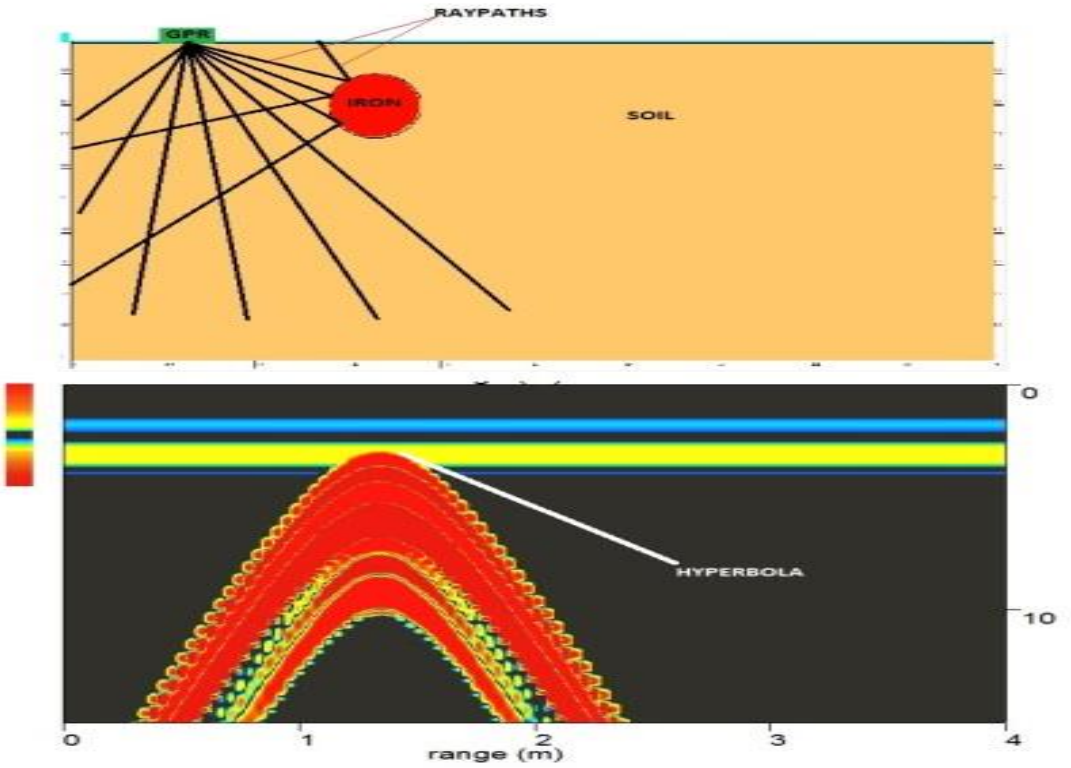

Figure 9: Simulated radargram showing characteristic reflection hyperbola

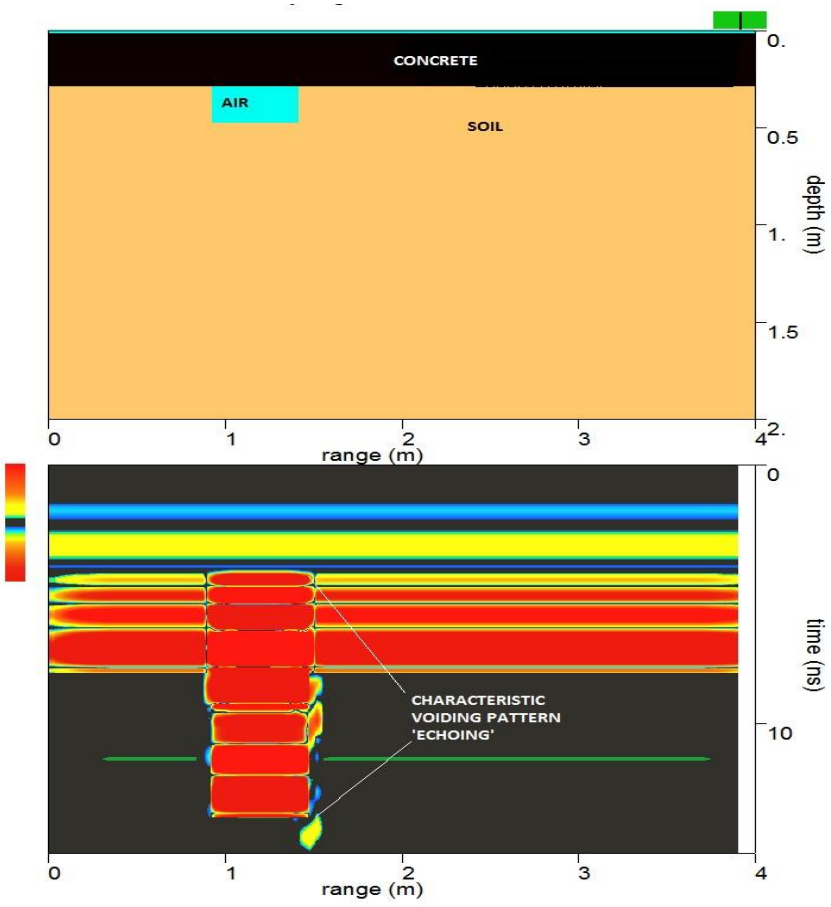

Figure 10: Simulated radargram showing characteristic voiding pattern 'echoing'

Figure 10 displays a simulated radargram for a small air void below a concrete slab on top of soil. Voiding has a particular pattern where the GPR detects several distinct banding where raypaths are 'echoing' within the void. As voids are generally filled with air / gas, the dielectric constant is usually the lowest when adjacent to solid layers and thus analysis of the adjacent polarity of reflections can identify voids (see Section 2.2).

4.2 FILTERS AND PROCESSING

Before interpreting GPR data, it is often helpful to process the data by applying filters to highlight features, removes noise and increase confidence in interpretations. Understanding what filter to apply is crucial as often incorrect interpretations from filters can be made.

4.2.1 Zero Time Correction

The zero time correction is a vertical filter that corrects for the air gap between the GPR antenna and the investigation surface. The first major reflection detected is usually the investigation surface and the data is vertically shift (time correction) to make this reflection zero time. This ensures that times measured are all relative to the investigation surface.

4.2.2 Band Pass

The band pass filter comprises a low pass and high pass frequency filter. This enables only a range of frequencies to be analysed. For example, frequencies detected may range from 12MHz to 3 GHz but as only reflections of sub-surface structure is important it is often helpful to restrict this range of frequencies detected (band pass). Low frequency noise from radio waves can create noise and often this is filtered out by removing all frequencies below a particular level. Similarly, other high frequency noise exists and by applying a high pass frequency will remove all frequencies above a particular level.

4.2.3 Deconvolution

Deconvolution is an inverse processing filter where the filter compresses the signal with the goal of removing shallow 'ringing' (often caused by metallic objects on the investigation surface) and displays data otherwise obscured by these ringing signals. Deconvolution should be applied with caution when investigating voiding as voiding also exhibits characteristic 'ringing' or 'echoing' (see Section 4.1).

4.2.4 Migration

Migration is an inverse processing filter which tries to produce a 2D model of the sub-surface by matching geometry features with radargram signals. Migration also includes a velocity analysis of the characteristic hyperbolas to determine velocity of layers to produce a depth profile.

4.2.5 Background

Horizontal banding from other sources, induction from objects moving near the GPR, and induction from other electromagnetic sources can occur within radargrams. A background filter removes the banding created from this by analysing horizontal banding and applying amplitude filters to remove these.

4.2.6 Hilbert

Hilbert filters reduce the reflection amplitudes to single amplitudes. A reflection on a GPR trace often has several small peaks of varying amplitude with a primary amplitude reflection which can often cloud where the reflection event occurs. The Hilbert filter averages out these amplitudes reducing it to one single amplitude

reflection event, preserving polarity. Figure 11 displays the effect of a Hilbert filter on a GPR trace.

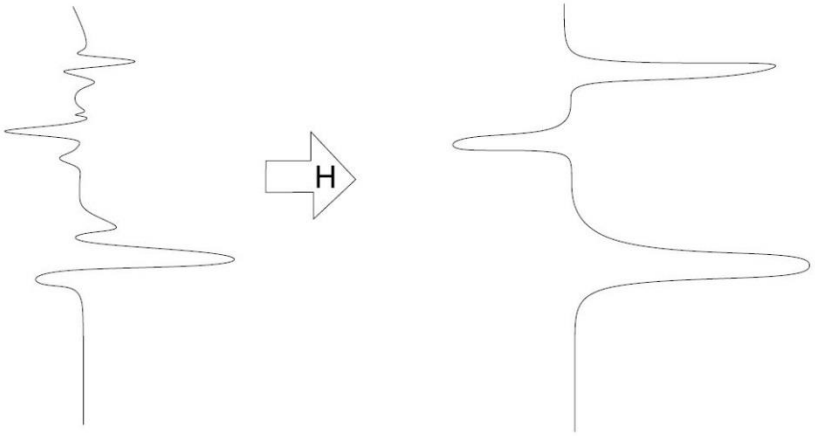

Figure 11: GPR trace before and after a Hilbert filter is applied

4.2.7 Gain

Gain filters apply a multiplier to the amplitude increasing or reducing the amplitudes of reflections. Gain filters allow us to identify reflection events or remove non-reflection event amplitudes and noise.

5 ULTRA WIDE BAND GPR FIELD TEST

5.1 OVERVIEW

Two sites were picked to perform a test on the viability of ultra-wide band GPR in its ability to determine sub-surface artefacts and voiding. Both sites are located in the Western Sydney region and are underlain by the Bringelly Shale geological unit with nearby Quaternary Alluvium. The goal was to perform a survey over the structures at the sites, determine from the data if any voiding or artefacts can be identified, and attempt to confirm the existence and extents of these artefacts or voids using drilling, probing etc. The data is processed using the software package GPR-SLICE (Version 7.0 - 2018). GPR-SLICE is a specialised GPR processing software designed for various levels of signal and image processing, import and export of GPR data, and 3D modelling of GPR data. Filter and data processing was applied (see Section 4.2) to aid analysis of data. Further filters are then applied to emphasise voiding based on a determined criteria.

When processing GPR data, the criteria for locating voiding is a combination of the following:

- Polarity change at first reflection (using Hilbert filters to help display this – see Section 4.2.6);
- Characteristic ‘echoing’ patterns (see Section 4.1) and;
- Amplitude of reflections consistent with air void/soil interface (see Section 4.1).

5.2 SITE A

Site A consists of four spill through abutments of a major highway overpass of a smaller road. A GPR survey of an approximate 15m x 4m area at the top of each spill through abutment was conducted. Figure 12 displays a description of the site and how it is configured and Figure 13 displays a description of the abutments.

Appropriate filters were applied to the GPR data as described in Section 4.2 using the criteria specified in Section 5.1 to help identify voiding within each abutment. A subsurface model was produced to identify likely areas of voiding which could be further assessed with direct intrusive investigations.

The spill through abutments consists of pavers (approximately 50mm depth) on top of sand base layer. The spill through abutments is likely comprised of general fill below this sand layer. Small diameter holes with a hand drill were drilled through the paver only and a dowel probe was inserted to detect the presence/absence of voiding in areas identified via the GPR processing. Figures 14a/14b/14c/14d to Figures 17a/17b/17c/17d show the processed GPR radargrams and interpreted voiding based on the criteria specified in Section 5.1. The XY plane on the figures represent the spill through surface.

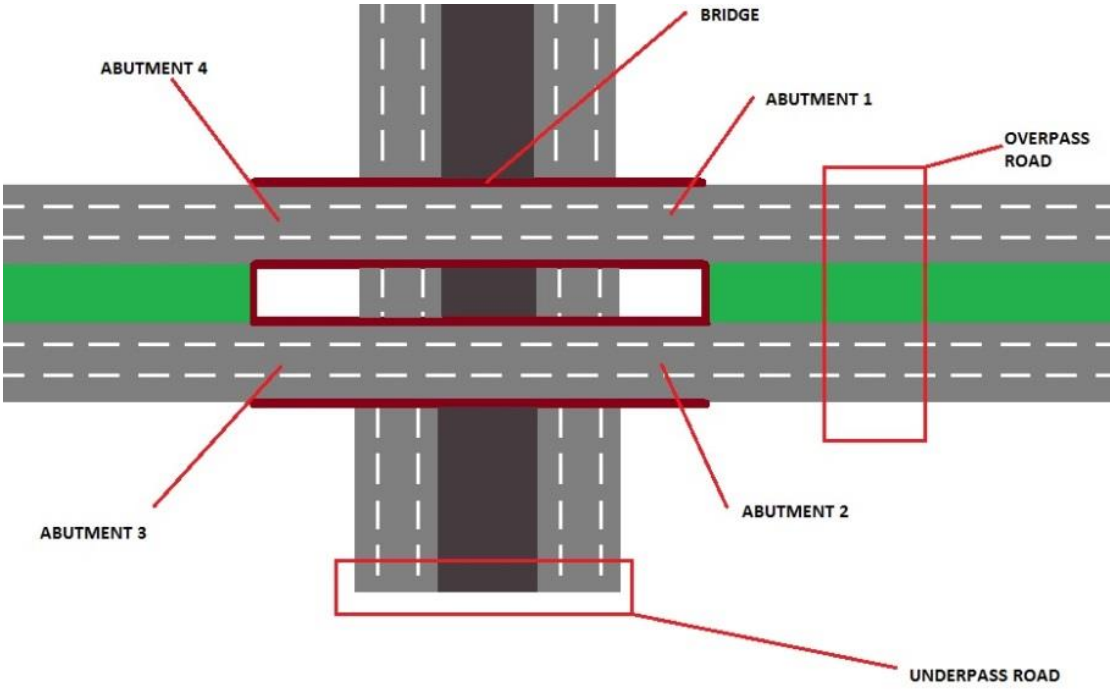

Figure 12: Site description of Site A

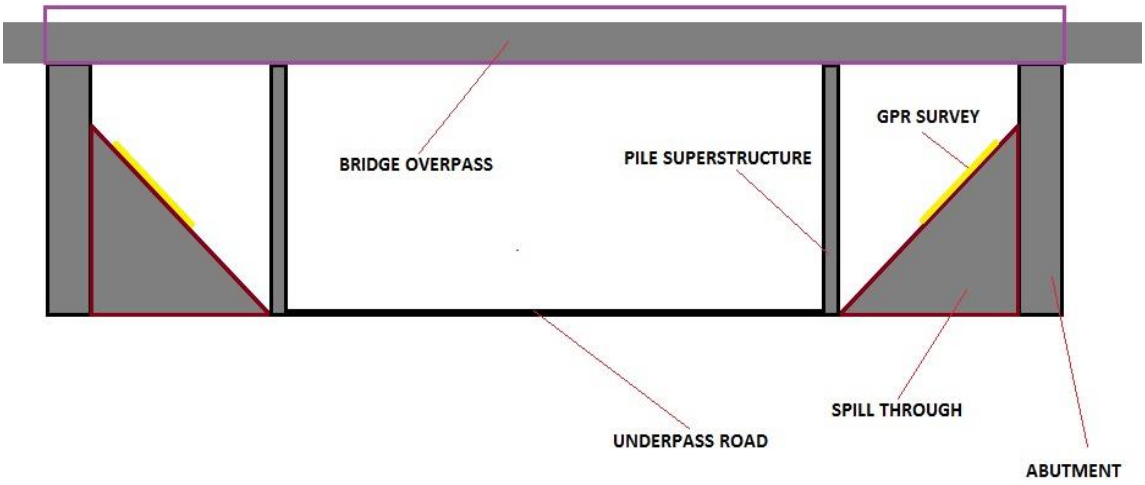

Figure 13: Abutment description site A

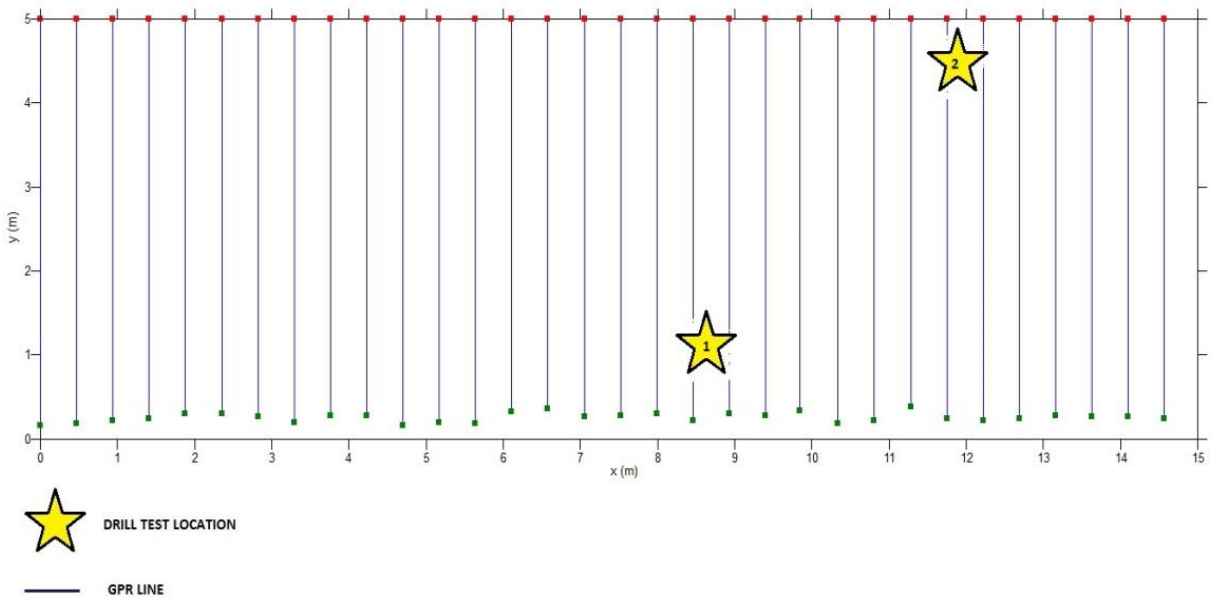

Figure 14a: GPR Scan lines and drill test points – Abutment 1, Site A

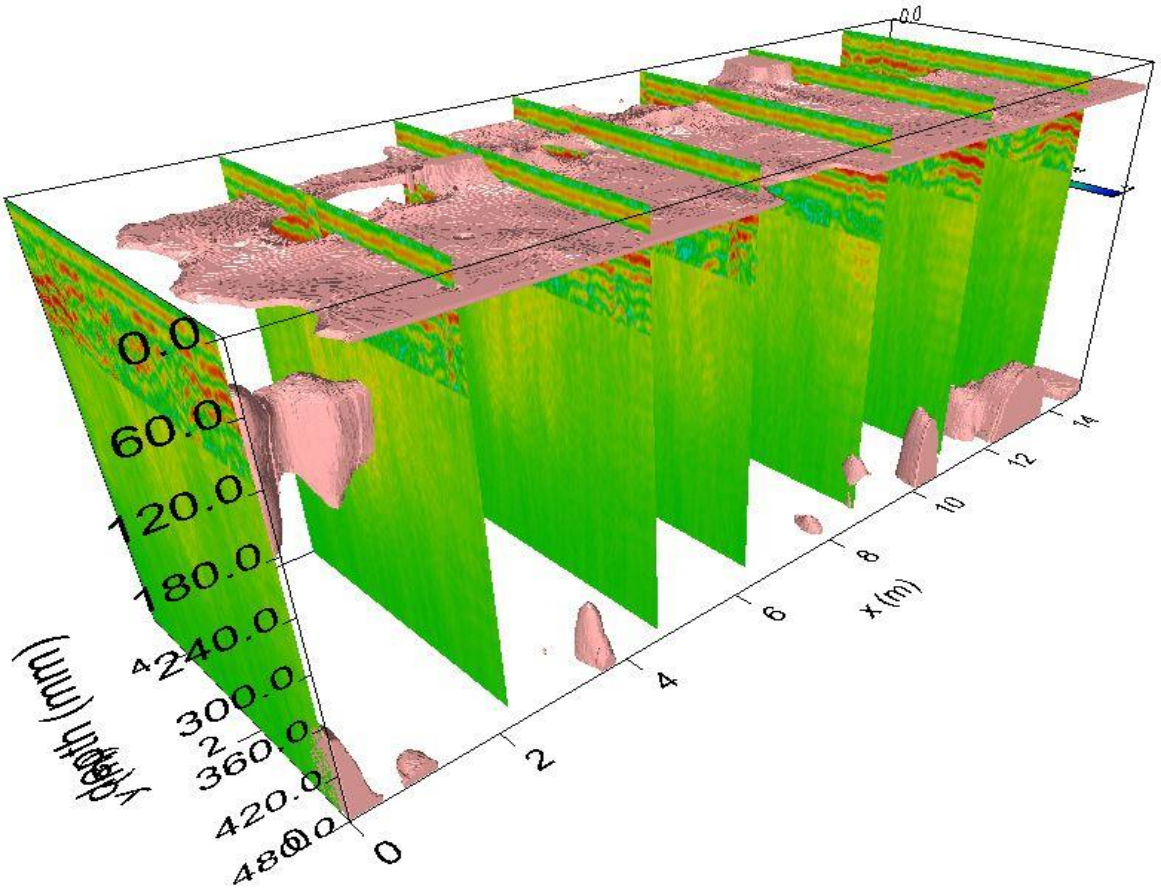

Figure 14b: GPR radargrams and voiding model – Abutment 1, Site A, View 1

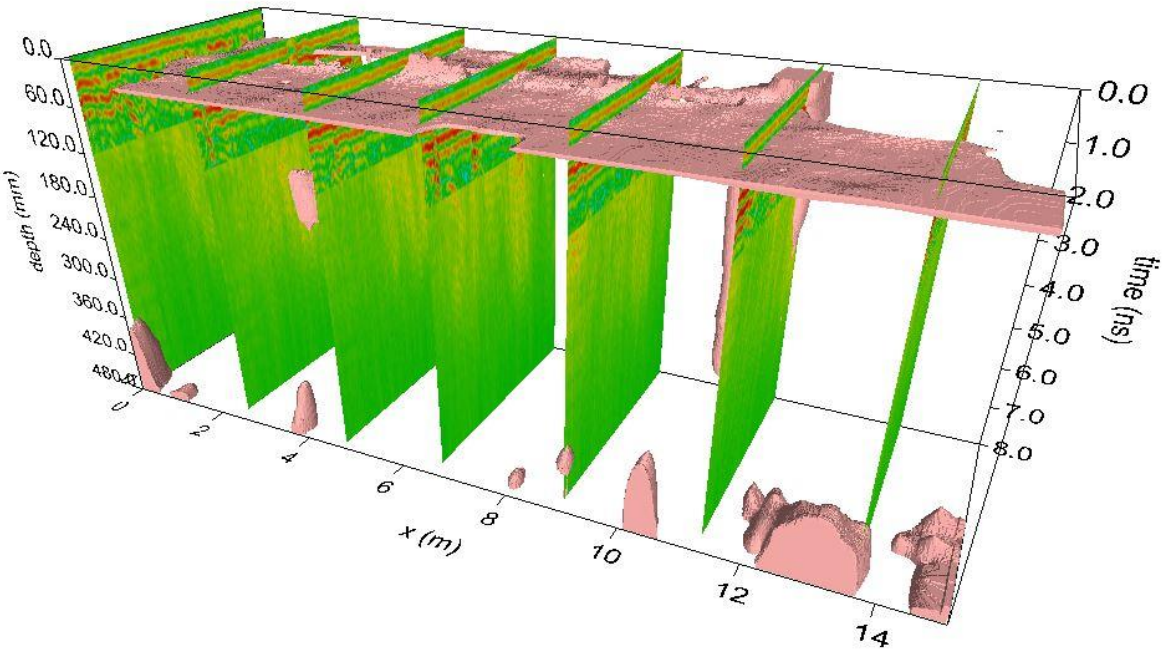

Figure 14c: ZGPR radargrams and voiding model – Abutment 1, Site A, View 2

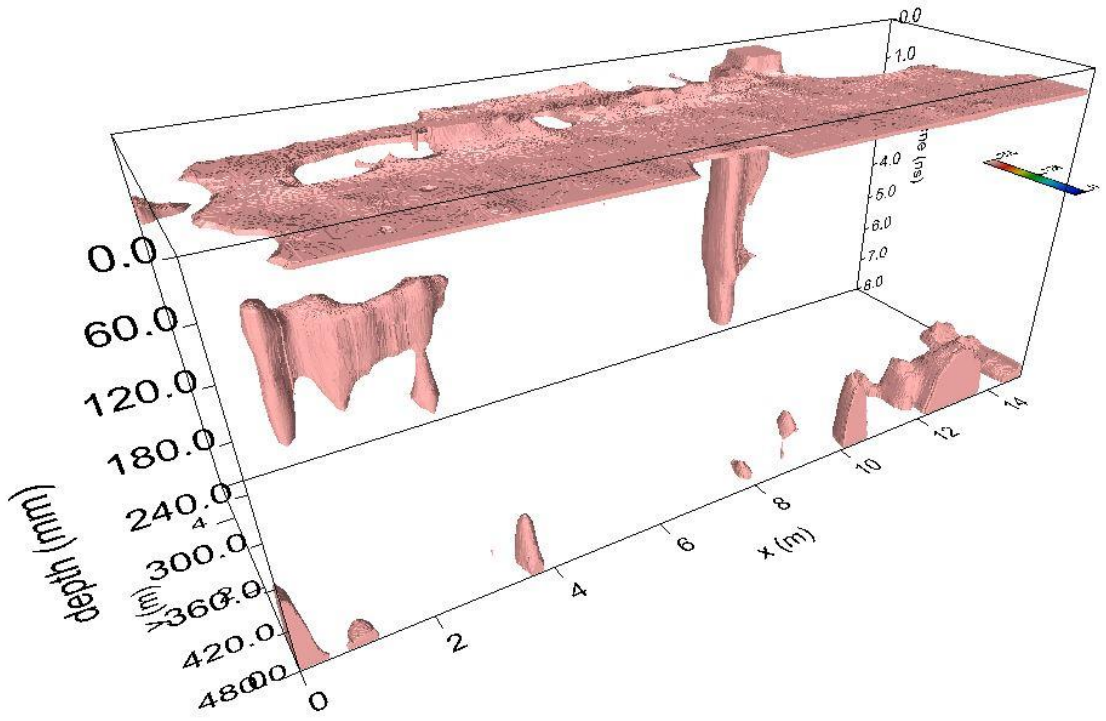

Figure 14d: Voiding model – Abutment 1, Site A

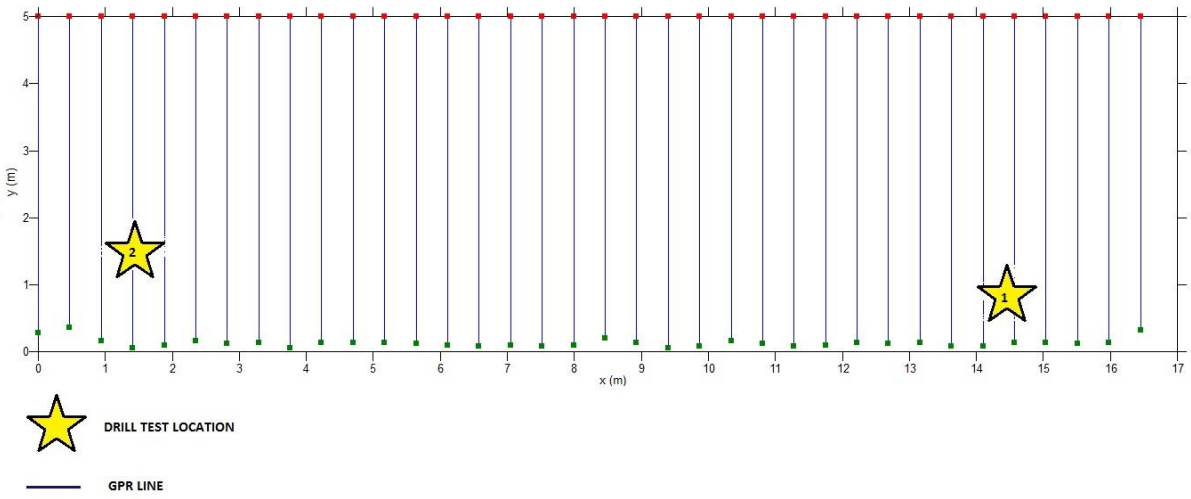

Figure 15a: GPR Scan lines and drill test points – Abutment 2, Site A

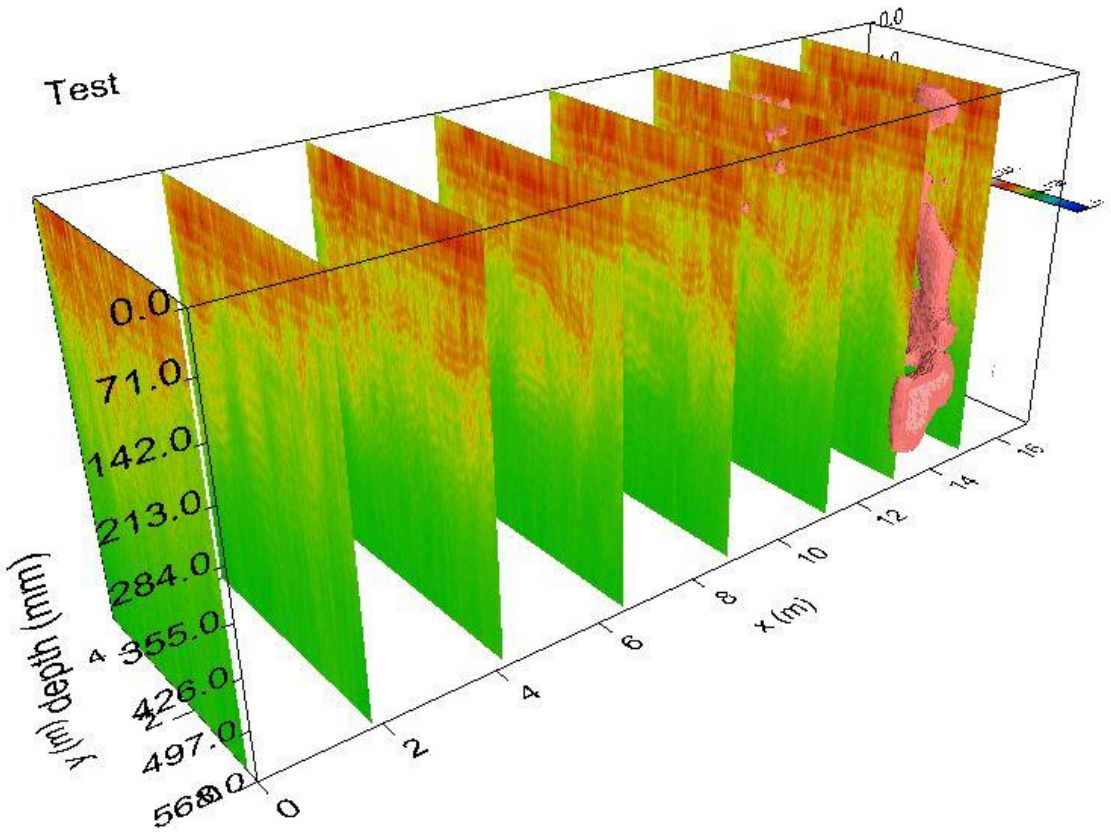

Figure 15b: GPR radargrams and voiding model – Abutment 2, Site A, View 1

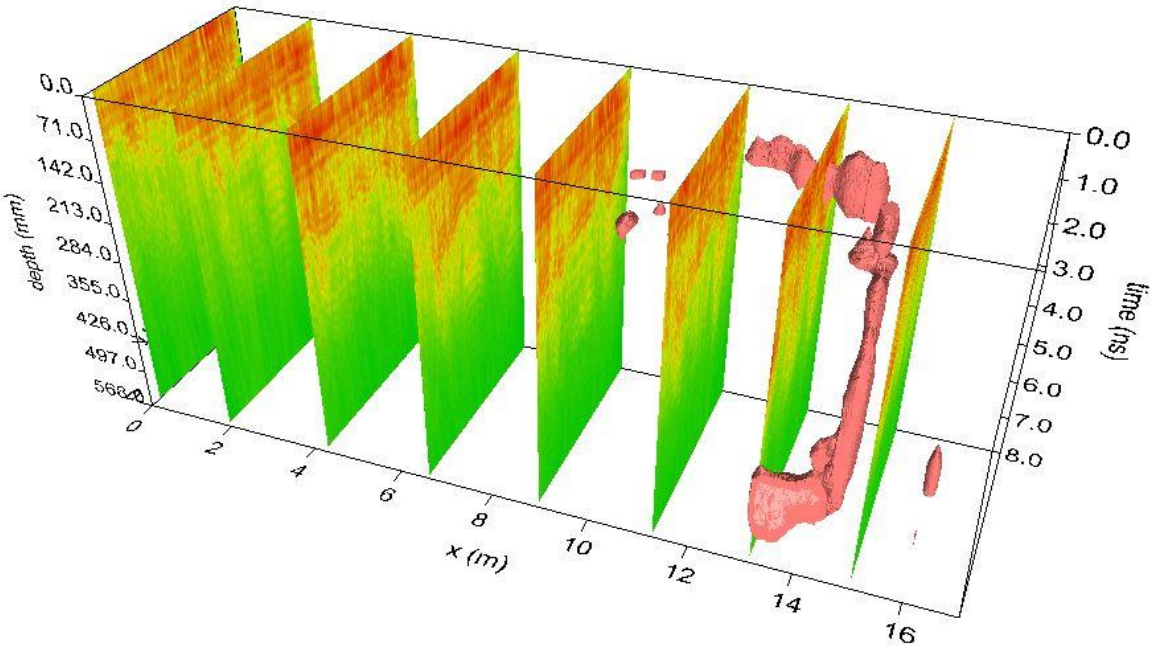

Figure 15c: GPR radargrams and voiding model – Abutment 2, Site A, View 2

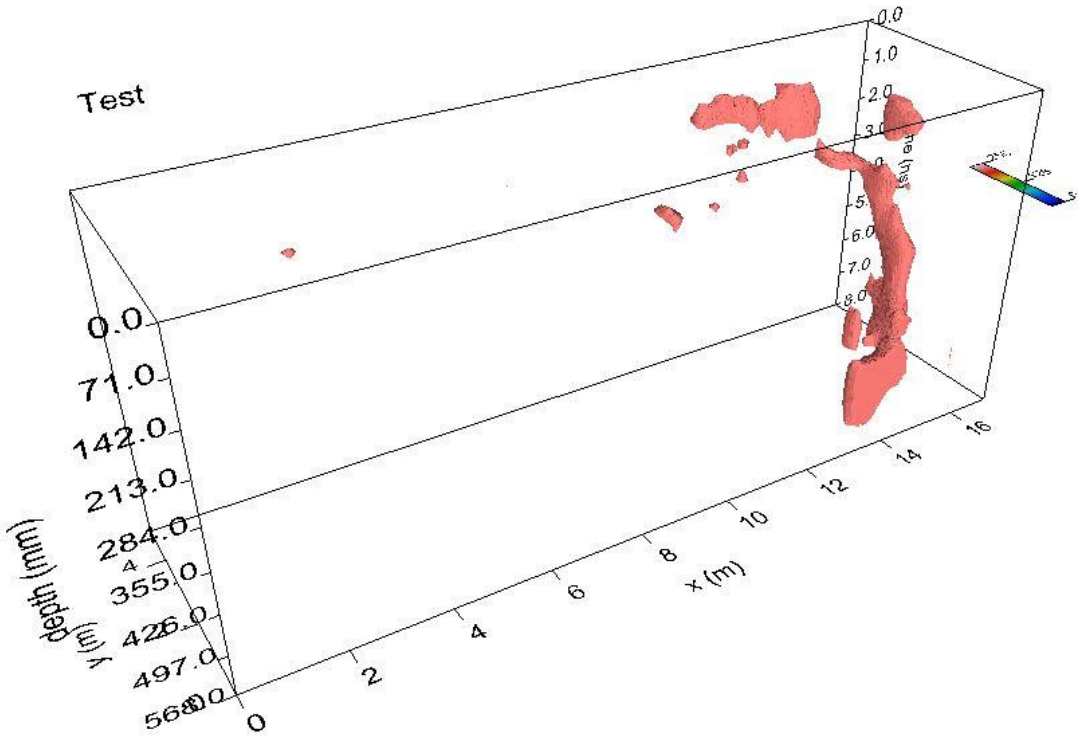

Figure 15d: Voiding model – Abutment 2, Site A

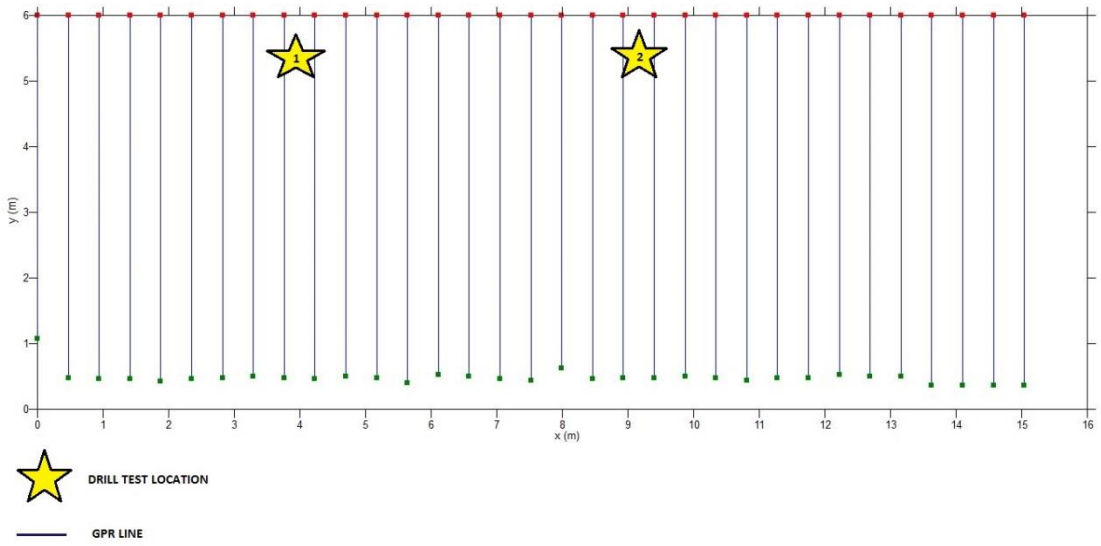

Figure 16a: GPR Scan lines and drill test points – Abutment 3, Site A

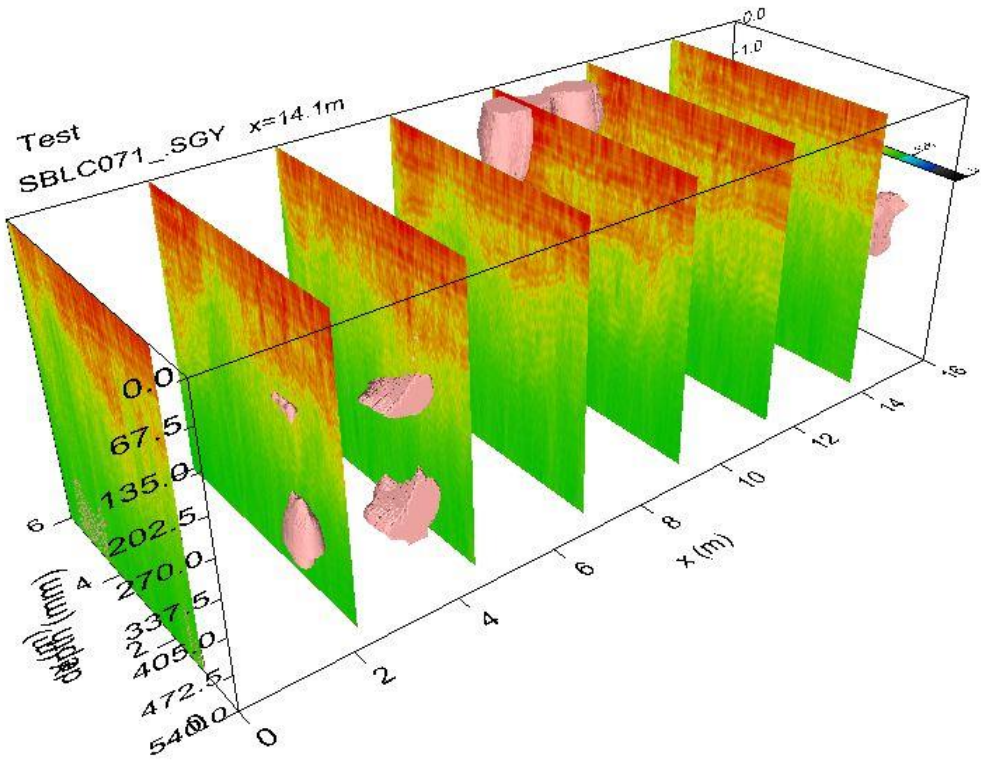

Figure 16b: GPR radargrams and voiding model – Abutment 3, Site A, View 1

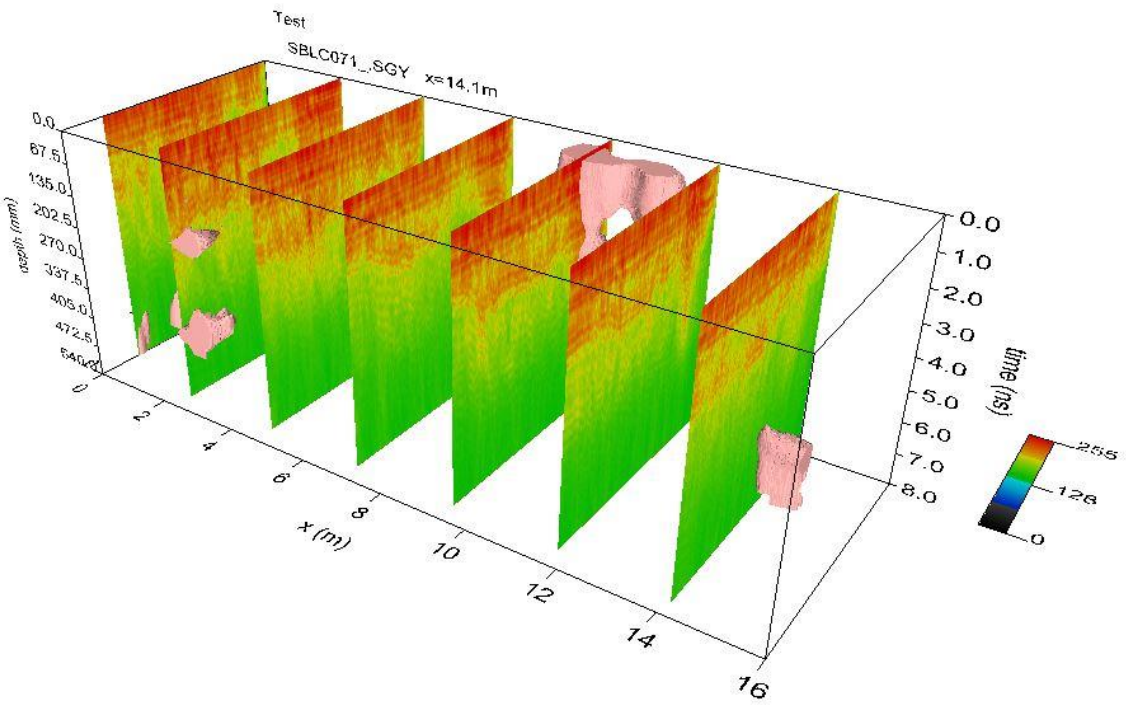

Figure 16c: GPR radargrams and voiding model – Abutment 3, Site A, View 2

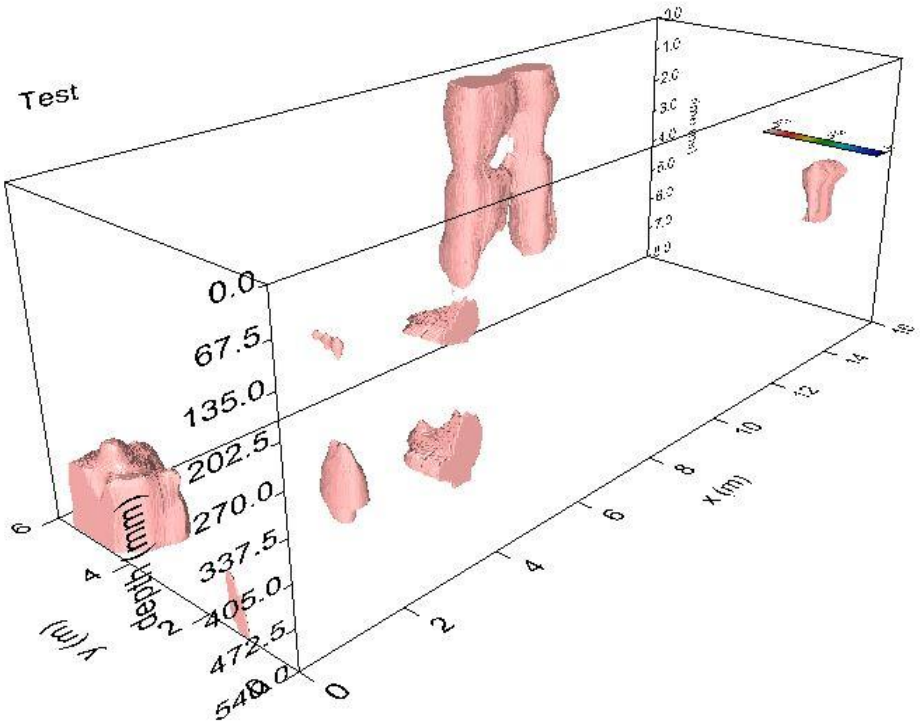

Figure 16d: Voiding model – Abutment 3, Site A

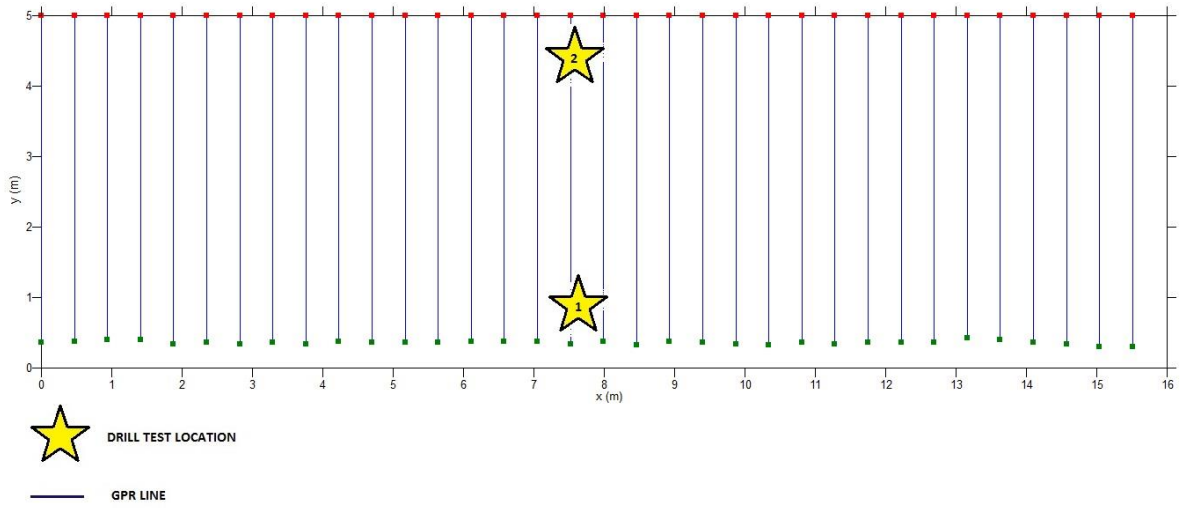

Figure 17a: GPR Scan lines and drill test points – Abutment 4, Site A

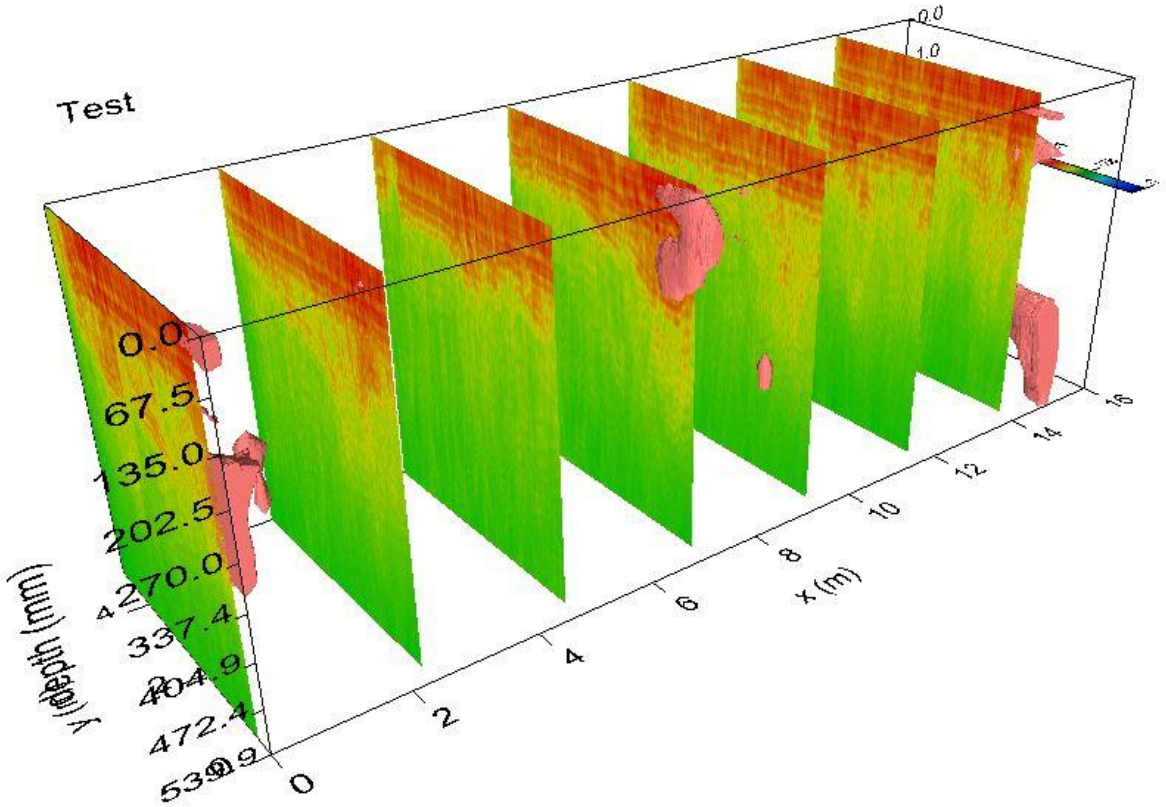

Figure 17b: GPR radargrams and voiding model – Abutment 4, Site A, View 1

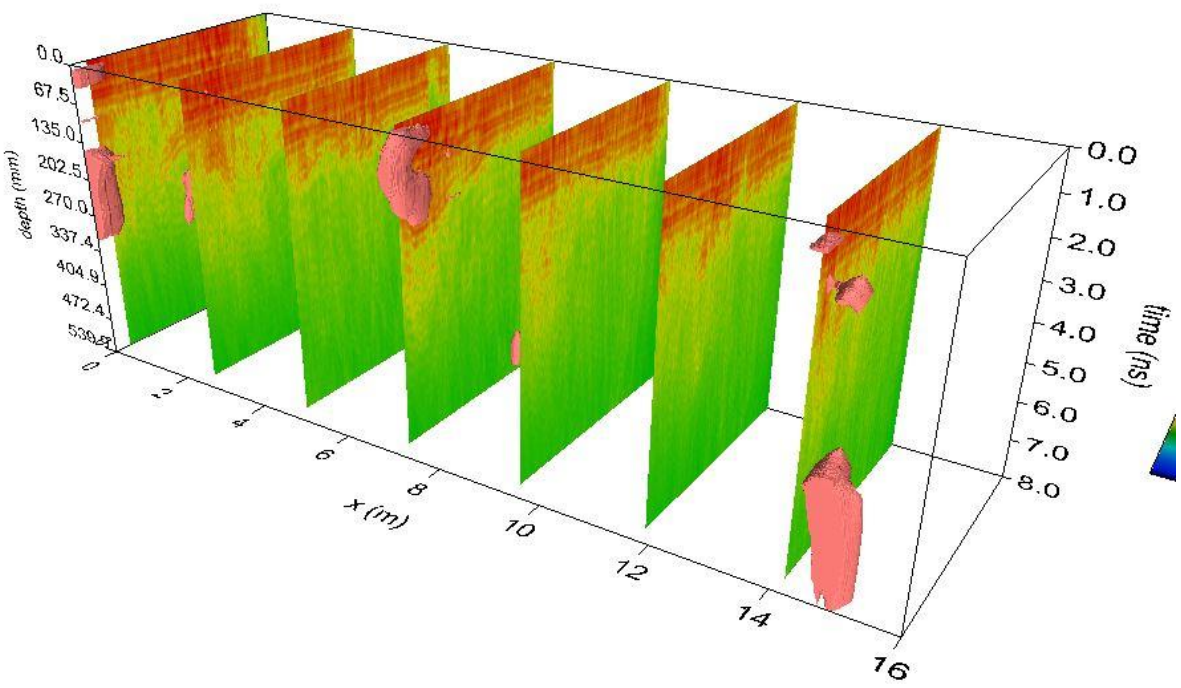

Figure 17c – GPR radargrams and voiding model – Abutment 4, Site A, View 2

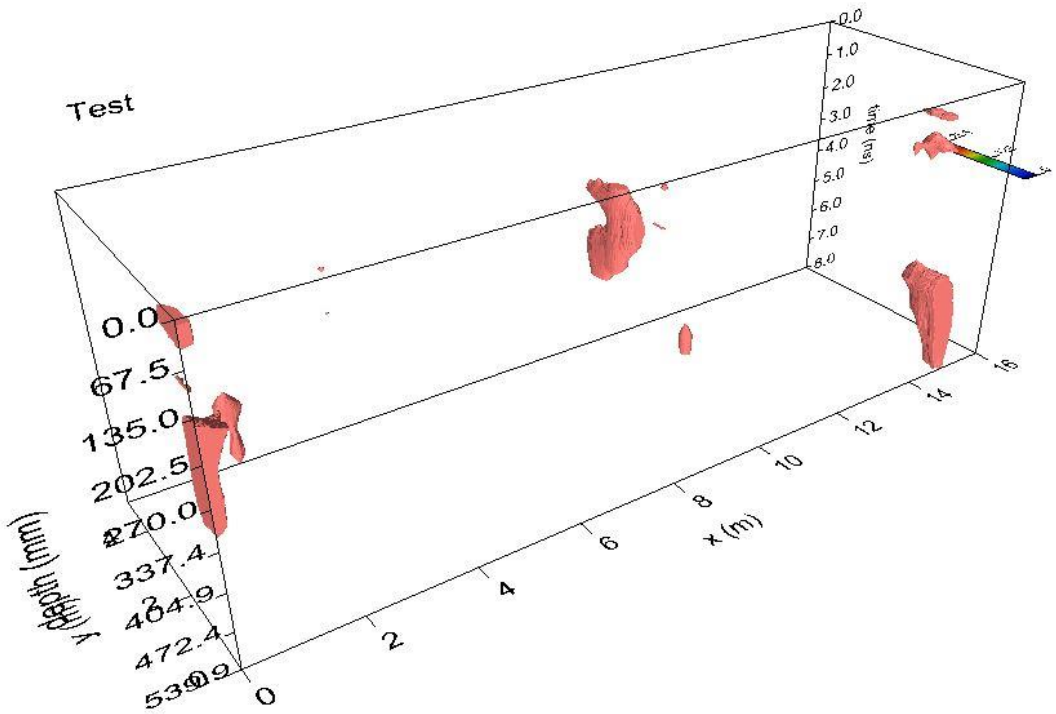

Figure 17d: Voiding model – Abutment 4, Site A

Table 1: displays the drill-hole results of suspected areas of voiding. As can be seen from the images, voiding is evident from the GPR models and confirmed by drill-holes for each of the GPR models produced.

Table 1: Comparison of voiding present between the GPR models and physical drill-holes – Site A

Abutment	Drill-hole	Voiding based on GPR (Y/N)	Voiding based on drill-hole (Y/N)
1	1	N	N
1	2	Y	Y
2	1	Y	Y
2	2	N	N
3	1	N	N
3	2	Y	Y
4	1	N	N
4	2	Y	Y

5.3 SITE B

Site B consists of a road bridge overpassing a railway. A GPR survey of the two abutments was carried out by scanning each abutment and part of the adjacent retaining structures. Figure 18 displays a description of the site and how it is configured. The abutment-retaining superstructure is a vertical concrete retaining wall, which extends to either side of the bridge approach as a soil retaining wall.

Appropriate filters were applied to the GPR data as described in Section 4.2 using the criteria specified in Section 5.1 to help identify voiding within each abutment. A subsurface model was produced to identify likely areas of voiding which could be further assessed with direct intrusive investigations.

As per Section 5.2, small diameter holes with a hand drill were drilled through the concrete and a dowel probe was inserted to detect the presence/absence of voiding in areas identified via the GPR processing. Unfortunately, compared to Site A, fewer drill holes were able to be carried out safely as the integrity of the existing structure and the presence of electrical utilities within the abutment retaining structure needed to be maintained. Figures 19a/19b/19c/19d to Figures 20a/20b/20c/20d show the interpreted sub-surface models based on GPR data and correlation with physical measurements. The XY plane in the figures represents the abutment wall plane.

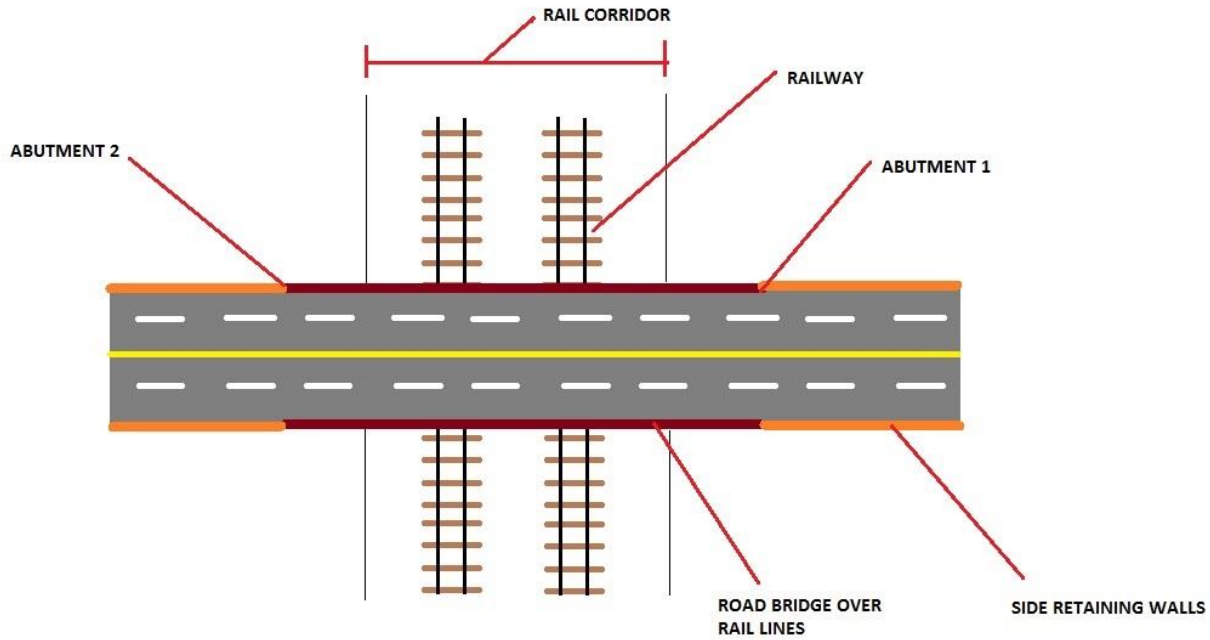

Figure 18: Site description of Site B

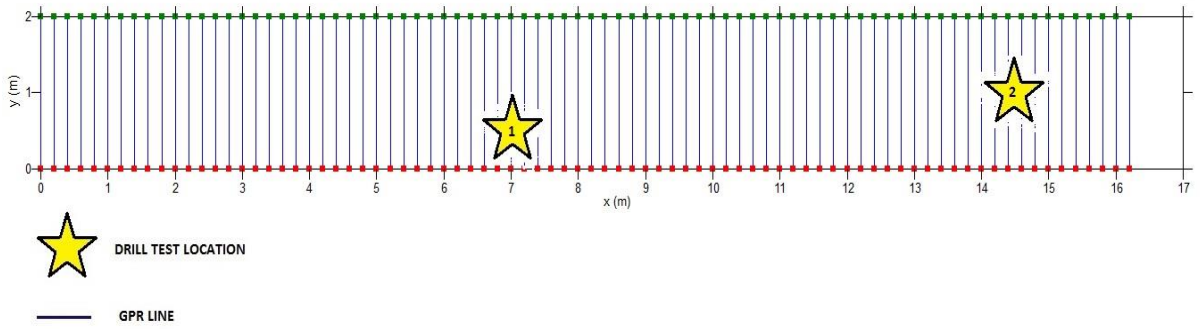

Figure 19a: GPR Scan lines and drill test points – Abutment 1, Site B

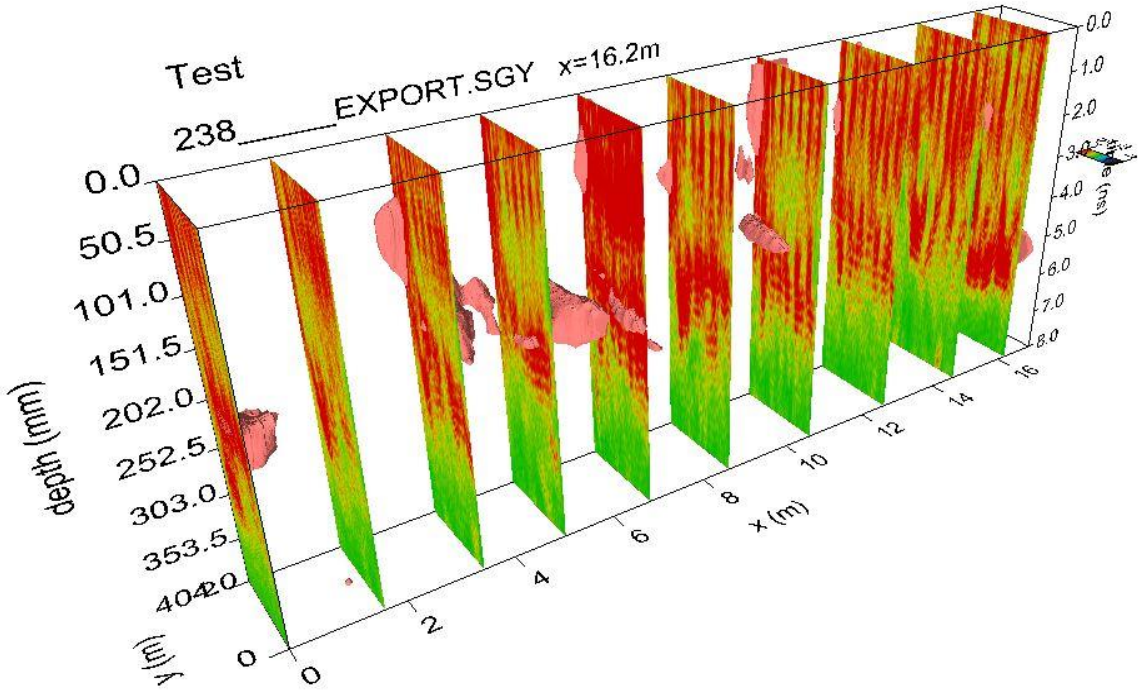

Figure 19b: GPR radargrams and voiding model – Abutment 1, Site B, View 1

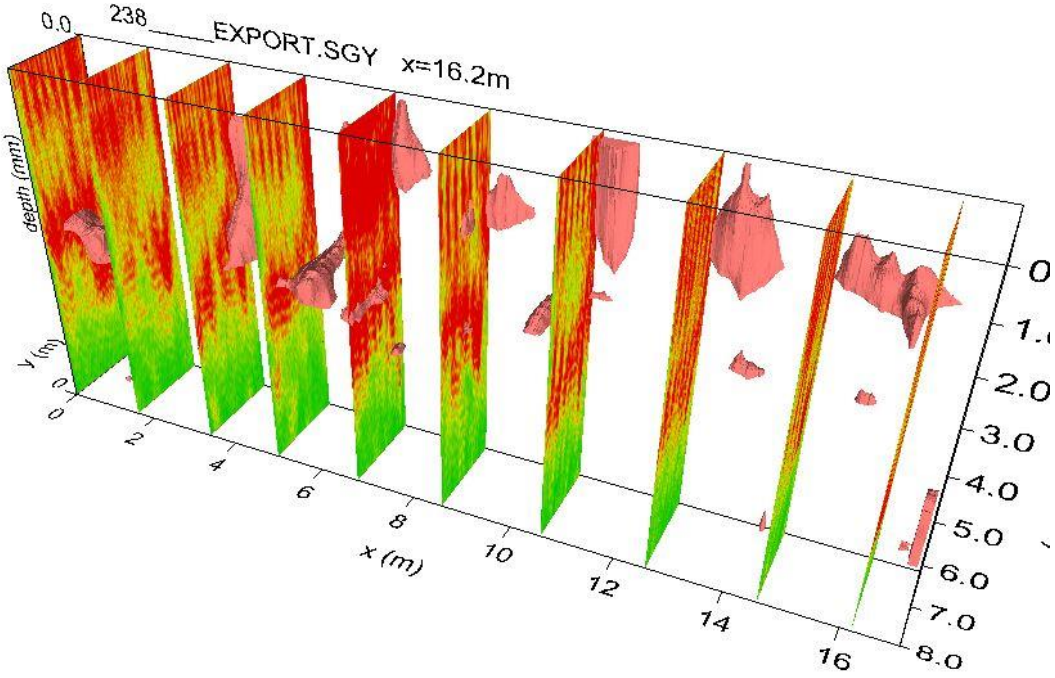

Figure 19c: GPR radargrams and voiding model – Abutment 1, Site B, View 2

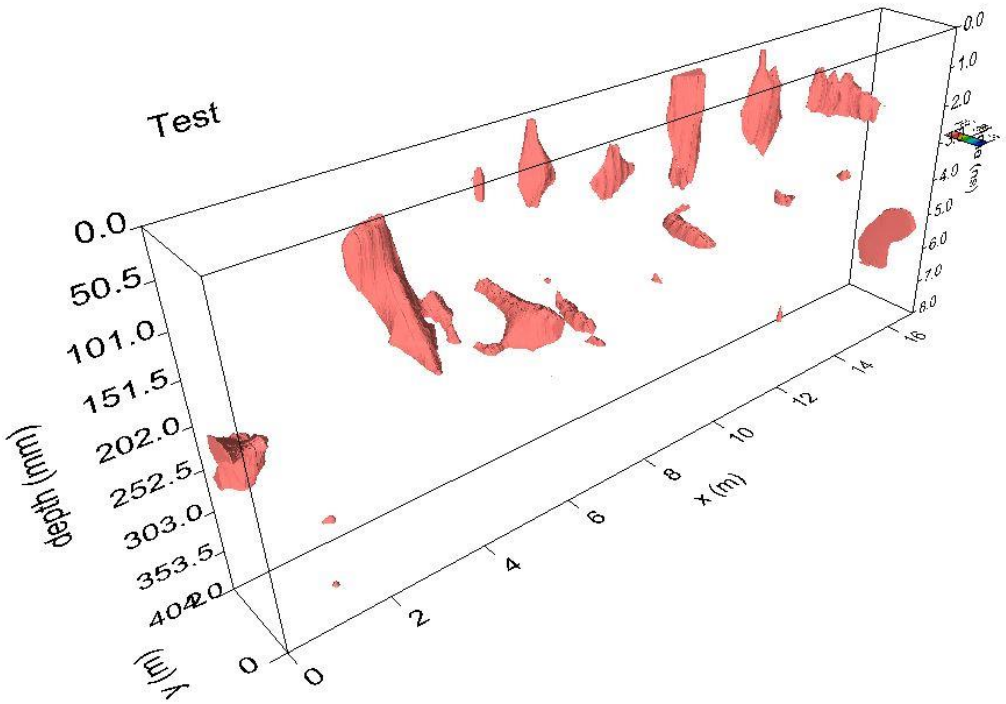

Figure 19d: Voiding model – Abutment 1, Site B

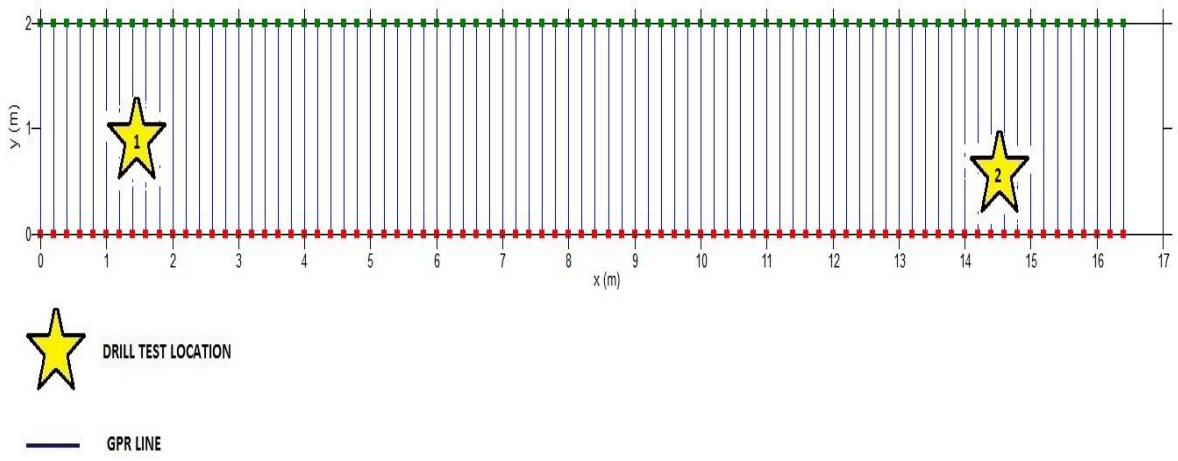

Figure 20a: GPR Scan lines and drill test points – Abutment 2, Site B

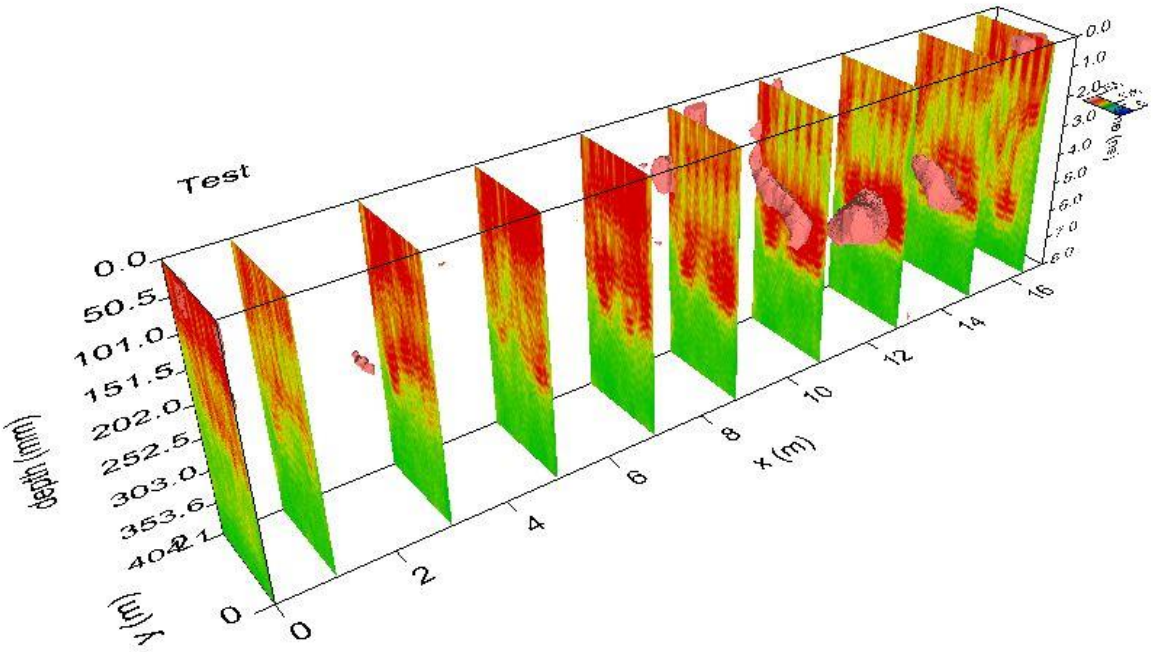

Figure 20b: GPR radargrams and voiding model – Abutment 2, Site B, View 1

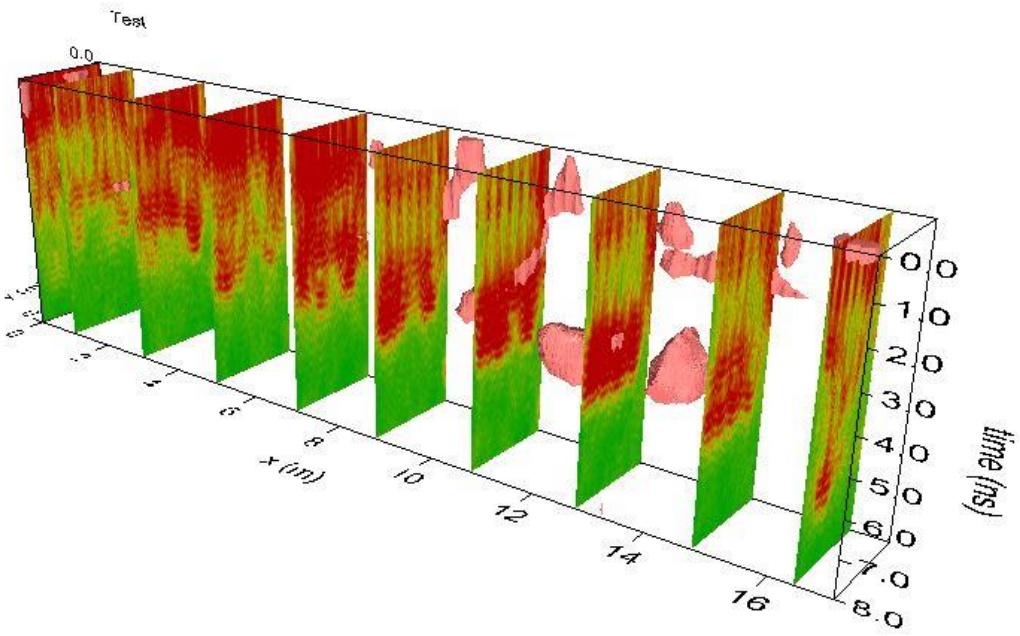

Figure 20c: GPR radargrams and voiding model – Abutment 2, Site B, View 2

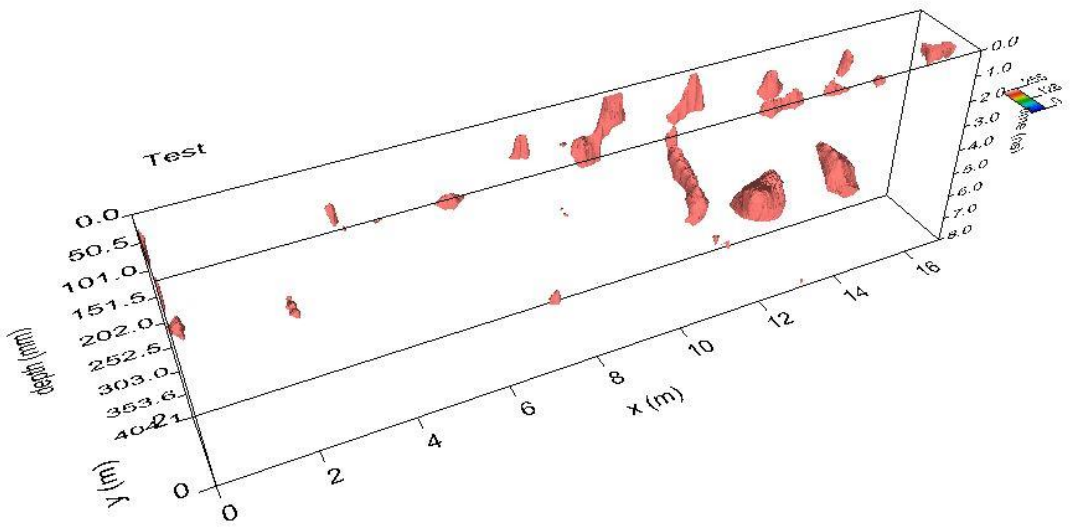

Figure 20d: Voiding model – Abutment 2, Site B

Table 2 displays the drill-hole results of suspected areas of voiding. The results are not as conclusive as Site A although the sample size is less than that of site A due to constraints in drilling.

Table 2 – Comparison of voiding present of GPR models and physical drill-holes – Site B

Abutment	Drill-hole	Voiding based on GPR (Y/N)	Voiding based on drill-hole (Y/N)
1	1	Y	Y
1	2	N	N
2	1	N	N
2	2	Y	N

6 DISCUSSIONS OF RESULTS

The ultra-wide band GPR method is shown to be able to detect the presence of voiding in bridge abutment and retaining structures and be confirmed via intrusive investigations.

In comparing Site A and Site B, Site A spill through appears not to have steel reinforcement as opposed to the concrete structure for the abutment in Site B. As steel reinforcement has a high amplitude reflection the comparison between voiding and steel reinforcement relies more heavily on polarity and echoing of the signal (see Section 5.1 criteria).

Sub-surface models produced from GPR data requires a specific skillset such as experienced interpretation, knowledge of the propagation of radar waves, knowledge of signal processing, and the physics of GPR. This broad interpretation and data processing stage can lead to mis-interpretations. Even when using filters, the wrong application of these filters could obscure relevant data required for accurate interpretation. The filters chosen to accent the criteria specified in Section 5.1 were selected based primarily on trial and error and past experience relating to detecting voiding on radargrams but unfortunately there is not a single set of filters to use for all given situations. The correct usage of filters will also depend on a specific data set with consideration to noise from varying factors at each location. In the case of the result in this paper, the Hilbert filter was particularly useful as it helped identify the dominant reflections while highlighting a polarity change.

The relative speed of GPR data collection makes it a cost effective and efficient way of collecting data with minimal impact to the community and traffic. Ultra-wide band GPR also provides more data for analysis over a larger area when compared to conventional drill hole and borescope inspections (which can only find information at a single point).

Ultimately a trade-off exists between covering a larger area efficiently and cost effectively with interpreted data against obtaining various discrete points of data using more accurate physical methods (drilling and borescope inspection).

In comparison with other GPR methods, ultra-wide band GPR has the advantage of providing high resolution over its depth range. However, other GPR methods with single or narrow band antenna provide high resolution of a target depth. In the case of void detection as the target depth is unknown, ultra-wide band GPR has this distinct advantage over traditional methods.

7 CONCLUSIONS

RMS continues to try and improve efficiency of bridge and retaining structure maintenance by investigating new technologies as part of its commitment to innovate. Ultra-wide band GPR could provide a cost effective method for the investigation of retaining structures to help supplement RMS' existing maintenance and inspection program. In its present form, ultra-wide band GPR should not replace existing investigation and inspection methods but rather supplement them. As the technology is also relatively new, higher accuracy (and deeper operating depth) GPR units utilising ultra-wide band technology may be developed. Given the benefits and the application displayed in this paper ultra-wide band GPR should be considered as a possible tool to increase the efficiency and effectiveness of RMS' maintenance and investigation programs.

8 ACKNOWLEDGEMENTS

The author would like to thank Matthew Dryburgh and Michael Hughes of RMS Geotechnical Science Unit for their assistance in data collection. The author would also like to thank Tak Ming Leung for technical review and Roads and Maritime Services for support in this paper.

9 DISCLAIMER

The views, opinions, considerations and conclusions expressed in this paper are strictly those of the author and do not necessarily reflect the views of Roads and Maritime Services.

10 REFERENCES

Conyers, L. & Goodman, D., (1997). *Ground-penetrating radar: an introduction for srchaeologists.* Walnut Creek(California): AltaMira Press.

Davis, J. & Annan, A., 1989. Ground Penetrating radar for high resolution mapping of soil and rock stratigraphy. *Geophysical Prospecting,* Volume 37, pp. 531-551.

Goodman, D. (2018), Version 3.0, June 11 2018. *GPRSIM: Ground penetrating Radar Simulation Software.* Woodland Hills, California: s.n.

Goodman, D., (2018) Version 7.0, June 12, 2018. *GPR-SLICE: Ground Penetrating Radar Imaging Software.* Woodland Hills, California: s.n.

Jol, H. M., (2009). Ground Penetratin Radar: Theory and Applications. In: *Elsevier.* s.l.:s.n.

Kruk, J.V.D., (2004). Three-dimensional GPR imaging in the horizontal wavenumber domain for different heights of source and receiver antenna. *Near Surface Geophysics,* Volume 2, pp. 23-29.

Mellet, J., (1995). Ground penetrating radar applications in engineering environmental management and geology. *Journal of Applied Geophysics,* Volume 33, pp. 69-77.

Sermal, A. I. A. & Setan, H., (2009). Ground Penetrating radar (GPR) for subsurface mapping: preliminary result. *Geoinformation Science Journal,* 9(2), pp. 45-62.

AN ADVANCED WEB-BASED MANAGEMENT SYSTEM FOR INSTRUMENTATION AND MONITORING DATA

Darren Huang[1], Idy Li[2] and Jeff Hsi[3]

[1] *Associate Principal – Instrumentation and Monitoring, EIC Activities, Level 6, HQ South Tower, 520 Wickham Street, Fortitude Valley, QLD 4006, Australia*

[2] *Associate Principal – Geotechnical, EIC Activities, Level 19, 177 Pacific Highway, North Sydney NSW 2060, Australia*

[3] *Technical Principal – Geotechnical, EIC Activities, Level 19, 177 Pacific Highway, North Sydney NSW 2060, Australia*

ABSTRACT

EIC GeoView is an advanced web-based management system for instrumentation and monitoring data that has been developed by EIC Activities, a member of CIMIC Group, for sole use on the Group's construction projects providing valuable competitive advantage. The System automates the processing of raw data and delivers graphical outputs of the information via an online portal. This system has the capacity to collate information from innumerable sources, then process and store the information via a cloud server. This paper presents how EIC GeoView has been used on three major projects in Australia to collate and process monitoring data to assess the performance and management of built structures. On the Torrens Road to River Torrens Project in South Australia, EIC GeoView was used to manage large quantities of movement data collected along a 3km long soil nail wall designed using unsaturated soil mechanics principles. Use of EIC GeoView allowed large volumes of data to be accurately delegated and processed with ease and minimal human effort. On Sydney Metro Northwest TSC, EIC GeoView was used to collate and process real-time rail track movements and ground surface deformation of existing structures relative to the progress of the underground tunnel, presenting the construction team with the ability to assess the impact of tunnel construction with up-to-the-minute accuracy. On the Frederickton to Eungai Pacific Highway Upgrade project, a considerable portion of the alignment involved construction upon soft soils. The grouping functionality in EIC GeoView was used to cluster different instrument readings on a single output, allowing engineers to observe and compare between linked phenomena, such as piezometer records, fill height, horizontal profile gauges and ground settlements from plate readings, all at the same time.

1 INTRODUCTION

Geotechnical engineers deal with non-uniform materials – earth and rock which have properties that can vary unexpectedly and behave in often unpredictable ways. To manage this risk, geotechnical engineers deploy instruments that are capable of providing quantitative measurements of the ground and associated built structures. Monitoring records from these instruments are interpreted by engineers to provide insight into the performance of as-built conditions. Thus, the application of instrumentation and monitoring (I&M) in geotechnical engineering plays a vital role in the management of built assets during construction and the operational phases. According to Transport for NSW (2016), instrumentation and monitoring in the rail environment is used as "a tool for asset integrity assurance, operational risk management of potential geotechnical hazards and construction control".

On large scale projects, vast numbers of instruments are often deployed, resulting in significant volumes of monitoring data. Project teams are faced with the challenge of effectively and efficiently, collecting, processing, presenting, distributing and storing the monitoring data, without mobilising a small army of engineers and surveyors. EIC GeoView is an in-house I&M database manipulation platform developed by EIC Activities, a member of CIMIC Group, to overcome this challenge.

2 EIC GEOVIEW DATABASE MANAGEMENT SYSTEM

2.1 OVERVIEW

EIC GeoView is a centralised database management system (DMS) which automates the processing of raw data and delivers outputs of the information in graphical formats. This web-based system has the capacity to collate information from numerous sources, then process and store the information via an online server.

The basic architecture of EIC GeoView follows a simple three-stage process, as shown in Figure 1. EIC GeoView has several built-in readers that allows data entries to be made from monitoring instruments such as standard data templates, data loggers, real-time instruments and automated total stations, etc. Inside the EIC GeoView core, there are several processors developed to process data in the background, and eventually present the data in the form of visual outputs such as reports, graphs, location maps, or deliver electronic notifications such as SMS or email.

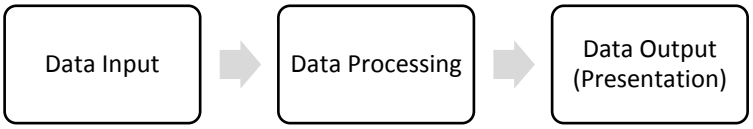

Figure 1: EIC GeoView System Architecture

EIC GeoView's capability extends beyond the management of I&M data with the ability to manage information arising from any asset where data acquisition, processing and reporting is required, such as site inspections, geotechnical data, and geological mapping records, etc. Thus, EIC GeoView can be used as a project management tool by virtue of its ability to provide users with real-time project status reports for large volumes of assets, all within a centralised platform. EIC GeoView also allows users to set predetermined targets and limits whereupon alert notifications can be sent to users, presenting itself as a useful tool for risk management.

Examples of applications where EIC GeoView has been used to manage other forms of construction data are shown below in **Figure 2**.

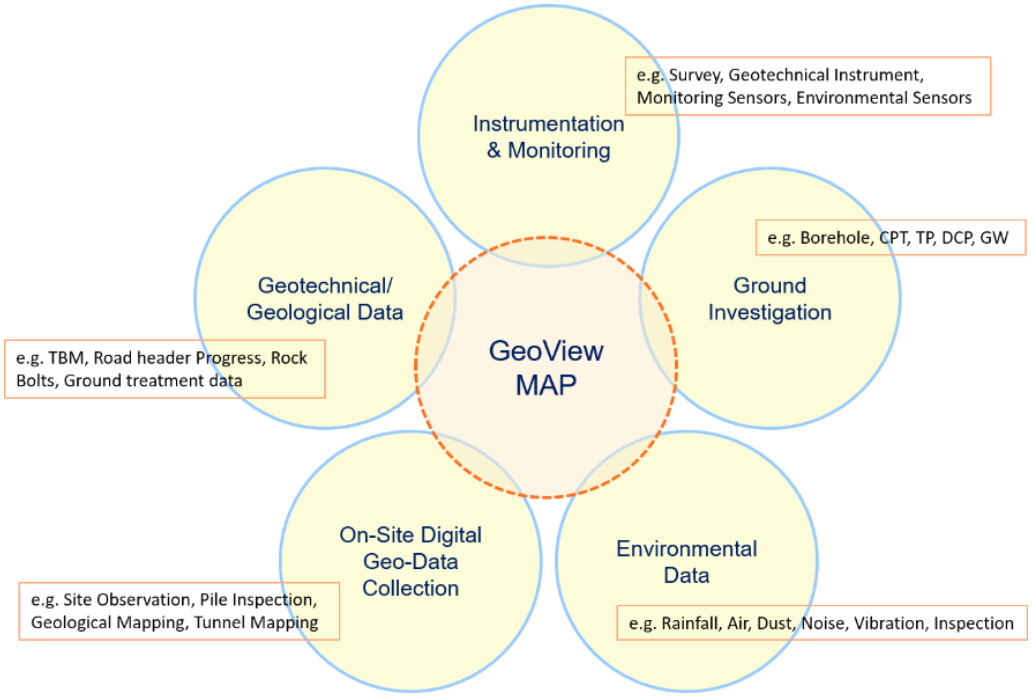

Figure 2: Applications of EIC GeoView as a management tool for other construction data

EIC GeoView has been used extensively on large scale infrastructure construction projects, including, railways, highways, tunnels and buildings. Projects of note include:

- Moreton Bay Rail Link, QLD (A$650m as at August 2013)
- Sydney Metro Northwest, NSW (A$1.15bn as at June 2017)
- WestConnex New M5, NSW (A$4.3bn as at November 2015),
- Torrens Road to River Torrens project, SA (A$896m as at July 2015),
- CityLink Tulla Widening, VIC (A$1.3bn as at February 2015),

- Transmission Gully, NZ (NZ$1.0bn as at July 2014),
- East Kowloon Cultural Centre, HK (HK$436m as at May 2017)

2.2 KEY FEATURES

In addition to providing automated data processing, monitoring and tracking of construction status, the key features of EIC GeoView are listed below in Table 1.

Table 1: Key features of EIC GeoView

Features	Characteristics
Customisable and scalable to meet project specific requirements	Offer users the flexibility to adapt to new instrument technologies. EIC GeoView can reformat input data from any survey or monitoring source into a standard that is consistent with EIC GeoView's database format
Automated alarm notification	Upon reaching pre-determined trigger limits for instruments, EIC GeoView will automatically generate SMS and/or email notifications to nominated recipients. The trigger limits are setup as Alert (Green), Alarm (Amber) and Action (Red). Once the trigger limits are applied to the monitoring points, the limits will be illustrated on graphs, colour coded data tables and reports. An example is provided in Figure 3. In the event anomalous data is entered into EIC GeoView, e.g. due to human error, or erroneous instrumentation data, EIC GeoView will alert users of such entries.
Web-based system	EIC GeoView is accessible from anywhere via the internet and web browsers. No additional software is required to be installed by users on local computers.
Availability and stability	EIC GeoView uses Cloud Services allowing for 24/7 operation and processing as well as to achieve 99.9% uptime. The centralised data storage uses the Microsoft SQL Server which has an unlimited capacity and regular data backup facilities
Integration with digital forms	Digital documents and forms which contain project data can be integrated to automatically upload onto EIC GeoView, allowing acquired information to be relayed to all members of the project team almost instantaneously. Examples include, collation of site inspection records, geological mapping, environmental quantity records etc.
GIS services integration	EIC GeoView can be integrated with interactive GIS maps with the most recent imagery, allowing users to visualise the location and records of the monitored instruments.
Account authentication system	EIC GeoView offers different levels of access and data manipulation to different users, enhancing protection of project data. For example, project administrators have the right to manage their own user access without any constraints. Restricted access may be provided to project clients to view the data and presented outcomes without affecting the underlying data operation.
Data presentation and reporting	There are four standard outputs provided in EIC GeoView: graphs, status map views, data tables and reports. The Grouping feature in EIC GeoView allows users to combine, arrange and produce combined charts and reports from multiple instruments and monitoring points. This feature provides an efficient means of viewing the trends of multiple data points for comparison. All reports and outputs can be setup to be automatically generated at specified frequencies, e.g. daily, weekly and monthly.

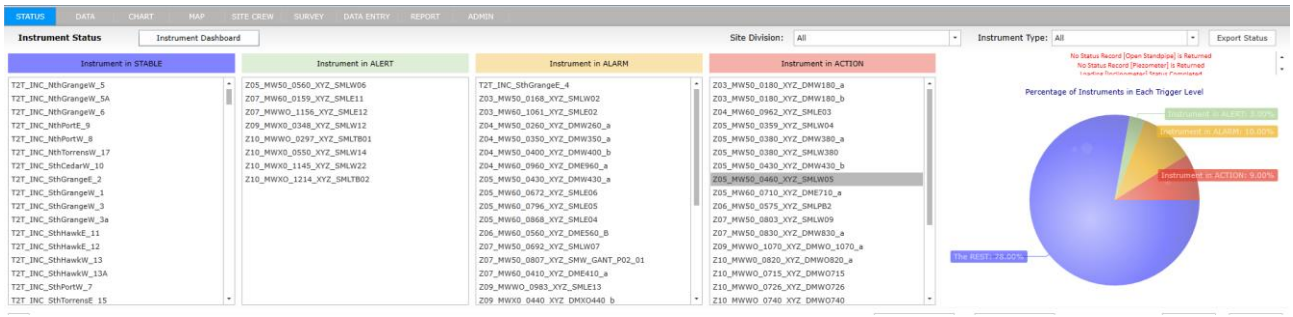

Figure 3: Snapshot of monitoring point status relative to trigger levels, Alert, Alarm and Action

3 I&M CASE STUDIES

The case studies below focus on examples of EIC GeoView used as a database management tool for instrumentation and monitoring only. However, EIC GeoView has also been used extensively in other projects such as Lam Tin Tunnel (Hong Kong), and Transmission Gully (NZ), where it was used as a construction and environmental data management tool.

3.1 TORRENS ROAD TO RIVER TORRENS PROJECT, SOUTH AUSTRALIA

Torrens Road to River Torrens project (T2T) is a road project currently being delivered by alliance partners CPB Contractors, York Civil, Aurecon Australia, and Department of Planning, Transport and Infrastructure in South Australia. One of the key features of the project is a depressed roadway 3km in length with a retained soil height of up to 8.9m. The retention support is partly provided by soil nails designed using unsaturated soil mechanics theories. The designed nail lengths are approximately 4m, which is significantly shorter than soil nails designed using conventional soil mechanics. The design was made particularly challenging due to the proximity of the excavation to an adjacent Arterial Road, South Road, located immediately upslope of the wall. This necessitated a project criterion of less than 30mm maximum lateral and vertical deformation at the excavation face.

More than 250 survey markers and 20 inclinometers were installed along the soil nail wall to monitor wall movement. Surveying of the monitoring points was captured using total stations and lowering of inclinometer probes. The data was then manually entered into spreadsheets and delivered as individual files to the design team on a daily or weekly basis. A typical cross section of the marker and inclinometer placement is provided in **Figure 4**.

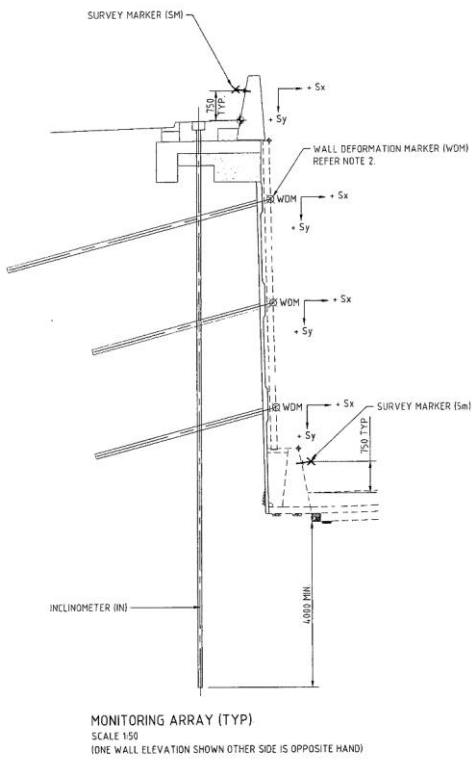

Figure 4: Typical cross section of survey markers and inclinometer placement on T2T

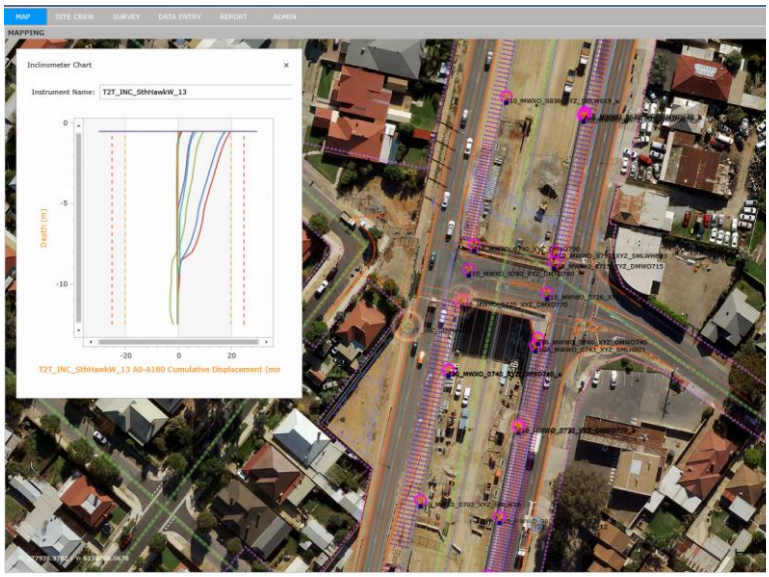

Figure 5: Example of aerial imagery overlain on top of instrumentation plan from T2T

In recognising the logistical challenges with handling and processing large volumes of survey data from multiple survey sources EIC GeoView was deployed, whereupon all survey data was uploaded into a consolidated online database. The automated formatting feature enabled survey data from different surveying companies (often adopting different data formats) to upload their data into EIC GeoView's unified database. The processor core allowed the uploaded data to be collated, processed and graphed almost instantaneously. Aerial imagery was overlaid onto the instrumentation plan allowing users to easily identify the location of the survey markers and view up-to-date survey results by selecting the marker point, such as that shown in **Figure 5**.

Use of EIC GeoView on T2T eliminated many hours of manual data processing and collation, thereby diminishing the risk of human error in what is, normally, a manipulation-heavy process. The automated notification system and status point summary portal allowed the movements of all monitoring points to be viewed at a glance, allowing the engineering team to focus their efforts in the required structures or areas.

3.2 SYDNEY METRO NORTHWEST TSC, NEW SOUTH WALES

Sydney Metro Northwest – Tunnels and Station Civil (TSC) formed part of the A$8.3bn (as at June 2017) Sydney Metro Northwest project located in the north-western suburbs of Sydney (formerly known as North West Rail Link, NWRL). TSC was delivered by the CPB Contractors, John Holland, and Dragados consortium and the works were completed in 2016. The key features of this project comprised 15km of twin TBM driven rail tunnels between Bella Vista and Epping, and civil works for five new stations and two services facilities.

Due to the scale of the project, up to 4700 instruments were deployed to monitor the numerous structural and geotechnical elements along the alignment. Use of EIC GeoView allowed significant volumes of instrumentation data to be stored in a single online database. Moreover, the centralised system allowed survey data from numerous surveying and monitoring parties (up to five parties), including manual and automated real-time data sources, to upload their data into a unified format.

The key feature of the project was the 15km twin 7m diameter tunnel constructed using four tunnel boring machines (TBM) which were mobilised simultaneously. The tunnel was up to 30m beneath heavily built up areas of suburban Sydney. Most of the tunnel alignment traversed through Sydney Sandstone and Siltstone, and beneath densely populated infrastructure such as Castle Towers Shopping Centre and Norwest Business Park, and came within close proximity of the existing rail crossing at Epping station where it had only 5m of rock cover.

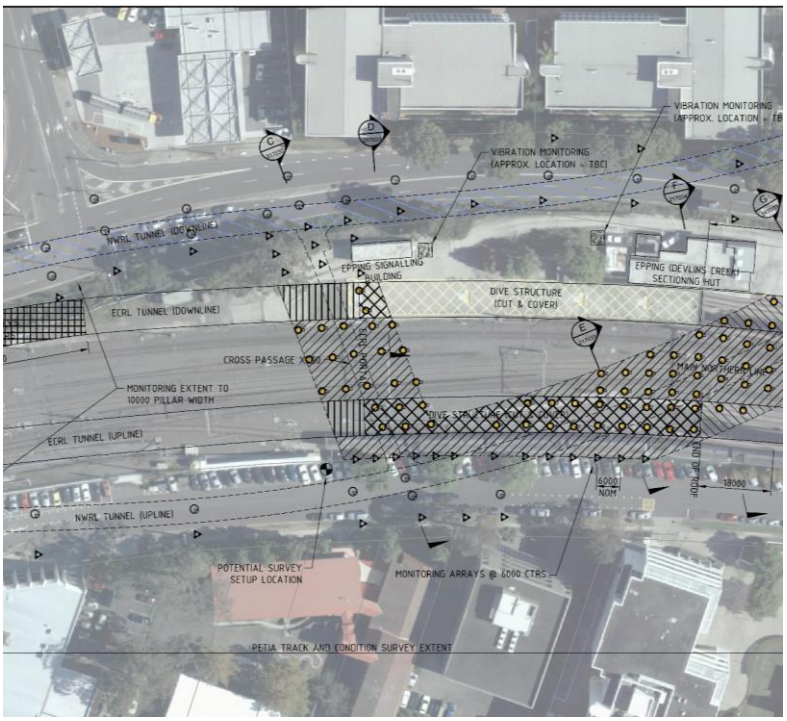

Figure 6: Survey markers and targets proposed close to Epping train station where the tunnel alignment of Sydney Metro Northwest TSC (NWRL) crosses beneath the existing train tracks of the Northern Line and Epping to Chatswood Rail Link (ECRL)

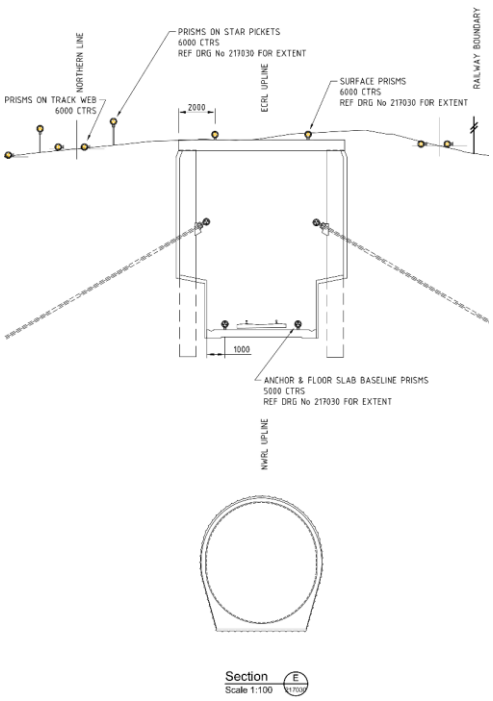

Figure 7: Cross section through Section E of Figure 6, illustrating relative elevations of the Sydney Metro Northwest TSC tunnel (NWRL) and the existing train tracks of the Northern Line and Epping to Chatswood Rail Link (ECRL)

The benefits of EIC GeoView were particularly apparent in the monitoring and assessment of tunnel induced deformation. As the tunnel alignment was constructed beneath well-established suburban areas, the impact of the tunnel construction on existing structures had to be captured with accuracy and efficiency. Instruments such as survey markers/targets, crack

pins and tilt beams were installed upon various structures located at the ground surface within the predicted zone of influence of the tunnel. An example of the monitoring plan for surface structures is provided in **Figure 6** and **Figure 7**, where TSC (NWRL) crosses beneath two existing rail lines at Epping, NSW (Northern Line, and Epping to Chatswood Rail Link, ECRL). Using EIC GeoView's customisable grouping function, the monitoring points at the ground surface could be viewed relative to the progress of the tunnel excavation. For example, **Figure 8** provides an illustration of the recorded settlement at the ground surface relative to the progress of the tunnel face passing beneath Edward Bennett Drive at Cherrybrook. This information allowed the engineers to assess whether the recorded settlements were related to the tunnel excavation, and whether the rate and magnitude of settlement were expected to trend along their predicted trajectory. As all records were time stamped it was simple for the engineers to determine the date/time at which certain monitoring values were registered. Moreover, the records provide the details of the user responsible for loading the input, fostering accountability and traceability of data. This degree of multi-point data assessment, efficiency and transparency could not have been done without the capabilities of an advanced instrumentation and monitoring data management system such as EIC GeoView.

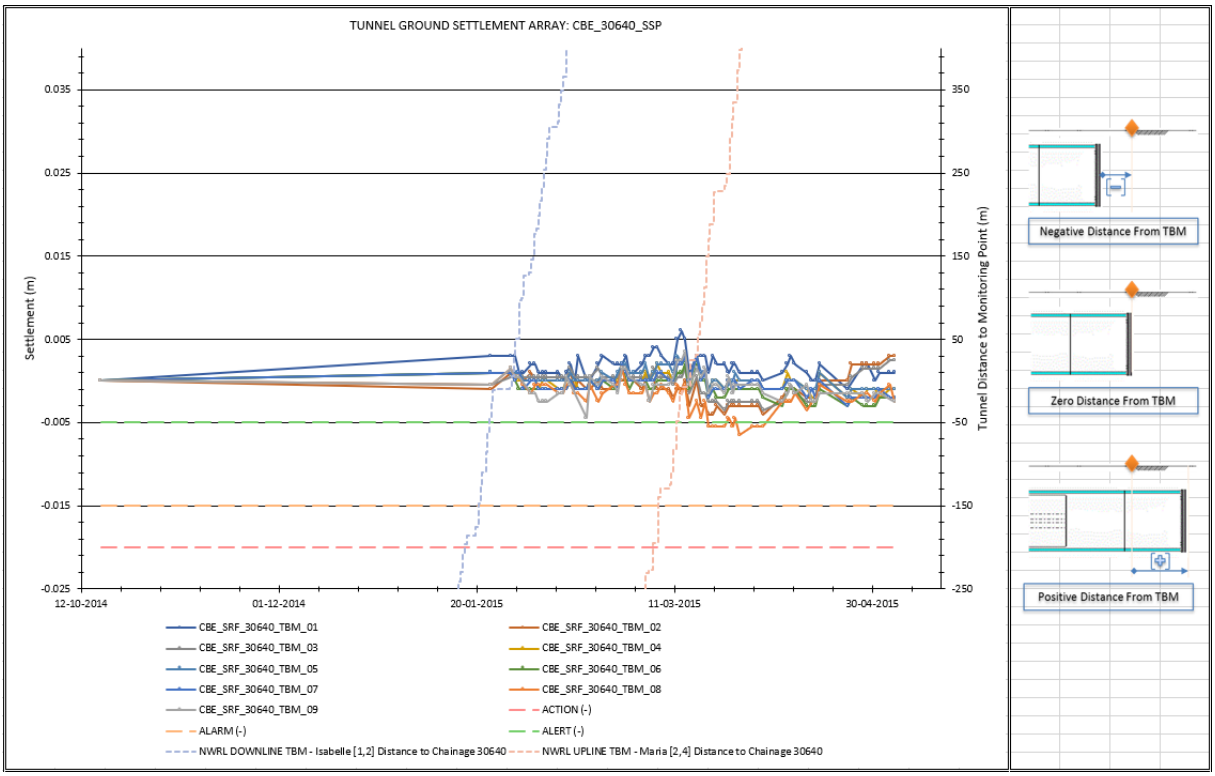

Figure 8: Illustration of recorded settlement at ground surface relative to the progress of the tunnel face at Edward Bennett Drive, Cherrybrook

Tunnel convergence was measured using optical prisms arranged around the internal perimeter of the tunnel excavation. The points were measured using automated total stations providing real-time records of the movement, allowing engineers to formulate an assessment of the tunnel stability. Once the tunnel face had progressed a certain distance from the convergence array and the magnitude and rate of deformation had dwindled the monitoring would then be ceased. An example of the monitoring records from a convergence array is provided in **Figure 9**.

On Sydney Metro Northwest ground investigation databases and associated functionalities were incorporated into EIC GeoView. This feature of the program allowed the plan locations of all the available ground data, such as boreholes, cone penetration tests and environmental test locations, etc., to be overlain onto aerial imagery and a plan of the alignment. A filtering function was incorporated to help the user search for the desired ground data. By selecting the ground investigation icon the investigation logs and related log files (such as laboratory test data) could be shown. **Figure 10** provides an example of the available ground investigation data overlain onto an aerial image at TSC. Further, with the inclusion of monitoring data in the same database, engineers could easily associate the available ground data with available monitoring information, e.g. correlating piezometer readings with the ground strata found in the borehole logs.

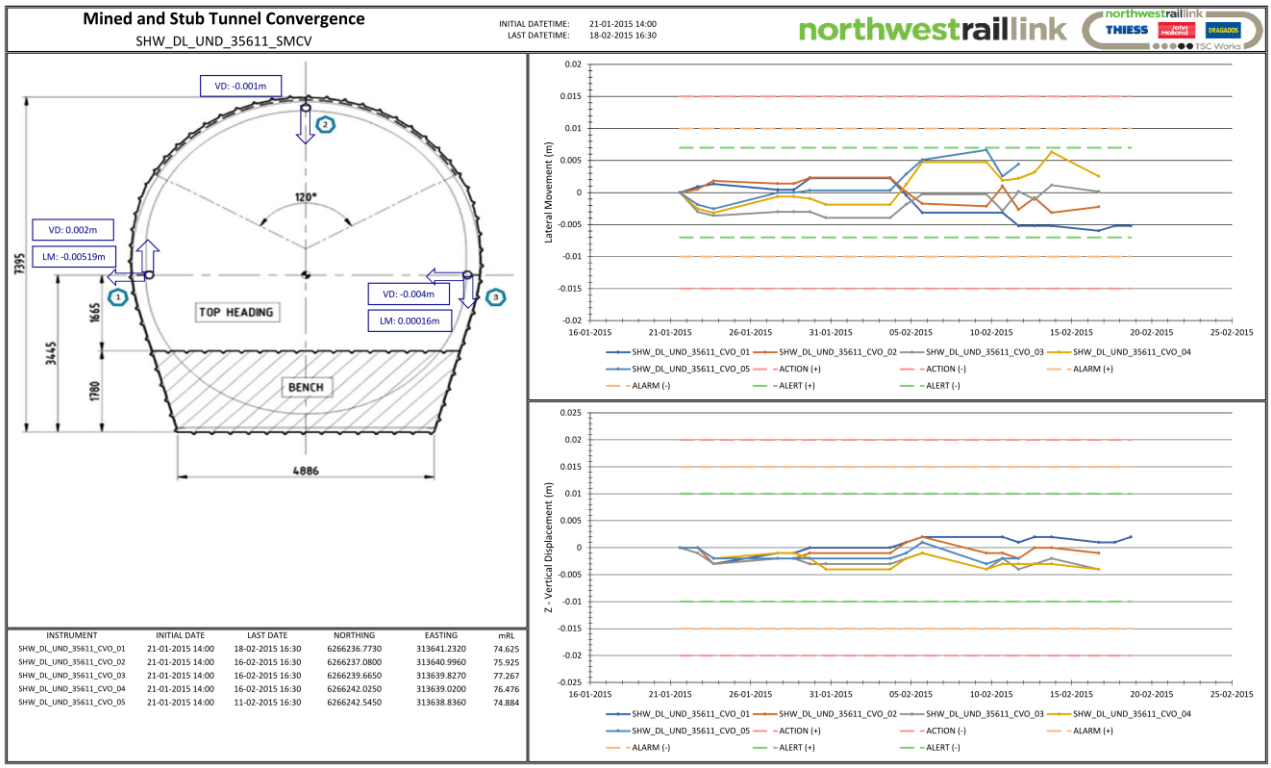

Figure 9: EIC GeoView portal illustrating outputs from tunnel convergence measurements adjacent to Showground station. VD: vertical displacement, LM: lateral movement

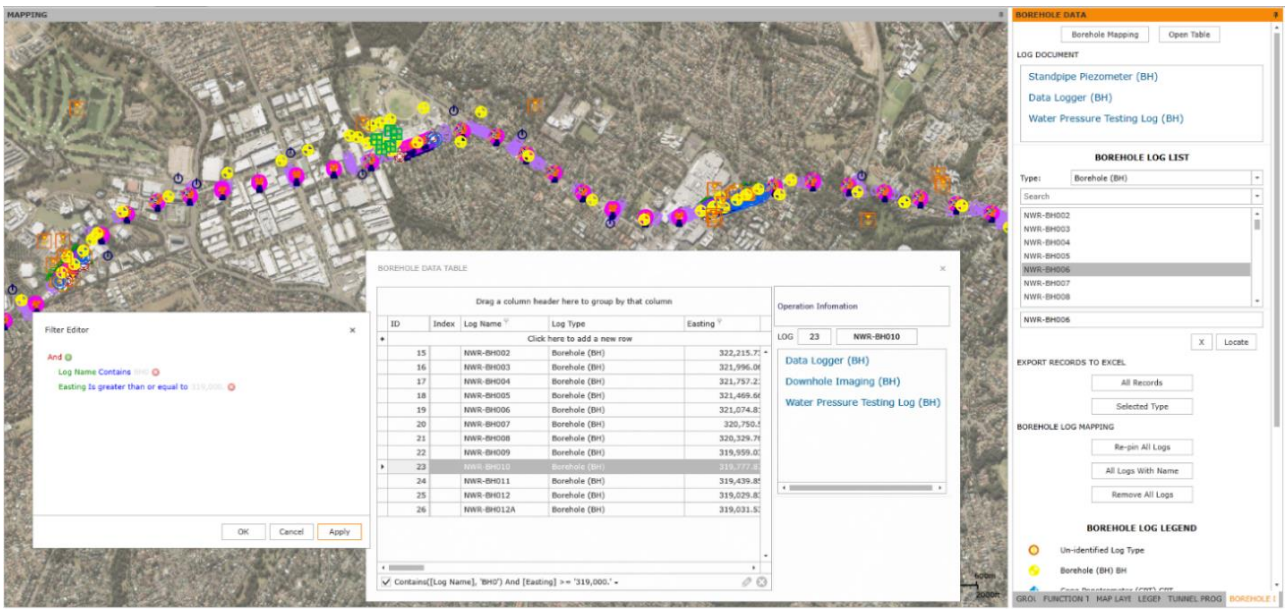

Figure 10: Illustration of ground investigation locations shown in the aerial map. Inset: Illustration of available logs associated with the user-selected investigation icon

Integrating the ground investigation data and instrumentation monitoring data into a single, easily accessible database brought unparalleled efficiencies to the engineers and the project as a whole.

3.3 FREDERICKTON TO EUNGAI PACIFIC HIGHWAY UPGRADE, NEW SOUTH WALES

Thiess Contractors were engaged by Roads and Maritime Services (Roads and Maritime) to deliver the Frederickton to Eungai Pacific Highway Upgrade (F2E) project which involved the upgrade of 26.5 kilometres of highway between

Frederickton interchange and Eungai Rail in New South Wales. Roads and Maritime were the principal for the design-and-construct contract worth A$762m (as at November 2012). The project was jointly funded by the Australian and NSW governments. One of the most geotechnically challenging aspects of the project was the treatment of soft soils covering up to 5km of the alignment. Road embankments up to 8m height were proposed upon these soft soils, placing the road pavement at risk of exceeding the residual settlement criteria of 100mm total settlement and 0.3% differential settlement, arising from long term compression of the underlying soft soils. In order to reduce post-construction settlement ground treatments using a combination of wick drains and surcharge were selected to accelerate consolidation of the soft soils prior to constructing the pavement. The additional weight of the surcharge on the embankment would hastened the consolation process, forcing the soils to consolidate more quickly than they otherwise would have under the embankment fill only.

The success of such ground treatments required the settlement of the soft soil layers to have achieved a certain degree of consolidation prior to removing the surcharge; whereupon the pavement would then be constructed on top of the embankment. Prediction of soft soil settlement is a particularly challenging and risky process, as numerous variabilities exist in soft soil geologies and treatment processes, many of which can significantly alter the consolidation rate and settlement magnitude.

To capture the settlement progress a series of instruments were installed as listed below. Typical cross sections illustrating the instruments and their placements in the embankments are provided in **Figure 11**.

- Horizontal profile gauges to measure settlement profiles at the base of the embankment;
- Settlement plates to measure settlement at the base of the embankment;
- Settlement markers to measure settlement;
- Vibrating wire piezometers to measure pore water pressure in the soft soils; and
- Inclinometers to measure lateral movements of the soils.

The "Observational Method" was adopted by the project engineers in the soft soil areas as an additional means of managing the risk posed by post-construction settlement magnitudes. This method relied on close monitoring of the instruments during construction, using the results of the monitoring to adjust the settlement predictions as construction progressed. The Observational Method affords early detection of an eventual settlement issue, allowing alterations to the ground treatment to suit the observed behaviour if deemed necessary.

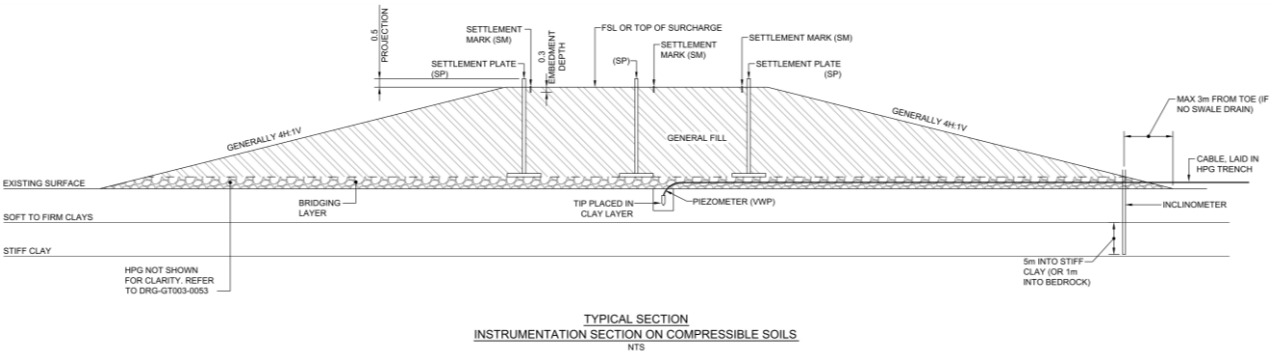

(a)

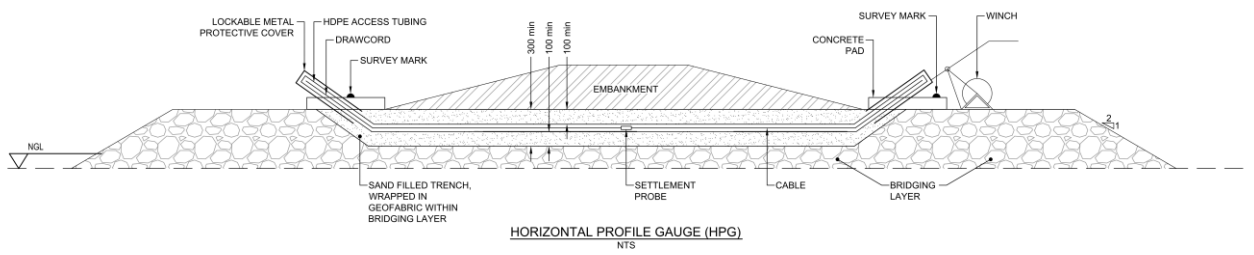

(b)

Figure 11: Typical cross section of instrumentation beneath embankments on soft soil, (a) settlement plates, vibrating wire piezometers and settlement markers and (b) horizontal profile gauge

This continual process of monitoring and refining the settlement prediction relied heavily on the monitoring records supplied by EIC GeoView. The Grouping function allowed numerous instruments to be viewed simultaneously to inform the engineers of the embankment performance, such as that shown in **Figure 12**. For example, determining the degree of consolidation in the soft soil could be assessed by observing behaviour in the settlement plate curves, then verified by the vibrating wire piezometer records.

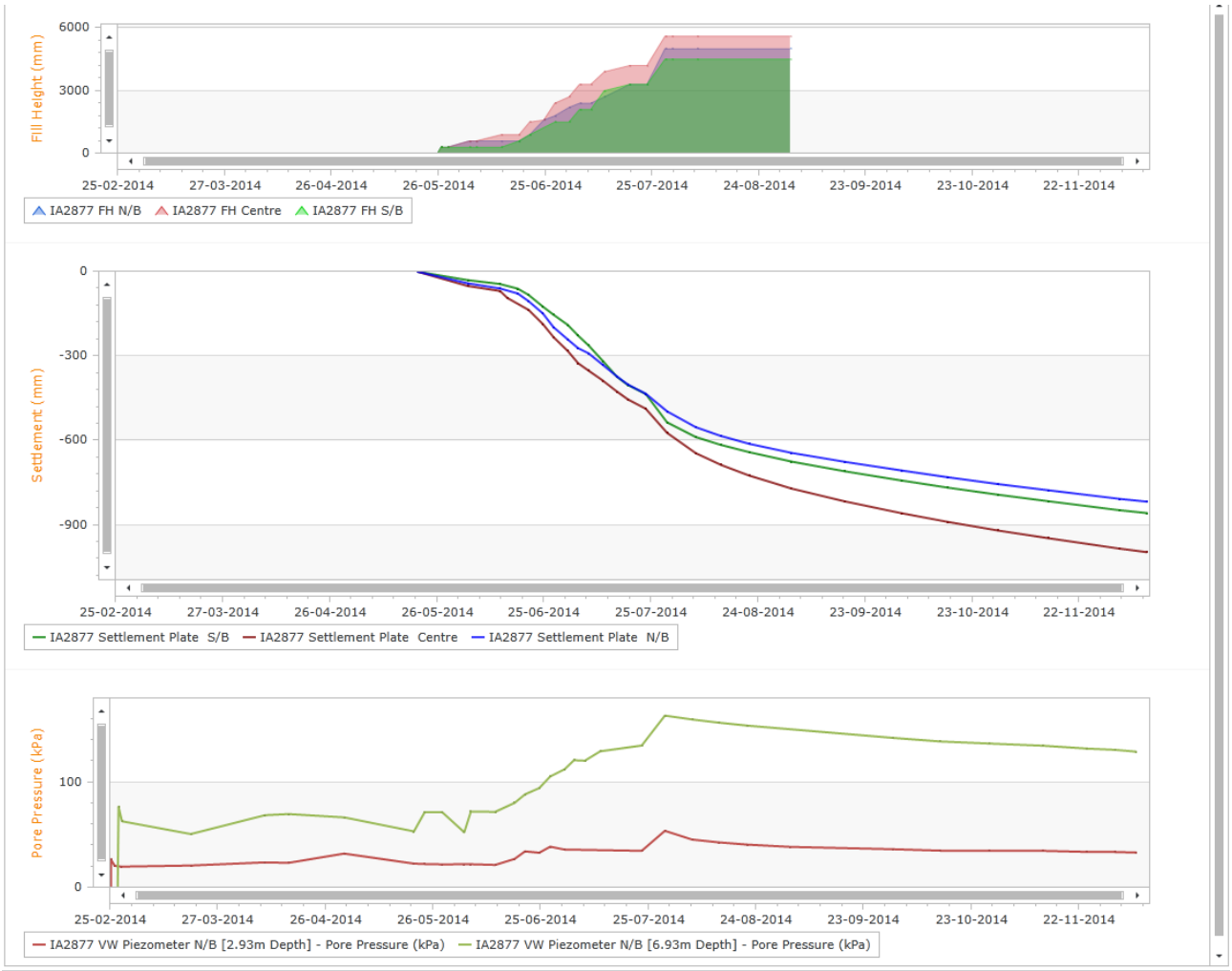

Figure 12: Viewing portal in EIC GeoView illustrating how multiple data sets from numerous sources can be viewed simultaneously to facilitate engineers with settlement predictions using the Observational Approach to soft soil treatment

Further, the automated processing core in EIC GeoView provided instantaneous calculations of differential settlement between the monitoring points each time the settlement data was updated. This resulted in significant time savings by the engineer to undertake manual assessments which would be prone to human-error. Graphs of total and differential settlement are provided in **Figure 13**.

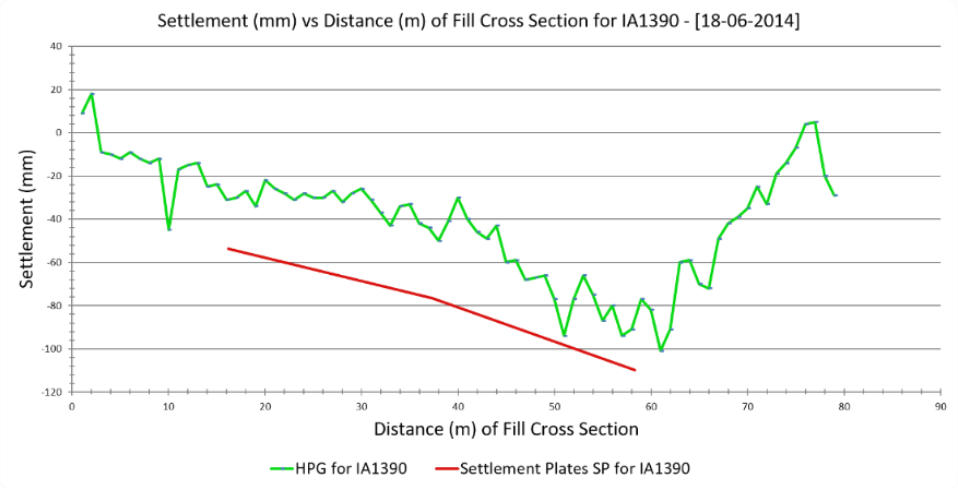

(a)

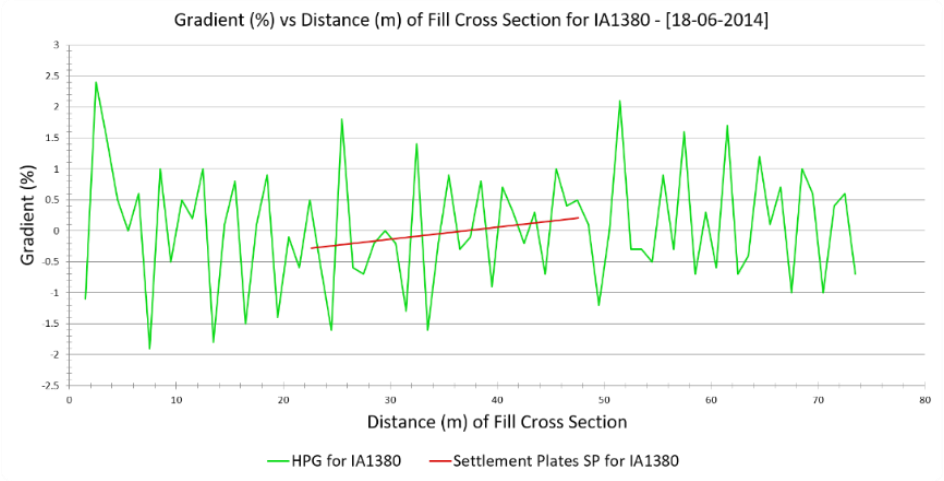

(b)

Figure 13: Graphs illustrating, (a) settlement versus distance and (b) differential settlement versus distance

Heat maps could also be automatically created based on the magnitude of the recorded values. On F2E heat maps such as that shown in **Figure 14** could be used to easily observe the magnitudes of settlement recorded at the settlement plate arrays.

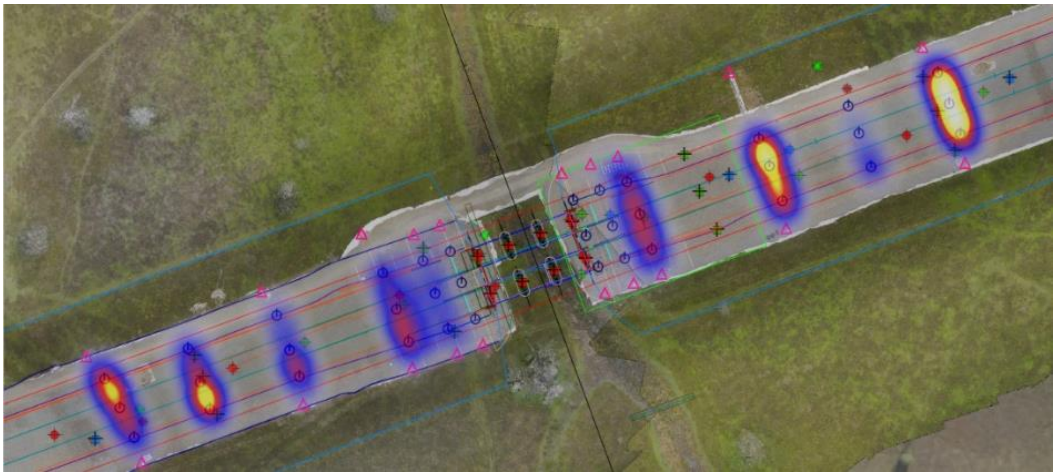

Figure 14: Heat map based on settlement values recorded from each settlement plate array on F2E

Given that the data was uploaded regularly and could be viewed simultaneously to inform the continual feedback loop required by the Observational Approach, EIC GeoView gave the engineers a degree of efficiency and up-to-date data which could not have been achieved by conventional manual methods of monitoring data management.

4 CONCLUSIONS

EIC GeoView is an advanced database management system which has been developed by EIC Activities to provide automated data processing, storage and visualisation of recorded data. This software has helped raise the transparency, processing efficiency and usability of recorded data allowing engineers to make informed decisions during and after construction. EIC GeoView has been used on numerous large-scale infrastructure projects in Australia, covering various built structures on road and rail projects. Use of the software provided the project teams with up-to-date performance of the as-built structures with unparalleled clarity and efficiency that could not have been achieved using conventional manual data collection and processing methods.

5 ACKNOWLEDGEMENTS

The authors wish to thank the CIMIC Group Clients and CPB Contractors construction teams from Torrens to Torrens Alliance, Sydney Metro Northwest TSC, and Frederickton to Eungai Pacific Highway Upgrade for their efforts in delivering these projects, and their approval to have the content of this paper published.

6 REFERENCES

Transport for NSW, (2016) “Guide – Geotechnical Instrumentation and Monitoring Guidelines”, T MU CI 12140 GU, version 1.0, 20 December 2016

A CASE STUDY – GEOTECHNICAL AND GEOPHYSICAL INVESTIGATIONS OF AN OLD STONE HERITAGE BRIDGE AT PARRAMATTA, GREATER WESTERN SYDNEY NSW, AUSTRALIA

Yogeshwaran Arumugam[1], Peter Hitchcock[2], Rolf Rohleder[3] and Simon Stewart[4]
[1]Geotechnical Engineer, [2]Geophysicist, [3]Principal Geotechnical Engineer, [4]Principal Geophysicist
Coffey Services Australia Pty Ltd, Level 19, Tower B - Citadel Tower, 799 Pacific Highway
Chatswood NSW 2067, Australia

ABSTRACT

This paper presents the methods used and results obtained from a combined geotechnical and geophysical investigation of Lennox Bridge located in Church Street Parramatta, NSW. Lennox Bridge is a Heritage-listed, 19th century, stone arch bridge spanning Parramatta River, constructed in 1839 and widened in 1934-35 under the direction of the Department of Main Roads, which included removal of a western footway and erecting a new reinforced concrete structure. Assessing the foundations and properties of a composite bridge constructed in different centuries presents significant challenges. A Borehole Ground Penetrating Radar (BGPR) technique was employed to assess the depth of the abutment foundations of the older sandstone bridge. A downhole magnetometer was used to determine the founding depth of the later concrete bridge by detecting the presence of rebar inside the concrete structure. Next to the sandstone bridge abutments, a set of boreholes were drilled at a distance of 1m and 4m from the edge of the abutment wall. The purpose of the furthest borehole was to provide a benchmark BGPR profile (without abutment) with which to compare the output from the sounding nearest the wall. The BGPR profiles of the two boreholes are compared to differentiate the presence of stone blocks used for the construction of the abutment and foundations embedded in an alluvial soil profile, down to bedrock. Boreholes were also drilled from the top of the bridge through the abutment to further confirm founding depths below the centre of the abutments.

1 HISTORICAL BACKGROUND OF LENNOX BRIDGE

The first bridge over the Parramatta River at this site, destroyed during floods in 1795, was constructed using timber with a replacement second bridge built between 1802 and 1804 on stone piers using timber railings. Later, single sandstone arch bridge spanning 91 feet (27.73m) was constructed in 1839 and became the third oldest surveying masonry bridge in New South Wales. In the early 1900's the internal structure of the bridge was strengthened to support a new tramway and in 1912 the western side parapet wall was removed to provide a continuous cantilever pedestrian footway of 1.6 m. In 1934-35, the Department of Main Roads extended the footway by reinforced concrete with a sandstone-faced abutment wall. During 1990's the bridge was proclaimed a Heritage structure within New South Wales. In 2012 Parramatta City Council approved the excavation of tunnels through the combined bridge structure on each bank (through the abutments) to create pedestrian access along the riverfront footpaths. Construction of the tunnels began in 2014 and was completed in September 2015.

2 BACKGROUND OF PARRAMATTA LIGHT RAIL

Transport for New South Wales (TfNSW) commissioned the geotechnical and environmental investigation for the design of the Parramatta Light Rail (PLR) project, which is required to meet the growing transportation needs of Western Sydney. The preferred corridor was announced by the NSW government in December 2015 and runs from Westmead to Strathfield via Parramatta Central Business District (CBD). The proposed works include environmental, heritage, geotechnical, geophysical and utility investigations required to inform the next stages of design. Lennox Bridge is situated within the Parramatta CBD area, connecting the suburbs north of the Parramatta River with the Parramatta CBD. The preferred PLR route is intended to cross over Lennox Bridge. Ministry of transport and infrastructure of NSW has announced PLR Stage 2 on October 2017, which connects Greater Parramatta to Sydney Olympic Park.

3 PURPOSE OF THE INVESTIGATION

As a part of the detailed investigations, TfNSW required that a structural and geotechnical investigation of Lennox Bridge be carried out. This technical paper focuses on the geotechnical and geophysical techniques employed as well as a brief overview on the structural investigation undertaken.

4 INVESTIGATION METHODOLOGY

There were three major components involved in the Lennox Bridge investigation, comprising:

Structural component, Geotechnical component and Geophysical component.

4.1 STRUCTURAL COMPONENT

The bridge consists of two major structural elements: an old sandstone bridge (eastern side) and a concrete bridge (western side) thus the approach of the investigation has been accordingly scheduled. The old sandstone bridge consists of a gallery inside and it is visually assessed for internal damages. A truck-mounted, specialised, extension gangway (known as an Under-Bridge Investigation Unit (UBIU)) was employed to inspect the abutment wall and the bridge arch. Figure 1 shows the UBIU on Lennox Bridge and Figure 2 shows the plan view of composite bridge.

4.1.1 Sandstone investigation

The sandstone blocks have undergone various chemical and physical weathering over a period. Following investigations has been undertaken to analyse the current integrity of sandstone blocks facing outside and inside the gallery.

4.1.1.1 Delamination survey

The sandstone bridge was visually inspected to assess the condition of the sandstone blocks and record any evidence of deterioration or defects. In general, the exposed surface of the sandstone abutment was gently tapped by steel mallet to remove the loose layers.

4.1.1.2 Petrographic analysis

The intact lime mortar between the sandstone blocks was cored below the ground level and analysed for minerals present in the mortar and presence of iron oxides.

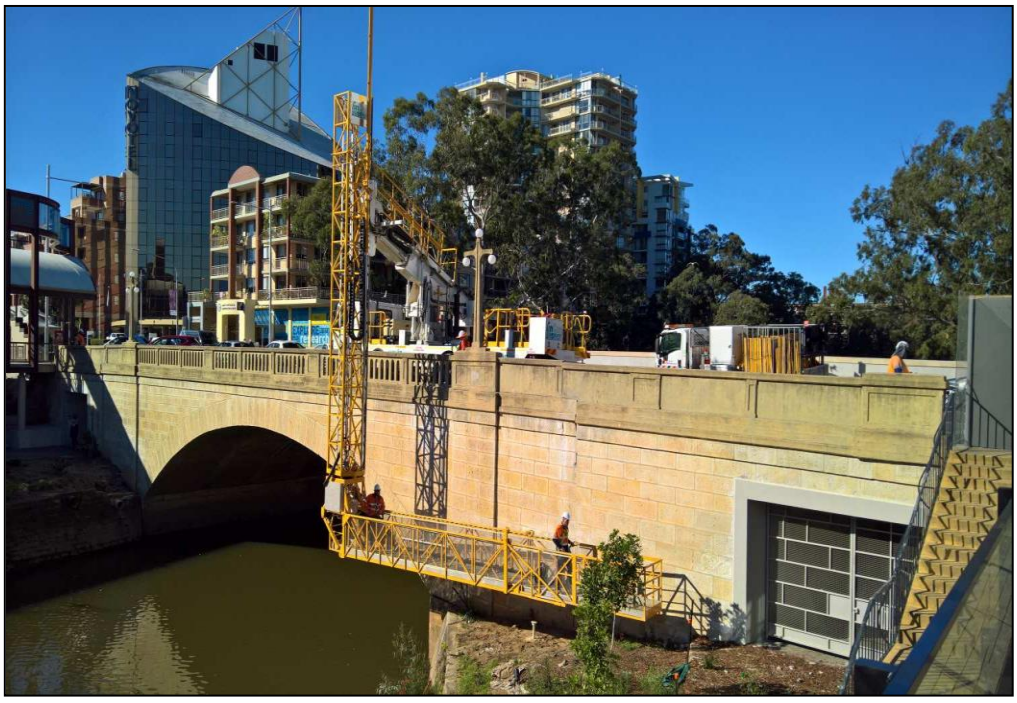

Figure 1: Structural investigation of Lennox Bridge using Under Bridge Inspection Unit (UBIU)

4.1.1.3 Gallery inspection

The sandstone bridge contains several internal galleries on both North and South abutments. Access was gained (by trained personnel) into one of the galleries for visual inspection of the internal sandstone blockwork. Numerous high-resolution photographs were obtained from this inspection.

4.1.2 Concrete investigation

Concrete bridge is covered by sandstone façade on western side of the bridge, however concrete at underside of the bridge is visible and mapped for investigation.

4.1.2.1 Crack mapping

The concrete surface of the balustrade and arch of the bridge was mapped for any cracks and the crack size was recorded.

4.1.2.2 Drumminess survey

The drumminess survey was carried out in the newer concrete bridge section by gently tapping the concrete surface with a small hammer to detect any cover separation from the reinforcement. These areas were mapped to identify the weak spots of the concrete.

4.1.2.3 Reinforcement bar detection

The reinforcement bars of the concrete bridge were detected on the abutment and arch surfaces by scanning with a non-intrusive GPR scanner in specific areas ranging from 1 m by 1 m to 1.8 m by 2.9 m.

4.1.2.4 Concrete coring

Concrete samples were cored from the abutment of the wall to identify the extent of carbonation and chloride ingress.

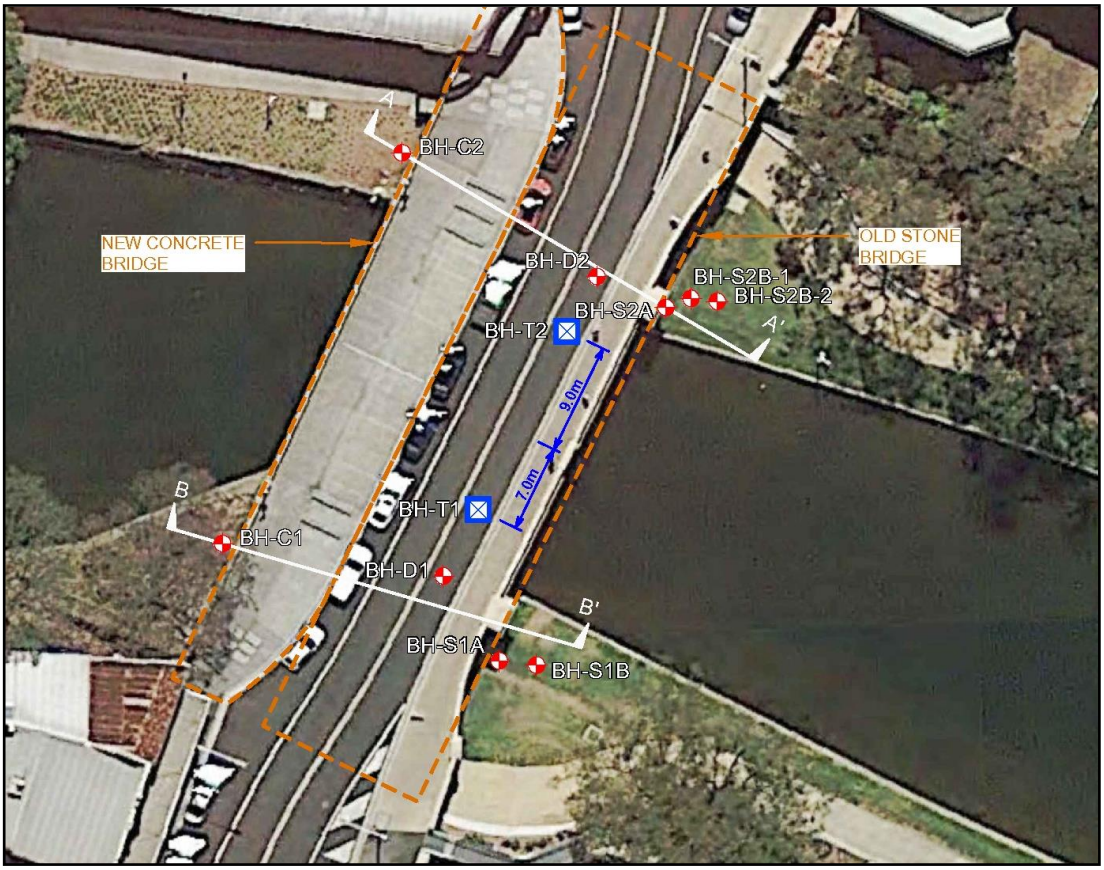

Figure 2: Geotechnical boreholes and trial pits at Lennox Bridge

4.2 GEOTECHNICAL COMPONENT

A total of 8 boreholes were drilled to identify the ground profile and founding depths of the bridge. Down-hole geophysics techniques were used in 6 of these boreholes, located in the riverbank areas next to each of the two abutment structures. A track mounted drilling rig was engaged to complete all boreholes.

Based on previous studies of the area, it was known that the ground profile beneath each river bank consists of a sequence of alluvial deposits over sandstone bedrock. It was anticipated that the bridge foundations (both for the older sandstone bridge and the later concrete bridge) were founded on the bedrock, however this needed to be verified.

4.2.1 Sandstone abutment boreholes

Two sets of boreholes were drilled adjacent to the two bridge abutments on the east side of the older stone bridge. One borehole was drilled approximately 1 m from the edge of the wall, and a second one positioned about 4 m from the edge of the wall. The purpose of first borehole (1 m away) was to carry out down-hole geophysics soundings using BGPR technique, to identify the founding depth of the bridge abutment. The purpose of the second borehole (4 m away) at each side was to provide a benchmark BGPR profile (without abutment) with which to compare the output from the sounding next to the wall. As the radial penetration of the BGPR is only about 2 m to 3 m, the second borehole BGPR sounding was expected to provide the profile through the alluvial sediments only.

The nearest BGPR sounding was expected to detect the abutment wall and foundation construction below ground level all the way down to top of bedrock, thus providing confirmation of minimum founding depth.

4.2.2 Boreholes through the sandstone bridge

Two boreholes were drilled through the abutments of the old sandstone bridge in order to confirm its construction materials and founding depth. Two boreholes were located approximately 14 m apart from the arch of the bridge. The boreholes were drilled into the asphalt of the road, fill materials followed by sandstone blocks and founding bed rock. The roughly rectangular-shaped sandstone blocks are separated by irregularly spaced lime mortar joints with a variable thickness ranging from 30 mm to 150 mm. In one particular zone, the mortar thickness was measured to be 490 mm thick.

4.2.3 Concrete abutment boreholes

On the concrete bridge side, a single borehole was located at each abutment, 1 m from the edge of the wall. Employing a downhole magnetometer probe to detect the presence of steel reinforcement within the concrete foundation, the results were used to infer the base of the bridge foundation.

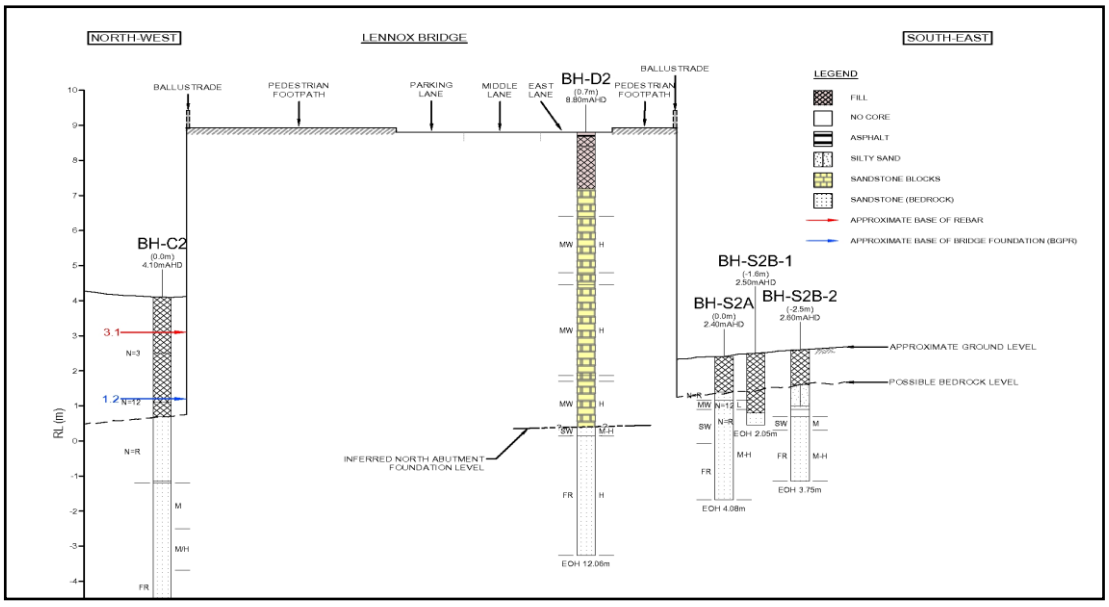

Figure 3: Northern sectional view (A-A') of the boreholes and the bridge.

4.2.4 Trial pits

Two trial pits were excavated on the old stone bridge deck approximately 7 m to 9 m from the middle of the bridge, on opposite ends. The dimensions of trial pits were 0.8 m × 0.6 m × 0.8 m (length × breadth × depth). The aim of the pits was to confirm and sample the fill material between the pavement and the upper surface of the stone arch. Due to Heritage-constraints, the pits were manually excavated using lightweight pneumatic tools. The pits revealed that the fill material is variable containing boulders and gravelly sand above the top of the arch blocks.

4.3 GEOPHYSICAL COMPONENT

The geophysical investigation undertaken at the bridge was carried out at several locations around the bridge. The varying construction methods used on either side of the bridge made it necessary to employ different geophysical survey methods to assist in identifying the foundation depth of the overall bridge structure.

4.3.1 Borehole ground penetrating radar

The BGPR survey was completed in four pre-drilled boreholes on the eastern (old) side of the bridge with the aim of identifying the depth of the bridges' sandstone foundation. Lack of steel reinforcement in the sandstone made other borehole techniques, such as magnetics, inappropriate to assist in identifying the foundation depth.

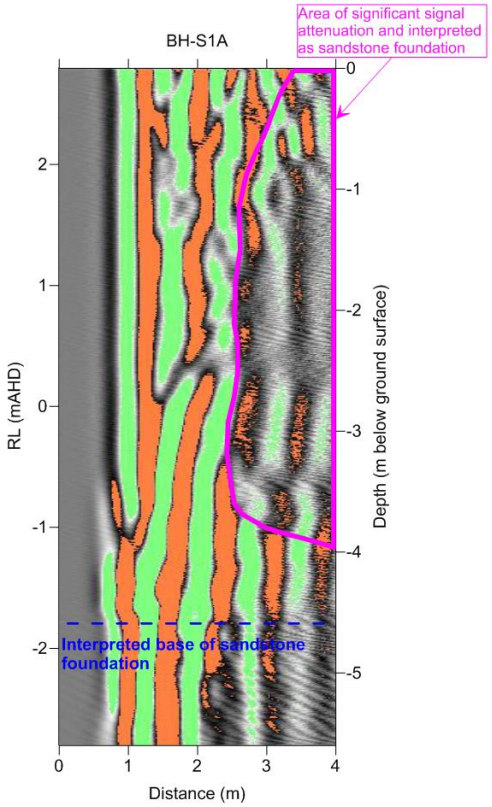

Figure 4: Sample BGPR profile with interpretation

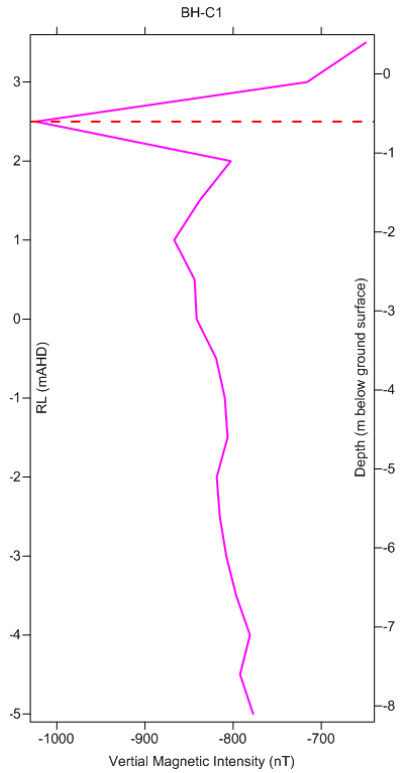

Figure 5: Sample downhole magnetics test result acquired adjacent to the concrete side of the bridge

The BGPR method is similar to surface GPR methods in that it passes radio frequency electromagnetic energy pulses into the ground. However, the equipment is deployed down a vertical borehole and signals are radiated omni-directionally, thus sampling a cylindrical shaped volume of material down the borehole with a radius (i.e. depth of penetration) that is dependent on the dielectric properties of the material. Reflection of BGPR energy occurs at interfaces where contrasting electrical properties exist, such as sub-surface construction layers and natural ground.

The acquired BGPR data were processed, analysed and interpreted using MALÅ Geoscience Radinter software. Where either a large reflector or signal attenuation occurred, this was interpreted as a result of the sandstone foundation of the bridge. Figure 4 shows the results of BGPR data at borehole BH-S1A.

These results of the BGPR corresponded with the base of the sandstone blocks as encountered in the geotechnical boreholes drilled through the bridge. The BGPR survey conducted down the borehole drilled 4 m from the bridge showed no interpretable foundation features and the foundation of the bridge was inferred to be beyond the depth of penetration of the BGPR system.

4.3.2 Downhole magnetometer testing

Downhole magnetometer testing was performed on the western (concrete) side of the bridge to identify the depth to the base of steel reinforcement in the concrete bridge foundation.

Downhole magnetic testing is a passive method based on the measurement of localised perturbations to the Earth's magnetic field measured in nanotesla's (nT). These may be caused by geological features and buried ferrous targets (eg, pipes, cables, drums, iron sheets, steel reinforcement).

Downhole magnetic testing was completed in-situ using pre-drilled, PVC cased boreholes. A Bartington 3-component Mag-03 fluxgate magnetometer was used to measure the magnetic field variations at 0.5m intervals to the maximum depth of the borehole. The magnetic data was acquired with Spectramag-6 software.

The vertical (Z) component of the magnetic field typically provides the clearest indication of the base of the steel reinforcement in the bridge foundation and hence the approximate depth of the foundation. Magnetic high anomalies present in the data usually indicates the approximate base of the steel reinforcement (Jo et. al, 2003).

The magnetic anomaly indicated by the red dotted line was interpreted as base of bridge foundation. Figure 5 shows a sample result of the downhole magnetic testing completed at the bridge site borehole BH-C1.

The downhole magnetic testing was considered successful in determining the base of the reinforcement within the concrete foundation of the western side of the bridge.

4.3.3 Ground penetrating radar (GPR) survey on bridge deck

As part of the overall investigation, a surface-based GPR survey of the bridge deck was completed to identify the top of the stone arch as well as provide preliminary assessment of the fill material beneath the road deck.

GPR data were collected along six (6) profiles parallel to the existing bridge alignment approximately 1.5m apart. The GPR identified variations in the fill material as well as larger boulder size objects within the fill. The GPR survey was also successful in identifying the stone arch of the bridge. The GPR data also showed various linear reflector within the fill material and likely indicate areas of differing fill material and filling 'event' during the bridge construction. Figure 6 shows the annotated GPR profile across the bridge.

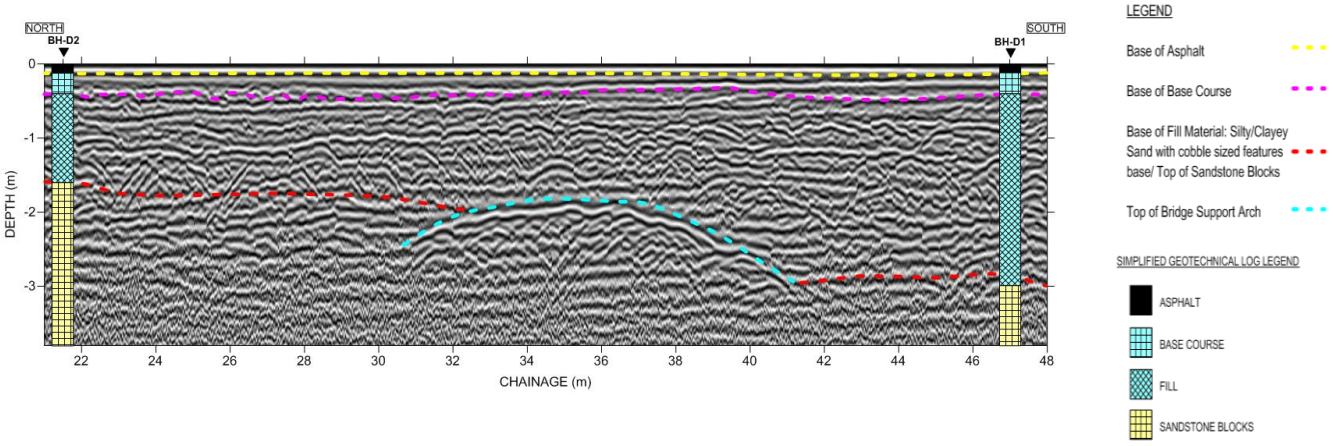

Figure 6: A sample annotated GPR profile acquired across the bridge.

5 DISCUSSIONS

5.1 FOUNDATION DEPTHS

Sandstone bedrock was encountered at variable depths across the two sides of the river. The depth to sandstone bedrock varied between 4.5 m and 5.3 m at the South abutment. In comparison, sandstone bedrock was encountered at much shallower depth at the North abutment, at between 1.0 m and 1.7 m depth on the NE side, and at 3.4 m on the NW side. Generally, the sandstone samples obtained from the bedrock in these boreholes indicate a medium to high intact rock strength based on the laboratory test results.

5.2 COMPARISON OF GEOTECHNICAL AND GEOPHYSICAL INVESTIGATION

The downhole geophysical methodologies provided consistent information on the depth of the old and new bridge foundations as did the GPR results acquired on the bridge deck.

The downhole magnetic testing results successfully identified the base of the concrete reinforcement and were in agreement with available reinforcement 'as built' drawings. Furthermore, the BGPR results were considered successful

in identifying the rock soil interface as well as the bridge sandstone foundation, particularly in holes that were drilled close (~1m) from the bridge sandstone foundation.

6 ACKNOWLEDGEMENT

We are grateful to officials, technical advisors and project members of Transport for New South Wales (TfNSW), PLR project team and Roads and Maritime Services (RMS) for providing support during site investigations and to publish this technical paper. We thank SAS TTI (Structural sub-contractor) for assisting us in gallery inspection and collecting samples. We extend our gratitude to the all Structural, Geotechnical and Geophysics staff members at Coffey for providing assistance during the course of investigation.

7 REFERENCES

Conservation Management Plan, Lennox Bridge over Parramatta River, Parramatta by Roads and Maritime Services (RMS) by Sydney region asset management branch, July 2012.

http://www.environment.nsw.gov.au/heritageapp

Jo, C.H.J., Y.H. Cha, and J.H Choi, Dec. 8-12, 2003. *A Borehole Magnetic Logging Tool for Estimating Unknown Foundation Depths*. Presented at the 3rd International Conference on Applied Geophysics.

Reinforcement drawings of concrete section of Lennox Bridge prepared for Department of Main Roads.

Road and Maritime Services (RMS) QA specification M209 edition 2 /Revision 0.

DEVELOPMENT AND APPLICATION OF GEOTECHNICAL MONITORING AND DATA MANAGEMENT FOR WOOLGOOLGA TO BALLINA PACIFIC HIGHWAY UPGRADE

[1]Henry Zhang, [1]Paul Hewitt, [2]Graham Yip, [2]Stephen Summerell, [1]Sudar Aryal, [3]Chris Davis, [2]David Groth, & [3]James Tyrrell

[1] WSP Australia; email: Henry.Zhang@wsp.com, [2] Roads and Maritime Services, [3] Laing O'Rourke

ABSTRACT

One of the major challenges on the Woolgoolga to Ballina Pacific Highway upgrade involved constructing more than 26 kilometres of road infrastructure over soft ground within 1 to 2 years, as part of upgrading 155 kilometres of the Pacific Highway. This included one of Australia's largest soft ground instrumentation programs.

As with many other sections of the Pacific Highway, the design required embankments on soft ground to meet pavement performance criteria, and address risks of instability of high fill embankments, and the potential impact of the new works on existing infrastructure. Data-management systems and automation maximized the value of site investigation data collected using GIS and document management capabilities. The project adopted web based real-time reporting which provided high information availability, transparency, efficiency and reliability. This paper provides a framework of the system with its unique features and functionalities. It demonstrates the monitoring and feedback process at several sections of the project, looks at innovations introduced as part of the work, discusses how monitoring could be improved, and describes applications of smart digital technology and high-performance computing which were used to facilitate early decision making, and enhance project and client outcomes.

Keywords: instrumentation and monitoring, soft ground, dashboard, ground improvement, slope instability

1 PROJECT BACKGROUND AND OVERVIEW

Woolgoolga to Ballina Pacific Highway upgrade (W2B) involves the duplication of 155 kilometres to a four-lane divided road on the Pacific Highway. The project starts about six kilometres north of Woolgoolga (north of Coffs Harbour) and ends about six kilometres south of Ballina. W2B bypasses the towns of South Grafton, Ulmarra, Woodburn, Broadwater and Wardell.

On behalf of the Australian and NSW governments, Roads and Maritime Services is progressively upgrading the Pacific Highway to dual carriageway between the Hunter and NSW/Queensland border. Roads and Maritime Services engaged Pacific Complete (PC), a joint venture between Laing O'Rourke and WSP (formerly Parsons Brinckerhoff), to partner with its Pacific Highway Project Office to deliver the W2B. PC works closely with Roads and Maritime to manage multiple contracts in delivering the design and construction of the W2B project.

W2B includes upgrading the highway to motorway (Class M) or arterial (Class A) standard over its 155kilometere length, nine grade-separated interchanges, 170 bridges, fauna crossings, three rest areas and a heavy vehicle checking station. Key elements of the project include the following:

- Over 90 cuttings with a maximum depth of up to 44 metres
- Over 143 embankments with a maximum fill height of 16 metres
- More than 60 bridge sites involving mainline carriageway overpasses of waterways, floodplains and local roads, and over 31 overbridges to maintain access to local roads that cross the highway.
- 110 hectares of soft soil sites over 26 kilometre cumulative route length, with compressible ground up to 23 metres thick.

This paper provides an overview of how challenge and innovation were addressed and managed in relation to geotechnical aspects of monitoring data management, and soft ground design across the project and summarises the benefits observed to date. Figure 1 shows the entire route of this project.

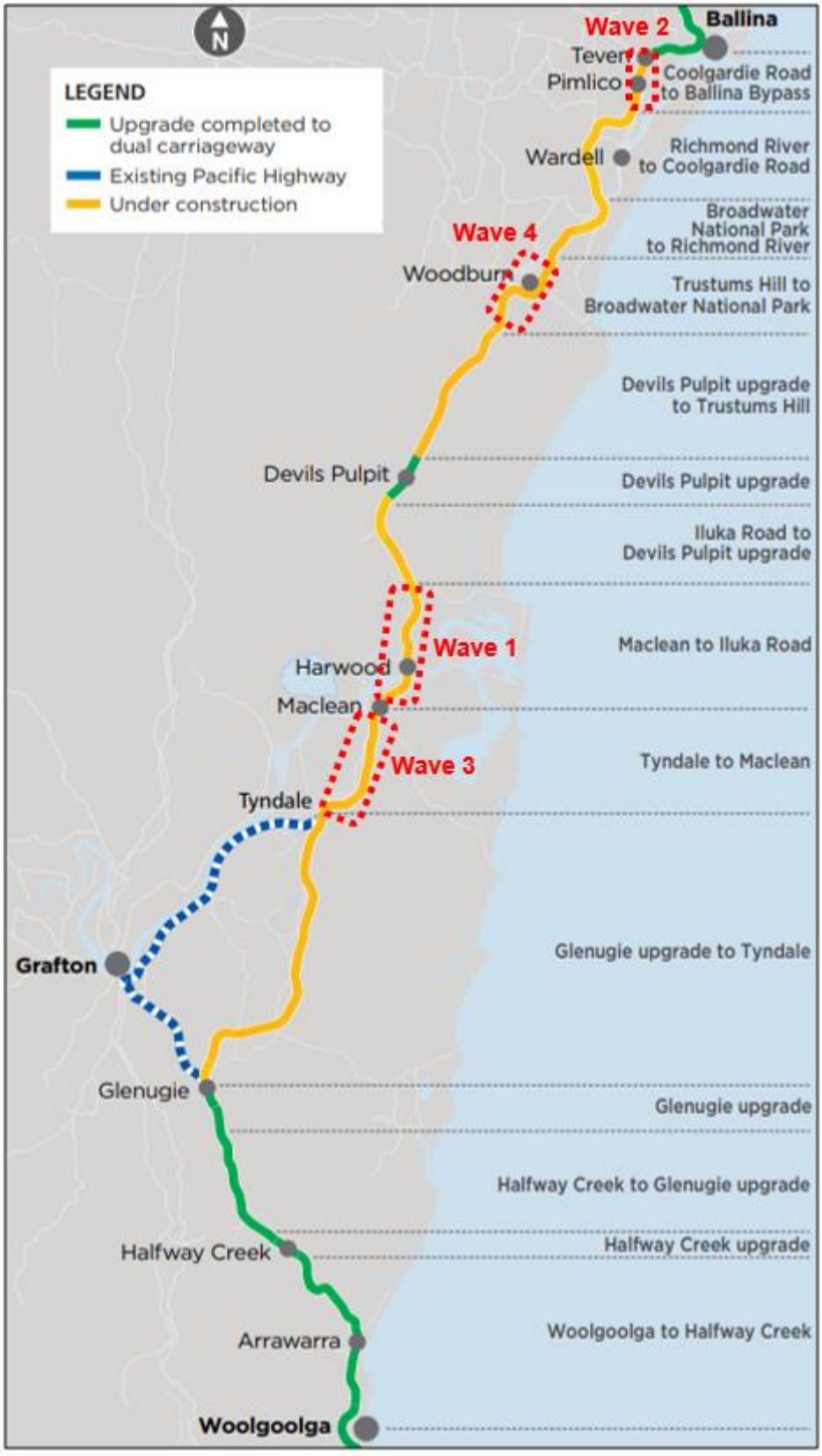

Figure 1: Woolgoolga to Ballina project map and early works "wave" package locations shown in red

2 VALUE ENGINEERING AND INNOVATION

From the earliest engagement of the delivery partner, significant effort was applied to value engineering of the existing owner-developed concept design. This value engineering effort was concentrated in key discipline areas and was proportionate to the cost and/or programme associated with that discipline. Review of value engineering and innovation around geotechnical aspects was completed by the project's Geotechnical Review Group (GRG), which comprised the writers, who were selected as technical experts representing senior leadership.

"Value engineering" was defined as those changes that yield quantity and/or programme reductions to provide some improved project outcome but did not require any change in Roads and Maritime standards or specifications. They may however have involved some change to the works brief. "Innovation" items are those that required some change to existing Roads and Maritime standards or specifications to yield some improved "public value" outcome. Both value engineering and innovation initiatives served to mitigate cost plan and programme challenges and better align cost plan with project budget.

A subset of value engineering achievements related to geotechnical issues is presented in Table 1.

Table 1: Value engineering achievements by Pacific Complete

Item	Benefit
Instrumentation and monitoring "dashboard"	Adopted web based real-time reporting which provided high information availability, transparency, efficiency and reliability. PC system automatically warehouses project data and presents real-time dashboard using GIS. Expected savings of $2.5 million in manual information handling costs alone.
Earthworks Volume Reductions	From award, reduced total cut volume by over 900,000m^3 and total fill volume by 1,500,000m^3
Rationalised Foundation Treatments	Set minimum embankment heights to minimise shallow embankments wherever possible. Raising embankments allowed cheaper foundation treatment options compared to tender stage design/cost with VE benefits of est $25m
Maximisation of Plain Concrete Pavement extents	Developed ground treatment solutions to maximise the area where the post construction settlement is anticipated to be less that 100mm in 40 years so rigid pavement can be constructed. Approx. 23% increase in Pacific Complete area from owner-developed concept design; 170km SPIR design v 210km final design.
Pavement re-use	Maximised re-use of existing concrete pavement where possible
Soft Soil Treatment	Design optimisation of soft soil treatment and surcharge designs including programme implications. Addressed as design development with emphasis on construction staging to significantly reduce hard treatment. Approximately $60m of hard treatment removed from initial concept design costing including: • Optimisation of stabilising berm requirements • Removal of high strength geotextile requirements • Rationalisation of high strength geotextile requirements in Maclean Interchange in Wave 3 (Figure 1) • Reduction of waiting periods for early works surcharged embankments
Instrumentation and monitoring	Optimisation of instrumentation and monitoring with: • reduced frequency of HPG, extensometers, settlement markers • reduced total number of HPG, extensometer and VW piezometer in general fills over relatively shallow soft ground with maintaining one settlement monitoring point at every 50m interval • grouping instruments into "banks" of instruments for better protection and access • Use of telemetry technique at critical structures that is expected to be affected by ground treatment
Replacing Culverts with Bridges	Replacing 24 No and 14 No. culvert banks with single 120m long plank bridge for improved ride quality and flooding outcomes at reduced cost. Use of bridges

	instead of large banks of box culverts on soft soil floodplains saved time in program / cost by removing pre-loading / ground treatment requirements.

3 GROUND CONDITIONS AND SOFT GROUND TREATMENT DESIGN

One of the key challenges on this project was the construction of embankments over deep soft and compressible soils that required ground treatment to address the long-term settlement problems. Soft soils are an important design consideration for the project as there are deep soft soils in floodplain areas along the upgrade. Key features of soft soils include high water content, low capacity for allowing water to pass through and low strength. Without soft soil treatment, there is the potential for highway foundations and main alignment to sink and crack because the bearing capacity of the soil is not strong enough to support the highway.

Treating soft soil before building the main alignment takes time but saves money. The aim was to consolidate the soil so it can be built on. Consolidation involves squeezing the water from the soil to make it stiffer. It will take about two and a half years for the soil to consolidate once the water is removed.

Figure 2: Early work construction on W2B (a) bogged excavator (b) wick drains installed

Prediction of the time dependent deformations of embankments constructed on soft and compressible ground is required when preload or surcharge design solutions are adopted, with or without the use of wick drains. Accurate predictions are essential to achieve cost-effective outcomes. If the settlements are underpredicted then the embankments will end up below design levels, leading to additional earthworks during construction or post construction performance not meeting the project criteria. If settlements are overpredicted, too much fill will be placed initially and more fill will need to be stripped and spoiled than expected after settlement has been completed. Either of these issues will result in additional construction time and unnecessary costs. Both underprediction and overprediction of embankment settlement has occurred on sections of the Pacific Highway upgrade between Sydney and the Queensland border. Underestimates or overestimates of the time-rate of settlement can also lead to opportunities for early completion of construction being missed; create a risk of excessive construction time, and in some cases cause stability problems.

On W2B, construction of embankments over these soils would cause significant settlement issues during construction and in the long term if the foundation is not treated prior to pavement. For this reason, soft soil treatments were started early using an early work contract. There were 11 soft soil sites with the majority covered in an early work "wave" package (Figure 1). For the soft ground outside the early work, PC provided preliminary design for tender and subsequently PSC provided detailed design after the tender was awarded. Soft ground treatment methods adopted on W2B were as follows.

1. Preload only (filling at pavement level at the end of preloading with no surcharge, no wick drains).
2. Surcharging (filling above pavement level at the end of preloading, no wick drains).
3. Surcharging with wick drains.
4. Concrete injection column (CIC) at critical bridge approaches and box culverts where the above solution was not viable

Figures 3 and 4 (Zhang et al, 2016) show the interpreted geotechnical long section and design parameters at Yamba, south of Harwood bridge, corresponding to one of the most challenging soft ground areas on this project.

3.1 DESIGN CRITERIA

Geotechnical design was developed to meet the requirements of the Pacific Highway Design Guidelines, RMS Standards and Technical Guidelines, and relevant Australian Standards. The following criteria were adopted in the design:

1. Total residual settlement (pavement settlement in 40 years): within 100mm and 200mm for rigid and flexible pavement respectively for general embankment; within 50mm in the 20m structural zone from a bridge abutment.
2. Differential settlement: 0.3% and 0.5% in both directions for rigid and flexible pavement respectively.
3. Slope stability: Factor of Safety (FOS) of any batters not less than 1.2 for short-term end of construction, flooding and earthquake cases; not less than 1.5 in the long-term drained case.
4. Culvert settlement: for pipe culvert 150mm in 100 years and for box culvert 110 mm in 100 years as a guidance. At culvert locations, pavement complies with the performance criteria in items 1 & 2 above. The culverts were also designed according to the supplier's recommendations.

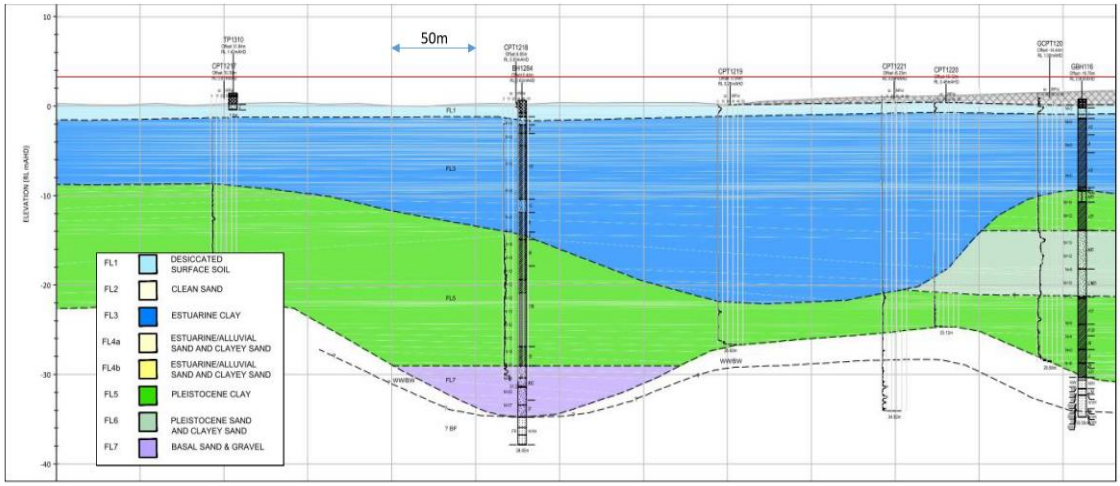

Figure 3: Geotechnical long section at south of Harwood bridge (FL3: very soft to firm clay)

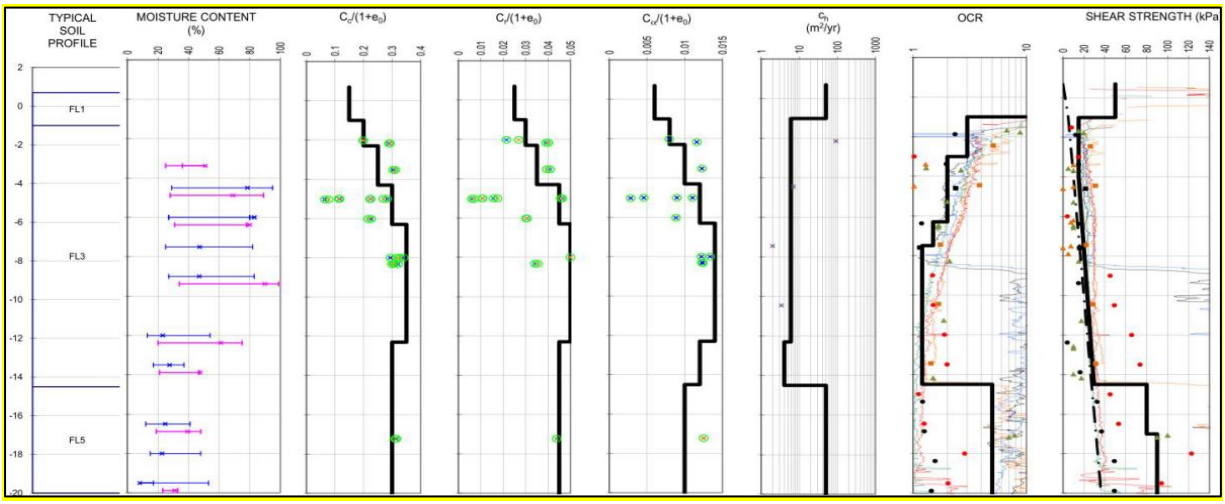

Figure 4: Profiles of material parameters with depth

3.2 SHORT TERM SLOPE STABILITY ASSESSMENT

Accurate prediction of embankment behaviour on soft soil requires a systematic process that ideally includes high quality sampling techniques in combination with high quality laboratory and in situ testing data, the adoption of an appropriate constitutive model, and calibration of the constitutive model. Short-term slope stability design requires analyses of settlement, lateral deformation and rate of pore water pressure dissipation. On W2B, short-

term slope stability was monitored and delivered adopting different trigger levels, which addressed the rate of lateral displacement as shown in Table 2. Parameters are defined in Figure 5. Two deformation ratios were assessed: total deformation ratio (= h_m/S) and incremental ratio (= $\delta_{hm}/\delta S$).

We assessed that the trigger levels achieved a minimum calculated FOS of 1.2 to meet design requirements. In addition to the trigger levels in Table 2 (Zhang et al., 2016), the trend of maximum lateral displacement versus fill height was monitored for a decision to slow down or stop filling. Three criteria (DRc, DRi and Di) were adopted for high risk areas (Yamba and Maclean Interchanges); while only two criteria (DRc and Di) were adopted for the remaining areas.

Table 2: Trigger levels for embankments with and without wick drains (Zhang et al., 2016)

Parameter	Wick drains		No wick drains	
	AL	WSL	AL	WSL
h_m/S (=DRc)	0.25	0.35	0.5	0.7
$\delta h_m/\delta S$ (=DRi)	0.5	0.7	N.A.	N.A.
δ_{hm}/δ_t (mm/day)	10	15	10	15
Action	Increase measurement frequency	Stop filling	Increase measurement frequency	Stop filling

Notes: h_m = max cumulative horizontal displacement from an inclinometer; S = cumulative settlement from adjacent settlement plate; δ = incremental; t = time in days; δ_{hm}/δ_t = daily lateral displacement; AL = Alert Level; WSL = Work Suspension Level; DRi only applies for high risk areas (Yamba and Maclean Interchanges)

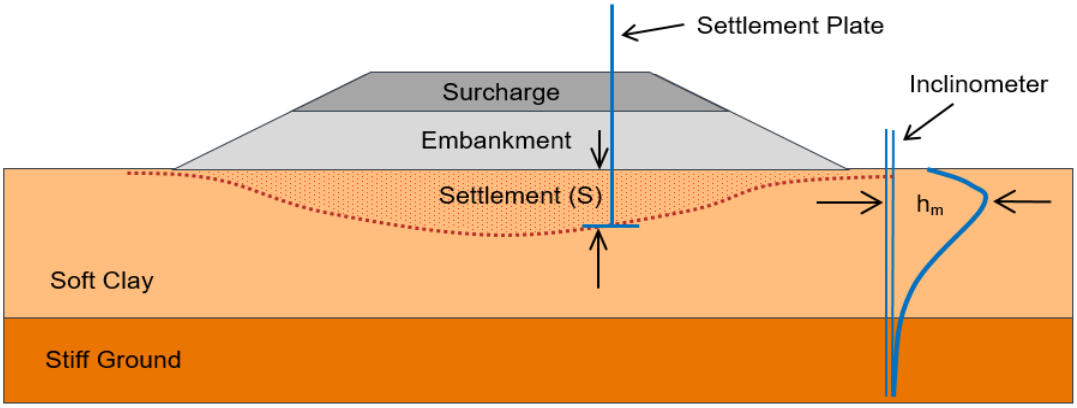

Figure 5: Definition of embankment deformation ratio

Analytical measures adopted by PC to address settlement and slope instability during design and construction included:

- "Field Deformation Analysis (FDA)," based on a simple concept dealing with lateral and vertical deformation characteristics of soft foundations under embankment stage loading. This method was used to delineate and quantify different settlement components, namely, immediate settlement, consolidation settlement, and creep settlement, from the total settlement measured during field observations, for the loading and consolidation stages (Loganathan, 1993).
- Changing the groundwater table with time to match measurements.
- Correcting pore pressure measurements for settlement and changes in the water table.
- Systematically modifying key parameters: a. Recompression ratio prior to the yield pressure being exceeded. b. Permeability / coefficient of consolidation prior to the yield pressure being exceeded. c. Yield stress ratio. d. Compression ratio over the stress range of interest. e. Permeability variation with stress level and permeability reduction in wick drain smear zone. f. Creep parameters.

Measuring the progress of consolidation during construction plays a critical role in the long-term success of embankments founded on soft soil. Records of its actual performance allow engineers to verify design assumptions and recommend early interventions if its as-built behaviour deviate from predictions. One of the most critical predictive decisions involves assessment of when residual settlements are sufficiently small to allow the construction of settlement-sensitive structures above the embankment, such as the overlying pavement. Accurately recorded consolidation measurements were used to predict embankment behaviour, and provide meaningful estimates of residual settlement.

4 PROGRAM DEVELOPMENT

4.1 FEATURES

Online monitoring systems were tried before on other Roads and Maritime projects but were only partially successful. For W2B an in-house online monitoring system was developed because of the scale of this project with extensive soft ground treatment work. The system development was funded by Roads and Maritime, and retained by Pacific Complete.

This system was developed by the PC who set up the format and calculation process for each instrument type and the link between different instrument types, e.g. inclinometer and settlement plate, piezometer and settlement plate. Review levels were set up to control short-term slope instability and hold-point release.

We then developed the system using a data application for data uploading/editing/downloading, a Microsoft SQL Server database for all calculations and the Qlik Sense dashboard with the QlikMap GIS extension for visualisation. A screenshot of the Geotech Dashboard is shown in Figure 7.

The tables, charts, graphs and maps used are interactively linked to the underlying data, so that selecting a project area, period, instrument type or instrument, will automatically filter the data being displayed on every control. The same session being open on multiple pages, screens or even computers and mobile devices will maintain a link to this dynamic filtering.

We structured the data management process to address the following:

- Alert system – allows anomalies to be reviewed to judge where settlement behaviour was of concern, and where unusual behaviour was caused by errors in the monitoring data. Information about the construction process was integrated with monitoring data to aid interpretation of movement ‘signatures’ in the data.
- Observational approach - to allow flexibility during construction to address unexpected behaviour and implementation of mitigation measures to rectify the as-built condition, and improve long-term project performance.
- Monitoring optimisation – based on historical monitoring data and on engineering judgment, it was possible to identify where there was redundancy in the monitoring system and reduce the amount of monitoring being carried out to reduce costs.
- Forecasting – it was possible to predict when settlement might exceed an acceptable level, thus allowing engineers to introduce contingencies in advance, such as reducing fill placement rate or adding an earthworks berm, and release of hold-points to release fills for pavement construction.

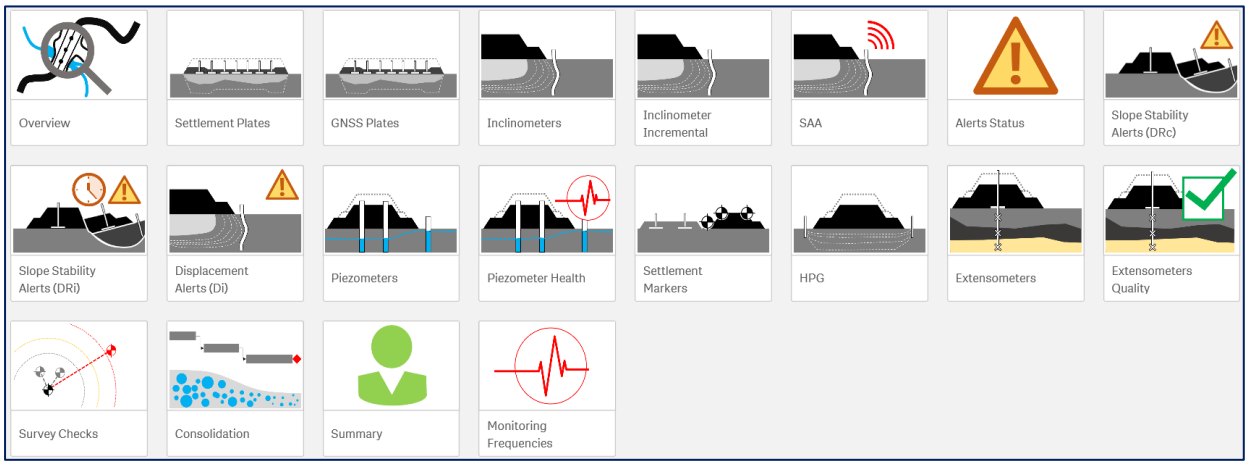

Figure 6: Geotechnical dashboards

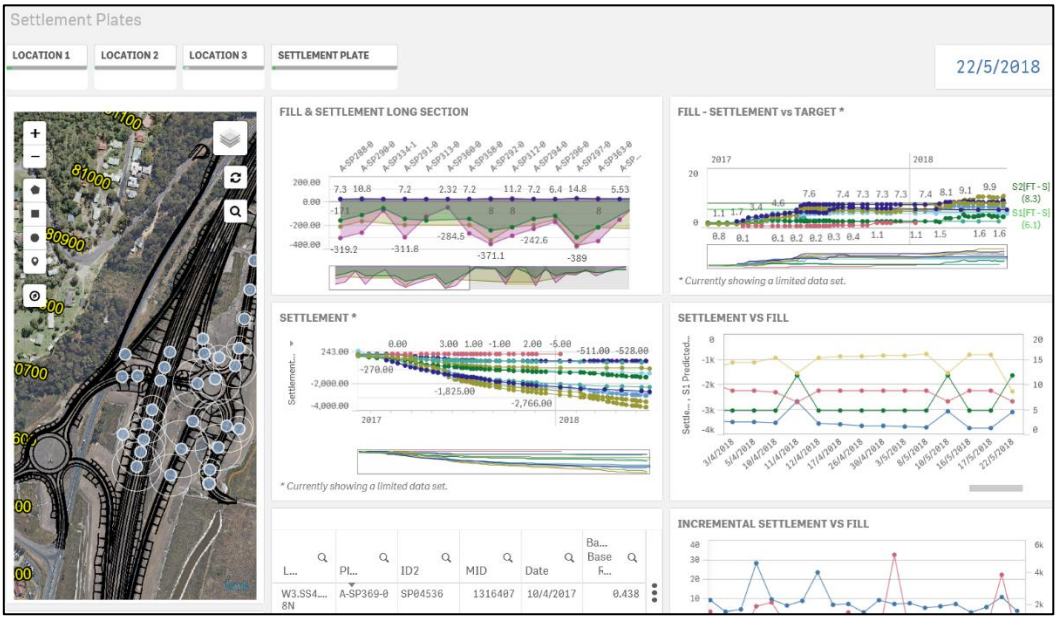

Figure 7: Example design vs measured fill height, settlement, settlement rate time plots

Features of this online monitoring system included:

- Automatic uploading using standard format for all instruments, via either an email or a third-party website (e.g. VW piezometers owned by the suppliers).
- Automatic Alert System: an email was automatically sent to all relevant parties once the predetermined Review Levels were exceeded.
- A quick comprehensive review of all relevant instruments linked with a GIS Map to enable a quick decision-making, which is critical for short-term slope stability.
- Open/flexible for further improvement.
- Automatic email reminders of late reading of any instruments.

4.2 APPLICATION

Part of the success of the geotechnical "dashboard" lay in effective visualisation of the data in a dashboard, allowing project managers to interpret and act quickly on settlement and groundwater data. The program took the data from each site and, with some complex statistical analysis, produced visualisations of the information to try to understand spatial and time-dependent correlation between monitoring points, and alert engineers to issues of

concern. A method of quality assurance was introduced: for each issue that was flagged up, engineers could enter in a box that they had reviewed the issue and dealt with it appropriately.

A higher-level view was also generated, allowing project managers to assess progress without needing to look at the detailed data. The application helped field engineers interpret and act on data, and in turn helped improve the risk management of field engineers' work.

With this system, the design team, with support from the construction team, has managed to build all the embankments safely without slip failure and 75% of all the preloading fills has been released for pavement construction.

5 INSTRUMENTATION AND MONITORING

5.1 OBJECTIVES

An objective of the project team was to streamline data collection to maximise the system and the project integration, and shorten the review and the decision-making process to improve construction safety.

As a general trend, advances in construction monitoring are moving away from physical measurements at a limited number of points, to widely distributed, wirelessly connected sensor networks, and to aerial scanning techniques. This data allows contractors to optimise construction processes and increase project safety performance. Integrating data from multiple sites can facilitate a quick overview of the whole project to pinpoint the sites with higher risk, improve performance prediction and understanding of zonation and ground properties. Monitoring for enhanced safety was also critical due to the project scale and proximity to existing infrastructure (e.g., bridges).

5.2 MONITORING DATA COLLECTION, DISTRIBUTION AND ACTION

The team carried out regular reviews of the collected data from instrumentation to check the actual ground movement performance against the design prediction. The process and associated responsibilities for collection, distribution and review/analysis of the monitoring data is outlined below:

- Instrumentation reader collects data in the field (the main contractor in the case of settlement plates, settlement markers and survey targets), review data for quality, consistency and reliability.
- Instrumentation reader compiles the measured data (the main contractor in the case of settlement plates, settlement markers and survey targets) using the template provided by Pacific Complete.
- Instrumentation reader to email the template with data, as soon as it is collected, to PC for automatic upload of data to the Data Warehouse.
- PC Geotechnical Team and or the Project / Site Engineers review data to check if actual movements being experienced by the embankment or structure is as expected and within the agreed trigger levels.
- During the settlement period, regular reviews occur to ensure that the performance of the embankment is occurring in accordance with the predicted design. This review addressed opportunities to reduce settlement period, increase the settlement period or increase the surcharge to maintain time.
- Where the performance trend lines up with design prediction indicating preload can be removed or the next lift can be placed, PC to liaise and share outcomes with the detailed designer and organise a hold point sign off from the designer.
- Where the actual performance does not follow design expectations, PC to consult with GRG and, if required, with the detailed designers, to develop a course of corrective actions/ intervention measures and submit action plan to GRG for approval. Once approved, PC will provide the plan to the contractor for implementation.

Extensive real-time data monitoring and centralized data management were critical parts of risk control and the processes to monitor construction progress and control of ground movement and surface settlement. For example, the geotechnical "Dashboard" brings together all data from geotechnical and construction instrumentation and monitoring into a centralised resource. This significantly shortens the geotechnical team's decision-making process on filling rate to control short-term slope stability, compared to conventional Spreadsheet.

Over 3000 instruments were installed on W2B and nearly 3 million measurements made up to mid July 2018. Based on the average manual processing time, automating the processing of the data would generate savings in the order of $A2.5M (Zhang, 2016). Instrument types and purpose are given in Table 3.

Table 3: Instrumentation schedule

Instrument Type	Monitoring Purpose	Number
Settlement plate	Settlement at ground surface	957
Multi-depth magnetic extensometers	Settlement at depth	94
Hydrostatic profile gauge (HPG)	Settlement profile across the embankment	107
Standpipe piezometer	Baseline ground water table	72
Vibrating wire piezometer	Pore pressure change due to embankment loading	362
Inclinometer	Horizontal ground displacement	468
Settlement marker	Settlement/lateral displacement at embankment top, existing structures and pavement	797

5.3 PERFORMANCE

The performance of various instruments on W2B is summarised below:

- Settlement plates and inclinometers generally gave accurate and reliable data for settlement and lateral displacement monitoring.
- Monitoring demonstrated that data from piezometers and extensometers is variable, with some giving accurate and reliable results while others giving unreliable results; the issues demonstrate that installation practice is inadequate which needs to change because it leads to uncertain decision making.
- Underestimation of field settlement led to separation of extensometer tubing making it unable to function (for extensometers).
- Project-wide issues with HPGs with the vast majority giving unrealistic or unreliable results; the root cause may be associated with poor installation practice and/or the quality of the readout unit.

6 CONCLUSIONS AND RECOMMENDATIONS

This paper summarises the use and value of data visualisation and geotechnical instrumentation for managing construction slope stability and embankment settlement performance for soft ground treatment on the 155-km Woolgoolga to Ballina Pacific Highway upgrade. This system is the first online monitoring system that has been implemented with full success on a Roads and Maritime project, and provided an excellent platform to identify the key elements required to successfully manage and help optimise the overall design process. At the time of writing, the team has avoided slope instability of all fills on soft ground and released 75% of the fills for pavement construction with both cost and timesavings.

This system was the key to the successful delivery of the soft ground treatment on time and on budget. Key features of this system are as follows:

- Shortened turnaround time from reading to uploading to the dashboard system for early decision-making.
- Online, user friendly, flexible dashboard to the whole team.
- Real time monitoring on critical structures, real-time VW piezometers.
- Automatic uploading using standardised format.
- Automatic alarming system for early intervention on site to avoid slip failure.
- Comprehensive visualisation of various instruments on GIS Map and grouping of relevant instruments to facilitate early decision-making.
- Fast processing of large data, downloading and screenshot of monitoring results for quick internal monitoring reporting and external party data distributing.
- System reliability, availability and data quality.
- Flexible platform to new instrument types and graphs.
- Additional functions e.g. curve fitting for predicting future settlement based on monitored data.

7 ACKNOWLEDGEMENTS

The authors acknowledge the contributions of the all parties involved in this technical paper. Any opinions, findings, conclusions and recommendations in this paper are those of the authors only, and do not necessarily reflect the views of NSW Roads and Maritime Services.

8 REFERENCES

AECOM (2016). Woolgoolga to Ballina Early Works Detailed Geotechnical Design for Wave 1 Soft Soil Sites SS-05 and SS-06

Asaoka A (1978). Observational procedure of settlement prediction. *Soils and Foundations*. 18(4), 87–101

Kelly RB, Sloan SW, Pineda JA, Kouretzis G, Huang J, (2018). Outcomes of the Newcastle symposium for the prediction of embankment behaviour on soft soil, *Computers and Geotechnics*, 93, 9-41

Ladd C (1991). Stability evaluation during staged construction. *Journal of Geotechnical Engineering*, 117(4), pp. 540-615

Loganathan N *et al* (1993). Deformation analysis of embankments, *Journal of Geotechnical Engineering*, 119(8) American Society of Civil Engineers

Matsuo M, Kawamura, K. (1977). Diagram for construction control of embankment on soft ground. *Soils and Foundations* 17(3), 37−52

Nicholson DP, Tse C, Penny C (1999), *The Observational Method in ground engineering - principles and applications*, Construction Industry Research and Information Association (CIRIA) Report 185, London, UK

Pacific Complete intranet https://reports.pacificcomplete.com.au

RMS 2018, http://www.rms.nsw.gov.au/projects/northern-nsw/woolgoolga-to-ballina/soft-soil-work/index.html, accessed July 2018.

Saye SR, Ladd CC (2004). A*nalysis of geotechnical instrumentation to assess foundation performance of I-15*, Geotechnical Engineering for Transportation Projects: 2103-2114

Tavenas F, Mieussens C, Bourges, F. (1979). Lateral displacements in clay foundations under embankments, *Canadian Geotechnical Journal*, 16, pp. 532-550.

Zhang H, Gombault N, Choi B. (2016). An innovative geotechnical monitoring system for soft ground treatment on W2B Pacific Highway upgrade project, AGS (Sydney Chapter) Symposium on ground stabilisation techniques for problematic soils and unstable rocks.

EXPERIENCE OF OVERCORING THE ANZI STRAIN CELL IN HQ EXPLORATION BOREHOLES TO DETERMINE THE THREE DIMENSIONAL IN SITU STRESSES AT DEPTHS APPROACHING 1KM

Kenneth W. Mills[1] and Jesse W. Puller[2]

[1]Principal Geotechnical Engineer, SCT Operations Pty Ltd, kmills@sct.gs, 0242222777
[2]Senior Engineering Geologist, SCT Operations Pty Ltd, jpuller@sct.gs, 0242222777

This paper describes recent use of the ANZI (Australia, New Zealand Inflatable) strain cell and the overcoring method of stress relief in an HQ exploration borehole at depths approaching 1km to determine the three dimensional in situ stress field in a one-day operation. The stages of a routine overcoring operation are presented to illustrate each step of the process. The results from a European metalliferous mining site are presented to illustrate the process of characterising the three dimensional in situ stress environment when multiple high confidence measurements are achieved.

The ANZI strain cell is an instrument system that uses the overcoring method of stress relief to determine the three dimensional in situ stresses in rock. The instrument has been used successfully for over three decades in numerous underground mining and civil projects but technical advances over the last decade have allowed the system to be deployed routinely in surface exploration boreholes. Recent development of a downhole electronic data logger, a wireline enabled drilling system and an instrument deployment system has simplified the process of obtaining three dimensional overcore measurements at previously inaccessible depths remote to any underground excavation.

The capability to deploy ANZI strain cells from surface exploration boreholes represents a significant breakthrough for the design of underground civil structures. High confidence characterisation of the in situ stresses at design stage provides the opportunity to design key infrastructure to take advantage of the in situ stress field from the outset before any excavation and construction activity even begins. Understanding the three dimensional in situ stress field not only provides a measure of the magnitude and direction of loads acting within the rock mass, it is also provided insight into the mechanics of the all the various processes driving ground deformations.

Keywords: overcore measurement, ANZI Strain Cell, three dimensional in situ stress.

1 INTRODUCTION

The overcoring method of stress relief is a method for determining three dimensional in situ stresses in rock. Overcoring the ANZI strain cell provides determination of the three dimensional in situ stress field, several independent estimates of the mechanical properties of the rock at a range of confining pressures, and importantly, an indication of the confidence that can be placed in each measurement.

A brief overview of the history of the ANZI cell is provided for context. The operation of the instrument and the various stages of testing used to provide confidence in the integrity of each measurement are described. Recent advances in the ANZI overcore system to enable measurements in surface exploration boreholes to depths approached 1km are also presented. These include:

- wireline enabled drilling techniques to prepare the pilot hole
- modular instrument deployment and pressurisation system
- high precision downhole strain, pressure and temperature logging
- increase in the number of axial gauges to measure axial strain variations.

Overcore measurements made in an underground European metalliferous mine illustrate the spatial and vertical variability in the stress field that can occur at the local and mine scale.

2 STRESS MEASUREMENT TECHNOLOGY AND LIMITATIONS

The concept of stress is a convenient engineering construct to link displacements and their derivative strain with forces through idealised models of material behaviour. Displacements and strain changes can be measured, but stresses cannot be measured directly. Changes in stress can be calculated from changes in strain by assuming a continuous, homogeneous, isotropic, linear elastic (CHILE) model of material behaviour.

To determine the in situ stress requires:

- a change in loading conditions, ideally from in situ conditions to conditions of zero stress
- the measurement of changes in six independent strains during stress relief
- an assumed material behaviour that relates stress to strain.

This relatively involved process means that in situ stresses determined from overcoring are in practice an estimate based on imperfect strain measurements and idealised rock behaviour. Although the term "stress measurement" is widely adopted, the limitations of the terminology should be recognised.

The overcoring process used with the ANZI strain cell allows a stress change in the rock, from the in situ state of stress at the start of overcoring to a zero state of stress at the end of overcoring. The strain changes measured by the ANZI strain cell during this process allow for the full three dimensional stress tensor to be determined based on an assumption of CHILE material behaviour. In practice, there are a variety of influences that are found to complicate this process, including drilling induced effects described by (Mills et al 2016), material behaviours that are not captured by the CHILE model described by (Mills and Gale 2016).

3 DEVELOPMENT OF DOWNHOLE OVERCORING USING THE ANZI STRAIN CELL

Mills and Puller (2017) provide a brief history of the overcoring method of stress relief from its beginnings by Lieurance (1933) in the 1930's, through to the use of strain gauged techniques in single boreholes from the 1950's onward. In the 1970's, Hiltscher et al (1979) developed an overcoring method for use in deep boreholes, where the pilot hole could be drilled without the need to withdraw drilling rods. This method is reported by Hallbjorn (1986) to have been successfully used to measure in situ stresses in exploration boreholes to depths of 500m. The ANZI overcoring system is similar to the method described by Hiltscher et al. (1979).

In 2014, a 48mm diameter (reduced from 58mm) version of the ANZI strain cell was developed to allow overcoring with a standard HQ coring bit. This version of the instrument was initially monitored using a data cable that ran to a logging system on the surface. Solid installation rods were initially used but these limited the installation depth to less than about 100m. These were replaced with a system using two cables deployed on a mechanised cable drum through the drill pipe. The first cable was connected to the instrument and monitored at the surface for the duration of the overcoring. The second cable was used to pressurise the instrument during installation and initial testing and then disconnected and withdrawn prior to overcoring. This approach was still somewhat cumbersome at depths greater than about 100m.

These various limitations were overcome with the development of:

- a drive sub installed behind the core barrel that provides for a wireline deployable downhole drilling system similar to the approach described by Hiltscher et al (1979)
- a high precision downhole data logging system fixed to the back of the ANZI strain cell
- a wireline enabled deployment system for the instrument and data logger
- an instrument pressurisation system that uses the drill pipe.

Mills and Puller (2017) describe in detail how these revised drilling, installation and data logging systems now enable routine overcore measurements at depths of 850m within a 12 hour shift.

4 OPERATION OF THE ANZI STRAIN CELL

The design of the ANZI strain cell is focused on providing systems to allow the confidence in each point measurement to be assessed. The confidence that can be placed in each estimate of the in situ stress varies for a range of reasons. The key is to be able to differentiate those as well as having sufficient duplication of measurement for rock behaviour to be characterised and departures from CHILE behaviour compensated for.

Figure 1 shows a photograph of the 48mm diameter version of the ANZI Strain Cell with the data logger attached prior to installation and one instrument after overcoring. The instrument has an inflatable polyurethane membrane with 18 electrical resistance strain gauges exposed on its outer surface. When the membrane is covered in epoxy cement and inflated during installation, the electrical resistance strain gauges become directly bonded to the wall of the pilot hole allowing direct measurement of strain changes in the rock as it is overcored. Further detail on the ANZI Strain Cell and its operation are provided in Mills (1997) and its specific application to overcoring in deep exploration boreholes is described in Mills and Puller (2017).

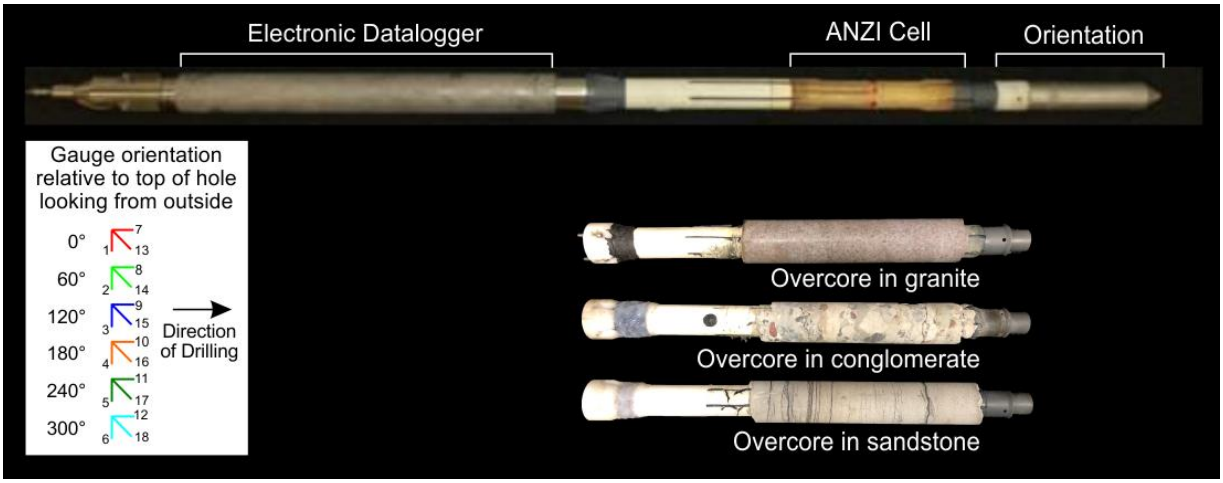

Figure 1: 48mm ANZI Strain Cell and downhole data logger prior to installation and recovered overcore, the result of which are used as examples throughout this report

There are six stages in the standard overcoring test procedure using the ANZI strain cell: preparation of the hole, installation, in situ pressure test, overcoring stress relief, biaxial pressure test and laboratory testing of the core recovered from the pilot hole. The following sections provide an overview of each of these stages.

5 BOREHOLE PREPARATION

A borehole is drilled to the measurement depth using standard drilling procedures. The borehole is commonly HQ size. A casing advancer drive sub is installed behind the core barrel. The end of the hole is prepared so that the HQ core stub is ground away and a centralising conical indentation is formed at the end of the hole. A small diameter pilot hole is then drilled concentrically from the end of the conical indentation in the end of the HQ hole, for a distance of 1m. The core from this pilot hole is inspected to determine the ideal horizon for instrument installation. The core from the pilot hole is retained for material testing in the laboratory.

6 INSTALLATION

Figure 2 shows a photograph of the instrument during installation. The outer surface of the ANZI strain cell is coated with a bespoke epoxy cement and deployed into the drill pipe on the wireline overshot with dry-release. Once the installation assembly is released from the overshot upon striking water, it floats downward until seating on the landing ring in the back of the core barrel. The pre-determined distance from the landing ring to the strain gauges positions the ANZI cell in the pilot hole at the target depth.

Figure 2: ANZI strain cell, data logger and installation assembly being readied for deployment in an inclined hole drilled to a depth of 740m. The collar of the hole is approximately 1340m below the ground surface.

Pressure is applied internally to the ANZI cell membrane by generating a positive pressure differential between the inside and the outside of the drill pipe. This pressure causes the strain gauges to be pressed directly against the pilot hole wall. Most of the epoxy cement coating is extruded away from the strain gauges and membrane under the pressure applied during installation. The membrane profile is designed to facilitate this process and leave a very thin (0.3-0.5mm) layer of cement between the gauges and the rock. When the cement has cured, typically 3-4 hours after installation depending on rock temperature, the strain gauges are bonded directly to the rock.

7 IN SITU PRESSURE TEST

Once the cement has cured, the internal pressure is varied to conduct a pressure test using the instrument as a dilatometer or pressuremeter. This test is used to:

- confirm that the strain gauges are well bonded to the rock
- provide an estimate of the in situ elastic properties of the rock under plane strain conditions prior to any disturbance that may be caused by drilling during the overcoring process
- provide, under some circumstances, independent confirmation of the in situ stress direction based in variation in elastic modulus around the borehole following the technique described by Mills and Gale (2016).

Figure 3 shows an example of a pressure test. The six circumferential gauges show the largest strain change. The six axial gauges show almost no change or a slight stretching consistent with the almost plane strain conditions at the centre of the pressurised length of borehole. The 45° gauges show a strain change midway between the circumferential gauges and axial gauges.

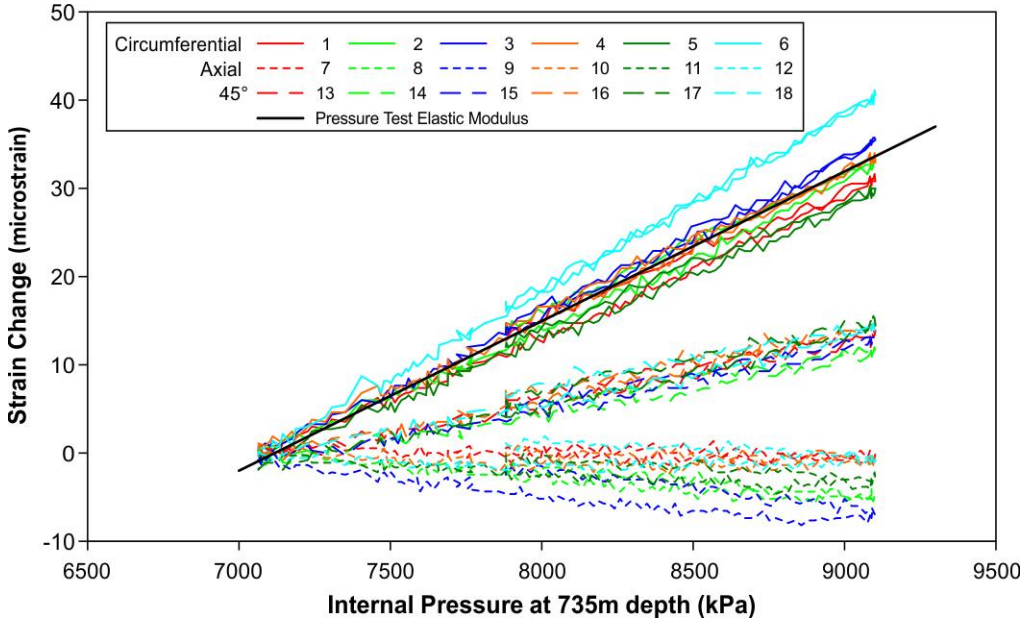

Figure 3: In situ pressure test result for ANZI instrument EMM5

8 OVERCORING

The ANZI strain cell overcoring operation is conducted in much the same way as for other instruments that use the overcoring stress relief method. Figure 4 shows an example of an ANZI overcoring result with the strain changes plotted relative to borehole depth/drilling distance. The final strains on all gauges are tensile, consistent with the relief of the compressive in situ stresses.

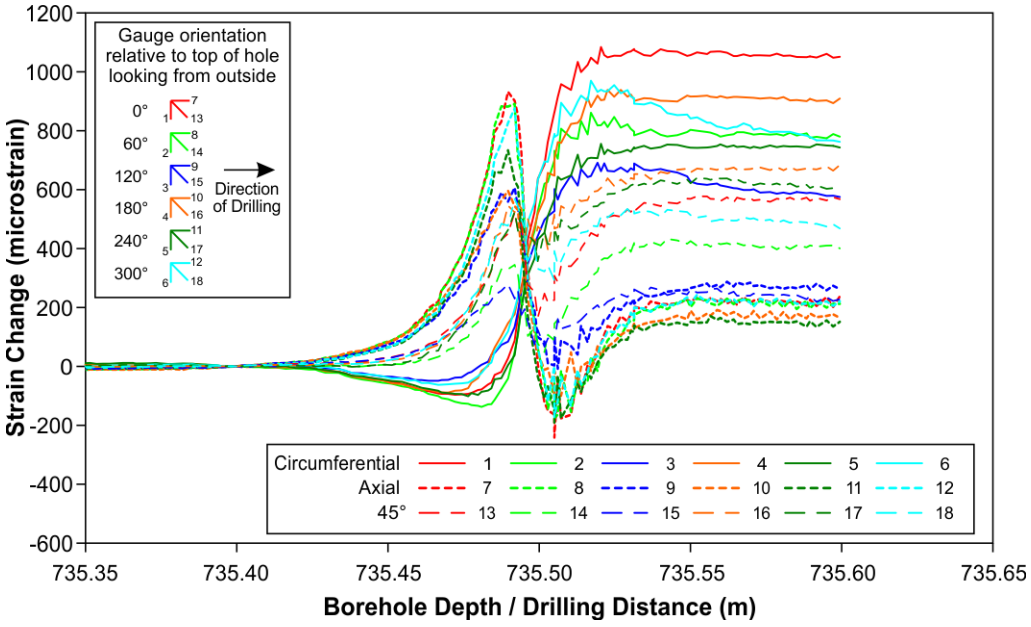

Figure 4: Strain changes observed during overcoring for ANZI instrument EMM5

The logger records strain, pressure and temperature every few seconds commencing before the instrument is deployed until it is recovered. The general form of the overcoring strain changes can be used as a basis to identify rosettes of strain gauges that may be behaving irregularly and should be ignored in the final analysis. Correlation of strains between opposing gauges and by the six independent measurements of axial strain provides an insight into rock behaviour during stress relief and an immediate indication of the level of confidence that can be placed in the strain data.

9 BIAXIAL PRESSURE TEST

A biaxial pressure test is conducted after the overcore is recovered. External pressure is applied incrementally to the outside of the rock annulus recovered when the pilot hole has been overcored with the instrument inside it. The elastic modulus and Poisson's ratio of the rock material can be estimated from this test at a range of different pressures. The strain changes measured provide not only an estimate of the CHILE rock properties but are also useful as an indicator of non-CHILE behaviour that may have been caused for example by permanent deformation during the overcoring process.

Figure 5 shows an example of a biaxial test result. The circumferential gauges show compressive strain changes consistent with the application of external pressure to the outside of the overcored rock annulus. The axial gauges show tensile going strain changes due to the Poisson's ratio effect of the external pressure being applied to the rock annulus.

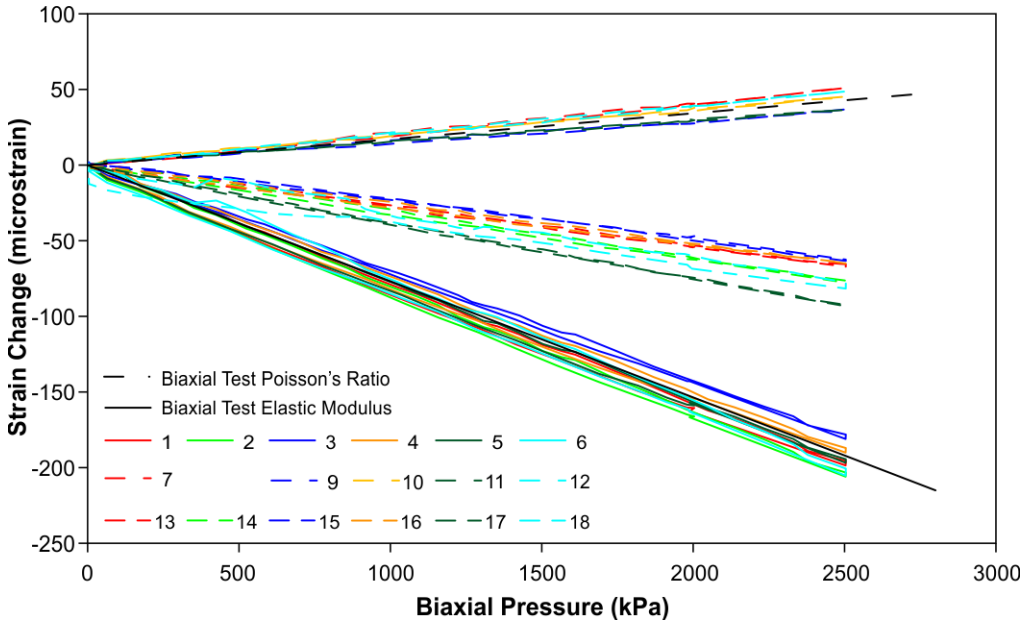

Figure 5: Biaxial test result for ANZI instrument EMM5

10 LABORATORY TESTING

Core recovered from the pilot hole at the location of the strain measurements is tested in a multi-stage uniaxial compression test to further confirm the elastic properties of the rock material. Axial and circumferential strain gauges and the load/displacement records of the compression test all the elastic properties of the rock to be estimated during three or more load/unload cycles up to failure in uniaxial compression.

11 ASSESSMENT OF ELASTIC PROPERTIES

The elastic properties of the rock are determined in three separate tests:

- in situ pressure test conducted prior to overcoring
- biaxial pressure test conducted after overcoring
- laboratory test on core recovered from the pilot hole.

These three tests are conducted on the rock at various stages of the measurement process and various confining stresses. In a CHILE material all three tests would indicate the same values of elastic properties but in practice there are commonly variations. These different conditions provide insight into the rock behaviour and the impact of drilling on the rock as it is unloaded and recovered from the hole.

Variations in elastic properties are commonly observed and these variations have provided useful insights into the processes that occur at the tip of a borehole during drilling and a range of factors that affect the behaviour of rock materials. Figure 6 shows an example of the elastic modulus variation at different confining pressures. The confining pressure is represented in Figure 6 as the first stress invariant which is the sum of the three principal stresses. A single value of elastic modulus is required to estimate the in situ stresses from the measured strains. Given the variation typically observed, an elastic modulus midway between the first stress invariant of the in situ stresses (pre-overcoring stress state) and zero (post-overcore stress state) is used in the analysis.

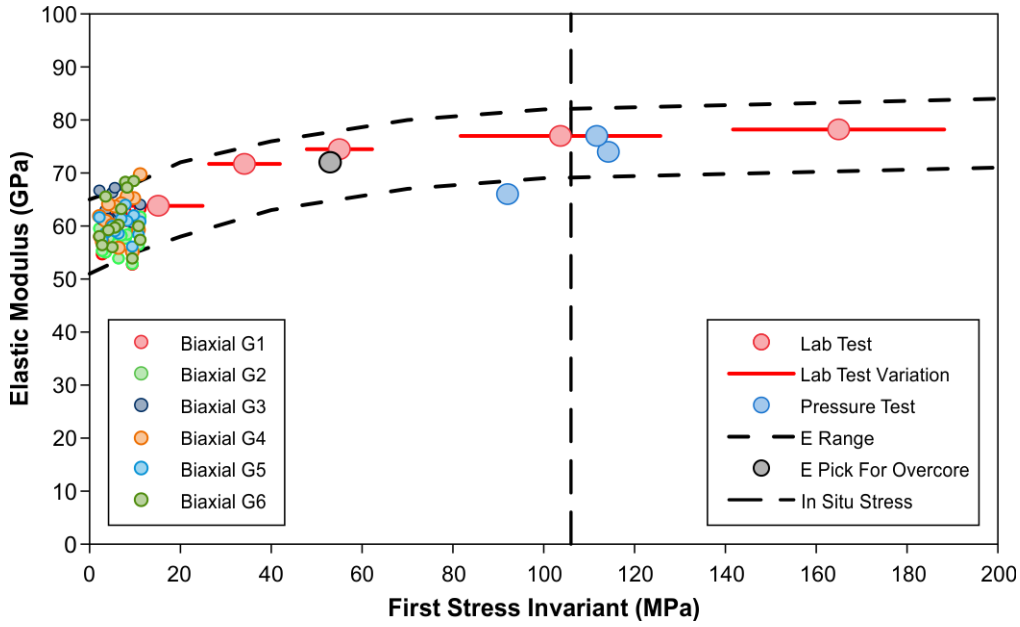

Figure 6: Variation of elastic modulus with first stress invariant (sum of the three principal stresses) for ANZI instrument EMM5

12 CASE STUDY OVERCORING AT A DEPTH OF 2050M BELOW SURFACE IN A METALLIFEROUS MINE

A single HQ borehole was collared from at 1340m below surface in an underground European metalliferous mine and drilled to a depth of 740m. The borehole dipped at an angle of 81°. Three campaigns of overcore measurements were conducted at depths in the borehole of approximately 50m, 350m and 740m. Two high confidence point measurements were made at each of the three measurement horizons. The stress field at this site was characterised using the results from these overcore measurements.

The interpreted in situ stress results from these six overcore measurements are summarised in Figure 7. There is close agreement of the in situ stresses indicating a stress field that is consistent in orientation over the length of the hole.

Four of the measurements also show close agreement in magnitude with the major principal stress having a well constrained magnitude of 53MPa, dipping 30° at a bearing of 195°. The other two overcore measurements, EMM4 and EMM5, indicate stresses that are consistent with the overall stress field in terms of orientation but show stress magnitudes that have been locally reduced at the point of measurement. These two measurements indicate the north-south major principal stress is 12MPa to 24MPa lower than the other point measurements, including those that are only 6m away. The cause of this variability is not known but anisotropy and differences in material properties of the rock between overcore locations are comparatively small and not thought to be responsible for stress reductions observed.

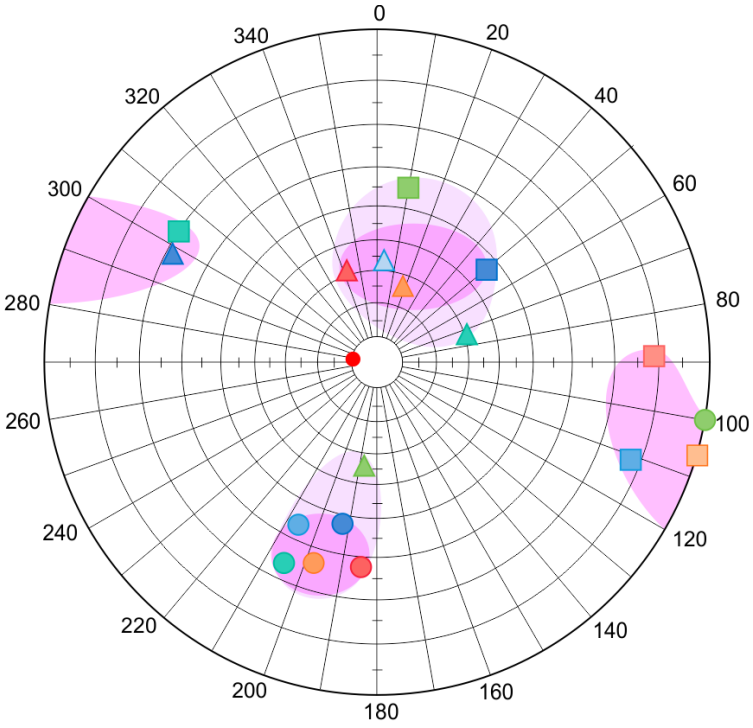

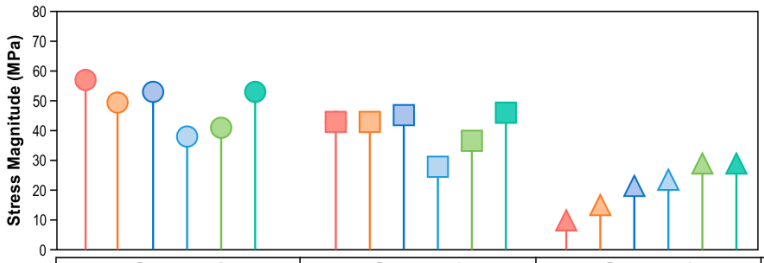

				Group 1			Group 2			Group 3			Sigma V	
Cell	Depth (m)	E	v	Mag. (MPa)	Dip (°)	Bearing (°GN)	Mag. (MPa)	Dip (°)	Bearing (°GN)	Mag. (MPa)	Dip (°)	Bearing (°GN)	Mag. (MPa)	I1 (MPa)
EMM1	57.5	62	0.22	59	29	185	43	11	89	10	59	341	23	112
EMM2	63.5	62	0.25	49	27	197	44	0	107	16	63	18	23	109
EMM3	345.5	73	0.23	53	32	209	45	12	111	21	56	3	31	118
EMM4	351.5	80	0.26	39	39	191	23	21	299	28	44	50	32	90
EMM5	735.5	72	0.23	29	56	189	41	0	100	36	34	10	31	106
EMM6	741.4	67	0.23	53	23	205	46	20	304	31	59	71	36	128

Figure 7: Stress measurement results from a European metalliferous mine

Figure 8 shows the depth/stress magnitude relationship for the principal stresses and for the first stress invariant. When EMM4 and EMM5 are ignored, the magnitudes of σ_1 and σ_2 are approximately constant at 53MPa and 44MPa respectively over the length of the borehole. The minor principal stress shows an approximately linear trend of increasing with depth consistent with increasing weight of overburden rock.

The ratio of σ_1 and σ_2 (i.e. the north-south and east-west stresses) is consistent with depth and averages approximately 1.2. This ratio is low when compared to other locations SCT have conducted overcoring measurements.

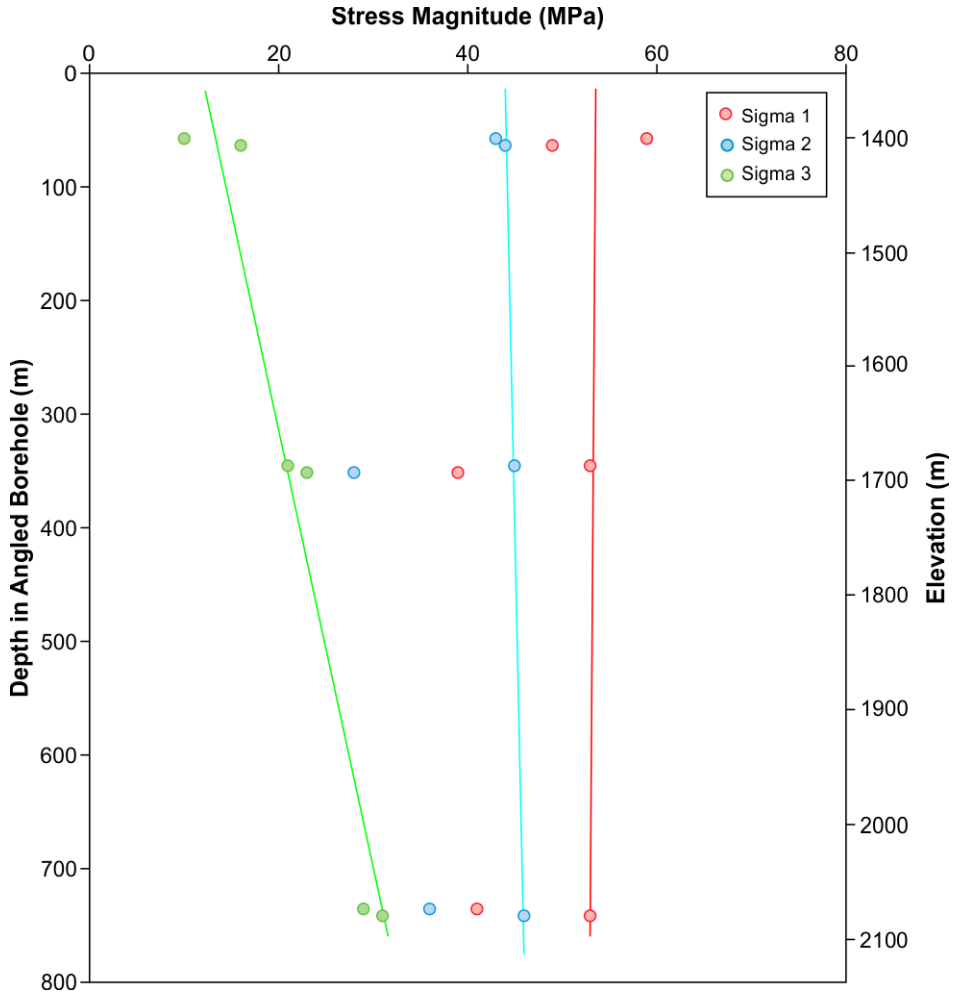

Figure 8: Depth/stress relationship for the three principal stresses and first stress invariant at a European metalliferous mine

13 CONCLUSIONS

The capability to deploy ANZI strain cells in exploration boreholes represents a significant technological breakthrough for the design of underground mines and underground excavations generally. Being able to obtain high confidence measurements of the three dimensional in situ stresses at the planning stage of any underground construction activity provides the opportunity to take advantage of these stresses in design of underground structures. Not only does it become possible to protect key infrastructure by locating it away from areas of stress concentration, advantage can be taken of the major stresses to promote caving through appropriate design.

The high levels of redundancy in both the instrument and the measurement technique are designed to provide an indication of the confidence that can be placed in each result and to enhance the understanding of material behaviour at the point of measurement and ground behaviour at the site more generally.

The ability to characterise the three dimensional in situ stresses at a site by making multiple point measurements is demonstrated. Understanding the spatial and depth related variability in the stress field at a local and mine scale becomes possible when multiple high confidence measurements are achieved.

14 REFERENCES

Hallbjorn L. (1986) Rock stress measurements performed by the Swedish Power Board. Proceedings of International Symposium on Rock Stress and Rock Stress Measurements, Stockholm, 1-3 September 1986 pp 197-205.

Hiltscher R, Martna J and Strindell L (1979) The measurement of triaxial rock stresses in deep boreholes. Proceedings of the 4th International Congress on Rock Mechanics, Montreaux, Switzerland 2-8 September 1979 pp 227-34.

Lieurance RS (1933) Stresses in the Foundation at Boulder Dam. Technical Memo. 346, Bureau of Reclamation, Denver, Colorado.

Mills KW (1997) In situ stress measurement using the ANZI stress cell. Proceedings of the International Symposium on Rock Stress, Editors K. Sugawara and Y. Obara, Balkema Rotterdam, P. 49-154.

Mills KW and Gale WJ (2016) In situ measurements of stress related elastic modulus variation using the ANZI strain cell. Proceedings of the 7th International Symposium on In-Situ Rock Stress, May 10-12, 2016 Tampere Finland P. 385-396.

Mills and Puller (2018) Experience of using the ANZI Strain Cell for three dimensional in situ stress determinations in deep exploration boreholes. Proceedings of 38rd International Conference on Ground Control in Mining Morgantown July 23-25 2018 in print.

Mills KW, Zoorabadi M, and Puller JW (2016) Strategy to compensate for axial strains induced by drilling during overcoring" Proceedings of the 7th International Symposium on In-Situ Rock Stress, May 10-12, 2016 Tampere Finland. P. 320-332.

VIBRATION TRANSFER MOBILITY MEASUREMENTS COMBINING FALLING WEIGHT AND IMPACT HAMMER EXCITATION METHODS

Giovanni Farotto and Alexis Bigot
SIXENSE, Lyon 69 - France, +33 (0)4 72 69 01 28

giovanni.farotto@sixense-group.com

ABSTRACT

For construction in an urban environment, vibration transfer mobility measurements are useful when developing detailed prediction of ground-borne vibration and ground-borne noise for underground or surface rail transit systems. These measurements typically use a large impact hammer to generate impulses in the soil and an array of accelerometers or velocimeters to measure the vibration response to the impulses. The correlation between the force and the vibration results is used to characterize the transfer function of the ground in a localized area.

The effectiveness of this approach is limited by the amplitude of the force impulse when dealing with larger zones and SSI attenuation, especially for larger buildings, where a satisfactory signal-to-noise ratio cannot be achieved with traditional methods. In some of these cases, a seismic vibrator truck can be deployed on site, but site specific constraints do not always make this possible.

To address these shortcomings, a double stage measurement method has been developed by using a "weight drop" approach combined with the impact hammer.

The methodology that combines the processes of the two impulse-inducing methods and controls the uncertainty of the measurement chain is presented in this paper. The technique will be detailed and an application case on a shaft of the "Grand Paris Express" project will be presented with emphasis on the added value for the parties involved.

1 INTRODUCTION

Detailed predictions of railway vibration for environmental assessments require knowledge of the specific ground vibration propagation characteristics of the soil in the project area. A method to measure the soil propagation characteristics ("transfer mobility") was developed by Nelson and Saurenman (1988). This method has been adopted by the Federal Transit Administration (FTA) (1995) and the Federal Railroad Administration (FRA) for detailed analysis of railway vibration. The transfer mobility measurement, as described in the FTA and FRA guidance, is carried out using a hammer to generate an impulsive force into the ground, of which the resulting vibration is measured at various locations near the point force using geophones.

A transfer function is calculated from the measured force and vibration data using Fast Fourier Transform (FFT) techniques. The transfer function calculation also generates a coherence function that can be used to verify the integrity of the recorded data. This data is then used to estimate the vibration propagation over distance as a function of frequency.

Some analysis methods such as the MLS vibration measurement method (Singleton Jr, 2005) are suitable for transfer mobility testing, but this system may not be suitable for measuring transmission into massive structures such as a cut-and-cover subway structure or masonry building.

Alternative methods have thus been developed for the purpose of this study.

2 CONTEXT

An exploratory shaft has been constructed in Saint-Cloud (France), where a metro station is to be constructed for the Grand Paris Express project in Paris.

Vibration transfer mobility measurements are being carried out to provide additional information for the model used to assess vibration impact of the construction works and the future metro line operation.

The distance between the exploratory shaft and sensitive receptors (hospital) is approximately 20 meters. The shaft and the hospital are on either sides of a street. Given the distance and the ambient vibration characteristics of the urban environment, it would be too difficult to carry out classic transfer mobility measurements with a traditional impact hammer.

Therefore, an alternative had to be sought and a combined mass / hammer method was developed to overcome the local restraints.

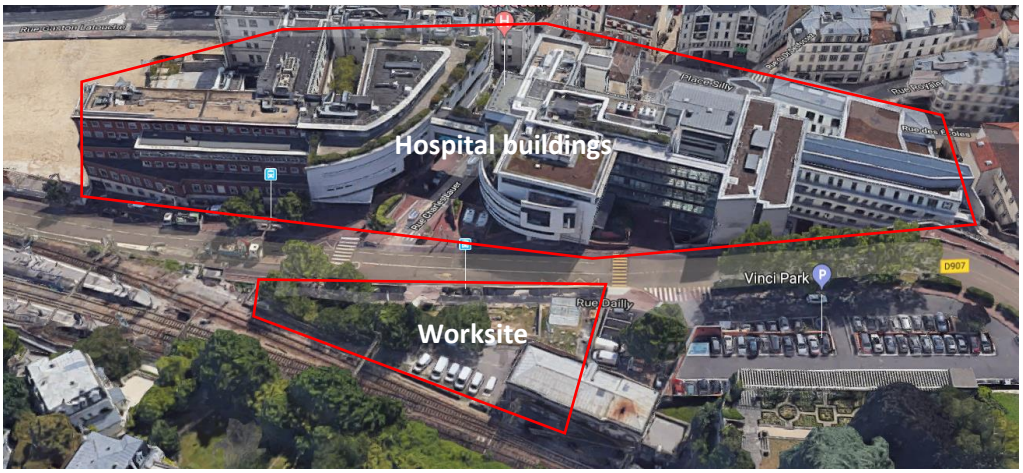

Figure 1: Aerial view of the worksite and sensitive buildings

3 MEASUREMENT METHODOLOGY

3.1 GENERAL PRINCIPLES

In order to measure the vibration response inside the sensitive buildings located on the other side of the road, the equipment chosen to induce the impulse in the ground is a 600 kg mass, falling from between 5 and 7 m high.

Since the impact force of the masses cannot be directly measured, an indirect approach was used and measurements were carried out at predefined reference points to establish the vibration responses of both the falling weight and impact hammer.

The force of the impact hammer was measured to determine the force of the falling mass.

The following pictures (Figure 1) show the installation of reference points (four sensors around the impact position) inside the exploratory shaft and the equipment used for the measurements.

Figure 1: Installation of reference points

3.2 SENSOR NETWORK

A network of vibration sensors was installed inside and outside sensitive buildings, as shown in the figure below. Sensors are tri-axial geophones (SYSCOM MR3000C), configured for continuous and synchronized vibration recording. The sensors have been installed inside the buildings on various floors.

For the purpose of this paper, we will focus on three measure points in particular (circled in the aerial view in the figure below), plus the reference point at the bottom of the shaft, as shown in the figure below. The other sensors are not relevant for this transfer mobility analysis and will be ignored.

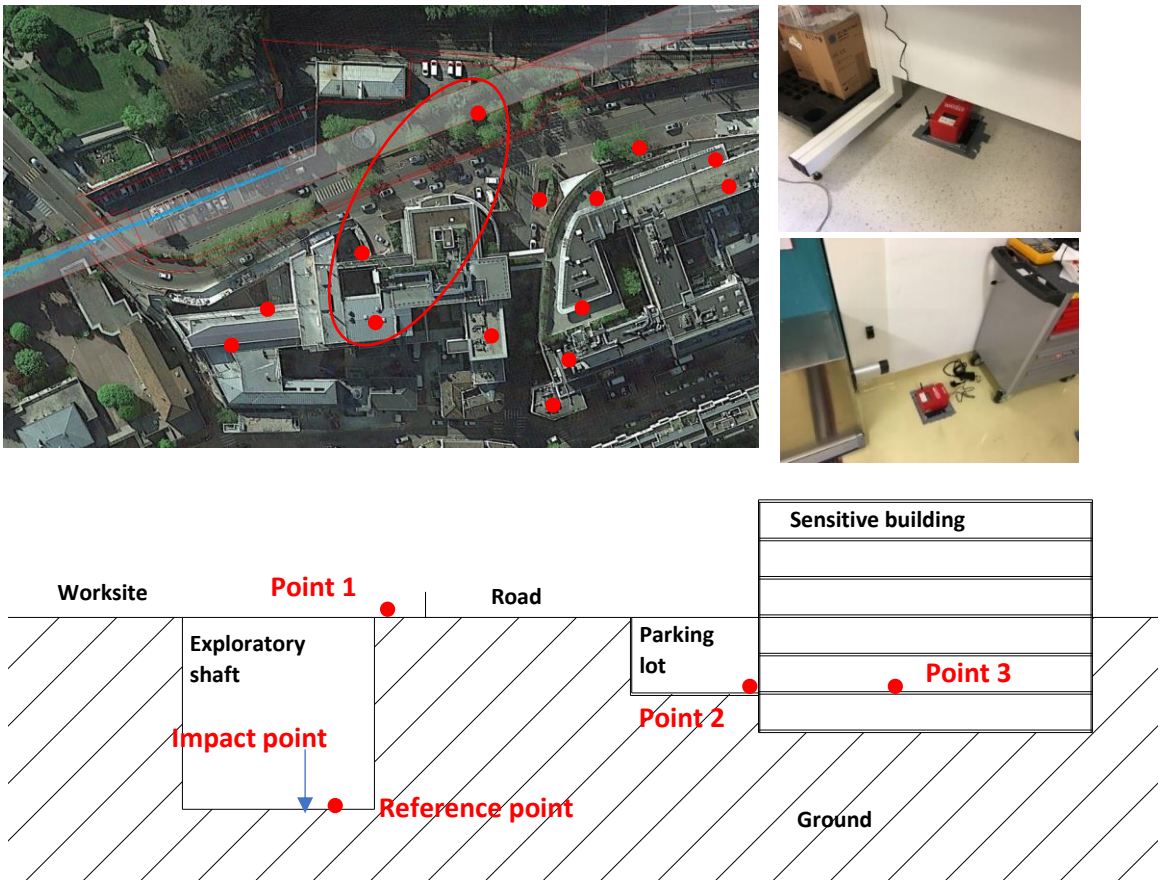

Figure 2: Sensors location

3.3 MEASUREMENT CONDITIONS

All sensors have been synchronized and installed with the same orientation (y-axis facing north).

The sensors inside the buildings were fixed to the floor using epoxy glue, while the sensors on the ground outside were fixed using metal spikes.

For the falling mass, a layer of sand was laid on the ground, to ensure some level of energy distribution over frequencies during the impact.

For the impact hammer, a metallic plate (200 x 200 x25 mm) was laid over the impact point in order to ensure wider shock distribution.

For improved repeatability, a series of at least 15 impacts were carried out for impact hammer tests and for falling weight tests. Each time, the falling height was set to approximately 7 m.

A set of four reference geophones were also deployed in four different directions, equidistantly around the impact point at the bottom of the shaft to account for heterogeneous soil response.

Other factors leading to measurement uncertainty due to technical constraints were:

- The geometrical precision of the point of impact of the falling weight, due to the difficulty of the weight drop installation inside the exploratory shaft.
- The background vibration, even though the test was carried out at night.

All measurements have been performed with a 1000 Hz sampling rate.

Results were given in 1/3 octave band within the 4 Hz – 315 Hz frequency range.

Each impact sample is set to 1-second duration for all measurements.

4 MEASUREMENT RESULTS REPEATABILITY AND PRECISION

In order to check the reliability of measurements in terms of repeatability and precision, two main controls were performed on each measurement: a coherence check and a background noise check.

For each velocity measurement, a control of signal over background noise was calculated by comparing the signal PSD (power spectral density) to the background noise PSD (background noise being the signal recorded by the sensor immediately after the impact response).

As for the impact mass measurements, the coherence function was calculated between the impact mass force and the velocity measured at each reference point.

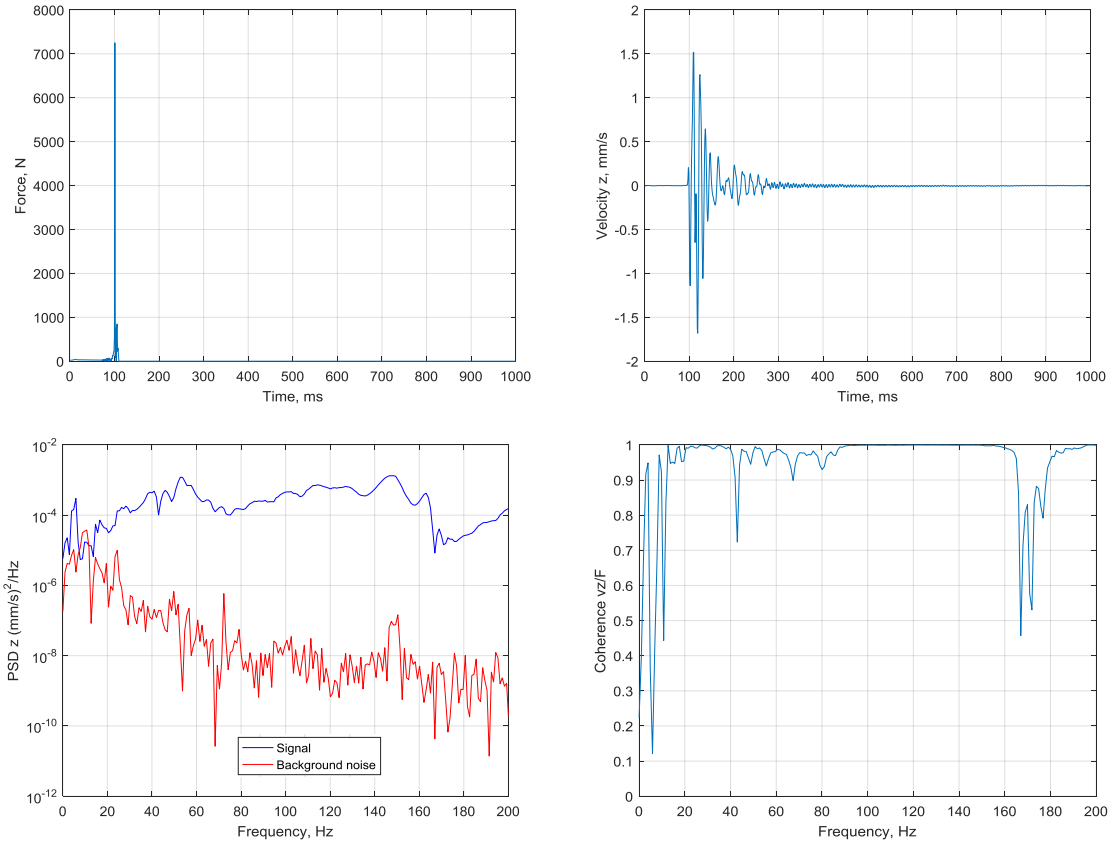

Figure 3: Falling weight measurement example.
(1) Force (2) Velocity at reference point on vertical axis (3) PSD on vertical axis (4) Coherence function (v/F)

For the falling weight measurements, the same function was calculated between the velocity measurements at the receiver point and each reference point.

An example of these calculations is shown below for the receiver point just outside the shaft (Point 1), on the surface.

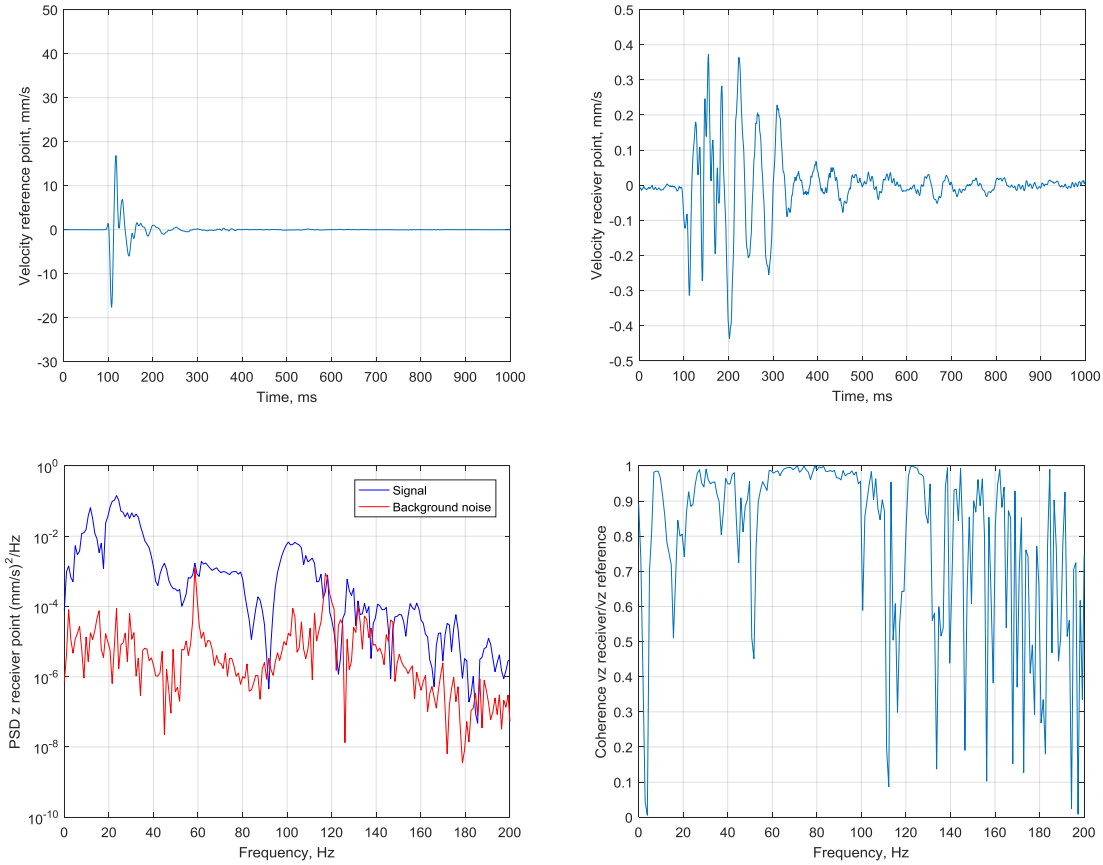

Figure 4: Coherence between a reference point and Point 1.
(1) Velocity at reference point (2) Velocity at receiver point (3) PSD on vertical axis (4) Coherence function (v/F)

Another set of results is given here for a receiver point just outside the nearest sensitive building (Point 2), on the base of one of the outer walls facing the worksite and the shaft.

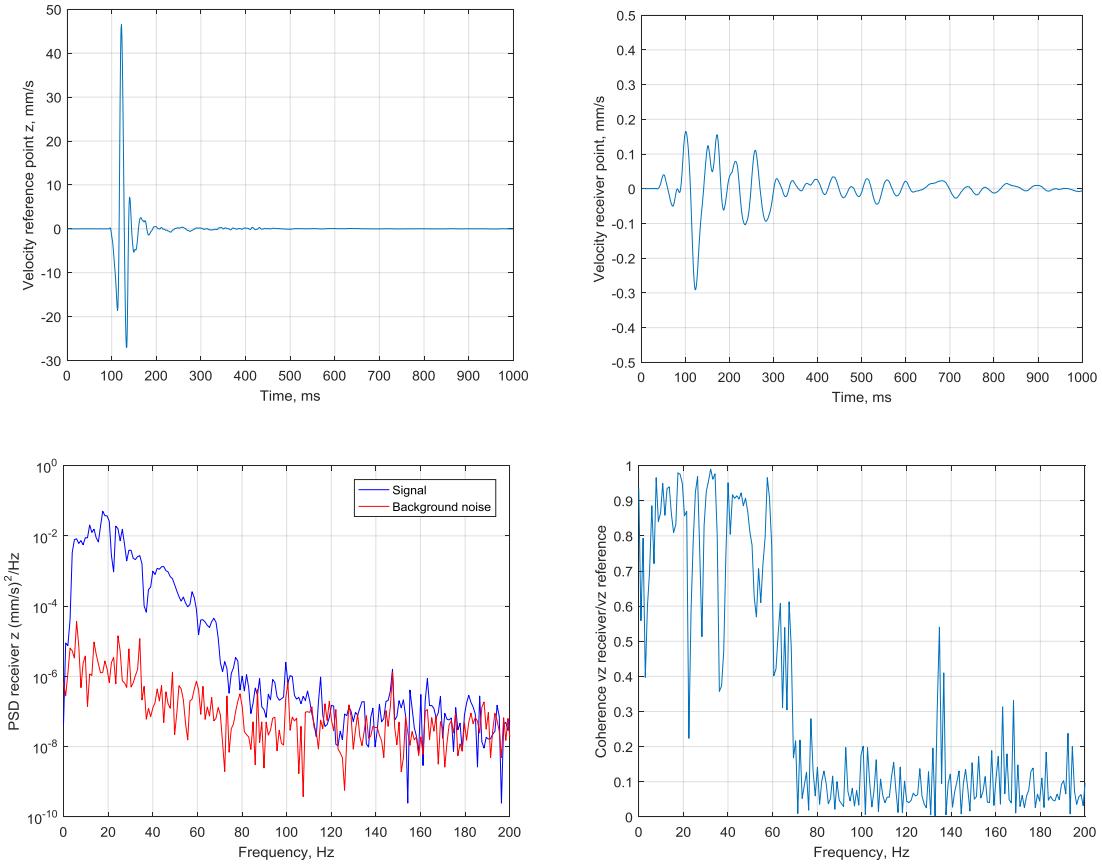

Figure 5: Coherence between a reference point and Point 2.
(1) Velocity at reference point (2) Velocity at receiver point (3) PSD on vertical axis (4) Coherence function (v/F)

The final example given below is for the receiver points inside the sensitive buildings (Point 3), approximately 40m from the impact point.

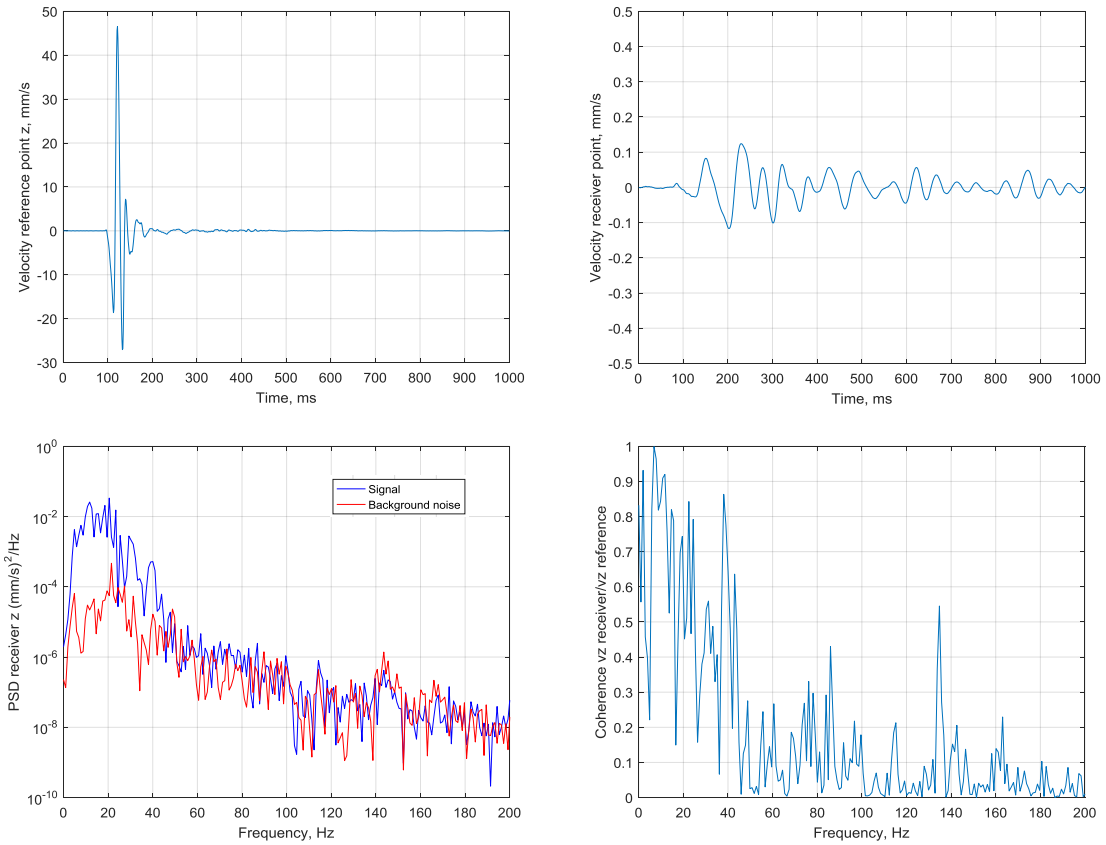

Figure 6: Coherence between a reference point and Point 3.
(1) Velocity at reference point (2) Velocity at receiver point (3) PSD on vertical axis (4) Coherence function (v/F)

Basic results remarks:

The comparison of the three sets of results shows that the energy of the falling weight is high enough to excite the building, but given the frequency response of the building itself and the background noise, the impact response at Point 3 is similar to the background noise for most of the frequency range over 50 Hz.

For the receiver point just outside the shaft (Point 1), the impact response is high enough compared to the background noise for most of the frequency range up to 200 Hz.

As for the receiver point halfway, on the outside wall of the building (Point 2), the impact response is higher than the background noise up to 120 Hz.

5 TRANSFER MOBILITY ANALYSIS

The analysis of the impact mass measurement results gives an indication of the local transfer mobility at the bottom of the shaft, between the reference point and the impact point. The calculation methodology applied (Verbraken, 2012) is the following:

$$\text{Transfer mobility} = L_{v\,ref} - F_{exc} \text{ (vibration level – excitation force level)} \quad (1)$$

This transfer mobility is plotted below for all impact hammer tests. The black dashed curve gives the average values of the transfer mobility over all the realized tests in vibration decibel (dBV, reference $5*10^{-8}$ m/s).

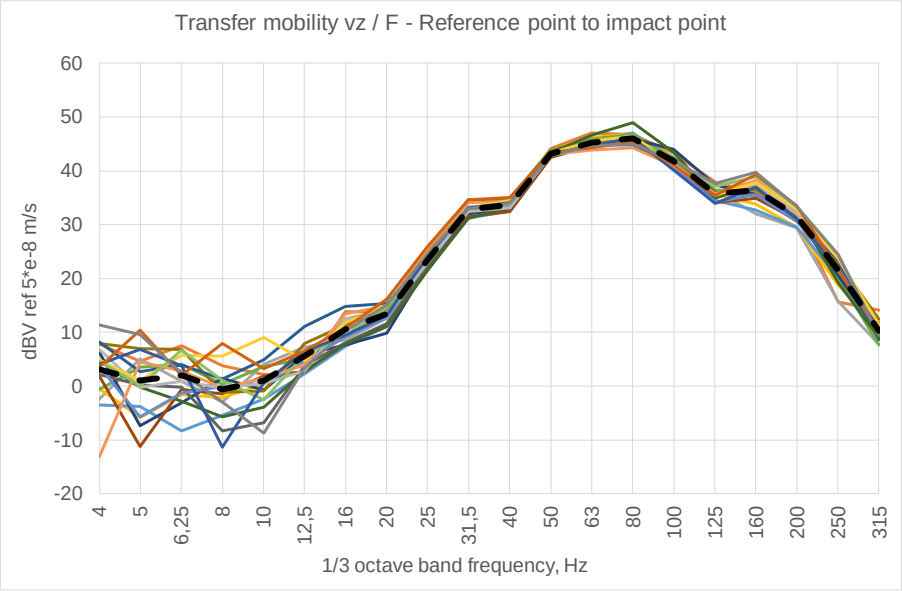

Figure 7: Transfer mobility vz/F – Reference point to impact point

As for the falling weight tests, by comparing the local transfer function and the vibration measurements at the reference point, we can estimate the falling weight impact force (F_{excW}).

$$F_{excW} = L_{v\ ref} \text{ - transfer mobility} \quad (2)$$

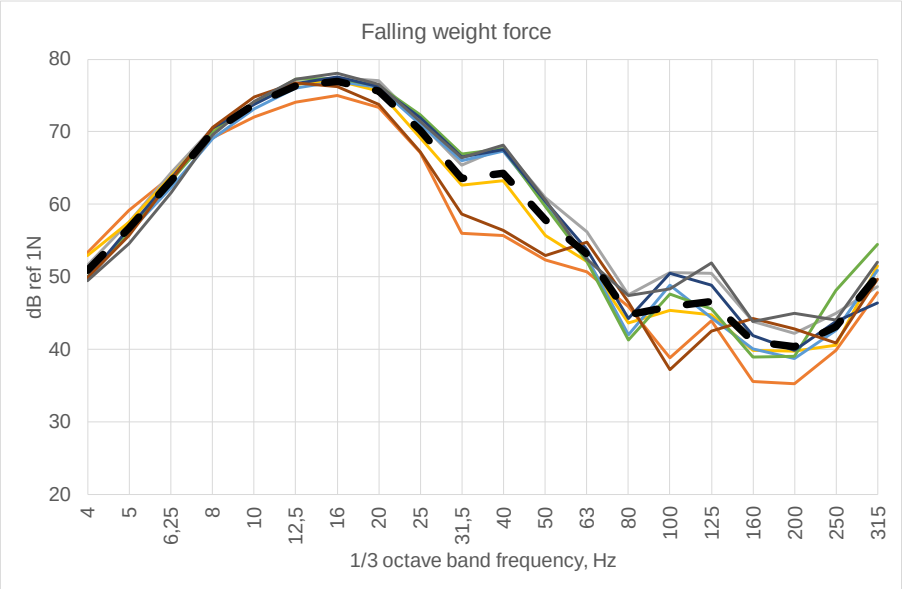

Figure 8: Falling weight force estimation

By applying the calculation methodology to measurement points located further away, we can estimate the transfer mobility for points 1, 2 and 3.

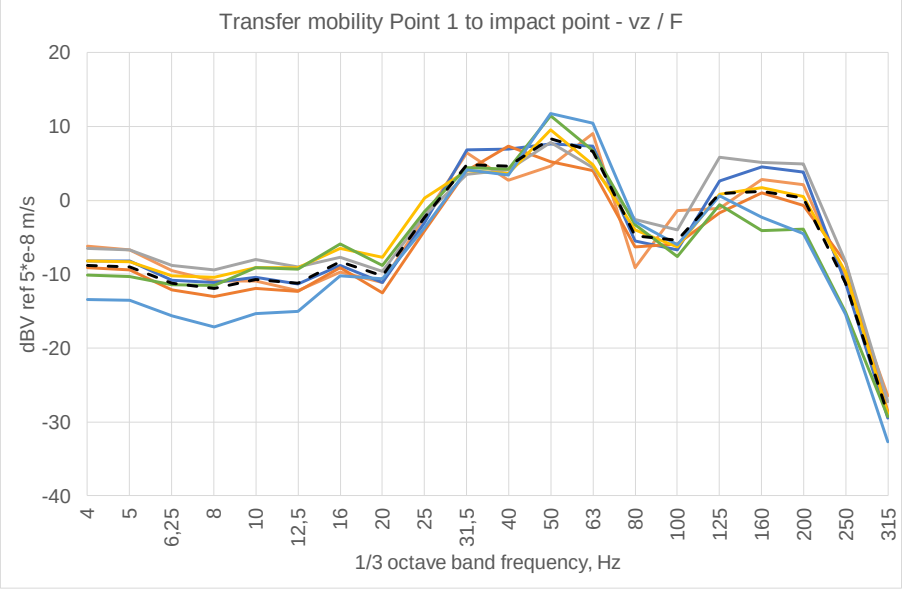

Figure 9: Transfer mobility vz/F – Point 1 to impact point

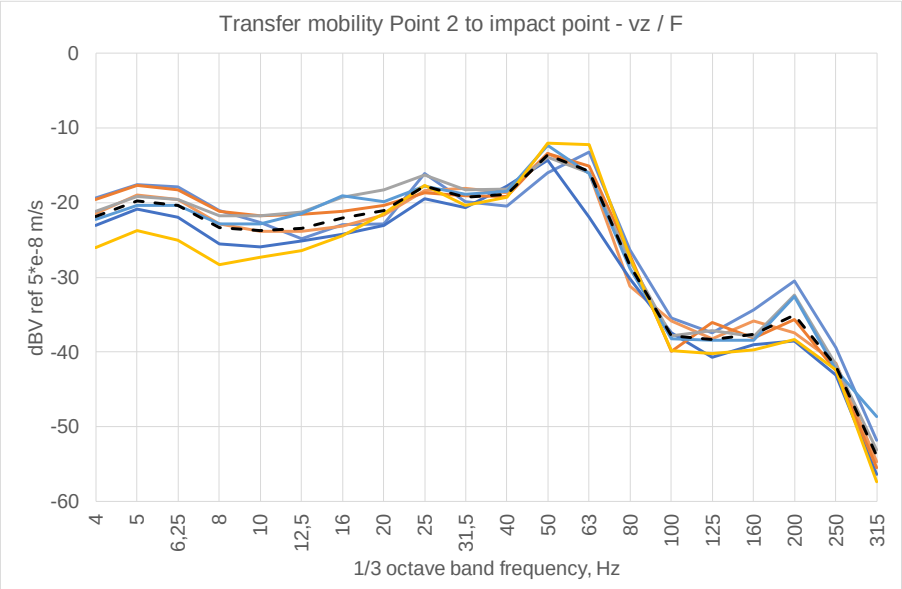

Figure 10: Transfer mobility vz/F – Point 2 to impact point

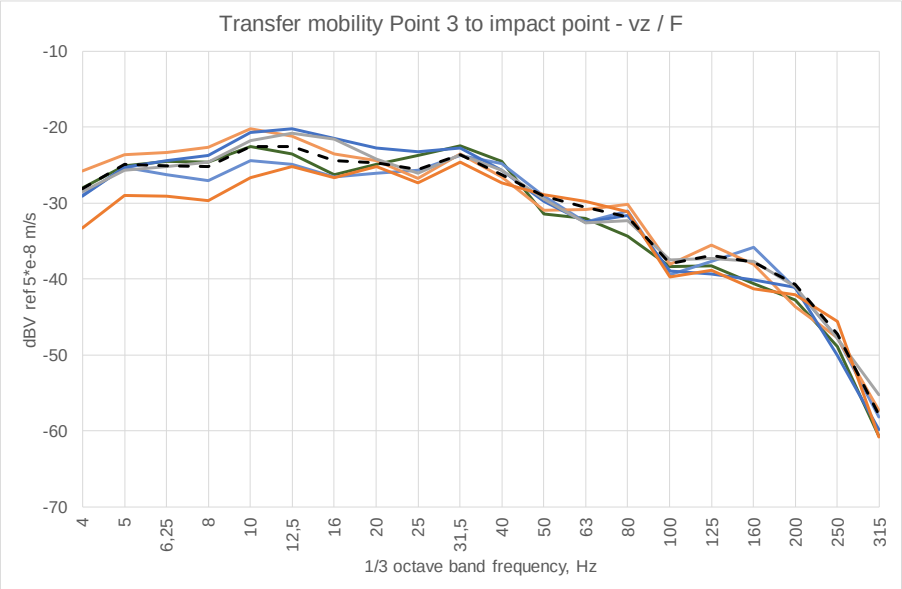

Figure 11: Transfer mobility vz/F – Point 3 to impact point

For easier comparison, we overlay the average of each point transfer mobility on the same graph. This comparison shows the different kind of attenuation between the measurement points:

- A higher energy loss between points 1 and 2, due to the ground attenuation over distance between the two points and to the soil structure interaction.
- A lower energy loss between points 2 and 3, due to the building structural response between the outer wall and the receiver room.

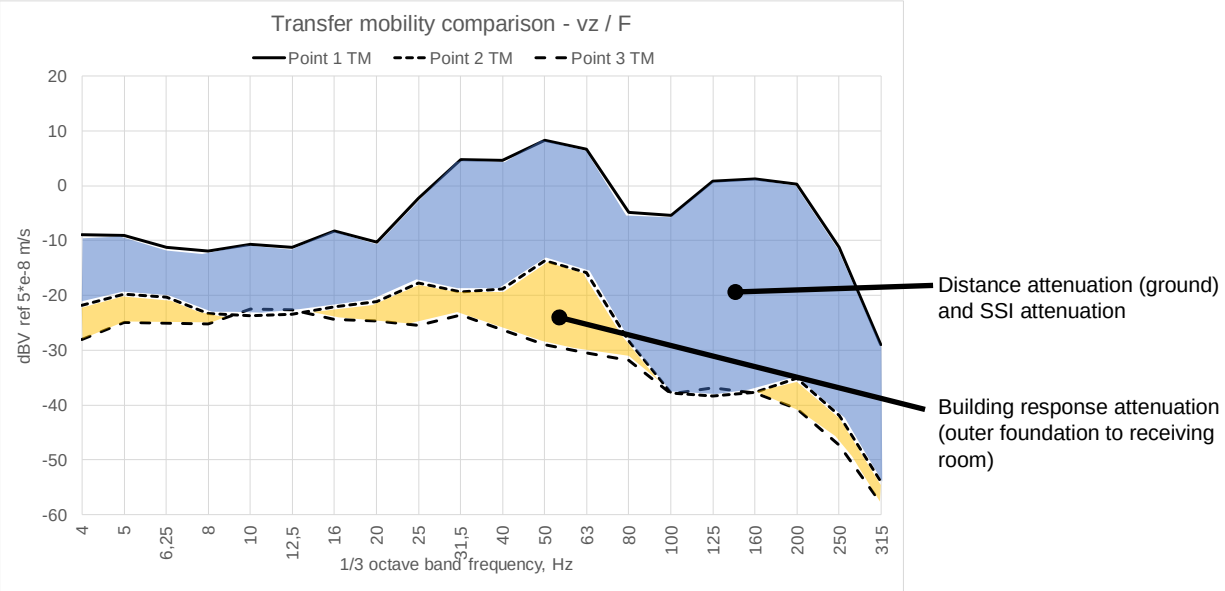

Figure 12: Transfer mobility comparison

Finally, the Point 3 TM curve gives an indication of the transfer mobility between a point located about 15 m underground in the worksite area and a point located in a sensitive room inside the nearest building.

This data is useful for assessing the impact of future works. By applying this transfer mobility to the force of each construction activity, the groundborne vibration impact inside the building can easily be estimated, as well as the groundborne noise impact.

6 BIBLIOGRAPHIC DATA COMPARISON

For comparison, we can estimate the transfer mobility by combining the available bibliographic data collected in the FTA transit noise and vibration assessment guide, as illustrated below.

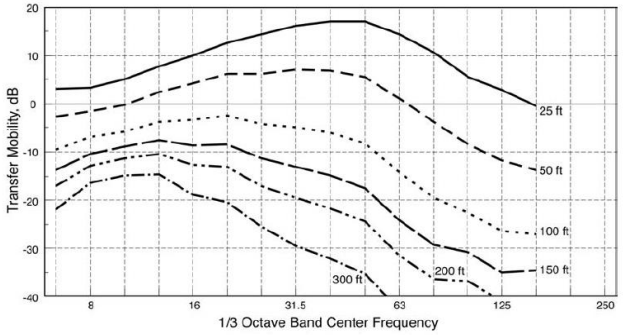

Figure 11-3. Example of Point-Source Transfer Mobility

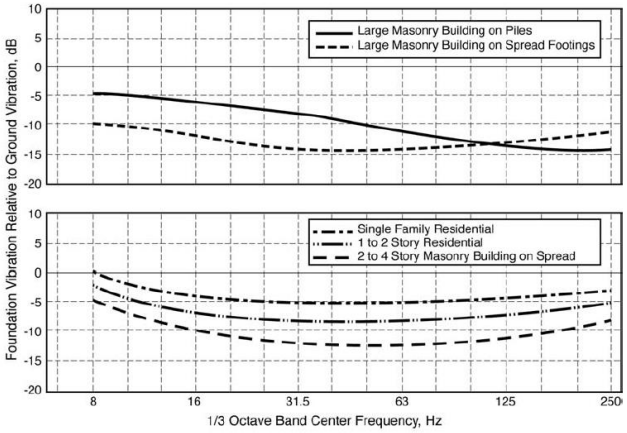

Figure 11-5. Foundation Response for Various Types of Buildings

Figure 13: Transfer mobility literature [2]#

The following graph compares the transfer mobility measured on site to the transfer mobility estimated based on the FTA curves for a large 2 to 4 stories masonry building on spread footings.

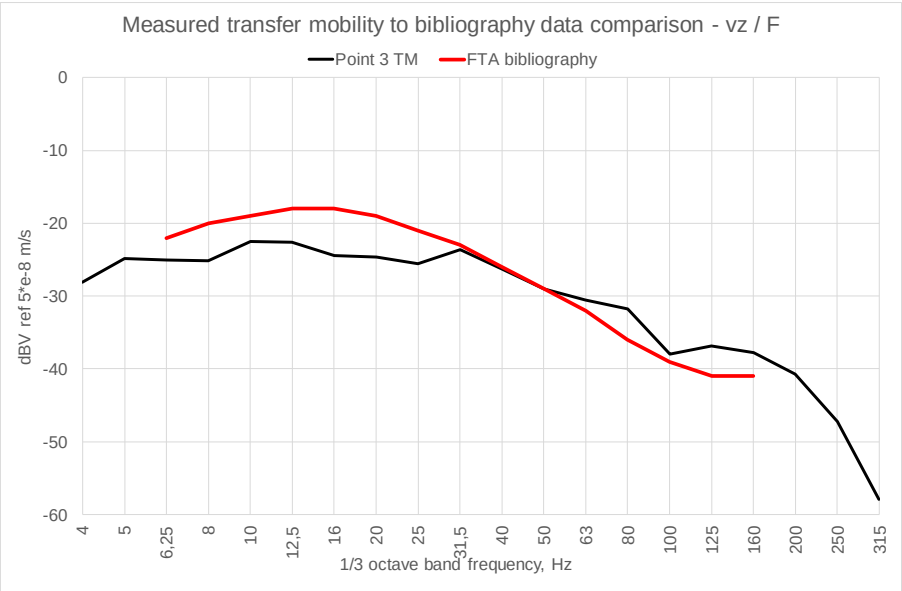

Figure 14: Measured transfer mobility compared to FTA data

As we can see, the two curves are quite similar, even though the FTA derived curve is ideal and given for homogeneous ground conditions.

Given the fact that the reference point is underground and that the test building has a complex morphology, the differences are not unexpected.

Moreover, test results provide a better knowledge of the transfer mobility for the test site and for a larger frequency range, which could be more suited for ground-borne noise analysis.

7 CONCLUSION

In this paper, we have discussed the results of a series of vibration transfer mobility tests on a worksite in Saint-Cloud (France). The focus of these tests was to estimate the transfer mobility over a large zone based on an alternative measurement method, using both an impact hammer and a falling weight.

The intermediate estimation of the local transfer mobility around the impact point can provide an approximation the falling weight force and on the global transfer mobility.

The test results are also compared to the bibliographic references available, and the similarity between the two sets of data confirms the general applicability of this kind of assessment.

8 REFERENCES

Federal Transit Administration, Transit Noise and Vibration Impact Assessment, (1995). Report DOT, Number DOT-T-95-16, April 1995.

Nelson, J.T. and Saurenman, H.J. (1988). "A Prediction Procedure for Rail Transportation Ground-Borne Noise and Vibration," Transportation Research Record 1143, August 1988 2. U.S.

Singleton Jr, H. L. (2005). "Vibration Transfer Mobility Measurements Using Maximum Length Sequences, NOISE-CON 2005

Verbraken, H., (2012), "Degrande, G. and Lombaert, G. Experimental and numerical determination of transfer functions along railway tracks". Volume 13, Issue 11, pp 802–813.

MONITORING OF SPRAYED CONCRETE LINED TUNNELS USING FIBRE BRAGG GRATING SENSORS

M Brunton, J Preston, BE Whelan
Monitor Optics Systems Pty. Ltd.

ABSTRACT

This paper outlines the use of Monitor Optics Systems' (MOS) Fibre Bragg Grating (FBG) sensor cables for convergence monitoring in tunnels made from sprayed concrete lining (SCL). The Crossrail project is currently installing the new Elizabeth line into the London rail network, and at Farringdon Station, the line will connect to both the London Underground and the Thameslink lines. Due to several of the new tunnels being in close proximity, as well as existing infrastructure and challenging geotechnical conditions, the decision was made to monitor the critical "RTE2" tunnel to ensure it was performing as designed. Pressure sensors and survey prisms were initially selected to monitor the tunnel's critical locations. However, as pressure sensors had a reputation for unreliable results due to difficulties with their installation, an additional method was sought out to validate the pressure and surveyed results. Following their successful use in a tunnel at Bond Street Station, MOS sensor cables were selected to monitor the tunnel in conjunction with the pressure sensors and survey prisms.

MOS sensor cables that incorporate a nylon coating are designed to survive direct embedment into the SCL of a tunnel and can provide real time monitoring of the lining immediately after embedment. Sensor cables with five FBGs were installed at two locations in the RTE2 tunnel, along with corresponding temperature sensor cables. The FBGs were monitored using an optical interrogator located outside of the installation area through the use of fibre optic signal cables. Data was available for visualisation and manipulation through the MOS web hosting site DaMiNs.

FBGs, survey prisms, and pressure sensors were located at the same locations, and the FBG results generally showed good agreement with the surveyed results. The majority of the pressure sensors were unable to capture reliable results but were also in good agreement with the FBG results where reliable data was captured. The monitoring results validated the tunnel design and allowed additional tunnel construction to continue without additional unnecessary concrete linings.

1 INTRODUCTION

Construction for the new Elizabeth line commenced in 2009 and will link London's east to London's west through the city, adding 10 new stations and upgrading 30 existing stations. Farringdon Station is one of the stations being upgraded and it will be the only link between the Elizabeth line and both the London Underground and the Thameslink lines.

The upgrade to Farringdon Station will include two large ticket halls and two new platform tunnels, as well as smaller linking tunnels, escalator inclines and escape shafts. The rail tunnels are being constructed using tunnel boring machines (TBM), which continue into where the new platforms are located to create "pilot tunnels" for the platforms. These pilot tunnels are then enlarged using sprayed concrete lining (SCL).

To allow for the simultaneous development of the underground tunnels and the adjoining ticket hall, the Main Contractor proposed abandoning the TBMs in the ground permanently following the excavation of the pilot tunnels instead of retrieving it through the ticket hall shaft. This "turn and bury" solution would allow the construction of the ticket hall to proceed unimpeded, reducing cost, time and risk. However, the simultaneous construction of the underground tunnels and the ticket hall shaft would pose several geotechnical challenges.

Figure 1 shows a plan view of the Farringdon tunnel network. Once the TBM was buried and backfilled with foam concrete, the "RTE2" tunnel was to be excavated from the "PL4" headwall to the "ETH" (Eastern Ticket Hall) shaft. Following the excavation of RTE2, the concourse "CH2" tunnel was to be excavated from the pilot tunnel to the ETH shaft while RTE2 SCL work was being completed. The CH2 construction was to end at a temporary headwall only 25mm from the extrados of RTE2. Finally, the escalator shaft "ES2" was to be excavated from the ETH shaft to the CH2 tunnel, with a "bench and invert" enlargement, and the lining of the ES2 tunnel almost coming within millimetres of the lining of the RTE2 tunnel. The secondary lining of RTE2 was to be installed during the construction of ES2.

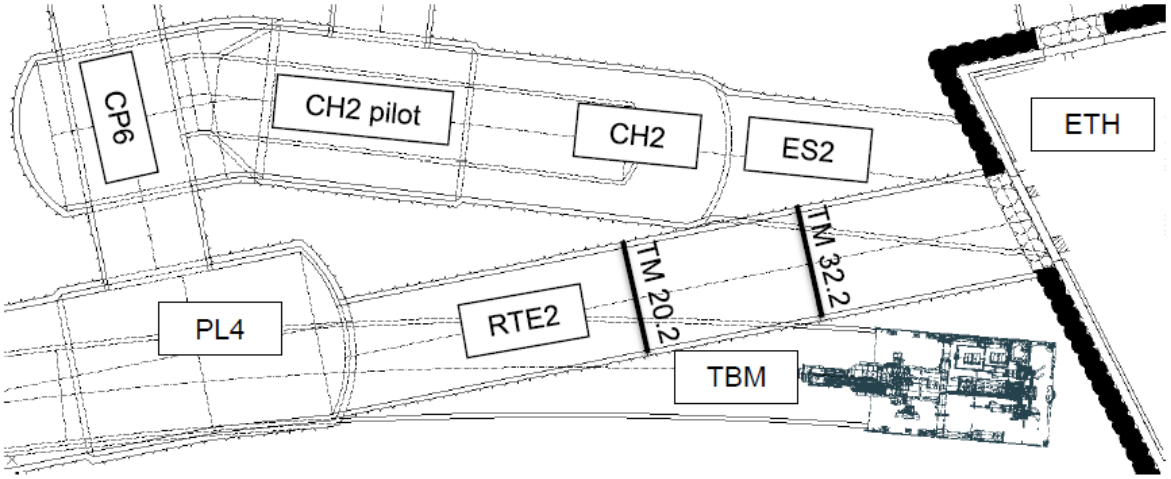

Figure 1: Plan view of Underground Tunnel Excavations

Further complicating the geotechnical conditions was a Listed Railway structure, the Lindsey Street Bridge (LSB), located directly above ES2, and 5 pre-existing major geological faults in the area.

A 3D Finite Element Analysis (FEA) was carried out to assess any ground movements and expected stresses and displacements in the tunnel network. From this, concerns were raised about the integrity of RTE2 with the construction of CH2 and ES2, and it was suggested that the secondary lining for RTE2 be installed prior to the excavation of ES2. This would have caused issues with the Contractor's program, so monitoring of RTE2 was proposed instead, with an overall increase in the thickness of the sprayed concrete lining of RTE2 in critical areas as well.

Survey prisms were considered adequate to monitor for changes in displacements for the majority of the tunnel, but a more direct and accurate method was sought to monitor the stress in the lining itself at key locations. Hydraulic concrete pressure (or stress) cells were suggested, but the Contractor had experienced difficulties with the installation and reading processes, causing many of the cells to yield incorrect or unreliable results. Embedded sensor cables were also suggested following a successful trial at Bond Street Station where Monitor Optics Systems (MOS) embedded their glass fibre reinforced composite (GFRC) sensor cables with Fibre Bragg Gratings (FBGs) into the SCL to measure strain. A compromise was reached to install all three systems at the key locations.

2 MONITORING OF SPRAYED CONCRETE LINING

Prior to the application of fibre optic sensor cables to monitor sprayed concrete linings, survey prisms and pressure cells were the common methods used to understand stress within the concrete linings. However, each of these methods had drawbacks. Survey prisms are only accurate to within a few millimetres, and the displacement results need to be converted to strain and then to stress, which is sensitive to any errors in the surveying measurements. Pressure cells measure pressure (and hence stress) directly from behind the concrete lining, so are ideal in this regard, but there are difficulties associated with their installation and data collection. The pressure cell needs to be set correctly against a mortar pad with good contact with the earth, which can be difficult to achieve, and the crimping (pressurisation) of the cells require a lot of precision and care from highly experienced personnel. Additionally, the results require complicated conversion formulae, making readouts difficult without software.

Embedded FBG sensors are well suited for tunnel monitoring. FBGs are periodic perturbations of an optical fibre that results in the reflection of a narrow bandwidth of light when illuminated by a broadband light. The reflected central peak wavelength is a function of both the grating's period and the refractive index of the fibre's core. If strain is applied to the grating, the grating period changes, changing the reflected wavelength as a linear function to the strain applied. If the fibre undergoes a temperature change, the refractive index of the fibre will change, which also changes the reflected wavelength as a linear function of temperature. This linear response makes FBGs ideal strain and temperature transducers. Some benefits include:

- They are passive and spark free, and are not influenced by EM noise
- They are self-referencing and experience zero drift, so no recalibration is ever required
- They have no moving parts and are of low impact, so they will not affect the structure
- They are highly resistant to the elements, allowing them to survive indefinitely in harsh environments
- They have high resolution and accuracy (typical 1-2με for strain, 0.1°C for temperature)

However, fibre optic FBG arrays are generally too delicate to survive the harsh sprayed concrete process when they are directly embedded. MOS's sensor cable consists of an optical fibre that is pultruded into a glass fibre reinforced composite cable (GFRC) which protects the fibre optic array while maintaining excellent strain transfer. A nylon coating can also be applied for further robustness.

MOS FBG Sensor cables were first tested with sprayed concrete at Cambridge University, and then installed at Bond Street Station in a full trial.

2.1 DIRECT EMBEDMENT OF SENSOR CABLES USING SPRAYED CONCRETE

Sprayed concrete is the process of projecting wet concrete through a nozzle with compressed air. This technique is often used for the containment and reinforcement of earth works in tunnels and underground structures. The sprayed concrete process is aggressive and can be damaging to sensitive instruments that are embedded using this technique.

In 2012, MOS carried out tests embedding their GFRC sensor cables in sprayed concrete at the University of Cambridge. The purpose of the this was to test the survivability of the MOS sensor cables under the harsh sprayed concrete process, and to demonstrate the capability of the embedded FBG sensor cables to accurately measure strains inside the concrete structure.

Three different sensor cables were installed into the framework of the concrete beam; one with one FBG, another with two FBGs and the last with three FBGs. This setup is shown in figure 2. Sensor cables with a protective nylon coating and no FBGs were also installed for validation purposes using OTDR. Sprayed concrete was then applied to the beam.

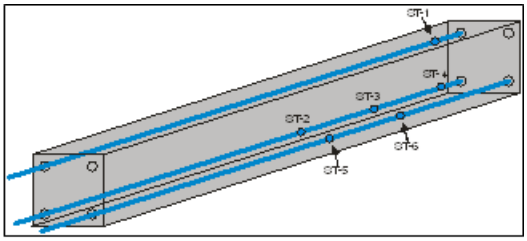

Figure 2: Sensor Cables Installed into Beam

The sensor cables survived the embedment process, with some losses to the FBG reflection levels, but the nylon coated sensor cables proved to be very robust during the installation process, with no losses. The sprayed concrete process is shown in figure 3. Load cells and vibrating wire sensors were then installed onto the beam for comparison to the FBG results.

Figure 3: Sprayed Concrete Applied to Beam

The beam was subject to a four-point bending load until failure. The FBGs results compared well with the other sensors attached to the outside of the beam as well as numerical simulations.

2.2 BOND STREET STATION INSTALLATION

Following the successful embedment tests, a trial installation of nylon coated sensor cables was carried out at the upgrade to Bond Street Station in 2013. Nylon coated sensor cables were selected because of their excellent performance at the University trials, and they were installed in two different locations. Each strain sensing cable had five FBGs, with all FBG positions corresponding to a desired position in the tunnel lining (as shown in figure 4). MOS temperature sensor cables with one FBG were installed alongside the strain cables to compensate for temperature induced changes to the strain values and to provide information on the temperature variance during the curing process.

All sensor cables survived the sprayed concrete application and provided information on the curing process. All results were set to zero at the conclusion of the spraying process, and the results for one of the installations can be seen in Figure 5. All FBGs showed tension in the lining which gradually turned compressive as the concrete cured. Additional compression was also noted at subsequent stages of tunnelling, most pronounced during the top heading excavation that occurred 21 and a half hours after the lining installation. This increase in compression is due to the lining taking the load from the surrounding London Clay.

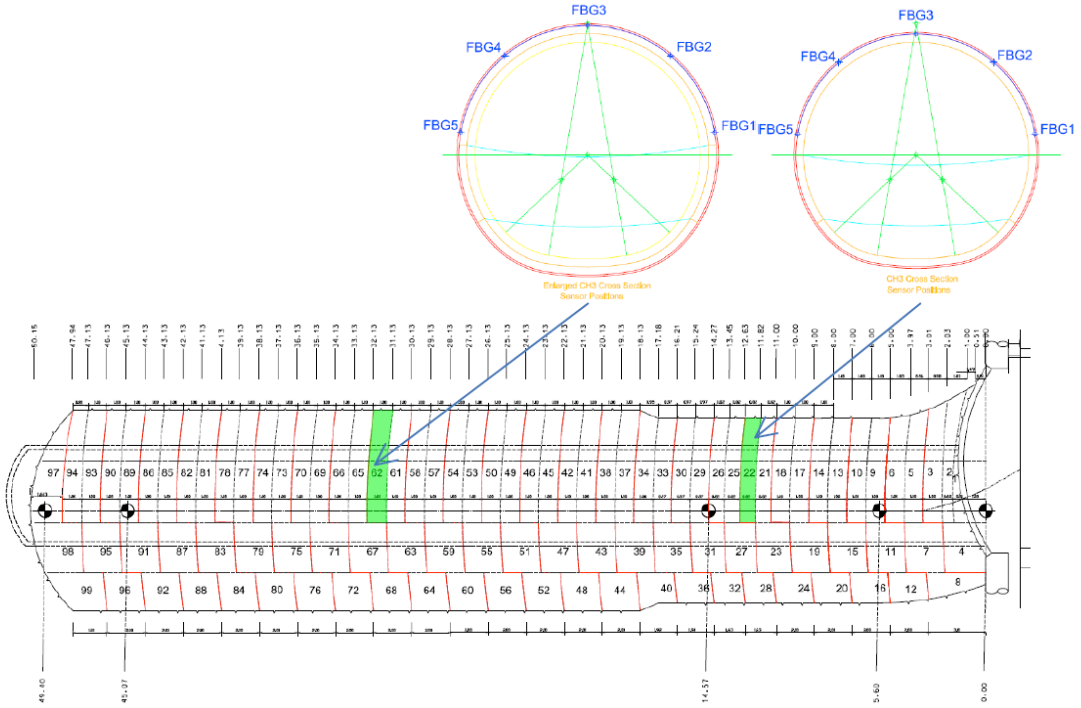

Figure 4: Section of Tunnel Monitoring Locations

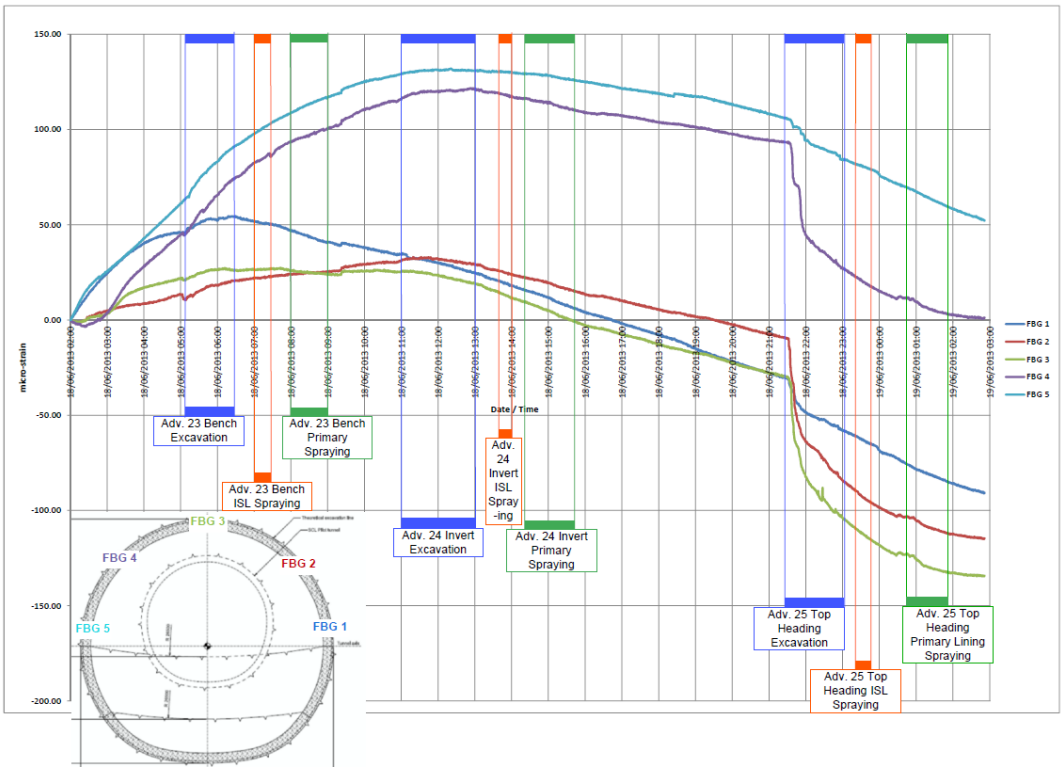

Figure 5: Results of Sprayed Concrete Lining Installation

3 FARRINGDON STATION INSTALLATION

The installation of all three monitoring systems occurred in late 2014.

3.1 FBG SENSOR INSTALLATION

FBG strain sensor cables with nylon coatings were installed at two tunnel locations, “TM20.2” and “TM32.2”. The strain sensor cables were paired with temperature sensor cables for temperature compensation. Following the initial boring of the tunnel, an initial sealing layer was applied for safety reasons, and once it had reached an appropriate strength, the sensor cables were installed.

The sensor cables were attached around the circumference of the tunnel using steel staples from an elevated work platform, with the identified FBGs positioned at their design location. A typical monitoring section is shown in figure 6. The FBG sensor cables had pigtails at each end of the cable, allowing redundancy in the event it became damaged. The pigtails were drawn back to the previous advance in conduit and protected using junction boxes. The sensor cable pigtail was connected to a signal cable that connected to a Micron Optics, Inc. sm130 dynamic interrogator located outside of the tunnel area in an office.

Data was automatically uploaded to MOS’s dedicated web server DaMiNs for visualisation and manipulation of data.

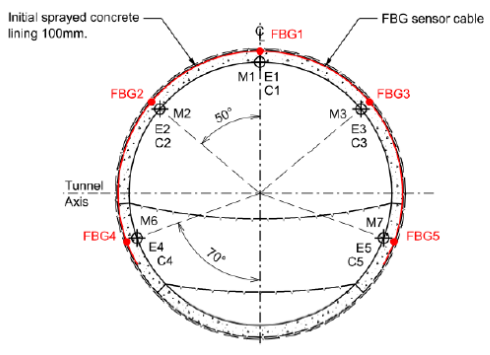

Figure 6: Section of Typical Instrumentation of RTE2

3.2 PRESSURE CELL INSTALLATION

The Contractor's in-house surveying team carried out the installation of the earth and concrete pressure cells. The team had experience with the installation of pressure cells and care was taken to install them correctly. The pressure cell mortar pads had to be fixed to the earth of the tunnel wall, meaning a suitable gap needed to be made from the sealing layer. The pressure cells were installed adjacent to the FBGs also using an elevated work platform and were pressurised according to the manufacturer's instructions. The pressure cells are also represented in figure 6 as C1 to C5 (concrete cells) and E1 to E5 (earth cells). A data logger was on hand to monitor the cells.

3.3 SURVEY PRISMS

The Contractor's in-house surveying team also carried out the installation of the prisms. A threaded rod that the survey prisms are attached to was installed following the sealing layer installation at the same location of the FBGs and pressure cells (M1 – M3 and M6 – M7 in figure 6). The primary lining was then applied, and the targets were installed onto the threaded rods after the lining had cured enough for safe access. Monitoring of these were then carried out by surveyors, relying on line of sight from the station setup to the target. The station was benchmarked against a static point in the tunnel away from the tunnel operations.

4 RESULTS

The FBG results generally compared well with the vertical displacement results. An example of the results is shown in figure 7. These results show point M2 of TM 32.2, which exhibited the largest changes in strain and displacement throughout the construction of CH2 and ES2.

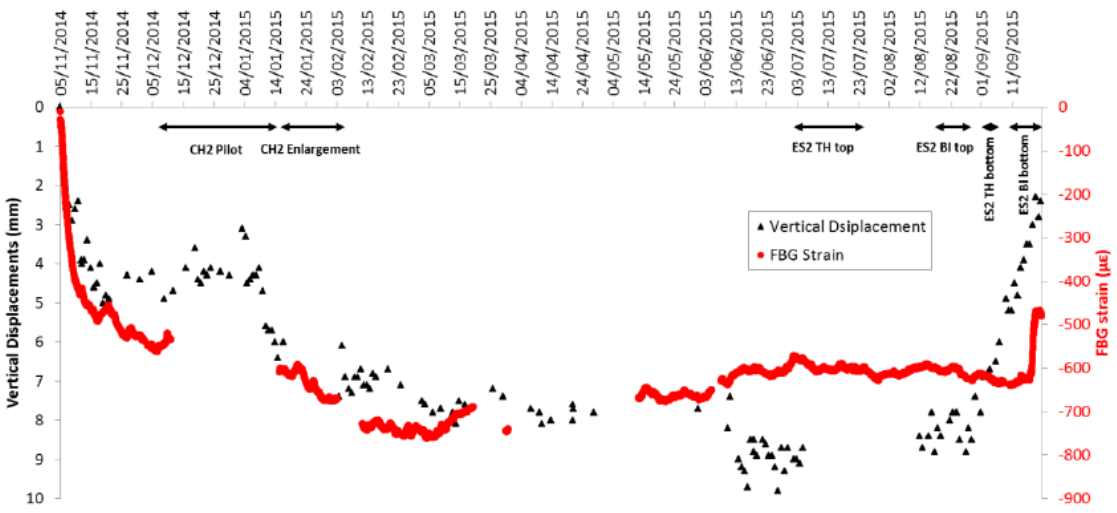

Figure 7: Vertical Displacement Vs FBG Strain Results at Point M2 of TM 32.2

In most cases the pressure cells were unable to capture reliable stress readings for the soil or concrete, but at M2 of TM 32.2, the data compared well between the first readings and steady state conditions. This is illustrated in Figure 8.

Figures 9 and 10 show FBG results for TM 20.2 and TM 32.2. Compression was observed for all FBG sensors during the initial stage, with additional compressive strains observed during the construction of CH2 and ES2.

The FBG results compared well with the FEA results, as shown in Table 1.

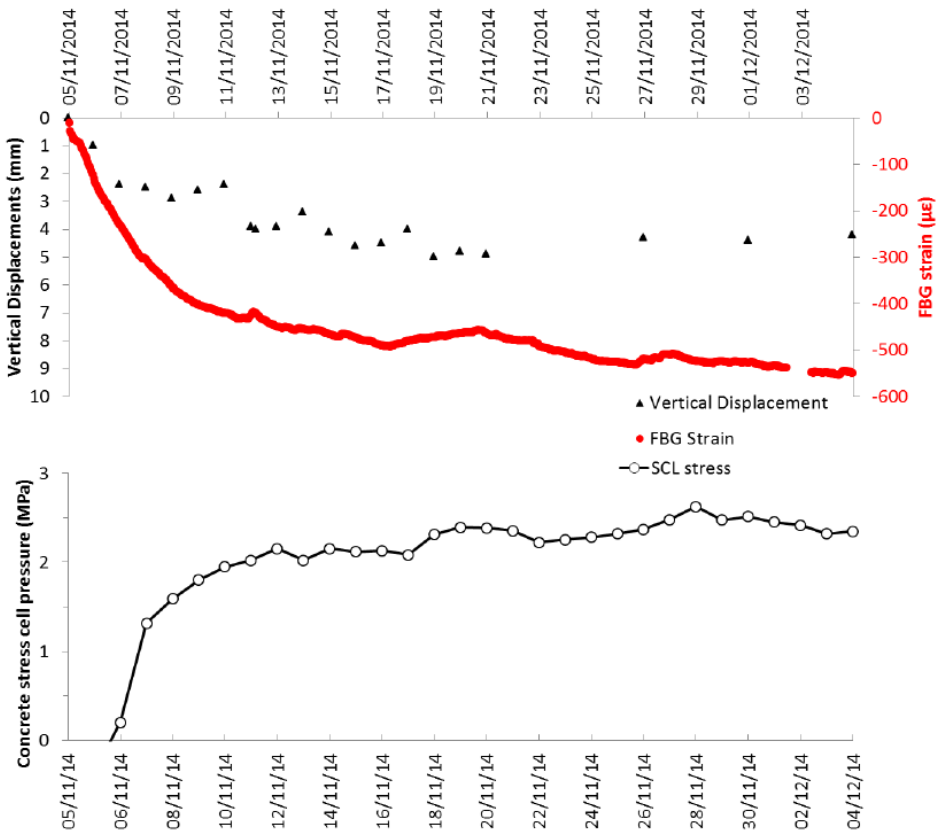

Figure 8: Agreement of Measurements between all sensors at M2 TM 32.2

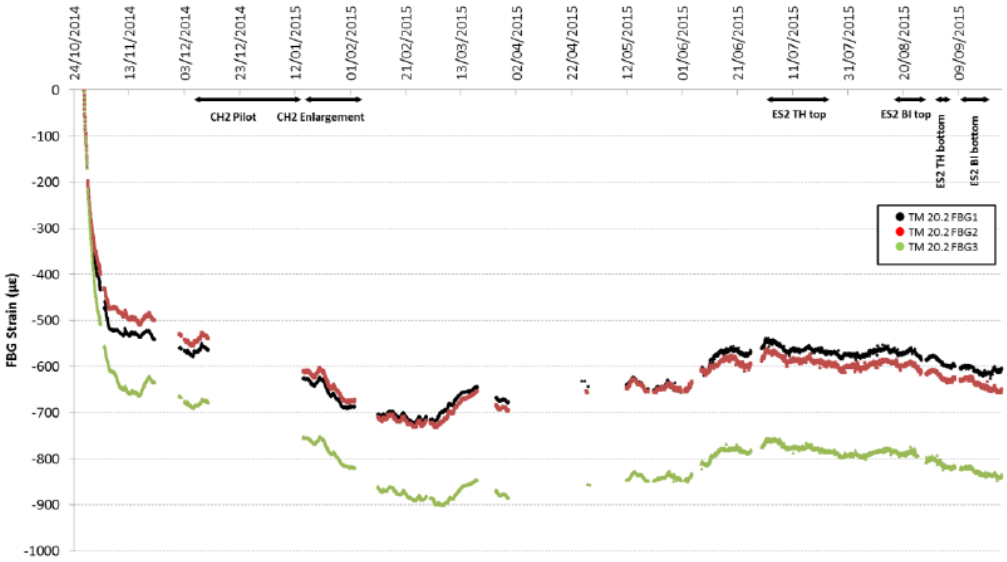

Figure 9: FBG Results at TM 20.2

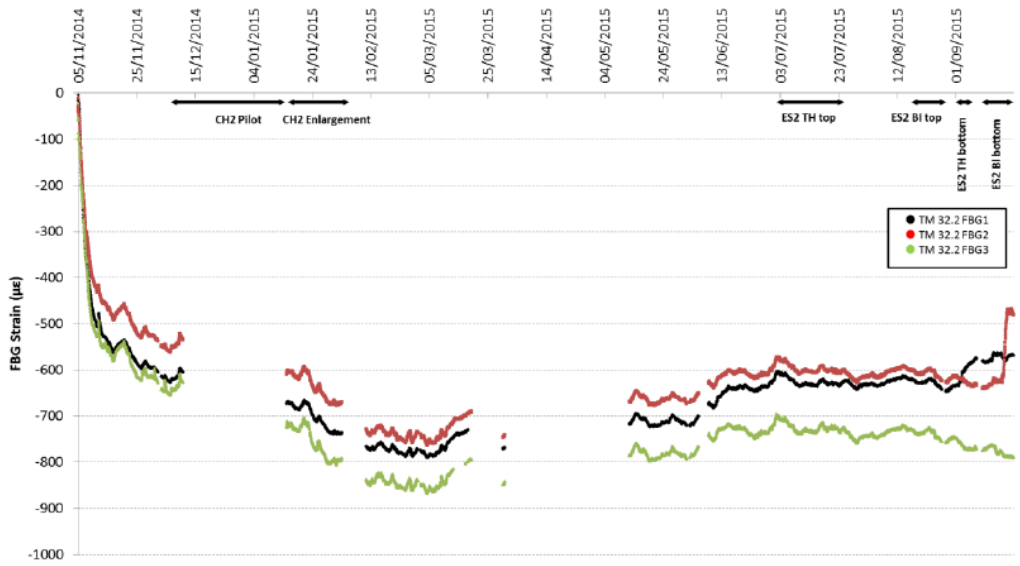

Figure 10: FBG Results at TM 32.2

Table 1: FEA VS FBG Results

		Radial Strains (με)					
		M1		M2		M3	
		FEA	FBG	FEA	FBG	FEA	FBG
TM 20.2	CH2 Pilot	-50	-65	-100	-75	-50	-80
	CH2 Enlargement	-100	-80	-150	-105	-50	-115
	CH2 Total	**-150**	**-145**	**-250**	**-180**	**-100**	**-195**
TM 32.2	CH2 Pilot	-20	-70	-50	-75	-20	-95
	CH2 Enlargement	-50	-100	-70	-125	-20	-120
	CH2 Total	**-70**	**-170**	**-120**	**-200**	**-40**	**-215**
	ES2 from Ticket Hall	50	60	150	-15	20	-10
	ES2 B&E Enlargement	50	5	250	160	30	-20
	ES2 Total	**100**	**65**	**400**	**145**	**50**	**-30**

5 COMPARISON BETWEEN SENSING METHODS

The Contractors made comparisons between each system, noting their strengths and weaknesses.

Aside from being a cost-effective option, the survey prisms were easy and safe to install, as this was done once the primary SCL had cured. Also, damaged prisms were easy to replace without any loss of data. However, the survey prisms are not autonomous, requiring manual labour for each reading, and they are limited by line of sight, need a static point away from tunnel operations, and require regular cleaning due to the large amount of dust in the tunnel.

The pressure cells were generally regarded as the weakest system as they are difficult to install and maintain, particularly with the crimping process, and many did not yield credible or reliable data.

The FBG system was considered safe and easy to install, and provided high precision, accurate and reliable data. All ten sensors remained functional throughout the monitoring period, and continuous access was provided by MOS's web-server DaMiNs. Their main weakness was considered to be the signal cables that ran between the sensors and the interrogator, as these were susceptible to damage from tunnelling machinery. However, damaged cables could easily be replaced, minimising data down-time.

Table 2 shows a summary of the pros and cons of each system according to the Contractor.

Table 2: Pros and Cons of Each Monitoring System

	Pros	Cons
Survey Prisms	• Cheapest system • Fast, easy and safe to install • Easily replaced if damaged without loss of data	• Limited by line of sight • Results depend on accuracy of levelling and control points • Manual operation • Targets get dirty and easily damaged • Least accurate system and can be affected by creep
Pressure Cells	• Most direct way to measure stress • Mid-range price • Very durable and robust once embedded • No maintenance required aside from crimping • Good accuracy (when installed correctly)	• No remote connection • Manual readings • Crimping process difficult • Difficult to obtain good contact with earth • Least safe option as it requires exposing earth • Slowest installation option • Signal cable can be frail and cannot be replaced • Complicated conversion formulae (although can be overcome with software) • Unreliable data
FBGs	• Reasonably fast, easy and safe to install • Very durable and robust when embedded • Signal cable can be replaced if damaged • DaMiNS provided easy and immediate access to data • Highest accuracy of each system • Reliable real-time data • Automated system	• Most expensive system • Signal cables can be frail

6 CONCLUSION

FBG sensor cables with nylon coatings were embedded into the SCL of the new RTE2 tunnel in Farringdon Station alongside survey prisms and pressure cells. Each monitoring system was installed in late 2014, and were used to monitor for changes to the SCL caused by the construction of adjacent tunnels CH2 and ES2.

The FBG sensors compared well with FEA models completed prior to the construction and to the data obtained by the survey prisms. The pressure cells were unable to yield reliable or credible data for the majority of cases, but the FBGs were in agreement with their results when reliable data was captured.

The Contractor concluded that FBGs are an effective tool to measure stress within concrete linings where survey prisms are not deemed accurate enough, and that it validated the design of RTE2.

7 ACKNOWLEDGEMENT

The authors would like to express their thanks to the members of Crossrail and the University of Cambridge that allowed these trials and eventual full installation to proceed.

8 REFERENCES

Masanari, N., Hammer, A.L., Thewes, M., Elshafie, M. Soga, K. (2015). Mechanical Behaviour of a Sprayed Concrete Lining Isolated by a Sprayed Waterproofing Membrane. *Tunnelling and Underground Space Technology 47*, 143-152.

Nosenzo, G., Whelan, B.E., Brunton, M., Kay, D., Buys, H. (2012). Continuous Monitoring of Mining Induced Strain in a Road Pavement Using Fiber Bragg Grating Sensors. *Photonic Sensors*, DOI: 10.1007/s13320-012-0077-0

O'Donnell, J., Nosenzo, G., Preston, J. And Sturman, T (2013). Installation of Optical Fibre based Sensors within Sprayed Concrete Lined Tunnels to measure Strain and Temperature *Crossrail Annual Technical Papers Competion*, London, U.K 2013

Salak, P., Gakis, A. and St.John, A. (2015). Taking the strain, coping with pressure or shooting targets? An objective comparison between monitoring solutions within sprayed concrete lined tunnels at Crossrail Farringdon Station, London. *Crossrail Technical Papers 2015*

ASSESSMENT OF METHODOLOGIES FOR REBURIAL OF EXCAVATED ACID SULFATE SOFT SOILS WITHIN SHELL COVE BOAT HARBOUR ZONE

Kourosh Kianfar[1], Scott Morrison[2], Glenn Colquhoun[3]

[1]Principal Geotechnical Engineer; [2]Principal Geotechnical Engineer
[2]SMEC, PPM Building, corner of Beach and Kembla Street, Wollongong NSW
[3]Shell Cove Boat Harbour Development Director, Frasers Property Australia, Shellharbour NSW

ABSTRACT

A study was carried out to assess the practical aspects of placement of excavated disturbed Acid Sulfate Soft Soils (ASSS) within the future Shell Cove Boat Harbour excavation zone at the proposed Shell Cove Boat Harbour development. The objective of the work was to assess and comment on the methodology from a geotechnical perspective for the placement of ASSS material 'in the moist' rather than as 'dredged slurry', during Stage 2 of construction. Two large field trial cells (approximately 15m by 15m at base, and 4.5m high) were constructed to practically observe, test and assess different placement scenarios. The following three scenarios were assessed:

- Placement of untreated ASSS material
- Placement of Agricultural lime treated ASSS material to modify soil shear strength and consistency
- Placement of Hydrated lime treated ASSS material to modify soil shear strength and consistency

Track rolling via long reach excavators and swampy dozers were utilised to place, spread and remove the large air voids between clumps/clods of the ASSS material within the trial cells. The neutralisation capacity of the various limes for treatment of Acid Sulfate Soil was also assessed in a preliminary manner. It should be noted that the focus of the work from the addition of lime was on geotechnical modification/stabilisation aspects rather than assessment of Acid Sulfate Soil neutralisation capacity.

Shear strength of ASSS material was assessed using a hand-held shear vane. The shear strength of the soils was measured at the borrow pits prior to excavation of material. It was then compared with the measured shear strength of the soil in different layers placed within the trial cells for different scenarios. Comments are provided in relation to the effects of the mixing agent on the shear strength of the soil.

Construction of bunds within harbour excavation zone including bund sizing and stability of bund to be used by earthmoving plant was also assessed and commented on. Change in soft soil pH due to addition of agricultural and Hydrated limes was also assessed. Waiting time to place subsequent layers within the cells and the effect of weather conditions on the placed soft soils within trial cells is also discussed to some extent in this paper.

Utilisation of a new type of long reach excavator not previously used in Australia is also discussed. This innovative construction technique enabled the excavator to travel directly onto soft disturbed soils and to spread the soils within the harbour excavation zone in a manner that provided enormous cost and time savings for the client.

1 INTRODUCTION

The Shell Cove Boat Harbour is a large integrated new harbour development located 100km south of Sydney, NSW. After commencement of Stage 1 of construction in 2013, and continuation of construction of Stage 2 in 2014, the site is now in the final stage of construction (Stage 3) and completion is due in late 2019. An extensive investigation and design program was carried out and a number of novel techniques were used to investigate and model the future design conditions. This paper discusses one aspect of this work.

This paper discusses the approach adopted, results of and lessons learnt from a full-scale field trial to assess the practical aspects of the placement of excavated disturbed Acid Sulfate Soft Soils (ASSS) within the future Shell Cove Boat Harbour excavation zone at the proposed Shell Cove Boat Harbour development. Large volumes of

ASSS material (about 500,000m^3) required excavation and reburial below the water table and ASSS management became an extremely important driver of construction activities.

The objective of the work was to assess and comment on the methodology from a geotechnical perspective for the placement of ASSS material 'in the moist' rather than as 'dredged slurry'. Two large field trial cells (approximately 15m by 15m at base, and 4.5m high) were constructed to practically observe, test and assess different placement scenarios. The following three scenarios were assessed:

- Placement of untreated ASSS material
- Placement of Agricultural lime treated ASSS material to modify soil shear strength and consistency
- Placement of Hydrated lime treated ASSS material to modify soil shear strength and consistency

The first aim of this trial was to establish whether the ASSS materials could be trafficked upon initial placement of non-treated Unit 3B ASSS material. If swampy dozers could not traffic the non-treated Unit 3B ASSS material, the second aim of the trial was to establish what form of stabilisation could potentially be used to allow swampy dozers to traffic the materials.

It should be noted that this paper does not discuss in detail the treatment of ASSS from an environmental/neutralisation perspective, but does comment on the effect of neutralisation in a preliminary manner. However, this aspect of work is acknowledged as highly important and should be evaluated in parallel to any geotechnical treatment measures where ASSS is to be treated.

2 BACKGROUND AND REVIEW WORK

3.1 PREVIOUS WORK

Morrison and Tait (2007) carried out an assessment of the consolidation behaviour of the Acid Sulfate Soil (ASSS) from the Shell Cove Boat Harbour. The assessment was in relation to removal of the ASSS material by a cutter-suction dredge, transported as a slurry by pipeline and then disposed into a dewatered disposal cell.

The following parameters were adopted:

- c_c is compression coefficient,
- e_0 is initial void ratio,
- c_v is coefficient of consolidation in vertical direction, and
- c_h is coefficient of consolidation in horizontal direction.

In their assessment, based on the laboratory and insitu testing results, different values of compression ratio ($c_c/(1+e_0)$) and coefficients of consolidation (c_v and c_h) were used to best estimate the self-weight consolidation behaviour of the ASSS material in form of slurry. To assess and estimate the duration of the consolidation, both cases for the vertical consolidation (without wick drains) and horizontal consolidation (with wick drains) were assessed and the outcomes discussed.

Morrison and Tait (2007) reported that for an initial thickness of the slurry ranging between 1.5m to 4.5m, the estimated time for 95% Degree of Consolidation (DOC) ranges between about 5 to 295 months and 4 to 26 months for the cases of vertical drainage and horizontal drainage, respectively (depending on the initial thickness of the slurry and the value of coefficient of consolidation, and whether wick drains were used or not).

Large volumes of water would be introduced to the material if a cutter-suction dredge is used, and wick drains would likely have been necessary to achieve practical consolidation timeframes. The technique was assessed as very costly. It was therefore decided to investigate alternative ASSS excavation and placement measures. It was decided to not place the ASSS material as slurry within the excavation zone and instead attempt to place the material "in the moist".

"In the moist" means excavating the ASSS material using conventional earthworks techniques such as excavators and transporting and tipping the soils within the excavation zone using dump trucks. This "in the moist' method results in different soil parameters than those reported by Morrison and Tait (2007).

It was theorised that:

- the rate of the material placement would increase dramatically if more conventional earthworks techniques are used.
- providing soil (treated or untreated) has an appropriate moisture content and shear strength when it is placed within the Boat Harbour excavation then it is possible that swampy dozers could potentially track over the soils in layers.
- using swampy dozers would allow some compactive effort to be imparted to the material and significantly speed up placement of the ASSS materials.

3.2 PLACEMENT OF NON-TREATED ASSS MATERIAL

Placement and subsequent performance of non-treated soft soil material within the Boat Harbour over-excavation zone depends on the following factors:

- Soil type and percentage of clayey material;
- Soil particle size;
- Insitu moisture content;
- Degree of disturbance;
- Thickness of each layer placed;
- Waiting time between the placement of each layer;
- Climate conditions;
- Machinery used for placement; and
- Experience of construction staff.

Insitu moisture content of soil is one of the most important factors affecting the practicality of the placement and compaction of soft soils due to its effect on undrained shear strength. Due to the soil being excavated from different depths with different void ratios and varying moisture content, assessment of the soil conditions when it is excavated, transported and placed within the excavation cell was foreseen as difficult to assess unless a field trial was carried out. In addition to the practical observation of the performance of a Swampy Dozer travelling over the material, measurement of the undrained shear strength of the disturbed and mixed soil was used as a key indicator of soil improvement.

The field trial attempted to assess the combined effects of all the above items in a practical way.

3.3 PLACEMENT OF LIME TREATED ASSS MATERIAL

Treatment using lime was chosen as the most likely technique for stabilisation due to the common use of lime to treat clay subgrades in pavements and the potential neutralising capacity of the lime to treat acidic soils such as the ASSS materials used onsite.

Based on published information from Austroads (2006), it was assessed that three different limes could potentially be used to modify, dry, and stabilise soft clayey soils as follows:

- Hydrated lime
- Quicklime
- Hydrated lime slurry

Table 2 summarises and compares some of the key parameters of different limes.

Table 2: Properties of Quicklime, Hydrated Lime, and Slurry Lime (from Austroads, 2006)

	Hydrated lime	Quicklime	Hydrated lime slurry
Composition	$Ca(OH)_2$	CaO	$Ca(OH)_2$
Form	fine powder	granular	slurry
Equivalent $Ca(OH)_2$/unit mass	1.00	1.32	0.33 to 0.56
Bulk density (t/m^3)	0.45 to 0.56	1.05	1.25

Quicklime (calcium oxide) is produced by heating limestone to temperatures above 900 °C to drive off carbon dioxide. The chemical equation is:

$$CaCO_3 \text{ (calcium carbonate/limestone)} + \text{Heat} \longrightarrow CaO \text{ (calcium oxide/quicklime)} + CO_2$$

Hydrated lime is produced at temperature below 350 °C when calcium oxide (quicklime) reacts with water. For the hydration of 1 tonne of pure quicklime (calcium oxide), approximately 320 litres of water is required. The chemical equation is:

$$CaO \text{ (calcium oxide/quicklime)} + H_2O \longrightarrow Ca(OH)_2 \text{ (calcium hydroxide)} + \text{Heat}$$

Application of any of the above limes has several advantages and disadvantages:

3.3.1 Quicklime:

Advantages: Compared to hydrated lime, quicklime is a more concentrated lime containing 20% to 24% more available lime oxide content. Therefore, if the moisture content of the mix is enough to allow full hydration of the lime, 3% of quicklime has an approximate effect as 4% of hydrated lime. Bulk density of quicklime is greater than hydrated lime (see Table 1), therefore less volume of quicklime is required. Quicklime is the best lime to be used for drying soft soils due to higher chemical reaction of lime with water and higher heat production. Compared to hydrated lime, quicklime has larger particles generating less dust during application.

Disadvantages: Approximately 32% (of lime weight) of water is required to convert quicklime to hydrated lime. This can be an issue in the areas where limited water sources are available. Quicklime is also much more dangerous when using as an additive. Reaction of lime, particularly quicklime, with water generates heat which can cause thermal burns to eyes and skin. This reaction and lime dust can create breathing issues if proper protective equipment is not worn.

3.3.2 Hydrated Lime

Advantages: Compared to the lime slurry, dry hydrated lime can be applied more rapidly and can be used to dry soft soils containing high moisture contents, but it is not as effective as quicklime unless higher percentage of lime is used. However, it is a safer product to use compared to Quicklime.

Disadvantage: Particles of the hydrated lime are fine and create dust during the application. Stray dust can drift offsite causing impacts to the general public (cases of washing on clothes lines damaged by drifting quicklime dust have been reported). Therefore, application of hydrated lime in populated zones is generally unsuitable.

3.3.3 Slurry Lime

Advantages: Slurry lime is a dust free lime and requires less additional water compared to quicklime and hydrated lime. It is also easier to spread it and to achieve even distribution through the soil.

Disadvantages: Higher cost and slower application rate are the main disadvantages of slurry lime. It is also not practical to use slurry lime to dry the soils and to modify soft soil with high moisture content.

3.3.4 Agricultural Lime

Based on experience with treatment and neutralisation of Acid Sulfate Soils, a fourth type of lime, fine powdered agricultural lime, was also investigated through the trial.

The effects of Agricultural (Ag) Lime on soil (Wikipedia, 2018) are:

- Increasing the pH of acidic soil - in other words, soil acidity is reduced and alkalinity increased
- Providing a source of calcium and magnesium for plants
- Permitting improved water penetration for acidic soils
- Improving the uptake of major plant nutrients (nitrogen, phosphorus, and potassium) of plants growing on acid soils

Fine powdered Agricultural Lime is commonly used to neutralise ASSS materials (ASSMAC 1998) but acts in a buffering capacity, active when the pH lowers. The Agricultural Lime used was pure ground calcium carbonate (limestone), unheated/treated, and comprises 98% $CaCO_3$ and 0.9% $MgC0_3$.

Ag Lime reacts with acids as follows:

$$CaCO_3(s) + 2H^+(aq) \rightarrow Ca^{2+}(aq) + CO_2(g) + H_2O\ (l)$$

It was assessed that whilst the use of Ag Lime to stabilise soils for geotechnical purposes is not commonly done and may not achieve any strength gain, a field check of this effect was assessed to be worthwhile given carrying out such a trial in conjunction with the main trial was relatively cost effective. Also, a field check of the effectiveness of the required percentage of Ag Lime necessary to achieve neutralisation of the ASSS was to be investigated which provided valuable data for future ASSS Management onsite.

3.3.5 Summary

Selection of any of the above limes depends on the following factors:

- Type of the soil requiring treatment;
- Soil moisture content;
- Climate conditions;
- Population in the proximity of the site;
- Workers experience;
- Cost of project;
- Available machinery;
- Volume of lime needed; and
- The purpose of treatment (Modification and drying and/or stabilisation, or neutralisation).

3.3.6 Summary

Of the three type of lime used for geotechnical treatment, Hydrated Lime was chosen as the preferred additive due to the relative safety of use in construction whilst also being able to dry the soil and increase soil strength.

Fine powdered agricultural lime (Ag Lime) was also chosen as an additional additive for the reasons stated above.

3 FIELD TRIAL WORKS

The future harbour floor was originally designed to be excavated to about RL -4.0m (AHD). However, the logistics of doing this in a complex geological environment were initially quite challenging and significant excess ASSS materials were to be produced from the harbour excavation.

It was known that high value engineering fill materials needed to be sourced for bridging, structural, and preload fills in adjacent areas. Therefore, rather than only excavating the harbour to RL-4.0m (AHD), it was theorised that over-excavation of the harbour floor area could be carried out to provide most of these high value engineering materials and to provide storage volume for disposal of ASSS materials below water level (rather than to offsite disposal areas). The main issue with doing this was how to emplace the ASSS materials in the harbour floor area.

The concept of staged over-excavation deeper than the harbour floor, removal and placement/stockpiling of the high value engineering fill materials and placement of ASSS within disposal cells was formulated, and this method of construction was investigated as part of the field trial.

At the time of the field trial, the proposed Boat Harbour was designed to be excavated to a depth of RL-8.5m (AHD). The excavated Boat Harbour zone was then designed to be refilled back to -4.0m RL mainly using ASSS material. The field trial was carried out to assess the practicality and workability of the placement of non-treated ASSS material and lime-treated ASSS material at these depths onsite.

4.1 TRIAL AREA, BUND SIZING AND GENERAL ARRANGEMENT

The trial area was carried out within the Stage 1 portion of the Boat Harbour construction site in 2013. The site was chosen as the trial floor and base areas were entirely within residual soil or weathered rock. Groundwater

continuously flowed upwards from the floor area but was being controlled through drainage to sumps and pumping.

Figure 1 shows the approximate location for the trial. It was divided into two cells which were located within excavated western portion of the Boat Harbour. The size of each cell was approximately 15m × 15m at the base. Coarse drainage rockfill was placed over the floor area of each cell and the rockfill was interconnected to allow dewatering to occur and prevent upwards saturation through from the floor of each bund.

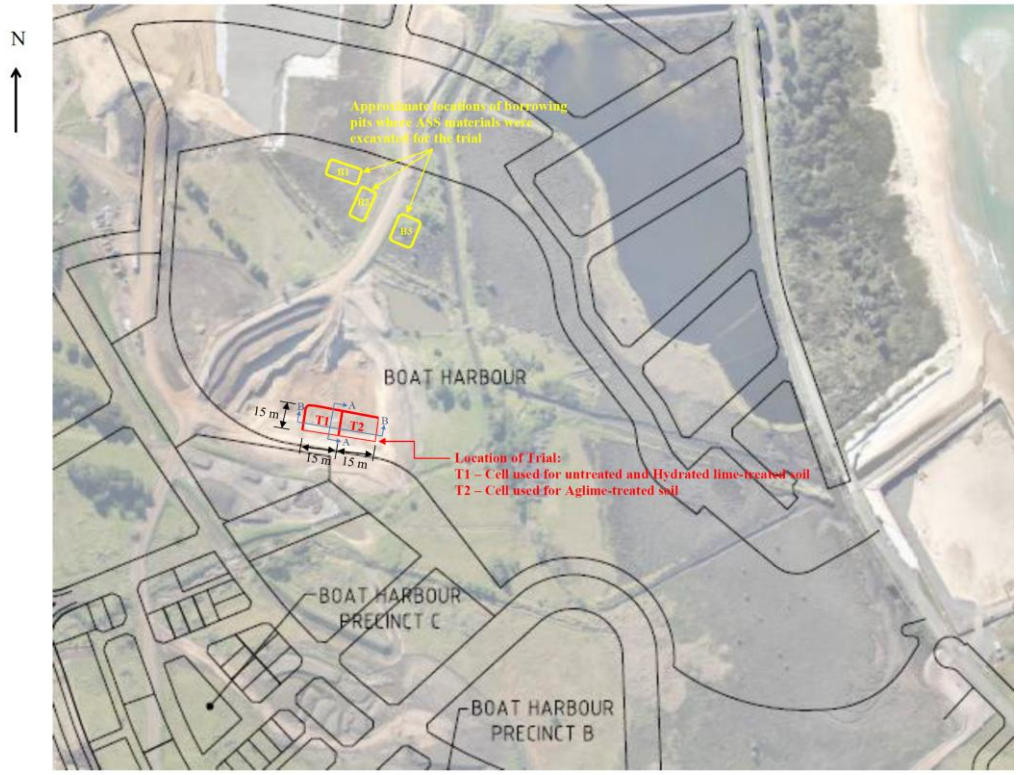

Figure 1- Location of Trial Cell and ASSS borrow areas within Shell Cove Boat Harbour footprint

Figures 2 and 3 show the typical cross sections of the cells and size of the bunds. These figures show the planned final cross sections of the cells filled with ASSS material and capped with a clayey capping layer. However, each cell was only filled by two soil layers having a total thickness of approximately between 1.5m to 2.0m.

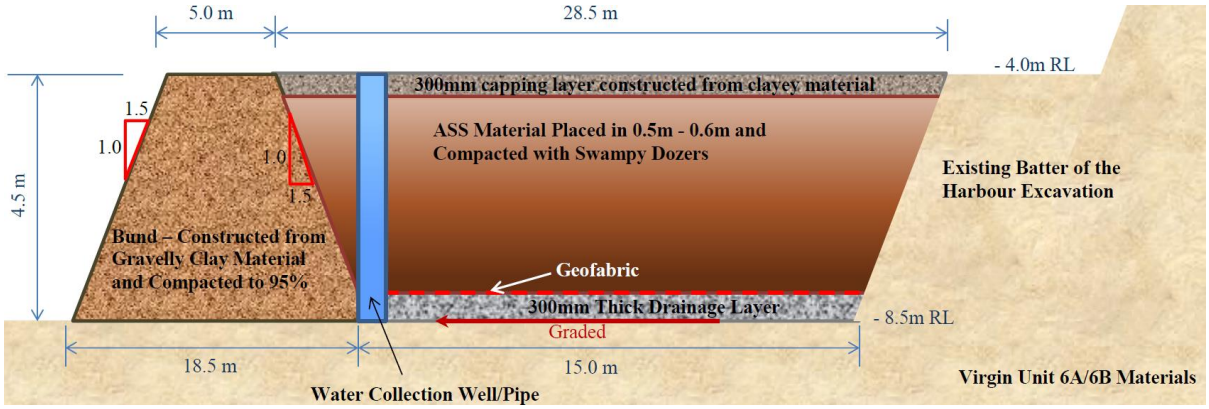

Figure 2 - Planned work - Section A-A of the Trial

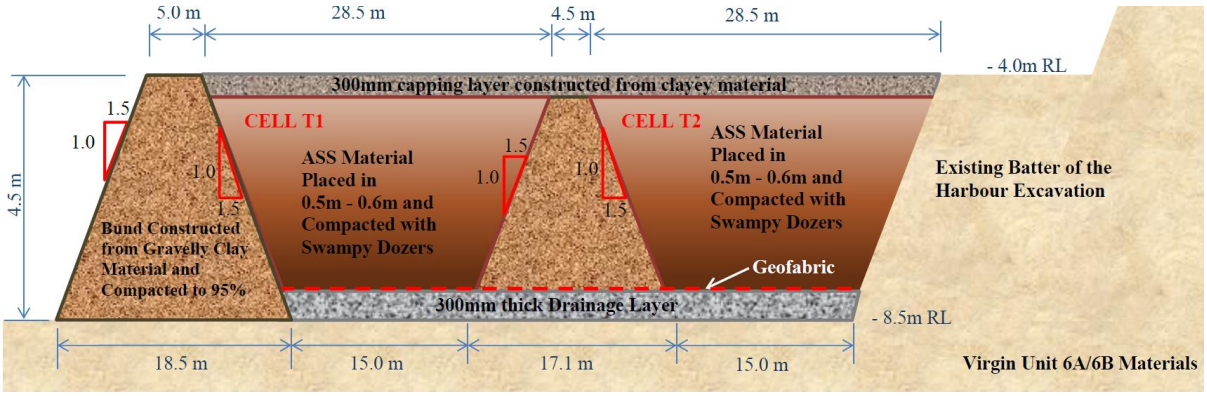

Figure 3 - Planned works - Section B-B of the Trial

The final thickness of fill material placed within each cell during trial work is shown in Figure 4.

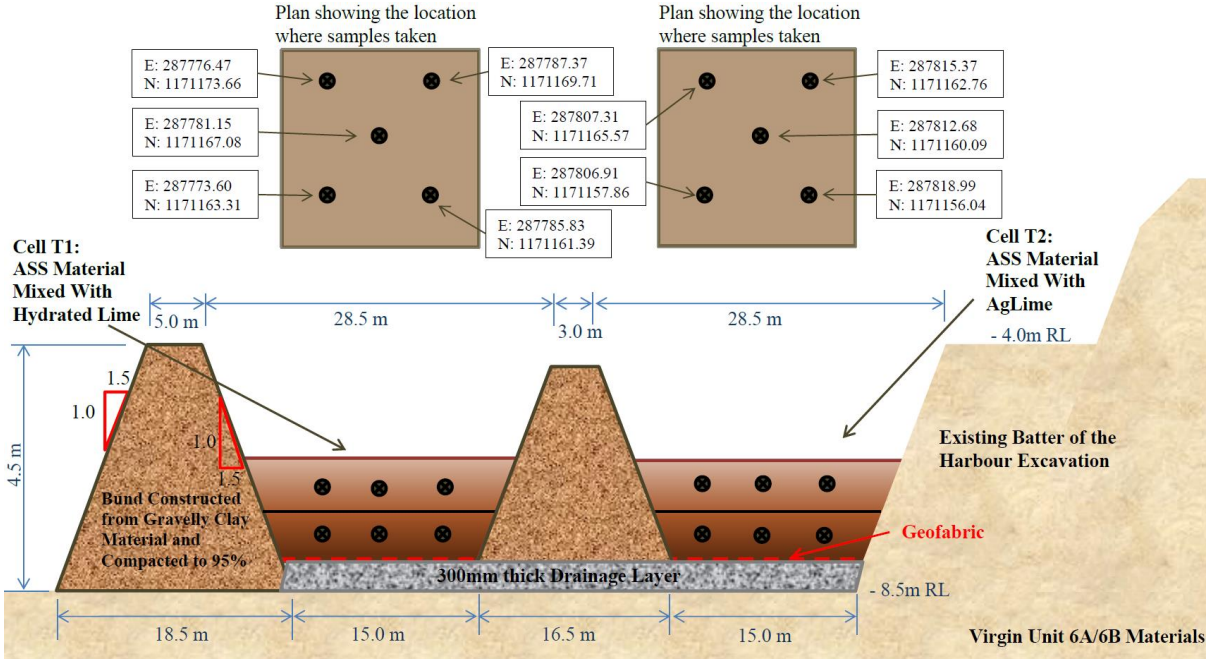

NOTE:
(1) Samples for pH testing were taken from app. 50mm to 100mm below the surface of each layer.

Figure 4 - Actual works - Section B-B of the Trial

Bunds were constructed using gravelly clay materials (Unit 4) by placing and compacting them in layers no more than 250mm thick. Each layer was compacted to a minimum dry density of 95% of Standard Compaction. Batter slopes of the bunds were constructed to a slope not greater than 1.5H:1V.

An assessment of the stability of the bund construction with Slope/W assuming a 25kPa uniformly distributed load at the crest assessed the Factor of Safety to be in excess of 1.3. It should be noted that during movement of the long reach excavator over the constructed bunds, some damage to the top of the bunds occurred. Formation of the bunds by leaving in-situ materials in place (rather than reconstruction of filled bunds) could potentially reduce this effect due to the presence of rock strength materials within some portions of the bunds.

4.2 GENERAL FILLING ACTIVITIES ADOPTED FOR PLACING ASS MATERIAL

To construct the bunds and to place the ASSS material within the trial cells, the following procedure and steps were adopted to best achieve the objective of the trial:

1) Three bunds (northern, western, and middle bunds, see Figure 1) were constructed to bund and divide the trial area to two cells (See Cells T1 and T2 in Figure 1 and Photo 1(a) and Photo 1(b)).
2) The southern and eastern bund walls and the bund floor comprised insitu soil and rock that had been formed as permanent works for the future harbour excavation. It should be noted that the floor of the bund area was at about RL-8.5mAHD. Significant groundwater was flowing out of the bund floor areas during the trial, requiring continual dewatering.
3) The northern, western and middle bund walls were constructed using controlled fill materials. In-situ density testing on the compacted material was carried out by the contractor to make sure that the adequate degree of compaction achieved for each layer before placing and compacting the next layer.
4) Photo 1(a) and Photo 1(b) shows the trial cells after completion of the bunds. Photo 1(b) shows the location of the pump that was installed at the north-east corner of cell T2 to pump the collected water out of the cells;
5) After constructing the northern and western bunds and before constructing the middle bund, a 300mm thick drainage layer was placed at the base of the cells passing under the middle bund (see Figures 2 and 3). This layer was placed to drain the water towards the water collection location at the north-east corner of the cell T2 (see Figure 2 and Photo 1) where the water was collected and pumped out of the cell and was tested for the acidity to be neutralised when and if necessary prior to discharge. This drainage layer was constructed using crushed rock;
6) A Geofabric layer was then placed on top of the drainage layer to prevent ASSS material migrating into and clogging the drainage layer (see Photo 1);
7) ASSS materials were then excavated from the borrow locations (see Figure 1 and Photo 2) using a long reach excavator and transported to the trial cells by trucks. The material was then dumped within the cells and spread by long reach excavator (see Photo 3 and 4);
8) For the lime-treated soils, a small excavator was used to spread one bag of Aglime or Hydrated lime (weighing about 1.0 tonne which was approximately 4% of the soil dry density) per truckload of ASSS materials. Each truckload was a Moxy truck capable of holding about 40 to 50 tonnes of soil. The lime was placed on top of the truck load when it was dumped within the cells, and then mixing of the soil with lime was carried out by a long reach excavator;
9) Following placement of enough material for one layer (approximately 1.0m thick) within each cell (and mixing with lime for the lime-treated cases), a long reach excavator was used to better mix the soil and spread it over the cell to achieve a relatively uniform thickness across the cell. The long reach excavator was also used to compress and compact the soil as much as possible using back of its bucket.
10) The above steps were repeated for the placement of second layer within each cell after carrying out pH and Hand Vane Shear testing from the already placed layer. Before placing the second layer, a swampy dozer was used on top of the first layer to see whether it could easily travel and properly move/push the material above the first layer.

(a)

(b)

Photo 1: Trial cells after completion of the bunds.

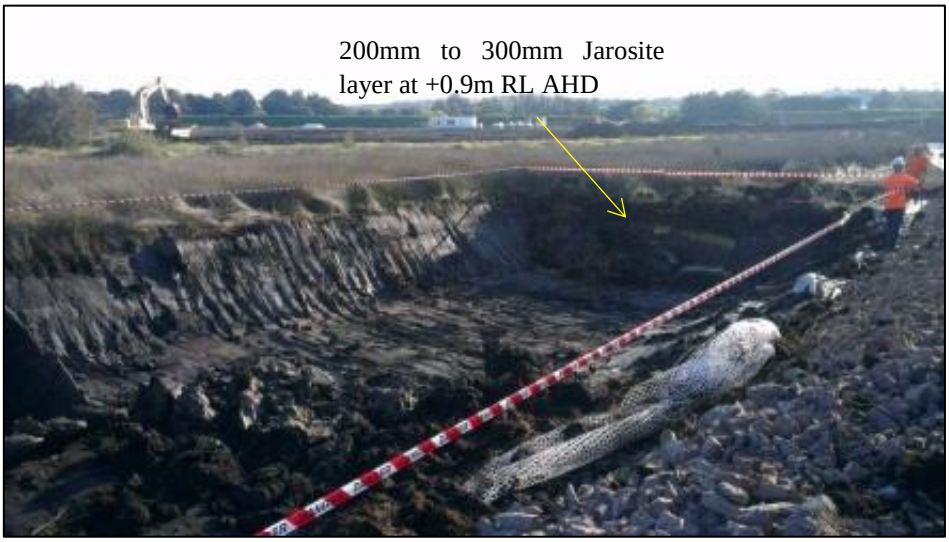

Photo 2: Extent of excavation for borrowing pit B1 and location of Jarosite layer.

Photo 3: ASSS material midway through being dumped within trial cell by trucks.

Photo 4: Long reach excavator spreading and compacting soils within trial cell T1.

4.3 DETAILED FILLING ACTIVITIES ADOPTED FOR PLACING ASS MATERIAL

Three borrow pits (B1, B2, and B3, see Figure 1 for the locations) were used to source the required ASSS material for the trial works. The borrow pits were generally excavated to a depth of 2.5m below the existing ground surface level (after stripping off the vegetation) at the time of excavation. The borrow pits excavated through Actual Acid Sulfate Soil (AASS) and Potential Acid Sulfate Soil (PASS). The following is a summary of the activities carried out in relation to the excavation of the borrow pits:

1) Excavation of the pits started at borrow pit B1. Excavation started from its western side and progressed towards the east on 2 September 2013. Photo 4 shows the excavated pit (completed to the entire extent on 3 September 2013) and the location of the Jarosite layer. Excavated material from this pit (which comprised a mixture of AASS and PASS) was transported and placed within cell T1 on the same day. After placing the material within cell T1, it was attempted to use a swampy dozer to spread and compact the material across the cell but this was not successful as the material was too moist, disturbed and had low shear strength (not enough to support the pressure of the swampy dozer), and the dozer sank into the material after few passes. Photo 5 shows the swampy dozer when it stuck within the material and attempted to get out of the cell.

Photo 5: Unsuccessful attempt of swampy dozer to spread and compact untreated material within cell T1

2) Following unsuccessful attempts of the swampy dozer to travel on top of the material, a long reach excavator was used to spread and compact the material within the cell. Photo 6 shows cell T1 after placement of the first layer (untreated ASSS material) which was spread and compacted using the long reach excavator. The average thickness of this layer was approximately 1.0m.

Photo 6: First layer of untreated ASSS material placed within cell T1

3) On 3 September 2013, excavation of the borrowing pit B1 continued further to the east and the excavated ASSS material (mixture of AASS and PASS) was transported to cell T2 where it was planned to place lime-treated material. Because of the availability of the Agricultural lime (which was already being used to neutralise the Acid Sulfate Soil) onsite, it was decided to initially examine the effectiveness of the Aglime to modify and dry the soil. It was already understood that Aglime is more environmentally friendly than hydrated or quicklime in terms of its ability to neutralise ASSS material whilst being much less soluble in water. However, the extent of its effectiveness from a geotechnical perspective was not clear. Following the placement of the material within the cell, adopting the same procedure as it was adopted for cell T1, approximately 4% (based on the soil dry density) Aglime was spread and mixed with the soil. A small excavator was used to spread and mix the lime with ASSS material. Photo 7 shows the process of spreading and mixing the lime with soil using a small excavator.

Photo 7: A small excavator spreading and mixing Aglime with ASSS material for the first layer placed within cell T2

4) After placing the material within the cell, a long reach excavator was used to better mix and then spread and compact the material across the cell to achieve a relatively uniform 1.0m thick Aglime-treated ASSS material layer. Photo 8 shows how the long reach excavator carried out mixing, spreading, and compacting the material within cell T2.

Photo 8: Long reach excavator mixing Aglime with ASSS material and then spreading and compacting it for the first layer placed within cell T2

5) The ASSS material used and placed for the first layers within both cells T1 and T2 was a mix of AASS and PASS. This mixture was placed within cell T1 without any treatment and within cell T2 as Aglime-treated material. It was then planned to use only PASS material and treat it with Aglime and then place it as second layer within cell T2. So, on 9 and 10 September 2013 the second borrowing pit (B2, see Figure 1) was excavated to source the PASS material required for the second layer to be placed within cell T2.
6) On 10 September 2013, the pump installed within cell T2 was not functioning for about 2 to 3 hours resulting ground water inflowing and filling both cells T1 and T2 and the water covered the surface of a portion of the material placed within these cells. Photo 13 shows the cells during the period when the pump was not functioning. The pump was fixed and started operating and the water was drained off the cells before placing additional material in. When the water was completely drained off the cells then PASS material excavated from borrowing pit B2 was transported, dumped, and mixed with about 4% Aglime and then spread and compacted into the trail cell T2 to form the second layer (approximately 1.0m thick) within this cell adopting exactly the same procedure as it was adopted to place the first layer within this cell.
7) As discussed above, the original plan was to use Hydrated lime to modify and dry the ASSS material for the trial works. After observing that the untreated and Aglime-treated ASSS materials did not obtain the minimum required shear strength (even after few days) to support the load of the swampy dozer, it was decided to change the functionality of the cell T1 to be used to test Hydrated lime-treated ASSS material. Therefore, following steps were carried out:
    - On 12 September 2013, about 4% Hydrated lime was mixed with the ASSS material already placed within cell T1 using a small and a long reach excavators. The small excavator first spread the lime on the surface of the material within the cell and then the long reach excavator was used to mix, spread and again compact the material within the cell. Photo 14 shows the long reach excavator during the process of mixing Hydrated lime with the first layer of ASSS material placed within cell T1;
    - It was decided then to leave this material for few days to dry out and to gain shear strength and then attempt the swampy dozer to see whether it can travel on top the material or not. Unfortunately, there was a heavy rain few days after placing this layer and water filled the cell (see Photo 15). As

a result, the material became too wet and the swampy dozer could not attempt to travel on top of the material as it was planned;

- The rain water gathered within the cells was pumped off the cells after being there for few days. Then, on 25 September 2013 (which was 13 days after mixing hydrated lime with the first layer placed within cell T1), a swampy dozer attempted trafficking on top of the treated material with success. It should be mentioned that at that time still some water existed within the north-east corner of the cell (that was not drained from the previous water covering the soil within the cell) and the material over there was completely loose in a form of a thick slurry; however, the rest of the material was dry enough and gained enough shear strength through addition of hydrated lime to support the pressure of the swampy dozer even after temporary burial beneath rain water (see Photo 16).

Photo 13(a): Cell T2 filled partially with groundwater that rose from the floor of the cell during a period on 10 September 2013 when pump was not functioning.

Photo 13(b): Cell T1 filled partially with groundwater that rose from the floor of the cell during a period on 10 September 2013 when pump was not functioning.

Photo 14: Long reach excavator mixing Hydrated lime with layer 1 of ASSS material within cell T1

Photo 15: Rain water that filled cell T1 after placing the first layer of Hydrated lime-treated ASSS material

Photo 16: Swampy dozer successfully travelling on top of the first layer placed within cell T1 and treated by Hydrated lime

8) On 26 and 27 September 2013, borrowing pit B3 was excavated (and also the southern side of the pit B2) taking both AASS and PASS material and mixing them with about 4% Hydrated lime and placing them within cell T1 as the second layer within this cell. The thickness of this layer was approximately 1.0m. The procedure adopted to place this layer was slightly different from the one adopted to place the previous layers within cells T1 and T2. This time, the Hydrated lime was spread over the dumped material within the cell and then swampy dozer was immediately used to mix, spread and compact the material. The reason doing that was to examine the immediate effect of the Hydrated lime on the material improvement. It was observed that the adopted procedure worked quite well and the swampy dozer could easily mix and spread the material without excessive sinking into the material. However, the following was noted:
   - pH testing was carried out onsite to distinguish AASS from PASS; however, the material encountered from borrowing pit B3 looked like there was some ASSS mixed with some alluvial brownish material and also the consistency was somewhat stiffer than the material encountered from borrowing pits B1 and B2;
   - The material encountered from pit B3 had a lower moisture content compared to the material excavated from pits B1 and B2; and
   - Because of the above two reasons, it was decided to excavate some material from pit B2 which was then mixed with the material sourced from pit B3 to achieve a more similar consistency and moisture content between these materials and the material placed within the trial cells for the previous layers.

Photo 17 shows the swampy dozer tracking on the second layer (Hydrated lime-treated ASSS material) placed within cell T1 and spreading and compacting the material.

Photo 17: Swampy dozer successfully travelling on top of the second layer placed within cell T1 (treated by Hydrated lime) immediately after placement

9) On 9 October 2013, 12 days after placing the second layer (Hydrated lime-treated) within cell T1 the swampy dozer was again driven on top of the material placed into this cell to examine any additional increase in shear strength of the soil. It was observed that the waiting time after mixing Hydrated lime with the soil is an important factor. With increasing the waiting time the material will further dry and gain additional shear strength enabling soil to carry out higher loads with less deflection. Photo 18 visually shows these improvements when the swampy dozer was moving on top of the second layer placed within cell T1. Comparing Photos 17 and 18 clearly shows the effect of time on moisture content decrease and gain in shear strength when soft soil material is mixed with Hydrated lime.
10) Considering the above (and noting that the swampy dozer successfully travelled on top of the first Hydrated lime-treated layer placed within this cell) indicates that the procedure adopted to dry and modify the ASSS material using Hydrated lime was successful for the adopted construction procedure and for the weather conditions when the trial work was carried out.

Photo 18: Swampy dozer successfully travelling on top of the second layer placed within cell T1 (treated by Hydrated lime), 12 days after placement. Note compared to Photo 17, soil surface is tight and strong.

4.4 TESTING AND RESULTS

Geotechnical testing included

- Vane Shear tests within borrowing pits B2 and B3 at different depths and within the material placed into the trial cells. In all locations, testing was carried out at about 200mm below the soil surface
- Within the borrow pits, testing was carried out on 'insitu' soils that had not yet been disturbed
- Hand Vane Shear testing was used to test the undrained shear strength of the first layers placed into the trial cells T1 (for untreated ASSS material) and T2 (for the Aglime-treated ASSS material).
- Hand Vane Shear Tests were carried out within the first and second layers of Hydrated lime-treated material placed into the trial cell T1 as follows:
    - For layer 1, shear vane strength testing was not carried out straight after mixing with hydrated lime and placement of the layer. Testing was going to be carried out several days afterwards to check the strength gain, but heavy rainfall occurred several days after placement. Testing of layer 1 was carried out on 27 September 2013 *after the layer had been buried/saturated from rainfall* (see photo 15). Therefore layer 1 was left until rainfall had finished and the accumulated water could be removed, which was 14 days after initial placement.
    - For layer 2, shear vane strength testing was carried out on 27 September, immediately after mixing with Hydrated Lime, about 15 minutes after initial placement and track rolling of layer 2 with the swampy dozer.

Figure 6 graphically shows the changes in undrained shear strength of the various soils observed as part of the trial. This figure compares the undrained shear strength within borrow pits and the measured undrained shear strength of the material placed within the trial cells for the cases of untreated and lime-treated material. The following observations are made:

- average shear strength of the in-situ material increased with depth within the borrow pits.
- The strength increase in layer 2 immediately after initial mixing with hydrated lime was significant. There was, on average, a 225% increase in undrained shear strength when comparing initial untreated strength (~20kPa) to strength immediately after mixing with Hydrated Lime (~45kPa). This amount of immediate strength increase made a significant difference to immediate traffickability.
- Based on observation carried out on 9 October 2013, the soil had increased in strength significantly even further. No testing was carried out, as based on visual observations the undrained shear strength was easily sufficient to allow passage of the swampy dozer. It was estimated that an undrained shear strength of greater than 150kPa was achieved in the mixed soil.

- The benefit of using Hydrated lime (compared to the untreated or Aglime-treated material) to increase the undrained shear strength is clear from this testing and from this Figure 6. Hydrated lime is effective in providing strength gain, whereas the addition of aglime treatment showed no increase in strength

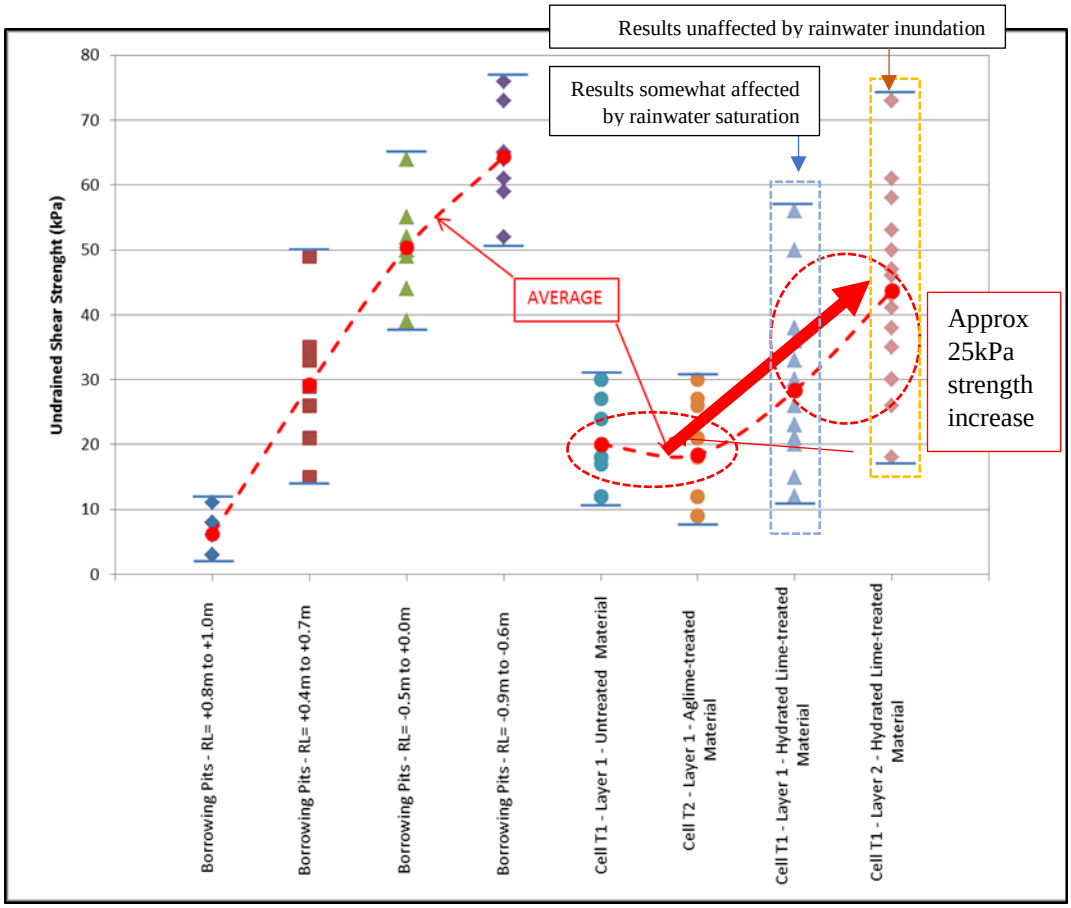

Figure 6: Undrained shear strength measured within borrowing pits and different layers placed within trial cells

4.5 ENVIRONMENTAL TESTING RESULTS

The pH of the material excavated from the borrowing pits was measured onsite at different depths to assess the approximate boundary between the Actual and Potential Acid Sulfate Soils and to obtain an understanding of the approximate average pH of the ASSS material as a base line before placing them within trial cells. In addition, the pH of the material was measured after a few days or immediately after placement of the material within the cells to assess the approximate average pH of the AASS and PASS material being mixed and placed into the cell with or without treatment with lime (including both Aglime and Hydrated lime). Also, some samples taken from the borrowing pits B1 and B2 were sent to the laboratory for Chromium Reducible Sulfur testing to assess the properties of the Acid Sulfate Soils and to recheck the presence of AASS and PASS material at the location of borrowing pits. During the progress of the trial works, the water collected at the north-east corner of cell T2 was also periodically tested (Testing carried out by Contractor) for acidity in case if neutralisation was necessary.

The pH testing results can be summarised as follows:

<u>Borrow Pits</u>

- The initial pH of the AASS ranged between 3.92 and 4.56;
- The initial pH of the PASS ranged between 4.99 and 7.04;

Trial Cells

Untreated ASSS materials:

- The initial pH of the untreated mixed AASS/PASS soil ranged between 4.45 and 6.63;

Aglime treated materials:

- The initial pH of the Aglime-treated mixed AASS/PASS soil ranged between 4.69 and 6.55;

Hydrated lime treated materials:

- The initial pH of the Hydrated Lime treated mixed AASS/PASS soil ranged between 10.99 and 11.67 within an hour of mixing
- The final pH of the Hydrated Lime treated mixed AASS/PASS soil measured between one to two weeks after initial mixing ranged between 9.20 and 11.30.

Groundwater:

- It should be noted that the main source of water from the pump-out well was the water flowing up and out of the formation (rock materials) below each cell. The volume of water pumped out of the dewatering well was a significant volume of water over the course of the field trial and therefore was expected to be close to pH neutral.
- The pH of the water measured from the pump-out well (as measured by Contractor) ranged between 6.2 and 6.5.

4 DISCUSSION

To place the soil "in the moist condition" within an excavation cell, ASSS material needs to be excavated, transported, dumped, spread, and compacted within the excavation zone as rapidly as practicable. This reduces the risk of the exposure of the ASSS material to air and subsequent production of acidic materials through oxidation of pyritic minerals within the soil.

The purpose of the trial was to assess the practicality and workability of the placement of ASSS material within the harbour excavation from a geotechnical point of view as the first priority. The secondary purpose of the trial was to also carry out some acidity testing (for environmental purposes) to generally estimate the effects of the adopted placement procedures on the production of acidic material. This testing was carried out to provide general information and inform responsible parties for the measurement and management of Acid Sulfate materials, as part of an overall Acid Sulfate Soil Management Plan (ASSMP).

5.1 GEOTECHNICAL ASPECTS

5.1.1 Workability of untreated, Aglime-treated, and Hydrated lime-treated ASSS material

It was visually and practically observed and assessed that if the ASSS material is placed within the Boat Harbour excavation as untreated or Aglime-treated material, the soil will not have the minimum required shear strength and bearing capacity to support the transferred load from the construction machinery such as swampy dozers. Therefore, after dumping the material within excavation zone, swampy dozers cannot track over and spread or compact the material.

Based on the reaction equation for Ag Lime, upon reaction with acids in the form of hydrogen ions (H^+), Ag Lime produces water. This is geotechnically adverse: additional water decreases undrained shear strength of soils. This is the reason that no additional strength benefit was gained from addition of Ag Lime to the soil. A slight decrease in strength from ~20kPa to ~18kPa was noted from addition of Ag Lime to the soil as seen in Figure 6 and this supports this conclusion. Therefore it is concluded that if strength increase in ASSS soils is desired, Ag Lime should not be added to soil emplacements as *if Ag Lime is added, a strength decrease below the initial strength* will likely occur.

To overcome this issue, if the material needs to be placed in untreated form and "in the moist" condition, the only practical method was thought to involve excavation of the Boat Harbour floor areas in 'cells' leaving in-situ bunds similar to those used in the trial work but comprising in-situ undisturbed soil and rock materials. These bunds can

then be used as access tracks for the trucks and long reach excavators to dump and spread the material. The minimum required width for the bund at the top should not be less than 6.0m to 8.0m to provide safe working access for machinery. The batter slope of bunds involving leaving insitu very stiff to hard soils/weathered rock insitu (compared to bunds constructed as filled bunds as was used for most bunds in this field trial) could allow steeper batters and increased storage volume. A proper arrangement of the bunds and cells needs to be designed to safely place the material within the excavation zone while providing maximum available volume to bury ASSS material under the water.

It was observed that mixing about 4% Hydrated lime with the ASSS material dries and modifies the material enabling swampy dozers to track on and spread and compact (to some extent) the material.

Also, for the Hydrated lime-treated material, the soil moisture content will further reduce with time and also its shear strength will further increase providing better working platform for the machinery. Therefore if a waiting time is planned between the placement of different layers within harbour excavation, this will help with ease of placement of subsequent layers. Comparing Photos 17 and 18 clearly shows the effect of waiting time.

The undrained shear strength increased from about 20kPa up to ~45kPa immediately after addition of Hydrated Lime, and higher strengths were achieved of >150kPa after a ~2 week waiting period. Undrained shear strength is an important factor for design of working platforms and is routinely used in BS8006 (2010). If Hydrated Lime can be successfully added to strengthen such soils then additional construction benefit for other temporary machinery such as tracked excavators and general construction vehicles could be possible.

This trial was limited in scope and different percentages of lime (different to the 4% adopted) could not be added to optimise the additive percentage. It could be possible that a slightly reduced concentration of Hydrated Lime (say 2% or 3%) may achieve a similar outcome to the 4% used in this trial. Further work would be necessary to confirm this. A slight reduction in concentration of added lime would reduce in significant cost savings for works.

5.1.2 Consolidation Settlement

Significantly less consolidation settlement is expected within soils placed “in the moist” compared to those placed in slurry form. Less consolidation settlement is expected from those soils treated with Hydrated Lime compared to those placed in untreated form.

Consolidation behaviour of the ASSS material was not of major interest as the soils were going to be placed within harbour excavation area and not beneath structures or settlement sensitive areas.

The consolidation parameters and behaviour of the following materials would be different:

1. the in-situ ASSS materials
2. the ASSS materials which are transferred to a slurry form
3. the ASSS materials placed into the excavation “in the moist” condition.

The properties of material type 1 and 2 are relatively well known based on insitu testing results and information Morrison and Tait (2007). If the consolidation behaviour of the material excavated and placed into the excavation “in the moist” condition is required, then further assessment would have been required.

5.2 ENVIRONMENTAL ASPECTS

It is known that the soils used for the trial were either Actual or Potential Acid Sulfate Soils.

The initial pH measurements carried out within the untreated and Aglime-treated ASSS mix AASS/PASS material placed within the trial cells does not show major changes compared to the average pH of the in-situ AASS and PASS materials. However, mixing 4% Hydrated lime with the mix AASS/PASS material placed within trial cell T1 shows considerable immediate increase of pH up to approximately 10 to 11.

If Hydrated Lime treatment is to be used for the disposal cells at any construction site, it is recommended that appropriate management measures be adopted to manage potential pH changes.

It is possible that if swampy dozers are used to push around and place the ASSS mixed with Hydrated Lime, that no lime would be necessary for the final layer, as no trafficking of the final layer would be necessary once the soils are filled to the harbour floor level. This also may have the added benefit of provision of an attenuation layer

to potential Hydrated Lime that may be released into the groundwater during subsequent construction flooding of the harbour and over the longer term. There would be cost savings if the final layer of mixed ASSS with the cells is placed without the addition of lime.

5.3 ALTERNATIVE METHODS USED DURING CONSTRUCTION

After this trial was carried out, the Contractor proposed a somewhat different method of placement of ASSS in the over-excavated portions of the Boat Harbour. This method involved using a very wide and long track 'swampy long reach excavator'. The ground pressure exerted on the ground underneath each track was less than the pressure of a human foot on the ground and less than that of a swampy dozer.

This long reach excavator was found to be able to work over the placed soils without using any additive. A photo of this equipment is shown in Photo 19.

The use of this equipment meant that significant efficiencies were gained and significantly larger storage of ASSS per metre of excavation depth was achieved. The bulk of ASSS materials were placed in over-excavation areas between 2014 and 2016 using this technique, and some ASSS materials continue to be placed in overexcavation areas in 2018. At the time that the ASSS placement work was first carried out (2014) the authors understood that this was the first time such 'swampy long reach excavator' equipment was used for a civil engineering application in Australia. This was an example of a 'win-win' for the project and the Contractor should be commended for their collaborative approach to developing an innovative solution and technique in this circumstance.

Photo 19: Picture of long reach excavator used by the Contractor with large, wide and long tracks used to track out over 'in the moist' ASSS untreated soils

5 CONCLUSIONS

This paper has presented information from a series of field trials for reburial beneath harbour water level of Acid Sulfate Soils. Trials were carried out of both untreated soils and soils treated with either hydrated lime or agricultural lime.

The results of the trials indicated that hydrated lime improved the geotechnical properties of these ASSS materials to a level sufficient for tracking over using a swampy dozer, and agricultural lime had no effect on soil strength at all.

During Construction, the Contractor proposed and used a very wide and long track 'swampy long reach excavator'. This long reach excavator was found to be able to work over the placed soils without using any additive. The use of this equipment meant that significant efficiencies were gained and significantly larger storage of ASSS per metre of excavation depth was achieved.

6 ACKNOWLEDGEMENTS

Authors 1 and 2 wish to thank Frasers Property (formerly Australand) for their support in the publication of this paper.

7 REFERENCES

Austroads, *Guide to Pavement Technology, Part 4D: Stabilised Materials, (2006)* Austroads Publication No. AGPT04D/06, ISBN 1 921139 38 2

British Standard BS8006, *Code of Practice for Strengthened/reinforced soils and other fill (2010)*, British Standards Institution.

Morrison, S.R. and Tait, A (2007) *Settling and consolidation behaviour of dredged cohesive estuarine soil using column testing apparatus,* 10th Australia/New Zealand Conference on Geomechanics - 'Common Ground', pp 336 - 341

Roads and Traffic Authority (2005) *Guidelines for the Management of Acid Sulfate Materials: Acid Sulfate Soils, Acid Sulfate Rock and Monosulfidic Black Ooze,* Roads and Traffic Authority of NSW

Stone, Y, Ahern C.R. and Blunden, B (1998) *Acid Sulfate Soils Manual,* Acid Sulfate Soils Management Advisory Committee, Wollongbar, NSW Australia

Wikipedia, *Agricultural Lime (2018)*, https://en.wikipedia.org/wiki/Agricultural_lime, Wikipedia, accessed August 2018

Wilmot, T.D., *Selection of Additives for Stabilisation and Recycling of Road Pavements, (1994)* http://citeseerx.ist.psu.edu/viewdoc/download?doi=10.1.1.586.4277&rep=rep1&type=pdf, accessed August 2018.

IGS

reducing geotechnical uncertainty

In Situ Testing

CPT, CPTu, SCPTu, Tee-Bar
DMT, SDMT, Vane Shear

Sampling

PPI Piston Sampler
Vibracore & other sediment samplers
Vertek & Window samplers, etc

Other Things

piezos, standpipes & permeabilities

0417-748-669
allan@insitu.com.au
www.insitu.com.au

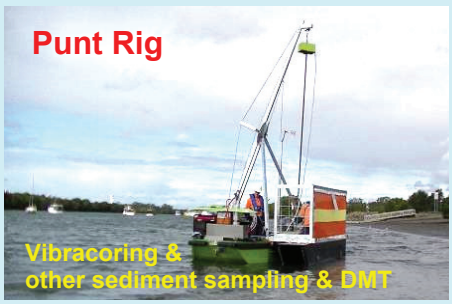

Melbourne *Sydney* *Newcastle* *Brisbane* *Townsville* *PNG*